Utilising CYP199A4 from *Rhodopseudomonas palustris* HaA2 for investigation of the mechanism of cytochrome P450-catalysed oxidations

Tom Coleman

A thesis submitted in fulfilment of the requirements
for the degree of Doctor of Philosophy

14th June, 2018

Supervisor: Assoc. Prof. Stephen G. Bell

THE UNIVERSITY of ADELAIDE

Department of Chemistry
The University of Adelaide
North Terrace Campus
Adelaide, South Australia 5005

Contents

Abstract

The work herein details efforts towards developing a system to better understand the mechanistic details of various oxidative reactions catalysed by cytochrome P450 enzymes (P450s). The bacterial P450 enzyme CYP199A4, from *Rhodopseudomonas palustris* HaA2, is highly selective for substrates with a *para*-substituted benzoic acid framework, such as 4-methoxybenzoic acid. The substrates are oxidised regioselectively at the *para*-substituent. For example, 4-methoxybenzoic acid is demethylated to 4-hydroxybenzoic acid. CYP199A4 has previously been shown to support other P450 mono-oxygenase reactions such as desaturation, heteroatom oxidation and dealkylation. The ready access to simple substrates compatible with CYP199A4, and the ease of purifying this enzyme in high yield, make it suitable for mechanistic study of P450-catalysed oxidations.

The effect of substituents at the benzene ring *ortho* and *meta* positions on the substrate's binding and enzyme activity have been investigated. These revealed that CYP199A4-catalysed demethylation outside of the *para* moiety was feasible with certain *meta*-substituted substrates but occurred with low activity. For example, it was found that CYP199A4 could catalyse the ring-opening of a 3,4-methylenedioxy bridge, but not the ring-opening of an ethylenedioxy substituent, which was hydroxylated to a cyclic hemiacetal.

Substrates containing nitrogen and sulfur moieties at the *para*-position were investigated to determine the catalytic parameters of N- and S-dealkylation versus heteroatom oxidation. CYP199A4 catalysed the sulfoxidation but not the S-dealkylation of sulfur substrates. Nitrogen substrates were N-dealkylated, and no N-oxidation was observed. CYP199A4 was able to generate an unexpected amide metabolite with ethylamino substituted benzoic acids. Halogen oxidation, which has also been previously observed in certain P450 systems, was studied. CYP199A4 did not show activity with 4-halobenzoic acids (F, Cl, Br, I) though these substrates did bind to the enzyme. Furthermore, alkyl substituents which contained halogens were investigated, and oxidative dehalogenation products were observed.

CYP199A4 has been shown to catalyse hydroxylation of the benzylic α-carbon and desaturation of the α,β-carbons of 4-ethyl- and 4-isopropyl-benzoic acids. The partition between hydroxylation and desaturation was investigated by employing substrates with longer and/or more substituted alkyl groups. The substrates tested were all hydroxylated at the benzylic α-carbon when a C$-$H bond was available. Otherwise, the β-carbon was hydroxylated. Additionally, α,β-desaturation was observed with the linear alkylbenzoic acid substrates. CYP199A4 was able to catalyse the oxidation of cycloalkane functional groups. Hydroxylation products were observed with 4-cyclopropyl- and 4-cyclohexyl-benzoic acids although there was very little desaturation.

It is hypothesised that desaturation by CYP enzymes proceeds from either a radi-

cal or cation species. *Meta*-substituted 4-isopropylbenzoic acids with various electron donating and withdrawing functional groups were employed to probe this mechanistic pathway by determination of the partition of hydroxylation and desaturation products. However, the results suggested that the steric properties of the *meta* groups were affecting substrate binding and complicating the analysis.

CYP199A4 possesses the highly conserved acid-alcohol pair (Asp251, Thr252), which facilitates dioxygen protonation and cleavage to generate the active oxidant, compound I (Cpd I). Oxygen activation by P450 enzymes is predominantly understood from work on $P450_{cam}$ and it is hypothesised that these results transfer directly to the majority of other P450s. Theoretical and experimental results differ in their interpretation of the nature of the active oxidant (either the spin states of Cpd I, or one of its precursors). Mutants of CYP199A4 (D251N, T252A) were used to investigate the oxidation of substrates which undergo different P450 reactions. With both mutants and with each substrate tested, the same reactions were observed as with the wild-type. The T252A mutant showed a decrease in activity and an increase in hydrogen peroxide formation with the majority of substrates, however the reduction in activity was not as drastic compared to $P450_{cam}$. The exception was 4-isopropylbenzoic acid, which was more active with the T252A mutant. The activity of the D251N mutant of CYP199A4 decreased dramatically as expected for this mutation, which is hypothesised to reduce the rate of proton delivery. Crystal structures of the CYP199A4 mutants revealed that protons are delivered to the active site via a water channel which extends directly from the surface of the enzyme to the D251 residue. The structural changes induced by the T252A mutation, especially in the I-helix, were less significant than in T252A-$P450_{cam}$. However, there was an additional water molecule found in the active site oxygen binding groove. These structural changes and the location of the water molecule may contribute to the lower than expected hydrogen peroxide uncoupling observed with this mutant.

A range of other *para*-functionalised benzoic acids was screened in order to expand the possible substrate range of CYP199A4. These included larger phenyl and heterocyclic functionalities. With the phenyl-containing substrates, α-benzylic hydroxylation was favoured where possible, and no aromatic oxidation was observed due to the high energy requirements of this transformation. Several of the heterocyclic substrates exhibited type II binding to CYP199A4. 4-(Furan-2-yl)benzoic acid underwent a set of hydroxylation and double bond reduction reactions *in vivo* with CYP199A4. These reactions probably required reduction of the aromatic system by an endogenous *E. coli* enzyme prior to P450 catalysed oxidation.

Overall, the utility of CYP199A4 for investigating diverse P450 oxidation mechanisms was demonstrated. Both the range of substrates as well as the diversity of activities that can be catalysed by this enzyme have been expanded.

Statement of Originality

I certify that this work contains no material which has been accepted for the award of any other degree or diploma in my name in any university or other tertiary institution and, to the best of my knowledge and belief, contains no material previously published or written by another person, except where due reference has been made in the text. In addition, I certify that no part of this work will, in the future, be used in a submission in my name for any other degree or diploma in any university or other tertiary institution without the prior approval of the University of Adelaide and where applicable, any partner institution responsible for the joint award of this degree.

The author acknowledges that copyright of published works contained within this thesis resides with the copyright holder(s) of those works.

I give permission for the digital version of my thesis to be made available on the web, via the University's digital research repository, the Library Search and also through web search engines, unless permission has been granted by the University to restrict access for a period of time.

I acknowledge the support I have received for my research through the provision of an Australian Government Research Training Program Scholarship.

Tom Coleman

14^{th} June, 2018

Acknowledgements

Thank goodness it's finally done. It's been quite a journey to get here and I owe many people my gratitude. Here are but a few.

My biggest thanks have to go to Stephen Bell for being patient in the face of my screw-ups, as well as for providing countless instances of feedback without which this document would be much less comprehensible.

The same has to be extended to the past and present members of the Bell group. Everyone has been supportive and absolutely fantastic to have around. Thanks to Emma, Stella, Sarah, Sam, Rebecca, Ian, Kai, Natasha, Joel, Raihan, Sherry, Matthew, Daniel and Saurabh. Also shoutouts to the summer students.

Second, to John Bruning and his research group in MLS, especially to both Andrews, Bec and Jia. Without John's support and generosity with his time there probably wouldn't be any successful crystallography in this document.

Thanks so much to my family for their continued support and motivation. Mum, Dad, Ella, Derek & the Rusts, Tracy & the Norrises, Zach.

Thanks to my close friends from undergrad and beyond. Alex, Vince, Kate, Peter, Simon, Jess, Sam, Sophie, the ABC Toms (feat. Tim), Tristan and Nick; anyone else whom I may have missed. Thanks to Patrick Tapping for his excellent LaTeX template, and thanks to Matthew Bull for keeping the department running.

Thanks to the lovely people from the RACI Young Chemists Group, especially James for being a very close friend during this time.

Big thanks to Katherine who kindly gave up her time to proofread my questionable grammar and sentence structure. Also thanks to Aaron and John for checking various organic and crystallographic details.

Thanks to musicians from all over the world for keeping me inspired. The list of people and groups I could credit is far too numerous, so here's a brief selection:

Air. Annie. Arcade Fire. The Avalanches. Burial. Can. Charlotte Gainsbourg. CoastDream. Daft Punk. DJ Healer. DJ Rashad. DJ Seinfeld. DJ Sports. Dorian Concept. Erykah Badu. Floating Points. Herbert. Goldie. Holy Ghost! Ikonika. LCD Soundsystem. Jamiroquai. Janelle Monae. Jessy Lanza. Justice. Kode9 & The Spaceape. Kyle Hall. Laurel Halo. Linkwood. LNRDCROY. LSD. MACINTOSH PLUS. Madonna. Marie Davidson. Martyn. Massive Attack. Miles Davis. Mogerlaine. Nicholas Jaar. Oneohtrix Point Never. Panoram. Pender Street Steppers. Project Pablo. Roxy Music. Ross From Friends. SebastiAn. Sinkane. Steven Julien. St Germain. St Plomb. Talking Heads. Theo Parrish. Toro y Moi. YACHT. Zomby.

Thanks to Adelaide, Melbourne, Sydney, Brisbane, London, Vancouver, Berlin and Zurich. Finally, thanks to video games, and to serendipity.

"The storm had now definitely abated, and what thunder there was now grumbled over more distant hills, like a man saying 'And another thing...' twenty minutes after admitting he'd lost the argument."

— Douglas Adams

Figures

Tables

Abbreviations

ACN	Acetonitrile
BA	Benzoic acid
$CDCl_3$	Deuterated chloroform
Cpd I	Compound I
CYP	Cytochrome P450
DFT	Density functional theory
d_6-DMSO	Deuterated dimethylsulfoxide
DTT	Dithiothreitol
E. coli	*Escherichia coli*
EMM	*E. coli* minimal media
EtOH	Ethanol
EtOAc	Ethyl acetate
FAD	Flavin adenine dinucleotide
FMN	Flavin mononucleotide
GC-MS	Gas chromatography-mass spectrometry
HAT	Hydrogen atom transfer
HCl	Hydrochloric acid
HPLC	High performance liquid chromatography
HRP	Horseradish peroxidase
HS	High spin
IPTG	Isopropyl β-D-thiogalactopyranoside
IS	Internal standard
LB	Lysogeny broth
LS	Low spin
NADH	Reduced form of nicotinamide adenine dinucleotide
NMR	Nuclear magnetic resonance
PEG	Polyethylene glycol
PDB	Protein Data Bank
RT	Retention time
SET	Single electron transfer
SOC	Super optimal broth with catabolite repression
TFA	Trifluoroacetic acid
WT	Wild-type

Chapter 1 Introduction

1.1 Cytochrome P450

Cytochrome P450s (CYPs or P450s) are a superfamily of heme cofactor-containing mono-oxygenases, which can be found across all domains of life with remarkably conserved overall fold and function.[1] In their ferric resting state, P450s absorb visible light at 419 nm which accounts for their distinctive red colouring. The name "P450" derives from the unique Soret absorbance band in the reduced CO-bound form (Figure 1, Species IIIa).[2] These systems were first identified in 1958 when Garfinkel and Klingenberg independently identified a unique CO-bound pigment at 450 nm in rat and pig liver microsomes.[3,4] Key work by Omura and Sato confirmed the hemoprotein nature of the pigment.[2]

The number of P450 isoforms in any given organism varies widely. For example, the human genome contains genes accounting for 57 unique P450 systems.[5] Rice contains 458 individual P450s,[6] the bacterium *Mycobacterium tuberculosis* contains 20 such genes,[7] while *Escherichia coli* contains no P450 systems.[8] Additional examples include 46 P450s found in *Apis mellifera* (honey bee),[9,10] 172 in *Nelumbo nucifera* (sacred lotus),[11] 98 sequences in *Laccaria bicolor* (a carnivorous mushroom),[12] 2 genes in the giant virus *Acanthamoeba polyphaga* mimivirus[13] and one from the acidothermophilic archaea *Sulfolobus acidocaldarius* (formerly *Sulfolobus solfataricus*).[14,15]

At the time of writing, there are currently more than 41,000 named and categorised P450s,[12,16] although genomic mining has revealed more than 300,000 total P450 sequences across all kingdoms of life, the majority of which remain uncategorised. Systematic naming of members of the P450 superfamily is based on sequence similarity and in some instances function.[17,18] The prefix CYP is followed by an alphanumerical string which denotes the family and subfamily of the enzyme. For example, the human CYP2E1 belongs to family 2 and subfamily E. CYP199A4 from the bacterium *Rhodopseudomonas palustris* HaA2 is a member of family number 199 and the subfamily A. CYP family members are defined as those with a similarity in amino acid sequence of > 40 %, while subfamilies have members with similarity > 55 %. Although sequence conservation between P450 proteins of different families may be less than 20 %, the overall structural fold is highly conserved between most P450 enzymes. However, the active site environment for substrate recognition differs significantly between P450s, which makes cytochrome P450 one of the most versatile biological catalyst superfamilies.

Certain bacterial P450s, such as $P450_{cam}$ from *Pseudomonas putida*,[19] have been extensively researched since their discovery because of the ease with which they can be expressed and purified in *E. coli*. P450s derived from plant or animal cells are anchored

in the cell membrane, and are often more difficult to express and purify. Furthermore, these P450s are prone to denaturing, which can make experiments employing these systems difficult to perform.

The primary function of P450s are as mono-oxygenases, which catalyse the cleavage of the O−O bond of molecular O_2 and insertion of an oxygen atom into a substrate C−H bond. This process occurs alongside formation of a H_2O molecule. Commonly, NADH or NADPH (subsequently NAD(P)H) is employed by the enzyme as the source of two electrons, and these are transferred one at a time by electron transfer partner proteins (Equation 1).[8,20]

$$\mathrm{R{-}H + NAD(P)H + O_2 + H^+ \longrightarrow R{-}OH + NAD(P)^+ + H_2O} \tag{1}$$

P450s catalyse a wide range of important transformations, including the synthesis of various metabolites and xenobiotic breakdown in the liver. Examples of these processes in mammalian systems include steroid biosynthesis,[21] drug metabolism[22,23] and vitamin D regulation,[24–26] making them of interest to fields such as biochemistry and medicinal chemistry. These outcomes are achieved by reactions such as dealkylation of methoxy and methylamino groups,[27,28] oxidation of sulfur atoms,[28] desaturation of alkyl chains to yield alkenes,[29,30] and further oxidation of alkenes and alkynes.[31,32]

More recently, P450s have become valuable for use in oxidative synthetic chemistry, because they can stereoselectively act on a specific C−H bond to efficiently produce compounds which are difficult to access via synthetic methods. P450s are attractive candidates for performing these reactions because of their high energy efficiency and low environmental impact, particularly the absence of waste products. The potential synthetic utility of cytochrome P450s in enzymatic oxidation and the numerous reactions they can catalyse has led to a significant body of research into the mechanisms of substrate binding and oxidation.[1,8,33]

The primary oxidant employed by P450s in substrate oxidation is compound I (Cpd I), which is a highly reactive Fe(IV)-oxo species capable of abstracting a hydrogen from a substrate C−H bond (Figure 1, Species VI).[34] The short lifetime of Cpd I made its characterisation difficult, although recently it has been investigated under cryogenic conditions which confirmed its nature as the key intermediate.[35]

Cpd I is generated during the P450 catalytic cycle as follows: The distal H_2O ligand dissociates upon binding of the substrate (Figure 1, Species I and II), shifting the P450 absorbance maximum from 419 to 390 nm. The ferric state heme is then reduced to ferrous Fe(II) by transfer of the first electron by a partner protein. Molecular oxygen then binds to the unoccupied distal site (Species IV). Subsequent transfer of a second electron and a proton results in a hydroperoxy species, Cpd 0 (Species V). A second proton transfer initiates O−O bond cleavage by release of H_2O, to form the highly reactive oxidant, Cpd I (Species VI).

Upon formation, Cpd I reacts rapidly with the substrate to release the hydroxylated product via a radical rebound mechanism (Figure 2), resulting in the oxidised substrate (Figure 1, Species VII).[34,36] The substrate C−H bond is homolytically broken by Cpd I, resulting in a substrate radical (Figure 2). The radical then recombines with the heme-bound hydroxy group to form the product (R−OH). This product leaves the P450 active site and H_2O binding regenerates the 6-coordinate ferric heme (Species I).

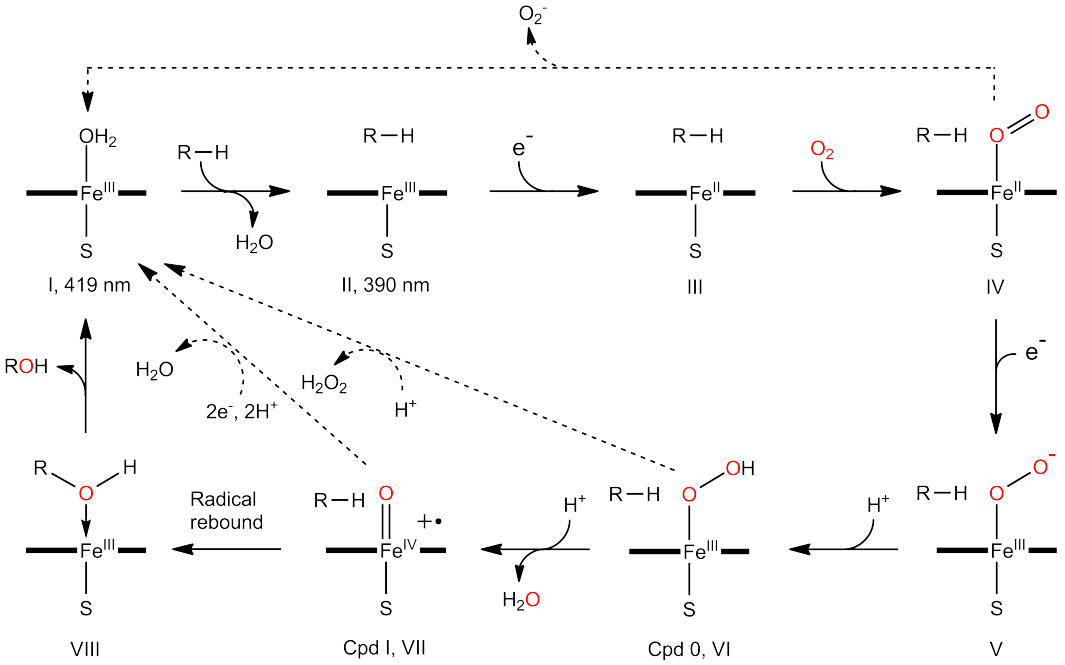

Figure 1. The catalytic cycle of P450 enzymes. Resting state (I) binds substrate (R−H), where controlled reduction by 2 H^+ and 2 e^- generates the reactive iron(IV)-oxo intermediate (Cpd I). Radical rebound generates hydroxylated product (R−OH). The fate of the two oxygen atoms of molecular O_2 is shown in red.

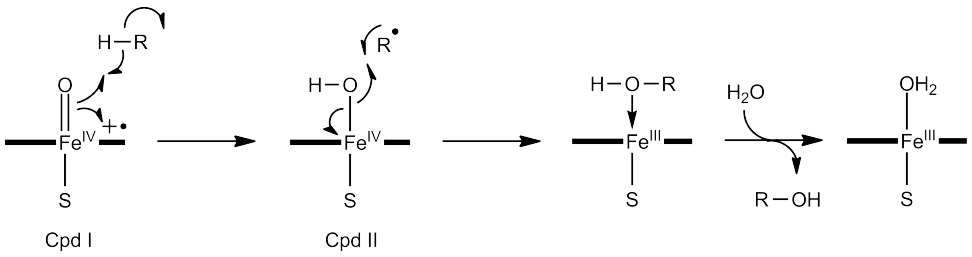

Figure 2: Oxidation of substrate (R−H) by Cpd I via radical rebound.[36]

1.2 P450 electron transfer systems

The majority of P450s are not able to source electrons directly from NAD(P)H, and hence require electron transfer systems for oxidative activity. Electron transfer systems consist of one or more partner proteins, the nature and number of which varies significantly between organisms.[20] Two broad classes, classes I and II, are found in the majority of studied P450 systems (Figure 3, top).

Class I includes most bacterial P450 systems and the mitochondrial P450s from eukaryotes. These employ a cytochrome P450 in conjuction with two redox partners. The first is a flavin adenine dinucleotide (FAD) domain reductase (a ferredoxin or adrenodoxin reductase), which transfers the NAD(P)H-derived reducing equivalents to an iron-sulfur cluster-containing protein (a ferredoxin or adrenodoxin). This ferredoxin then directly reduces the cytochrome P450. Bacterial class I systems are cytosolic; in eukaryotic class I systems only the ferredoxin protein is soluble and the reductase and P450 are both membrane-associated. Despite these two class I systems functioning in a similar manner, most ferredoxins are not capable of efficiently reducing P450s derived from a different system. For example, a bacterial ferredoxin may not function effectively with a eukaryotic P450, or vice versa (although exceptions are known).[20]

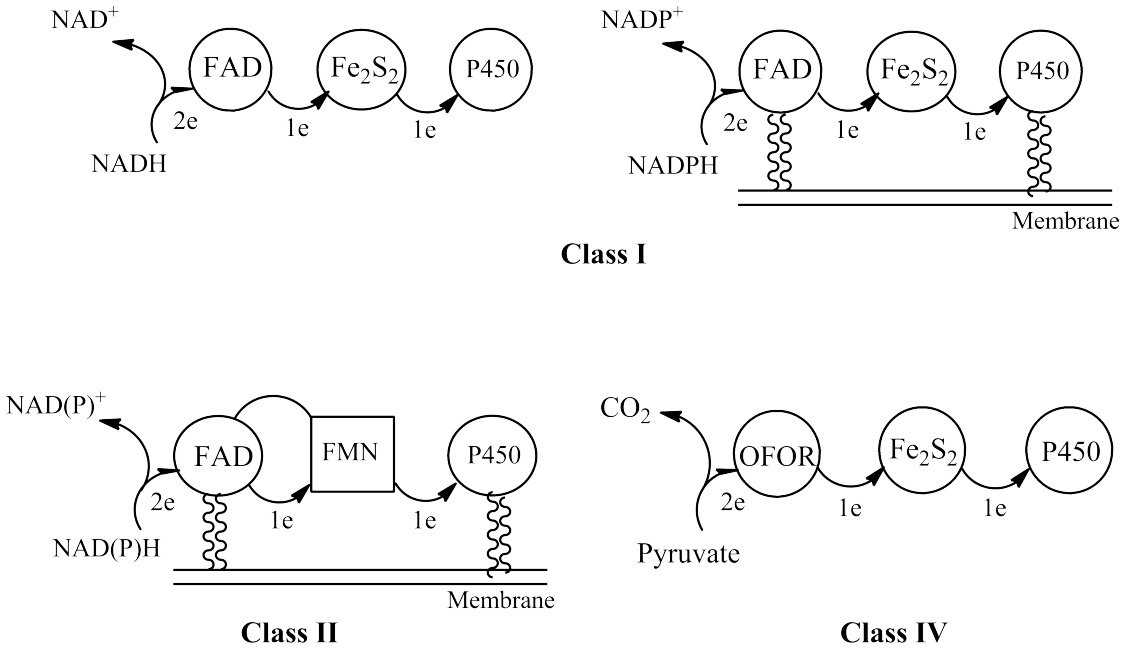

Figure 3. Electron transfer systems of cytochrome P450s. Shown are classes I, II and IV. Top left shows the bacterial class I system; top right, the eukaryotic membrane-associated class I system. Bottom left, class II, a diflavin-driven membrane-bound system. Shown in the bottom right is an example of a more unusual system, derived from *S. acidocaldarius*, which is driven by an oxoacid ferredoxin oxidoreductase domain (OFOR), employing pyruvate rather than NAD(P)H. This system has been designated as class IV.[20,37]

Class II P450 systems are found in various eukaryotes such as mammals, fungi and plants, and thus are associated with diverse metabolic pathways. Class II systems consist of a P450 and an NADPH powered diflavin reductase (containing the FAD and FMN domains) which is responsible for tranferring all required reducing equivalents to the P450 enzyme (Figure 3, bottom left). Being eukaryotic in origin, class II systems are membrane-bound and thus typically have lower water solubility and stability compared to class I systems.

In the remaining classes III-X, the electron transfer systems are typically derived from bacterial, fungal or plant origins, and contain less common electron transfer systems with unique structural features or novel mechanisms of action.[20] For example, the class IV system which supports CYP119A1 from the acidothermophilic archaeon *Sulfolobus acidocaldarius* (Figure 3, bottom right) does not contain an NAD(P)H-dependant flavoprotein, and instead employs pyruvic acid along with a ferredoxin and an FMN domain protein to supply CYP119A1 with electrons.[14,37,38]

1.3 Oxygen activation by P450 enzymes

The use of atmospheric dioxygen by P450s allows for events where reductive equivalents of NAD(P)H are not successfully channelled towards substrate oxidation. These points of stoichiometric inefficiency, known as uncoupling pathways, can result in the release of superoxide immediately after molecular oxygen binding (Figure 1, Species IV), generation of hydrogen peroxide (H_2O_2) from Cpd 0, or water from the reduction of Cpd I prior to radical rebound (Figure 1).

The controlled delivery of both protons to the active site is thus crucial to facilitate the successful activation of molecular oxygen. Protonation of Cpd 0 can occur at either the distal oxygen, resulting in homolytic O−O bond cleavage, or at the proximal oxygen, which results in the generation of hydrogen peroxide. These protonation events are facilitated by a highly conserved acid-alcohol pair of amino acid residues found in the I-helix, commonly aspartic acid/glutamic acid (Asp/Glu) and threonine/serine (Thr/Ser). Although these residues are highly conserved across P450 systems, variations are known to exist.[39] For example, $P450_{cin}$ (CYP176A1) contains asparagine in place of the conserved alcohol threonine (Asp241 - Asn242).[40]

Much of the current understanding of the roles of these residues in the protonation steps is derived from $P450_{cam}$. This enzyme rapidly hydroxylates camphor to 5-*exo*-hydroxycamphor (product formation $> 1000\,\mathrm{min}^{-1}$), with nearly all of the reductive equivalents channelled into substrate oxidation.[41–43] Roles for both key residues have been proposed based on extensive studies. The Asp251 residue is believed to be involved in proton transfer to the Fe(III)-peroxy complex (Figure 1, Species V),[44,45] whereas Thr252 is thought to stabilise Cpd 0 in order to facilitate O−O bond cleavage.[41,42]

The T252A mutant of $P450_{cam}$, in which Thr252 is substituted for an alanine residue, displayed 95 % H_2O_2 uncoupling and 1 % wild-type product formation, although the NADH oxidation rate (a measure of the turnover of the catalytic cycle) remained comparable to the wild-type.[41,42] This appeared to implicate the OH group of Thr252 as a direct proton source for the protonation of the hydroperoxy intermediate. This hypothesis was later questioned by the high activity of a Thr252-MeO-Thr mutant,[46] which possesses an oxygen atom that could act as a hydrogen bond acceptor but not as a donor. Additional studies with the Thr252-Asn and -Ser mutants showed retention of camphor hydroxylation activity, albeit with varied turnover rates.[33,39] The crystal structures of camphor-bound $P450_{cam}$ variants provided an explanation for their high degree of uncoupling. In the wild-type enzyme, the Thr252 alcohol group hydrogen bonds to a water molecule and to the carbonyl group of a glycine, Gly248 (Figure 4a). In the T252A mutant structure, there is no G248-A252 hydrogen bond, allowing an additional water to enter the active site and bind near camphor (Figure 4b). This suggested that hydrogen peroxide uncoupling may be caused by a mis-protonation

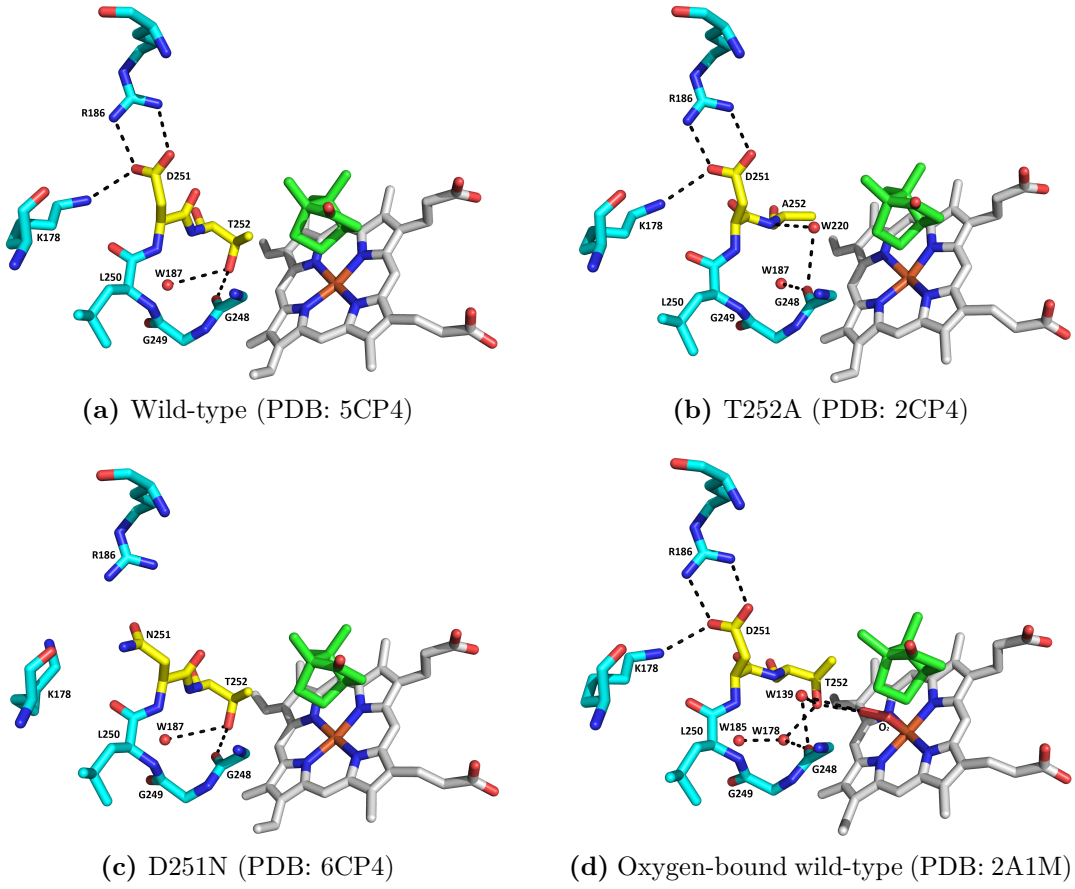

(a) Wild-type (PDB: 5CP4)

(b) T252A (PDB: 2CP4)

(c) D251N (PDB: 6CP4)

(d) Oxygen-bound wild-type (PDB: 2A1M)

Figure 4. Active site and oxygen binding groove of the crystal structures of $P450_{cam}$ variants.[44,45,47] Shown are (a) the wild-type, (b) T252A mutant, (c) D251N mutant and (d) O_2-bound wild-type. Camphor is green, the heme group is grey, the 251 and 252 residues are yellow, and water molecules are red spheres. Shown in cyan are the residues comprising the O_2 binding loop and the salt bridge network of $P450_{cam}$.

event due to the presence of this additional water molecule in the active site (W220) rather than the threonine side chain.

The T252A variant showed similar structural changes to those observed in the O_2-bound wild-type $P450_{cam}$ structure (Figure 4d). Upon O_2 binding to the heme iron, a conformational change is induced in the D251 and T252 residues.[45] The I-helix groove widened due to a disrupted H-bond between G248 and T252, which allowed water to enter the active site. The D251 residue's backbone carbonyl group undergoes a 90° rotation so that it can adopt an α-helix H-bonding pattern. In the wild-type O_2-bound structure, an extra water molecule was observed to directly interact with the distal oxygen. There is also an extra water molecule held near the groove that forms a solvent network to the nearby E366. It has been suggested that this network is important to proton delivery.[33] Based on these studies, the proposed role for T252 in oxygen activation by $P450_{cam}$ is to stabilise the hydroperoxy intermediate (Cpd 0) by functioning as a hydrogen bond acceptor to the heme-bound O_2.[45,47,48]

Mutagenesis studies of the highly conserved Asp251 indicated that this residue was also important to $P450_{cam}$'s activity. For $P450_{cam}$, the D251N mutation displayed turnover activity which was reduced by two orders of magnitude, but with high coupling, which suggested that the rate of protonation of the peroxy species to form Cpd 0 (and eventually Cpd I) was being dramatically decreased (Figure 1).[49–51] In the wild-type crystal structure of $P450_{cam}$, the Asp251 residue forms a salt bridge to nearby Lys178 and Arg186 (Figure 4a). However, in the structure of D251N-$P450_{cam}$, these salt bridges are broken as a result of a 90° rotation in the Asn251 residue (Figure 4c). Notably, the Gly248-Thr252 H-bond is not broken in the D251N structure, nor is it upon binding of O_2 to the D251N mutant.[44,45] Thus, the role proposed for D251 in $P450_{cam}$ is part of a proton delivery system to dioxygen.[33] The D251N mutant exhibits a solvent kinetic isotope effect ≈ 6 times that observed for the wild-type, which indicates that the mechanism of proton delivery is altered for this mutant. Additionally, density functional theory (DFT) studies demonstrated the favourable energetics of proton transfer by the D251 residue.[52]

Although the acid-alcohol pair is most commonly Asp-Thr, functional variations are also known. The $P450_{cin}$ D241N mutant displayed a significant reduction in NADH oxidation rate, which was similar to D251N-$P450_{cam}$, in addition to low coupling efficiency.[40]

1.4 Reactions catalysed by P450 enzymes

1.4.1 C–H hydroxylation

Oxidation of a C−H bond is chemically difficult due to the high energy requirements of breaking this bond.[53] However, this is the most common reaction catalysed by the P450 enzyme superfamily. Hydroxylation is thought to occur by a radical rebound process (Figure 2),[36,54] and the majority of research supports the involvement of a carbon radical-containing species in the radical rebound mechanism.[39] High kinetic isotope effects were observed in hydrocarbon hydroxylations, and were interpretated as the O−H−C transition state possessing a linear geometry.[36,55,56] This was used as evidence in support of a hydrogen abstraction mechanism. Independently, a mechanism involving a radical formation step was supported by the observation of stereochemical scrambling in certain hydroxylations.[39] This finding indicated the presence of a species, presumed to be a radical intermediate, which permitted the inversion of carbon stereochemistry before the hydroxyl rebound step.[36,57,58] The involvement of a radical species would suggest that loss of stereochemistry would be observed during substrate hydroxylation. However, most P450 hydroxylations proceed with retention of stereochemistry, implying that the radical very rapidly recombines in the same orientation.[36,39,54]

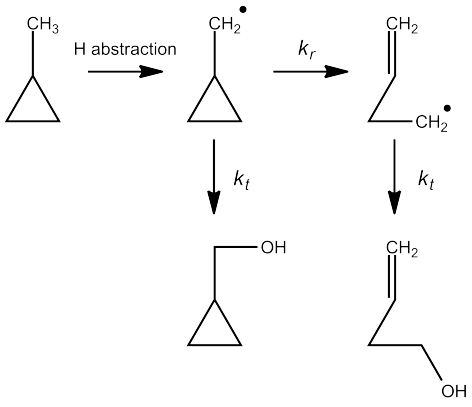

Figure 5. Function of radical clocks. Radical trapping (k_t) and rearrangement (k_r) result in different products.

Radical clock substrates, containing strained cyclopropyl ring systems, have been extensively employed to determine the rate of radical rebound in C−H hydroxylations (Figure 5). These substrates can undergo one of two competing reactions upon radical formation. If rebound occurs at the initial site of H-abstraction, hydroxylation product results (Figure 5, rate=k_t). Alternatively, the radical can undergo a rearrangement (k_r) followed by trapping of the radical, thus yielding a different hydroxylated product. This allows calculation of the rate of radical trapping using the ratio of the products. Radical lifetimes were measured for norcarane and bicyclo[2.1.0]pentane when oxidised by P450s CYP2B1, CYP2E1, $P450_{cam}$ and $P450_{BM3}$. These results supported the proposal of a radical intermediate in the hydroxylation pathway ($\sim$ 50 ps).[59–62] However, more recent studies have suggested that the norcarane radical lifetime may have been significantly overestimated due the prevalence of minor products. This allowed the radical lifetime to be recalculated as 0.5–25 ps, suggesting the determination of the radical lifetime and its subsequent interpretation to be nontrivial.[63] Furthermore, several "ultrafast" clocks displayed extremely short radical lifetimes, which seemed to indicate the radical to be a transition state rather

than a reaction intermediate.[64–67]

Although Cpd I is widely acknowledged as the key oxidising species, many experiments have also been interpreted as evidence that multiple oxidants, namely the nucleophilic ferric peroxy anion and the electrophilic ferric-hydroperoxy Cpd 0 (Figure 1, Species V and VI), are able to catalyse certain mono-oxygenase activities that do not involve C−H bond abstraction.[68–78] Due to their different relative reactivities, these species may have preferences for certain reactions over others.[70,71] For example, Cpd 0 is proposed to facilitate alkene epoxidation[70,71,76] whereas the ferric peroxy species has been implicated in aldehyde oxidation.[69]

Theoretical studies, however, have provided a rationale for the short lifetime of the radical clocks discussed. The electronic configuration of Cpd I can be either a doublet or quartet,[79–82] accounted for by two unpaired electrons on the iron centre in 3d π^* orbitals, and one in the porphyrin a_{2u} π^* orbital (Figure 6, inset). In the high-spin quartet state ($^4A_{2u}$), these three spins are parallel, while the electron in the porphyrin orbital is inverted in the low-spin doublet state ($^2A_{2u}$). When a radical intermediate is considered, these two states display different energy barriers towards the C−H hydroxylation pathway (Figure 6).[81,83–85] Both the doublet and quartet states have similar

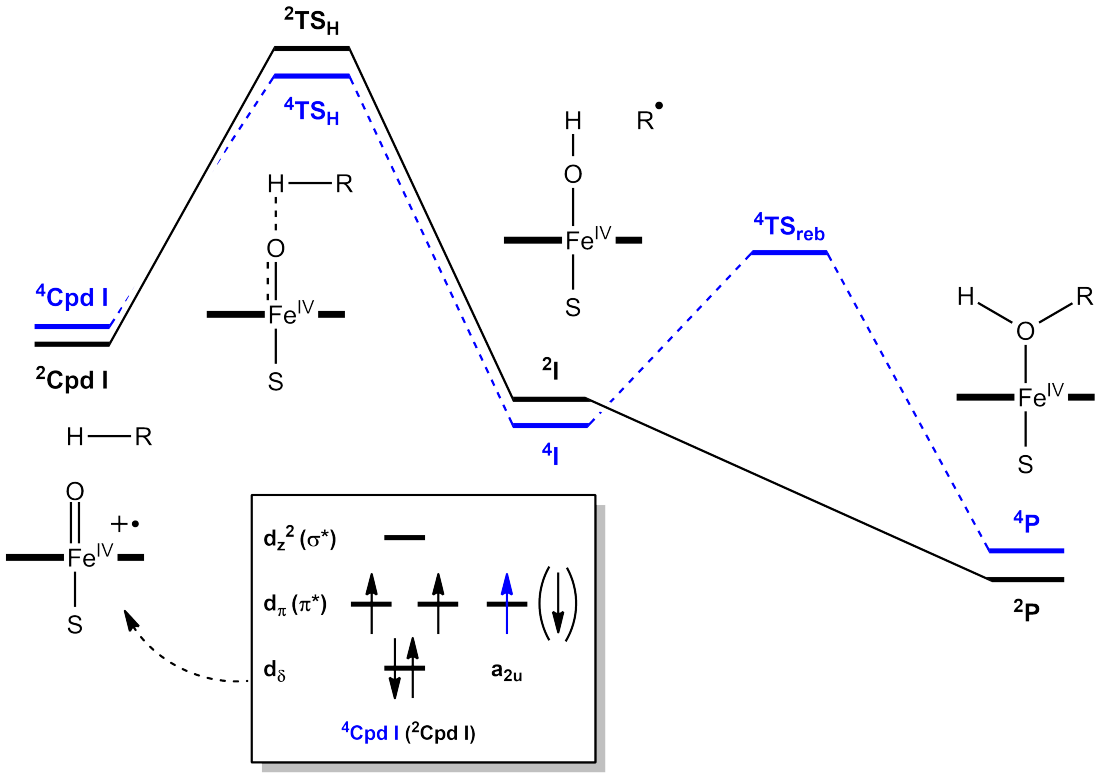

Figure 6. Overall reaction mechanism for alkyl hydroxylation of substrate (R−H) by compound I (Fe^{IV}=O) using the two-state reactivity model.[81] The relative energy of the doublet (^{2}Cpd I, **black**) and quartet (^{4}Cpd I, blue) pathways are shown in the main figure. TS_H represents the transition state to hydrogen abstraction, I represents the hydrogen abstraction intermediate, TS_{reb} the cation intermediate during radical rebound and P is hydroxylated product. The inset shows the electronic configuration of Cpd I in both states.

energy barriers to hydrogen abstraction; however the quartet state displays a high energy barrier for radical rebound, whereas the doublet state shows a negligible barrier for this step. These studies accounted for the short radical lifetimes observed experimentally. Likewise, DFT studies disagree with the proposed involvement of Cpd 0, as the redox potential of Cpd 0 is insufficient to facilitate C−H bond abstraction.[76,86–88] This theoretical observation was also supported by experimental studies, which employed synthetic Cpd 0 mimics for substrate hydroxylation and epoxidation.[89]

Recent theoretical studies towards identification of the P450 active oxidant(s) implicates the close-lying spin states of Cpd I as the most likely candidates.[87] This theory is named the "two-state" reactivity model, and hypothesises that the intermediate involved (either a radical or a cation species) is controlled by the dominant spin state of Cpd I. DFT calculations show a significant energy barrier to radical rebound when Cpd I is a high-spin quartet, whereas this barrier is small for the low-spin doublet species.[81,90–92] In the contrasting "two-oxidant" model, the most abundant species (e.g. Cpd I or Cpd 0) dictates the resulting product distribution.

1.4.2 Dealkylation of oxygen, nitrogen, and sulfur substrates

P450 enzymes are widely known to catalyse the dealkylation of substrates containing oxygen or other heteroatoms. Oxygen dealkylation appears to proceed similarly to C−H hydroxylation, by initial hydrogen abstraction (HAT) at the carbon adjacent to the oxygen (Figures 2 and 7a). The second step is the loss of an aldehyde by decomposition of the unstable hemiacetal.[8,39,93,94]

Heteroatom dealkylation reactions can potentially proceed via a single electron transfer (SET) as an alternative first step to the HAT process. In this mechanism, the heteroatoms of lower electronegativity (N and S) allow transfer of an electron to Cpd I yielding a substrate radical cation (Figure 7b).[39] Subsequently, a proton can be abstracted and rearrangement of the electrons results in a carboradical intermediate, which can be stabilised across the heteroatom and adjacent carbons. Rebound of the hydroxyl from compound II (Cpd II), followed by decomposition of the hemiaminal/hemithioacetal, results in the dealkylated product. There is ongoing debate concerning the relative roles of the SET and HAT mechanisms in nitrogen and sulfur dealkylation reactions.

Experimental evidence for the single electron transfer mechanism (SET) includes low kinetic hydrogen isotope effects (KIE ≈ 2) for N-demethylation of *para*-substituted N,N-dimethylanilines (Figure 7b).[39,95,97,98] These low KIE values are believed to arise from the ease of proton abstraction from the substrate radical.[8] Further evidence in support of the SET mechanism includes the strong correlation between rates of N-demethylation of N,N-dimethylanilines with their respective Hammett substituent parameters and redox potential values.[39,81] The negative σ values indicated that N-

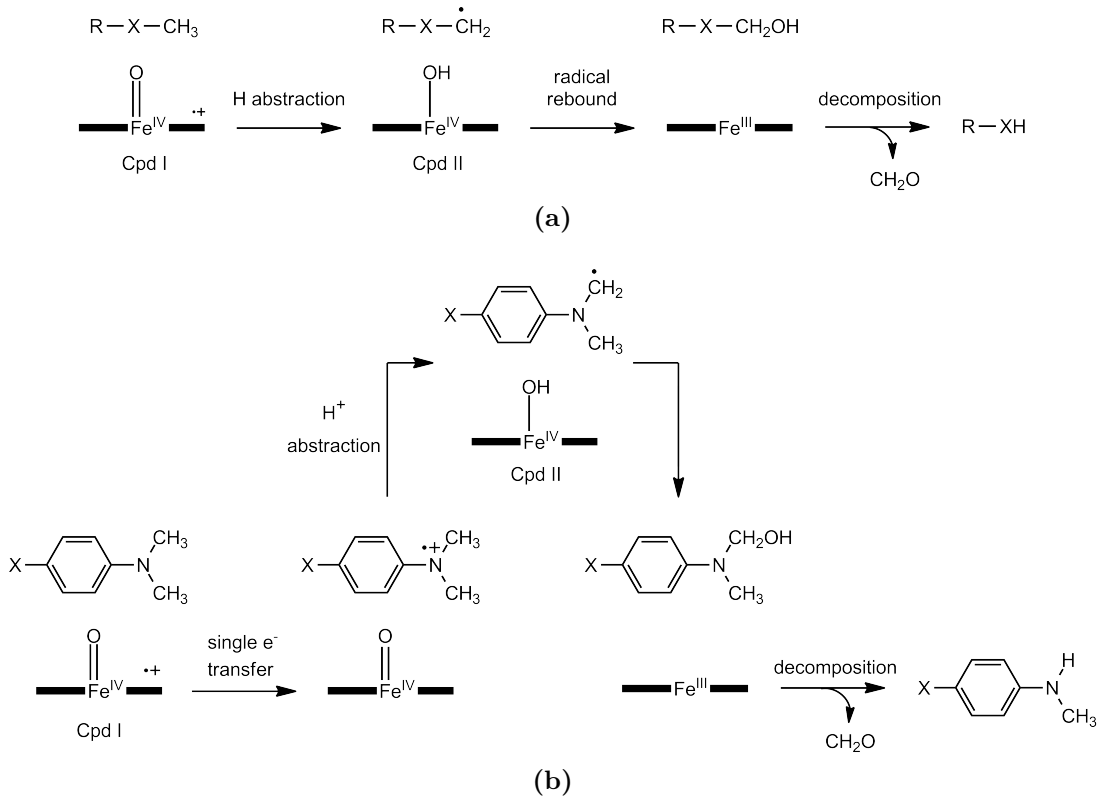

Figure 7. Mechanisms for P450-catalysed dealkylation. Shown are a) Hydrogen abstraction (HAT) pathway for dealkylation of O or N containing substrates, and b) Single electron tranfer (SET) mechanism towards demethylation of *para*-N,N-dimethylalinine substrates.[95,96]

demethylations accelerate in the presence of electron donating substituents, which is consistent with the formation of a nitrogen radical cation via a SET mechanism.[39,81]

Evidence for the HAT mechanism (Figure 7a) has been provided in the form of large intramolecular isotope effects observed for amide N-dealkylations (KIE $\approx$ 13). Additionally, DFT studies are generally in favour of the HAT mechanism for nitrogen and oxygen dealkylation.[8,81,99–101] DFT calculations on *para*-substituted N,N-dimethylanilines showed that the radical cation arising from the first single electron transfer on the SET pathway was significantly higher in energy than its radical counterpart on the HAT pathway (Figure 7).[100,101] The same study also found that dealkylation products can arise (via the HAT pathway) from either of the two spin-states of Cpd I, depending on the nature of the substrate's substituent: the doublet state is preferred when the *para*-substituent of the N,N-dimethylaniline is H or Cl.[81] The gap between doublet and quartet states was also found to decrease with increasing electron withdrawing power of the substituent (X = H < Cl < CN < NO_2, Figure 7b), such that the two spin-states become very close in energy.[100,101]

1.4.3 Desaturation/dehydrogenation

The majority of P450-catalysed reactions result in an oxygen atom in the product. However, desaturation of alkyl chains to form alkenes is an exception which is an important reaction in many metabolic pathways. Key examples include the formation of the hepatotoxic valproic acid desaturation product, Δ^4-valproic acid (Figure 8, top)[102] and metabolism of the capsaicin family of compounds (Figure 8, bottom).[103] In each of these cases, the expected hydroxylation products also form. Crucially, the ratio of hydroxylation to desaturation differs dramatically between substrate/enzyme pairs. For example, a 2:1 ratio of hydroxylation:desaturation is observed with valproic acid and CYP4B1, but increases to 37:1 for CYP2B1.[104,105]

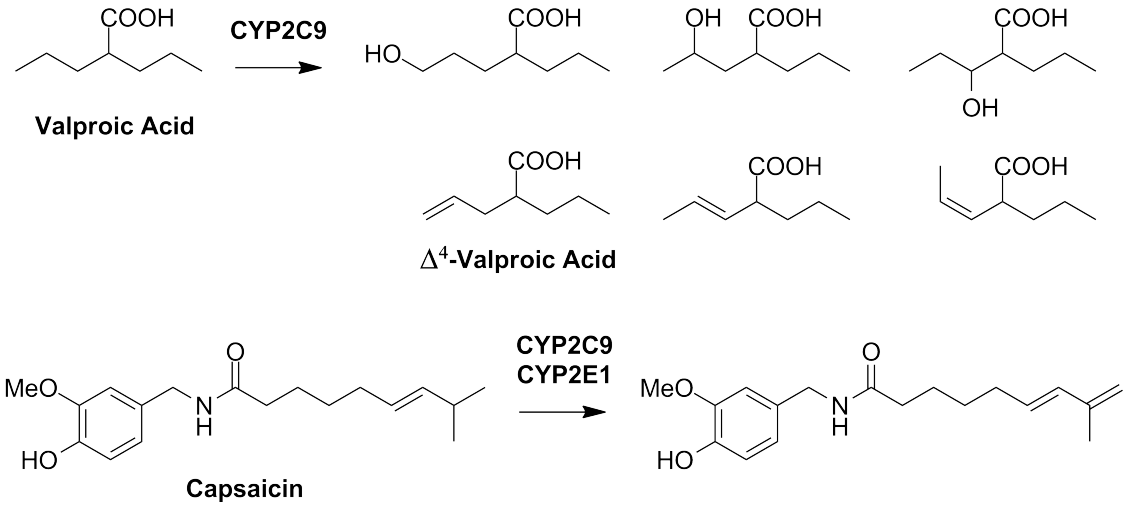

Figure 8. Examples of P450-catalysed desaturations. Shown are the hydroxylation and desaturation metabolites of valproic acid (top), including the liver-toxic terminal olefin Δ^4-valproic acid; and one of the common desaturation metabolites of capsaicin (bottom).

These observations inspired the hypothesis that hydroxylation and desaturation pathways are in direct competition following the initial hydrogen abstraction step by Cpd I. The proposed mechanism for alkene formation branches from this point (Figure 9, left pathway). Radical rebound leads to the expected hydroxylated product; alternatively, the radical species could undergo a second hydrogen abstraction step to form the desaturated product. Conversely, a single electron loss yielding a cation followed by loss of a proton leads to formation of the alkene. These competing steps must proceed at a comparable rate to radical rebound for desaturation to be observed.[94] The initial hydrogen abstraction that results in dehydrogenation can occur at different carbons, depending on the substrate's position relative to Cpd I in the P450 active site (Figure 9, right pathway).[39,94] The partition between hydroxylation and desaturation also depends on the relative stabilities of the radical or cation species formed.[105]

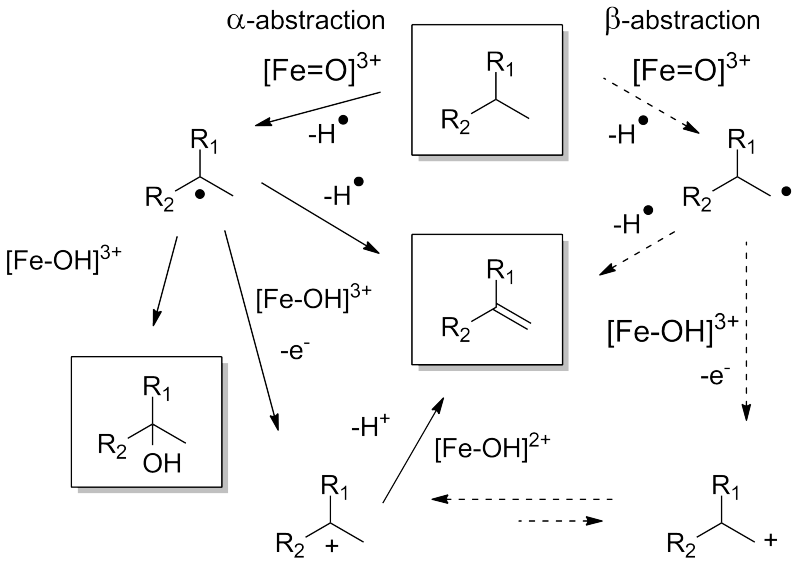

Figure 9. Mechanism of P450-catalysed desaturation. Initial H abstraction occurs at either the α or β carbon. The second step is either a second H abstraction to produce the alkene, or electron transfer to form a cation. Proton loss from the cation generates the alkene.

The two-state reactivity model has also presented a theoretical explanation for the formation of desaturation product that is consistent with that of hydroxylation. In the cases of both the desaturation and hydroxylation products, the doublet state Cpd I provides a lower energy barrier to initial hydrogen abstraction than the quartet state, and subsequently no energy barrier for a second hydrogen atom loss from the radical intermediate. A significant energy barrier exists with the quartet state, indicating that the desaturation should be expected to proceed via the doublet state of Cpd I.[81,85,106–108]

1.4.4 Carbon-carbon bond cleavage

P450s involved in biosynthesis pathways have been shown to catalyse cleavage of carbon-carbon bonds. There are three known types of C-C bond cleavage reactions, including those which involve a carbonyl adjacent to a carbon, a carbonyl adjacent to a hydroxyl, or two adjacent hydroxyls (Figure 10).[39] In each case the P450 generates one of these moieties by successive oxidation events, and these species are able to undergo C-C bond-breaking reactions. Key examples include cleavage α to a carbonyl in lanosterol,[109] wherein the methyl group is oxidised twice in succession, first to an alcohol then an aldehyde (Figure 10, top). The final step is believed to be nucleophilic addition of the peroxy species (pre-Cpd 0) to the aldehyde group, followed by a fragmentation event which also generates a carboxylic acid.[110]

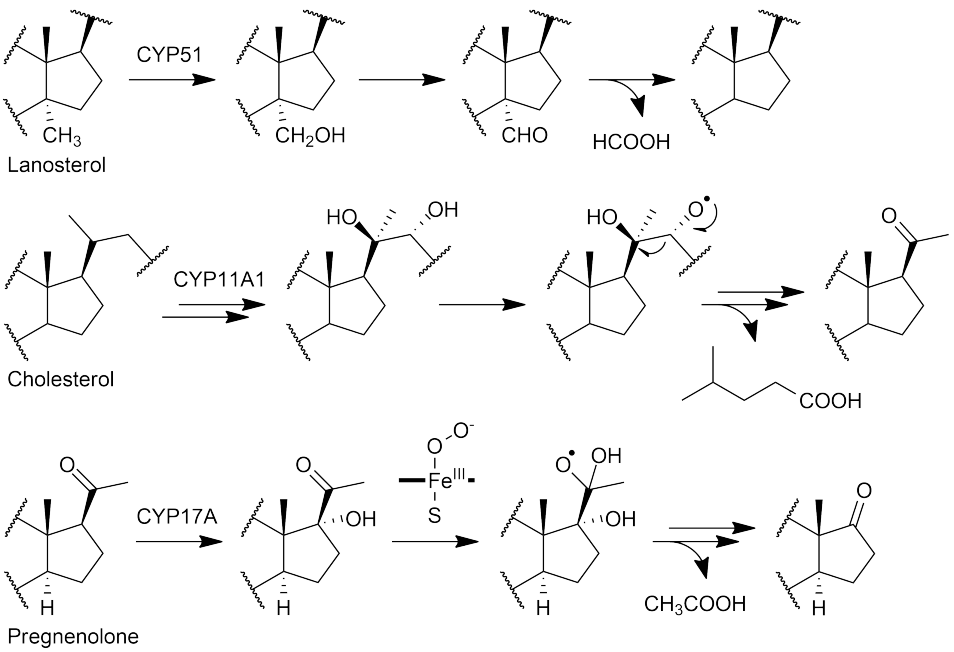

Figure 10. Examples of P450-catalysed carbon-carbon bond cleavage reactions. Shown (top to bottom) are details from the metabolisms of lanosterol, cholesterol and pregnenolone. In each case, a carboxylic acid compound is generated as a result of the cleavage step.

Generation of a diol, as seen in the metabolism of cholesterol by CYP11A1 (Figure 10, middle), can also initiate C-C bond breaking.[111,112] This is believed to occur via an alkoxy radical formed by Cpd I, which then fragments to form a molecule of 4-methylpentanal and a radical precursor to pregnenolone. The ketone product can then form via electron transfer from the radical to the enzyme. However, studies of different CYP11A1 substrates suggested the possibility that a Cpd I-hydroperoxy intermediate is involved in this transformation.[39] Similarly to CYP11A1, the synthesis of pimelic acid (a precursor to biotin) by prokaryotic $P450_{BioI}$ (CYP107H1) from *Bacillus subtilis* proceeds via a diol intermediate. Initial hydroxylation at the carbon α to the hydroxyl group, and subsequent C-C bond cleavage between the diol, generates two aldehydes which undergo further oxidation.[113,114]

Cleavage between a carbonyl and hydroxyl has been observed for the CYP17A-pregnenolone system.[115] Initial hydroxylation at the carbon adjacent to the carbonyl yields an intermediate which can undergo nucleophilic attack by the ferric peroxy species (Figure 1, Species V), producing a radical that rearranges to eliminate acetic acid and a diol (Figure 10, bottom). This diol then undergoes dehydration to form a ketone.

1.4.5 Halogen oxidation

The oxidation of halogens (R−X) is a much rarer P450 activity due to the very high electronegativity of halogen atoms. Dodecanoic acid undergoes hydroxylation at the ω-carbon when oxidised by CYP4A1 and CYP52A21. When a hydrogen at the ω-carbon is substituted with a halogen, the activity dramatically changes, resulting in a partition between C−H hydroxylation and halogen oxidation (Figure 11a, top). Hydroxylation adjacent to the halogen proceeds with corresponding elimination of HX (X = Cl or Br) to yield an aldehyde.[116,117] Alternatively, a halonium $R{-}X^{+}{-}O^{-}$ species can be formed from oxidation of the halogen, followed by hydrolysis to yield an ω-hydroxylation product and HOX (Figure 11a, bottom). Dehalogenation has also been observed with chloramphenicol, where the terminal $CHCl_2$ group undergoes hydroxylation followed by elimination of HCl to produce a ketone.[118,119]

Some substrates that undergo halogen oxidation require circumstances where alternate oxidation sites are sterically or electronically disfavoured. For example, the I-oxidation of aryl iodides by rat liver P450 most likely proceeds only because there are no other oxidisable positions on this substrate (Figure 11b).[120]

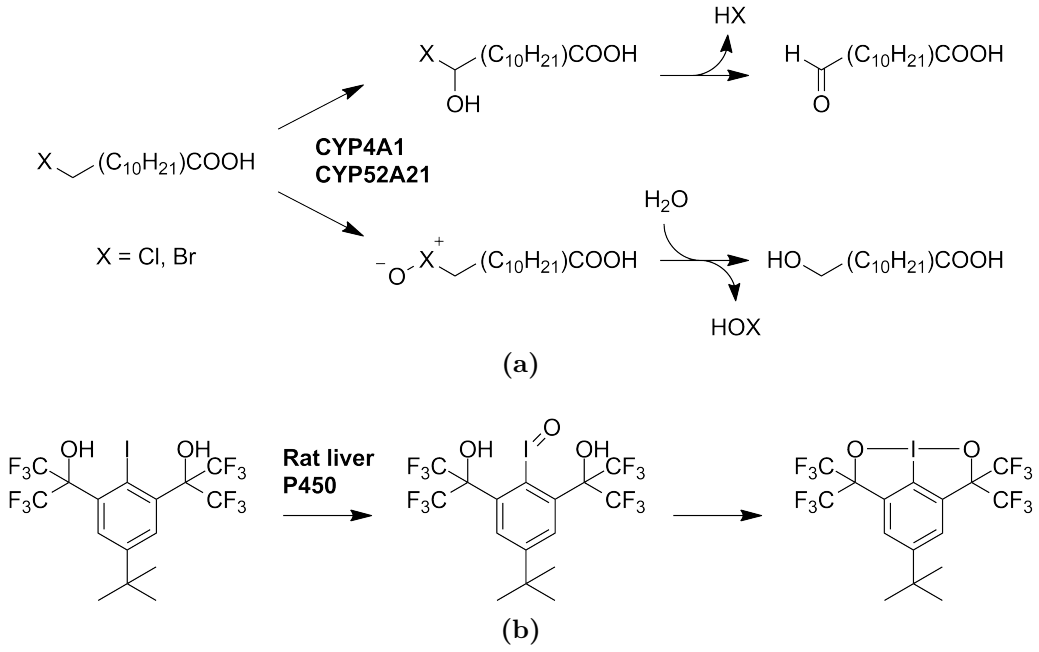

Figure 11. Examples of P450-catalysed halogen oxidations. Shown in (a) are the oxidation of 12-halododecanoic acids by CYPs 4A1 and 51A21, yielding dehalogenation products by two differing pathways. Shown in (b) is the I-oxidation of an aryl iodide compound.

1.5 CYP199A4, a cytochrome P450 from *Rhodopseudomonas palustris* HaA2

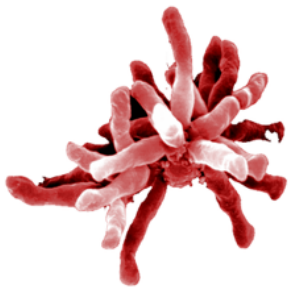

Figure 12. *R. palustris* HaA2 cells under SEM.[121]

Rhodopseudomonas palustris is a gram-negative purple non-sulfur phototrophic bacterium, which has been found to inhabit diverse environments, such as pond water and earthworm droppings.[122] These bacteria display extraordinary metabolic diversity, and dynamically adapt their metabolism to their local environment. This allows them to function using any of the four modes of metabolism: photoautotropic or photosynthetic (energy from light and carbon from CO_2), chemoheterotropic (carbon and energy from organic compounds) and chemoautotropic (energy from inorganic compounds and carbon from CO_2).[122] Hence, these organisms can grow with or without light or oxygen, can fix nitrogen, produce hydrogen gas, and biodegrade a wide range of substrates.[23,30,122–127]

The genome of different strains of *Rhodopseudomonas* changes based on the bacteria's microenvironment; consequently, *R. palustris* strains contain varied numbers of P450 genes with diverse metabolic functions. Genomic analyses indicate that P450s from this bacterium belong to several CYP families, which suggests that *R. palustris* P450s can metabolise a range of substrates.[23] The CGA009 strain of *R. palustris* was the first to have its genome fully sequenced, and was found to possess seven P450 genes, including CYP199A2, CYP195A2 and CYP203A1.[122] CYP199A2 can be reconstituted with a class I electron transfer system which allows it to metabolise *para*-substituted benzoic acids.

Strain HaA2 of *R. palustris* was isolated from freshwater pond sediment obtained near Haren, The Netherlands (Figure 12). This strain functions via light driven aerobic respiration rather than anaerobically and heterotrophically.[128,129] One P450 from the HaA2 strain, CYP199A4, is a close relative of CYP199A2. However, CYP199A4 and its electron transfer partners are easier to produce in *E. coli* compared to CYP199A2.[27]

CYP199A4 can catalyse a wide variety of mono-oxygenase reactions with different *para*-substituted benzoic acid substrates. Mono-oxygenase function can be observed when CYP199A4 is reconstituted with its class I electron transfer system: a ferredoxin containing a [2Fe-2S] cluster (HaPux) and a ferredoxin reductase (HaPuR), alongside NADH as an electron source.[27] CYP199A4 tightly binds substrates with a *para*-substituted benzoic acid framework, such as 4-methoxybenzoic acid and 4-ethylbenzoic acid (Figure 13). This enzyme regioselectively oxidises these substrates at the *para*-substituent; for example 4-methoxybenzoic acid is demethylated to 4-hydroxybenzoic acid (Figure 13). Oxidation of 4-ethylbenzoic acid yields two products: 4-(1-hydroxyethyl)benzoic acid and 4-vinylbenzoic acid, in respective yields of 51 % and 38 % respectively (Figure 13).[27] Furthermore, CYP199A4 has been shown to

support catalytic activity of heteroatom-containing substrates such as 4-methylamino- and 4-methylthio-benzoic acids, with N-demethylation being the observed outcome for 4-methylaminobenzoic acid and sulfoxidation the only product resulting from 4-methylthiobenzoic acid.[28,130]

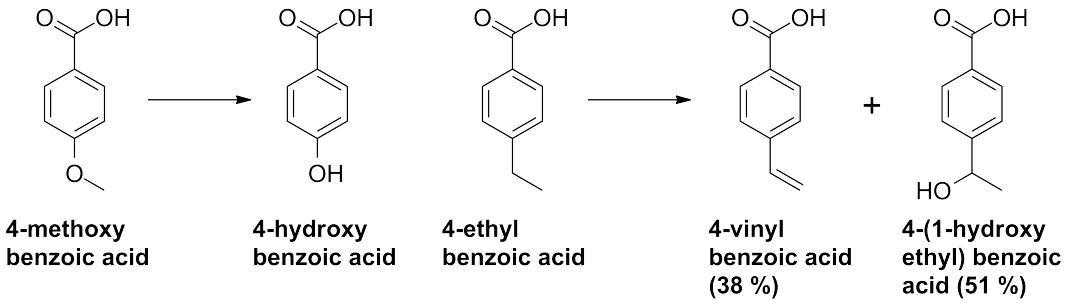

Figure 13. Previously determined CYP199A4 oxidation products of *para*-substituted benzoic acid substrates.[27]

The substrate preferences of CYP199A2 and CYP199A4 have been rationalised using macromolecular X-ray crystallography. The crystal structures of 4-methoxy- and 4-ethyl-benzoic acid-bound CYP199A4 (PDBs: 4DO1 and 4EGM)[30,131] indicate that the carboxylate group of the substrate interacts with the active site residues Arg92, Ser95, Arg243 and Arg244 (Figure 14). The planar benzene ring interacts with the hydrophobic residues V181, F182, F185, V295 and F298. Subsequently, the *para* substituent is held over the heme accounting for the regioselectivity of the enzyme for this position. These interactions are important for tight binding of the substrate and explain the highly selective nature of this enzyme for *para*-substituted benzoic acids.

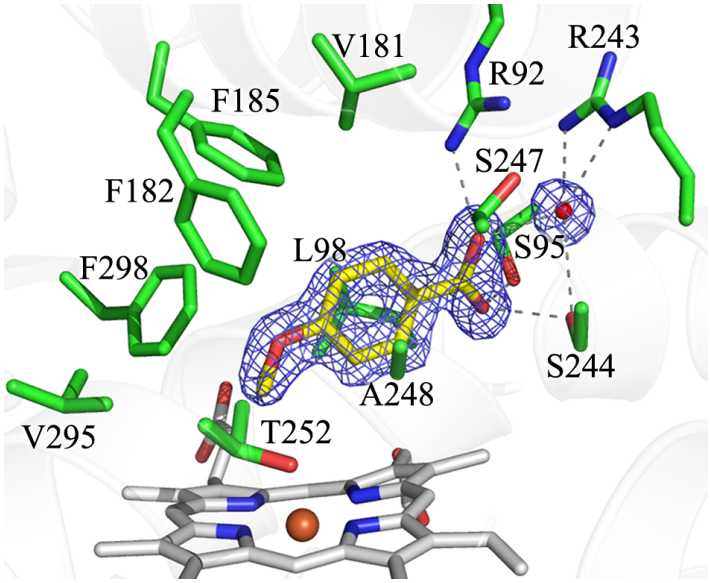

Figure 14. The active site of 4-methoxybenzoic acid-bound CYP199A4 (PDB: 4DO1).[131] 4-Methoxybenzoic acid is shown in yellow, active site amino acids are green and the heme is shown in grey. The *para*-position methyl group is close to the Fe centre of the protein (3.9 Å), and has induced dissociation of the distal H_2O ligand.

Replacement of the carboxylate moiety of *para*-substituted benzoic acid substrates with other functional groups demonstrated its importance to binding and enzyme activity. Compared to 4-methoxybenzoic acid, 4-methoxybenzaldehyde and 4-methoxybenzamide displayed reduced binding affinity and turnover efficiency for CYP199A4, although a small amount of demethylation product was still formed.[132] Methyl 4-methoxybenzoate and 4-methoxybenzyl alcohol did not bind to the enzyme.[132] Similar effects were observed when the aromatic benzene ring was modified to a cyclohexane ring, with significantly reduced enzyme activity and binding affinity.[30] More recently, an S244D mutant of CYP199A4 has allowed the efficient and selective oxidative demethylation of *para*-substituted benzene derivatives such as 4-methoxyphenol and 4-methoxynitrobenzene.[133]

Mammalian P450s (particularly human P450s) oxidise a wide variety of functional groups in drug metabolism pathways. By understanding the mechanisms of these oxidations, future drug design could be improved by enabling better prediction algorithms for preventing unwanted side-reactions. The design of substrates to probe P450 oxidation mechanisms can be difficult, due to the complexity of the substrate framework that many P450s typically require to generate tight binding and high turnover activity.

The recombinant CYP199A4-HaPux-HaPuR system is high yielding in *E. coli* and simple to purify and handle.[27,30,134] Mechanistic probe substrates can be purchased or easily synthesised due to the simplicity of the *para*-substituted benzoic acid framework. Thus, CYP199A4 presents the possibility of exploring in detail the mechanistic pathways of various CYP-catalysed oxidations by systematic substrate engineering. Mutagenesis of the key acid-alcohol pair will also allow investigation of the mechanism of oxygen activation by CYP199A4.

1.6 Thesis Objectives

The exploration of potential substrates for CYP199A4 will allow the mechanism of P450 transformations to be investigated in detail. CYP199A4 and the required partner proteins will be purified in order to perform enzyme-substrate binding and turnover studies. Protein X-ray crystallography will be employed to elucidate the active site binding orientation of these substrates and rationalise the products formed in assays. These experimental procedures are described in Chapter 2.

In Chapter 3, the effect of substituents at the *ortho* and *meta* positions of the benzoic acid on the substrate binding and O-dealkylation activity of CYP199A4 are studied. This will provide additional insights into the range of oxygen dealkylation activities catalysed by CYP199A4 (Figure 15).

In Chapter 4, substrates containing nitrogen and sulfur moieties at the *para*-position will be investigated, to probe the capability of CYP199A4 to catalyse N- and S-dealkylation and heteroatom oxidation (Figure 15). These substrates will include

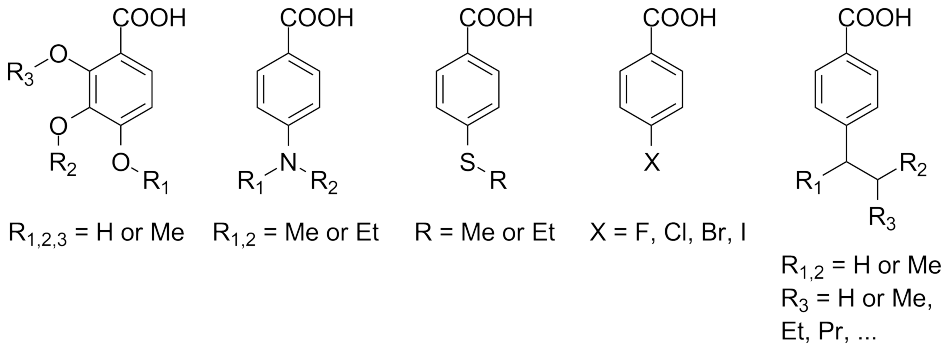

Figure 15. Families of *para*-substituted benzoic acid substrates to be investigated with CYP199A4.

compounds such as 4-methylamino-, 4-ethylamino-, 4-dimethylamino-, 4-methylthio- and 4-ethylthio-benzoic acids.

Halogen oxidation has been previously observed in substrates where the oxidation of C−H bonds is highly disfavoured by electronic or steric effects, or due to the position of the substrate in the active site. Since the activity of CYP199A4 with halogen substrates has not yet been determined, 4-halobenzoic acids (F, Cl, Br, I) will be employed as substrates. Furthermore, the oxidation of substrates containing alkyl chains substituted with halogens will also be explored. Both 4-halomethyl- and 4-(2-haloethyl)-benzoic acids (Cl, Br) might be expected to undergo dehalogenation, or may result in similar activities to 4-methyl- and 4-ethyl-benzoic acids.

4-Methylbenzoic acid undergoes hydroxylation to 4-hydroxymethylbenzoic acid. By extending the *para*-alkyl substituent, CYP199A4 has been shown to catalyse both α-hydroxylation and α,β-desaturation reactions in 4-ethyl- and 4-isopropyl-benzoic acids. The partition between the two products changes between these substrates, with the isopropyl generating a higher proportion of hydroxylation product than 4-ethylbenzoic acid.[30] In Chapter 5, the partition between hydroxylation and desaturation in response to extension of the carbon chain will be determined by employing substrates with longer and/or more substituted alkyl groups. Also of interest is whether CYP199A4 can catalyse oxidation of cycloalkane functional groups. 4-Cyclopropyl- and 4-cyclohexyl-benzoic acids will be investigated to determine if both hydroxylation and desaturation activities are supported. These substrates will be studied using X-ray crystallography to rationalise the activities observed.

4-Isopropylbenzoic acid undergoes both hydroxylation and desaturation. CYP199A4 is capable of accommodating benzoic acid substrates containing certain *meta*-functional groups. A series of *meta*-substituted isopropylbenzoic acids with various electron donating and withdrawing groups will be employed as mechanistic probes to investigate the desaturation reaction catalysed by CYP199A4 (Figure 16).

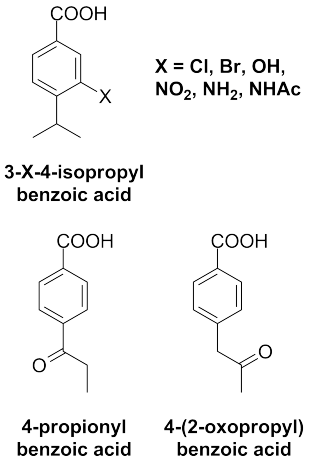

Figure 16. *Meta*-substituted 4-isopropyl- and carbonyl-benzoic acid substrates.

Carbon-carbon bond cleavage reactions have yet to be investigated with CYP199A4. These reactions are of significant physiological interest and CYP199A4 could be employed as a useful probe system for investigating mechanistic details. 4-Propionyl- and 4-(2-oxopropyl)-benzoic acids contain precursors to the α-hydroxycarbonyl group, which is known to undergo carbon-carbon bond cleavage (Figure 16). These substrates will exploit the regioselectivity of CYP199A4 at the *para*-position functional group to determine whether α-hydroxycarbonyl species can be generated by CYP199A4 and if they can undergo further reactions such as C-C bond cleavage.

CYP199A4 possesses the highly conserved acid-alcohol pair (Asp251, Thr252) found in most P450s. Oxygen activation by P450 enzymes is predominantly understood from studies of $P450_{cam}$. Cpd I is the active oxidant responsible for C−H bond abstraction. The T252A variant of $P450_{cam}$ has been used to study the involvement of Cpd 0 as an oxidant for epoxidation. Although the results from experiments using $P450_{cam}$ have been generally applied to other P450s, the precise details may vary in other enzymes. In Chapter 6, turnovers of a selection of substrates (Figure 15) will be performed with the equivalent CYP199A4 mutants (D251N, T252A), which will allow the role of the acid-alcohol pair in this P450 system to be investigated. The roles of these active site residues will also be investigated using X-ray crystallography of the substrate-bound CYP199A4 mutants. The turnovers of these mutant CYP199A4s will also allow the role of alternative oxidants in different P450 catalysed transformations to be assessed.

In Chapter 7, a range of other *para*-functionalised benzoic acids will be investigated in order to explore the potential substrate range of CYP199A4. Phenyl and heterocyclic functionalities such as *para*-methoxyphenyls, pyridines, thiophenes and furans will be explored. These substrates may exhibit activities such as aromatic oxidation, or have the potential to interact with the heme iron of the P450.

Finally, concluding remarks, along with future directions, will be presented in Chapter 8.

Chapter 2 Experimental

2.1 General

Organic substrates, general laboratory reagents, HPLC solvents and derivatisation agents were purchased from Sigma-Aldrich, TCI, Merck and Alfa-Aesar. Buffer components, NADH and isopropyl-β-D-thiogalactopyranoside (IPTG) were from Astral Scientific, Australia. The 3-X-4-isopropylbenzoic acids (X = Cl, Br, OH, NO_2, NH_2, NHAc), employed in Chapter 5, were synthesised by the research group of James J. De Voss (University of Queensland).

UV-Vis spectra and activity assays were recorded at 30 ± 0.5 °C on a Varian CARY 60 or CARY 5000 spectrophotometer. Analytical liquid chromatography was performed on an Agilent 1260 Infinity pump equipped with an autoinjector and a Phenomenex Kinetex 5u XB-C18 100A column (250 × 4.6 mm, 5 µm). A gradient of MilliQ water/trifluoroacetic acid (TFA, 0.1 %) to acetonitrile/TFA (0.1 %) was used. The gradients employed were 0-50 %, 0-80 % and 20-95 %, and these are specified in each figure legend when presented. The wavelength used to monitor the chromatogram is also provided in each figure legend. Chiral chromatographic analysis was performed using a Phenomenex Lux 3u Cellulose-1 column. The flow rate was controlled at 0.4 mL min^{-1}. The solvent system was MilliQ water/TFA (0.1 %) to acetonitrile/TFA (0.1 %). Gradients are provided where necessary. Prep-scale liquid chromatography was undertaken using a Gilson GX Prep with a Gilson 322 pump system with an autoinjector and fraction collector with a Kinetex 5u EVO C18 column (150 × 21.2 mm, 5 µm). Fractions were combined and the solvent was removed using an Alpha 2-4 LDplus freeze dryer (Christ, Germany). Chiral HPLC analysis to determine the enantiospecificity of 4-ethyl- and 4-ethylthio-benzoic acids was performed by the research group of James J. De Voss (University of Queensland). The method used was 5 % isopropanol in hexane, isocratically for 60 min.

Gas chromatography experiments were performed on a Shimadzu GC-17A with a QP5050A GC-MS detector, equipped with a DB-5 MS fused silica column (30 m × 0.25 mm, 0.25 µm). The injector was held at 250 °C and the interface was 280 °C. The column temperature was held at 120 °C for 3 min and then increased at 6 °C min^{-1} until it reached 230 °C. The column was held at this temperature for 6 min. Peak integrations were determined using the total ion count.

2.2 Enzyme production and molecular biology

Transformations for protein expression and purification were performed by mixing competent cells (50 µL) with DNA (70–100 ng). This mixture was held at 0 °C for 60 min followed by heat shock at 42 °C for 1 min. After cooling in ice for 2 min, 250 µL SOC media was added to the mixture and it was shaken at 37 °C at 200 rpm for 1 h. Cells were then spread onto a LB plate containing the appropriate antibiotics; kanamycin (30 mg L^{-1}) and/or ampicillin (100 mg L^{-1}); and incubated for 18 h at 37 °C. The media solutions used for cell growths are listed in Table 1.

Table 1: Growth media constituents.

Medium	Constituents (L^{-1})
LB	tryptone (10 g), yeast extract (5 g), NaCl (10 g)
SOC	tryptone (20 g), yeast extract (5 g), $MgCl_2$ (1 g), NaCl (0.5 g), KCl (0.2 g), glucose (0.2 % w/v)
Trace Elements	Na_2EDTA (20.1 g), $FeCl_3.6H_2O$ (16.7 g), $CaCl_2.H_2O$ (0.74 g), $CoCl_2.6H_2O$ (0.25 g), $ZnSO_4.7H_2O$ (0.18 g), $MnSO_4.4H_2O$ (0.132 g), $CuSO_4.5H_2O$ (0.10 g)
EMM	K_2HPO_4 (7 g), KH_2PO_4 (3 g), $(NH4)_2SO_4$ (1 g), $Na_3Citrate$ (0.5 g), $MgSO_4$ (0.1 g), 20 % glucose (20 mL)

2.2.1 CYP199A4 (Wild-type, D251N and T252A isoforms)

The pET28 CYP199A4 plasmid construct, containing the CYP199A4 gene inserted between the NcoI and HindIII restriction sites, has been described previously.[27] Plasmid DNA for the D251N and T252A mutants of CYP199A4 were made by Dr Jeanette Stok (University of Queensland) using the Quikchange site directed mutagenesis methodology (Agilent).

Competent *E. coli* or BL21(DE3) was transformed with the CYP199A4 plasmid and plated onto LB_{kan}. Single colonies were then grown in 2 × 500 mL LB_{kan} media at 37 °C at 120 rpm for 8 h. After this time, the temperature was reduced to 18 °C. To each flask, benzyl alcohol (100 µL) and ethanol (10 mL) were added to induce expression of *E. coli* chaperone proteins and aid protein folding.[135] Trace elements solution (1.5 mL.L^{-1} of media) was added to aid heme iron incorporation. After 30 min, 50 µL of 0.5 M IPTG was added to each flask to induce protein production. The mixture was shaken at 18 °C and 105 rpm for a further 24 h. The red cell pellet was harvested by centrifugation (5000 *g*, 10 min) and resuspended in Tris buffer (pH 7.4, 50 mM) containing 1 mM DTT (dithiothreitol; this buffer is subsequently referred to as Buffer T). The cells were kept on ice and lysed by sonication (20 kHz using a VC505 Ultrasonic Processor and an Autotune CV334 probe, both from Sonics & Materials, USA) using

30 × 20 s pulses with 40 s between each pulse. The cell debris was removed by centrifugation at 40,000 *g* for 30 min at 4 °C and the supernatant was subject to ammonium sulfate precipitation and centrifugation (0-25 % and 25-50 % fractions). The pelleted protein containing fraction (25-50 %) was then dissolved in Buffer T, and desalted using a Sephadex G-25 course grain column (250 × 40 mm) and the same buffer. The protein was concentrated using a Vivacell 100 centrifugal concentrator cell at 2500 rpm (10 kDA membrane, Sartorius, UK). It was then was loaded onto a DEAE fast flow Sepharose column (XK50, 200 × 40 mm, GE Healthcare) and eluted using a linear salt gradient of 100–400 mM KCl in Buffer T at 6 mL min^{-1}. The red fractions were collected and desalted using a Sephadex G-25 medium grain column (250 × 40 mm), then concentrated and loaded onto a Source 15Q column (XK26, 80 × 30 mm, GE Healthcare). The protein was eluted using a 40–160 mM KCl gradient at 6 mL min^{-1}. The red fractions were combined and concentrated. The final A_{419}/A_{280} ratio of > 1.75 indicated the protein was > 90 % pure.[27] The protein concentration was determined using the extinction coefficient, $\varepsilon_{419} = 119\,\text{mM}^{-1}\,\text{cm}^{-1}$.[131] The protein was further purified using an ENrich SEC 650 (10 × 300 mm) size exclusion column at a flow rate of 1 mL min^{-1} using Tris (pH 7.4, 50 mM) as the elution buffer, which increased the A_{419}/A_{280} ratio to ≈ 2. The protein was concentrated and an equal volume of 80 % glycerol was added, then the solution was filtered through a 0.22 µm aqueous filter and stored at −20 °C.

To determine whether the P450 was active, CO difference assays were performed.[2,136] To an aliquot of P450, sodium dithionite was added until the resting state peak ($\approx$ 419 nm) was shifted to the reduced ferrous form ($\approx$ 416 nm). CO gas was gently bubbled to shift the absorbance to the distinctive Soret peak ($\approx$ 450 nm).

2.2.2 Ferredoxin reductase (HaPuR)

Competent *E. coli*, BL21(DE3) was transformed with the plasmid pET26-HaPuR containing the HaPuR gene and plated onto LB_{kan}.[27] Isolated colonies were then grown in 3 × 0.5 L LB_{kan} at 37 °C at 120 rpm for 8 h. After this time, the temperature was reduced to 18 °C. To each flask, benzyl alcohol (100 µL) and ethanol (10 mL) were added. After 30min, 50 µL of 0.5 M IPTG was added. The incubated culture was grown for a further 24 h at 18 °C at 105 rpm, then the yellow cell pellet was harvested by centrifugation (5000 *g*, 10 min) and resuspended in Buffer T. The cells were kept on ice and lysed by sonication using 30 × 20 s pulses with 40 s between each pulse. The cell debris was removed by centrifugation at 40,000 *g* for 30 min at 4 °C. The protein-containing supernatant was loaded onto a DEAE Sepharose column (XK50, 200 × 40 mm, GE Healthcare) and eluted using a linear salt gradient of 100–350 mM KCl in Buffer T, at a flow rate of 6 mL min^{-1}. The yellow fractions were combined

and concentrated at 2500 rpm using a Vivacell 10 kDA concentrator cell. The protein was desalted by two successive dilution (to 50 mL total) and concentration steps. The concentrated protein was then loaded onto a Source 15Q column (XK26, 80 × 30 mm, GE Healthcare). The protein was eluted using a salt gradient of 75–300 mM KCl in buffer T, at 6 mL min^{-1}. The yellow fractions were collected and the absorbance ratio measured ($A_{280}/A_{454} < 6.0$) indicated the protein was > 90 % pure.[27] An equal volume of 80 % glycerol was added and the solution was filtered through a 0.22 µm aqueous filter and stored at −20 °C. The final protein concentration was determined using the extinction coefficient, $\varepsilon_{454} = 10\,mM^{-1}\,cm^{-1}$.[23]

2.2.3 Ferredoxin (HaPux)

Competent *E. coli* BL21(DE3) was transformed with the plasmid pCW-HaPux containing the HaPux gene using the methodology as described earlier (Chapter 2.6.1) and plated onto LB_{amp}. Single colonies were grown into 10 × 0.5 L LB_{amp} at 37 °C at 120 rpm for 5 h. After this time, the temperature was reduced to 18 °C. To each flask, benzyl alcohol (100 µL), ethanol (10 mL) and trace elements solution (1.5 mL) were added. After 30 min, 50 µL of 0.5 M IPTG was added. The incubated culture was inoculated for a further 24 h at 18 °C at 105 rpm. The brown cell pellet was collected by centrifugation (5000 *g*, 10 min) and resuspended in 300 mL of 10 mM Tris pH 7.4 containing 20 % v/v glycerol, 2 mM DTT, 1 % v/v β-mercaptoethanol and 1 mg mL^{-1} lysozyme. After stirring at 4 °C for 1 h the cells were kept on ice and lysed by sonication using 30 × 20 s pulses with 40 s between each pulse. The cell debris was removed by centrifugation at 40,000 *g* for 30 min at 4 °C. The collected brown supernatant was loaded onto a DEAE fast flow Sepharose column (XK50, 200 mm × 40 mm, GE Healthcare) and eluted using a linear salt gradient of 150–400 mM KCl in buffer T, at a flow rate of 6 mL min^{-1}. The brown fractions containing the protein were collected and concentrated at 2500 rpm using a Vivacell 10 kDA concentrator cell. The protein was then desalted using a Sephadex G-25 medium grain column (250 mm × 40 mm). This was concentrated then loaded onto a Source-Q column (XK26, 80 mm × 30 mm, GE Healthcare) and the protein was eluted using a salt gradient of 40–160 mM KCl in buffer T, at a flow rate of 6 mL min^{-1}. Fractions with $A_{325}/A_{280} > 0.65$ were combined and concentrated. The protein concentration of HaPux was determined using $\varepsilon_{416} = 11.2\,mM\,cm^{-1}$.[27] An equal volume of 80 % glycerol was added and the solution was filtered through a 0.22 µm aqueous filter and stored at −20 °C.

2.3 Substrate binding assays

Before use in assays, glycerol was removed from proteins using a 5 mL gel filtration column (PD-10, GE Healthcare). CYP199A4 was diluted in Tris buffer (50 mM, pH 7.4). To 1 mL of protein, 1 µL aliquots of substrate from a 100 mM stock solution were added using a 5 µL Hamilton glass syringe. The resulting change in absorbance was recorded on a UV-Vis spectrophotometer (from 300–600 nm) until the peaks did not change upon further addition of substrate. The high-spin heme content was estimated (± 5 %) by comparison with a set of spectra generated from the sum of the appropriate percentages of the spectra of the substrate-free (> 95 % low-spin, Soret maximum at 418 nm) and camphor-bound (> 95 % high-spin, Soret maximum at 392 nm) forms of $P450_{cam}$.[30]

For dissociation constant analysis (K_d), aliquots of substrate from a stock solution were added to 2.5 mL of CYP199A4 (0.5–2.5 µM) in Tris buffer (50 mM, pH 7.4) using a 5 µL Hamilton glass syringe. The peak-to-trough difference spectrum (trough at ≈ 419 nm and peak at ≈ 390 nm) for a type I shift was recorded on a UV-Vis spectrophotometer from 300–600 nm. Further aliquots of substrate were added to the mixture until the peak-to-trough difference did not increase. The data was analysed by fitting the difference in absorbance (ΔA_{max}) vs substrate concentration (S) to a hyperbolic function[137,138] (Equation 2):

$$\Delta A = \frac{\Delta A_{max} \times [S]}{K_d + [S]} \tag{2}$$

where ΔA represents the peak-to-trough absorbance, ΔA_{max} represents the maximum peak-to-trough absorbance, $[S]$ is the substrate concentration and K_d is the dissociation constant. For cases where the substrate bound extremely tightly (K_d < 10 µM), data was instead fit to a tight-binding equation to determine K_d (Equation 3):[139]

$$\Delta A = \Delta A_{max} \frac{[E] + [S] + K_d - \sqrt{([E] + [S] + K_d)^2 - 4\,[E]\,[S]}}{2} \tag{3}$$

where ΔA represents the peak-to-trough absorbance, ΔA_{max} represents the maximum peak-to-trough absorbance, $[S]$ is the substrate concentration, $[E]$ is the concentration of CYP199A4 enzyme and K_d is the dissociation constant.

2.4 *In vitro* NADH oxidation assays

Before use in NADH oxidation assays, glycerol was removed from proteins using a 5 mL gel filtration column (PD-10, GE Healthcare) and the concentration of each protein was quantified using UV-Vis spectrophotometry. In a final volume of 1.2 mL, oxygenated Tris buffer (50 mM, pH 7.4), CYP199A4 (0.5 µM), ferredoxin (HaPux, 5 µM), ferredoxin

reductase (HaPuR, 0.5 µM) were combined and equilibrated at 30 °C for 2 min. NADH was added to $A_{340} \approx 2.0$ (≈ 320 µM). Substrate was then added to a final concentration of 1 mM and the absorbance at 340 nm was monitored. The rate of oxidation of NADH was determined from the gradient of the plot of A_{340} vs time (Figure 17), using the extinction coefficient of NADH, $\varepsilon_{340} = 6.22\,\mathrm{mM^{-1}\,cm^{-1}}$.

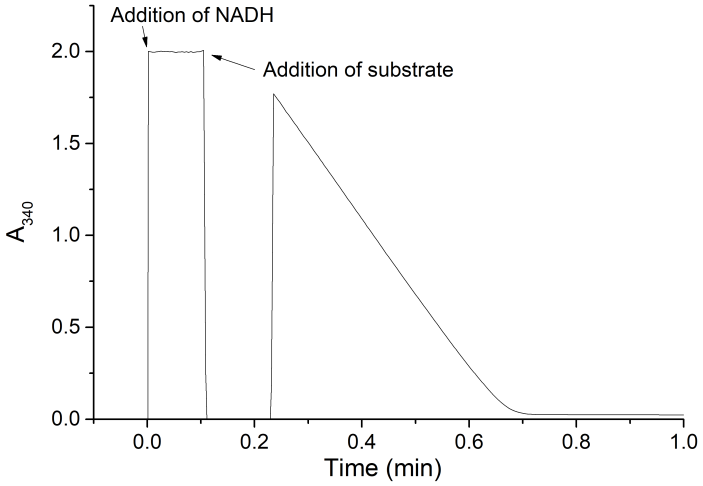

Figure 17. Example plot of an *in vitro* NADH oxidation assay. The absorbance of NADH at 340 nm was recorded over time after addition of 4-methoxybenzoic acid, and the gradient was used to calculate the rate of NADH oxidation by CYP199A4.

2.5 Analysis of metabolites and substrate coupling

For HPLC analysis, the *in vitro* reaction mixture (132 µL) was combined with acetonitrile (66 µL) and internal standard (2 µL, 10 mM 9-hydroxyfluorene or biphenylmethane in EtOH). This mixture was centrifuged (13,000 rpm, 3 min) to remove particulate matter from the sample. This mixture was used directly for HPLC analysis (Chapter 2.1). The product was quantified using 20–500 µM calibration solutions containing 2 µL of 10 mM internal standard. Where an authentic sample of the oxidation product was available, calibrations were performed using these samples. Where this was not possible, the product was isolated and purified after a large scale whole-cell turnover, or the calibration was performed using a closely related compound (Table 2). The HPLC samples for calibration were prepared using the same method as described above.

GC-MS was used to identify turnover products that could not be identified by HPLC coelution, or where insufficient product could be isolated for NMR analysis. The *in vitro* reaction mixture (990 µL) was combined with internal standard (9-Hydroxyfluorene, 10 µL of 10 mM in EtOH) and acidified using HCl (20 µL, 3 M). The mixture was extracted three times with ethyl acetate (400 µL) and the organic extracts were dried over $MgSO_4$. Solvent was evaporated under a stream of N_2 and the sample was dissolved in anhydrous acetonitrile (200 µL). BSTFA/TMCS (99:1, 25 µL) was added and the mixture was left for 2 h at 37 °C to derivatise the benzoic acid and hydroxyl groups

to trimethylsilyl esters. This mixture was used directly for GC-MS analysis (Chapter 2.1). The amount of product was quantified using 20–500 µM calibration solutions containing 2 µL of 10 mM internal standard (Table 2). These were extracted using the same method as described above for the GC-MS turnover samples.

Table 2. Selected examples of calibration factors used to determine coupling and product formation rates.

Technique	Compound	Internal standard[a]	Calibration factor[b]
HPLC	4-(1-hydroxyethyl)benzoic acid	9-hydroxyfluorene	0.0045
		biphenylmethane	0.0019
	4-(2-hydroxyethyl)benzoic acid	9-hydroxyfluorene	0.0073
	4-vinylbenzoic acid	9-hydroxyfluorene	0.0185
		biphenylmethane	0.0075
GC-MS	4-isopropylbenzoic acid	(9-hydroxyfluorene)	0.00805
	4-ethylbenzoic acid		0.00901
	4-(1-hydroxyethyl)benzoic acid		0.00938
	4-vinylbenzoic acid		0.00684
	3-chloro-4-isopropylbenzoic acid		0.00893
	3-bromo-4-isopropylbenzoic acid		0.00992
	3-hydroxy-4-isopropylbenzoic acid		0.01079
	3-nitro-4-isopropylbenzoic acid		0.00383

[a] 2 µL of a 10 mM stock solution in EtOH was used. Biphenylmethane was used in several instances where a metabolite coeluted with 9-hydroxyfluorene. [b] The calibration slope was derived from plots of the ratio of the compound peak to the internal standard peak against concentration. The R^2 of each was ≥ 0.98.

2.6 Whole-cell substrate oxidation systems (*in vivo* turnovers)

2.6.1 *In vivo* oxidation systems

Competent *E. coli* cells were transformed with the DNA vectors pETDuet and pRSF-Duet (containing the genes encoding HaPuR and HaPux genes on the former, and CYP199A4 and HaPux on the latter) were plated onto $LB_{amp/kan}$.[30] One colony from the incubated plate was added to 500 mL $LB_{amp/kan}$, and the mixture was shaken at 37 °C at 120 rpm for 8 h. After this time, the temperature was reduced to 18 °C. To each flask, benzyl alcohol (100 µL), ethanol (10 mL) and trace elements solution (1.5 mL) were added. After 30 min, 50 µL of 0.5 M IPTG was added. The mixture was left overnight at 18 °C and 105 rpm. The supernatant was removed using centrifugation (5000 *g*, 10 min) and the resultant cell pellet was resuspended in 200 mL of *E. coli* minimal medium (EMM, Table 1). This volume was divided equally between flasks and diluted to a final volume of 200 mL using additional EMM. Substrate was then

added to a final concentration of 2 mM to each flask. The whole-cell reaction mixture was allowed to proceed at 30 °C, 200 rpm. An additional 2 mM of each substrate was added after 5 h and the reaction mixtures were left overnight. Aliquots of the turnover mixture were taken at 1 h and 24 h time intervals for analysis. After removal of the cells by centrifugation (6000 rpm, 10 min) the supernatant was used to prepare samples for HPLC and GC-MS analysis as described previously (Chapters 2.1 and 2.5).

2.6.2 Analysis of *in vivo* systems

Where the reaction product was available from a commercial source, the product(s) were identified by coeluting an *in vitro* or *in vivo* turnover reaction against the authentic sample using HPLC/GCMS.

To isolate and characterise products of *in vivo* systems where authentic samples could not be obtained for coelution, cells were removed by centrifugation (5000 *g*, 10 min). The supernatant was then freeze-dried for 12 h. The products were separated using preparative HPLC (Chapter 2.1) and freeze-dried to yield the isolated products, which were then characterised using a combination of NMR, GC-MS and HPLC (details in their respective sections).

2.7 Hydrogen peroxide uncoupling assays

The concentration of hydrogen peroxide generated during *in vitro* NADH turnover assays was determined using a horseradish peroxidase (HRP)/phenol/4-aminoantipyrine (4-AP) assay.[140] To 400 µL of an *in vitro* turnover, 200 µL of 50 mM phenol (pH 7.4, Tris buffer) and 200 µL of 5 mM 4-AP (pH 7.4, Tris buffer) were added. The absorbance at 510 nm was zeroed, and 1 µL of 20 mg mL^{-1} HRP was added. The absorbance at 510 nm was used to calculate the concentration of hydrogen peroxide ($\epsilon_{510} = 6580\,\mathrm{M^{-1}\,cm^{-1}}$).

2.8 Formaldehyde and formic acid assays

The amount of formaldehyde generated during certain turnovers was determined using 600 µL mixtures containing Tris buffer (pH 7.4, 50 mM, 312 µL), *in vitro* turnover mixture (240 µL) and Purpald (168 µM, 48 µL).[141,142] The reaction of formaldehyde and Purpald was allowed to develop by shaking for 15 min before measuring the absorbance at 550 nm. A calibration curve was produced using 20–500 µM solutions of formaldehyde and the resulting extinction coefficient, $\epsilon_{550} = 3450\,\mathrm{M^{-1}\,cm^{-1}}$, was used to quantify the amount of formaldehyde-Purpald complex in each turnover.

Formic acid content was determined using a formic acid assay kit from Megazyme (Ireland). The turnover (1.1 mL), H_2O (0.8 mL), phosphate buffer (pH 7.6, 0.2 mL) and β-NAD (0.2 mL) were combined and equilibrated for 5 min. The absorbance at 340 nm was measured and formate dehydrogenase (50 µL) was added to consume formic acid,

producing NADH. This was allowed to react for 15 min and the increase in absorbance at 340 nm was used to quantify the formic acid.[143]

2.9 Substrate docking studies

Computational studies were performed by manually docking small molecule substrates into the active site of CYP199A4. The protein model file (PDB: 4DO1, available from www.rcsb.org or www.wwpdb.org) was prepared by removing the 4-methoxybenzoic acid using WinCoot.[144] Ligand coordinates and restraints were created using eLBOW, available in the PHENIX suite of programs.[145] The protein-ligand complexes were subjected to 300 rounds of Cartesian MMFF energy minimization using ICM Pro (Molsoft LLC, USA). Side chains were globally optimized and the backbone was annealed to improve the model using the ICM Pro Monte Carlo algorithm.

2.10 Protein X-ray crystallography

Crystallisation experiments were performed with WT, D251N and T252A isoforms. Prior to use, glycerol was removed from CYP199A4 using a 5 mL gel filtration column (PD-10, GE Healthcare). Immediately before preparation of crystal trays, the protein was eluted through an ENrich SEC 650 (10 × 300 mm) size exclusion column at a flow rate of 1 mL min^{-1} using Tris (pH 7.4, 50 mM) as the elution buffer. CYP199A4 was then concentrated to approx. 30–35 mg mL^{-1} in 50 mM Tris, pH 7.4 to increase the likelihood of crystallisation.[146]

Initial screening of conditions was performed using the Crystal Screen HT, SaltRX HT and PEG/Ion HT kits available from Hampton Research (USA). Crystal growth was observed with several conditions from the PEG/Ion screen and were optimised further. Crystals were obtained using the hanging-drop vapour diffusion method at 16 °C using 1 µL of protein mixed with 1 µL of reservoir solution and equilibrated with 500 µL of reservoir solution. Large crystals (200–300 µm by 100–150 µm by 20–30 µm) were obtained in 1-2 weeks from reservoir solutions containing 0.2 M magnesium acetate tetrahydrate, PEG-3,350 and 0.1 M Bis-Tris. Details are provided in their results sections.

Crystals were harvested using a nylon loop (Hampton Research) or micromount (Mitegen), cryoprotected by immersion in Parabar 10312 (Paratone-N, Hampton Research, USA) and flash cooled in *l.* N_2. X-ray diffraction data were collected at 100 K on the MX1 beamline at the Australian Synchrotron.[147,148]

Diffraction data for the majority of structures were indexed and integrated using iMosflm.[149] For 4-*n*-heptylbenzoic acid with wild-type CYP199A4, the data were indexed and integrated using HKL.[150] Scaling, merging and R_{free} flag labelling (5 % of reflections, randomly selected) were performed using Aimless,[151] available in the CCP4

suite of programs.[152] The phase was solved using molecular replacement with Phaser[153] in CCP4 using 4-methoxybenzoic acid-bound CYP199A4 (PDB: 4DO1) as the initial search model. All ligands and solvent molecules were removed from the model prior to phasing to reduce model bias. Electron density maps (weighted $2mF_o$-DF_c map, and F_o-F_c difference map) were obtained after initial model building, and the model was manually rebuilt using WinCoot.[144] Structural refinements were performed over multiple iterations under the guidance of the F_o-F_c difference maps using phenix.refine (Phenix Refine), available in the Phenix suite of programs.[145] Reduced bias maps for inspection of ligand binding were generated using either a composite omit map or a feature enhanced map (presented in the individual chapters where relevant).[154,155] Inspection of the reduced bias maps in each structure unambiguously revealed the locations of all substrate atoms. Polder omit maps, generated by excluding bulk solvent and calculating omit maps for the ligand, also revealed the same binding location for all structures.[156]

Detailed data collection and structural refinement statistics for each data set are summarised in tables in the results section of each chapter. The coordinates for the crystal structures have been deposited in the wwPDB (Worldwide Protein Data Bank),[157,158] freely available to download at www.rcsb.org or www.wwpdb.org. Individual PDB accession codes have been presented where relevant.

Images were produced in PyMol.[159] To model the location of the Cpd I oxygen, the CreateAtomAlongBond script was employed. Computational studies of Cpd I have calculated that the Fe=O bond length is very consistent at 1.62 Å. This was determined both in absence and in presence of substate for CYPs 2C9, 2D6, 3A4 and $P450_{cam}$;[160,161] as well as a model system of Cpd I in chloroperoxidase.[162] The oxygen atom was thus positioned 1.62 Å from the heme iron of the CYP199A4 structures.[i]

[i]The Cpd I Fe=O bond length has been experimentally determined to be 1.63 Å using X-ray crystallography of several non-P450 heme enzymes.[163] This value is in close agreement with the computational results for P450 enzymes (1.62 Å).

Chapter 3 Dealkylation of *para*-methoxy substituted benzoic acids by CYP199A4

3.1 Introduction

CYP199A4, from the bacterium *R. palustris* strain HaA2, and the closely related CYP199A2 from strain CGA009, have high affinities for 4-methoxybenzoic acid and related benzoic acids.[23,27,28,164] 4-Methoxybenzoic acid has been shown to induce a $\geq$ 95 % type I spin state shift.[23] 4-Methoxybenzoic acid also bound very tightly to the active site of CYP199A4 ($K_d = 0.28\,\mu M$). The benzoic acid skeleton is important for binding, and replacing the carboxylate group with a benzyl alcohol, benzamide or a benzaldehyde reduces the strength of substrate binding dramatically.[23,28,30] Altering the benzene ring to a saturated cyclohexyl system or removal of the substituent at the *para*-position also has a deleterious effect on substrate binding and activity.[23,30] As well as 4-methoxybenzoic acid, CYP199A4 can bind and O-demethylate 3,4-dimethoxybenzoic acid solely at the *para* methoxy group to yield 3-methoxy-4-hydroxybenzoic acid.[27] With 3,4-dimethoxybenzoic acid, the spin state shift of CYP199A4 is reduced (70 % vs $\geq$ 95 %) and the binding is not as tight (29.5 µM vs 0.28 µM). The product formation is also lower due to the additional *meta*-methoxy group.[27] CYP199 family enzymes have also been reported to be active with related aromatic carboxylic acids including 2-naphthoic acid,[165,166] indole-6-carboxylic acid,[167] and *para*-substituted cinnamic acids.[31,32]

The crystal structure of 4-methoxybenzoic acid-bound CYP199A4 has been determined (PDB: 4DO1).[30,131,164] In this crystal structure, the substrate carboxylate group directly hydrogen bonds to the side chains of Arg92, Ser95 and Ser244 and, via a bridging water molecule, Arg243 (Figure 18). Hydrophobic interactions between Leu98, Val181, Phe182, Phe185, Val295 and Phe298 with the benzene ring help hold the substrate in position.[131] A chloride ion caps the entrance to the active site and protects the heme from external solvent entering the active site. The methyl group of the *para*-methoxy substituent is oriented towards the heme iron (3.9 Å), which is consistent with exclusive attack at this position, resulting in demethylation to form 4-hydroxybenzoic acid. These interactions rationalised the enzyme's selectivity for the benzoic acid *para*-substituent.

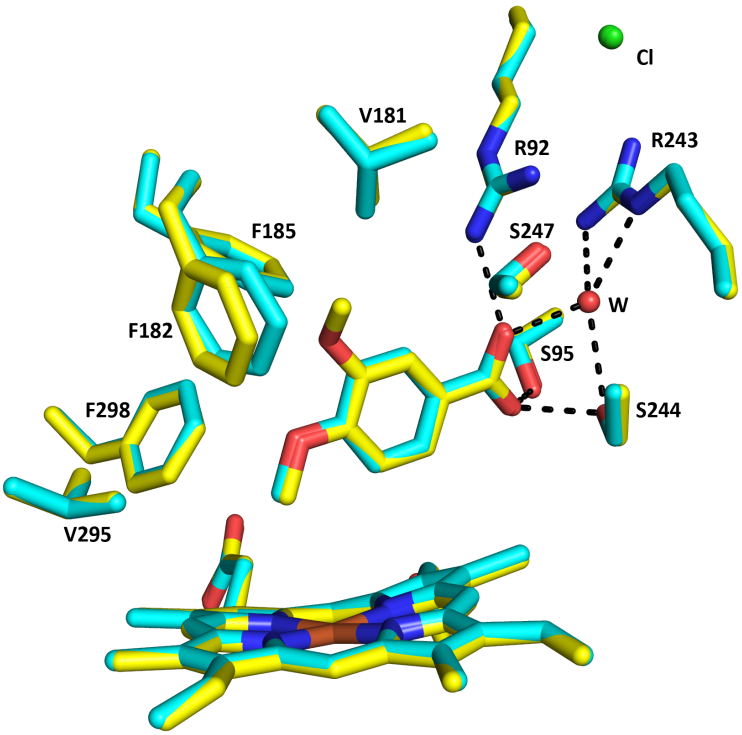

Figure 18. Comparison of the active site of 3,4-dimethoxybenzoic acid (yellow, PDB: 4EGN) with 4-methoxybenzoic acid (cyan, PDB: 4DO1). The F182 residue has moved slightly due to the *meta*-position methoxy group of 3,4-dimethoxybenzoic acid.

The crystal structure of CYP199A4 with 3,4-dimethoxybenzoic acid (PDB: 4EGN) revealed that the positions of the benzene ring, carboxy group and 4-methoxy group were superimposable with that of 4-methoxybenzoic acid.[131] However, the 3-position methoxy group of 3,4-dimethoxybenzoic acid pointed away from the heme, towards the active site residues Phe185 and Phe182, causing a movement in the F182 residue (Figure 18). This steric clash accounted for the weaker binding of the substrate and provided further evidence for the enzyme's preference towards *para*-substituted substrates.[30]

Removal of methyl groups in synthesis often requires harsh conditions and unselective reagents and very few catalysts are available for this reaction.[168] Alkyl methyl ethers usually require a Lewis acid and a nucleophile[169,170] for efficient demethylation while aryl methyl ethers can be demethylated in the absence of the Lewis acid[168] but in both instances elevated temperatures are required. Additionally these reagents generate significant volumes of hazardous waste and proceed with low atom economy.[ii] The CYP enzyme-catalysed O-demethylation reaction proceeds under ambient conditions, and thus these enzymes can potentially be applied as biocatalysts for selective dealkylation.

[ii] Atom economy is defined as the proportion of atoms present in the reactants that are incorporated into the product.[171,172]

Related to oxidative demethylation mono-oxygenase activity are the reactions of several plant-based CYPs, such as CYP81Q1 and the CYP719A subfamily. These enzymes have been shown to catalyse the ring-closing of *ortho*-hydroxymethoxy-containing substrates to yield methylenedioxy rings.[173,174] These ring-closing reactions must proceed via an unconventional mechanism as there is no incorporation of oxygen into the final product (Figure 19).

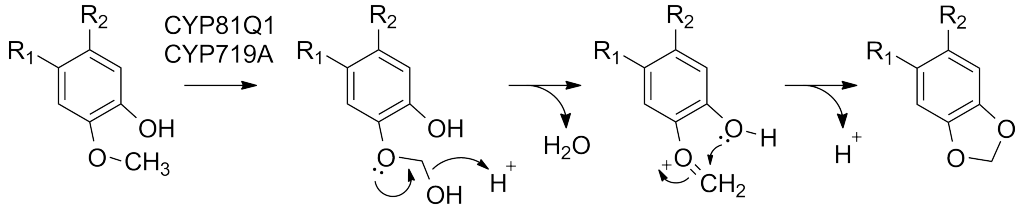

Figure 19. Proposed mechanism for CYP719A and CYP81Q1-mediated ring closing of *ortho*-hydroxymethoxy-containing substrates.[173,174]

The proposed mechanism for this reaction involves formation of a hemiacetal, similar to normal demethylation activity. The key step is proposed to be formation of a methylene-oxonium intermediate along with a molecule of water, followed by an intramolecular attack on the resultant methylene carbon by the adjacent *ortho*-hydroxy group.[174] Proton abstraction yields the methylenedioxy bridge-containing product.

The reverse ring-opening reaction has been observed in various (methylenedioxy)phenyls with rabbit liver and lung microsomal P450s,[175] with the dihydrofuran moiety of the drug darifenacin,[176] and in 3,4-(methylenedioxy)benzoic acid with CYP199A4 (Figure 20).[177]

This was postulated to proceed via a hemiacetal intermediate, followed by addition of water to induce ring-opening. Attack of the resultant carbonyl by H_2O would result

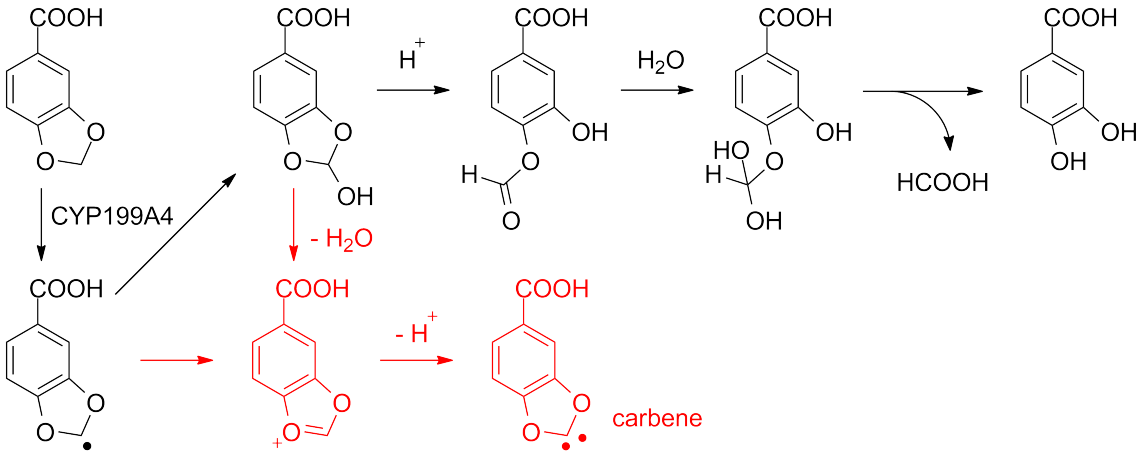

Figure 20. Proposed mechanism for methylenedioxy deprotection by mammalian P450s.[175] Also shown in red is the proposed formation of a carbene intermediate, which can bind to the heme iron and inhibit further catalysis.[178] This carbene was not observed in the turnovers of 3,4-(methylenedioxy)benzoic acid by CYP199A4.[177]

in generation of formic acid and the methylenedioxy bridge-deprotected product.[175] In the CYP2A6 metabolism of paroxetine, there was evidence of inhibition of the turnover rates after initial oxidation of the methylenedioxy group, which was proposed to be due to binding of a carbene species to the heme iron (Figure 20).[178]

The binding and turnover activity of CYP199A4 with a range of mono-, di- and tri-substituted methoxybenzoic acid substrates will be determined (Figure 21). These studies will elucidate how benzoic acids with differently sized substituents at the *ortho*-, *meta*- and *para*-positions or a heteroatom in the benzene ring interact with the enzyme. Of interest was to determine whether CYP199A4 could catalyse ring-closing and ring-opening reactions as observed with other P450s. Several benzoic acids containing *ortho*-hydroxy-methoxy functional groups were investigated to determine if CYP199A4 can catalyse ring-closing reactions. To extend the understanding of the ring-opening transformation, 3,4-ethylenedioxybenzoic acid was investigated to determine if an equivalent ethylene bridge deprotection reaction could be catalysed by CYP199A4. These studies will provide a basis for the future choice or synthesis of small molecule probes designed to investigate the mechanism of action of CYP enzymes.

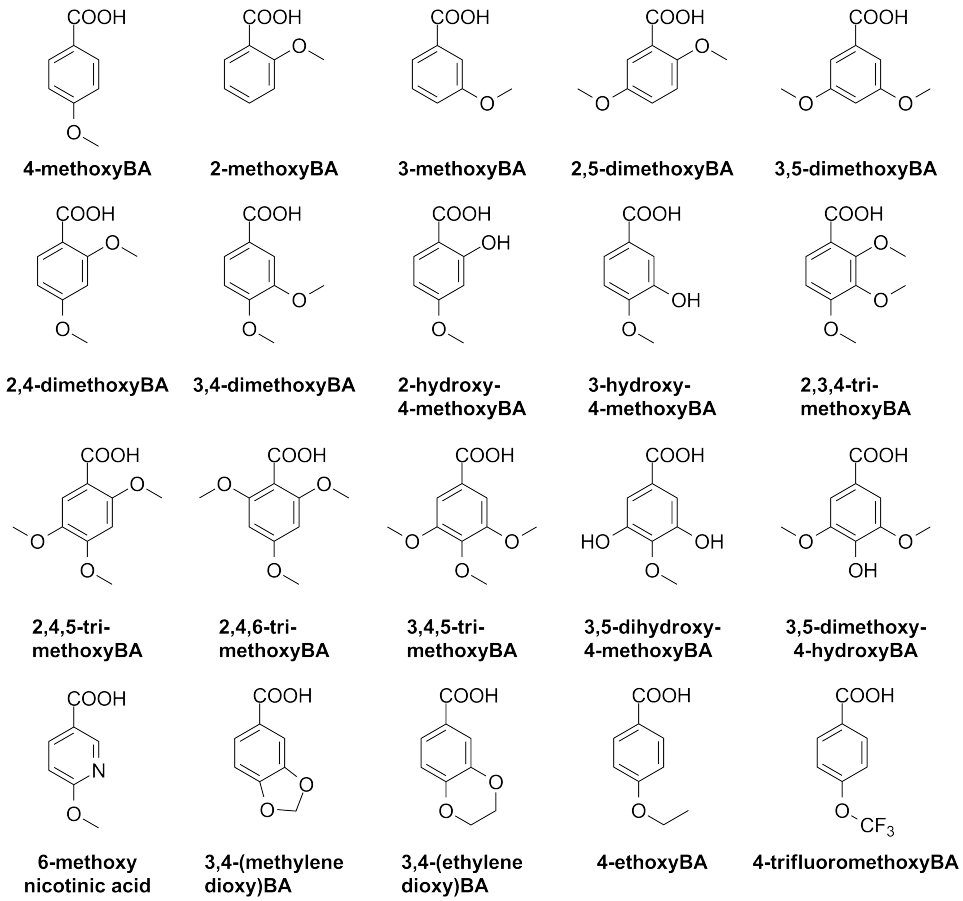

Figure 21. Multiply-substituted methoxy and ring-containing substrates investigated with CYP199A4.

3.2 Results

3.2.1 Substrate binding assays

Analysis of the spin state shift (Chapter 2.3) gives an indication of the ability of a substrate to induce dissociation of the distal heme water ligand, and hence if the substrate fits in the active site.[iii] Therefore, the proportion of high spin heme (denoted % HS) was assayed with each substrate as an initial screening method. The substrates without a *para*-methoxy group induced very low spin state shifts in CYP199A4 compared to the high shift induced by 4-methoxybenzoic acid ($\geq$ 95 % HS, Table 3). 2-Methoxy induced a lower shift than 3-methoxybenzoic acid (10 % and 40 % HS respectively, Table 3, Figure 22a, Appendix A.1). In comparison, benzoic acid induced a 30 % shift while 3,4-dimethoxybenzoic acid shifted the spin state to 70 % high spin. Dimethoxybenzoic acids which did not have a *para*-position methoxy substituent also displayed minimal spin state shifts with CYP199A4, 10 % HS for both 2,5- and 3,5-dimethoxybenzoic acids. These results emphasised the importance of the *para*-position methoxy group for inducing dissociation of the distal water bound to the heme iron. The presence of additional *ortho* and *meta* groups reduced the spin state shift and therefore would be expected to be detrimental towards substrate binding.

Motivated by the preference of substrates with a *para* substituent towards substrate binding, several di- and tri-substituted benzoic acids containing additional *ortho* and *meta* substituents of different sizes were investigated. 2,4-Dimethoxybenzoic acid induced a marginally lower spin state shift than 4-methoxybenzoic acid but higher than 3,4-dimethoxybenzoic acid (90 % HS, Figure 22c, vs $\geq$ 95 % and 70 % respectively). Both 2-hydroxy- and 3-hydroxy-4-methoxybenzoic acids induced spin state shifts $\geq$ 90 %, indicating the smaller hydroxy group was better tolerated than a methoxy substituent at these positions by the enzyme active site. The greater spin state shifts of 2,4-dimethoxy- and 2-hydroxy-4-methoxybenzoic acids over the substrates with *meta*-substitutions implied an *ortho* substituent was less disruptive to active site binding. This contrasted with the results of 2- and 3-methoxybenzoic acids, where the *meta* substituted benzoic acid induced a greater spin state shift.

[iii] It is important to note that in certain instances the spin state shift is not indicative of displacement of the distal water ligand. For example, the distal water is still bound to the heme iron in the X-ray crystal structure of adamantane-bound $P450_{cam}$.[48,179]

Table 3. Binding and turnover parameters determined for methoxybenzoic acid (BA) analogues investigated with CYP199A4. Shown are spin state shift and dissociation constant analyses (% HS and K_d, Chapter 2.3), NADH oxidation rates (Chapter 2.4), product formation rates (PFR, Chapter 2.5) and resulting coupling efficiency (%). Rates are given as mol (molCYP)$^{-1}$ min^{-1}.

Substrate	HS (%)	K_d (µM)	NADH[a]	PFR[b]	Coupling[c]
4-methoxyBA [28]	≥ 95	0.28 ± 0.01	1340 ± 28	1220 ± 120	91 ± 2
2-methoxyBA	10	n.d.[d]	-[e]	-[f]	-
3-methoxyBA	40	69 ± 2	498 ± 5	-[f]	-
2,5-dimethoxyBA	10	n.d.[d]	-[e]	-[f]	-
3,5-dimethoxyBA	10	1500 ± 200	49 ± 2.0	7 ± 2	14 ± 4
2,4-dimethoxyBA	90	47 ± 1	664 ± 32	384 ± 21	58 ± 1
3,4-dimethoxyBA	70	30 ± 3[g]	807 ± 35	626 ± 100	77 ± 9
2-hydroxy-4-methoxyBA	≥ 95	0.16 ± 0.01	483 ± 32	271 ± 20	56 ± 4
3-hydroxy-4-methoxyBA	90	1.7 ± 0.1	847 ± 60	663 ± 75	75 ± 8
2,3,4-trimethoxyBA	5	n.d.[d]	54 ± 5	-[h]	-
2,4,5-trimethoxyBA	0	n.d.[d]	-[e]	-[f]	-
2,4,6-trimethoxyBA	0	n.d.[d]	-[e]	-[f]	-
3,4,5-trimethoxyBA	10	n.d.[d]	9.7 ± 1.9	-[f]	-
3,5-dihydroxy-4-methoxyBA	5	n.d.[d]	10 ± 1	-[f]	-
3,5-dimethoxy-4-hydroxyBA	5	n.d.[d]	163 ± 12	-[f]	-
6-methoxynicotinic acid	≥ 95	0.46 ± 0.05	353 ± 6	286 ± 32	81 ± 8
4-trifluoromethoxyBA	≥ 95	0.43 ± 0.05	294 ± 8	-[f]	-
4-ethoxyBA	≥ 95	0.17 ± 0.02	527 ± 10	527 ± 38	100 ± 8
3,4-(methylenedioxy)BA	70	0.17 ± 0.05	265 ± 7.2	158 ± 19	59 ± 7
3,4-(ethylenedioxy)BA	70	50 ± 1.5	437 ± 7	332 ± 57	76 ± 2
benzoic acid	30	13 ± 0.2	257 ± 2	-[f,i]	-

[a]NADH oxidation rate. [b]PFR: product formation rate. [c]% of NADH consumed that led to formation of substrate metabolite. [d]Not able to be determined due to low spin state shift. [e]No significant NADH oxidation activity above the leak rate (≈ 9 min^{-1}). [f]no detectable levels of product formation. [g]This dissociation constant was determined previously.[27] [h]Product detectable in *in vivo* turnovers only, hence was not quantified. [i]Hydrogen peroxide levels in the turnover were 18 ± 0.6 µM (4.7 ± 0.3 %). In the 4-methoxybenzoic acid turnover, it was 5.5 ± 0.5 µM of H_2O_2.

A series of tri-substituted benzoic acid substrates were investigated (2,3,4-, 3,4,5-, 2,4-5- and 2,4,6-trimethoxybenzoic acids; 3,5-dihydroxy-4-methoxy- and 3,5-dimethoxy-4-hydroxybenzoic acids). None of these substrates were able to induce a significant shift of CYP199A4 to the high spin state (all ≤ 10 % HS). The highest shift was observed with 3,4,5-trimethoxybenzoic acid (10 %, Figure 22). 3,5-Dihydroxy-4-methoxybenzoic acid, containing two *meta*-hydroxy groups, demonstrated that three substituents could not easily be accommodated in the active site of CYP199A4 despite the smaller size of the hydroxy groups (Table 3). In line with the results for substrates without a *para*-position methoxy group, 3,5-dimethoxy-4-hydroxybenzoic acid induced

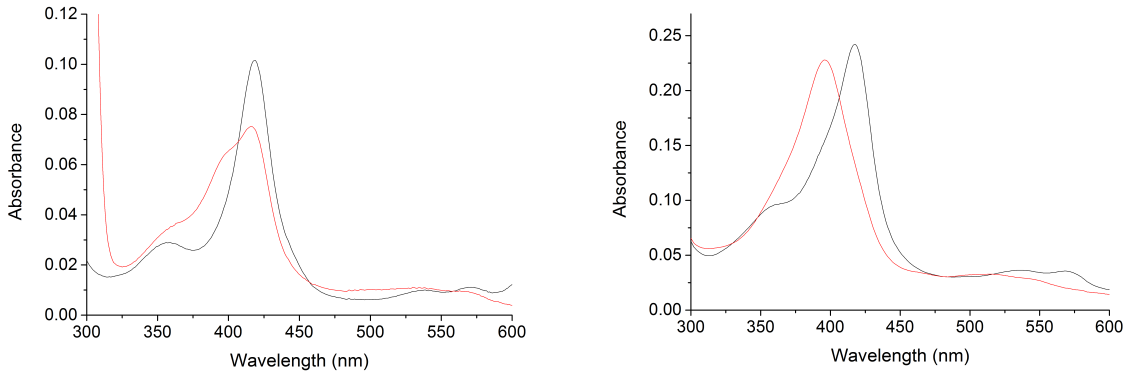

(a) 3-methoxyBA

(b) 4-ethoxyBA

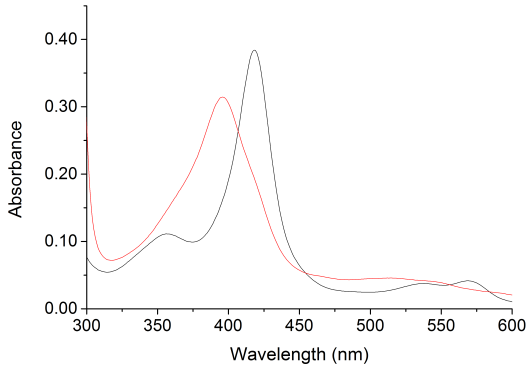

(c) 2,4-dimethoxyBA

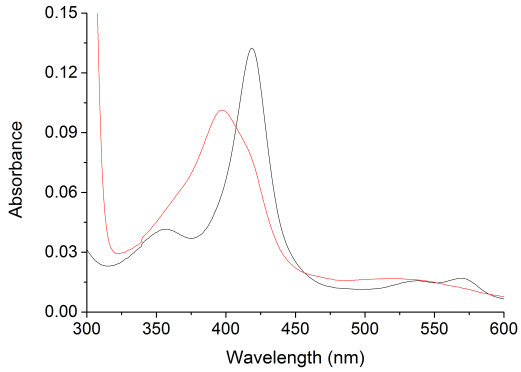

(d) 3,4-(methylenedioxy)BA

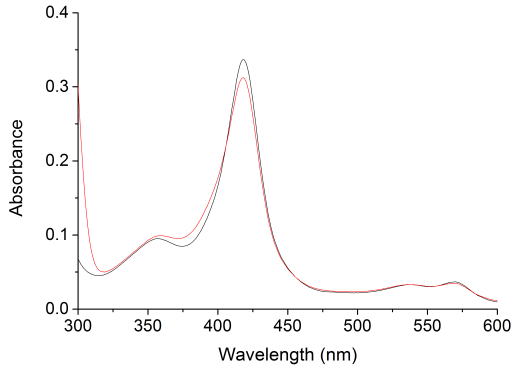

(e) 3,4,5-trimethoxyBA

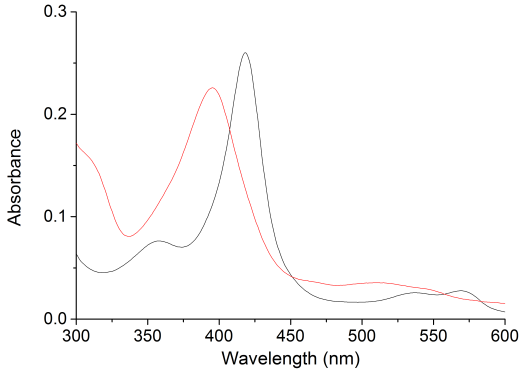

(f) 4-trifluoromethoxyBA

Figure 22. Spin state shifts of substituted benzoic acid substrates investigated with CYP199A4. Black shows CYP199A4 in its resting state, while red shows the maximum absorbance shift obtained upon addition of substrate.

a minimal spin state shift (5 %, Table 3). Overall, the inclusion of multiple *ortho* and *meta* substituents is detrimental to the binding of benzoic acids to CYP199A4.

The effect of inserting a heteroatom at the *meta*-position of the benzene ring was investigated using 6-methoxynicotinic acid. A $\geq$ 95 % spin state shift was observed suggesting that modification of the benzene to a pyridine does not dramatically impact binding. 4-Trifluoromethoxybenzoic acid, in which the hydrogens of the methoxy moiety have been replaced by similarly sized fluorine atoms, was then investigated. The $\geq$ 95 % spin state shift observed suggested that the trifluoromethoxy group did not

impair binding (Figure 22f).

To further investigate the size of the substrate and range of functional groups that can be accommodated by the CYP199A4 active site, 4-ethoxy-, 3,4-(methylenedioxy)- and 3,4-(ethylenedioxy)-benzoic acids were investigated. 4-Ethoxybenzoic acid, which is similar to 4-methoxybenzoic acid but with an additional methylene carbon at the *para*-position, generated a ≥ 95 % spin state shift, revealing that the additional steric bulk at the *para* position was able to be accommodated in the active site. 3,4-(Methylenedioxy)benzoic acid induced a 70 % spin state shift (Figure 22d),[177] lower than the structurally related 3-hydroxy-4-methoxybenzoic acid but comparable to 3,4-dimethoxybenzoic acid[27] (Table 3). 3,4-(Ethylenedioxy)benzoic acid also induced a 70 % spin state shift. The 3,4-(ethylenedioxy)benzoic acid would be a comparable size to 2-napthoic acid, which contains a planar benzene ring fused to the 3,4-position. However, 2-napthoic acid only induced a 5 % HS shift.[30]

In order to assay the affinity of each substrate for CYP199A4 binding, dissociation constants (K_d) were determined (Chapter 2.3, Table 3). A small absorbance change in CYP199A4 upon substrate addition, in line with the spin state shifts measured, was observed for 2-methoxy- and 2,5-dimethoxybenzoic acids. This prevented determination of the dissociation constant but again demonstrated that the *ortho*-substituted benzoic acids do not appear to bind to CYP199A4 (Appendix A.2). 3-Methoxybenzoic acid bound ≈ 200 times less tightly than 4-methoxybenzoic acid (69 µM vs 0.28 µM, Figure 23a). The binding affinity was lower than that of benzoic acid (13 µM), despite the higher spin state shift for 3-methoxybenzoic acid. 3,5-Dimethoxybenzoic acid (Figure 23b) bound even more weakly than 3-methoxybenzoic acid (1500 µM).

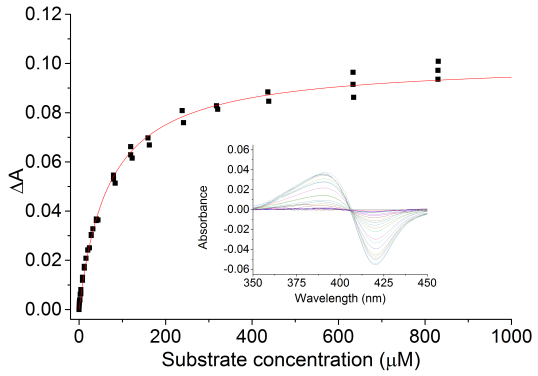

(a) 3-methoxyBA (420 nm, 390 nm, 1.7 µM)

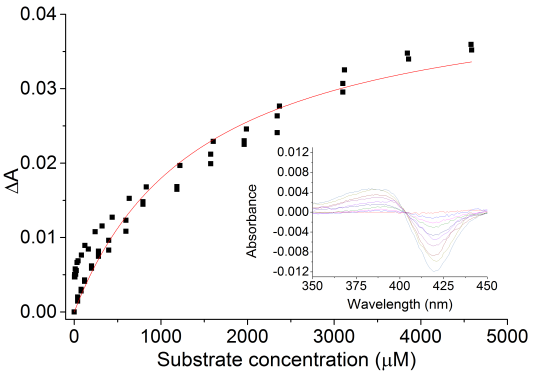

(b) 3,5-dimethoxyBA (420 nm, 386 nm, 1.9 µM)

Figure 23. Dissociation constant determination of 3-methoxy- and 3,5-dimethoxybenzoic acids investigated with CYP199A4. The inset image shows the UV-Vis response to successive addition of substrate aliquots. Shown in brackets are the wavelengths of the trough and peak, and the enzyme concentration used for dissociation constant analysis (trough, peak, µM-P450).

The *ortho*- and *meta*-substituted substrates also containing a *para*-methoxy moiety bound more tightly than the equivalent substrates without a *para* substituent (2,4-dimethoxyBA, 47 µM; 3,4-dimethoxyBA, 30 µM, Appendix A.2), but less tightly than benzoic acid (13 µM) and 4-methoxybenzoic acid (0.28 µM). These results indicated that the *ortho*- and *meta*-position methoxy groups were interacting unfavourably with active site amino acid residues, or potentially the heme moiety.

The substrates containing *ortho*- or *meta*- hydroxy groups bound more tightly than their dimethoxy analogues (2-hydroxy-4-methoxy-, 0.16 µM; 3-hydroxy-4-methoxy-, 1.7 µM, Appendix A.2), highlighting that the smaller hydroxy group was better accommodated in the active site of CYP199A4. With all of the tri-substituted substrates investigated, no dissociation constant could be determined due to the negligable spin state shift and low response upon substrate addition to CYP199A4.

6-Methoxynicotinic acid bound tightly (0.46 µM, Appendix A.2), marginally weaker than 4-methoxybenzoic acid, illustrating that the heterocyclic ring does not significantly impair substrate binding. 4-Trifluoromethoxybenzoic acid bound comparably tightly (0.43 µM). 4-Ethoxybenzoic acid bound tighter than 4-methoxybenzoic acid (0.17 µM), which combined with its spin state shift emphasised that the ethoxy group is a good fit for the CYP199A4 active site (Figure 24a).

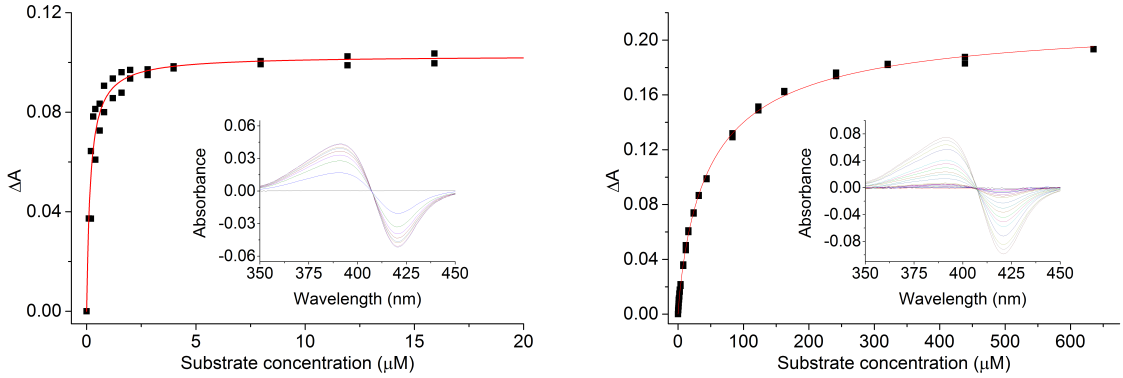

(a) 4-ethoxyBA (421 nm, 391 nm, 0.9 µM)

(b) 3,4-(ethylenedioxy)BA (421 nm, 391 nm, 2.0 µM)

Figure 24. Dissociation constant determination of 6-methoxynicotinic acid and 3,4-(ethylenedioxy)benzoic acid with CYP199A4. Shown in brackets are the wavelengths of the trough and peak, and the enzyme concentration used for dissociation constant analysis (trough, peak, µM-P450).

3,4-(Methylenedioxy)benzoic acid bound more tightly (0.17 µM, Appendix A.2) than both 3,4-dimethoxybenzoic acid and 3-hydroxy-4-methoxybenzoic acid, despite inducing a lower spin state shift than 3-hydroxy-4-methoxybenzoic acid. The smaller size and increased rigidity of a methylenedioxy ring compared to these substrates may account for the tighter binding observed. 3,4-(Ethylenedioxy)benzoic acid, despite inducing the same 70 % spin state shift, bound approximately 300 times less tightly to CYP199A4 (Figure 24b) than 3,4-(methylenedioxy)benzoic acid. The larger ethylene-

dioxy ring may induce steric clashes between active site residues, but is still able to displace the heme distal water ligand.

The binding studies revealed that *para*-substituted benzoic acids containing small *ortho* and *meta* substituents can be accommodated by CYP199A4, although tri-substituted benzoic acids were too large for the active site. Substrates with five and six membered ring systems at the *meta* and *para* positions or those with larger *para*-substituents can also be accommodated. The *para*-position substituent is crucial for high spin state shift and tight binding.

3.2.2 Activity and product formation

In order to quantitate the activity of CYP199A4 with each substrate, *in vitro* assays were performed to determine the rate of NADH oxidation. This is indicative of the turnover rate of the catalytic cycle under conditions where the first electron transfer to the P450 is expected to be rate determining (Chapter 2.4, Figure 25). The amount of product formed was then quantified by using HPLC or GCMS, using coelution studies with authentic standards of the P450 oxidation product where available (Chapter 2.5). The product formation rate (mol (molCYP)$^{-1}$ min^{-1}, henceforth abbreviated to min^{-1}) could then be determined from the NADH oxidation rate and total coupling efficiency (channelling of NADH equivalents into substrate oxidation). Where reaction products were obtained and a standard was not available for identification purposes, *in vivo* turnover reactions (Chapter 2.6) were used to generate product followed by purification using semi-prep HPLC and characterisation using NMR and MS.

The rates of NADH oxidation and product formation for each substrate with the CYP199A4 enzyme varied significantly, although all were lower in activity compared to 4-methoxybenzoic acid (Figure 25, Table 3). CYP199A4 showed little to no NADH oxi-

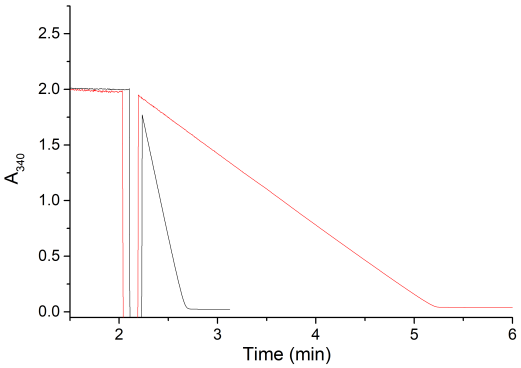

(a) 4-methoxybenzoic acid (**black**) and 6-methoxynicotinic acid (red)

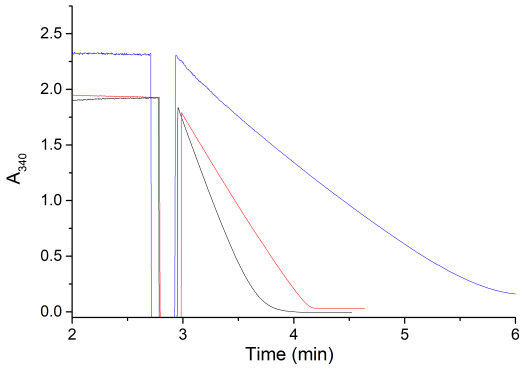

(b) 3-hydroxy-4-methoxyBA (**black**), 2-hydroxy-4-methoxyBA (red) and 3,4-(methylenedioxy)BA (blue)

Figure 25. NADH oxidation assays with selected benzoic acid CYP199A4 substrates. The NADH oxidation rate induced by each substrate was slower than with 4-methoxybenzoic acid, which is shown in (a) in black.

dation activity and no evidence of product formation with 2-methoxy-, 2,5-dimethoxy-, 2,4,5-trimethoxy-, 2,4,6-trimethoxy-, 3,4,5-trimethoxy-, and 3,5-dihydroxy-4-methoxybenzoic acids (Figure 25, Appendix A.3). This was in agreement with the low spin state shifts and binding affinity of these substrates.

3-Methoxybenzoic acid displayed moderate NADH oxidation that was slower than 4-methoxybenzoic acid (Table 3, 498 vs 1340 min^{-1}). No product was detected in the *in vitro* turnovers, indicating that the NADH consumed was being channelled into uncoupling pathways. Hydrogen peroxide was only detected in low quantities (2 % of the NADH reducing equivalents, Chapter 2.7), and thus the oxidase pathway was the most likely source of this uncoupling (Chapter 1.3, Figure 1). 3,5-Dimethoxybenzoic acid with CYP199A4 showed tenfold slower NADH consumption (49 min^{-1}) than 3-methoxybenzoic acid. Significantly, a metabolite was detected in the GC-MS trace of the *in vitro* turnovers (Figure 26). This was identified by GC-MS as a demethylation product (MS m/z = 342.35 vs expected 342.13, Appendix A.4) so must be 3-hydroxy-5-methoxybenzoic acid. Of all the substrates investigated, this was the only incidence of oxidative demethylation at a *meta*-methoxy group, and additionally was the only substrate without a *para* substituent that generated any significant levels of product. The coupling efficiency, which is a measure of the amount of NADH that resulted in product formation, was 14 %, which resulted in a product formation rate of 7 min^{-1}. These findings suggest an alternative binding orientation in the active site for 3,5-dimethoxybenzoic acid compared to the other *meta*-substituted substrates.

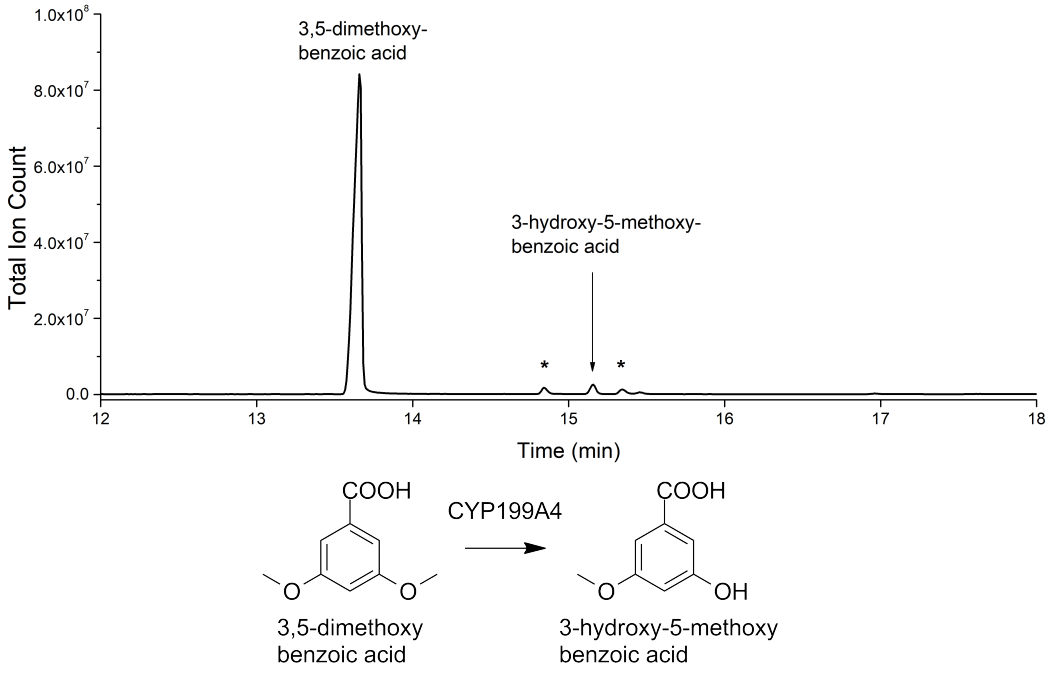

Figure 26. GC-MS analysis of 3,5-dimethoxybenzoic acid turnover with CYP199A4. Impurity peaks (present in control reactions with no P450) are marked with an asterix (*). Mass spectrum of the 3-hydroxy-5-methoxybenzoic acid product is presented in Appendix A.4.

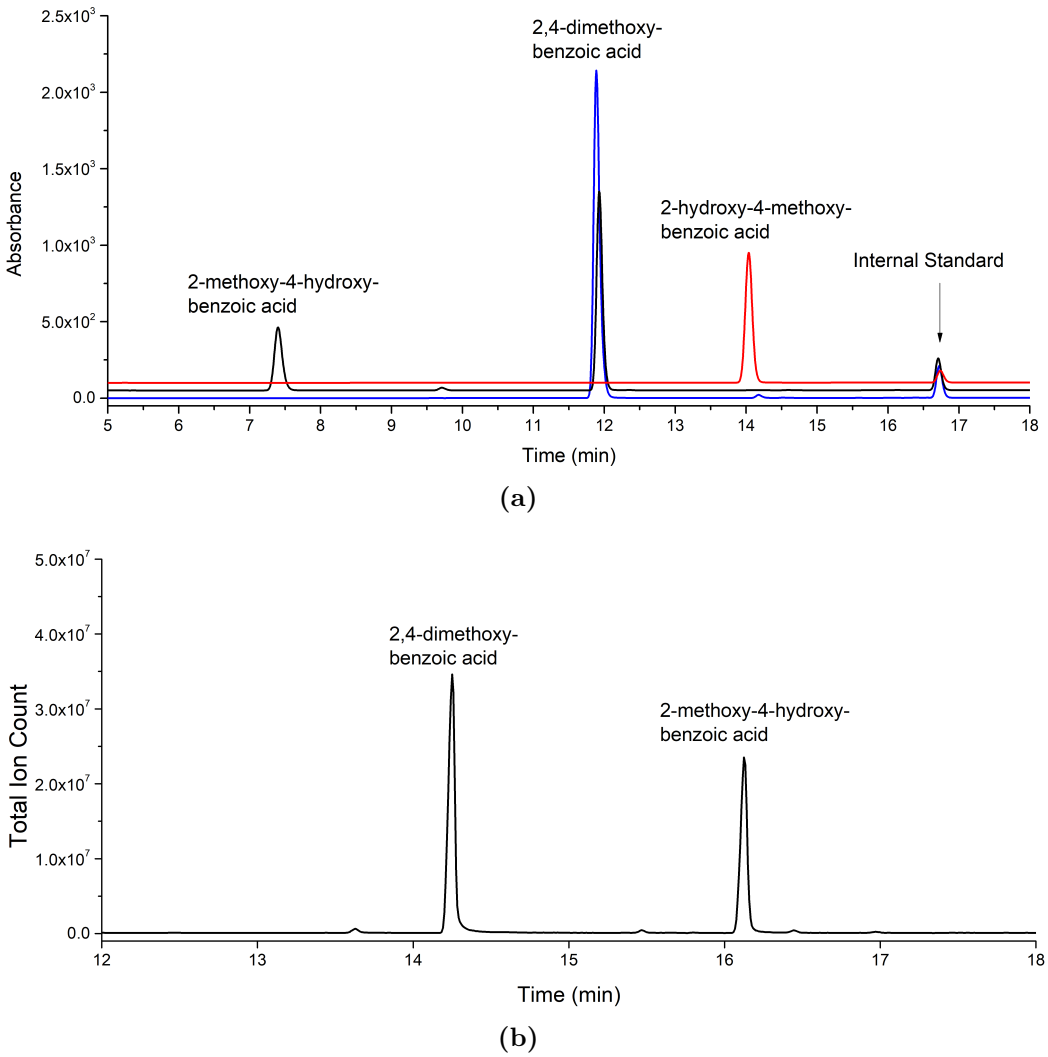

Figure 27. Analysis of 2,4-dimethoxybenzoic acid turnover with CYP199A4. Shown are (a) HPLC analysis: **black**, *in vitro* turnover; red, 2-hydroxy-4-methoxybenzoic acid control; blue, substrate control. The gradient of H_2O:ACN was 20-95 %, and the chromatogram was monitored at 254 nm. (b) GC-MS analysis. The product mass spectrum is presented in Appendix A.4.

2,4-Dimethoxybenzoic acid displayed a high product formation rate with CYP199A4 (384 min^{-1}) although this was lower than both 4-methoxybenzoic acid (1220 min^{-1}) and 3,4-dimethoxybenzoic acid (626 min^{-1}). The product did not coelute with 2-hydroxy-4-methoxybenzoic acid using HPLC (Figure 27), and GCMS analysis indicated the product mass was that of a TMS-derivatised demethylation product (MS m/z: 312.05 vs expected 312.12), thus the product was assigned as the expected 2-methoxy-4-hydroxybenzoic acid.

2-Hydroxy-4-methoxybenzoic acid underwent oxidative demethylation at the *para*-position by CYP199A4 to yield 2,4-dihydroxybenzoic acid as the sole reaction product. This was confirmed by HPLC coelution experiments with an authentic standard (Appendix A.3), and by GC-MS of the *in vitro* turnover mixture (Appendix A.4). The product formation rate observed in turnovers of 2-hydroxy-4-methoxybenzoic acid was

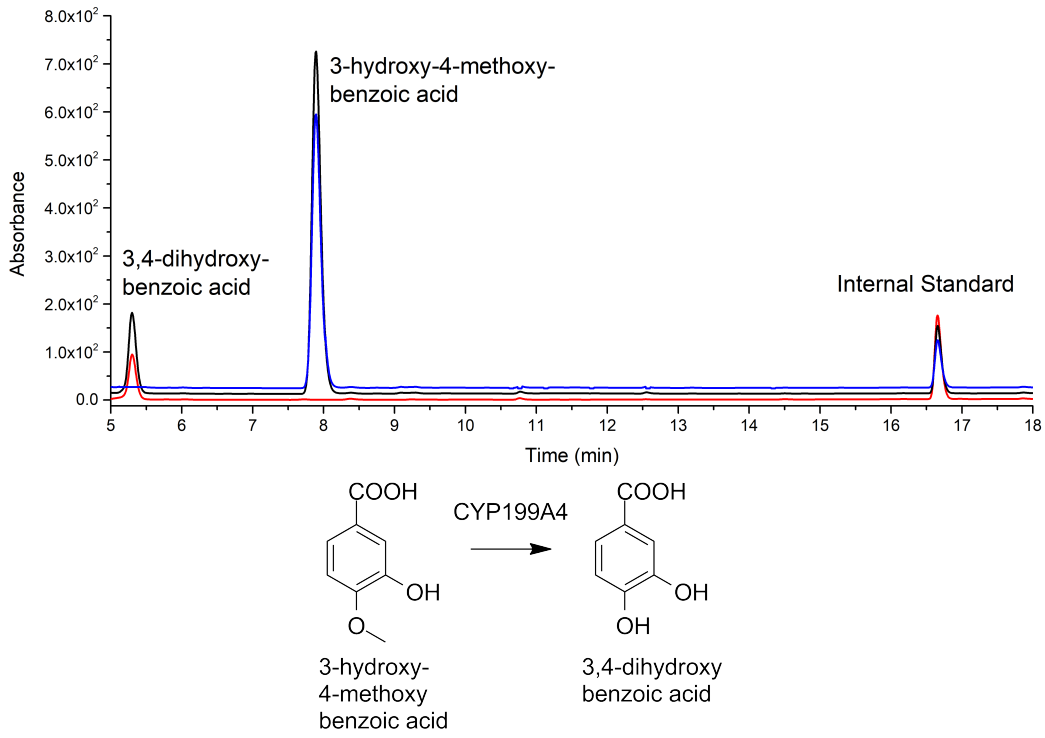

Figure 28. HPLC analysis of 3-hydroxy-4-methoxybenzoic acid turnover with CYP199A4. **Black**, *in vitro* turnover; blue, substrate control; red, 3,4-dihydroxybenzoic acid control. A 20-95 % gradient of H_2O:ACN was used, and the chromatogram was monitored at 254 nm.

slower than 2,4-dimethoxybenzoic acid (271 min^{-1} vs 384 min^{-1}). This was unexpected given the higher spin state shift and tighter binding of 2-hydroxy-4-methoxybenzoic acid. The coupling efficiency was 56 %.

3-Hydroxy-4-methoxybenzoic acid displayed a high product formation rate (663 min^{-1}). The single reaction product was 3,4-dihydroxybenzoic acid which was determined by HPLC coelution experiments (Figure 28). No enzyme-mediated ring-closing reaction between the *para*-methoxy and *meta*-hydroxy groups was observed,[174] which would yield 3,4-(methylenedioxy)benzoic acid which had a HPLC retention time of 12.3 min (Figure 28).

3,5-Dimethoxy-4-hydroxybenzoic acid induced moderate NADH oxidation activity in CYP199A4 (163 min^{-1}, Table 3) despite the negligable substrate binding and spin state shift. This was faster than 3,5-dimethoxybenzoic acid and all tri-substituted benzoic acids tested. However, unlike 3,5-dimethoxybenzoic acid, no products were detected by GC-MS or HPLC analysis (Appendix A.4).

Of the trimethoxybenzoic acids investigated, the highest NADH oxidation activity was observed with 2,3,4-trimethoxybenzoic acid (54 min^{-1} vs $< 10\,min^{-1}$, Table 3). No products were observed in the HPLC or GC-MS of *in vitro* incubation mixtures of any of the trimethoxybenzoic acids. The *in vivo* turnovers of 2,3,4-trimethoxybenzoic acid displayed a peak with a retention time indicative of a demethylation product (Figure 29, RT = 15.8 min). This metabolite was isolated by semi-prep HPLC and

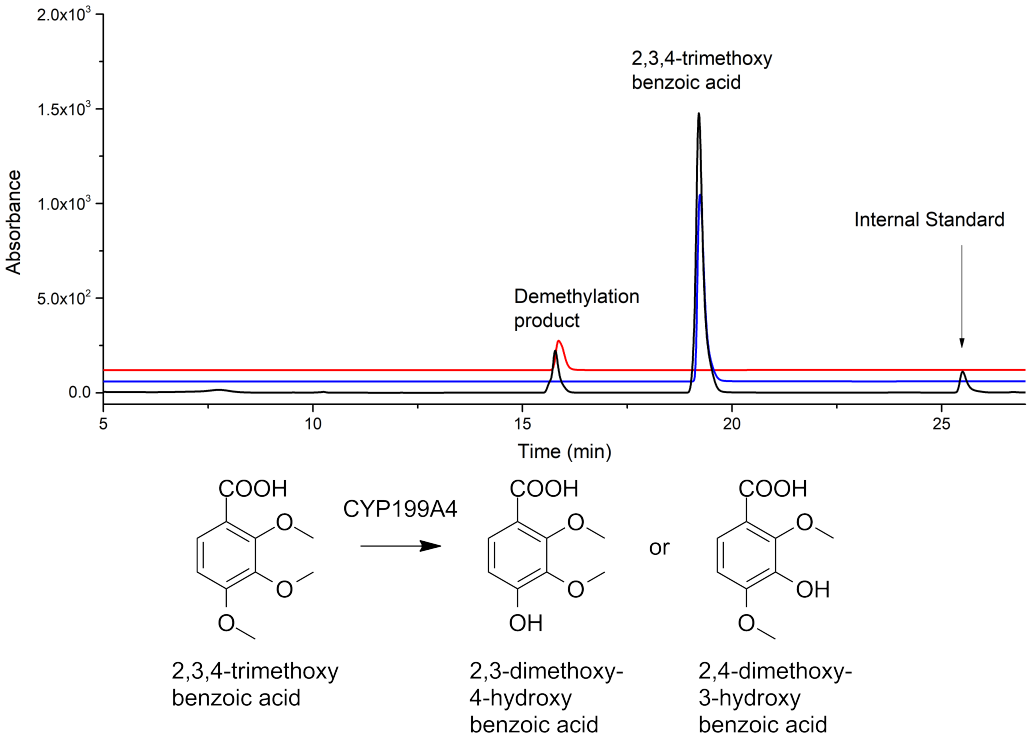

Figure 29. HPLC analysis of 2,3,4-trimethoxybenzoic acid turnover. **Black**, *in vivo* turnover; blue, substrate control, RT = 19.2 min; red, isolated demethylation product, RT = 15.8 min. The chromatogram was monitored at 254 nm and the gradient was 0-50 % of H_2O:ACN.

characterised by GC-MS (Appendix A.4, MS m/z = 342.35 vs expected 342.13). This confirmed it was a demethylation product. NMR analysis of the product was able to rule out 2-hydroxy-3,4-dimethoxybenzoic acid, which has been reported previously.[180] The product was thus either demethylation at the *meta*- or *para*-methoxy. A combination of ^{1}H-^{13}C (HSQC) and through-bond ^{1}H-^{13}C (HMBC) NMR spectroscopies were unable to definitively assign the site of demethylation (Appendix A.5). Based on the selective activity of CYP199A4 for the *para*-substituent observed with other substrates, the product was expected to be 2,3-dimethoxy-4-hydroxybenzoic acid. This could be confirmed by small-molecule X-ray crystallography of the isolated product. The presence of even a small amount of oxidative demethylation showed that the active site of CYP199A4 can accommodate this large, highly substituted substrate, albeit with much lower binding affinity.

4-Trifluoromethoxybenzoic acid, which does not contain any abstractable hydrogen atoms on the *para*-trifluoromethoxy group, was not dealkylated by CYP199A4 due to the strong C−F bonds (Appendix A.3), although NADH was consumed at a moderate rate (294 min^{-1}). The lack of any significant levels of hydrogen peroxide formation suggested that uncoupling events were likely occurring via the oxidase uncoupling pathway (Figure 1).

CYP199A4 with 6-methoxynicotinic acid displayed moderate NADH oxidation (353 min^{-1}, Figure 25) and product formation rates (286 min^{-1}) that were significantly lower than 4-methoxybenzoic acid (NADH, 1340 min^{-1}; PFR, 1220 min^{-1}). It was oxidatively demethylated to 6-hydroxynicotinic acid as identified by HPLC coelution experiments (Figure 30). There was no evidence of a product arising from aromatic N-oxidation. The overall coupling efficiency was comparable to 4-methoxybenzoic acid (81 % vs 91 %). The reduced product formation rate compared to 4-methoxybenzoic acid indicated that the pyridine ring had some effect on the enzyme's activity, despite the binding data suggesting that 6-methoxynicotinic acid binds effectively to CYP199A4.

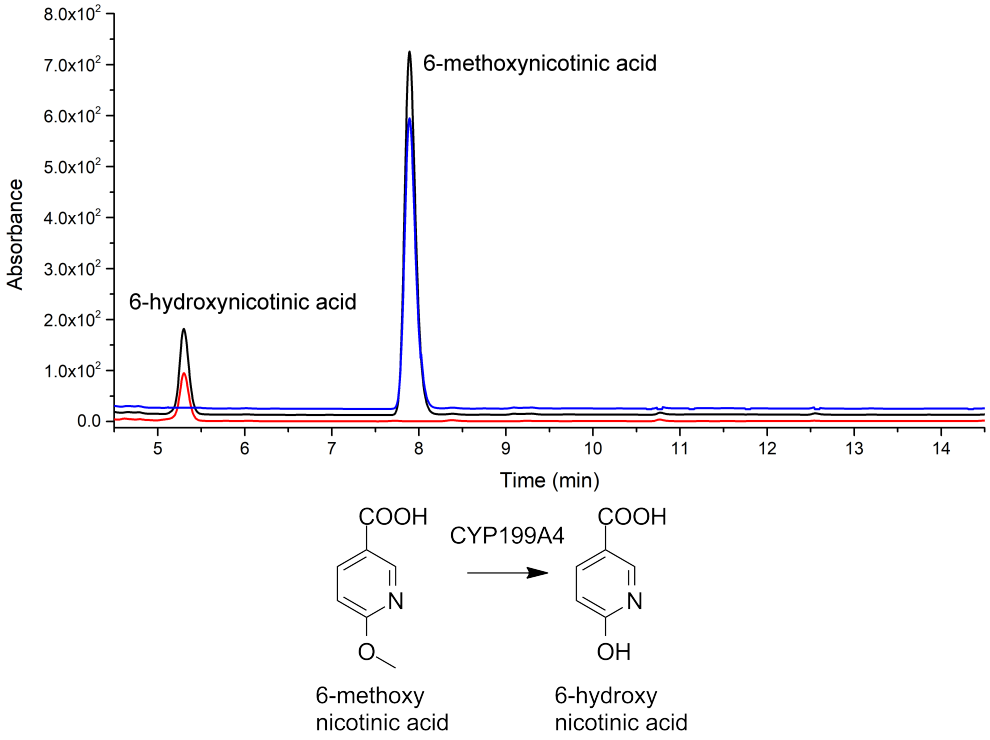

Figure 30. HPLC analysis of 6-methoxynicotinic acid with CYP199A4. **Black**, *in vitro* turnover; blue, substrate control; red, 6-hydroxynicotinic acid control.The gradient was 20-95 % of H_2O:ACN, and the chromatogram was monitored at 254 nm.

Despite the higher binding affinity of 4-ethoxybenzoic acid compared to 4-methoxybenzoic acid, the product formation rate observed was less than half that of 4-methoxybenzoic acid (527 min^{-1} vs 1220 min^{-1}). HPLC analysis showed formation of 4-hydroxybenzoic acid, via oxidative deethylation (Figure 31). Of the substrates investigated, 4-ethoxybenzoic acid displayed the highest coupling (100 %), indicating the ethoxy group methylene CH_2 is ideally positioned in the active site to undergo oxidation. Oxidative O-deethylation can be added to the set of transformations catalysed by CYP199A4.

3,4-(Methylenedioxy)benzoic acid displayed lower product formation and coupling (265 min^{-1}, 59 %, Table 3), compared to the structurally related 3,4-dimethoxybenzoic acid and 3-hydroxy-4-methoxybenzoic acids. The turnover product was identified by

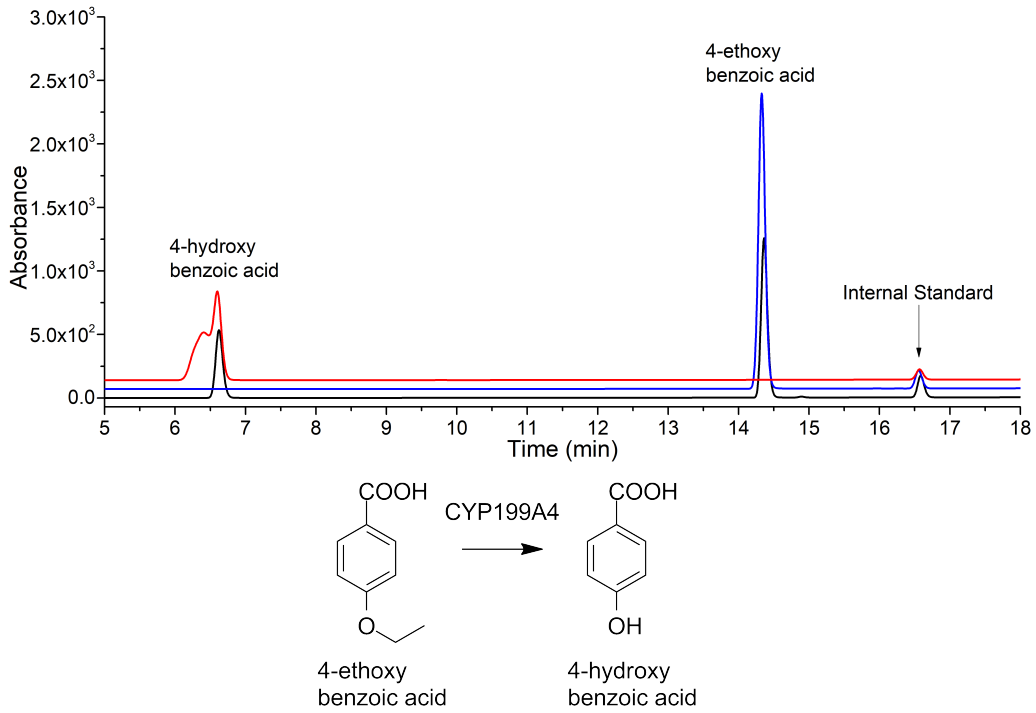

Figure 31. HPLC analysis of 4-ethoxybenzoic acid with CYP199A4. **Black**, *in vitro* turnover; blue, substrate control; red, 4-hydroxybenzoic acid control (double peak). A 20-95 % gradient of H_2O:ACN was used, and the chromatogram was monitored at 254 nm.

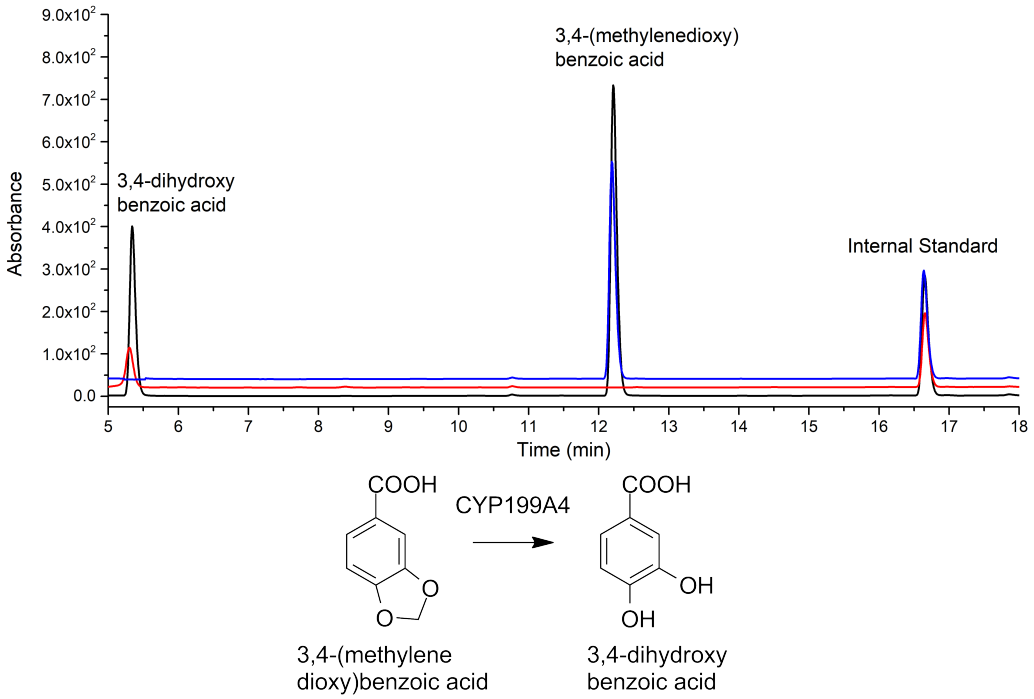

Figure 32. HPLC analysis of 3,4-(methylenedioxy)benzoic acid with CYP199A4. **Black**, *in vitro* turnover; blue, substrate control; red, 3,4-dihydroxybenzoic acid control. A 20-95 % gradient of H_2O:ACN was employed. The chromatogram was monitored at 254 nm.

HPLC coelution experiments as 3,4-dihydroxybenzoic acid (Figure 32). This would have arisen via demethenylation of the methylenedioxy bridge.

3,4-(Ethylenedioxy)benzoic acid displayed higher coupling and product formation (332 min^{-1}, 76 %) compared to 3,4-(methylenedioxy)benzoic acid. HPLC analysis showed the formation of a single *in vitro* product (Figure 33), which was isolated by semi-prep HPLC and characterised by NMR spectroscopy as 3,4-(2′-hydroxyethylenedioxy)benzoic acid (Appendix A.5). The key feature used to assign the regiochemistry of the OH was the HMBC spectrum, where through-bond interactions were observed between the ethylenedioxy bridge carbons and the quaternary carbons on the benzene ring (Figure 34, HMBC cross peaks: **8** ↔ **4**; **9** ↔ **5**).

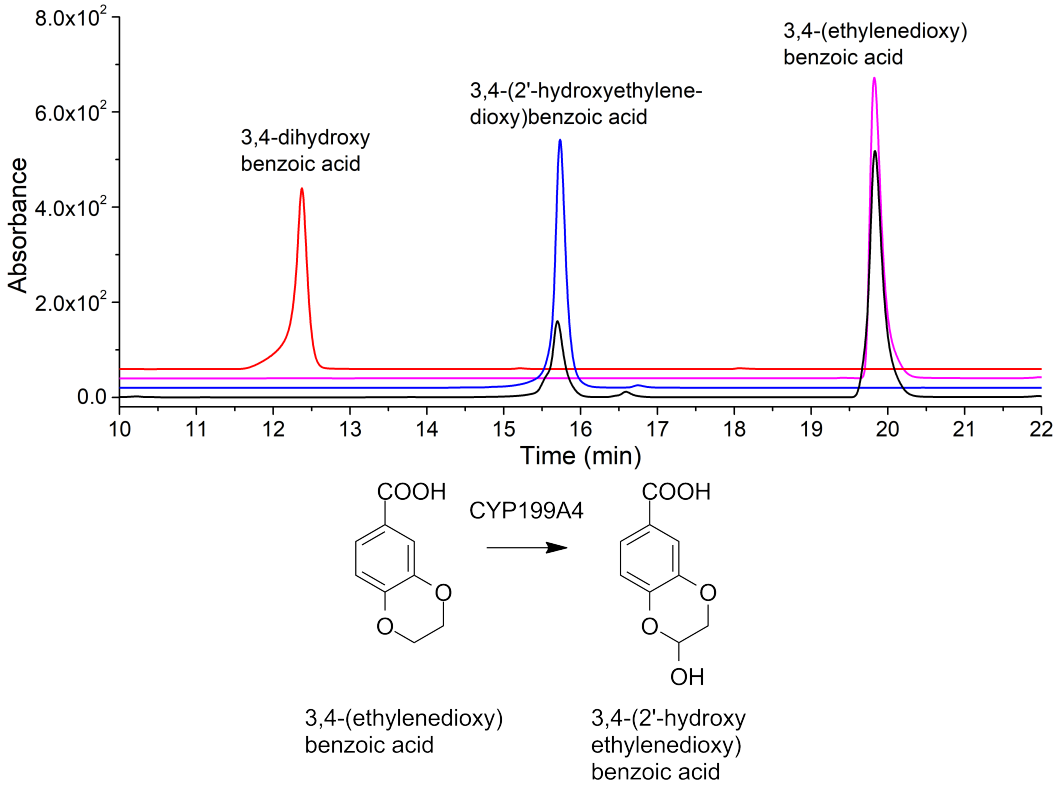

Figure 33. HPLC analysis of 3,4-(ethylenedioxy)benzoic acid with CYP199A4. **Black**, *in vitro* turnover; blue, isolated 3,4-(2′-hydroxyethylenedioxy)benzoic acid product; pink, substrate control; red, 3,4-dihydroxybenzoic acid control. A 0-50 % gradient of H_2O:ACN was used, and the chromatogram was monitored at 254 nm. Chiral HPLC was also performed to investigate the enantioselectivity of the reaction, however the enantiomers could not be resolved (Appendix A.3).

This product could have formed via hydroxylation with no subsequent ring-opening, or it could be in equilibrium with a ring-opened product. The cyclic hemiacetal was unexpected given that ring-opening was observed with the methylenedioxy substrate. The presence of the additional methylene was presumed to stabilise the cyclic hemiacetal, similar to the stability of cyclic sugars.[181] The reaction product is chiral, however chiral HPLC was unable to separate the enantiomers as indicated by the single broad peak observed (Appendix A.3). The product possibly exists in an equilibrium between the ring-closed hemiacetal and ring-opened forms, which would mask any enantioselective hydroxylation by the enzyme. The results indicated that both methylenedioxy and

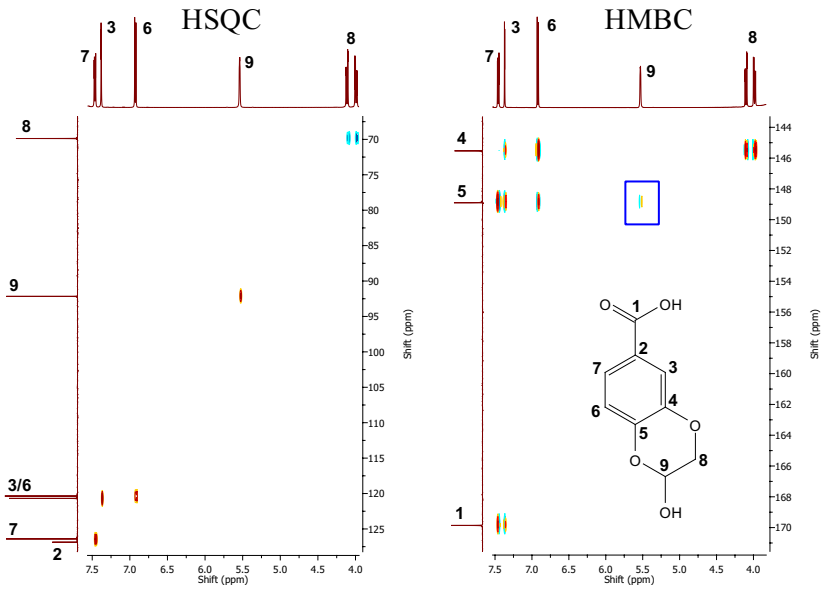

Figure 34. NMR analysis of 3,4-(2′-hydroxyethylenedioxy)benzoic acid. Shown are (left) ^{1}H-^{13}C HSQC and (right) ^{1}H-^{13}C HMBC. After assignment of the quartenary carbons attached to the oxygen atoms using the HSQC spectrum, the site of the hydroxylation was inferred using the HMBC cross-peak which is highlighted with a blue rectangle.

ethylenedioxy bridges could be accommodated and oxidised by CYP199A4, although the activity of each differed dramatically. It might also be possible to include larger ring systems in CYP199A4 substrates.

To confirm the mechanism of oxidative demethylation, the amount of formaldehyde and formic acid were measured in turnovers of 4-methoxy-, 3,4-dimethoxy-, 3-hydroxy-4-methoxy- and 3,4-(methylenedioxy)-benzoic acids. The Purpald assay was employed to measure formaldehyde.[141] Purpald reacts in a 1:1 stoichiometric ratio with formaldehyde to form a complex that strongly absorbs at 550 nm (Chapter 2.8).[141,142] A significant amount of formaldehyde was detected in the turnovers of each of 4-methoxy-, 3,4-dimethoxy- and 3-hydroxy-4-methoxy-benzoic acids (Table 4). This was in agreement with the mechanism of oxygen dealkylation, which proceeds with loss of an aldehyde from the substrate (Chapter 1.4.2).[8,39,93,94]

However, the quantity of formaldehyde observed did not agree with the product

Table 4. Selective assay data for methoxybenzoic acid substrates of CYP199A4. Shown are the % coupling of NADH that could be quantified as reaction product, formaldehyde and formic acid. Each assay is described in Chapter 2.8.

Substrate	Coupling efficiency	Formaldehyde	Formic acid
4-methoxyBA	91 ± 2	46 ± 2	9 ± 4
3,4-dimethoxyBA	77 ± 9	50 ± 8	8 ± 3
3-hydroxy-4-methoxyBA	75 ± 8	43 ± 7	7 ± 3
3,4-(methylenedioxy)BA	59 ± 7	5 ± 1	56 ± 5

coupling for each substrate turnover. The formaldehyde and reaction product should be found in a 1:1 stoichiometric ratio. It is possible that the volatile formaldehyde was lost during the NADH oxidation turnover assay, prior to measurement using the Purpald assay. Alternatively, the development of the Purpald-formaldehyde complex during the assay did not proceed to completion. This may be improved by employing an oxidant such as sodium periodate ($NaIO_4$).[142]

The turnovers were then investigated using a selective assay for formic acid (Chapter 2.8, Table 4).[143] None of 4-methoxy-, 3,4-dimethoxy- and 3-hydroxy-4-methoxy-benzoic acids produced significant levels of formic acid. The turnovers of 3,4-(methylenedioxy)benzoic acid however showed there were comparable amounts of formic acid and the demethenylation product (56 % vs 59 % respectively, Table 4) which in conjunction with the lack of formaldehyde for this substrate agreed with the proposed mechanism for methylenedioxy bridge deprotection.[175]

3.2.3 Substrate docking studies

In the 4-methoxy- and 3,4-dimethoxybenzoic acid bound CYP199A4 crystal structures, the benzoic acid components of each substrate were superimposed (Chapter 3.1, Figure 18).[131] The substituent at the *para* position is held above the heme iron allowing for selective oxidation, while the 3-methoxy group of 3,4-dimethoxybenzoic acid points away from the heme towards F182. This observation was consistent with the product arising by demethylation occurring exclusively at the *para*-substituent. Given that substrates without a 4-methoxy substituent typically displayed no formation of product, it is likely that these substituents also point away from the heme iron. However, 3,5-dimethoxybenzoic acid displayed small amounts of a *meta*-O-demethylation product. This presumably results from a different substrate binding orientation. In order to investigate the possible binding orientations for this substrate, docking studies were performed using the 4-methoxybenzoic acid-CYP199A4 system as the initial model (Chapter 2.9).

3,5-Dimethoxybenzoic acid was manually built into the CYP199A4 active site and energy minimised to determine the likely binding orientation (PDB: 4DO1 with the 4-methoxybenzoic acid substrate removed). Compared to the orientation of 3,4-dimethoxybenzoic acid and other analogues, the lowest energy structure showed that the benzoic acid moiety was tilted by $\approx 15°$ (Figure 35). In this position the 3-methoxy methyl carbon is 5.0 Å from the heme iron (the oxygen of this methoxy group is 0.2 Å closer) although still significantly further than the 4-methoxy carbon of 4-methoxybenzoic acid (4.1 Å). The 3-methoxy carbon is also 2.8 Å from both Leu98 and the closest heme carbon atom, and 3.0 Å from a heme nitrogen. The 5-methoxy group points towards Phe182 with both the oxygen and methyl carbon being 2.9 Å from the closest atom of this residue. This altered binding orientation, compared to the mono *para*-substituted benzoic acids, may explain the observation of a *meta*-O-

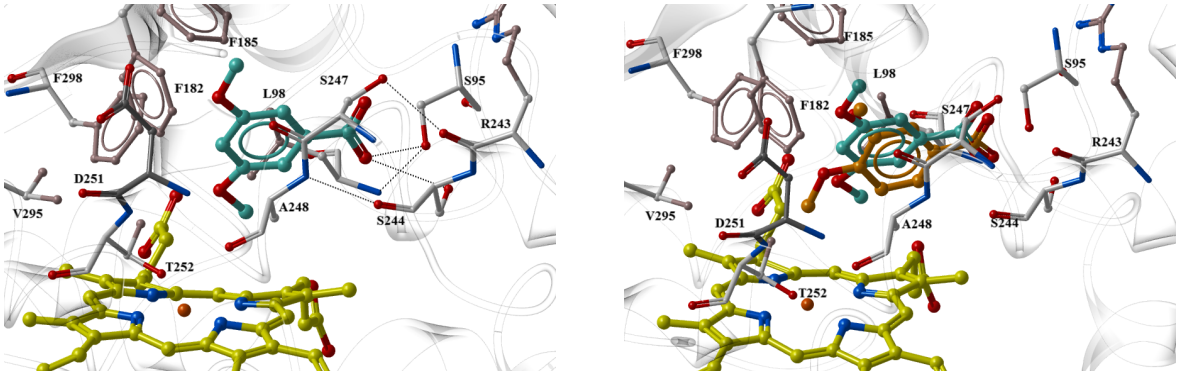

(a) **(b)**

Figure 35. Computational model of 3,5-dimethoxybenzoic acid (dark green) docked into the active site of CYP199A4. Shown in (b) is an overlay with 3,4-dimethoxybenzoic acid (orange).

demethylation product. It may also account for the low binding affinity and the greatly reduced product formation rate of this substrate when compared to 4-methoxybenzoic acid (Table 3).

3-Hydroxy-4-methoxybenzoic acid induced a larger spin state shift and bound more tightly to CYP199A4 than 3,4-dimethoxybenzoic acid (90 %, 1.7 µM vs 70 %, 30 µM, Table 3) In addition, the NADH oxidation and product formation rates were slightly higher with the former substrate (847 min^{-1}, 663 min^{-1} vs 807 min^{-1}, 626 min^{-1}). The 3-hydroxy group may be pointing in one of two orientations, either towards the heme group (subsequently named the "down" orientation) or towards the roof of the active site ("up" orientation). In order to ascertain the likely effect of the different binding orientations, two CYP199A4 models were created where the 3-hydroxy group of 3-hydroxy-4-methoxybenzoic acid was pointing "up" or "down". This was followed by energy minimisation of the structures.

In the docked structure with the 3-hydroxy group in the down position (Figure 36a), the 3-hydroxy oxygen was only 3.1 Å from the heme iron, which was significantly closer than the distance between the 4-methoxy group carbon and the heme iron (3.9 Å). In the up position, however, the 3-hydroxy group was found to be 4.3 Å from the heme, minimising steric clashes with active site residues and allowing access of the 4-methoxy carbon to the heme iron. This seems likely to be the preferred binding orientation of this substrate and rationalises the high product formation rate observed, which was the highest of the disubstituted benzoic acids (663 min^{-1} vs 3,4-dimethoxyBA, 626 min^{-1}, Table 3).

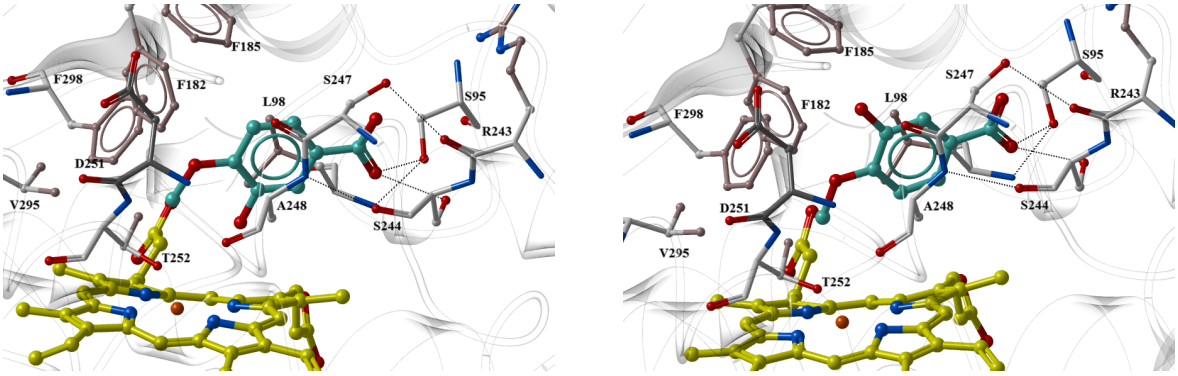

Figure 36. Computational model of 3-hydroxy-4-methoxybenzoic acid docked into the active site of CYP199A4. Shown are two energy minimised orientations of the substrate, with the 3-hydroxy substituent pointing (a) down and (b) up.

The nitrogen in the pyridine ring of 6-methoxynicotinic acid could also point towards the heme, or towards F182 and F185. The substrate was docked, and the nitrogen was only 3.9 Å from the heme iron when directed towards it (Figure 37). Turnover studies indicated there was no product arising from N-oxidation at the pyridine nitrogen, thus the nitrogen is either pointing away from the heme or simply not close enough to compete with the 4-methoxy carbon for oxidation by CYP199A4.

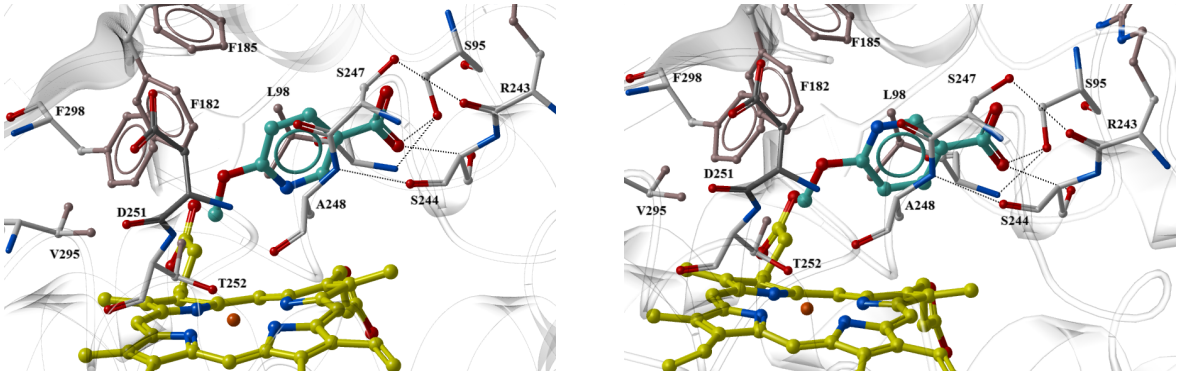

(a) **(b)**

Figure 37. Computational model of 6-methoxynicotinic acid docked into the active site of CYP199A4. Shown are two energy minimised orientations of the substrate, with the pyridine ring nitrogen pointing (a) down and (b) up.

Docking of 3,4-(methylenedioxy)benzoic acid indicated that, with the methylenedioxy bridge pointing towards the heme, it could be bound in a similar orientation to indole-6-carboxylic acid (PDB: 4EGO).[30] This positions the methylenedioxy bridge carbon 4.0 Å from the heme iron. Alternatively, if the methylenedioxy group points away from the heme, the binding orientation could be similar to 3,4-dimethoxybenzoic acid (Figure 38a).[30] In this orientation, the methylenedioxy bridge carbon is 5.7 Å from the heme iron which would presumably not allow for efficient substrate oxidation at

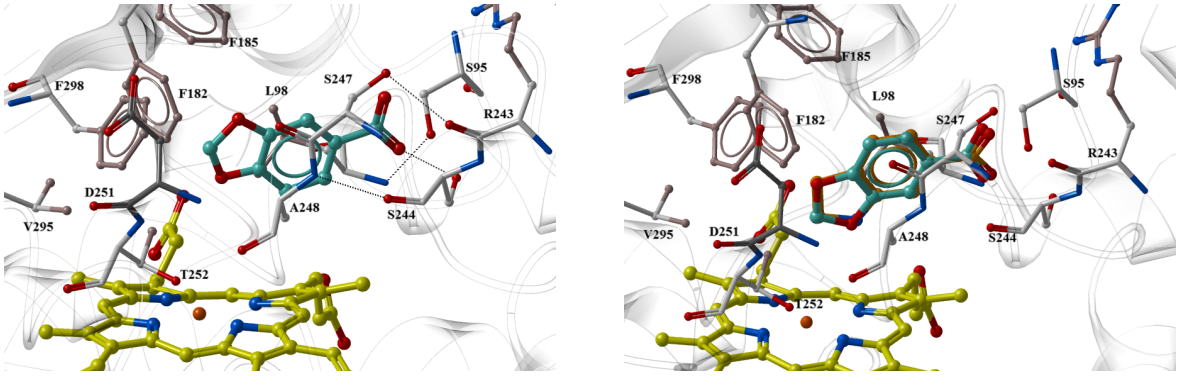

(a) **(b)**

Figure 38. Computational model of 3,4-(methylenedioxy)benzoic acid docked into the active site of CYP199A4. Shown are two energy minimised orientations of the substrate, with the methylenedioxy ring pointing (a) up and (b) down. In the down orientation (b), the substrate (green) is shown overlaid with indole-6-carboxylic acid, PDB: 4EGO (orange).

the methylene C−H bonds. Given that the enzyme forms product with relatively high coupling efficiency, the substrate seems likely to be bound in the "down" orientation, which would be similar to the binding observed with indole-6-carboxylic acid (Figure 38b).

It is likely based on these results that disubstituted benzoic acids will bind in the active site of CYP199A4 with the *meta*-substituent pointing up, into the enzyme binding pocket, to minimise clashes with the heme group and any nearby active site residue side chains. This may also be the case with the pyridine nitrogen of 6-methoxynicotinic acid, given that there is no N-oxidation observed. The 3,4-(methylenedioxy)benzoic acid substrate must be bound in the down orientation, as this orientation explains the observed activity with CYP199A4. The smaller hydroxy group of 3-hydroxy-4-methoxy compared to the dimethoxy equivalent would reduce steric clashes between the substrate and active site of CYP199A4, rationalising the higher spin state shift and tighter binding compared to 3,4-dimethoxybenzoic acid. Further work to try and obtain structures of CYP199A4 with these substrates would confirm these hypotheses. However, some substrates such as 3,5-dimethoxybenzoic acid bind with low affinity.

3.2.4 Crystal structure of 4-ethoxybenzoic acid-bound CYP199A4

The structure of 4-methoxybenzoic acid-bound CYP199A4 has been previously reported[131] (Chapter 3.1 and Figure 14). This enabled the binding orientation of the *para*-position methoxy group relative to the heme iron to be determined, and explained the observed *para*-O-demethylation activity. 4-Ethoxybenzoic acid, which also underwent exclusive O-deethylation, was studied to determine the binding position of the *para*-ethoxy substituent, and if there were changes in the enzyme structure upon binding of the substrate.

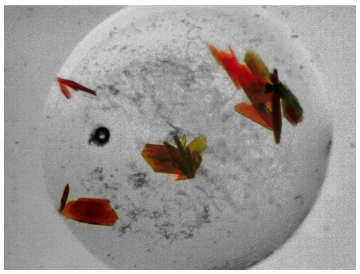

Figure 39. Crystals of CYP199A4. The background colour has been desaturated for clarity.

Crystals of CYP199A4 with 4-ethoxybenzoic acid (1 mM) were obtained in 2 weeks from a 500 µL reservoir solution containing 0.2 M magnesium acetate tetrahydrate, 29 % w/v PEG-3,350 and 0.1 M Bis-Tris pH 5.75 (Figure 39). X-ray diffraction data were collected at 100 K on the MX1 beamline at the Australian Synchrotron[147,148] and the structure was solved at 1.94 Å resolution. A model was developed using WinCoot[144] (Chapter 2.10), and the structure was deposited in the wwPDB database[157,158] (www.wwpdb.org) with accession code 5U6T (Table 5).

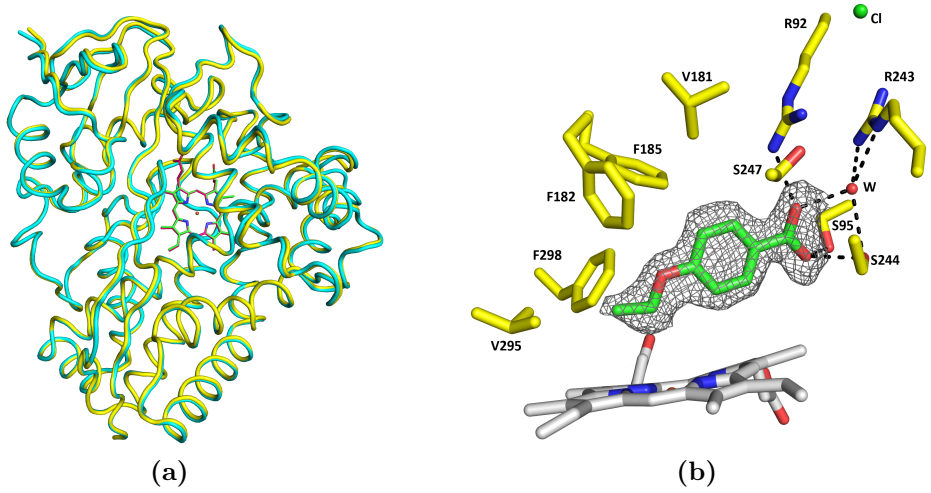

Figure 40. Crystal structure of 4-ethoxybenzoic acid-bound CYP199A4 solved at 1.94 Å resolution. Shown are (a) three-dimensional fold (yellow tube and magenta heme) overlaid with structure of 4-methoxybenzoic acid (cyan tube and green heme) and (b) reduced bias $2mF_o$-DF_c composite omit map[154] of 4-ethoxybenzoic acid-bound CYP199A4. The electron density map for 4-ethoxybenzoic acid is shown contoured as a grey mesh at the 1 σ level.

Table 5. Structural refinement and data collection statistics for 4-ethoxybenzoic acid. 4-Methoxybenzoic acid (PDB: 4DO1) is shown for comparison.[131]

	4-methoxyBA[131]	4-ethoxyBA
PDB code	4DO1	5U6T
X-ray wavelength (Å)	0.9796	0.9537
Unit cell (a/b/c)	107.0/143.5/172.8	44.4/51.4/79.1
($\alpha/\beta/\gamma$)	90/90/90	90/92.0/90
Space group	$P2_12_12_1$	$P12_11$
Molecules per unit cell	4	1
Resolution range[a]	50.0 - 2.00	44.42 - 1.94
	(2.03 - 2.00)	(1.98 - 1.94)
$<I/\sigma(I)>$[a]	28.5 (5.2)	8.4 (2.1)
Unique reflections	179187	26777
Completeness[a]	100.0 (100.0)	99.8 (96.9)
Multiplicity[a]	7.1 (6.1)	7.4 (7.2)
R_{merge}[a,b] (%)	9.8 (31.9)	16.8 (78.8)
R_{pim}[a,b] (%)	N/A[c]	6.6 (31.2)
$CC_{1/2}$[a,d] (%)	N/A[c]	99.5 (77.4)
R_{work}	0.154	0.133
R_{free}[e]	0.189	0.184
Ramachandran plot[f]		
Most favoured	98.5	98.0
Allowed	1.5	2.0

[a]Highest resolution shell is shown in parentheses where applicable. [b]all I+ and I-. [c]Not reported in previous work. [d]Half-correlation coefficient.[182,183] [e]5 % of total reflections, randomly selected. [f]% of all amino acid residues.[184] There were no Ramachandran outliers.

Previously, the 4-methoxybenzoic acid-CYP199A4 complex was crystallised with the $P2_12_12_1$ space group, and the model consisted of 4 identical subunits of the enzyme. The newly solved 4-ethoxybenzoic acid structure contained only a single molecule in the asymmetric unit, and crystallised with lower cell symmetry ($P12_11$). The constructed models when overlaid indicated that the positions of all active site residues are functionally superimposable (rmsd = 0.550 Å over 392 of 393 residues, Figure 40a) The electron density observed in the active site was successfully modelled as a bound 4-ethoxybenzoic acid molecule (Figure 40b).

The substrate carboxylate and benzene groups were superimposable with 4-methoxybenzoic acid's, as was the water molecule that is part of the substrate carboxylate hydrogen bonding network (Figure 41). The chloride ligand that caps the active site from solvent access was found in an nearly identical position. This indicated that the lower symmetry space group was acceptable for use as a comparative

model (Table 5). The ethoxy methylene C_α is held at a comparable distance from the heme iron (4.1 Å) to the methyl of 4-methoxybenzoic acid (4.2 Å). The methyl C_β is held 4.3 Å from the heme and points towards V295. These observations are consistent with and rationalise the substrate's observed C_α-deethylation activity. There was no oxidation at the C_β methyl, which was slightly further away. It would also be less likely to undergo hydrogen abstraction, due to the stronger C−H bonds of a methyl group compared to that of a methylene adjacent to an oxygen atom.

Computational studies have suggested that a linear angle of approach of the substrate to the Cpd I Fe=O may be important to activity.[185] The ferryl oxygen of Cpd I was modelled into the crystal structures of CYP199A4 (Chapter 2.10). The C_α of 4-ethoxybenzoic acid was closer to the Cpd I oxygen than the C_β (2.8 Å vs 3.0 Å). The Fe=O-C angles for 4-ethoxybenzoic acid were also significantly lower than that of 4-methoxybenzoic acid (4-methoxy C_α, 140.7°; 4-ethoxy C_α, 144.8°; C_β, 137.3°, Table 6). The angle of the Fe=O to the substrate *para* oxygen atom was found to be closer to this range (4-methoxy, 158.3°; 4-ethoxy, 163.4°), however this was not a viable position for oxidation by the enzyme.

Table 6. Distances and angles between structural features of 4-ethoxybenzoic acid-bound CYP199A4. The ferryl Cpd I oxygen was modelled 1.62 Å from the heme iron.[160,161]

Distance (Å)	4-methoxyBA	4-ethoxyBA
C_α - Fe	4.1	4.2
C_α - **O**=Fe	2.7	2.8
C_β - Fe	-	4.3
C_β - **O**=Fe	-	3.0
O - Fe	5.2	5.1
C_X - F298	(X = α) 3.8	(X = α,β)[a] 3.6
Angle (°)		
C_{04}-O-C_α	118.6	118.9
O-C_α-C_β	-	105.3
Dihedral C_{09}-C_{04}-O-C_α	2.1	9.2
Fe=O-C_α	140.7	144.8
Fe=O-C_β	-	137.3
Fe=O-O (Me)	158.3	163.4

[a]Both were the same distance from the F298 residue.

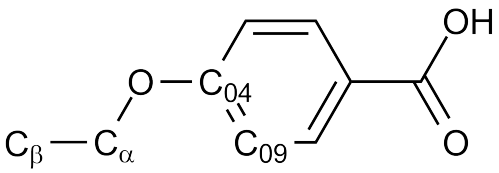

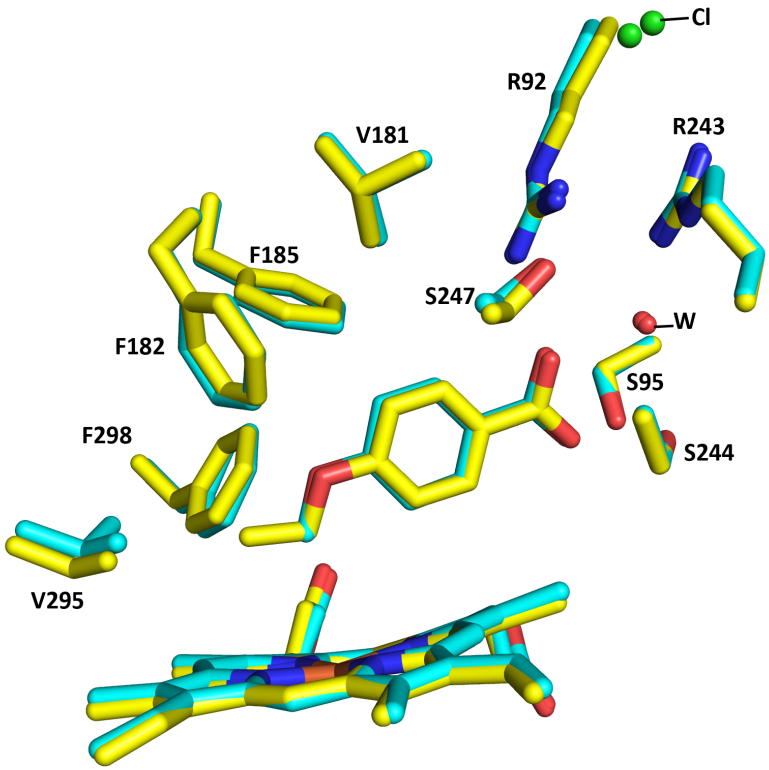

Figure 41. Comparison of the active site of the 4-ethoxy- and 4-methoxy-benzoic acid-bound CYP199A4 structures. 4-Methoxybenzoic acid (cyan) is overlaid with 4-ethoxybenzoic acid (yellow). Water molecules are shown as red spheres and the chloride ligands are green spheres. Those that are labelled (Cl, W) correspond to the 4-ethoxybenzoic acid structure.

3.3 Discussion

The results reinforced the importance of the *para* functional group for benzoic acid substrates of CYP199A4. Most substrates without a *para* substituent did not bind effectively and hence were not oxidised by CYP199A4. Substrates containing *ortho* or *meta* position functional groups could be accommodated but always with a decrease in both binding affinity and oxidation activity. The observation of a turnover product with 3,5-dimethoxybenzoic acid indicated the enzyme can facilitate *meta*-demethylation in certain instances. The size of the substrate necessitated a different binding orientation, where the 3-methoxy group points towards the heme iron.

CYP199A4 was able to accommodate *para*-methoxybenzoic acid substrates with an additional *ortho*- and *meta*-methoxy or hydroxy group, as indicated by oxidative demethylation at the *para*-position in each of 2,4-dimethoxy-, 2-hydroxy-4-methoxy-, 3,4-dimethoxy- and 3-hydroxy-4-methoxy-benzoic acids.

Tri-substituted benzoic acids overall were poor substrates for CYP199A4. It is likely they do not fit into the enzyme's active site. 3,4,5-Trimethoxy- and 3,5-dimethoxy-4-hydroxy-benzoic acids were not turned over, despite CYP199A4 accommodating 3,5-dimethoxybenzoic acid. 2,3,4-Trimethoxybenzoic acid was the only tri-substituted substrate where a miniscule amount of product was detectable after whole-cell oxidations. Based on substrate docking studies, and the crystal structure of 3,4-dimethoxybenzoic acid, it seems plausible that the 2-methoxy and 3-methoxy groups of 2,3,4-trimethoxybenzoic acid point away from the heme iron to avoid steric clashes with the heme. From this, and from the NMR spectra obtained, it follows that demethylation is most likely at the *para* methoxy group.

Some plant P450 enzymes have been shown to catalyse the oxidative ring-closing reaction of *ortho*-hydroxymethoxy substrates[173,174] (Chapter 3.1), however no ring-forming products were observed with any of the substrates tested here. 3-Hydroxy-4-methoxybenzoic acid can be oriented with the *meta* substituent pointing either towards the heme or towards the active site binding pocket. If the substrate was bound similarly to 3,4-dimethoxybenzoic acid (Figure 18), with the *meta*-substituent pointing away from the heme iron, demethylation by CYP199A4 would be the only expected activity. If the hydroxyl moiety points towards the heme iron, ring-closing might be competitive with oxidative demethylation. Plant P450s, which are highly substrate specific, often have specialised active sites which facilitate the unusual reactions observed. This is possibly achieved by holding the substrate *ortho*-hydroxymethoxy moiety close to the heme iron. Of note in these plant P450s is the replacement of the highly conserved Thr252 (CYP81Q1, Ala252; CYP719A, Ser252), which may play a role in catalysing this unique family of transformations.[174]

4-Ethoxybenzoic acid bound tighter to CYP199A4 than 4-methoxybenzoic acid and was deethylated to 4-hydroxybenzoic acid, although the product formation rate was

significantly lower than 4-methoxybenzoic acid. The product would have arisen from C_α-hydroxylation followed by cleavage of the hemiacetal to release acetaldehyde and 4-hydroxybenzoic acid. There was no product observed arising from oxidation at the terminal C_β. This was rationalised by the closer proximity of the methylene C_α to the heme iron and the more linear approach of this carbon to the heme iron. Further crystallographic studies into substrates such as the di- and tri-methoxybenzoic acids may provide further insight into substrate binding, activity patterns and selectivity of these reactions. The study of these substrates by crystallography may be hampered by the typically low binding affinities. Additionally, these substrates may move to adopt a different orientation in the active site of CYP199A4 after oxygen binding and activation, and these details would not be revealed by the crystal structures.

3,4-(Methylenedioxy)benzoic acid underwent demethenylation, comparable to a reaction studied with methylenedioxy bridge-containing drug molecules.[175] The presence of formic acid in the turnovers supported the postulated mechanism of demethenylation[175] (Figure 20), where a hemiacetal forms by oxidation of the methylene carbon, followed by ring-opening induced by addition of water. A second addition of water results in loss of a molecule of formic acid and deprotection of the methylene group. The demethenylation reaction proceeds with lower activity than the demethylation of 4-methoxy-, 3,4-dimethoxy- and 3-hydroxy-4-methoxy-benzoic acids and has a lower coupling efficiency. This would be unexpected if hydrogen abstraction was the rate determining step, as the two oxygen atoms would weaken the methylene C−H bonds. The methylene C−H bonds must be located in a less favourable position for hydrogen abstraction by compound I. This may be due to the more constrained nature of the ring structure. 3,4-(Ethylenedioxy)benzoic acid showed much weaker binding but higher product formation than 3,4-(methylenedioxy)benzoic acid. The product was unusual, but the stability of 3,4-(2′-hydroxyethylenedioxy)benzoic acid could be explained by analogy to the stability of cyclic sugars.[181] The inability to determine the enantioselectivity of hemiacetal formation using chiral chromatography may be explained by rapid ring opening and closing, scrambling the stereochemistry of the product (Appendix A.3).

6-Methoxynicotinic acid bound tightly and was turned over with high coupling efficiency, suggesting that replacement of the benzene ring with a pyridine in the substrate could be accommodated in the active site of the enzyme. The reduced product formation and coupling of this substrate relative to 4-methoxybenzoic acid were presumably due to replacement of a carbon with a nitrogen atom. The nitrogen is electron-withdrawing, and thus nicotinic acid substrates could be employed to investigate reaction pathways that proceed via a cation or radical intermediate. For example, the partition between the hydroxylation and desaturation pathways of substrates such as 4-ethylbenzoic acid could be compared to 6-ethylnicotinic acid.

Chapter 4 Heteroatom dealkylation and oxidation by CYP199A4

4.1 Introduction

P450 enzymes catalyse oxygen dealkylation reactions (Chapter 3). They are also capable of metabolising substrates containing heteroatoms such as nitrogen and sulfur (Chapter 1.4.2) and less commonly, halogens (Chapter 1.4.5). Nitrogen-containing drug molecules are important in biological pathways, and cytochrome P450 oxidation of these substrates typically results in nitrogen dealkylation or direct oxidation of the nitrogen atom.[39,186,187] For example, CYP3A4 catalyses two successive N-deethylations of lidocaine (Figure 42, top).[188] In contrast, one of the bridge nitrogens of strychnine[189] and the pyridine of sorafenib[190] are converted to N-oxides (Figure 42, middle and bottom). Other types of N-oxidations are also known, such as the generation of an oxime from the primary amine of Nocardicin C by *Nocardia uniformis*.[191,192] Members of the CYP79 family are also capable of similar transformations, producing oximes that are important defence molecules in the plant *Arabidopsis thaliana*.[193–195]

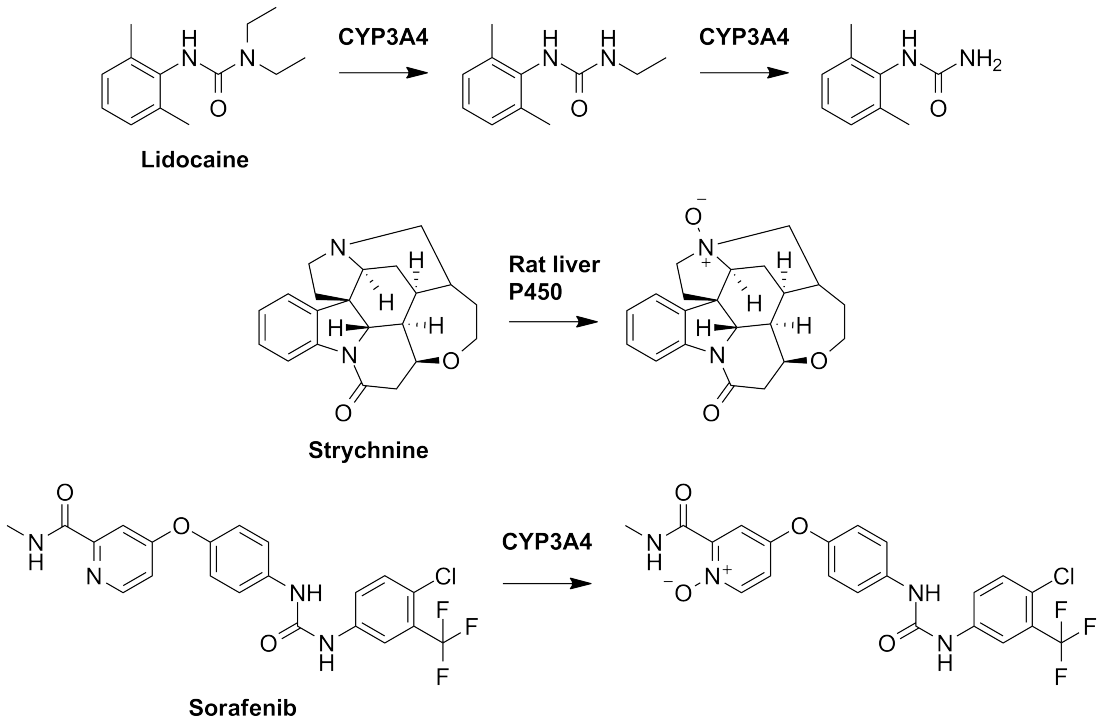

Figure 42. Examples of P450-catalysed nitrogen dealkylation and N-oxidation reactions. Shown are the N-deethylation steps in lidocaine metabolism (top), the metabolism of strychnine in rats to an N-oxidation product (middle) and the N-oxidation of the pyridine moiety of the kidney cancer drug, sorafenib (bottom).

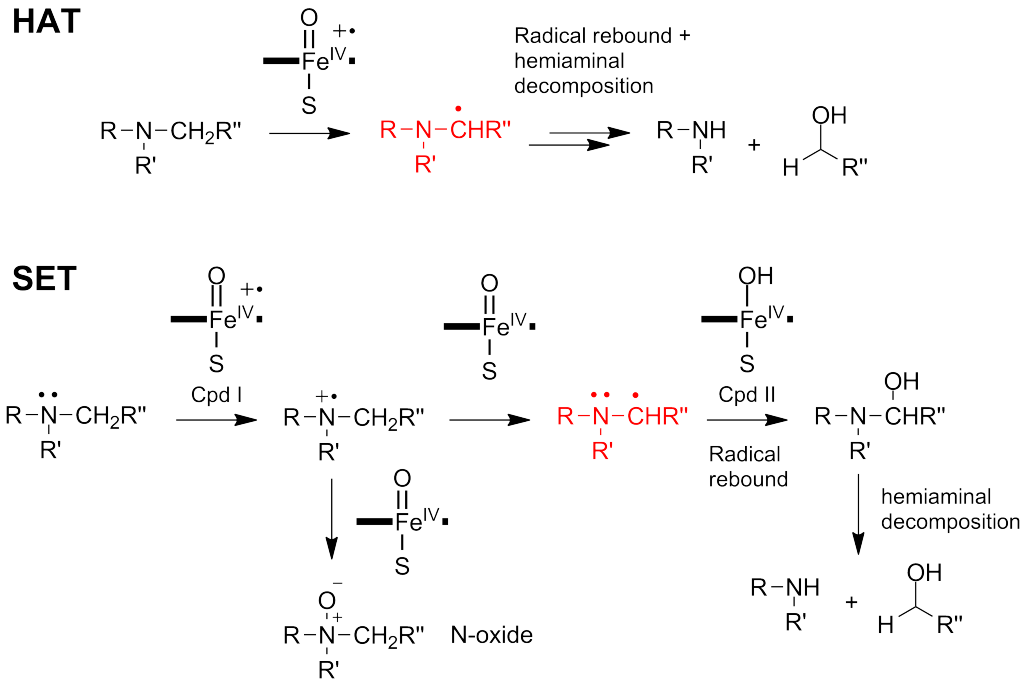

Figure 43. The mechanism of nitrogen dealkylation and oxidation by P450s via different initial steps. Top, hydrogen abstraction (HAT); bottom, single electron transfer (SET). HAT leads to dealkylation, while SET can lead to either N-oxidation or dealkylation. Shown in red is the radical intermediate that is common in both pathways.

Hydroxylation adjacent to a nitrogen can proceed via a hydrogen abstraction (HAT) or single electron transfer (SET) mechanism due to the lower electronegativity of nitrogen relative to oxygen.[39] Hydrogen abstraction can occur in a similar manner to the mechanism of oxygen dealkylation (HAT mechanism, Figure 43). Alternatively, single electron transfer from the nitrogen to Cpd I results in a nitrogen radical cation (SET mechanism, Figure 43). This is followed by proton removal from the carbon adjacent to the nitrogen, and rearrangement of the electrons generates a carbon radical species.[8] Rebound of the Cpd II hydroxy group produces the hydroxylated hemiaminal intermediate, and subsequent decomposition of the hemiaminal results in the dealkylation product. Two distinct mechanisms of direct nitrogen oxidation have been proposed. Single electron transfer followed by direct transfer of the iron-bound oxygen to the nitrogen radical cation leads to nitrogen oxidation (Figure 43). Alternatively, a substrate N−H bond can undergo hydroxylation to a hydroxylamine, in a reaction analogous to normal C−H bond hydroxylation[39,186,187] (Figure 44).

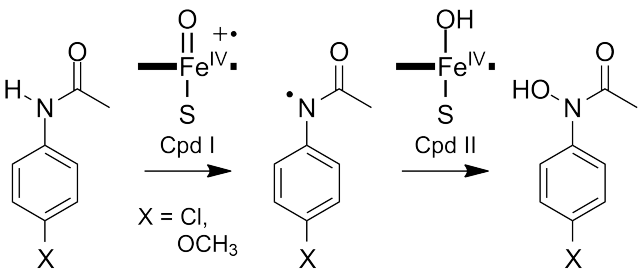

Figure 44. The mechanism of N−H bond oxidation of *para*-substituted acetanilides by P450s.[186,187]

In cases where either one of the N-dealkylation or N-oxidation pathways could occur, the dealkylation reaction tends to be favoured.[39] DFT

calculations of a model system containing Cpd I in complex with trimethylamine have shown that there is a lower activation energy barrier to N-demethylation via a HAT pathway compared to N-oxidation via a direct O transfer mechanism (34.7 kJ mol^{-1} vs 53.3 kJ mol^{-1}).[196]

Examples of nitrogen oxidation are less common than dealkylation, which suggests that N-oxidation reactions are more substrate specific.[39] One such case is the N−H bond hydroxylation of *para*-substituted acetanilides.[186,187] These are substrates where the nitrogen lone pair is delocalised and thus the N−H bond undergoes oxidation (Figure 44). N-oxide products are observed as the metabolites of nitrogen-containing substrates that contain a strained ring system, a nitrogen lone pair and no N−H bonds. Examples include N-oxidation of the pyridine moiety of sorafenib and the strained ring system of strychnine (Figure 42).[189,190]

The reaction outcome (either N-oxidation or dealkylation) can thus be summarised as follows. N-oxidation is more likely to occur when:

The carbons attached to the nitrogen do not possess a C−H bond;

There is a C−H bond but it is not ideally positioned to be abstracted by Cpd I;

There is an N−H bond that can be hydroxylated to a hydroxylamine, or the nitrogen lone pair of electrons is localised.

Both S-oxidation and dealkylation pathways are viable with sulfur-containing substrates. Sulfur dealkylation can occur via initial hydrogen abstraction at the carbon adjacent to the sulfur atom, similar to oxygen dealkylation.[39] The initial step could alternatively be a single electron transfer, which would result in a sulfur radical cation intermediate, similar to the proposed formation of a nitrogen radical cation (Figures 7b, 42). Rearrangement of the electrons followed by radical rebound then results in the hydroxylation product, a hemithioacetal, which is analogous to formation of a hemiacetal or hemiaminal. The hemithioacetal can then decompose into the deprotected thiol and an aldehyde.

Several mechanisms for sulfoxidation have been proposed. Single electron transfer, followed by subsequent transfer of the ferryl oxygen to the sulfur heteroatom would result in a sulfoxide product. Alternatively, the Cpd I oxygen could directly react with the substrate in a single step, two-electron transfer process.[39] Other studies have suggested that the hydroperoxy intermediate, Cpd 0, may also contribute to sulfur oxidation.[76] A DFT model system containing Cpd I in complex with dimethylsulfide demonstrated that the energy barrier for S-oxidation is lower than that of S-dealkylation.[196] This contrasted with results from the same study showing that it is more energetically favourable for trimethylamine to undergo N-demethylation rather than N-oxidation.

Although there are reported examples of sulfur dealkylation (Figure 45),[197–199] sulfur oxidation appears to be more common.[39] This suggests that oxygen transfer to the sulfur is more favourable than C−H abstraction in these cases. The experimental anti-cancer drug OSI-930 undergoes sulfur oxidation by CYP3A4 (Figure 46, top).[200] A cyclopropyl-containing thioether, developed as a radical clock substrate to test for the sulfur radical cation intermediate, has been shown to undergo sulfoxidation when oxidised by a P450 from the fungus *Mortierella isabellina*, with no competing cyclopropyl ring-opening (Figure 46, bottom).[201] It is possible that the cyclopropyl ring-opening reaction is slower than oxygen transfer to the sulfur radical cation; alternatively a sulfur radical cation is not formed and the reaction proceeds via direct two-electron sulfoxidation.

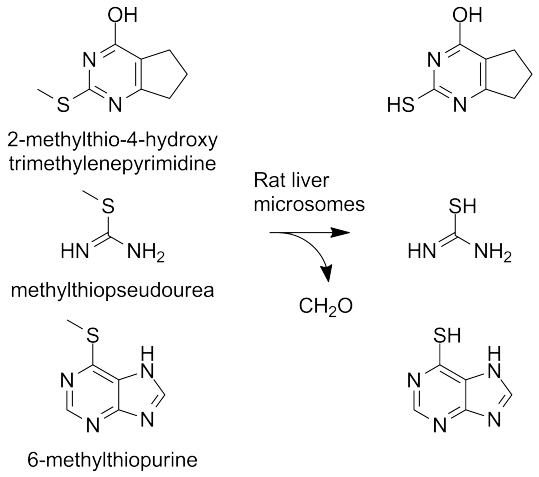

Figure 45. Examples of sulfur dealkylations catalysed by P450s in rat liver microsomes.[197–199]

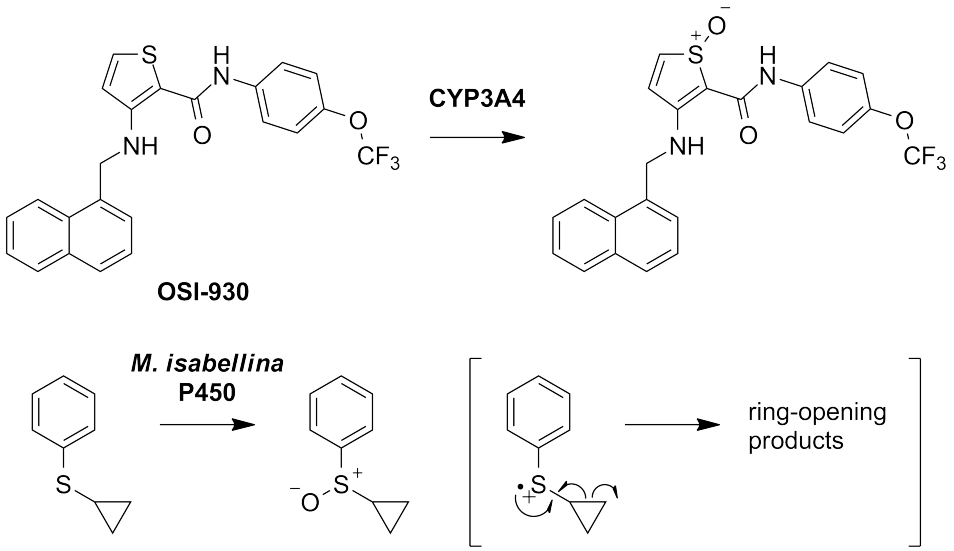

Figure 46. Examples of P450-catalysed sulfur oxidations. Shown are (top) the sulfoxidation of the anti-cancer agent OSI-930; and (bottom) cyclopropyl thioether sulfoxidation by a P450 from *M. isabellina*. In brackets is shown the sulfur radical cation intermediate which would lead to cyclopropyl ring-opening products (not observed).

The turnover activity of CYP199A4 with nitrogen and sulfur substrates has been investigated previously. Preliminary studies have shown that 4-methylaminobenzoic acid undergoes N-demethylation at the *para*-methylamino group, while 4-methylthiobenzoic acid exclusively undergoes oxidation to a sulfoxide.[28] However, other nitrogen and sulfur containing substrates have not been investigated.

P450 catalysed halogen oxidation reactions are rare and have been observed with very specific substrates, such as an aryl iodide compound, where there are no other available sites for oxidation (Chapter 1.4.5, Figure 11b).[120] Direct oxidation of a halogen, which produces a halonium ion, can also lead to dehalogenation and formation of an alcohol alongside a hydroxylated halogen. Oxidation can also occur on a carbon to which a halogen is attached, which can lead to dehalogenation and generation of a carbonyl (Figure 11a).[116,117]

4-Methyl- and 4-ethyl-benzoic acids have been shown previously to undergo hydroxylation (Chapter 1.5). 4-Ethylbenzoic acid also undergoes a more unusual desaturation metabolism with CYP199A4, yielding an alkene where there is no oxygen incorporated into the final product (Chapter 1.4.3). The presence of a halogen at the *para* alkyl substituent could impact the hydroxylation and desaturation pathways.

The binding, turnover kinetics and products of a range of *para*-substituted benzoic acids containing nitrogen, sulfur and halogen containing moieties will be determined (Figure 47). *Para*-substituted halogen-containing benzoic acid substrates will be studied in order to determine if halogen oxidation can be catalysed by CYP199A4. Several haloalkyl-substituted benzoic acids will also be investigated. The heteroatoms present in these substrates could also interact with the heme iron.

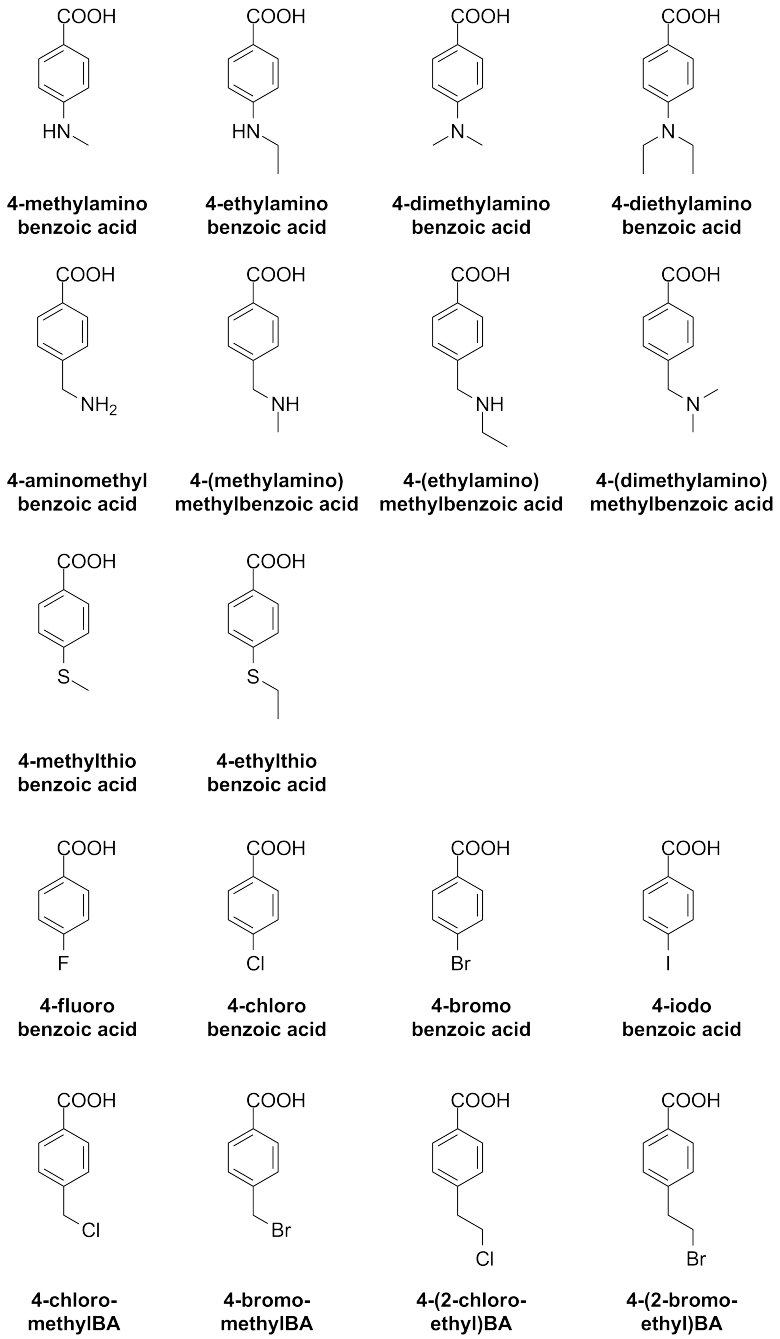

Figure 47. Heteroatom-containing substrates (X = N, S, F, Cl, Br, I) investigated with CYP199A4.

4.2 Results

4.2.1 Binding and activity of nitrogen-containing benzoic acid substrates

The spin state shift induced in CYP199A4 by each nitrogen-containing substrate was first assayed (Chapter 2.3). 4-Methylaminobenzoic acid has been shown to induce a 70 % shift to high spin heme in CYP199A4 (Table 7, Figure 48a).[28] This was lower than that of 4-methoxybenzoic acid ($\geq$ 95 %).

Table 7. Binding and turnover parameters determined for nitrogen-containing benzoic acid substrates investigated with CYP199A4. Shown are spin state shift and dissociation constant analyses (% HS and K_d, Chapter 2.3), NADH oxidation rates (Chapter 2.4), product formation rates (PFR, Chapter 2.5) and coupling efficiency (%). Rates are given as $\mathrm{mol\,(molCYP)^{-1}\,min^{-1}}$. Several oxygen-containing substrates (Chapter 3) are shown for comparison. Benzoic acid is abbreviated to BA; methylbenzoic acid to mBA.

Substrate	HS (%)	K_d (µM)	NADH[a]	PFR[b]	Coupling[c]
4-methoxyBA[28]	$\geq$ 95	0.28 ± 0.01	1340 ± 28	1219 ± 120	91 ± 2
4-ethoxyBA	$\geq$ 95	0.17 ± 0.02	527 ± 10	527 ± 38	100 ± 8
4-methylaminoBA[28]	70	1.6 ± 0.07	923 ± 200	669 ± 15	64 ± 2
4-ethylaminoBA[d]	40	0.92 ± 0.02	197 ± 8	112 ± 10	57 ± 3
4-dimethylaminoBA[d]	50	20 ± 2	284 ± 4	239 ± 16	84 ± 4
4-diethylaminoBA[d]	80	11 ± 1	332 ± 17	298 ± 8	90 ± 4
4-aminomethylBA[28]	20	11500 ± 400	13 ± 1	0.3 ± 0.1	2.0 ± 0.1
4-(methylamino)mBA	419 nm[e]	n.d.[f]	24 ± 3	1.3 ± 0.1	5.6 ± 0.8
4-(ethylamino)mBA	< 5	n.d.[f]	15 ± 1	0.4 ± 0.1	2.9 ± 0.1
4-(dimethylamino)mBA	10	n.d.[f]	24 ± 2	2.9 ± 0.2	12 ± 1

[a]Rate of turnover of NADH during the reaction. [b]Product formation rate. [c]% of NADH consumed that led to formation of substrate metabolite. [d]These turnovers contained a product that must have resulted from two full P450 catalytic cycles. This was taken into account during determination of the total coupling efficiency and product formation. [e]A red shift was observed, however the difference spectrum was type I (Figure 48d). [f]Could not be determined accurately as a minimal change in absorbance on addition of substrate was observed.

4-Ethylaminobenzoic acid displayed a shift to only 40 % high spin heme with CYP199A4 (Figure 48b), lower than 4-ethoxy- and 4-methylamino-benzoic acids which shifted the spin to $\geq$ 95 % and 70 % high spin respectively. With 4-dimethylaminobenzoic acid, a 50 % shift was observed (Figure 48c), smaller than 4-methylaminobenzoic acid. 4-Diethylaminobenzoic acid shifted the high spin content of CYP199A4 to 80 % (Appendix B.1), a larger shift than the methylamino, dimethylamino and ethylamino substrates.

4-Aminomethylbenzoic acid, containing a terminal amino group, displayed only a 20 % spin state shift with the enzyme (Appendix B.1).[28] The secondary amine, 4-(methylamino)methylbenzoic acid, caused the spin state of CYP199A4 to red-shift from 418 to 419 nm (Table 7), which suggested that the nitrogen lone pair may be

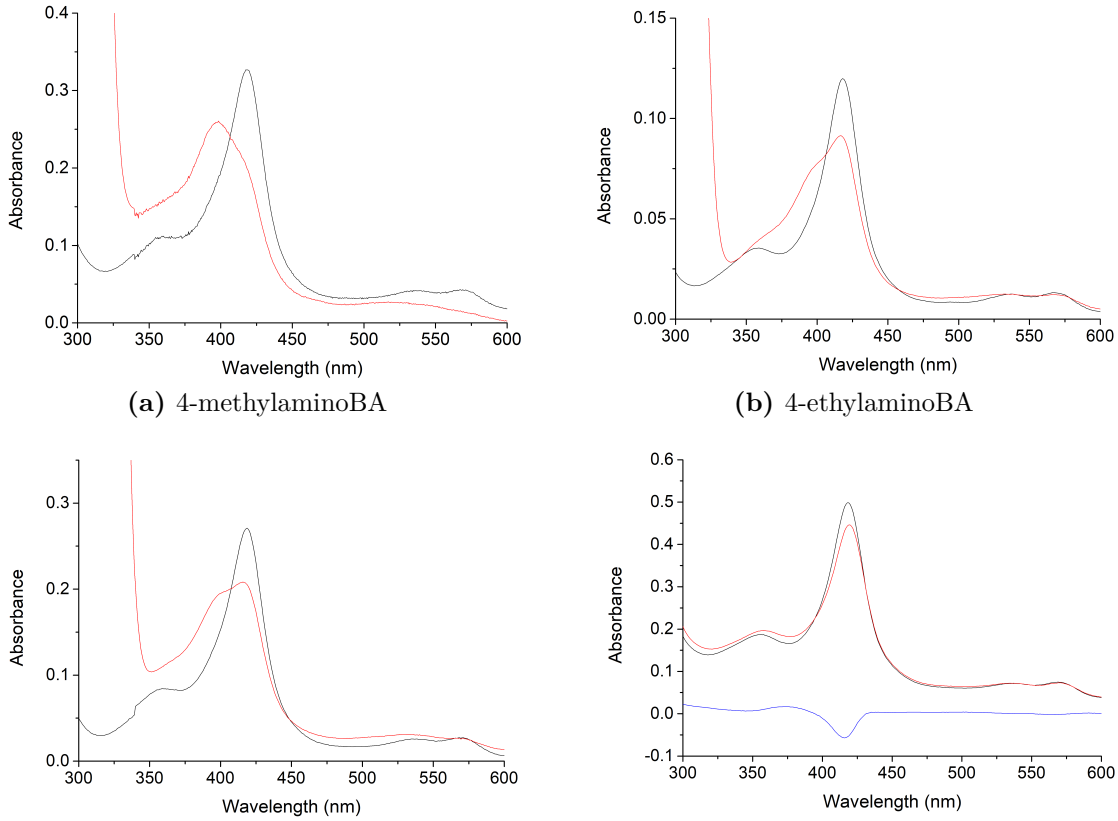

(a) 4-methylaminoBA **(b)** 4-ethylaminoBA

(c) 4-dimethylaminoBA **(d)** 4-(methylamino)methylBA

Figure 48. Spin state shifts of selected nitrogen-containing substrates investigated with CYP199A4. Black shows CYP199A4 in its resting state, red shows the maximum absorbance shift obtained upon addition of substrate, and in (d), blue shows the difference spectrum observed, which was indicative of a type I shift.

interacting either directly or indirectly with the heme iron.[202] However, the resulting difference spectrum was more indicative of a type I binding pattern (Figure 48d). Both 4-(ethylamino)methyl- and 4-(dimethylamino)methyl-benzoic acids induced very small type I spin state shifts (< 5 % and 10 % respectively, Appendix B.1).

The dissociation constant was then determined for each substrate with CYP199A4, to gain insight into how tightly each was binding in the active site (Chapter 2.3). 4-Methylaminobenzoic acid bound with lower affinity to CYP199A4 than 4-methoxybenzoic acid (1.6 µM vs 0.28 µM), in line with the reduced spin state shift of the former (Figure 49a).[28] 4-Ethylaminobenzoic acid bound more tightly to CYP199A4 (0.92 µM) than 4-methylaminobenzoic acid despite its lower spin state shift (Figure 49b). The binding affinities of CYP199A4 to the tertiary amine substrates, 4-dimethylamino- and 4-diethylamino-benzoic acids, were an order of magnitude weaker than their secondary amine equivalents (4-Dimethylamino-, 20 µM; 4-diethylamino-, 11 µM, Figures 49c and d respectively).

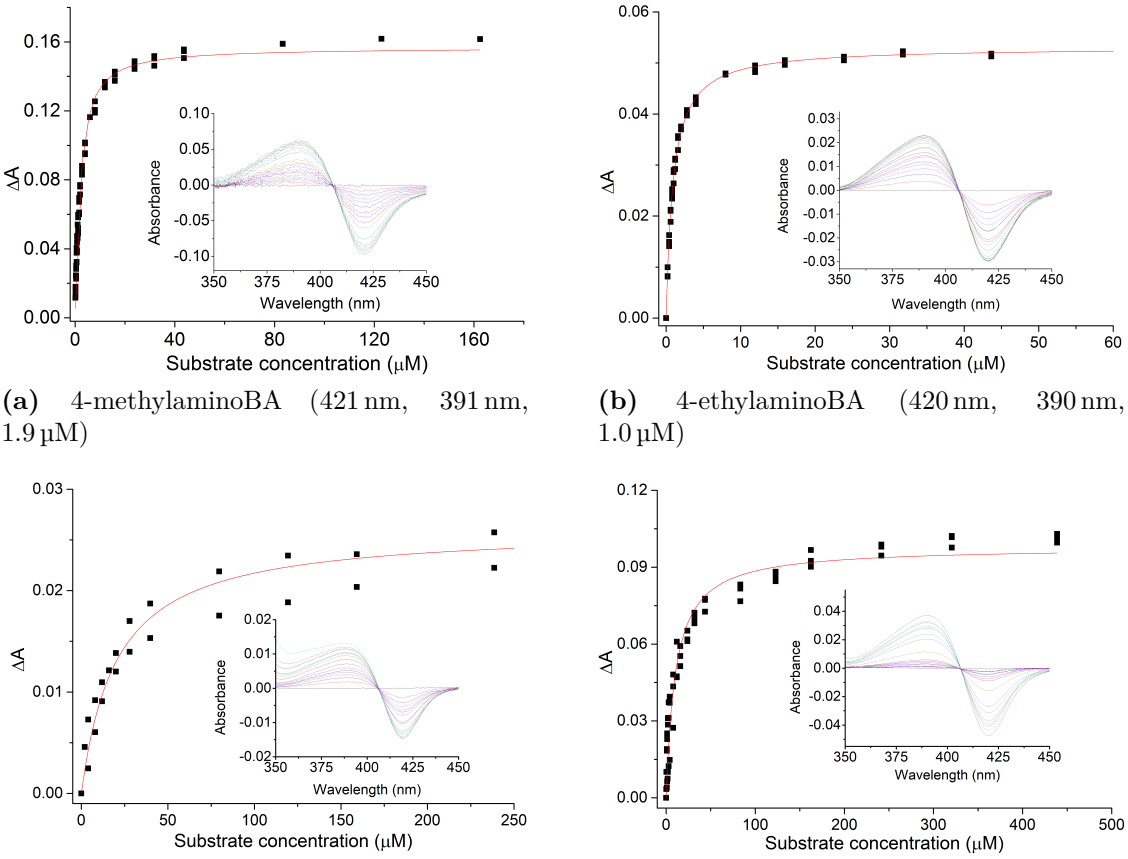

(a) 4-methylaminoBA (421 nm, 391 nm, 1.9 µM)

(b) 4-ethylaminoBA (420 nm, 390 nm, 1.0 µM)

(c) 4-dimethylaminoBA (419 nm, 389 nm, 1.5 µM)

(d) 4-diethylaminoBA (420 nm, 390 nm, 1.5 µM)

Figure 49. Dissociation constant determination of selected nitrogen-containing substrates investigated with CYP199A4. The inset image shows the UV-Vis response to successive addition of substrate aliquots. Shown in brackets are the wavelengths of the trough and peak, and the enzyme concentration used for dissociation constant analysis (trough, peak, µM-P450).

The binding of 4-aminomethylbenzoic acid to CYP199A4 was more than four orders of magnitude weaker than 4-methylaminobenzoic acid (11,500 µM vs 0.92 µM). A dissociation constant could not be determined for 4-(methylamino)methyl-, 4-(ethylamino)methyl- and 4-(dimethylamino)-methylbenzoic acids due to the low absorbance change on addition of substrate aliquots, suggestive of low binding affinity (Table 7). This indicated that moving the amino group to the β-position of the *para* substituent interfered with heme iron water displacement or the observable spin state. Alternatively it could be detrimental to substrate binding.

Turnovers of each substrate by CYP199A4 were undertaken and analysed for metabolite formation using HPLC (Chapter 2.1). Previously, 4-methylaminobenzoic acid was shown to be oxidatively demethylated by CYP199A4 to 4-aminobenzoic acid[28] (Appendix B.3). In summary the NADH oxidation rate and the coupling efficiency of CYP199A4 with 4-methylaminobenzoic acid were lower than that of 4-methoxybenzoic acid (Table 7, PFR, 923 min^{-1} vs 1340 min^{-1}; coupling efficiency, 64 % vs 91 %). The resulting product formation rate was approximately half that of 4-methoxybenzoic acid

($669\,\mathrm{min}^{-1}$ vs $1219\,\mathrm{min}^{-1}$).

4-Ethylaminobenzoic acid, when turned over by CYP199A4, formed two products (Figure 50). These were identified as the expected deethylation product, 4-aminobenzoic acid (47 % of total product), and an unusual metabolite, 4-acetamidobenzoic acid (53 %). Both were characterised by HPLC coelution using authentic samples, and 4-acetamidobenzoic acid was also confirmed after isolation using NMR spectroscopy (Appendix A.5). The acetamido product was hypothesised to have arisen from hydroxylation of 4-ethylaminobenzoic acid to a hemiaminal, followed by a second oxidative cycle by CYP199A4 to form the amide. The NADH oxidation rate by CYP199A4 with 4-ethylaminobenzoic acid was five-fold lower than 4-methylaminobenzoic acid ($197\,\mathrm{min}^{-1}$ vs $923\,\mathrm{min}^{-1}$) and the coupling efficiency was reduced (57 % vs 64 %). The product formation rate was also slower ($112\,\mathrm{min}^{-1}$ vs $669\,\mathrm{min}^{-1}$).

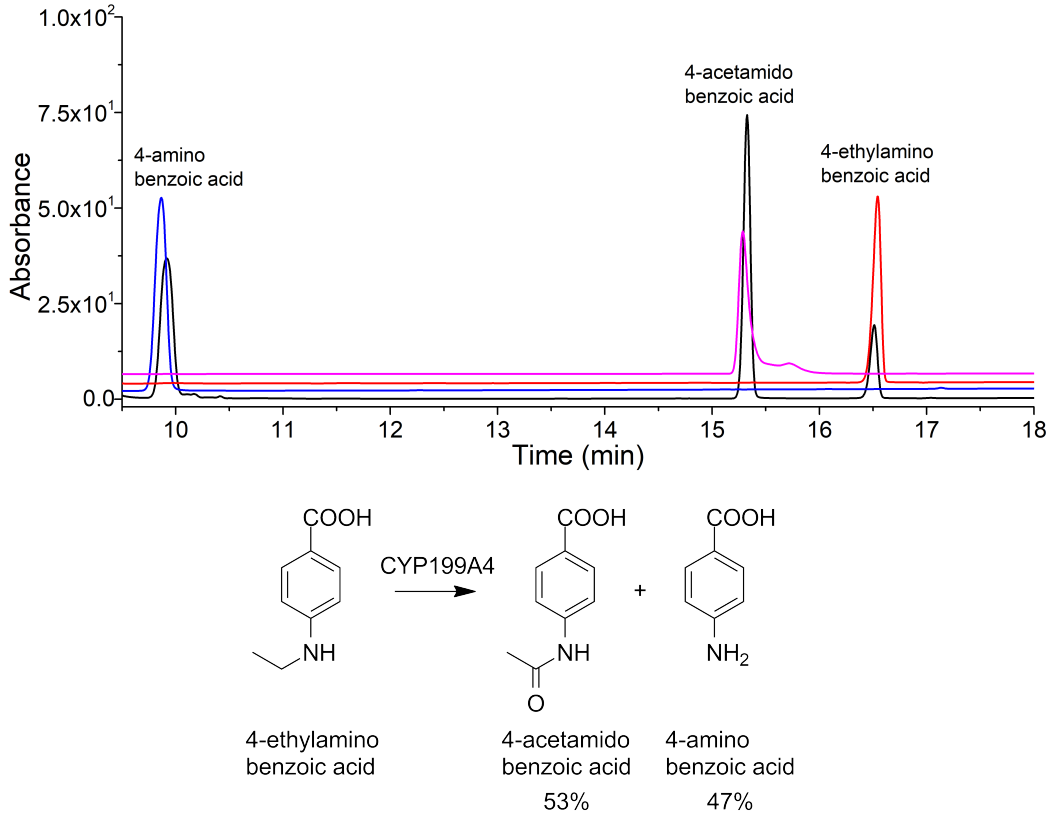

Figure 50. HPLC analysis of 4-ethylaminobenzoic acid turnover with CYP199A4. **Black**, *in vitro* turnover; blue, 4-aminobenzoic acid control, RT = 9.8 min; red, substrate control, RT = 16.5 min; pink, 4-acetamidobenzoic acid control, RT = 15.3 min. The gradient employed was 0-50 % of H_2O:ACN and it was monitored at 254 nm.

Two products were observed in the HPLC analysis of the CYP199A4 turnover of 4-dimethylaminobenzoic acid, both resulting from N-demethylation steps (Figure 51). These were 4-methylaminobenzoic acid (8 % of total product) and 4-aminobenzoic acid (92 %). The 4-aminobenzoic acid major product would have formed from two successive CYP199A4-catalysed N-dealkylations (Table 7). The NADH oxidation ac-

tivity of CYP199A4 with 4-dimethylaminobenzoic acid was significantly lower than with 4-methylaminobenzoic acid (284 min^{-1} vs 923 min^{-1}). The coupling efficiency of the NADH reducing equivalents towards substrate oxidation was higher than with 4-methylaminobenzoic acid (84 % vs 64 %), and the product formation rate was 239 min^{-1} (vs 669 min^{-1}). No products resulting from N-oxidation could be detected.

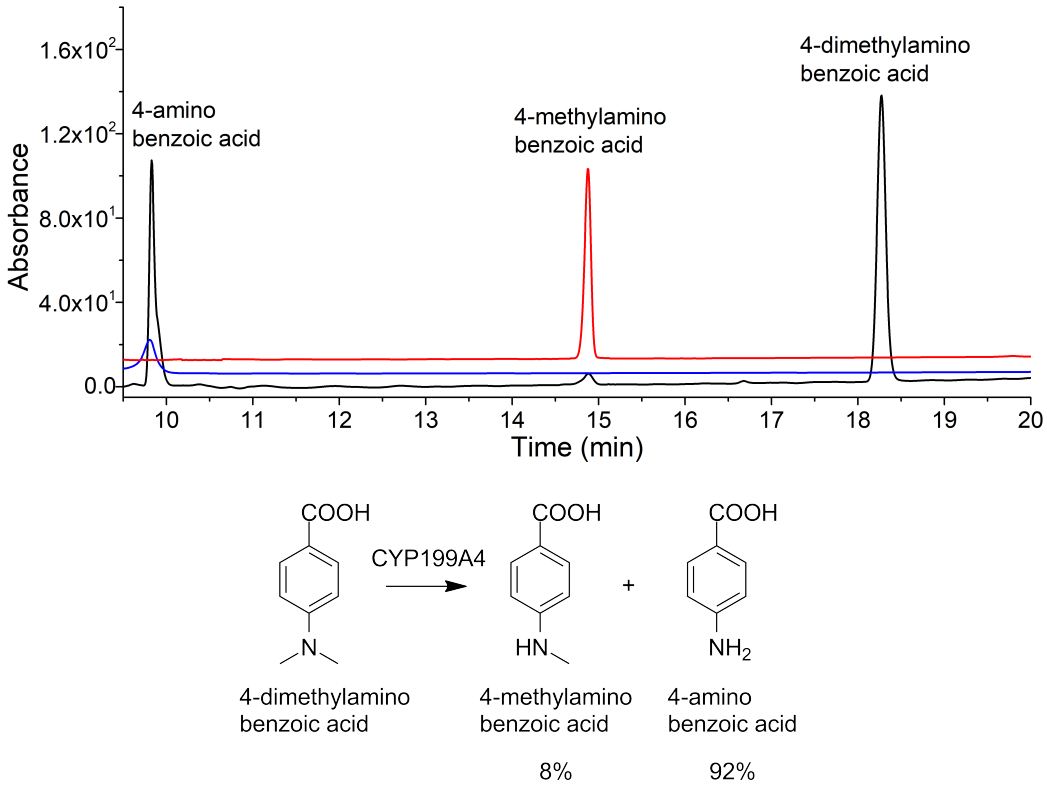

Figure 51. HPLC analysis of the turnover of 4-dimethylaminobenzoic acid with CYP199A4. **Black**, *in vitro* turnover; blue, 4-aminobenzoic acid control, RT = 9.8 min; red, 4-methylaminobenzoic acid control, RT = 14.9 min. A 0-50 % gradient of H_2O:ACN was used. The chromatogram was monitored at 254 nm.

In turnovers of 4-diethylaminobenzoic acid, the same two products were observed as in the turnovers of 4-ethylaminobenzoic acid (Figure 52). The double dealkylation metabolite, 4-aminobenzoic acid, constituted 80 % of the total turnover products and 4-acetamidobenzoic acid accounted for the remaining 20 %. There was little evidence of 4-ethylaminobenzoic acid, via a single deethylation, or a product containing both ethyl and acetamido groups. The NADH oxidation rate of CYP199A4 with 4-diethylaminobenzoic acid was faster than 4-ethylaminobenzoic acid (197 min^{-1} vs 332 min^{-1}). The total coupling efficiency and product formation rate were both higher than 4-ethylaminobenzoic acid (90 %, 298 min^{-1}; vs 57 %, 112 min^{-1}).

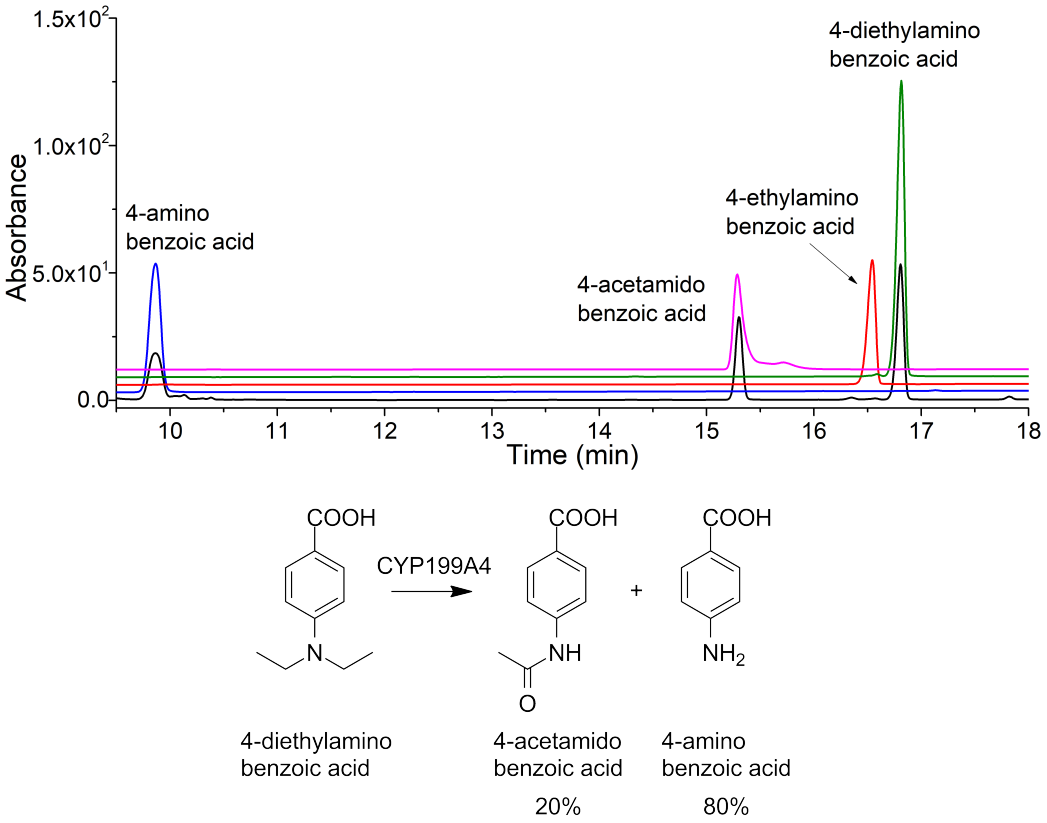

Figure 52. HPLC analysis of 4-diethylaminobenzoic acid turnover with CYP199A4. **Black**, *in vitro* turnover; blue, 4-aminomethylbenzoic acid control, RT = 9.8 min; red, 4-ethylaminobenzoic acid control, RT = 16.5 min; green, substrate control, RT = 16.8 min; pink, 4-acetamidobenzoic acid control, RT = 15.3 min. A 0-50 % gradient of H_2O:ACN was used and the chromatogram was monitored at 254 nm.

In the turnovers of all nitrogen substrates, the total uncoupling due to hydrogen peroxide was < 5 %. This indicated that the majority of NADH equivalents, which were not used for product formation, were likely being channelled into the oxidase uncoupling pathway, with formation of water as a by-product (Figure 1, Chapter 2.7).

The spin state shift induced in CYP199A4 by these substrates (4-ethylamino-, 4-dimethylamino- and 4-diethylamino-benzoic acids) correlated with the NADH oxidation and product formation activity observed. Since substrate binding displaces the distal water ligand bound to the heme iron (measurement of % HS), which facilitates the first electron transfer step in the P450 catalytic cycle, the relative rates of NADH oxidation and product formation suggested that these reactions are gated by substrate binding.[203,204]

The NADH oxidation rate of CYP199A4 with substrates containing β-amino substituents (4-aminomethyl-, 4-(methylamino)methyl-, 4-(dimethylamino)methyl- and 4-(ethylamino)methyl-benzoic acids) were only slightly higher than the passive leak rate oxidation of NADH (Table 7, leak rate $\approx 9\,\text{min}^{-1}$). Analysis of the enzyme turnovers in each case indicated the formation of small amounts of terephthalic acid and 4-formylbenzoic acid (Figure 54, Appendix B.3). These were identified using coelution

experiments with authentic standards. With each substrate, the product formation rate and coupling efficiency were very low ($< 3\,\mathrm{min}^{-1}$, < 12 %, Table 7). The low levels of high spin heme correlated with the low NADH oxidation rate by the enzyme, and suggested that these secondary and tertiary aminomethylbenzoic acid substrates are not oxidised effectively by CYP199A4.

In the turnovers of 4-aminomethyl- and 4-(methylamino)methyl-benzoic acids there were additional peaks in low concentration at 14.2 min, 16.4 min and 17.2 min that could not be identified as obvious P450 oxidation products. As such, these peaks were not included in the calculation of coupling efficiency of the turnovers. There was no formation of 4-aminomethylbenzoic acid, expected from N-dealkylation, in any of the turnovers. The 4-formylbenzoic acid would have arisen from oxidation at the benzylic methylene carbon, followed by rearrangement of the unstable hemiacetal. Further oxidation to terephthalic acid may have occurred either by the P450 or by air oxidation (Figure 53). Further investigation of these substrates is required to fully elucidate the identity and amount of the products which arise from P450 activity. However it is clear that these are not as effective substrates with CYP199A4 as their methylaminobenzoic acid equivalents.

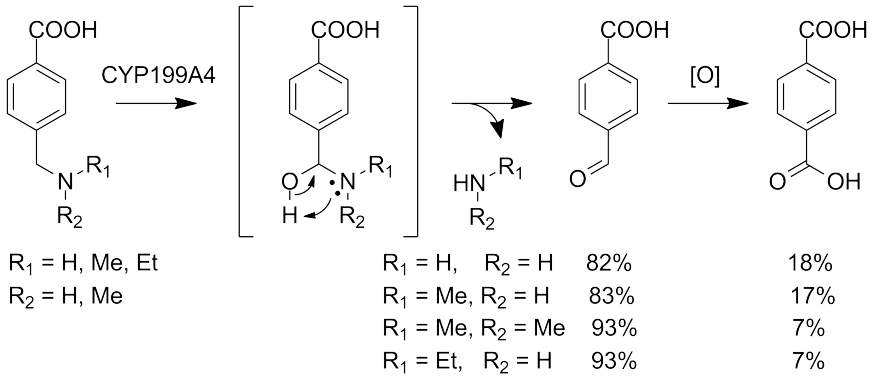

Figure 53. Mechanism of 4-formylbenzoic acid and terephthalic acid formation by CYP199A4. The 4-formylbenzoic acid oxidation step may either be P450-catalysed or due to air oxidation.

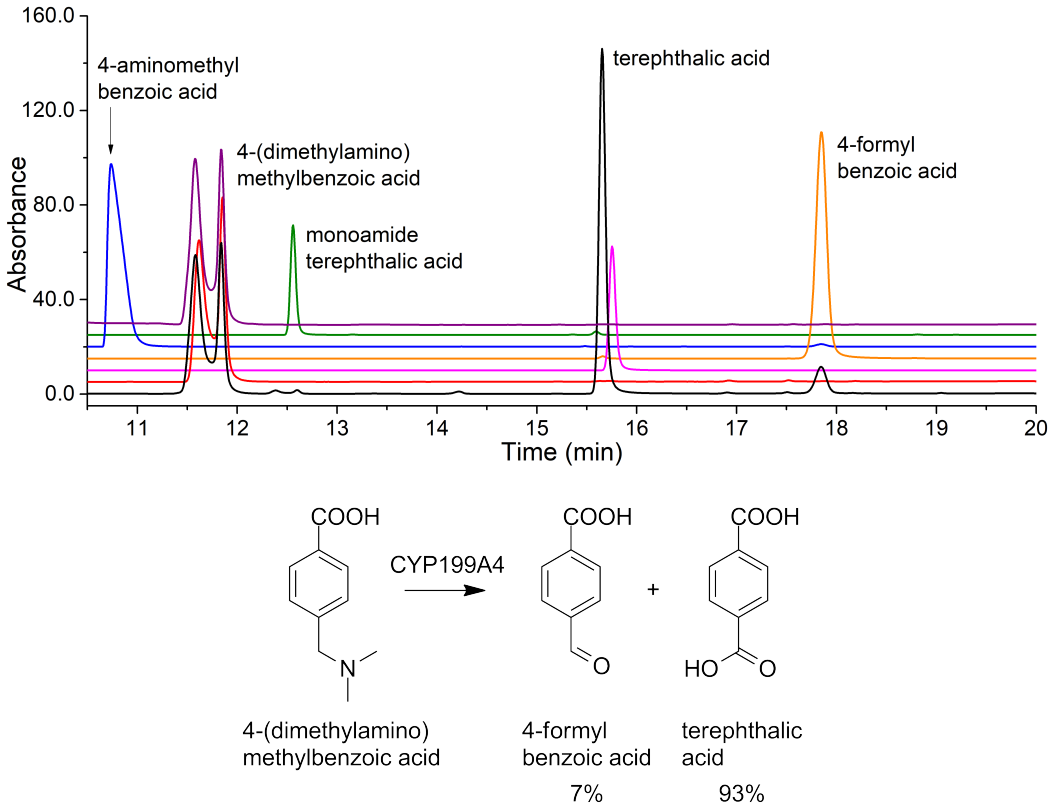

Figure 54. HPLC analysis of 4-(dimethylamino)methylbenzoic acid turnover with CYP199A4. **Black**, *in vitro* turnover; red, substrate control, RT = 11.6 min and 11.9 min double peak; pink, terephthalic acid control, RT = 15.8 min; orange, 4-formylbenzoic acid control, RT = 17.8 min; blue, 4-aminobenzoic acid control, 10.8 min; green, monoamide terephthalic acid control, RT = 12.6 min; purple, no P450 control reaction. The gradient used was 0-50 % H_2O:ACN. The chromatogram was monitored at 254 nm. HPLC analyses of the other β-amino substrates are presented in Appendix B.3.

4.2.2 Crystal structure of 4-methylaminobenzoic acid-bound CYP199A4

4-Methylaminobenzoic acid and related substrates underwent efficient N-dealkylation with CYP199A4. In order to gain insight into how the nitrogen *para*-substituents are orientated in the active site relative to the methoxy group of 4-methoxybenzoic acid, the substrate-bound forms of CYP199A4 were studied using crystallography. Crystals of CYP199A4 containing 4-methylaminobenzoic acid (1 mM) were obtained in 3 weeks from a 500 µL reservoir solution containing 0.2 M magnesium acetate tetrahydrate, 23 % w/v PEG-3,350 and 0.1 M Bis-Tris pH 5.5. X-ray diffraction data were obtained at 100 K on the MX1 beamline at the Australian Synchrotron[147,148] and the structure was solved at 2.63 Å resolution. Models were developed for each structure using WinCoot[144] (Chapter 2.10), and the data were then deposited in the wwPDB[157,158] (www.wwpdb.org) with accession code 5U6W (Table 8).

Table 8. Structural refinement and data collection statistics for 4-methylaminobenzoic acid. 4-Methoxybenzoic acid (4DO1) is shown for comparison. Benzoic acid is shortened to BA.

	4-methoxyBA[131]	4-methylaminoBA
PDB code	4DO1	5U6W
X-ray wavelength (Å)	0.9796	0.9537
Unit cell (a/b/c)	107.0/143.5/172.8	44.4/51.2/78.9
($\alpha/\beta/\gamma$)	90/90/90	90/92.0/90
Space group	$P2_12_12_1$	$P12_11$
Molecules per unit cell	4	1
Resolution range[a]	50 - 2.0	44.34 - 2.63
	(2.03 - 2.00)	(2.76 - 2.63)
$<I/\sigma(I)>$[a]	28.5 (5.2)	6.9 (1.8)
Unique reflections	179187	10517
Completeness[a]	100.0 (100.0)	98.6 (89.4)
Multiplicity[a]	7.1 (6.1)	7.4 (7.0)
R_{merge}[a,b] (%)	9.8 (31.9)	25.0 (88.6)
R_{pim}[a,b] (%)	N/A[c]	9.9 (35.7)
$CC_{1/2}$[a,d] (%)	N/A[c]	99.0 (77.9)
R_{work}	0.154	0.224
R_{free}[e]	0.189	0.261
Ramachandran plot[f]		
Most favoured	98.5	97.7
Allowed	1.5	2.3

[a]Highest resolution shell is shown in parentheses where applicable. [b]all I+ and I-. [c]Not reported in previous work. [d]Half-correlation coefficient.[182,183] [e]5 % of total reflections, randomly selected. [f]% of all amino acid residues.[184] There were no Ramachandran outliers.

The 4-dimethyl- and 4-diethyl-aminobenzoic acid substrates with CYP199A4 were not able to be crystallised when conditions similar to those above were employed. Small crystals of CYP199A4 complexed with 4-ethylaminobenzoic acid were obtained, and a data set was collected. However, the resulting model displayed very high R factors which were not able to be reduced and was not considered fit for analysis (R_{work}, $R_{free} > 0.4$; for further details and data collection statistics refer to Appendix B.6). Further optimisation of the conditions are required to solve these structures of these substrate-CYP199A4 complexes.

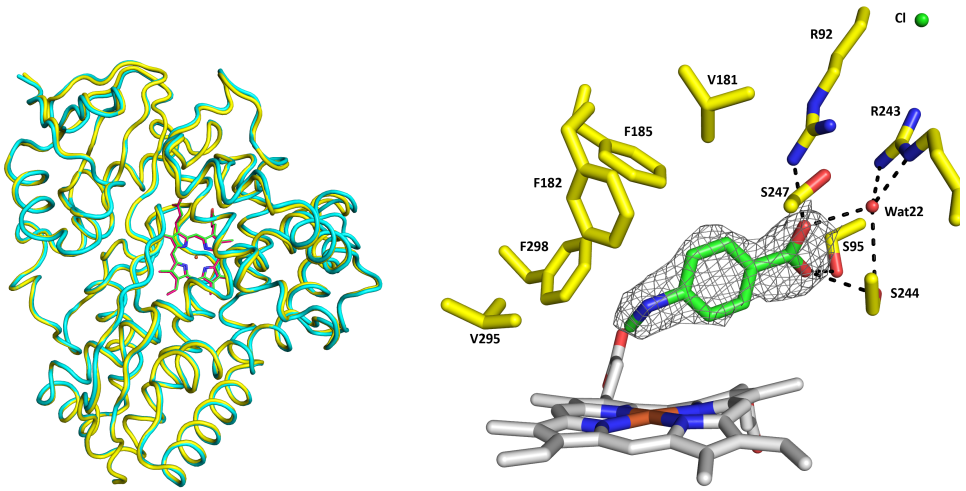

Figure 55. Crystal structure of 4-methylaminobenzoic acid-bound CYP199A4 solved at 2.63 Å resolution. Shown are (a) overlay of the three-dimensional fold (yellow tube and magenta heme, rmsd = 0.539 Å over 392 of 393 residues) with structure of 4-methoxybenzoic acid (cyan tube and green heme) and (b) feature-enhanced $2mF_o$-DF_c map[155] of 4-methylaminobenzoic acid-bound CYP199A4. The electron density map for 4-methylaminobenzoic acid is shown contoured as a grey mesh at the 1 σ level.

Compared to the crystal structure of the 4-methoxybenzoic acid-CYP199A4 complex, which crystallised in the $P2_12_12_1$ space group with 4 identical subunits,[131] the 4-methylaminobenzoic acid-bound CYP199A4 contained a single molecule in the asymmetric unit, and crystallised with lower cell symmetry ($P12_11$), similar to that observed in Chapter 3 with 4-ethoxybenzoic acid. The electron density in the active site was modelled as 4-methylaminobenzoic acid (Figure 55).

The benzoic acid moiety of 4-methylaminobenzoic acid and 4-methoxybenzoic acid were bound in comparable orientations, as were the chloride ligand and carboxylate bridging water molecule. In both structures, the active site residues were also found in similar positions. However, the 4-methylamino moiety of the substrate is orientated differently to that of the methoxy group of 4-methoxybenzoic acid (Figure 56). The methylamino moiety is rotated relative to the benzoic acid, causing the C_{09}-C_{04}-X-C_α dihedral angle to be much larger than the equivalent dihedral of 4-methoxybenzoic acid (50.0° vs 2.1°). As such the nitrogen atom is significantly closer to the heme than

the oxygen in 4-methoxybenzoic acid (4.2 Å vs 5.2 Å). However, the distance from the methyl group to the heme iron is the same in both structures (4.1 Å, Table 9).

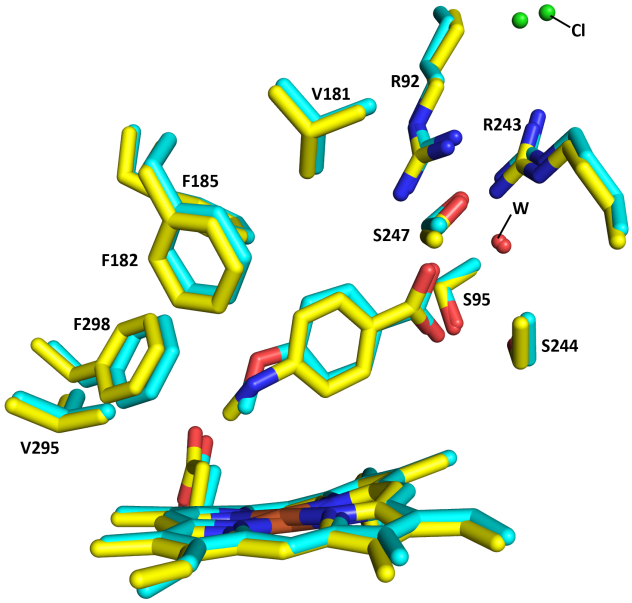

Figure 56. Comparison of the active site of 4-methylaminobenzoic acid-CYP199A4 (yellow) and 4-methoxybenzoic acid (cyan). Water molecules are shown as red spheres and the chloride ligands are green spheres. Those that are labelled (Cl, W) correspond to the 4-methylaminobenzoic acid structure.

Table 9. Distances and angles between structural features of 4-methylaminobenzoic acid-bound CYP199A4. The ferryl Cpd I oxygen was modelled 1.62 Å from the heme iron.[160,161] X refers to the O or N heteroatom.

Distance (Å)	4-methoxyBA	4-methylaminoBA
C_α - Fe	4.1	4.1
C_α - **O**=Fe	2.7	3.1
X - Fe	(X = O) 5.2	(X = N) 4.2
X - **O**=Fe	3.6	3.0
C_α - closest F298 C	3.8	3.5
Angle (°)		
C_{04}-X-C_α	118.6	120.3
Dihedral C_{09}-C_{04}-X-C_α	2.1	50.0
Fe=O-C_α	140.7	133.0
Fe=O-X	158.3	158.4

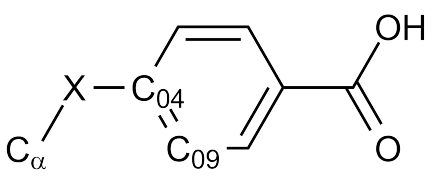

X = O or NH

The angle of the methylamino carbon to the O=Fe was determined to be lower than that of 4-methoxybenzoic acid (4-methoxy, 140.7°; 4-methylamino, 133.0°; Fe=O-C_α, Table 9). Despite the close approach of the N atom of 4-methylaminobenzoic acid to the ferryl oxygen (4-methylamino, 3.0 Å; 4-methoxy, 3.6 Å; X-Fe, Table 9), there was no detectable N-oxidation product in the turnovers, nor was there any evidence from the spin state shift and dissociation constant analyses that the nitrogen atom was interacting with the heme iron.

4.2.3 Binding and turnover activity of sulfur-containing benzoic acid substrates

The turnover activity of CYP199A4 with 4-methylthiobenzoic acid has been previously characterised.[28] The reaction product, 4-methylsulfinylbenzoic acid, was formed by oxidation of the sulfur atom. To compare and contrast this activity with the ethoxy- and ethylamino- deethylation activities of the O and N equivalents, 4-ethylthiobenzoic acid was investigated.

The spin state shift induced by 4-ethylthiobenzoic acid was significantly lower than 4-methylthiobenzoic acid (20 % vs 70 %, Table 10, Figure 57a,c), although the binding affinity of CYP199A4 with 4-ethylthiobenzoic acid was higher (0.99 µM vs 2.3 µM, Figure 57b,d).

Table 10. Binding and turnover parameters determined for the sulfur-containing benzoic acid substrates with CYP199A4. The equivalent oxygen containing substrates are shown for comparison (Chapter 3). Benzoic acid is abbreviated to BA. Rates are given as mol (molCYP)$^{-1}$ min^{-1}.

Substrate	HS (%)	K_d (µM)	NADH[a]	PFR[b]	Coupling[c]
4-methoxyBA[28]	$\geq$ 95	0.28 ± 0.01	1340 ± 28	1220 ± 120	91 ± 2
4-ethoxyBA	$\geq$ 95	0.17 ± 0.02	527 ± 10	527 ± 38	100 ± 8
4-methylthioBA[28]	70	2.3 ± 0.32	1430 ± 178	1180 ± 133	83 ± 3
4-ethylthioBA	20	0.99 ± 0.05	132 ± 6	64 ± 6	50 ± 3

[a]Rate of turnover of NADH during the reaction. [b]Product formation rate. [c]% of NADH consumed that led to formation of substrate metabolite.

The NADH oxidation rate for the CYP199A4 turnover of 4-ethylthiobenzoic acid was an order of magnitude lower than 4-methylthiobenzoic acid (132 min^{-1} vs 1430 min^{-1}, Table 10). This was consistent with the reduced spin state shift. HPLC analysis was performed on the *in vitro* CYP199A4 turnovers of 4-ethylthiobenzoic acid (Figure 58). The reaction product was initially assigned as 4-ethylsulfinylbenzoic acid by comparing the HPLC retention time (RT = 6.7 min) to that of 4-methylsulfinylbenzoic acid product generated in the 4-methylthiobenzoic acid turnover (RT = 5.6 min, Appendix B.3). A very small peak which coeluted with 4-mercaptobenzoic acid was also observed in the HPLC, however this peak was also

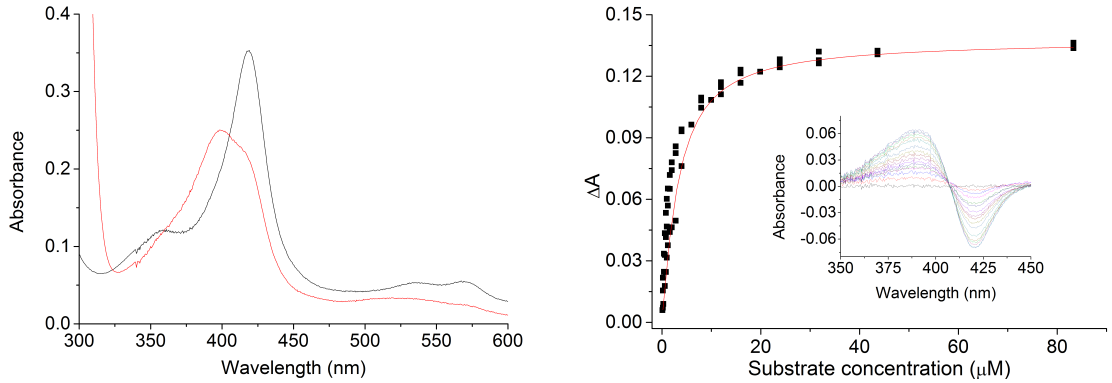

(a) 4-methylthioBA (420 nm, 390 nm, 1.6 μM)[28]

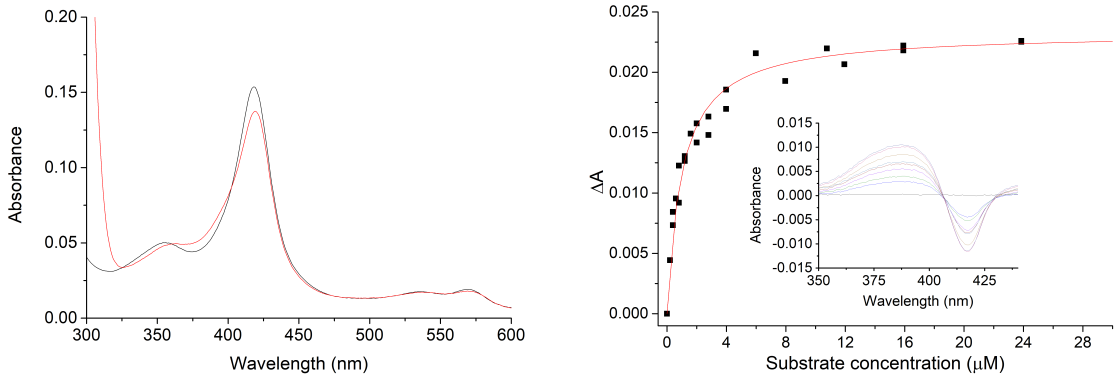

(b) 4-ethylthioBA (417 nm, 388 nm, 1.5 μM)

Figure 57. Spin state shift and dissociation constant analysis of 4-methylthio- and 4-ethylthio-benzoic acids with CYP199A4. Left column: spin state shift analysis; black shows CYP199A4 in its resting state, red shows the maximum absorbance shift obtained upon addition of substrate. Right column: dissociation constant determination; the inset image shows the UV-Vis response to successive addition of substrate aliquots. Shown in brackets are the wavelengths of the trough and peak, and the enzyme concentration used for dissociation constant analysis (trough, peak, μM-P450).

present in control experiments that contained no P450 enzyme. The same was found to be true with 4-methylthiobenzoic acid (Appendix B.3), indicating that CYP199A4 was not catalysing the S-dealkylation reaction. The coupling efficiency of the 4-ethylthiobenzoic acid turnover was lower than 4-methylthiobenzoic acid (50 % vs 83 %), and the product formation rate was more than an order of magnitude reduced (64 min^{-1} vs 1174 min^{-1}). In the turnovers of both 4-methylthio and 4-ethylthiobenzoic acids, the uncoupling due to hydrogen peroxide was < 5 %, which suggested the oxidase pathway as the source of unproductive coupling of NADH (Figure 1, Chapter 2.7).

The sulfoxides which are generated in the turnovers of both 4-methyl- and 4-ethylthiobenzoic acids are chiral. Therefore, chiral HPLC was used in an attempt to determine the enantiospecificity of each turnover. The methyl esters of the racemic alkylsulfinylbenzoic acids and those generated by the CYP199A4 turnovers were synthesised for analysis by chiral HPLC at the laboratory of James J. De Voss, University of Queensland (Chapter 2.1). The enantiomers in the racemic mixture of the methylsulfinyl metabolite could not be resolved, preventing further analysis. The ethylsulfinyl

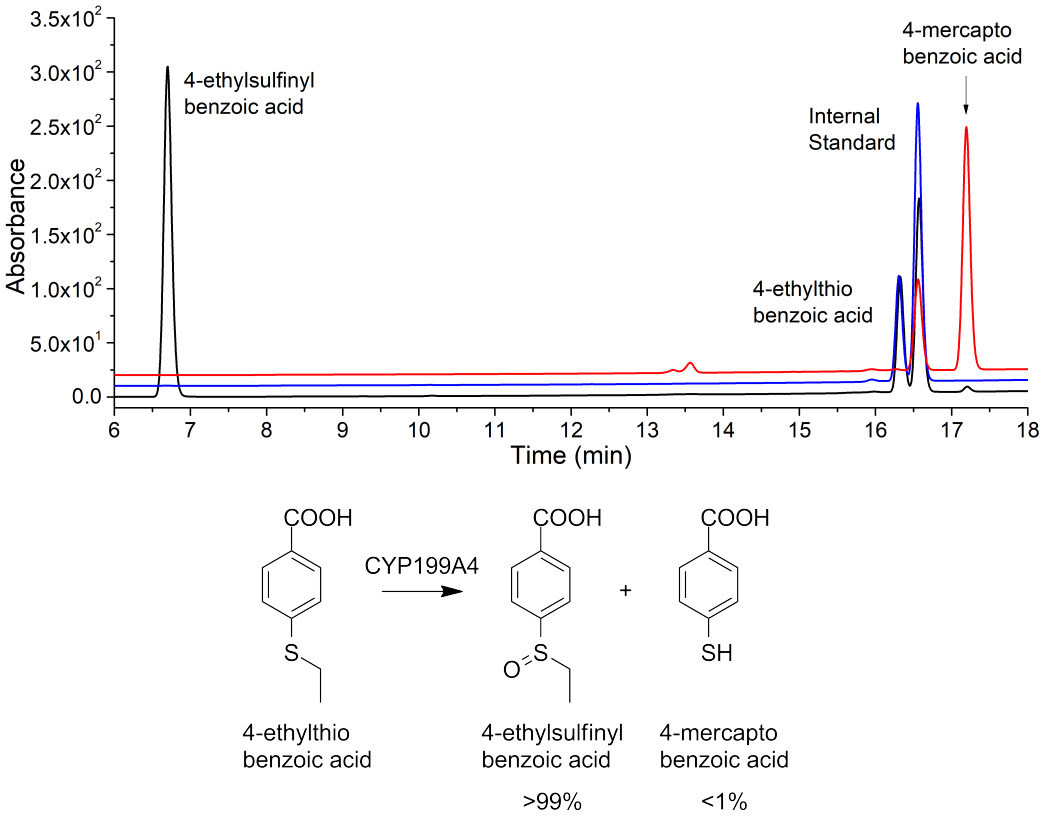

Figure 58. HPLC analysis of 4-ethylthiobenzoic acid turnover with CYP199A4. **Black**, in vitro turnover; blue, substrate control; red, 4-mercaptobenzoic acid control. A 20-95 % gradient of H_2O:ACN was employed, and the chromatogram was monitored at 254 nm.

enantiomers were able to be separated (Appendix B.3). In the CYP199A4 turnovers one enantiomer was highly favoured (91 % vs 9 %) although the stereochemistry of the product has not yet been confirmed. In order to compare the enantioselectivity of the sulfoxidation reaction to hydroxylation, the stereoselectivity of the CYP199A4 catalysed turnover of 4-ethylbenzoic acid was also determined (Appendix B.3). The hydroxylated metabolite forms the (S)-enantiomer in preference (87 % vs 13 %).

The results reinforced the observation that sulfur oxidation is highly favoured over dealkylation. It would be expected that C−H abstraction at the methylene carbon of 4-ethylthiobenzoic acid, leading to dealkylation, would be energetically more feasible than abstraction of the methyl carbon of 4-methylthiobenzoic acid, however neither reaction was observed.

4.2.4 Crystal structures of 4-methylthiobenzoic acid and 4-ethylthiobenzoic acid-bound CYP199A4

Both sulfur substrates exclusively underwent S-oxidation with CYP199A4. In order to ascertain if there were changes in the relative orientation of the sulfur containing substrates in the enzyme active site, CYP199A4 was co-crystallised with 4-methylthio- and 4-ethylthio-benzoic acids. Crystals of CYP199A4 with both substrates (1 mM) were obtained in 2 weeks from a 500 µL reservoir solution containing 0.2 M magnesium acetate tetrahydrate, 23 % w/v PEG-3,350 and 0.1 M Bis-Tris (4-methylthioBA, pH 5.5; 4-ethylthioBA, pH 5.25). X-ray diffraction data were obtained at 100 K on the MX1 beamline at the Australian Synchrotron[147,148] and the structures were solved to high resolution (4-methylthioBA, 2.01 Å; 4-ethylthioBA, 1.79 Å). Models were developed for each structure using WinCoot[144] (Chapter 2.10), and the data were deposited in the wwPDB[157,158] (www.wwpdb.org). The structures were assigned PDBs: 4-methylthioBA, 5KT1; 4-ethylthioBA, 5U6U (Table 11).

The structures of 4-methylthio and 4-ethylthiobenzoic acid-bound CYP199A4 both contained a single molecule in the asymmetric unit and crystallised with cell symmetry $P12_11$. As with the crystal structures of CYP199A4 with 4-ethoxy- and 4-methylaminobenzoic acids, the overall enzyme structure was similar to that of the 4-methoxybenzoic acid-bound CYP199A4[131] (4-methylthio, rmsd = 0.299 Å; 4-ethylthio, rmsd = 0.300 Å). The electron density observed in the active site could be modelled as a bound substrate molecule in both structures (Figures 59b and 61b).

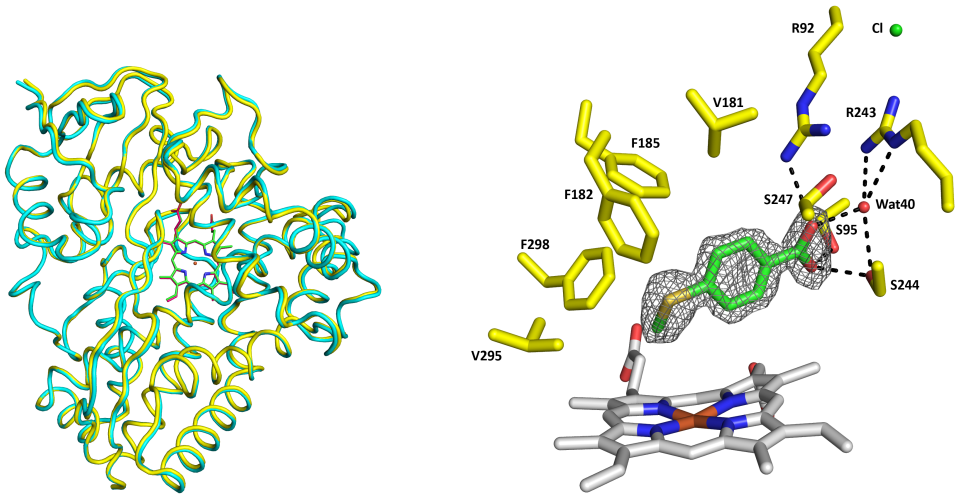

Figure 59. Crystal structure of 4-methylthiobenzoic acid-bound CYP199A4 solved at 2.01 Å resolution. Shown are (a) three-dimensional fold (yellow tube and magenta heme) overlaid with structure of 4-methoxybenzoic acid (cyan tube and green heme) and b) reduced bias $2mF_o$-DF_c composite omit map[154] of 4-methylthiobenzoic acid-bound CYP199A4. The electron density map for 4-methylthiobenzoic acid is shown contoured as a grey mesh at the 1 σ level.

Table 11. Structural refinement and data collection statistics for 4-methylthio and 4-ethylthiobenzoic acids crystallised with CYP199A4. 4-Methoxybenzoic acid (4DO1) is shown for comparison. Benzoic acid is shortened to BA.

	4-methoxyBA[131]	4-methylthioBA	4-ethylthioBA
PDB code	4DO1	5KT1	5U6U
X-ray wavelength (Å)	0.9796	0.9537	0.9537
Unit cell (a/b/c)	107.0/143.5/172.8	44.1/51.3/80.0	44.2/51.4/79.9
($\alpha/\beta/\gamma$)	90/90/90	90/91.8/90	90/92.1/90
Space group	$P2_12_12_1$	$P12_11$	$P12_11$
Molecules per unit cell	4	1	1
Resolution range[a]	50 - 2.0	44.05 - 2.01	44.15 - 1.79
	(2.03 - 2.00)	(2.07 - 2.01)	(1.82 - 1.79)
$<I/\sigma(I)>$[a]	28.5 (5.2)	7.2 (2.1)	12.0 (2.1)
Unique reflections	179187	23479	33670
Completeness[a]	100.0 (100.0)	99.7 (97.2)	99.8 (97.7)
Multiplicity[a]	7.1 (6.1)	7.1 (6.7)	7.4 (7.1)
R_{merge}[a,b] (%)	9.8 (31.9)	29.7 (89.4)	10.7 (81.8)
R_{pim}[a,b] (%)	N/A[c]	11.9 (36.7)	4.2 (32.5)
$CC_{1/2}$[a,d] (%)	N/A[c]	98.4 (82.8)	99.8 (97.7)
R_{work}	0.154	0.156	0.152
R_{free}[e]	0.189	0.223	0.202
Ramachandran plot[f]			
Most favoured	98.5	97.2	97.2
Allowed	1.5	2.8	2.5

[a]Highest resolution shell is shown in parentheses where applicable. [b]all I+ and I-. [c]Not reported in previous work. [d]Half-correlation coefficient.[182,183] [e]5 % of total reflections, randomly selected. [f]% of all amino acid residues.[184] There were no Ramachandran outliers.

In the 4-methylthiobenzoic acid-bound CYP199A4 structure, all the active site residues, along with the chloride and carboxylate-bound water molecule, and the benzoic acid moiety of the substrate, reside in similar positions to those of structures determined previously. The sulfur atom is held 4.9 Å away from the heme (Table 12), closer than the oxygen of 4-methoxybenzoic acid (5.2 Å, Figure 60). The methyl carbon is held 4.4 Å from the heme iron, further away than the methyl carbon of 4-methoxybenzoic acid (4.1 Å).

The active site orientation of 4-ethylthiobenzoic acid shows significant differences in the location of the longer *para* substituent, which contains an additional methylene unit. The sulfur atom is 4.7 Å from the heme iron, closer than the equivalent sulfur of 4-methylthiobenzoic acid. The methylene C_α is held 5.2 Å from the heme iron, while the methyl C_β is even further away (6.7 Å), and it points away from the heme. These

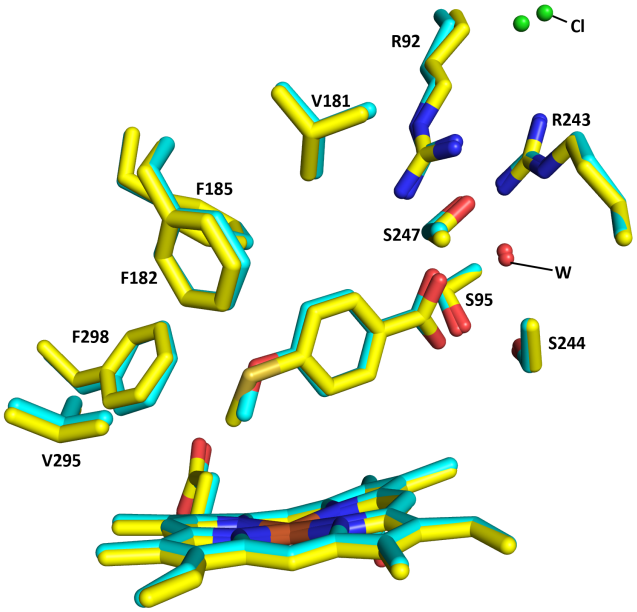

Figure 60. Comparison of the active site of 4-methylthiobenzoic acid-CYP199A4 complex (yellow) with 4-methoxybenzoic acid (cyan). Water molecules are shown as red spheres and the chloride ligands are green spheres. Those that are labelled (Cl, W) correspond to the 4-methylthiobenzoic acid structure.

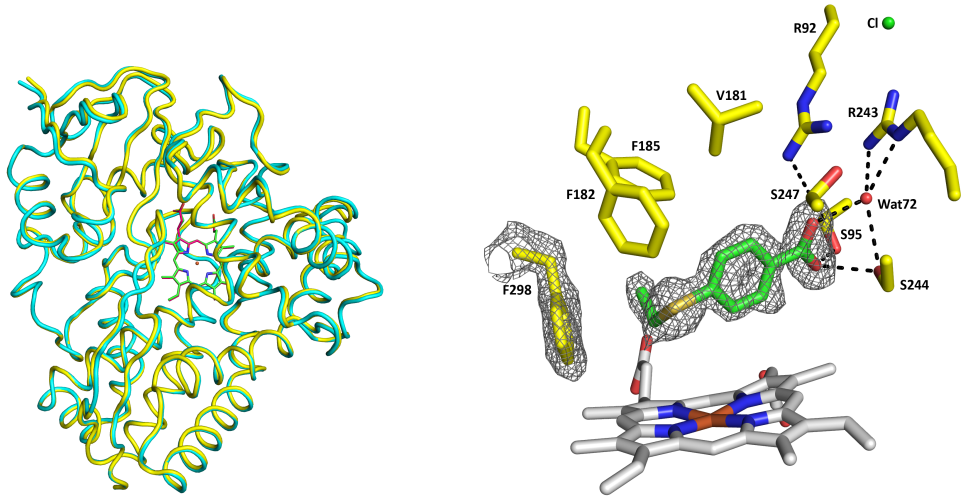

Figure 61. Crystal structure of 4-ethylthiobenzoic acid-bound CYP199A4 solved at 1.79 Å resolution. Shown are (a) three-dimensional fold (yellow tube and magenta heme) overlaid with structure of 4-methoxybenzoic acid (cyan tube and green heme) and (b) reduced bias $2mF_o$-DF_c composite omit map[154] of 4-ethylthiobenzoic acid-bound CYP199A4. The electron density map of 4-ethylthiobenzoic acid and the F298 residue is shown contoured as a grey mesh at the 1 σ level. The V295 residue has been removed for clarity.

observations help explain the selective S-oxidation activity over S-dealkylation. The closer approach of the sulfur may also contribute to the lower spin state shifts observed with the sulfur substrates.

In the 4-ethylthiobenzoic acid-CYP199A4 crystal structure, the F298 residue has moved in order to accommodate the ethylthio moiety (Figure 61b). All other active site

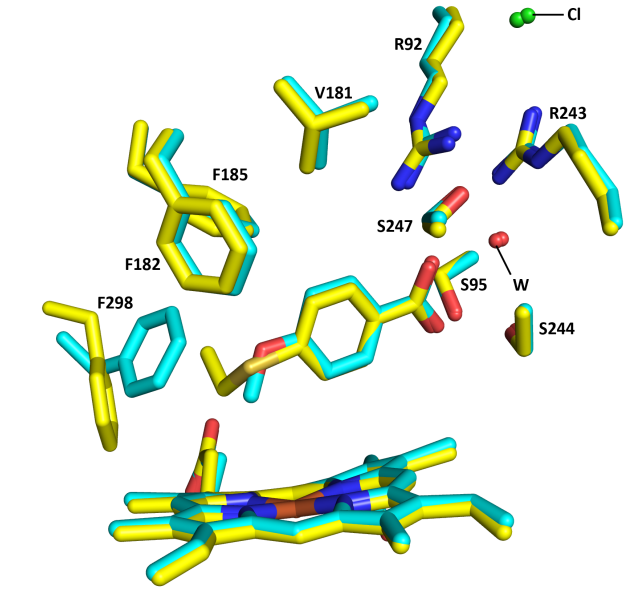

(a)

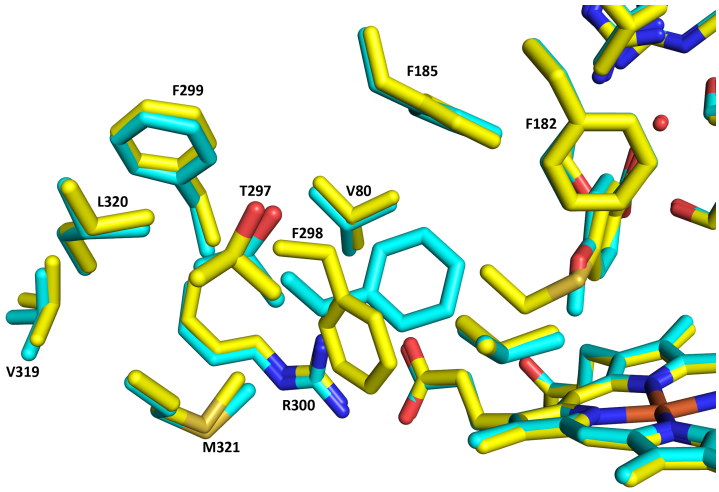

(b)

Figure 62. Comparison of the active site of 4-methylthiobenzoic acid-CYP199A4 complex (yellow) with 4-methoxybenzoic acid (cyan). Water molecules are shown as red spheres and the chloride ligands are green spheres. Those that are labelled (Cl, W) correspond to the 4-methylthiobenzoic acid structure. In (a), the active site environment is depicted (The V295 residue has been removed for clarity); in (b) an alternate view showing the residues nearby to F298, highlighting that only the F298 residue has moved significantly.

residues are found in a similar location to those found in the other structures (Figure 62). This suggests that the F298 residue in CYP199A4 can move to accommodate larger substrates. It is of note that 4-ethoxybenzoic acid did not induce a similar movement in the F298 residue (Chapter 3.2.4). The C_β of 4-ethylthiobenzoic acid is 1.1 Å from the closest carbon of F298 in the 4-methoxybenzoic acid structure, while in the 4-ethylthiobenzoic acid structure it is 4.0 Å away, reducing steric clashes with the ethylthio moiety (Figure 62a).

In both the 4-methylthio- and 4-ethylthio-benzoic acid structures, the sulfur atom

was closer to the Cpd I oxygen (4-methylthio-, 3.4 Å; 4-ethylthio-, 3.3 Å) than the equivalent oxygen atoms of 4-methoxy- and 4-ethoxy-benzoic acids (4-methoxy- and 4-ethoxy-, both 3.6 Å). Conversely, the C_α was closer to the Cpd I oxygen for the 4-methoxy- and 4-ethoxy-benzoic acids (4-methoxy-, 2.7 Å; 4-ethoxy-, 2.8 Å) than for the 4-methylthio- and 4-ethylthio-benzoic acids (4-methylthio-, 3.3 Å; 4-ethylthio-, 4.0 Å). The C_β of 4-ethylthiobenzoic acid was significantly further from the Cpd I oxygen than the C_β of 4-ethoxybenzoic acid. In addition, the Fe=O - - - S angle was larger (4-methylthio-, 162.5°; 4-ethylthio-, 159.2°) than the Fe=O - - - C_α angle (4-methylthio-, 131.9°; 4-ethylthio-, 133.7°, Table 12). There was no significant difference between the Fe=O - - - X angle for the sulfur (X = S) and oxygen substrates (X = O). These observations provide additional insight into why the oxidation of sulfur was preferable to carbon hydroxylation for these substrates.

Table 12. Distances and angles between structural features of 4-methylthio and 4-ethylthiobenzoic acid-bound CYP199A4s. The ferryl Cpd I oxygen was modelled 1.62 Å from the heme iron.[160,161] X refers to the O or S heteroatom.

Distance (Å)	4-methoxyBA	4-ethoxyBA	4-methylthioBA	4-ethylthioBA
C_α - Fe	4.1	4.2	4.4	5.2
C_α - **O**=Fe	2.7	2.8	3.3	4.0
C_β - Fe	-	4.3	-	6.7
C_β - **O**=Fe	-	3.0	-	5.5
X - Fe	(X = O) 5.2	(X = O) 5.1	(X = S) 4.9	(X = S) 4.7
X - **O**=Fe	3.6	3.6	3.4	3.3
C_X - F298	(X = α) 3.8	(X = α,β) 3.6	(X = α) 3.2	(X = β) 4.0
Angle (°)				
C_{04}-X-C_α	118.6	118.9	104.3	106.1
Dihedral (*) C_{09}-C_{04}-X-C_α	2.1	9.2	33.9	55.2
Fe=O-C_α	140.7	144.8	131.9	133.7
Fe=O-C_β	-	137.3	-	137.9
Fe=O-X	158.3	163.4	162.5	159.2

(*) The dihedral angle, C_{09}-C_{04}-X-C_α, is represented below.

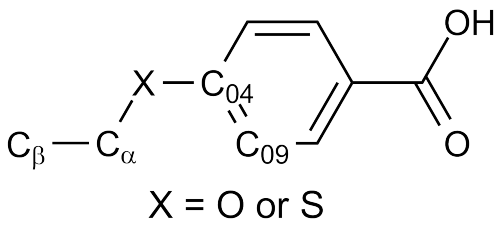

4.2.5 Investigation of halo- and haloalkyl-benzoic acid substrates

The activity of CYP199A4 with halogen-containing substrates has not yet been determined. Halogen oxidation is a difficult reaction due to the high electronegativity of halogen atoms.[39] 4-Fluoro, 4-chloro, 4-bromo and 4-iodobenzoic acids were investigated with CYP199A4, first using spin state shift analysis to determine if the heme distal water ligand could be dissociated upon substrate binding.

Table 13. Binding and turnover parameters determined for halogen-containing benzoic acid substrates investigated with CYP199A4. Rates are mol (molCYP)$^{-1}$ min^{-1}.

Substrate	HS (%)	K_d (µM)	NADH^{a,b}
4-fluoroBA	50	7.5 ± 0.1	359 ± 12
4-chloroBA	70	2.0 ± 0.1	436 ± 10
4-bromoBA	80	1.5 ± 0.3	523 ± 32
4-iodoBA	≥ 95	0.58 ± 0.02	577 ± 49

[a]Rate of turnover of NADH during the reaction. [b]No products were detected in any of the turnovers.

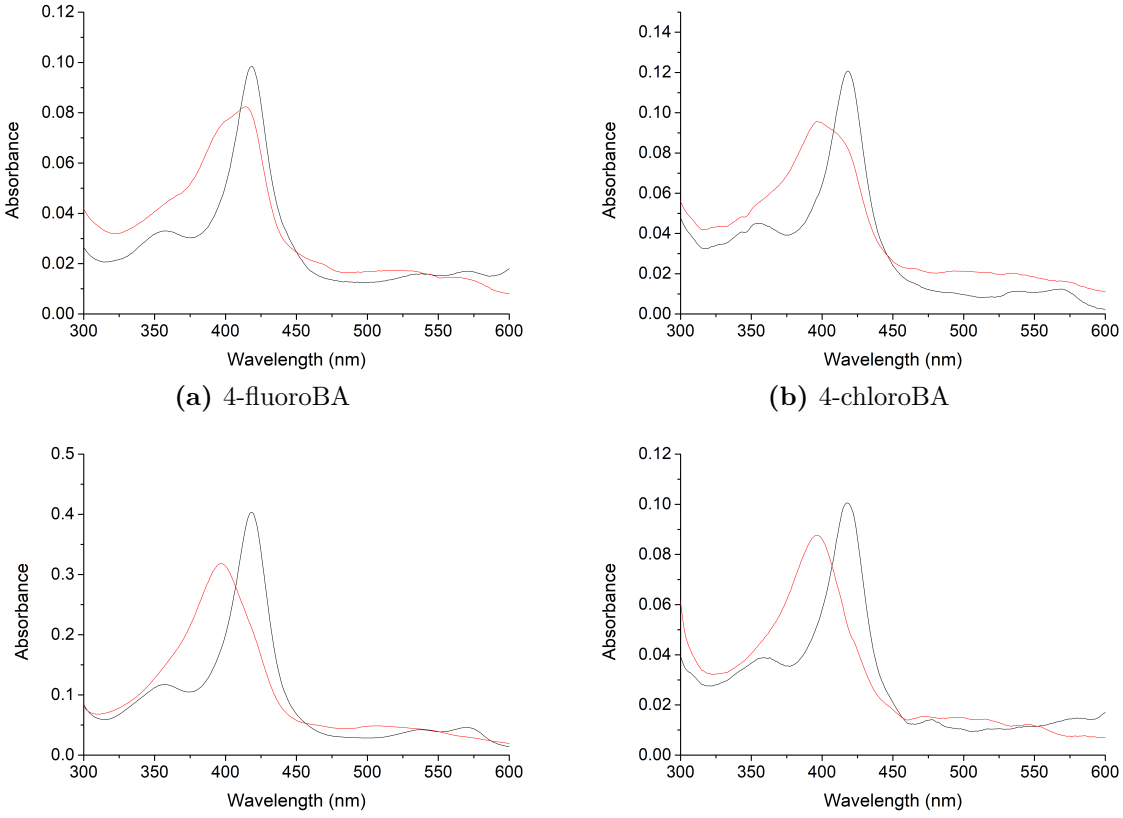

(a) 4-fluoroBA **(b)** 4-chloroBA

(c) 4-bromoBA **(d)** 4-iodoBA

Figure 63. Spin state shifts of halogen-containing substrates investigated with CYP199A4. Black shows CYP199A4 in its resting state, red shows the maximum absorbance shift obtained upon addition of substrate.

A type I spin state shift was observed when each substrate was added to CYP199A4 (Table 13, Figure 63). The trend that emerged was that the shift to high spin heme correlated with the size of the halogen. 4-Fluorobenzoic acid gave the smallest shift of the four (50 % HS), followed by 4-chloro- (70 %), 4-bromo- (80 %) and 4-iodo-benzoic acid ($\geq$ 95 %).

The binding affinity of each substrate to CYP199A4 was then determined (Figure 64). The tightest binding was observed with 4-iodobenzoic acid (0.58 µM), and the affinity decreased as the halogens became smaller (F, 7.5 µM; Cl, 2.0 µM; Br, 1.5 µM). The trend in binding affinity was similar to that observed with the magnitude of the spin state shift. This indicated that the larger *para* substituted halobenzoic acids were a better fit for the active site of CYP199A4.

In order to determine if CYP199A4 was capable of oxidising these substrates, *in vitro* turnovers were performed (Chapter 2.4). Oxidation of NADH was observed with each substrate, and those with the larger halogen substituents displayed faster rates. These correlated with the spin state shifts (Table 13); in order from slowest to fastest: 4-fluorobenzoic acid (359 min^{-1}), 4-chlorobenzoic acid (436 min^{-1}), 4-bromobenzoic acid

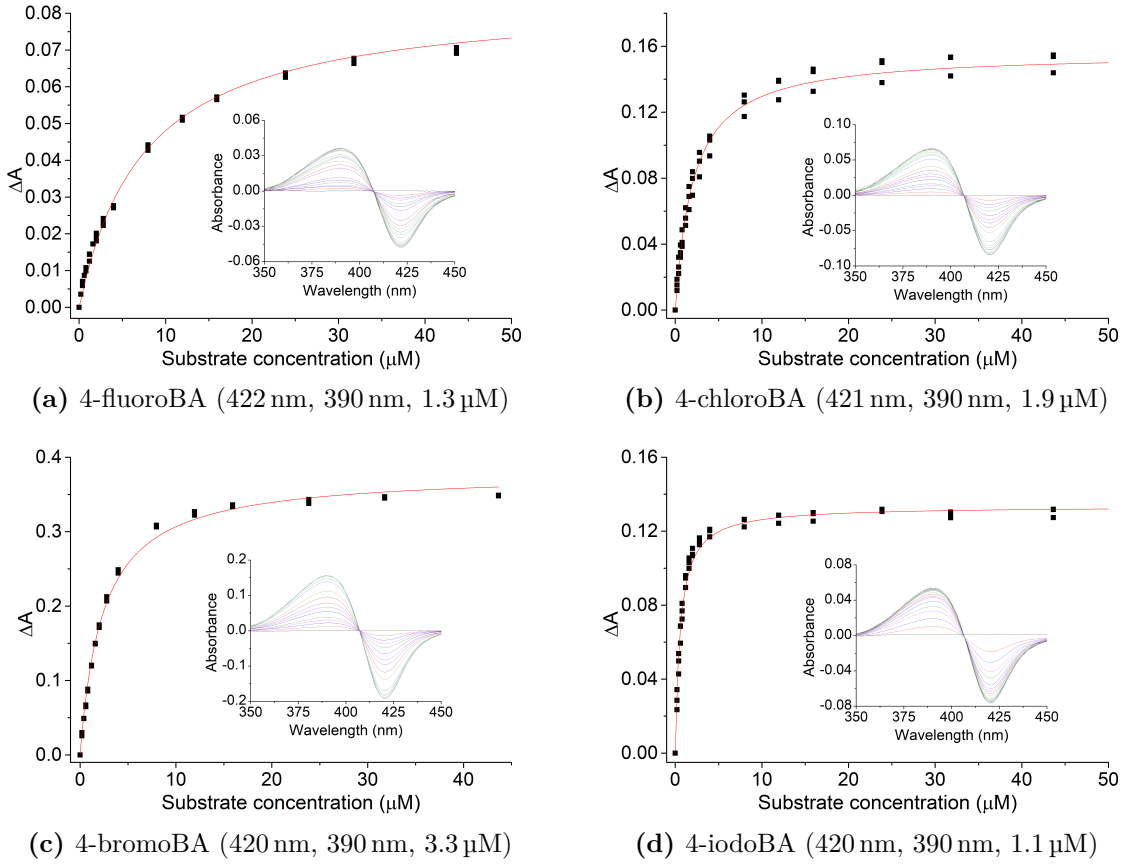

(a) 4-fluoroBA (422 nm, 390 nm, 1.3 µM)

(b) 4-chloroBA (421 nm, 390 nm, 1.9 µM)

(c) 4-bromoBA (420 nm, 390 nm, 3.3 µM)

(d) 4-iodoBA (420 nm, 390 nm, 1.1 µM)

Figure 64. Dissociation constant determination of halogen-containing substrates investigated with CYP199A4. The inset image shows the UV-Vis response to successive addition of substrate aliquots. Shown in brackets are the wavelengths of the trough and peak, and the enzyme concentration used for dissociation constant analysis (trough, peak, µM-P450).

($523\,\mathrm{min}^{-1}$) and 4-iodobenzoic acid ($577\,\mathrm{min}^{-1}$). The amount of hydrogen peroxide formed during each turnover was determined to be $< 2\,\%$ (Chapter 2.7), which indicated that there was minimal uncoupling via the hydrogen peroxide pathway (Figure 1). It is likely the reductive equivalents were channelled towards the formation of water via the oxidase pathway.

HPLC analysis was employed to search for P450 oxidation products in the turnovers (Chapter 2.1). In each, there were no observable peaks apart from that of the substrate (Figure 65, Appendix B.3), indicating that CYP199A4 was not capable of oxidising *para*-halogen benzoic acids to any significant degree (Figure 66).

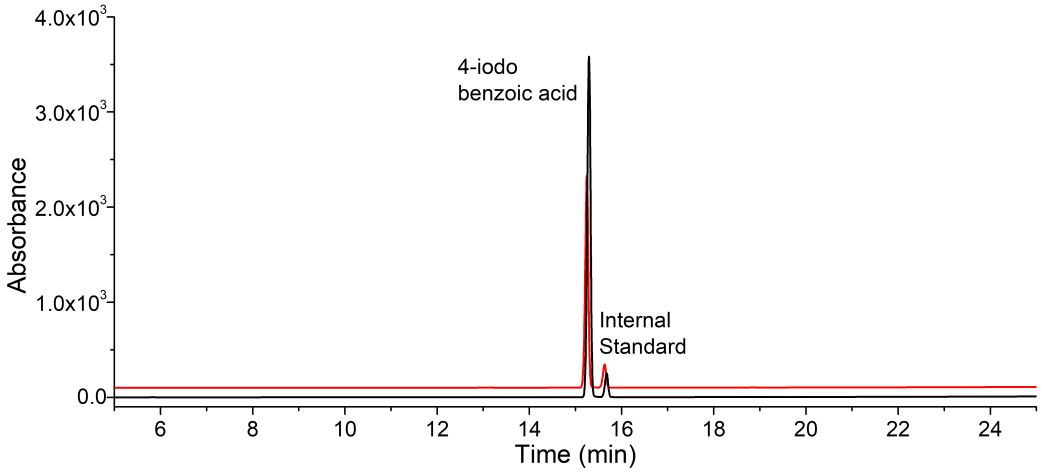

Figure 65. HPLC analysis of 4-iodobenzoic acid turnover with CYP199A4. **Black**, *in vitro* turnover; red, substrate control, RT = 15.3 min. The retention time of 4-hydroxybenzoic acid is 6.6 min. A 20-95 % gradient of H_2O:ACN was employed, and the chromatogram was monitored at 254 nm. The remaining chromatograms are presented in Appendix B.3.

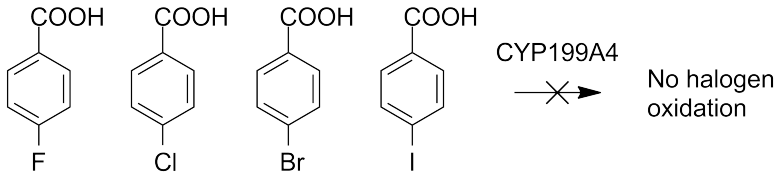

Figure 66. Summary of 4-halobenzoic acid substrates substrate activity with CYP199A4. No P450 oxidation products were observed.

Previously, 12-chloro- and 12-bromo-dodecanoic acids have been shown to undergo P450-catalysed dehalogenations (Figure 11a, Chapter 1.4.5).[116,117] While CYP199A4 does not perform these reactions with 4-halobenzoic acids, the enzyme hydroxylates 4-methylbenzoic acid to 4-hydroxymethylbenzoic acid, and both hydroxylates and desaturates 4-ethylbenzoic acid.[30] To determine if CYP199A4 can support oxidative dehalogenation or halogen oxidation on aliphatic rather than aromatic carbons, halomethyl and haloethyl substrates were investigated with CYP199A4 (Figure 67). 4-Chloromethyl- and 4-bromomethyl-benzoic acids will allow the partition between C−H bond abstraction and halogen oxidation to be determined. The competition between desaturation, hydroxylation and oxidation of halogens will be assessed using 4-(2-chloroethyl)- and 4-(2-bromoethyl)-benzoic acids.

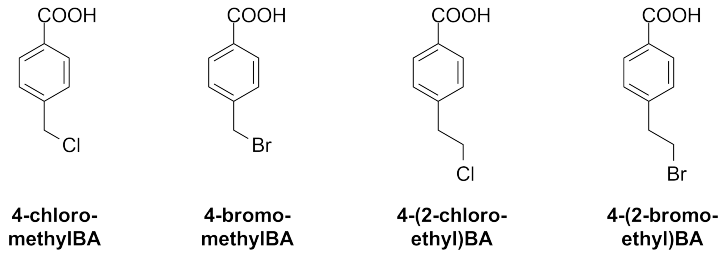

Figure 67: Alkyl halide substrates (X = F, Cl) investigated with CYP199A4.

Addition of all the alkyl halide substrates to the enzyme resulted in a large shift in CYP199A4 from the low to the high spin state. 4-Chloromethyl-, 4-bromomethyl- and 4-(2-chloroethyl)-benzoic acids induced ≥ 95 % HS shifts in CYP199A4, while 4-(2-bromoethyl)benzoic acid shifted the spin state to 90 % HS (Table 14, Figure 68). The HS shifts of both halomethyls were larger than 4-methylbenzoic acid (70 %), while those of the haloethyls were comparable to 4-ethylbenzoic acid (≥ 95 %). The halomethyl substrates would be expected to be of a similar size as 4-ethylbenzoic acid.

Table 14. Binding and turnover parameters determined for chloro- and bromo-alkylbenzoic acid (BA) analogues investigated with CYP199A4. Rates are given as mol (molCYP)$^{-1}$ min^{-1}.

Substrate	HS (%)	K_d (µM)	NADH[a]	PFR[b]	Coupling[c]
4-methylBA[30]	70	0.66 ± 0.05	444 ± 8	397 ± 22	89 ± 4
4-ethylBA	≥ 95	0.34 ± 0.02	812 ± 7	515 ± 88	63 ± 10
4-chloromethylBA	≥ 95	0.75 ± 0.1	165 ± 2	161 ± 4	97 ± 2[d]
4-bromomethylBA	≥ 95	24 ± 2	69 ± 2	54 ± 8	93 ± 3[d]
4-(2-chloroethyl)BA	≥ 95	0.33 ± 0.09	453 ± 24	15 ± 2	3 ± 0.3
4-(2-bromoethyl)BA	90	0.87 ± 0.08	338 ± 6	52 ± 1.1	16 ± 0.5

[a]NADH oxidation rate. [b]PFR: product formation rate. [c]% of NADH consumed that led to formation of substrate metabolite. [d]The terephthalic acid product resulted from two full P450 catalytic cycles. This was taken into account during determination of the total coupling and product formation.

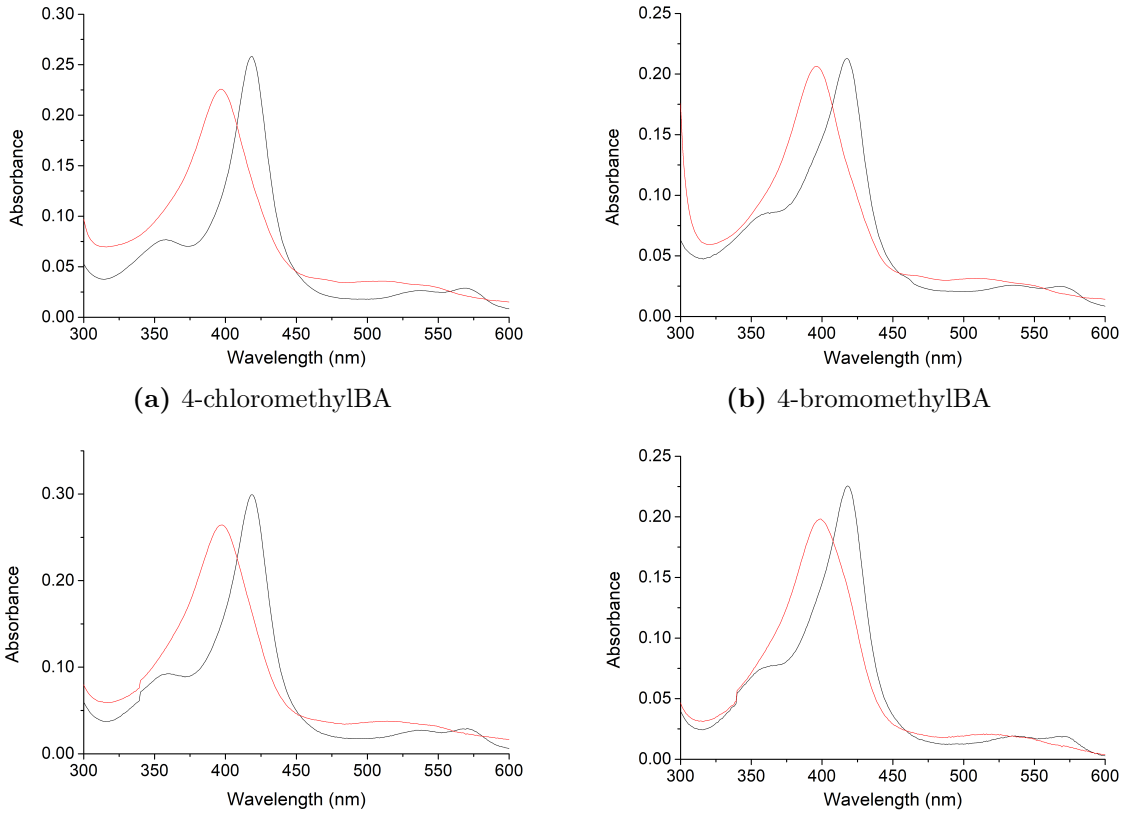

(a) 4-chloromethylBA **(b)** 4-bromomethylBA

(c) 4-(2-chloroethyl)BA **(d)** 4-(2-bromoethyl)BA

Figure 68. Spin state shifts of alkyl halide substrates investigated with CYP199A4. Black shows CYP199A4 in its resting state, red shows the maximum absorbance shift obtained upon addition of substrate.

4-Chloromethylbenzoic acid bound less tightly than 4-ethylbenzoic acid (0.75 µM vs 0.34 µM, Figure 69). The binding affinity of 4-bromomethylbenzoic acid was several orders of magnitude lower (24 µM). The haloethyl substrates would be comparable in size to 4-*n*-propylbenzoic acid.[28] The affinities of 4-(2-chloroethyl)- and 4-(2-bromoethyl)-benzoic acids for CYP199A4 were also high (0.33 µM and 0.87 µM respectively), which indicated that the bromo and chloro substituted alkyl benzoic acids could be readily accommodated in the active site of CYP199A4.

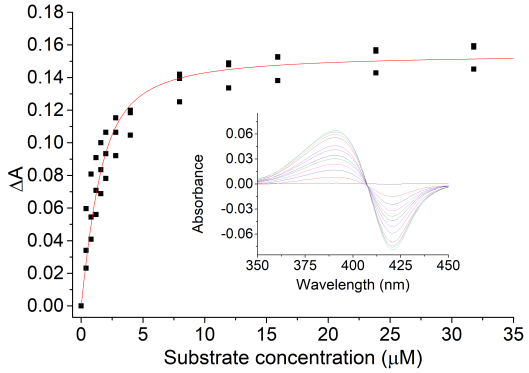

(a) 4-chloromethylBA (421 nm, 391 nm, 1.3 μM)

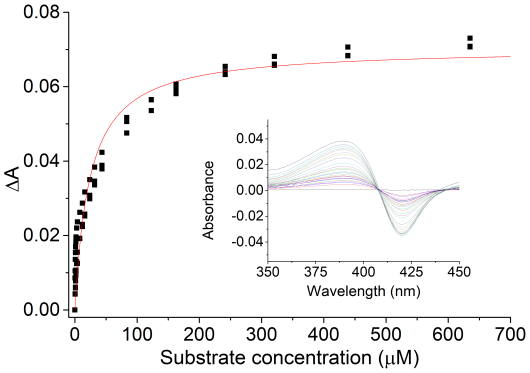

(b) 4-bromomethylBA (420 nm, 389 nm, 1.1 μM)

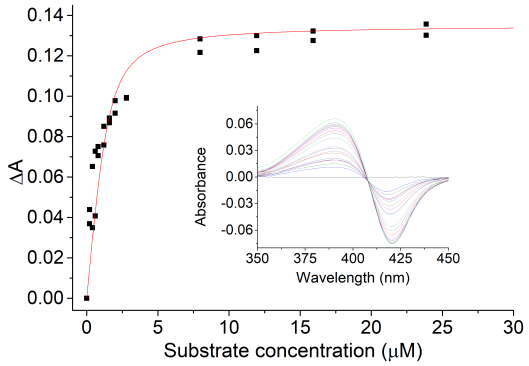

(c) 4-(2-chloroethyl)BA (421 nm, 391 nm, 1.5 μM)

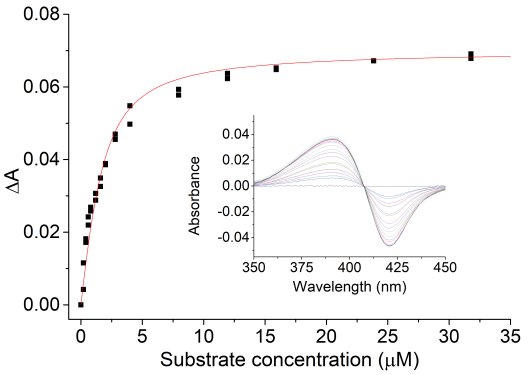

(d) 4-(2-bromoethyl)BA (421 nm, 391 nm, 1.4 μM)

Figure 69. Dissociation constant determination of alkyl halide-containing substrates investigated with CYP199A4. The inset image shows the UV-Vis response to successive addition of substrate aliquots. Shown in brackets are the wavelengths of the trough and peak, and the enzyme concentration used for dissociation constant analysis (trough, peak, μM-P450).

In vitro assays were performed with each substrate and then analysed by HPLC. The NADH oxidation rates of CYP199A4 with the halomethyl substrates were lower than 4-methylbenzoic acid (4-chloromethyl-, 165 min^{-1}; 4-bromomethyl-, 69 min^{-1} vs 4-methyl-benzoic acid, 444 min^{-1}, Table 14). This contrasted with the spin state shifts, which were higher for both halomethyls than 4-methylbenzoic acid. The NADH oxidation rates of the CYP199A4-catalysed turnovers of 4-(2-chloroethyl)benzoic acid (453 min^{-1}) and 4-(2-bromoethyl)benzoic acid (338 min^{-1}) were both lower than with 4-ethylbenzoic acid (812 min^{-1}).

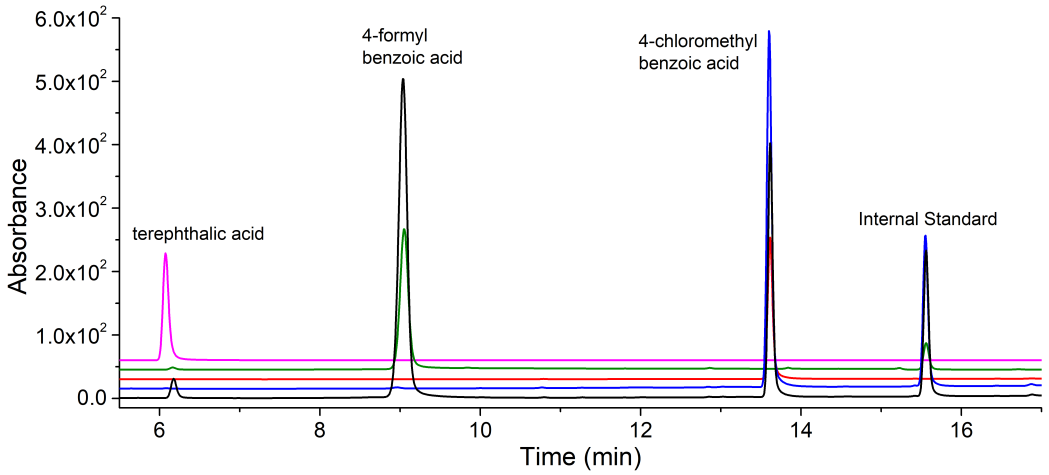

Figure 70. HPLC analysis of 4-chloromethylbenzoic acid turnover with CYP199A4. **Black**, *in vitro* turnover; blue, no P450 control reaction; red, substrate control, RT = 13.7 min; green, 4-formylbenzoic acid control, RT = 9.0 min; pink, terephthalic acid control, RT = 6.1 min. A 20-95 % gradient of H_2O:ACN was used. The chromatogram was monitored at 254 nm. The substrate may have degraded to form 4-hydroxymethylbenzoic acid (RT = 5.1 min).

In the HPLC and GC-MS chromatograms of *in vitro* turnovers of the halomethyl substrates, P450 oxidation products were observed. 4-Chloromethylbenzoic acid (Figure 70) and 4-bromomethylbenzoic acid (Figure 71) were both oxidised to the same major product, 4-formylbenzoic acid. This was identified using HPLC coelution experiments against authentic standards (Chapter 2.1) and by GC-MS analysis (Appendix B.4). 4-Chloromethylbenzoic acid turnovers with CYP199A4 were highly coupled (97 %) with a product formation rate of 161 min^{-1}. Along with the 4-formylbenzoic acid, a small amount of terephthalic acid was detected. The distribution of products was 96 % 4-formylbenzoic acid and 4 % of terephthalic acid as determined using HPLC calibrations of authentic standards (Figure 72). Control reactions with 4-bromomethylbenzoic acid, which contained no P450 enzyme, indicated there was a small amount of terephthalic acid formed (either during the turnovers or the HPLC analysis). The coupling of 4-bromomethylbenzoic acid was also high (93 %) with a resulting product formation rate of 54 min^{-1}, and there was $>$ 99 % 4-formylbenzoic acid with the remainder terephthalic acid ($<$ 1 %, Figure 71).

The 4-formylbenzoic acid product presumably arose via hydroxylation at the

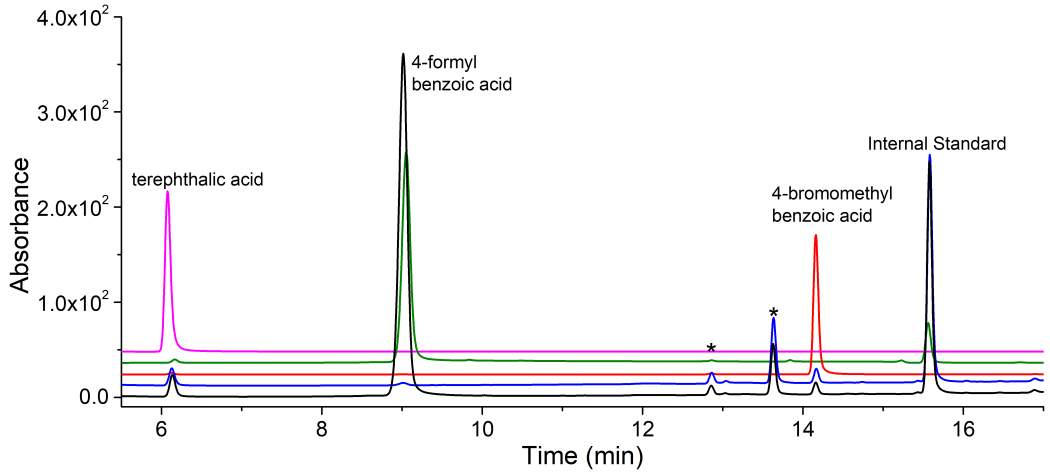

Figure 71. HPLC analysis of 4-bromomethylbenzoic acid turnover with CYP199A4. **Black**, *in vitro* turnover; blue, no P450 control reaction; red, substrate control, RT = 14.2 min; green, 4-formylbenzoic acid control, RT = 9.0 min; pink, terephthalic acid control, RT = 6.1 min. A 20-95 % gradient of H_2O:ACN was used, and monitored at 254 nm. Additional unidentified peaks which were present in the no P450 control reaction are denoted (*). The substrate may have degraded in the no P450 turnover mixture to form these peaks as well as 4-hydroxymethylbenzoic acid (RT = 5.1 min).

para-methyl group, followed by intramolecular loss of a molecule of HX (Figure 72, top pathway). The terephthalic acid would have resulted from either a second P450-catalysed oxidation of 4-formylbenzoic acid, or by air oxidation. 4-Hydroxymethylbenzoic acid was observed at 5.1 min in the HPLC chromatograms of both *in vitro* halomethyl turnovers. This could arise from oxidation of the halide to

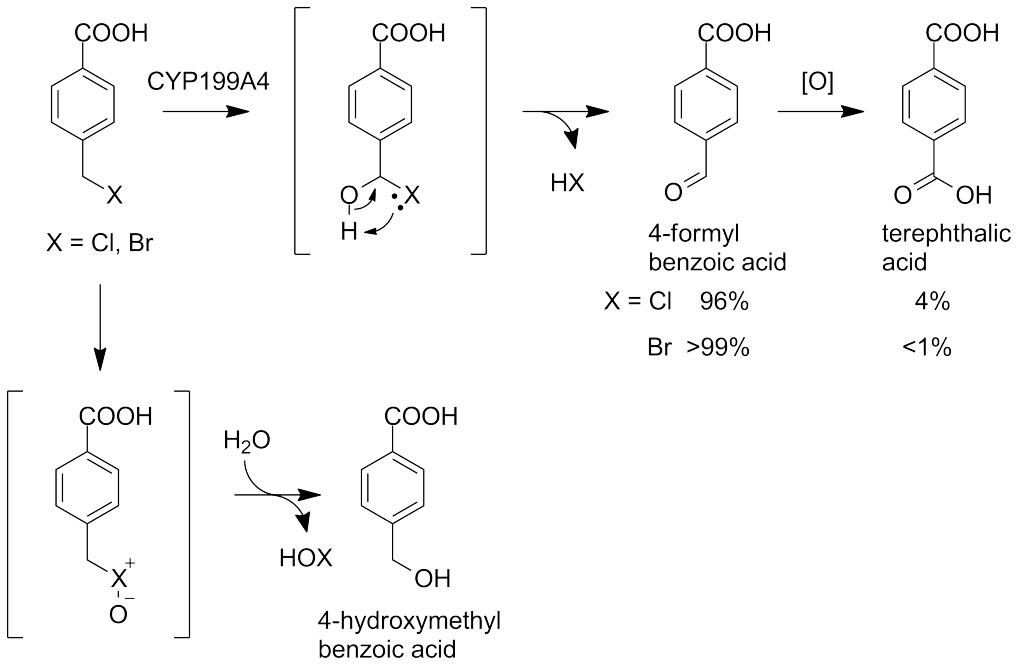

Figure 72. Oxidation of halomethylbenzoic acid substrates by CYP199A4. The proposed mechanisms of dehalogenation, either via halohydroxy or halonium intermediates, are shown.

X^+-O^-, followed by hydrolysis to the alcohol (Figure 72, bottom pathway). However, a comparable amount of this metabolite was found in the HPLC chromatograms of control reactions containing no P450 enzyme. There was also a small amount in the substrate control. The 4-hydroxymethylbenzoic acid was not observed in the GC-MS analysis (Appendix B.4). This indicated that P450 activity was not likely to be responsible for formation of this product and that it arises from hydrolysis of the substrate during HPLC analysis.

The *in vitro* CYP199A4 turnovers of 4-(2-chloroethyl)benzoic acid were analysed which indicated that there were three potential oxidation products formed in low yield (Figure 73, Appendix B.4).[iv] One of these products was identified using HPLC coelution experiments as 4-(2-hydroxyethyl)benzoic acid. However, controls with no P450 enzyme showed formation of this product ($\approx$ 50 %), suggesting a proportion of this was also formed by non-enzymatic means.

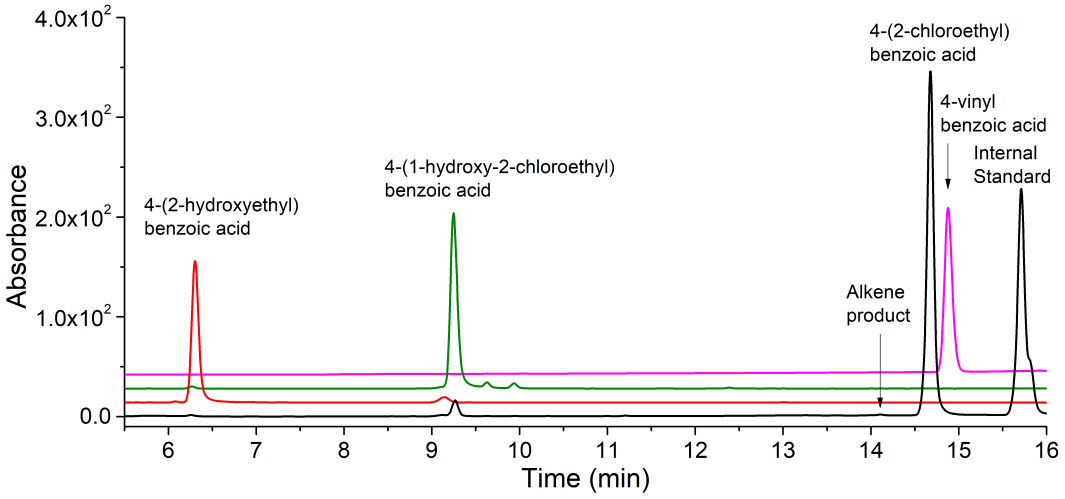

Figure 73. HPLC analysis of 4-(2-chloroethyl)benzoic acid turnover with CYP199A4. **Black**, *in vitro* turnover; red, 4-(2-hydroxyethyl)benzoic acid control, RT = 6.3 min; green, isolated 4-(1-hydroxy-2-chloroethyl)benzoic acid control, RT = 9.3 min; pink, 4-vinylbenzoic acid control, RT = 14.9 min. The gradient employed was 20-95 % of H_2O:ACN and the chromatogram was monitored at 254 nm.

To identify the remaining products, an *in vivo* turnover culture was performed and the supernatant was extracted. The metabolites were purified by semi-prep HPLC (Chapter 2.1). NMR analysis indicated that the major product was 4-(1-hydroxy-2-chloroethyl)benzoic acid (Figure 74). The doublet at 5.9 ppm corresponded to the hydroxy group which was coupling to the connected α-carbon. This proton did not have an associated ^{13}C signal in the HSQC spectrum which confirmed it was an OH group. The minor product, 4-(2-hydroxyethyl)benzoic acid, was also confirmed by NMR (Appendix B.5). The third product (RT = 14.1 min) was not isolated in sufficient

[iv] Only two product peaks were observed via GC-MS. The retention times were 12.9 min and 16.4 min.

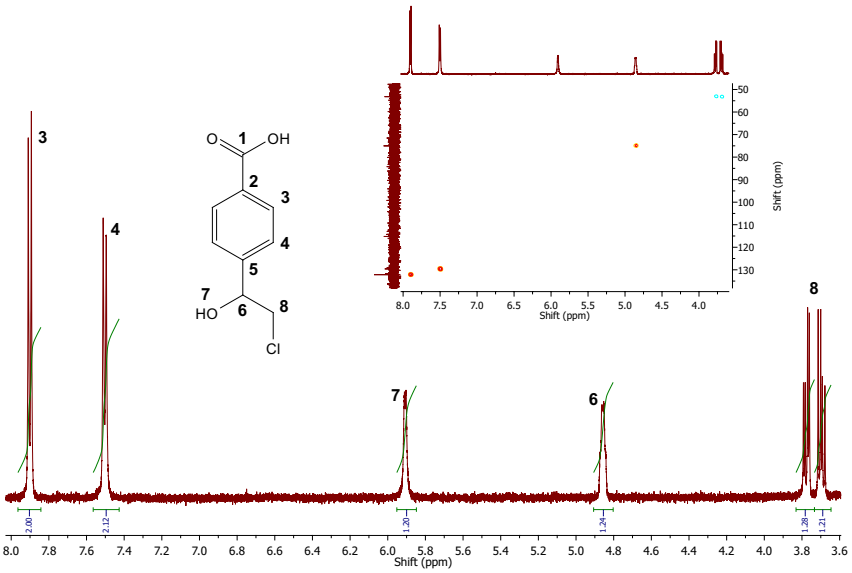

Figure 74. NMR analysis of 4-(1-hydroxy-2-chloroethyl)benzoic acid. Shown are ^{1}H and (inset) ^{1}H-^{13}C HSQC. The doublet at 5.9 ppm (**7**) had no associated ^{13}C signal and thus corresponded to the hydroxy group on the α-carbon.

amounts to obtain an NMR spectrum. In the GC-MS chromatogram of the *in vitro* turnover, the 4-(1-hydroxy-2-chloroethyl)benzoic acid was detected (m/z = 343.05 and 329.00, loss of Me; vs expected 344.10, Appendix B.4). This mass was indicative of a doubly-TMS derivatised hydroxylation product with the chlorine substituent still attached. A peak at 12.9 min was also detected, which was assigned as an alkene with the chlorine attached (m/z = 254.00 vs expected 254.05, Appendix B.4). The potential alkene peak in the HPLC chromatogram could be observed but not confirmed (Figure 73). The E/Z stereochemistry of the alkene could not be confirmed as it was not produced in sufficient quantities to permit NMR characterisation. The product peaks were calibrated using HPLC. The coupling efficiency was low (3 %) and the resulting product formation rate was more than an order of magnitude slower than 4-ethylbenzoic acid (15 min^{-1} vs 515 min^{-1}). The distribution of products was 4-(1-hydroxy-2-chloroethyl)benzoic acid, ≈ 80 %; 4-(2-hydroxyethyl)benzoic acid[v], ≈ 10 %, and the remaining ≈ 10 % the chloro alkene.

The *in vitro* CYP199A4 turnovers of 4-(2-bromoethyl)benzoic acid indicated there were three oxidation products (Figure 75 and Appendix B.4). Isolation of the products after an *in vivo* turnover, and subsequent HPLC purification and NMR characterisation, revealed the major product was 4-(1-hydroxy-2-bromoethyl)benzoic acid (Figure 76). The hydroxy group attached to the α-carbon appeared as a doublet with no corresponding ^{13}C signal, similarly to the hydroxylated chloroethyl product. The minor product, 4-(2-hydroxyethyl)benzoic acid (Appendix C.4), also appeared in turnovers

[v]There was little evidence to suggest that the 4-(2-hydroxyethyl)benzoic acid was formed by P450-catalysed oxidation.

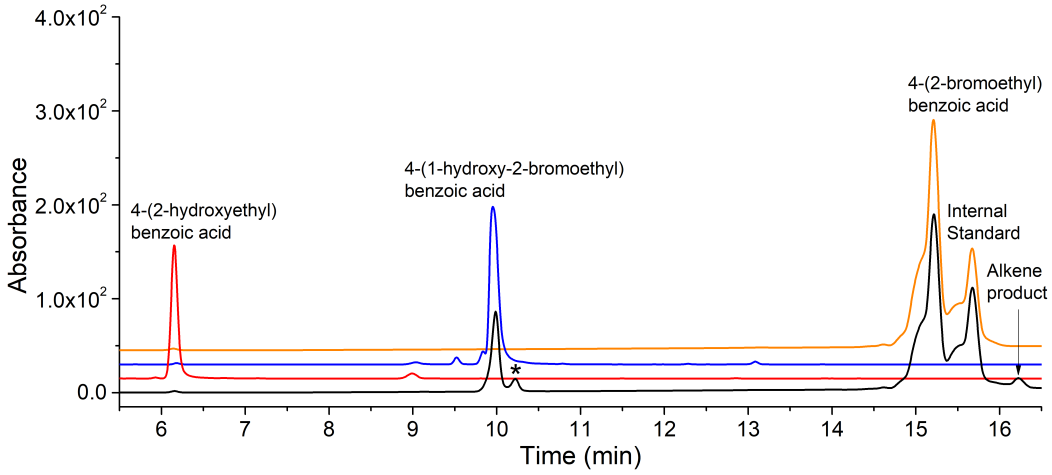

Figure 75. HPLC analysis of 4-(2-bromoethyl)benzoic acid turnover with CYP199A4. **Black**, *in vitro* turnover; red, 4-(2-hydroxyethyl)benzoic acid control, RT = 6.3 min; blue, isolated 4-(1-hydroxy-2-bromoethyl)benzoic acid control, RT = 10.2 min; orange, no P450 control reaction. An unidentified peak is denoted (*), which could be a further oxidation product. A 20-95 % gradient of H_2O:ACN was used and the chromatogram was monitored at 254 nm.

with no P450 enzyme (≈ 50 % of the amount observed in the turnover), similar to the turnovers of 4-(2-chloroethyl)benzoic acid with no P450. The mass spectrum of 4-(1-hydroxy-2-bromoethyl)benzoic acid showed a 1:1 ratio of the ^{79}Br and ^{81}Br isotope peaks, indicating the bromo substituent was still attached (Figure 77a, Appendix B.4). This product would have resulted from α-carbon hydroxylation, similar to the major product from the turnover of 4-(2-chloroethyl)benzoic acid.

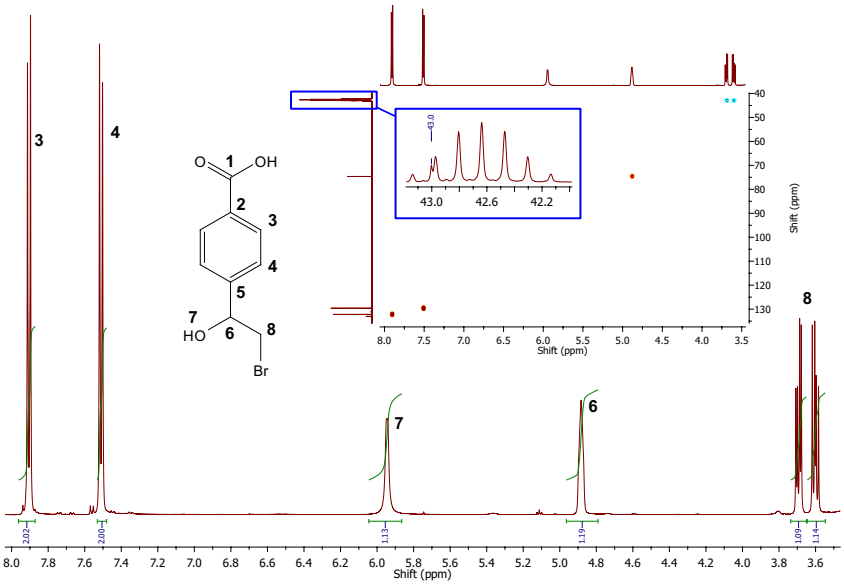

Figure 76. NMR analysis of 4-(1-hydroxy-2-bromoethyl)benzoic acid. Shown are ^{1}H and (inset) ^{1}H-^{13}C HSQC. The d_6-DMSO signal overlaps the carbon signal at 43.0 ppm which corresponds to the CH_2Cl (blue expansion). The doublet at 5.95 ppm (**7**) had no associated ^{13}C signal and thus corresponded to the hydroxy group on the α-carbon.

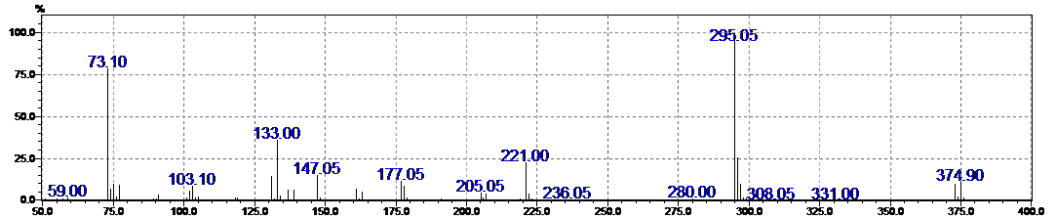

(a) 4-(1-Hydroxy-2-bromoethyl)benzoic acid. Observed m/z = 372.90/374.90 (1:1, - Me) vs expected 388.05/390.05.

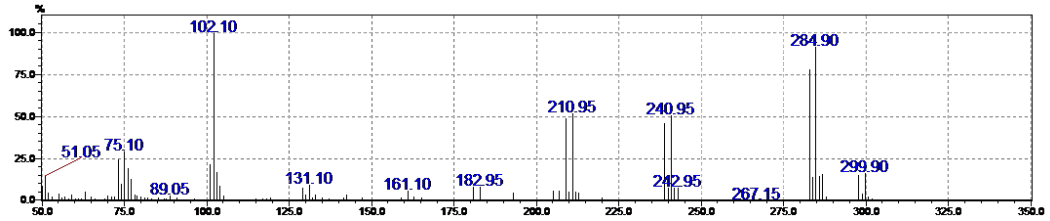

(b) 4-(2-Bromovinyl)benzoic acid. Observed m/z = 297.90/299.90 (1:1) vs expected 298.00/300.00.

Figure 77. MS analysis of 4-(2-bromoethyl)benzoic acid products. The distinctive 1:1 ratio of the ^{79}Br and ^{81}Br isotopes indicated the bromine substituent was still attached. The gas chromatogram is shown in Appendix B.4.

There was also a peak in the HPLC at 10.2 min that could potentially be a further oxidation product such as an epoxide or a ketone. Another peak had a retention time of 16.2 min, which may be a desaturation product (Figure 75). In the GC-MS, a small peak at 14.8 min with a mass indicative of a bromo alkene was observed (Figure 77b, Appendix B.4). This could be the metabolite observed in the HPLC at 16.2 min. The amount of bromo alkene product was calibrated using 4-vinylbenzoic acid via HPLC. The product formation rate and coupling were higher for 4-(2-bromoethyl)benzoic acid than 4-(2-chloroethyl)benzoic acid (52 min^{-1}, 16 % vs 15 min^{-1}, 3 %). The product distribution was 4-(1-hydroxy-2-bromoethyl)benzoic acid, ≈ 82 %; 4-(2-hydroxyethyl)benzoic acid[v], ≈ 2 %; bromo alkene, ≈ 16 %.

The 4-(1-hydroxy-2-haloethyl)benzoic acid products presumably arose by hydroxylation of the α-carbon, similar to formation of 4-(1-hydroxyethyl)benzoic acid in the turnovers of 4-ethylbenzoic acid. The 4-(2-hydroxyethyl)benzoic acid may have arisen by halogen oxidation followed by hydrolysis to the alcohol (Figure 78), but also appeared to form by hydrolysis during the HPLC analyses of both the haloethyl substrates.

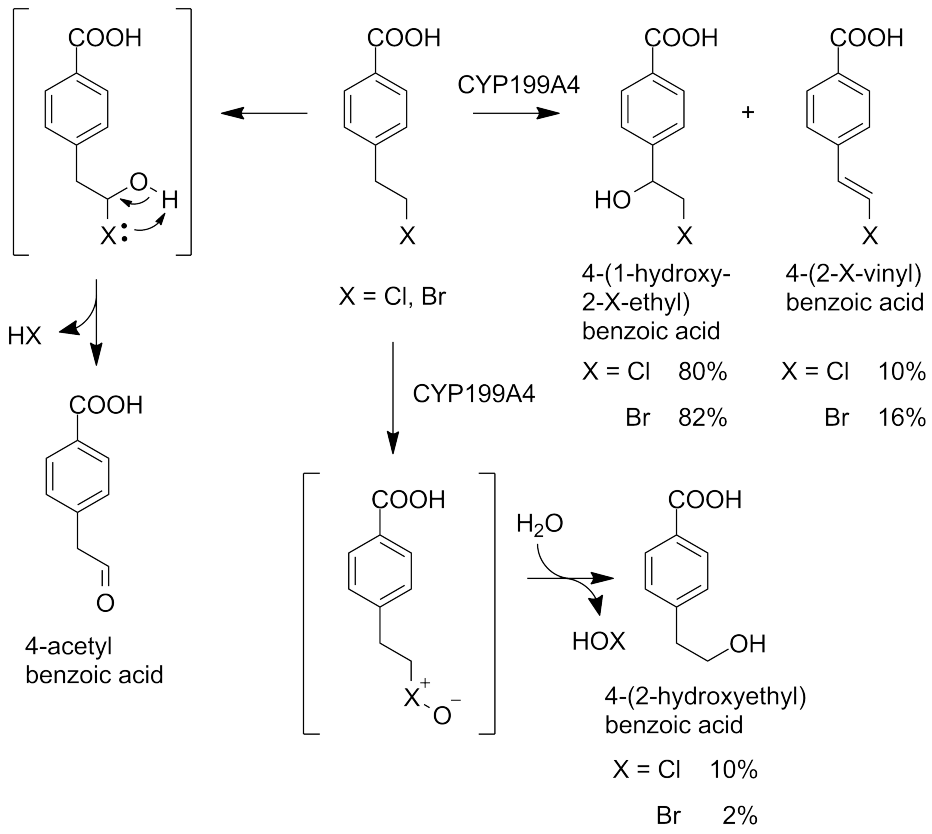

Figure 78. Oxidation of haloethylbenzoic acid substrates by CYP199A4. The proposed dehalogenation mechanisms to 4-(2-hydroxyethyl)benzoic acid and 4-acetylbenzoic acid are shown.

There were no significant levels of H_2O_2 in any of the turnovers (< 2 % of total NADH coupling). The halomethyls were dehalogenated to 4-formylbenzoic acid and the activity of CYP199A4 with these substrates was high. The haloethyls showed poor turnover activity with limited halogen oxidation. It is possible the haloethyl substrates bind in the active site in an orientation that reduces mono-oxygenase activity and the coupling efficiency. Crystal structures of CYP199A4 with these substrates could help elucidate the reasons behind the low activity and the selectivity of these reactions.

4.3 Discussion

The current work has further elucidated the substrate range and expanded the known activities of CYP199A4 with *para*-substituted benzoic acids. A variety of nitrogen and sulfur containing substrates were all able to be efficiently oxidised by CYP199A4, although substituted aminomethylbenzoic acids were not effective substrates. Single and double N-dealkylation, sulfoxidation and amide formation can be added to the known activities of the enzyme. The fastest reaction catalysed by CYP199A4 was sulfoxidation, although the reaction rate decreased dramatically if the alkyl chain was lengthened from methylthio to ethylthio.

4-Methoxybenzoic acid, 4-methylaminobenzoic acid and related nitrogen-containing substrates all underwent dealkylation reactions with CYP199A4. The orientation of the *para* substituent of 4-methylaminobenzoic acid in the active site of CYP199A4 was different to that of the methoxy substituent of 4-methoxybenzoic acid, despite the structural similarities of these compounds. The methyl group and nitrogen atom of 4-methylaminobenzoic acid were held at a comparable distance from the heme iron, unlike in the 4-methoxybenzoic acid structure where the methyl group was held significantly closer. Despite this orientation of the methylamino moiety, no N-oxidation products (either N-oxides or hydroxylamines) were detected in agreement with previous studies on the relative energetics of these reactions. It is important to note that the binding of molecular oxygen and the subsequent oxygen activation steps may result in changes in the orientation of this substituent prior to oxidation.

In the turnovers of 4-dimethylamino-, 4-ethylamino- and 4-diethylamino-benzoic acids, several of the oxidation products are themselves substrates of CYP199A4. These are presumably retained in the active site of CYP199A4, leading to further oxidation. For example 4-methylaminobenzoic acid, formed in the 4-dimethylaminobenzoic acid turnover, binds tightly to CYP199A4 and the rate of product formation is fast (1.6 µM, 669 min^{-1}, Table 7). This accounted for the presence of the 4-aminobenzoic acid double oxidation product. 4-Diethylaminobenzoic acid is deethylated to 4-ethylaminobenzoic acid, which binds more tightly in the enzyme active site than the diethylamino (0.92 µM vs 11 µM).

4-Acetamidobenzoic acid was formed in the turnovers of 4-ethyl- and 4-diethylamino-benzoic acids. Amide formation by other P450 enzymes does not seem to have been previously reported, although hemiaminal (carbinolamine) metabolites have been identified in turnovers of compounds such as N-methylcarbazole,[205–207] propranolol[208] (Figure 79), and more.[209,210] The formation of 4-acetamidobenzoic acid in the CYP199A4 turnovers of the ethylamine substrates could have arisen from hydroxylation to a hemiaminal precursor followed by further oxidation. Hemiaminals typically decompose to a primary amine and an aldehyde.[205,206,208,209] In these cases, there was no report of further oxidation to an amide in competition with dealkylation.

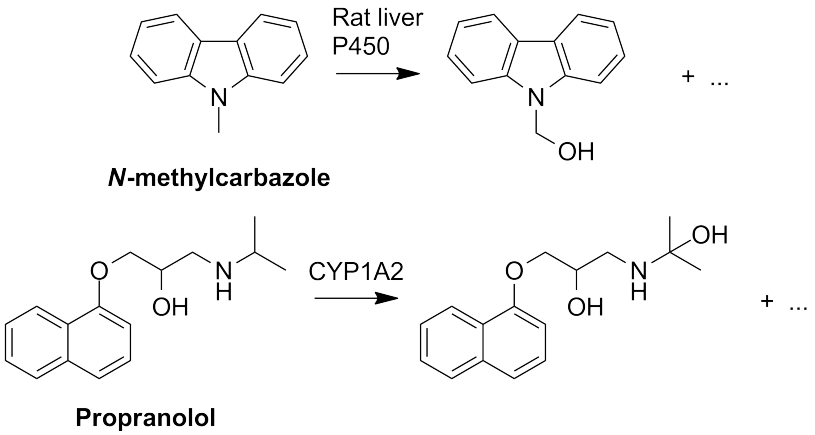

Figure 79. Characteristic examples of hemiaminal formation in P450-catalysed metabolisms.[205–209] In both cases, the hemiaminal was sufficiently stable such that it could be characterised, although subsequently it underwent dealkylation. There was no observation of further oxidation to an amide with these compounds. Other P450 oxidation activities were also reported with these substrates.

Evidentally, the hemiaminal species formed in the turnovers of 4-ethylamino- and 4-diethylaminobenzoic acids was more stable, or was trapped in the enzyme active site long enough to undergo further oxidation by CYP199A4 before hemiaminal decomposition (Figure 80). By way of contrast, 4-formamidobenzoic acid was not observed in the turnovers of either 4-methylamino- or 4-dimethylamino-benzoic acids. The ethylamino hemiaminal must be more stable than the methylamino hemiaminal. The product distribution in the turnovers of N-ethyl substrates indicated that the further oxidation step was able to compete with product release and cleavage of the N−C bond.

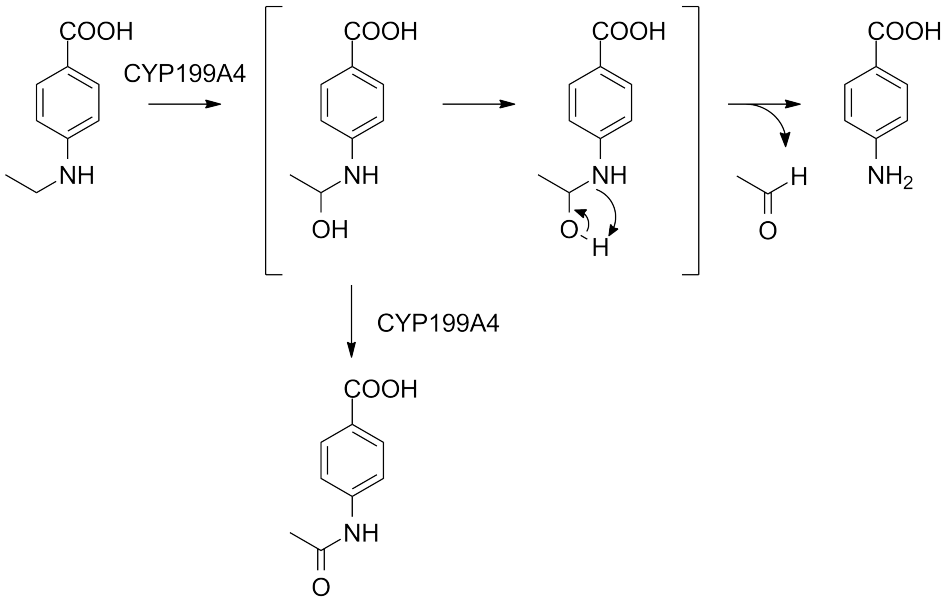

Figure 80. Proposed mechanism for 4-acetamidobenzoic acid formation by CYP199A4 with 4-ethylaminobenzoic acid. The proposed hemiaminal intermediate may be bound to CYP199A4 such that it can undergo a second P450 oxidation. Alternatively, it decomposes to 4-aminobenzoic acid as per the expected dealkylation pathway.

The binding affinity of 4-acetamidobenzoic acid to CYP199A4 is several times weaker than 4-ethylamino- and 4-diethylamino-benzoic acids (62 µM vs 0.92 µM and 11 µM) and has been shown previously to be an inhibitor of CYP199A4 mono-oxygenase activity.[32] In the turnovers of 4-ethylamino- and 4-diethylamino-benzoic acids, the 4-acetamidobenzoic acid may accumulate and bind to the heme, eventually inhibiting CYP199A4. This could be probed further using EPR spectroscopy, which provides information on whether the substrate is interacting with the heme iron.[211]

In the case of formation of 4-acetamidobenzoic acid from 4-diethylaminobenzoic acid, one ethyl group was always removed by the enzyme along with formation of the hemiaminal precursor. Additionally, there was no evidence of diacetamido formation in the 4-diethylaminobenzoic acid turnovers. Co-crystallisation of the 4-ethylamino-, 4-dimethylamino- and 4-diethylamino- substrates with CYP199A4 was unsuccessful. More work towards the solution of these crystal structures would help to elucidate details of the binding of these substrates, and may provide insight into the observed activity and product distributions.

The sulfur-containing substrates underwent oxidation to chiral sulfoxides. The addition of the methylene unit in 4-ethylthiobenzoic acid, which might be expected to facilitate C−H bond abstraction such that dealkylation could occur, did not change the product selectivity, but had the effect of reducing the product formation and enzyme activity. The selectivity for sulfur oxidation was explained in part by the binding orientations of 4-methylthio- and 4-ethylthiobenzoic acids in the crystal structures. The α-carbons were held further from the heme iron than the equivalent of 4-methoxy- and 4-methylamino-benzoic acids (Table 12). The binding of 4-ethylthiobenzoic acid to CYP199A4 resulted in the phenyl ring of F298 moving to accommodate the ethyl group of the *para* substituent. 4-Ethoxybenzoic acid bound in a similar orientation to 4-methoxybenzoic acid, however no movement of any active site residues was required to accommodate it (Chapter 3, Figure 41).

The chiral analysis of the sulfoxidation of 4-ethylthiobenzoic acid demonstrated that one enantiomer was favoured. The enantioselectivity of 4-methylthiobenzoic acid oxidation could not be determined, but would be expected to be similar to 4-ethylthiobenzoic acid. This was rationalised by the position of the sulfur in each crystal structure, where the same face of the sulfur was pointing towards the heme iron (Figures 60 and 62).

There were no oxidation products in the CYP199A4 turnovers of the 4-halobenzoic acids. The *para*-halogen substituent must be unreactive towards Cpd I. The high spin state shifts and tight binding observed in CYP199A4 with each substrate suggest that binding was not the limiting factor. The lack of hydrogen peroxide detected in these turnovers suggested that reductive equivalents were being directed into the formation of water via the oxidase pathway.

Replacement of the *para*-halogen substituent with a halomethyl group led to highly efficient oxidative dehalogenation activity. The major product, 4-formylbenzoic acid,

would arise via hydroxylation of the α-carbon, followed by formation of hydrogen bromide/hydrogen chloride (HX) along with the 4-formylbenzoic acid (Figure 72). The halomethyl substrates may be bound in the enzyme active site in a similar orientation to 4-ethylbenzoic acid[30] (PDB: 4EGM), and hydrogen abstraction at the benzylic C−H bonds must be feasible.

In the turnovers of the 4-(2-haloethyl)benzoic acids, there was a small amount of product arising from halogen oxidation alongside the α-hydroxylation and desaturation activities normally observed with 4-ethylbenzoic acid. The formation of small amounts of haloalkene product in the turnovers indicated that the desaturation pathway is disfavoured compared to 4-ethylbenzoic acid. The low levels of product formation in these substrates compared to 4-ethylbenzoic acid suggests the orientation of the *para*-substituent may be different and has a deleterious effect on the P450 activity. This may be due to the electron-withdrawing halogen atom. The 4-(2-hydroxyethyl)benzoic acid product was presumed to have arisen via hydroxylation of the halogen to a halonium, followed by hydrolysis and formation of a molecule of HOX (Figure 78). Further studies would be required to confirm this reaction pathway. The active site binding orientation of the 4-(2-haloethyl)benzoic acids may position the halogen atom close to the heme iron, enabling this reaction, but may decrease other activities. Crystal structures of the 4-(2-haloethyl)benzoic acid-bound forms of CYP199A4 may explain the lower activity and coupling efficiency observed.

These *para*-substituted haloalkylbenzoic acid substrates could be used to further study the mechanism of halogen oxidation; however the low coupling efficiency and product formation may be a limiting factor. These studies showed that CYP199A4 is capable of supporting limited oxidative dehalogenation activity with very specific substrates, and emphasised the difficulty of halogen oxidation by P450 systems. Reductive dehalogenation activities are also possible with CYP enzymes.[212–216] These haloalkylbenzoic acid substrates could be used to investigate reductive dehalogenation activities with CYP199A4.

Chapter 5 Investigation of the partition of desaturation and hydroxylation

5.1 Introduction

4-Ethyl-, 4-*n*-propyl- and 4-isopropyl-benzoic acids have been shown to undergo both hydroxylation and desaturation reactions with CYP199A4.[27] The latter reaction, yielding an alkene, does not result in oxygen being incorporated into the product (Chapters 1.4.3 and 1.5).[27,28,30] After the initial abstraction of hydrogen, there are two possible alternative steps to radical rebound that result in the alkene: either a second hydrogen abstraction by Cpd II ($[Fe{-}OH]^{3+}$); or electron abstraction by Cpd II to yield a cation and $[Fe{-}OH]^{2+}$ species (Figure 81, labelled in red). The cation would then lose a proton to generate the alkene. The rate of these steps must be comparable to the rate of radical rebound, such that desaturation is competitive with hydroxylation. The ratio of alkene to alcohol is thought to be controlled by the relative stability of the carbocation or radical intermediate (or transition states) formed after the initial hydrogen abstraction.[94,105]

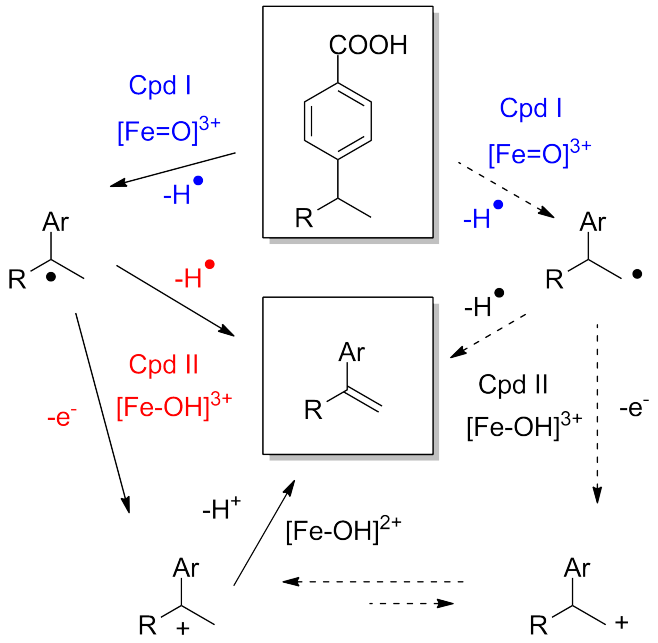

Figure 81. Possible mechanistic pathways for CYP199A4-catalysed desaturation (dehydrogenation) of *para*-substituted benzoic acid substrates. Initial H abstraction occurs at either the α or β carbon (blue). The second step is either a second H abstraction to produce the alkene, or electron transfer to form a cation (red). Proton loss from the cation generates the alkene.

In turnovers of 4-ethyl and 4-isopropylbenzoic acids with CYP199A4, there were α-hydroxylation as well as α,β-desaturation products. In the 4-ethylbenzoic acid turnover, there was also a limited amount of β-hydroxylation (< 5 %). The alkene

product could form from initial abstraction at either the α- or β-carbon (Figure 81, labelled in blue). Abstraction at the benzylic α-carbon would be favoured due to the stability provided by the aromatic system, but the β-carbon is known to be closer to the heme iron from the crystal structure of 4-ethylbenzoic acid-bound CYP199A4.[30] 4-*t*-Butylbenzoic acid has also previously been investigated, and the only product was 4-(1,1-dimethyl-2-hydroxyethyl)benzoic acid, which was unsurprising given the absence of hydrogens on the α-carbon.[28] However, this demonstrated that CYP199A4 could hydroxylate β-methyl groups. 4-*n*-Propylbenzoic acid was oxidised by CYP199A4 to α- and β-hydroxylation products (40 % and 26 %), and there was also a significant amount of α,β alkene formed (34 %).[28] These reactions showed that abstraction from a β-carbon is feasible. No β,γ-alkene or terminal γ-alcohol were generated with 4-*n*-propylbenzoic acid, which suggested that the α- and β- methylene carbons were the preferred sites of oxidation by CYP199A4.[28]

In order to better determine the selectivity of C−H bond abstraction by CYP199A4, a selection of alkyl substituted benzoic acids will be analysed (Figure 82). These substrates will also provide a better understanding of the factors which determine the partition between hydroxylation and desaturation. 4-*n*-Butylbenzoic acid and 4-*n*-heptylbenzoic acid were selected to determine the impact of a longer alkyl chain on product formation. Both substrates contain methylene groups at the β- and γ-positions. 4-Isobutylbenzoic acid will be used to probe the effects of increased branching at the β-position, which would energetically favour oxidation at this position. 4-Cyclopropyl- and 4-cyclohexylbenzoic acid will be used to investigate how cycloalkane moieties effect the hydroxylation and desaturation activities.

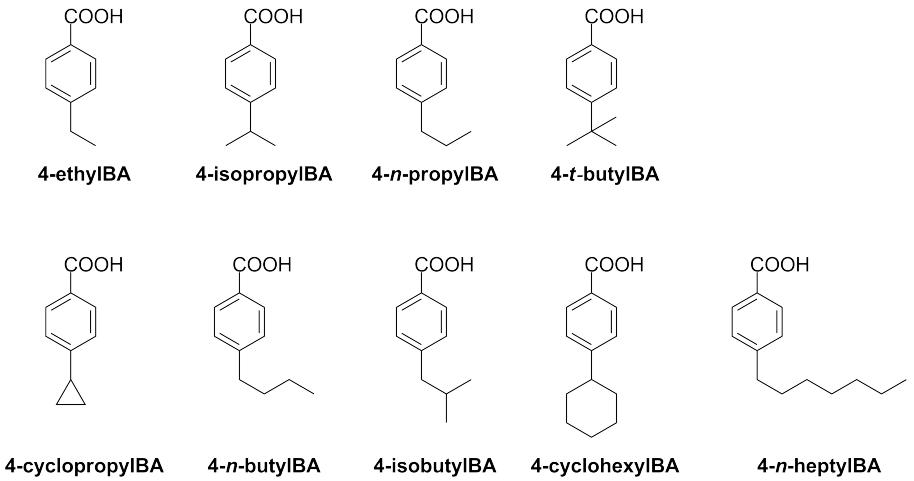

Figure 82. *Para*-alkyl substituted benzoic acid substrates investigated with CYP199A4. The top row have been previously investigated.[27,28,30]

5.2 Results

5.2.1 Substrate binding assays

To assess if each substrate could bind in the active site and displace the distal heme water ligand of CYP199A4, the spin state shift was determined (Chapter 2.3). 4-Ethyl and 4-isopropyl-benzoic acids have already been shown to induce $\geq$ 95 % spin state shifts in CYP199A4,[30] suggesting that the distal water ligand was effectively removed. When the other substrates were investigated, it was found that each displayed a spin state shift that was 90 % or larger (Table 15, Figure 83 and Appendix C.1). 4-*t*-Butylbenzoic acid, which possessed a fully substituted quaternary carbon, shifted the spin state of CYP199A4 to 90 %, which was the same shift observed with the linear 4-*n*-butylbenzoic acid. The largest substrates, 4-cyclohexyl- and 4-*n*-heptyl-benzoic acids, induced $\geq$ 95 % spin state shifts.

Table 15. Spin state shift and dissociation constant analyses (% HS and K_d, Chapter 2.3) for alkyl substituted benzoic acids (BA) investigated with CYP199A4.

Substrate	HS (%)	K_d (µM)
4-ethylBA[27]	$\geq$ 95	0.34 ± 0.02
4-isopropylBA	$\geq$ 95	0.29 ± 0.01
4-*n*-propylBA[28]	$\geq$ 95	0.04 ± 0.02
4-*t*-butylBA[28]	90	39 ± 2
4-cyclopropylBA	$\geq$ 95	0.28 ± 0.02
4-*n*-butylBA	90	0.39 ± 0.04
4-isobutylBA	$\geq$ 95	0.59 ± 0.03
4-cyclohexylBA	$\geq$ 95	0.45 ± 0.05
4-*n*-heptylBA	$\geq$ 95	0.16 ± 0.03

The binding affinity of CYP199A4 for each substrate was investigated by determining the dissociation constants with CYP199A4 (K_d, Table 15, Chapter 2.3). The *para*-alkyl substrates displayed tight binding, which was similar to results for 4-ethylbenzoic acid (0.34 µM) and 4-isopropylbenzoic acid (0.29 µM). 4-*n*-Propylbenzoic acid bound several times tighter than either (Appendix C.2, 0.04 µM),[28] which signified that an *n*-propyl moiety is preferred over the more substituted isopropyl group. The binding affinity of 4-*t*-butylbenzoic acid (Appendix C.2, 39 µM) was 100-fold weaker than 4-isopropylbenzoic acid,[28] presumably due to the steric bulk caused by the tertiary *t*-butyl moiety.

4-Cyclopropylbenzoic acid bound comparably tightly to 4-isopropylbenzoic acid (Figure 84a, 0.28 µM vs 0.34 µM), revealing that the cyclopropyl ring was a good fit in the active site of CYP199A4. The binding affinity of CYP199A4 for 4-*n*-butylbenzoic acid was also high (Figure 84b, 0.39 µM), with that of the more sub-

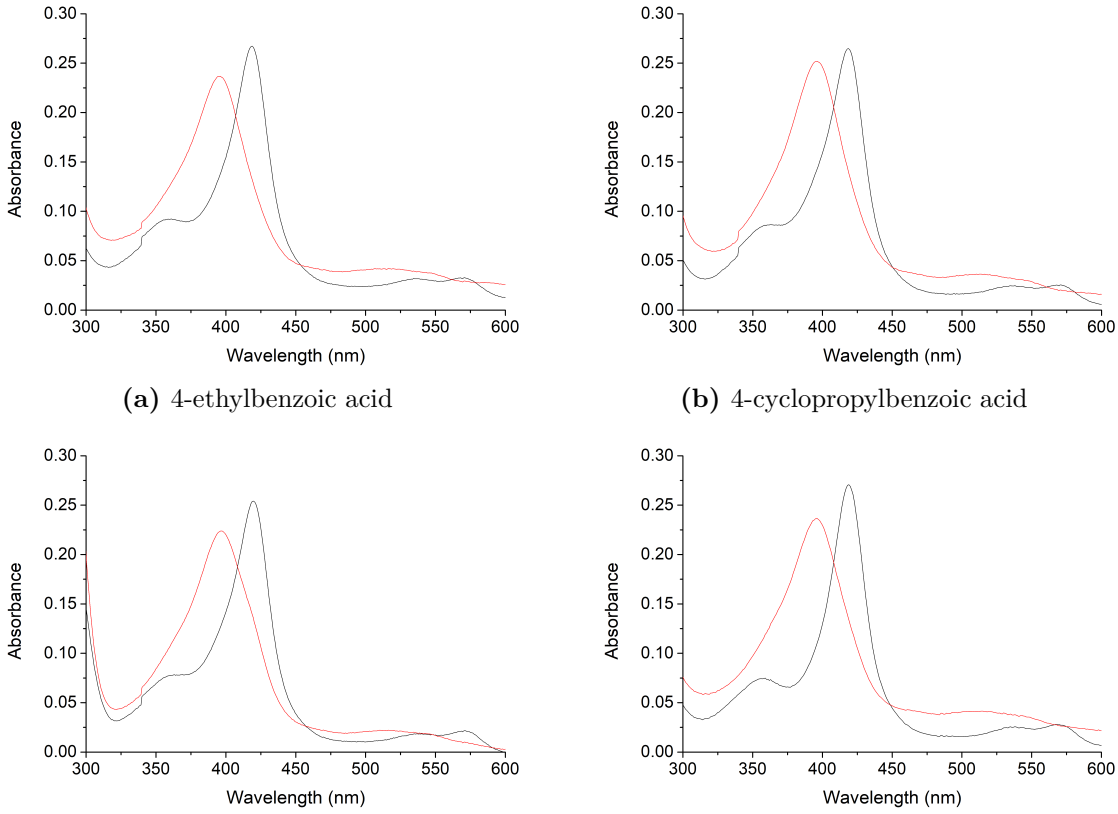

(a) 4-ethylbenzoic acid

(b) 4-cyclopropylbenzoic acid

(c) 4-*n*-butylbenzoic acid

(d) 4-*n*-heptylbenzoic acid

Figure 83. Spin state shifts of selected *para*-alkyl substituted benzoic acid substrates with CYP199A4. Black shows CYP199A4 in its resting state, red shows the maximum absorbance shift obtained upon addition of substrate.

stituted 4-isobutylbenzoic acid being marginally lower (Appendix C.2, 0.59 µM). 4-Cyclohexylbenzoic acid bound to CYP199A4 with almost as high affinity (Figure 84c, 0.45 µM) as 4-ethylbenzoic acid and 4-cyclopropylbenzoic acid. CYP199A4 was also able to bind 4-*n*-heptylbenzoic acid very tightly (Figure 84d, 0.16 µM). The enzyme must possess a degree of flexibility in its active site to be able to accommodate the substrates with these larger *para*-alkyl groups.

Overall, the binding studies showed that longer alkyl chain benzoic acids could be substrates of CYP199A4. The substrate which contained a more highly substituted tertiary group displayed significantly lower binding affinity.

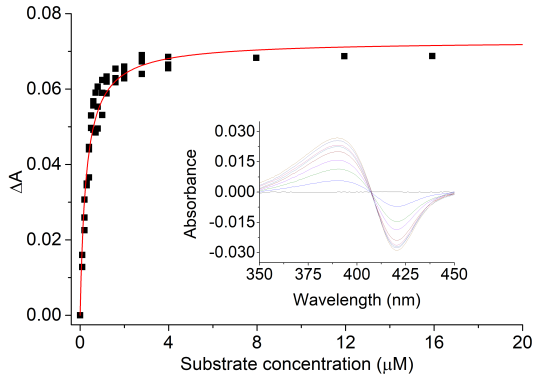

(a) 4-cyclopropylbenzoic acid (420 nm, 390 nm, 0.5 µM)

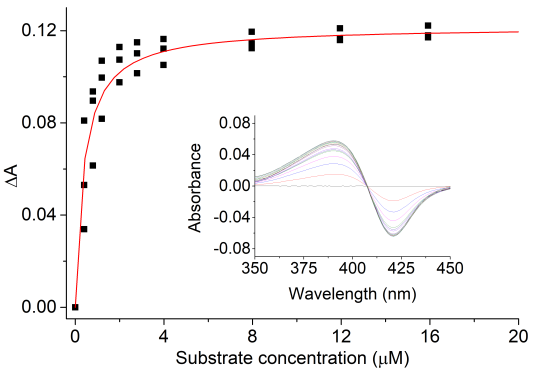

(b) 4-*n*-butylbenzoic acid (421 nm, 391 nm, 1.2 µM)

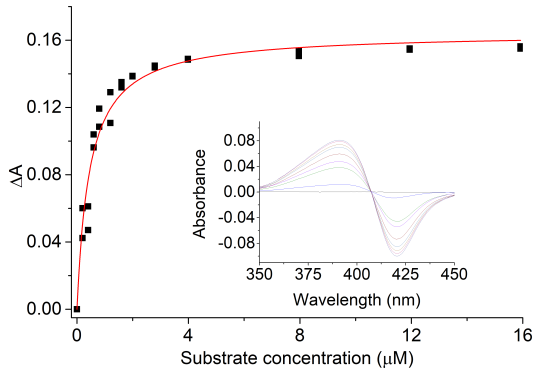

(c) 4-cyclohexylbenzoic acid (421 nm, 391 nm, 1.5 µM)

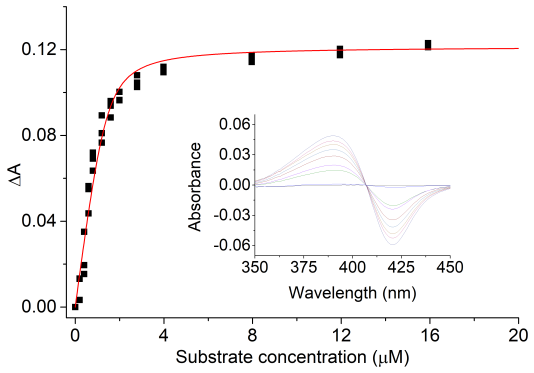

(d) 4-*n*-heptylbenzoic acid (420 nm, 390 nm, 1.2 µM)

Figure 84. Dissociation constant determination of selected alkylbenzoic acid benzoic acids investigated with CYP199A4. The inset image shows the UV-Vis response to addition of aliquots of substrate. Shown in brackets are the wavelengths of the trough and peak, and the enzyme concentration used for dissociation constant analysis (trough, peak, µM-P450).

5.2.2 Activity and product formation

In vitro oxidation assays using the CYP199A4 system were performed with each substrate, using NADH as the source of reducing equivalents (Chapter 2.4). The turnovers were then analysed for product formation by HPLC and GC-MS. Semi-prep HPLC was used to isolate the products, followed by characterisation using NMR spectroscopy. The isolated products were then coeluted using HPLC to confirm the identity of each peak in the turnover. The product distribution and coupling efficiency were then calculated (Chapter 2.5).

Table 16. Turnover parameters determined for alkyl substituted benzoic acid (BA) analogues investigated with CYP199A4. Shown are NADH oxidation rates (Chapter 2.4), product formation rates (PFR, Chapter 2.5) and coupling efficiency (%). Rates are given as mol (molCYP)$^{-1}$ min^{-1}.

Substrate	NADH[a]	PFR[b]	Coupling[c]
4-ethylBA [27]	812 ± 7	525 ± 88	64 ± 4
4-isopropylBA	325 ± 36	221 ± 27	68 ± 1
4-*n*-propylBA [28]	688 ± 24	594 ± 72	86 ± 8
4-*t*-butylBA [28]	227 ± 4	227 ± 32	100 ± 13
4-cyclopropylBA	383 ± 8	170 ± 22	45 ± 5
4-*n*-butylBA	167 ± 6	67 ± 3	40 ± 1
4-isobutylBA	359 ± 46	146 ± 21	41 ± 5
4-cyclohexylBA	169 ± 11	52 ± 6	33 ± 2
4-*n*-heptylBA	278 ± 15	147 ± 12	53 ± 2

[a]NADH oxidation rate. [b]PFR: product formation rate. [c]% of NADH consumed that led to formation of substrate metabolite. In each case, these metabolites were calibrated using HPLC against the closest available of the following: 4-(1-hydroxyethyl)BA, 4-(2-hydroxyethyl)BA or 4-vinylBA.

The NADH oxidation rate of CYP199A4, which is used as a measure of the turnover frequency of the P450 catalytic cycle, was the highest with 4-ethylbenzoic acid of all those measured at 812 mol (molCYP)$^{-1}$ min^{-1} (Henceforth abbreviated to min^{-1}). All other substrates induced slower oxidation rates (Table 16), which varied from 167 min^{-1} to 688 min^{-1}. There was no obvious trend between the binding affinity, size or degree of substitution of the *para*-alkyl substituent with the NADH oxidation rate. HPLC and GC-MS analysis showed that all substrates investigated were oxidised by CYP199A4 to yield one or more oxidation products. To determine the coupling efficiency, calibrations were performed using HPLC against the most similar of the following compounds: 4-(1-hydroxyethyl)-, 4-(2-hydroxyethyl)- or 4-vinyl-benzoic acid (Chapter 2.5, Table 2). In all cases, a small amount of H_2O_2 ($\leq$ 2 % of NADH equivalents) was detected at the conclusion of the *in vitro* turnovers (Chapter 2.7) and thus there was minimal uncoupling via the hydrogen peroxide pathway. Therefore, any remaining uncoupling was most probably accounted for by the oxidase pathway (Chapter 1.3).

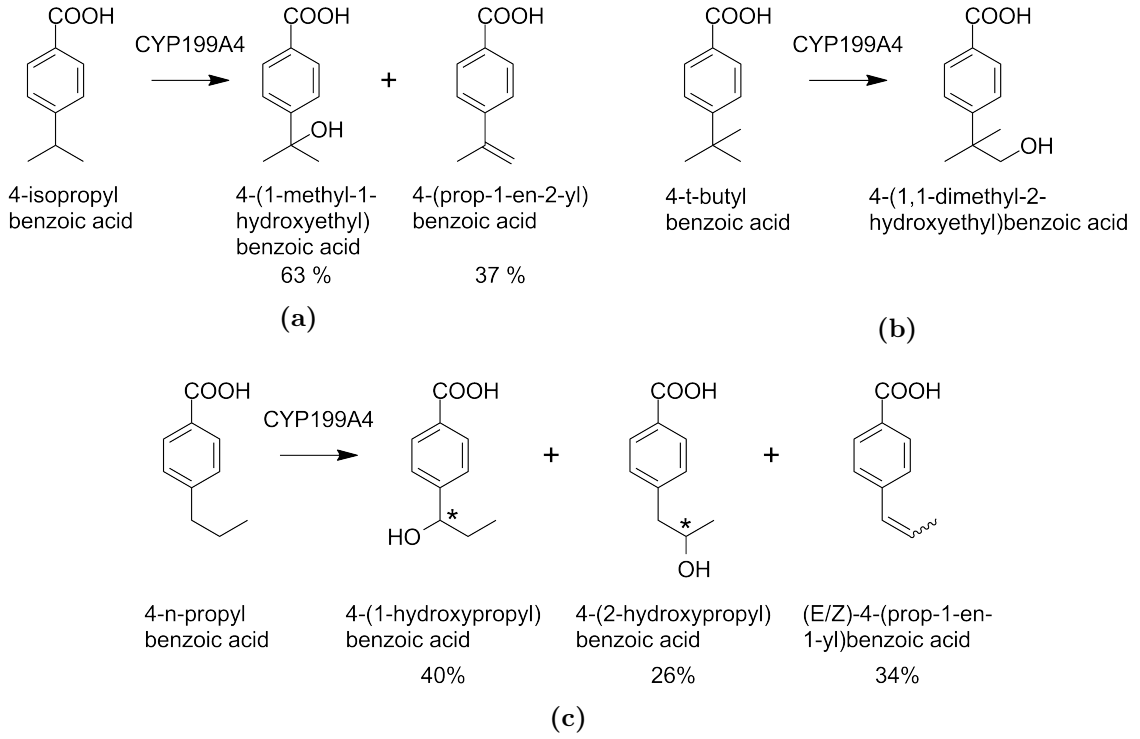

Figure 85. Turnover products of (a) 4-isopropyl-, (b) 4-*t*-butyl- and (c) 4-*n*-propyl-benzoic acids by CYP199A4.[28] The 4-*n*-propyl alkene was assigned using GC-MS, and the stereochemistry was not able to be determined using the NMR spectrum obtained previously.[28] The stereocentres are labelled (*).

The CYP199A4 oxidation products of 4-isopropylbenzoic acid have been previously reported (Figure 85a)[30] as 4-(1-methyl-1-hydroxyethyl)benzoic acid (63 %), and 4-(prop-1-en-2-yl)benzoic acid (37 %). The oxidation products of 4-*n*-propylbenzoic acid have been determined (Figure 85c)[28] to be 4-(1-hydroxypropyl)benzoic acid (40 %), 4-(prop-1-en-1-yl)benzoic acid (34 %) and 4-(2-hydroxypropyl)benzoic acid (26 %). The *in vitro* CYP199A4 turnover of 4-*t*-butylbenzoic acid formed one product (Figure 85b), 4-(1,1-dimethyl-2-hydroxyethyl)benzoic acid (100 %). The turnover data for these substrates have been included in Table 16 for comparison.

The major products of 4-ethylbenzoic acid oxidation by CYP199A4 have been previously reported by GC analysis as 4-(1-hydroxyethyl)benzoic acid and 4-vinylbenzoic acid.[28,30] The majority of the reducing equivalents of NADH were channelled into product formation (PFR, 525 min^{-1}, 64 % coupling of NADH). The products were confirmed against authentic standards using HPLC (Figure 86). 4-(2-Hydroxyethyl)benzoic acid, 4-acetylbenzoic acid, and 4-(oxiran-2-yl)benzoic acid were also detected by HPLC. The 4-(1-hydroxyethyl)benzoic acid product (42 %) and 4-(2-hydroxyethyl)benzoic acid (3 %) are formed by hydroxylation. Desaturation of the α,β carbons would have formed 4-vinylbenzoic acid (37 %). Further oxidation of 4-(1-hydroxyethyl)benzoic acid would form 4-acetylbenzoic acid (1 %), while further oxidation of 4-vinylbenzoic acid would yield 4-(oxiran-2-yl)benzoic acid (17 %). The presence of the 2-hydroxyethyl hydroxylation product indicated that initial radical abstraction was, to a limited extent, occurring at the β-carbon.

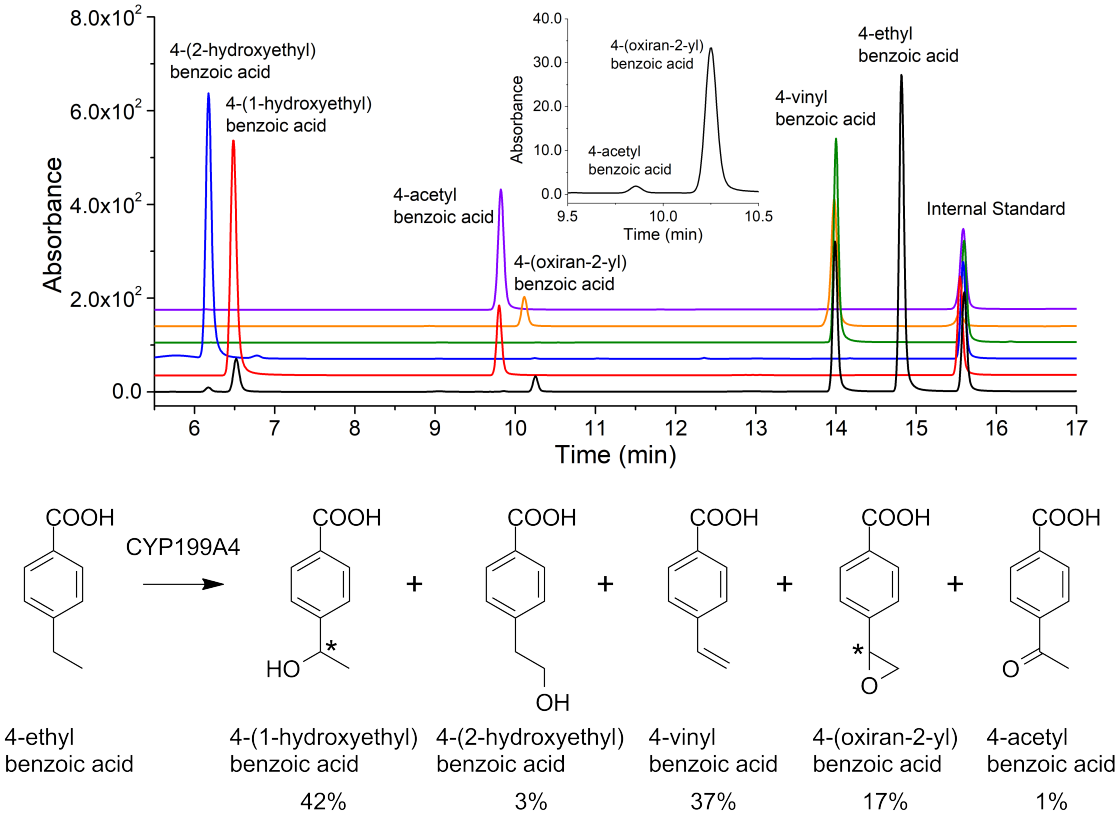

Figure 86. HPLC analysis of 4-ethylbenzoic acid turnover by CYP199A4. **Black**, *in vitro* turnover; red, 4-(1-hydroxyethyl)benzoic acid, RT = 6.5 min; blue, 4-(2-hydroxyethyl)benzoic acid, RT = 6.2 min; green, 4-vinylbenzoic acid, RT = 14.0 min; orange, turnover of 4-vinylbenzoic acid showing 4-(oxiran-2-yl)benzoic acid peak at 10.2 min;[32] purple, 4-acetylbenzoic acid control, RT = 9.8 min. A 20-95 % gradient of H_2O:ACN was used and the chromatogram was monitored at 254 nm. The inset shows the further oxidation products in the *in vitro* turnover, highlighting the small amount of 4-acetylbenzoic acid formed.

4-Cyclopropylbenzoic acid was oxidised by CYP199A4 at a lower product formation rate than 4-ethyl and 4-isopropylbenzoic acids (170 min^{-1} vs 525 min^{-1} and 221 min^{-1}, respectively). The coupling efficiency of the 4-cyclopropylbenzoic acid turnover was also reduced compared to these substrates (45 % vs 64 % and 68 %, respectively).

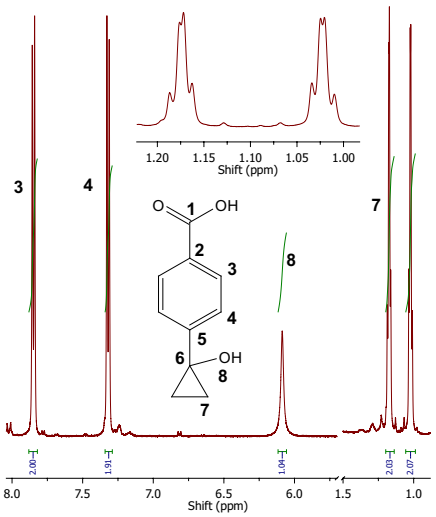

Figure 87. ^{1}H NMR spectrum of 4-(1-hydroxycyclopropyl)benzoic acid.

HPLC analysis showed a single product with a retention time characteristic of an alcohol (Figure 88, RT = 9.8 min). This was supported by GC-MS of the TMS-derivatised turnover (m/z = 322.00 vs expected 322.14, Appendix C.3). NMR analysis confirmed the product was 4-(1-hydroxycyclopropyl)benzoic acid (Figure 87). The ^{13}C signal at 57.41 ppm (C_α), no longer had an associated ^{1}H signal (Appendix C.4). The aromatic and cyclopropyl ring β-hydrogen signals were retained, which permitted simple characterisation. There was no evidence of any alkene (or desaturation) metabolites.

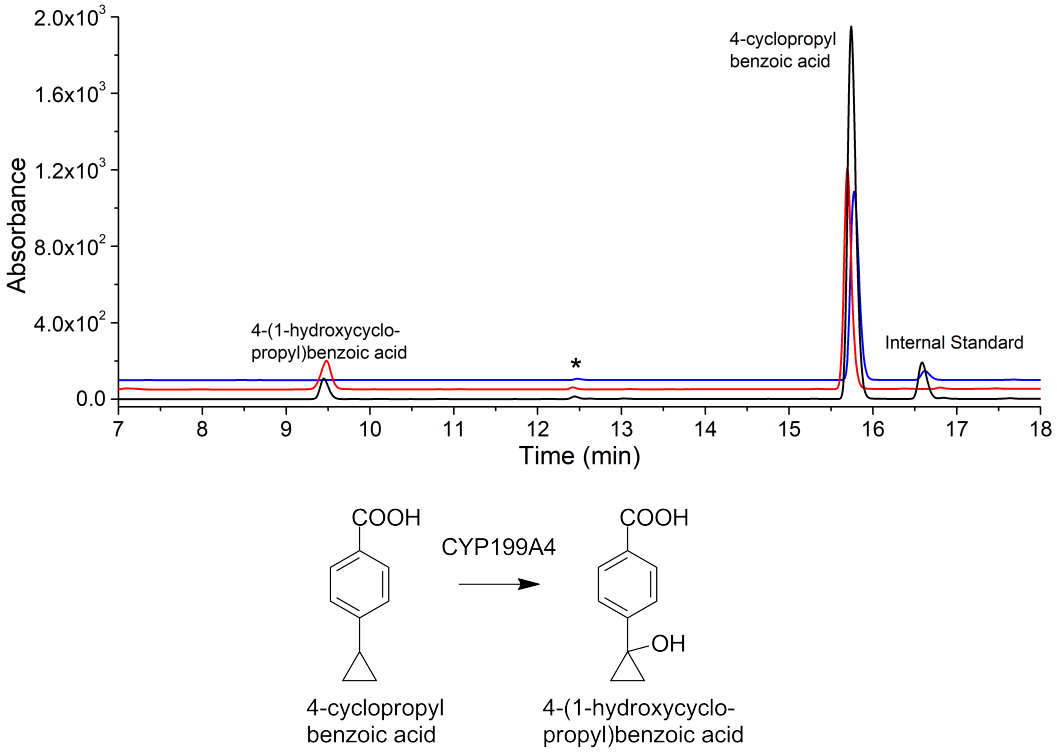

Figure 88. HPLC analysis of 4-cyclopropylbenzoic acid turnover with CYP199A4. **Black**, *in vitro* turnover; red, *in vivo* turnover; blue, substrate control, RT = 15.8 min. An impurity in the substrate is marked (*). A 20-95 % gradient of H_2O:ACN was employed. The chromatogram was monitored at 254 nm.

CYP199A4 oxidised 4-*n*-butylbenzoic acid with a slower NADH oxidation rate (167 min^{-1}) and product formation rate (67 min^{-1}) than the shorter linear alkyl substrates, 4-ethyl- and 4-*n*-propyl-benzoic acids (NADH, 812 min^{-1}, PFR, 525 min^{-1}; NADH, 688 min^{-1}, PFR, 594 min^{-1}, respectively). The coupling efficiency was 40 % (Table 16). HPLC analysis of the *in vitro* turnover revealed four peaks arising from enzymatic oxidation of the substrate (Figure 89). These were produced using an *in vivo* turnover (Chapter 2.6), and three were able to be isolated and characterised using NMR (Appendix C.4). They were (E)-4-(but-1-en-1-yl)benzoic acid (50 %), 4-(1-hydroxybutyl)benzoic acid (46 %) and (E)-4-(3-hydroxybut-1-en-1-yl)benzoic acid (4 %). The masses of the TMS-derivatised products observed via GC-MS supported these product assignments (Appendix C.3).

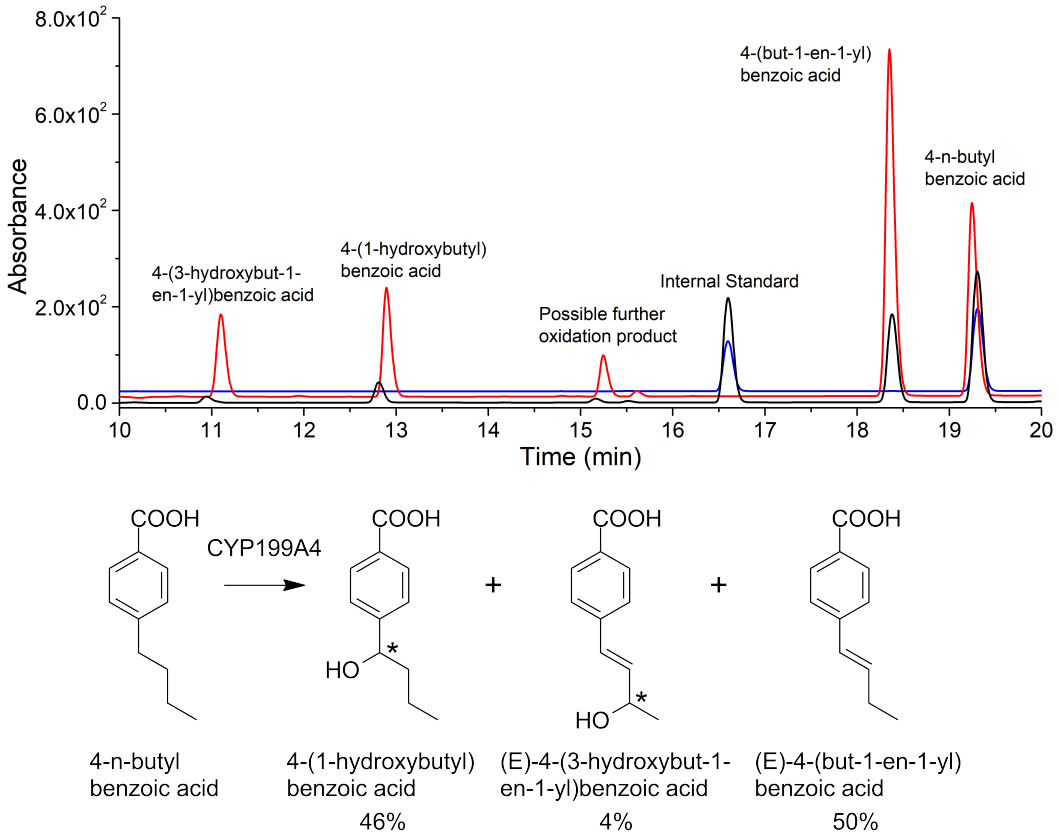

Figure 89. HPLC analysis of 4-*n*-butylbenzoic acid turnover with CYP199A4. **Black**, *in vitro* turnover; red, *in vivo* turnover; blue, substrate control, RT = 19.4 min. There was an unidentified product peak at 15.2 min. The gradient was 20-95 % H_2O:ACN, and the chromatogram was collected at 254 nm.

The (E) stereochemistry of the alkene was assigned based on the large coupling constant observed for the vinylic protons of 4-(3-hydroxybut-1-en-1-yl)benzoic acid (J = 15.9 Hz, Figure 90, Appendix C.4), and by comparison of the 4-(but-1-en-1-yl)benzoic acid product to literature for alkylbenzoic acids. It was found that (E)-alkenes displayed overlapping vinylic ^1H signals while (Z)-alkene signals were clearly separated.[217,218]

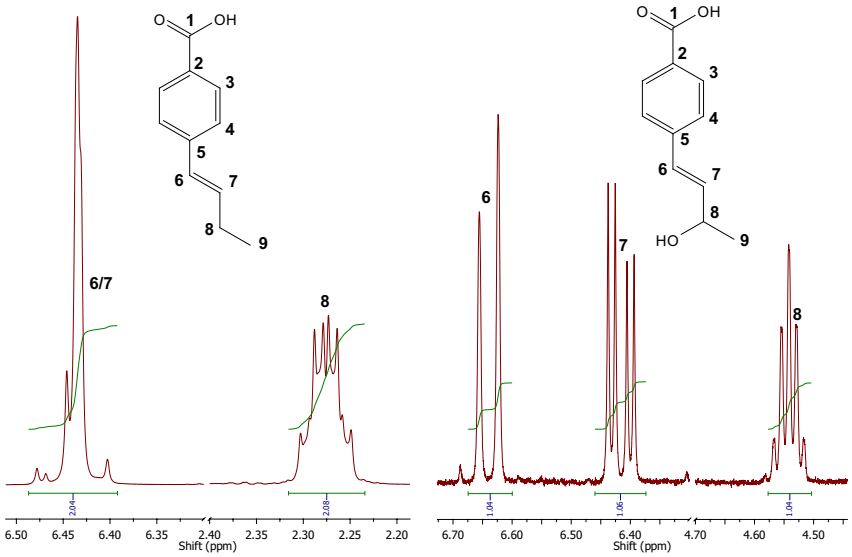

Figure 90. A portion of the ^{1}H NMR spectra of the 4-*n*-butylbenzoic acid alkene products. Shown are (left), 4-(but-1-en-1-yl)benzoic acid and (right), 4-(3-hydroxybut-1-en-1-yl)benzoic acid. The large coupling constant observed for the γ-hydroxylated alkene (right) indicated an (E)-alkene geometry, which suggested the alkene product (left) was probably also an (E)-alkene. Literature for benzoic acid (E)-alkenes shows that the vinylic protons are usually overlapped.[217,218]

In contrast to the other linear alkylbenzoic acids (C_2, C_3, C_7), no formation of a β-hydroxylation product was detected. The major product was α,β-desaturation, with the α-hydroxylation product being formed in a comparable yield. The double oxidation minor product, (E)-4-(3-hydroxybut-1-en-1-yl)benzoic acid, presumably arose from hydroxylation of the alkene product at the γ-carbon. The alkene product must bind or be retained in the active site such that another oxidation cycle can occur, and it must bind in a position which favours γ-hydroxylation over epoxide formation. The peak at 15.2 min in the HPLC of both *in vitro* and *in vivo* turnovers was not able to be isolated, and was not observed in the *in vitro* GC-MS chromatogram. Based on its HPLC retention time, combined with the increase in yield during the *in vivo* oxidation (Figure 89), this peak was probably a further oxidation product such as an epoxide or ketone.

4-Isobutylbenzoic acid CYP199A4 turnovers displayed a higher product formation rate than 4-*n*-butylbenzoic acid and a comparable coupling efficiency (146 min^{-1}, 41 %, vs 67 min^{-1}, 40 %, Table 16). HPLC analysis of the *in vitro* turnovers indicated three products were formed (Figure 91). These were isolated using semi-prep HPLC and characterised using NMR to be 4-(1-hydroxy-2-methylpropyl)benzoic acid (54 %), 4-(2-hydroxy-2-methylpropyl)benzoic acid (41 %) and 4-(2-methylprop-1-en-1-yl)benzoic acid (5 %). The masses observed using GC-MS in a TMS-derivatised

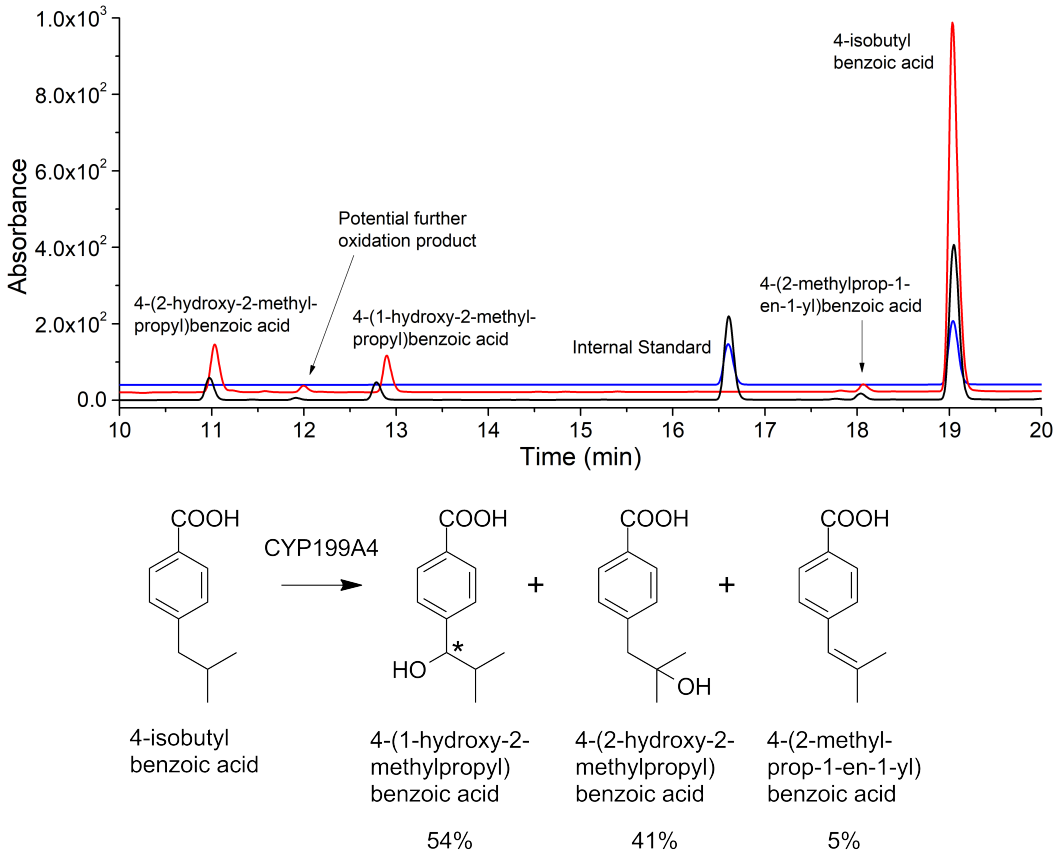

Figure 91. HPLC analysis of 4-isobutylbenzoic acid turnover with CYP199A4. **Black**, *in vitro* turnover; red, *in vivo* turnover; blue, substrate control, RT = 19.1 min. A 20-95 % gradient of H_2O:ACN was employed, and the chromatogram was monitored at 254 nm.

turnover supported these product assignments (Appendix C.3). The mass of 4-(2-hydroxy-2-methylpropyl)benzoic acid was 251.20 (rather than the expected mass of 338.17), which suggested it was undergoing only a single derivatisation rather than the expected double derivatisation (Appendix C.3). Presumably the reactive carboxylate group has been derivatised while the alcohol at the sterically hindered β-carbon has not. An additional product peak at 12.0 min, which was formed in the *in vivo* turnover, was observed but was too low yielding to isolate (Figure 91). It was not observed in the GC-MS chromatogram and was suspected to be either a further oxidation product such as an epoxide or ketone, or a γ-alcohol of the substrate or alkene. It is noteworthyl that with this substrate there was a larger amount of β-hydroxylation product compared to other turnovers.

CYP199A4 oxidation of 4-cyclohexylbenzoic acid proceeded with a product formation rate of 52 min^{-1}, and the coupling was 33 % (Table 16). HPLC analysis of the *in vitro* turnovers of 4-cyclohexylbenzoic acid displayed three products (Figure 92), two of which were likely to be alcohols (RT = 14.6 min, 33 %; and RT = 13.7 min, 66 %) and a third which could be an alkene (RT = 20.2 min, < 1 %).

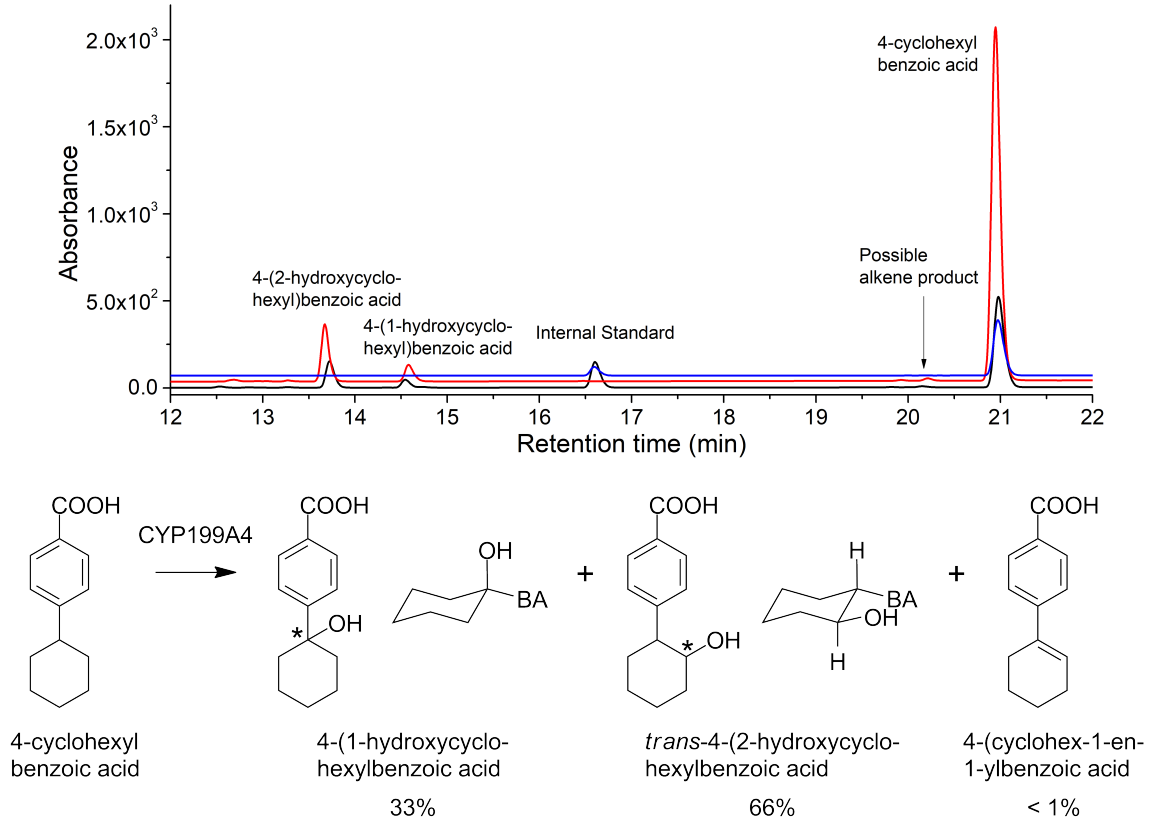

Figure 92. HPLC analysis of 4-cyclohexylbenzoic acid turnover with CYP199A4. **Black**, *in vitro* turnover; blue, substrate control, RT = 21.0 min. A 20-95 % gradient of H_2O:ACN was monitored at 254 nm. The two additional small peaks at 12.5 min and 13.3 min may be minor products. The chair conformers show the relative stereochemistry of the cyclohexyl ring of each product, as determined by NMR analysis.

Using an *in vivo* turnover, sufficient amounts of the two alcohols were obtained for NMR characterisation, which confirmed these products were 4-(1-hydroxycyclohexyl)benzoic acid and 4-(2-hydroxycyclohexyl)benzoic acid (Appendix C.4). The alkene product was not formed in large enough yield to be characterised, but was presumed to be 4-(cyclohex-1-en-1-yl)benzoic acid based on the positions of hydroxylation and desaturation observed with the other alkylbenzoic acids. GC-MS analysis of the TMS-derivatised turnover (Figure 93) showed a small peak at 18.6 min with a mass corresponding to the alkene (m/z = 274.10 vs expected 274.14). The major product masses were 364.10 (RT = 19.5 min) and 364.05 (RT = 20.0 min) compared to the expected mass of a double TMS-derivatised hydroxylation metabolite, 364.19 (Appendix C.3). Compared to the HPLC, the product peak for the 1-hydroxy product was very small. A larger peak, which corresponded to the singly TMS-derivatised 4-(1-

hydroxycyclohexyl)benzoic acid product, suggested that the sterically hindered alcohol was difficult to derivatise.

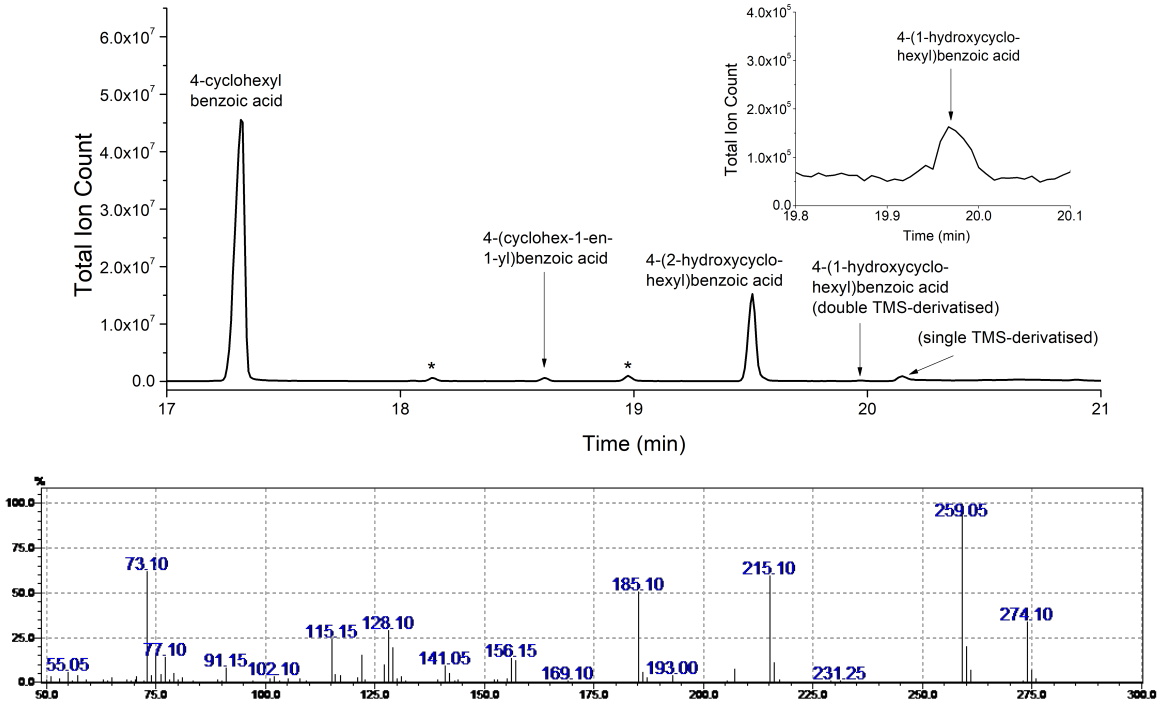

Figure 93. GC-MS analysis of *in vitro* 4-cyclohexylbenzoic acid turnover with CYP199A4. Impurity peaks (present in no P450 control reactions) are marked with an asterix. The mass spectrum of 4-(cyclohex-1-en-1-yl)benzoic acid is also shown (RT = 18.6 min). The loss of 2 mass units from the substrate was indicative of an alkene product. Observed m/z = 274.10 vs expected 274.14. The remaining mass spectra are presented in Appendix C.3.

^{1}H NMR coupling constants were used to assign the relative stereochemistry of the benzoic acid and hydroxyl groups in the case of the 2-hydroxycyclohexyl product. The peak at 2.42 ppm, which corresponds to the benzylic hydrogen, appears as as a multiplet. It has two comparably large coupling constants (J = 11.1 Hz) and one smaller (J = 2.9 Hz). This implies there were two axial-axial interactions with adjacent axial hydrogens (Figure 94, Appendix C.4). One of these axial-axial couplings is derived from the β-carbon where the OH is attached and thus the product was assigned as *trans*-4-(2-hydroxycyclohexyl)benzoic acid. The benzoic acid moiety in both hydroxylation products would be positioned equatorially and would prevent ring-flipping.[181]

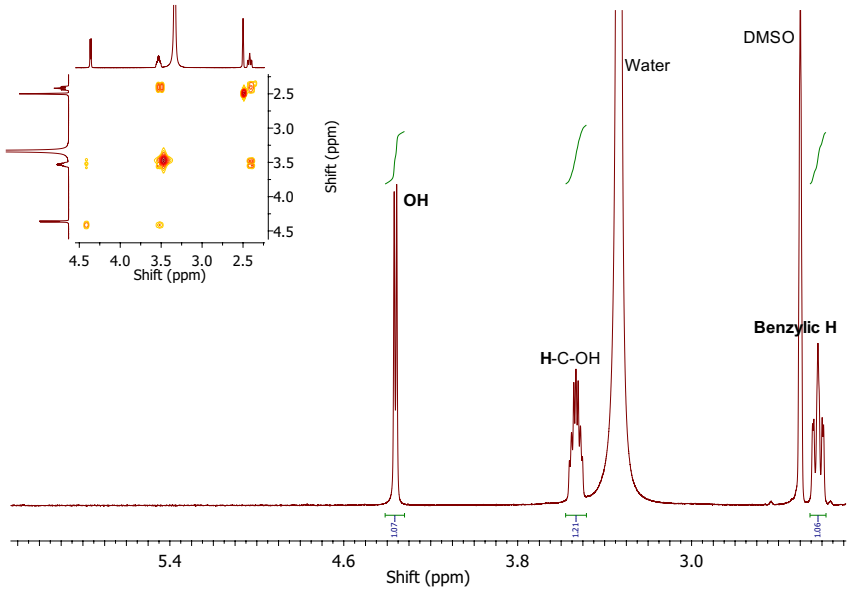

Figure 94. NMR analysis of 4-(2-hydroxycyclohexyl)benzoic acid. Shown are the ^{1}H and ^{1}H-^{1}H COSY (inset), highlighting the benzylic hydrogen (2.42 ppm, J = 2.9, 11.1, 11.1 Hz). The two large couplings observed suggested that there were two axial-axial interactions.

The total coupling efficiency of the CYP199A4 catalysed 4-*n*-heptylbenzoic acid oxidation was 53 %, and the product formation rate was 147 min^{-1}. This was faster than 4-*n*-butylbenzoic acid (67 min^{-1}) but slower than both 4-ethyl- and 4-*n*-propylbenzoic acid (525 min^{-1} and 594 min^{-1} respectively). HPLC analysis of the *in vitro* turnovers revealed at least 5 identifiable product peaks (Figure 95). These were produced in higher yield using an *in vivo* turnover, were isolated by semi-prep HPLC and characterised using a combination of GC-MS (Appendix C.3) and NMR (Appendix C.4). Two additional peaks which had the potential to be oxidation products were found in the whole-cell turnovers (Figure 95, RT = 15.5 min and 16.2 min), but these were

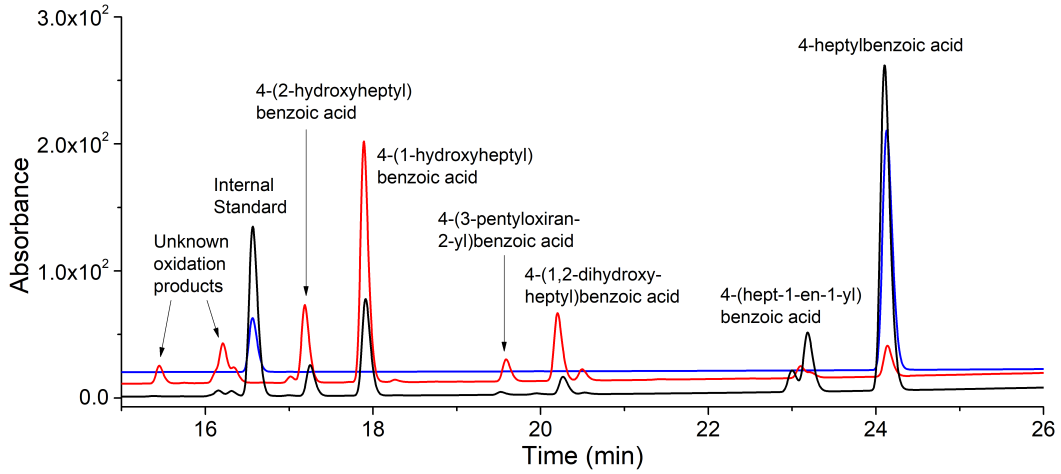

Figure 95. HPLC analysis of 4-*n*-heptylbenzoic acid turnover with CYP199A4. **Black**, *in vitro* turnover; red, *in vivo* turnover; blue, substrate control, RT = 24.2 min. A 20-95 % gradient of H_2O:ACN was employed, and the chromatogram was collected at 254 nm.

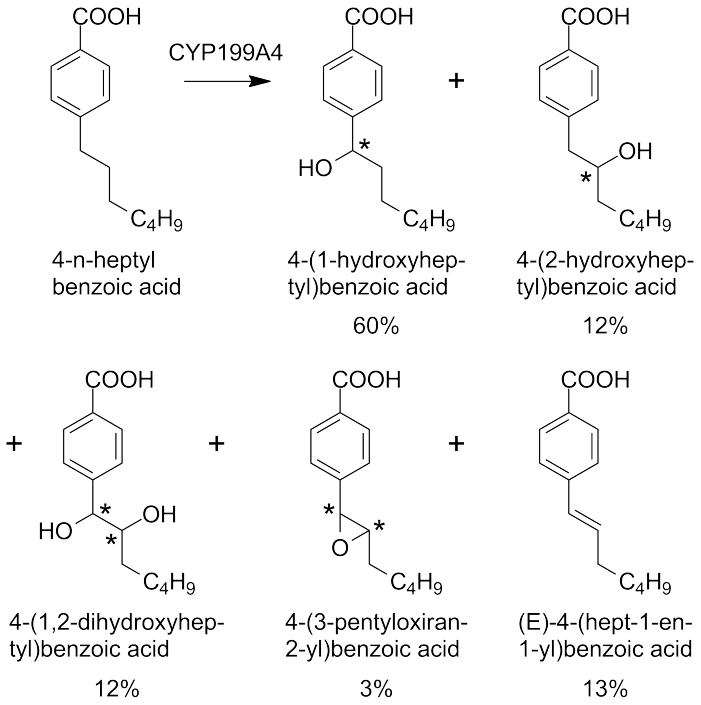

Figure 96. Products of 4-*n*-heptylbenzoic acid turnover. The α,β-alkene stereochemistry was rationalised by comparison to literature data, where the ^{1}H signals of (E)-alkenes tended to overlap.[217,218]

not able to be isolated in sufficient yield to allow their characterisation by NMR or GC-MS. The products were identified as 4-(1-hydroxyheptyl)benzoic acid (60 %), 4-(2-hydroxyheptyl)benzoic acid (12 %), 4-(1,2-dihydroxyheptyl)benzoic acid (12 %), 4-(3-pentyloxiran-2-yl)benzoic acid (3 %) and (E)-4-(hept-1-en-1-yl)benzoic acid (13 %, Appendix C.4). The primary product was hydroxylation at the α-carbon, with smaller amounts of β-hydroxylation and α,β-desaturation (Figures 96, 97, 98). The amount of β-hydroxylation product observed (12 %) was less than that found in turnovers of 4-*n*-propylbenzoic acid (26 %), but more than the turnovers of 4-ethyl- (3 %) and 4-*n*-butylbenzoic acid (no β-hydroxylation).

The alkene stereochemistry was assigned as the (E)-isomer by comparison to literature data for alkylbenzoic acids, where the vinylic ^{1}H signals of (E)-alkenes tended to overlap (Figure 98). In contrast, (Z)-alkene signals were typically able to be resolved.[217,218] Also observed in the ^{1}H spectrum for the alkene product were signals at 5.78 ppm, 7.39 ppm and 7.91 ppm which could be a small amount of a (Z)-alkene (Figure 98). There were two products that would have arisen from double oxidations. The epoxide, 4-(3-pentyloxiran-2-yl)benzoic acid, would have arisen from oxidation of the 4-(hept-1-en-1-yl)benzoic acid product. The other double oxidation product, 4-(1,2-dihydroxyheptyl)benzoic acid, may have formed by two successive hydroxylation steps. Alternatively, it may have arisen from epoxidation followed by a non-enzymatic hydrolysis, resulting in ring opening of the epoxide.

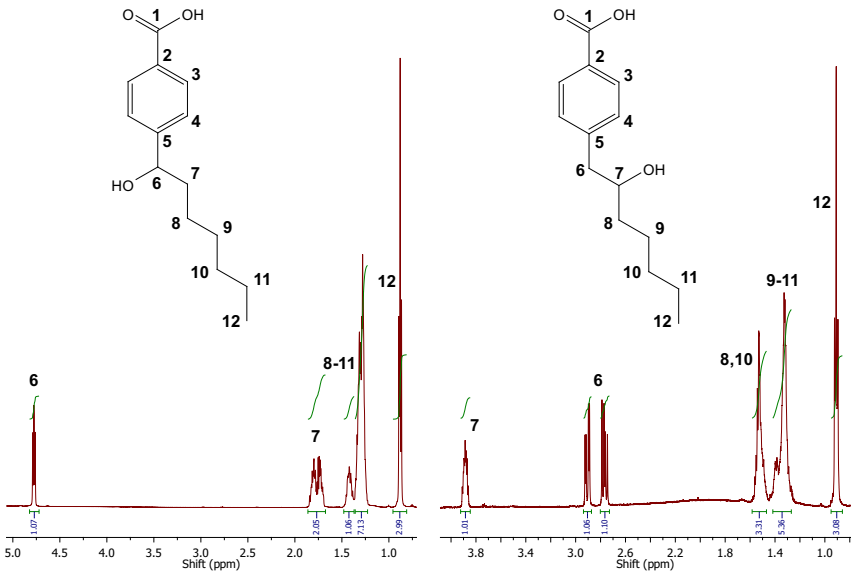

Figure 97. A portion of the ^{1}H NMR spectra of (left) 4-(1-hydroxyheptyl)- and (right) 4-(2-hydroxyheptyl)-benzoic acids.

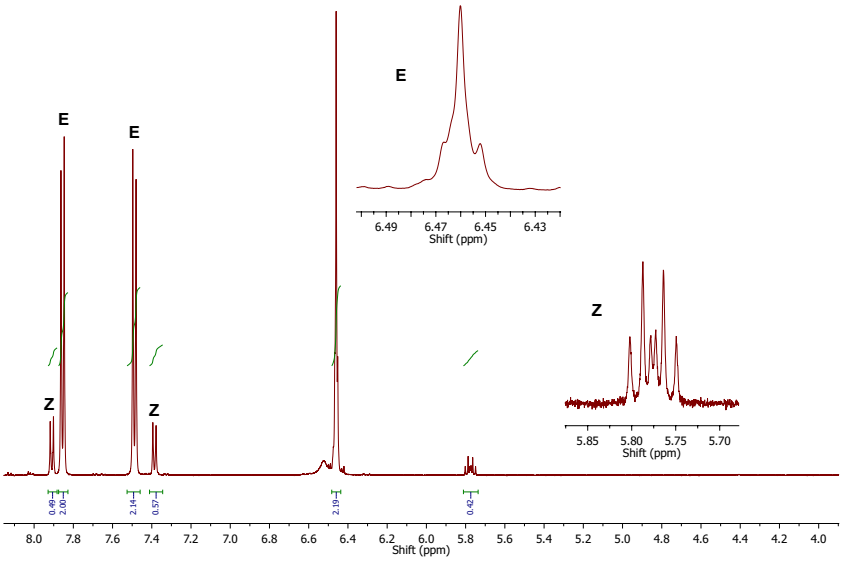

Figure 98. The aromatic and alkene region of the ^{1}H NMR spectrum of 4-(hept-1-en-1-yl)benzoic acid. The 2H multiplet at 6.45 ppm, which was likely to be two overlapped 1H signals, was characteristic of an (E)-alkene. The smaller signals (5.78 ppm, 7.39 ppm and 7.91 ppm) likely corresponded to a small amount of (Z)-alkene. There was likely to be an additional 1H (Z)-alkene signal embedded in the (E)-alkene signal at 6.46 ppm. Each peak is labelled with its respective isomer.

In the *in vitro* turnover, there was a comparable amount of the alkene and the dihydroxy product, and a small amount of the epoxide. In the *in vivo* turnover, the amount of alkene was reduced while that of the further oxidation products increased. This suggested that these products may arise from oxidation of the alkene. There was

also an increase in the amount of hydroxy metabolites.

In summary, each substrate was hydroxylated at either the α- or β-carbon, and there was formation of a varying amount of an α,β-alkene product with the linear and branched alkylbenzoic acids. There was no alkene formation with the cyclopropyl moiety and only a very limited amount with the cyclohexyl, suggesting the desaturation pathway was unfavourable in these cyclic systems.

5.2.3 Crystal structures of alkylbenzoic acid-bound CYP199A4

Despite the differences in size of the *para*-substituents, the binding affinities of CYP199A4 for all these substrates was high, with the exception of 4-*t*-butylbenzoic acid (Table 15). The CYP199A4 catalysed oxidation of all the alkylbenzoic acids generated products which would arise from initial abstraction of the C_α- or C_β-hydrogens. The distribution of α-hydroxylation, β-hydroxylation and α,β-desaturation products would depend on the energetics of C−H bond abstraction and the distances of the C_α and C_β hydrogens from the iron-oxo moiety of the reactive Cpd I intermediate. The activities and product distributions observed with the alkylbenzoic acids suggested that the *para*-alkyl group may be orientated in different positions relative to the reactive intermediate in the substrate binding pocket. 4-Ethylbenzoic acid has previously been co-crystallised with CYP199A4[30,131] (Figure 99). The α-carbon was found to be held 4.7 Å from the heme iron while the β-carbon was held significantly closer (3.2 Å). Despite this, there was very little product arising from hydroxylation at the β-carbon compared to the α- (α, 42 %; β, 3 %). The desaturation product (37 %) could arise from initial hydrogen abstraction at either the α- or β-carbon.

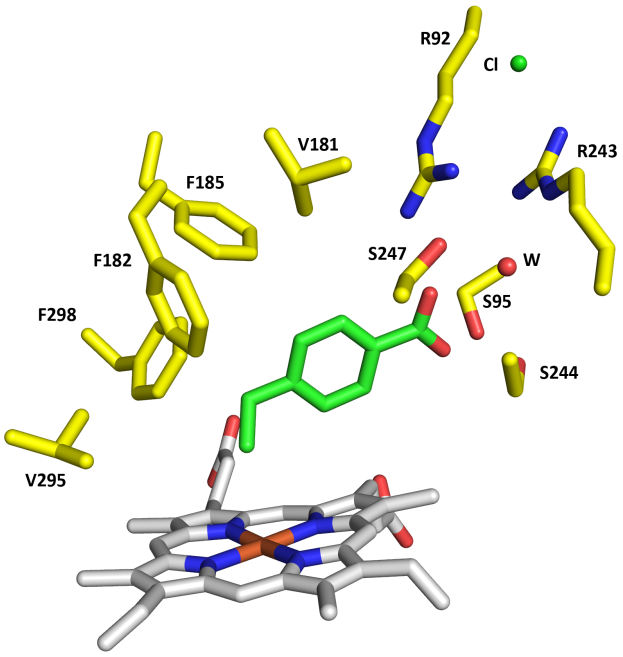

Figure 99. The active site of 4-ethylbenzoic acid-bound CYP199A4 (PDB: 4EGM). The heme is grey, 4-ethylbenzoic acid is green, and the active site amino acid residue side chains are yellow. The water molecule is a red sphere and the chloride ligand is a green sphere. The α-carbon is 4.7 Å from the heme iron, and the β-carbon is held significantly closer at 3.2 Å.

In order to rationalise the binding affinity of these alkylbenzoic acids to the enzyme, and the selectivity of C−H bond abstraction, crystallography of the substrate-bound CYP199A4 forms was attempted. These structures could help explain the ratio of hydroxylation and desaturation products observed in turnovers with CYP199A4, by providing information on the position of the substrate carbons relative to the heme

iron. Crystals of CYP199A4 mixed with 4-isopropyl-, 4-cyclopropyl-, 4-cyclohexyl- and 4-heptyl-benzoic acids (1 mM) were successfully obtained. These grew in 2 weeks from a 500 µL reservoir solution containing 0.2 M magnesium acetate tetrahydrate, 23-26 % w/v PEG-3,350 and 0.1 M Bis-Tris pH 5.25-5.75. High resolution data (Table 17, < 1.8 Å) was obtained at 100 K on the MX1 beamline at the Australian Synchrotron[147,148] and deposited online in the wwPDB[157,158] (Table 17). The remaining substrate-CYP199A4 combinations did not produce crystals under these conditions (4-*n*-butyl-, 4-isobutyl- and 4-*t*-butyl-benzoic acids). A completed, unpublished structure for 4-*n*-propylbenzoic acid bound to CYP199A4 at 1.38 Å resolution was also provided by Weihong Zhou (Nankai University) for analysis and comparison[219] (Data collection and refinement statistics are presented in Appendix C.5).

Table 17. Structural refinement and data collection statistics for CYP199A4 wild-type structures with alkyl chain substituents. All data were collected using 0.9537 Å X-rays and the space group for each structure was $P12_11$. In all cases, there was one molecule in the asymmetric unit.

	4-isopropylBA	4-cyclopropylBA	4-cyclohexylBA	4-*n*-heptylBA
PDB code	5KDB	5UVB	6C2D	6C3H
Unit cell (a/b/c)	44.3/51.5/79.3	44.2/51.3/78.3	44.2/51.4/79.7	44.5/51.4/78.5
($\alpha/\beta/\gamma$)	90/91.9/90	90/92.1/90	90/92.0/90	90/92.7/90
Resolution range[a]	44.29 - 1.64	43.08 - 1.54	44.12 - 1.79	78.45 - 1.71
	(1.67 - 1.64)	(1.56 - 1.54)	(1.82 - 1.79)	(1.74 - 1.71)
$<I/\sigma(I)>$[a]	10.2 (1.8)	10.7 (1.8)	11.0 (2.0)	19.7 (1.6)
Unique reflections	43487	48030	33615	38848
Completeness[a]	99.5 (92.3)	96.8 (45.1)	98.7 (76.8)	99.4 (94.6)
Multiplicity[a]	7.2 (6.8)	7.4 (6.8)	7.4 (6.9)	4.1 (3.4)
R_{merge}[a,b] (%)	11.2 (75.4)	10.9 (76.3)	13.4 (76.7)	14.2 (77.7)
R_{pim}[a,b] (%)	6.8 (45.9)	6.5 (46.1)	7.9 (46.3)	8.2 (48.2)
$CC_{1/2}$[a,c] (%)	99.8 (77.3)	99.8 (71.8)	99.6 (76.6)	99.3 (64.2)
R_{work}	0.145	0.142	0.126	0.159
R_{free}[d]	0.186	0.179	0.173	0.203
Ramachandran plot[e]				
Most favoured (%)	98.5	98	98.2	97.7
Allowed (%)	1.5	2	1.8	2.3

[a]Highest resolution shell is shown in parentheses where applicable. [b]all I+ and I-. [c]Half-correlation coefficient.[182,183] [d]5 % of total reflections, randomly selected. [e]% of all amino acid residues.[184] There were no Ramachandran outliers.

In each substrate-CYP199A4 complex, the overall protein fold was very similar to the 4-ethylbenzoic acid and 4-methoxybenzoic acid-bound CYP199A4 structures[30,131] (Appendix C.5, each case, rmsd < 0.350 Å). All of the structures were monomers with $P12_11$ symmetry (Table 17). In all structures, there was electron density in the active

site that was readily modelled as the appropriate substrate molecule (Figure 100).

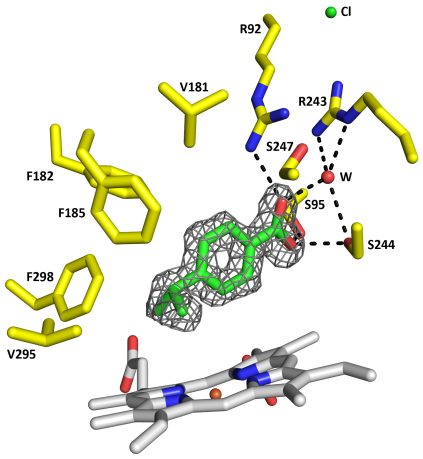

(a) 4-isopropylbenzoic acid

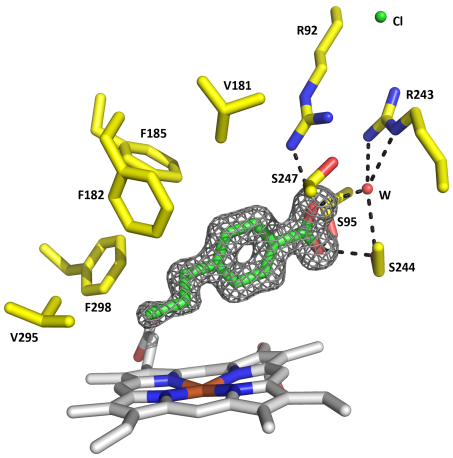

(b) 4-*n*-propylbenzoic acid[219]

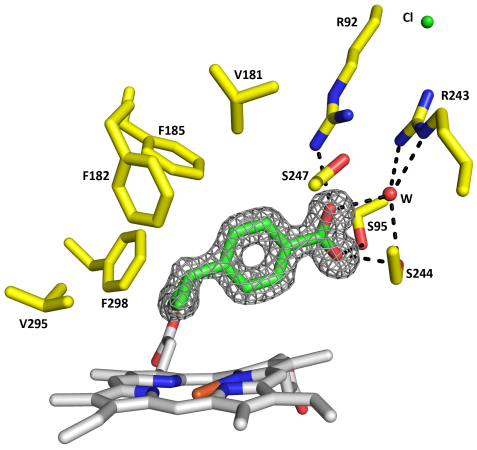

(c) 4-cyclopropylbenzoic acid

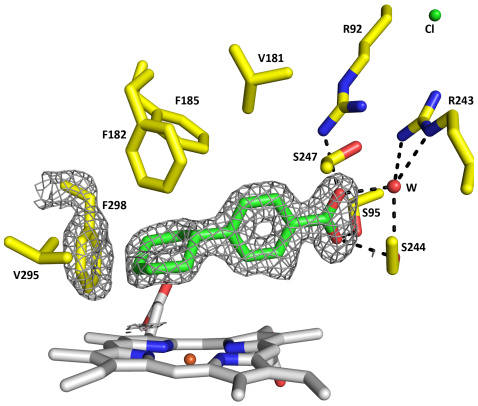

(d) 4-cyclohexylbenzoic acid

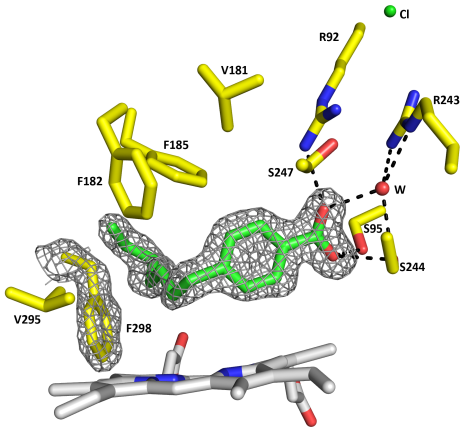

(e) 4-*n*-heptylbenzoic acid

Figure 100. Composite omit maps of alkyl-benzoic acid-CYP199A4 complexes. The heme is grey, the substrate is green and the active site amino acid residue side chains are yellow. The water molecule is a red sphere and the chloride ligand is a green sphere. The electron density of the substrate and, in (d) and (e) the movement of the F298 residue, are shown contoured as a grey mesh ($\sigma = 1.2$) using a reduced bias $2mF_o$-DF_c composite omit map.[154]

The carboxylate and benzene ring moieties of each substrate were found in comparable positions to that of 4-ethylbenzoic acid. The water molecule that hydrogen bonds to the carboxylate moiety, as well as the chloride ligand that caps the active site, were also found in similar locations.

In the crystal structure of 4-isopropylbenzoic acid (PDB: 5KDB), the substrate molecule was bound in a nearly identical orientation to 4-ethylbenzoic acid (Figure 101). The 4-isopropyl *para* position α-carbon was held slightly further from the heme iron than the 4-ethyl equivalent (Table 18, 4.9 Å vs 4.7 Å). One β-carbon was held pointing towards the heme iron but was further away than the equivalent atom of the 4-ethylbenzoic acid structure (3.7 Å vs 3.2 Å). The dihedral angle to the benzene ring (C_{09}-C_{04}-C_{α}-C_{β}, Table 18) was larger (4-isopropylBA, 72.0°; vs 4-ethylBA, 50.2°). The other β carbon points away from the heme iron and is a distance of 5.0 Å away.

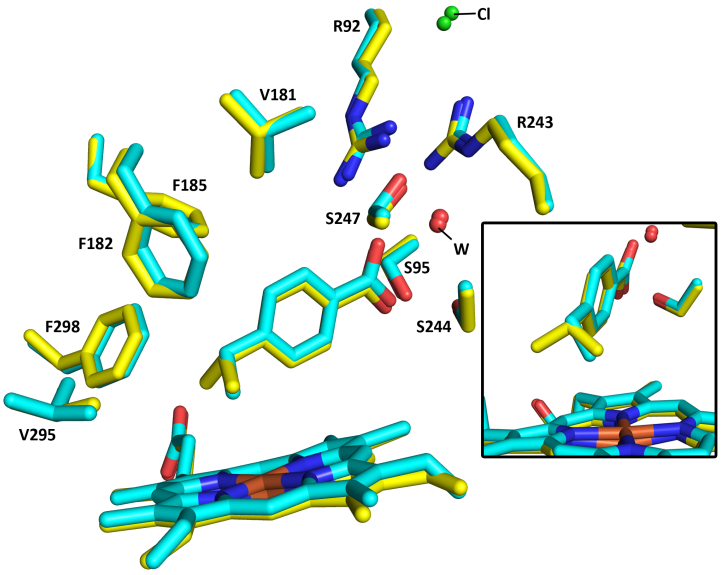

Figure 101. Comparison of the active site of the 4-isopropyl- and 4-ethyl-benzoic acid-bound forms of CYP199A4. 4-Ethylbenzoic acid (cyan) is overlaid with 4-isopropylbenzoic acid (yellow). The water molecule is shown as a red sphere and the chloride ligand is a green sphere. The labels (W, Cl) point to those bound in the 4-isopropylbenzoic acid structure. The inset shows that one methyl of the isopropyl group points towards the heme iron, while the other points away.

Desaturation of 4-isopropylbenzoic acid by CYP199A4 involves removal of two hydrogens from the substrate. The crystal structure shows that one of the two methyl groups bound significantly closer to the heme iron than the other (Figure 101). The alkene would presumably form via removal of a hydrogen from the β-carbon that is held 3.7 Å from the heme iron.

Hydroxylation of 4-isopropylbenzoic acid results in an alcohol at the α-carbon. There is no product observed from hydroxylation at the β-carbon despite its close proximity to the heme iron. Based on the crystal structure, the α-hydrogen would be directed away from the heme iron. Evidentally, abstraction of this hydrogen by Cpd I

is feasible, and this can be rationalised by the benzylic nature of the α-hydrogen, which means it would be energetically more favourable to abstract than the β-hydrogens. It is important to note that the substrate may move to adopt a different orientation after oxygen binding and activation in order to facilitate this.

In order to mimic Cpd I, an oxygen atom was modelled 1.62 Å away from the heme iron in each alkyl-benzoic acid-bound CYP199A4 structure[185] (Chapter 2.10). The carbons of the isopropyl moiety where oxidation activity was observed, C_α and C_{β_a}, are orientated such that the Fe=O-C angle was comparable to that of 4-ethylbenzoic

Table 18. Distances and angles between structural features of alkylbenzoic acid-bound CYP199A4s. Each substrate's name is shortened (4-ethyl-, 4-EtBA; 4-isopropyl-, 4-iPrBA; 4-*n*-propyl-, 4-*n*-Pr; 4-cyclopropyl-, 4-cPrBA; 4-cyclohexyl-, 4-cHxBA; 4-*n*-heptyl-, 4-*n*-HpBA). For substrates with an R group such that two of the same carbon designation exist, these are designated (e.g. C_β) β_a and β_b. The "a" carbon in each case is the carbon closer to the heme iron, while "b" the one further away.

Distance (Å)	4-EtBA	4-iPrBA β_a (β_b)	4-*n*-PrBA	4-cPrBA β_a (β_b)	4-cHxBA $(\beta/\gamma)_{a/b}$	4-*n*-HpBA
C_α - Fe	4.7	4.9	5.1	4.9	5.4	4.5
C_α - **O**=Fe	3.5	3.4	3.7	3.4	3.9	3.1
C_{β_X} - Fe	3.2	3.7 (5.0)	3.8	3.7 (4.2)	4.0 (6.1)	4.7
C_{β_X} - **O**=Fe	2.0	2.1	2.3	2.1 (2.9)	2.5 (4.8)	3.5
C_γ - Fe	-	-	3.9	-	4.2 (6.2)	6.2
C_γ - **O**=Fe	-	-	2.6	-	2.8 (4.9)	4.9
C_X - F298	X=α, 3.9	X=β_b, 3.1	X=α, 3.6	X=β_b, 3.4	X=γ_b, 4.1	X=ω-1, 2.9
Angle (°)						
C_{04}-C_α-C_β	113.7	113.3 (110.0)	112.6	126.4 (126.5)	114.9	113.3
Dihedral (*) C_{09}-C_{04}-C_α-C_β	50.2	72.0 (52.6)	68.4	54.8 (22.9)	45.3	64.0
C_α-C_β-C_γ	-	-	108.8	-	110.8	110.7
Fe=O-C_α	161.6	151.9	156.2	155.5	156.1	158.7
Fe=O-C_{β_X}	162.1	166.5 (129.0)	165.6	157.7 (131.0)	156.5 (140.8)	136.3
Fe=O-C_{γ_X}	-	-	138.8	-	137.8 (133.7)	139.3

(*) The dihedral angle, C_{09}-C_{04}-C_α-C_β, is represented below.

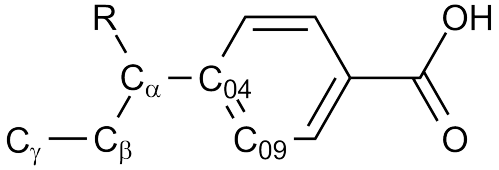

acid (α, 151.9° and β, 166.5°, vs α, 161.6° and β, 162.1°; Table 18). The angle made by the C_{β_b} carbon was significantly smaller (129.0°). The distance from the Cpd I oxygen to the isopropyl carbons was also similar to that of the ethyl carbons (difference ≈ 0.1 Å).

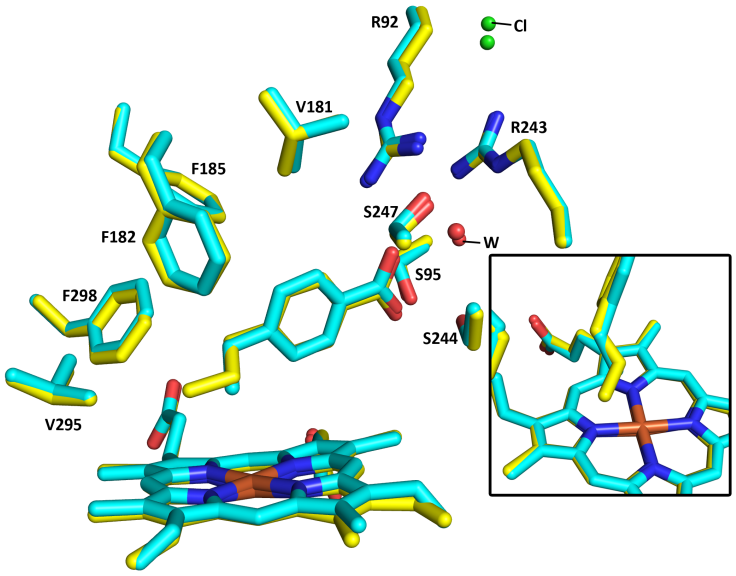

Figure 102. Comparison of the active site of the 4-*n*-propyl- and 4-ethyl-benzoic acid-bound forms of CYP199A4. 4-Ethylbenzoic acid (cyan) is overlaid with 4-propylbenzoic acid (yellow). The water molecule is shown as a red sphere and the chloride ligand is a green sphere. The labels (W, Cl) point to those of the 4-*n*-propylbenzoic acid crystal structure. The inset shows the relative positions of the *n*-propyl group relative to the heme iron.

In the 4-*n*-propylbenzoic acid-bound CYP199A4 crystal structure (Figure 102), the positions of the α- and β-carbons were similar to the equivalent atoms of 4-ethylbenzoic acid, with the γ-carbon pointing towards the V295 residue. The α-carbon was found slightly further from the heme iron than in 4-ethylbenzoic acid (5.1 Å vs 4.7 Å), as was the β-carbon (3.8 Å vs 3.2 Å). The dihedral angle was higher than the equivalent in 4-ethylbenzoic acid (68.4° vs 50.2°). The γ-carbon was 3.9 Å from the heme iron. The Fe=O-C_X angles of the 4-*n*-propylbenzoic acid were comparable to those of 4-ethylbenzoic acid (X = α, 156.2°; β, 165.6°, Table 18) but the angle of the γ-carbon was much lower (138.8°). The major product in the turnover of 4-*n*-propylbenzoic acid was hydroxylation at the α-carbon (40 %), which can be rationalised by the ease of abstracting a benzylic secondary C−H bond. The β-hydroxylation product was slightly lower yielding (26 %) but was formed in greater amounts compared to 4-ethyl- and 4-isopropyl-benzoic acid. With 4-ethylbenzoic acid, there was only a very small amount of methyl β-hydroxylation product compared to the α-hydroxylation product (α, 42 %; β, 3 %), and with 4-isopropylbenzoic acid, there was no β-hydroxylation. The 4-*n*-propylbenzoic acid β-carbon is a methylene and C−H bond abstraction should be more facile. The amount of α,β-alkene in the 4-*n*-propylbenzoic acid turnover was also comparable with 4-ethylbenzoic acid and 4-isopropylbenzoic acid (34 % vs both

37 %). There was no product resulting from γ-hydroxylation of the primary CH_3 of 4-*n*-propylbenzoic acid. This can be rationalised by the higher bond strength of a methyl C−H bond compared to a methylene, in combination with the lower Fe=O-C_γ angle and closer position of the C_β to the O=Fe (Table 18).

In the crystal structure of CYP199A4 bound with 4-cyclopropylbenzoic acid, the α-carbon and one of the β-carbons (designated β_a) of the cyclopropyl group are in similar positions to the equivalent carbons of 4-isopropyl- and 4-ethyl-benzoic acids (Figure 103). The cyclopropyl moiety is held with the α-carbon 4.9 Å from the heme iron (Table 18), the same distance as the α-carbon in 4-isopropylbenzoic acid. The β_a carbon is also held at an equivalent distance to the β-carbon of 4-isopropylbenzoic acid (3.7 Å). The dihedral angle the carbon makes with the benzene ring is smaller (54.8° vs 72.0°).

The other β-carbon of 4-cyclopropylbenzoic acid, designated β_b, is closer to the heme iron than that of 4-isopropylbenzoic acid (4.2 Å vs 5.0 Å), due to the constrained nature of the cyclopropyl moiety. Despite the proximity of both β-carbons to the heme iron, there was no oxidative activity at these positions, from either hydroxylation or desaturation. Cyclopropyl rings have stronger C−H bonds making hydrogen abstraction more difficult, although cyclopropyl cations are aromatic and thus are stabilised.[181,220] The lack of desaturation could also be rationalised due to ring strain in the expected alkene product. As with the 4-isopropylbenzoic acid structure, the α-hydrogen of 4-cyclopropylbenzoic acid would be pointing away from the heme iron, but must be more readily abstracted by Cpd I due to its benzylic nature. The angle to the modelled Cpd I Fe=O of the cyclopropyl moiety carbons were less than that of 4-ethylbenzoic acid (α, 155.5° and β_a, 157.3°, vs α, 161.6° and β, 162.1°; Table 27). The angle made by the β_b carbon was significantly smaller (121.0°). The distance from the Cpd I oxygen to the cyclopropyl carbons was comparable to the equivalent carbons in the 4-ethylbenzoic acid structure (α, 3.4 Å, β_a, 2.1 Å, β_b, 2.9 Å, vs α, 3.5 Å, β, 2.0 Å).

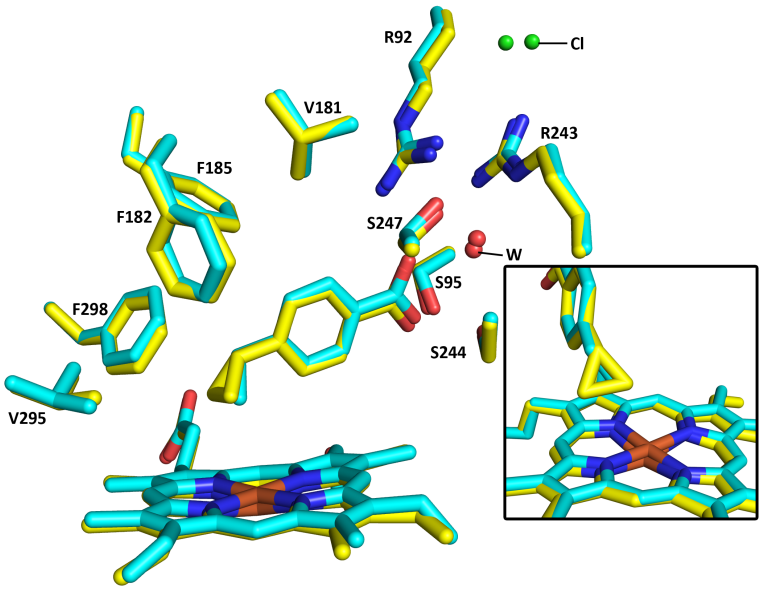

(a) Overlay with 4-ethylbenzoic acid

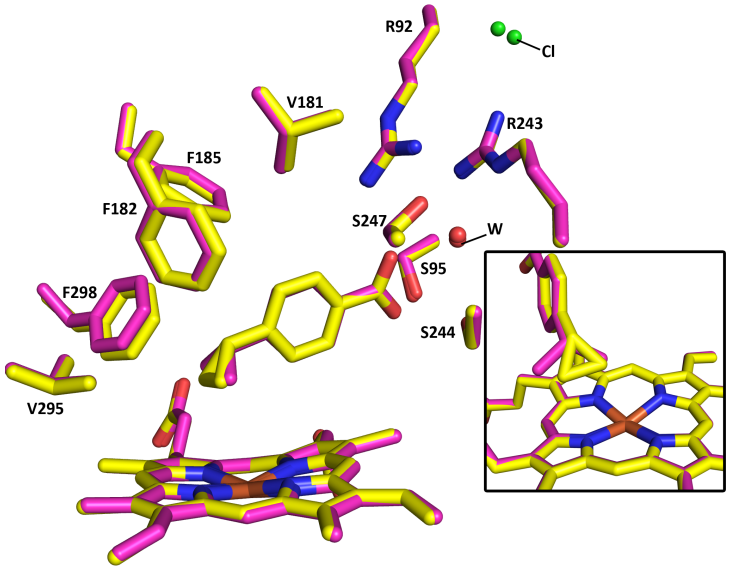

(b) Overlay with 4-isopropylbenzoic acid

Figure 103. Comparison of the active site of the 4-cyclopropyl- with the 4-ethyl- and 4-isopropyl-benzoic acid-bound forms of CYP199A4. 4-Cyclopropylbenzoic acid (yellow) is overlaid with (a) 4-ethylbenzoic acid (cyan) and (b) 4-isopropylbenzoic acid (magenta). The water molecule is shown as a red sphere and the chloride ligand is a green sphere. The labels (W, Cl) point to those bound in the 4-cyclopropylbenzoic acid structure. The insets show the orientation of the cyclopropyl moiety relative to the heme iron.

In the crystal structure of 4-cyclohexylbenzoic acid, the cyclohexyl group adopted a chair conformation within the active site of CYP199A4. The benzoic acid moiety of 4-cyclohexylbenzoic acid occupied an equatorial bond (Figure 105). The α-carbon was held 5.4 Å away from the heme (compared to 4-ethyl, 4.7 Å; 4-*n*-propyl, 5.1 Å). The β carbon is the closest carbon to the heme iron at 4.0 Å (compared to 4-ethyl, 3.2 Å; 4-*n*-propyl, 3.8 Å), and the γ carbon was further away (4.2 Å, compared to 4-*n*-propyl, 3.9 Å). Due to the additional steric bulk of the cyclohexyl ring, the F298 residue occupied a different conformation in the active site of CYP199A4 (Figures 100d, 105). The closest cyclohexyl carbon to the F298 residue was γ_b (4.1 Å). If this distance was measured to the location of the equivalent atom of F298 in the 4-ethylbenzoic acid structure, it would be 1.7 Å which would result in a steric clash of the large F298 residue. The movement would minimise potential steric clashes with the cyclohexyl ring. All other active site amino acid residues are otherwise found in identical positions. Hydroxylation at both the α- and β-carbons was observed, with β-hydroxylation being the major product (66 %). This was rationalised by the fact that the β-carbon is the closest to the heme iron. Both the axial and equatorial hydrogens would be held close to the heme iron, thus abstraction by Cpd I would be favoured. The axial hydrogen would be closest (Figure 104, 3.5 Å), although NMR analysis showed that there was a *trans* relationship between the benzoic acid and hydroxyl groups. The cyclohexyl ring would be conformation-locked due to the bulky benzoic acid moiety,[181] which would place the hydroxyl group in an equatorial position (Figure 94, Appendix C.4).

Hydroxylation at the benzylic α-carbon was observed in a lower yield (33 %). The α-carbon hydrogen points axially towards the roof of the enzyme active site, and it is further away from the heme iron compared to the other alkylbenzoic acids, which would make abstraction of the hydrogen more difficult (Figure 104). Despite the secondary γ-carbon being only 0.2 Å further from the heme iron than the β-carbon (4.2 Å), and the equatorial hydrogen of the γ-carbon being only 3.5 Å from the heme (Figure 104), there was no γ-hydroxylation observed. This is similar to the results for 4-*n*-propylbenzoic acid, where hydroxylation was also at the secondary α- and β- carbons and not at the primary γ-carbon. The angles made by the Cpd I Fe=O to the cyclohexyl carbons were lower than 4-ethyl- and 4-*n*-propyl-benzoic acids; for C_α it was 156.1° (4-ethyl-, 161.6°; 4-*n*-propyl-, 156.2°), for C_β, 156.5° (4-ethyl-, 162.1°; 4-*n*-propyl-, 165.6°). For the cyclohexyl C_γ it was 156.5° which was higher than that of 4-*n*-propylbenzoic acid (138.8°). These carbons, however, were held further from the

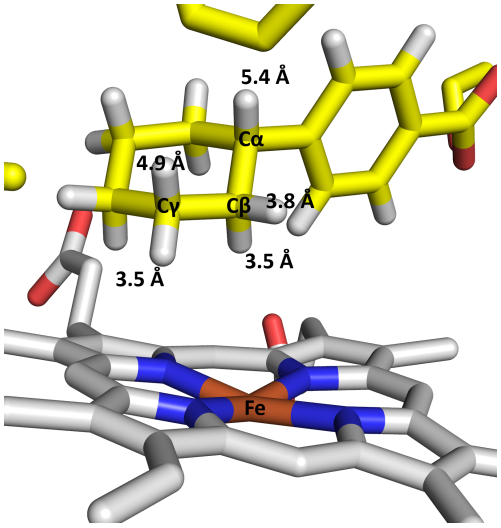

Figure 104. Distances of the cyclohexyl group hydrogens to the heme iron (See Figure 105).

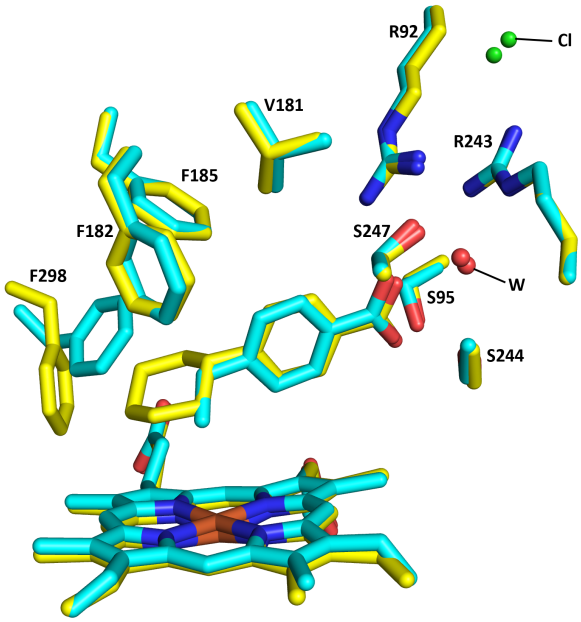

(a) Overlay with 4-ethylbenzoic acid

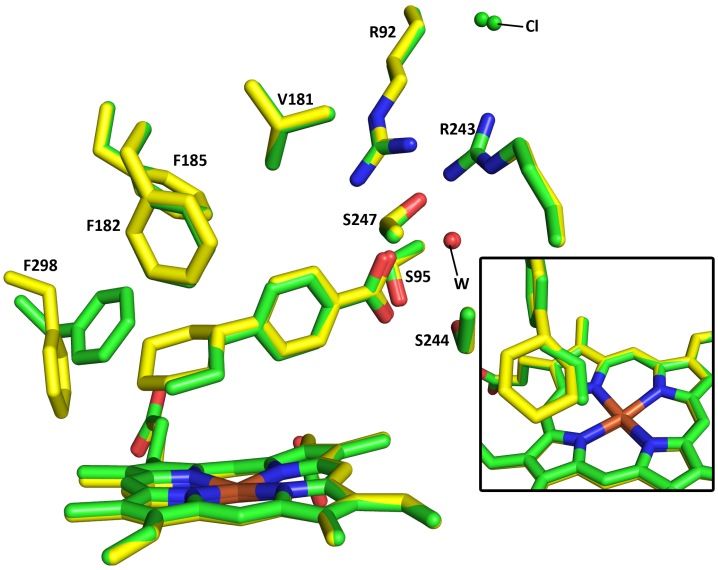

(b) Overlay with 4-*n*-propylbenzoic acid

Figure 105. Comparison of the active site of the 4-cyclohexyl- with the 4-ethyl- and 4-*n*-propyl-benzoic acid-bound forms of CYP199A4. 4-Cyclohexylbenzoic acid (yellow) is overlaid with (a) 4-ethylbenzoic acid (cyan) and (b) 4-*n*-propylbenzoic acid (green). The water molecule is shown as a red sphere and the chloride ligand is a green sphere. The labels (W, Cl) point to those bound in the 4-cyclohexylbenzoic acid structure. The V295 residue has been removed for clarity. The inset in (b) shows the cyclohexyl group from above, emphasising the similar positions of several of the cyclohexyl carbons when compared to the *n*-propyl carbons.

Cpd I oxygen than those of 4-*n*-propylbenzoic acid (4-cyclohexyl-, α, 3.9 Å, β, 2.5 Å, γ, 2.8 Å, vs 4-*n*-propyl-, α, 3.7 Å, β, 2.3 Å, γ, 2.6 Å).

In the CYP199A4 crystal structure with 4-*n*-heptylbenzoic acid bound, the orientation of the *para*-heptyl group in the active site was different to those of the ethyl or *n*-propyl moieties (Figure 100e). The α-carbon of 4-heptylbenzoic acid was held closer to the heme iron than either of those from 4-ethyl- and 4-*n*-propyl-benzoic acids (Figure 106, 4.5 Å vs 4.7 Å and 5.1 Å). The β-carbon was further away than the α (4.7 Å), compared to both 4-ethyl- and 4-*n*-propyl-benzoic acids (4-ethyl-, 3.2 Å; 4-propyl-, 3.8 Å). The longer alkyl side chain is orientated such that the γ carbon is held at a distance of 6.2 Å compared to 3.9 Å with 4-*n*-propylbenzoic acid. To accommodate the four remaining carbons, the F298 residue has moved into a similar orientation to that observed in the 4-cyclohexylbenzoic acid bound structure (Figure 105). The remainder of the heptyl group occupies the space vacated by F298 (Figure 106). In this orientation, the ω-1-carbon is 3.5 Å from the closest carbon of the F298 residue. The terminal methyl carbon of the *n*-heptyl group is 3.2 Å from the F185 residue.

The angle formed between the C_α and the modelled Fe=O was 158.7°, similar to that of 4-ethylbenzoic acid (160.1°, Table 18). For the C_β, it was significantly lower (136.3°). The four remaining carbons each formed an angle to the Fe=O which increased down the *n*-heptyl chain (δ, 126.8°; ϵ, 130.5°; ω-1, 132.0°; ω, 139.5°).[vi] The α-carbon was closer to the Cpd I oxygen than the 4-ethylbenzoic acid α-carbon (3.5 Å vs 3.1 Å), but the β- and all subsequent carbons were held further away (β, 3.5 Å, γ, 4.9 Å).

The activity of CYP199A4 with 4-*n*-heptylbenzoic acid resulted predominantly in oxidation at the α- and β-carbons (4-(1-hydroxyheptyl)- and 4-(2-hydroxyheptyl)-benzoic acids respectively). The major product was α-hydroxylation (60 %). There was a smaller amount of β-hydroxylation and α,β-desaturation (both 13 %). The observed product distribution can be rationalised by the α-carbon being closer to the heme iron and the β-carbon being further away than those of the 4-ethyl- and 4-*n*-propyl-benzoic acid structures. Overall, the crystal structures of these alkylbenzoic acids provided a rationale for the binding and product selectivity observed in the substrate turnovers. They will also provide valuable data for future experimental and theoretical studies into the mechanism and selectivity of these enzymes.

[vi] The ω-1 and ω positions could alternatively be referred to as ζ and η respectively.

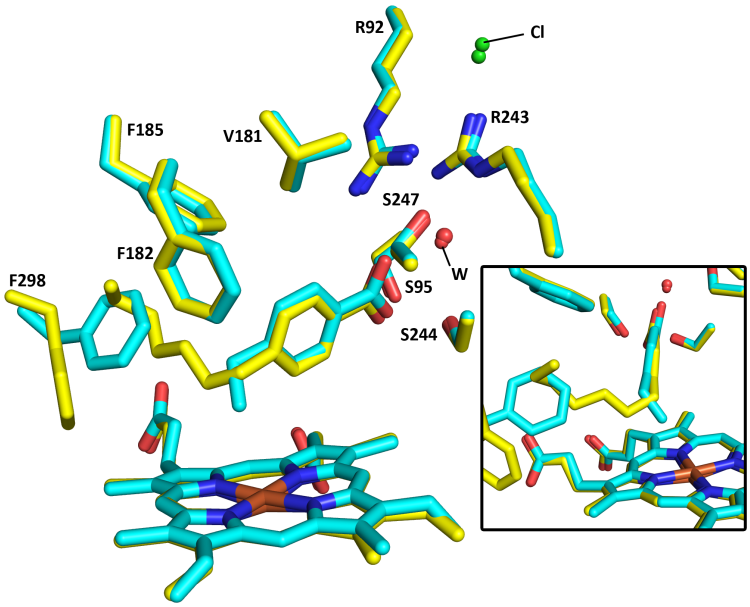

(a) Overlay with 4-ethylbenzoic acid

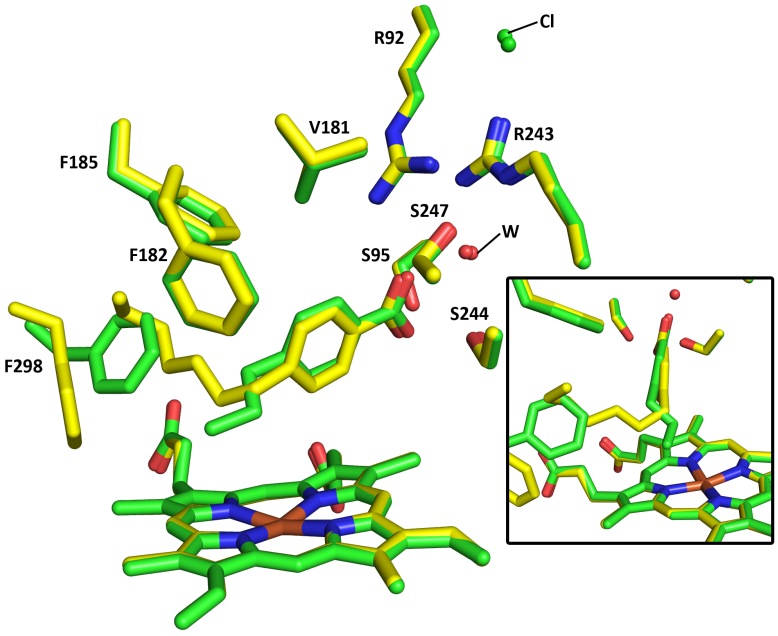

(b) Overlay with 4-*n*-propylbenzoic acid

Figure 106. Comparison of the active site of the 4-*n*-heptyl- with the 4-ethyl- and 4-*n*-propyl-benzoic acid-bound forms of CYP199A4. 4-*n*-Heptylbenzoic acid (yellow) is overlaid with (a) 4-ethylbenzoic acid (cyan) and (b) 4-*n*-propylbenzoic acid (green). The water molecule is shown as a red sphere and the chloride ligand is a green sphere. The labels (W, Cl) point to those bound in the 4-*n*-heptylbenzoic acid structure. The V295 residue has been removed for clarity. The inset highlights the orientation of the *n*-heptyl group, which is located in the space vacated by the F298 residue.

5.2.4 *Meta*-substituted 4-isopropylbenzoic acids as mechanistic probe substrates

The mechanism of the P450-catalysed desaturation pathway is not fully characterised. After the initial hydrogen abstraction step, it is unclear whether the alkene forms formed by a second H atom abstraction or by electron transfer followed by proton removal (Chapter 5.1). In Chapter 3, data was presented demonstrating that CYP199A4 substrates can accommodate additional small functional groups at the benzene ring *meta*-position. To further probe the factors controlling the partition between the hydroxylation and desaturation products, *meta*-substituted *para*-alkylbenzoic acids containing various electron-withdrawing and electron-donating groups could be employed. The ratio of alcohol to alkene product would determine the impact of each *meta* functional group. The electron withdrawing or donating properties of each substituent would impact the relative stabilities of a cation or radical species at the benzylic C_α carbon. If desaturation proceeds via a cationic mechanism, an increase in alkene formation would be expected for electron donating groups with a corresponding decrease for electron withdrawing groups.

A series of 3-X-4-isopropylbenzoic acids (Figure 107, X = Cl, Br, OH, NO_2, NH_2, NHAc) were synthesised by the research group of James J. De Voss, University of Queensland (Chapter 2.1). Substrate binding assays (Chapter 2.3) were performed and *in vitro* turnovers (Chapter 2.4) were analysed using GC-MS (Chapter 2.1) to determine the hydroxylation and desaturation products.

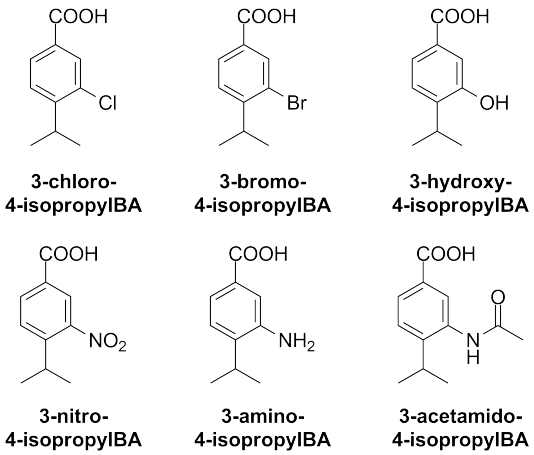

Figure 107: 3-X-4-isopropylbenzoic acid substrates investigated with CYP199A4.

The spin state shift of CYP199A4 was determined to be high on addition of the majority of these substrates (3-chloro-, 3-bromo- and 3-amino-, all $\geq$ 95 %; 3-hydroxy-, 70 %, 3-nitro-, 80 %). The 3-acetamido substrate gave only a 20 % spin state shift (Figure 108 and Appendix C.1). This suggested that the 3-acetamido group could be too large for the active site of CYP199A4 (Chapter 3.2.3), or may interact with the heme iron (potentially in a similar manner to 4-acetamidobenzoic acid, Chapter 4.3).

Table 19. Binding and turnover parameters determined for 3-X-4-isopropylbenzoic acid (3-X-4-iBA) substrates investigated with CYP199A4. Shown are spin state shift and dissociation constant analyses (% HS and K_d, Chapter 2.3), NADH oxidation rates (Chapter 2.4), product formation rates (PFR, Chapter 2.5) resulting coupling efficiency (%) and partition of hydroxylation (OH), desaturation (D) and epoxidation (E) products. Rates are mol (molCYP)$^{-1}$ min^{-1}.

Substrate	HS (%)	K_d (µM)	NADH[a]	PFR[b]	Coupling[c]	OH:D:E[d]
4-isopropylBA	≥ 95	0.29 ± 0.01	325 ± 36	221 ± 27	68 ± 1	63:37
3-chloro-	≥ 95	0.49 ± 0.04	90.1 ± 2.2	48.6 ± 4.2	53 ± 6	77:20:3
3-bromo-	≥ 95	0.27 ± 0.04	95.1 ± 2.5	34.4 ± 4.1	38 ± 3	89:11
3-hydroxy-	70	52 ± 4	98.5 ± 1.0	21.4 ± 3.3	21 ± 4	77:16:7
3-nitro-	80	35 ± 2	45.9 ± 6.1	6.2 ± 1.3	14 ± 1	94:6
3-amino-	≥ 95	34 ± 2	294 ± 32[e]	-[f]	-	-
3-acetamido-	20	n.d.[g]	133 ± 10[e]	-[f]	-	-

[a]NADH oxidation rate. [b]PFR: product formation rate. [c]% of NADH consumed that led to formation of substrate metabolite. [d]Partition of turnover products - α-hydroxylation (OH):α,β-desaturation (D):epoxide (E). [e]These NADH oxidation rates were significantly higher than the other 3-X-4iBA substrates. Turnover mixtures with the P450 removed were able to oxidise NADH at a rate much higher than the usual leak rate (≈ 9 min^{-1}). These were: 3-amino-, 251 min^{-1}; 3-acetamido-, 115 min^{-1}. [f]no detectable levels of product formation. Significant levels of H_2O_2 were detected in these turnovers: 3-amino-, 37 %; 3-acetamido-, 54 %. In the turnovers with no P450, this changed to: 3-amino-, 100 %; 3-acetamido-, 41 %. [g]Not able to be determined due to low absorbance change upon addition of substrate aliquots.

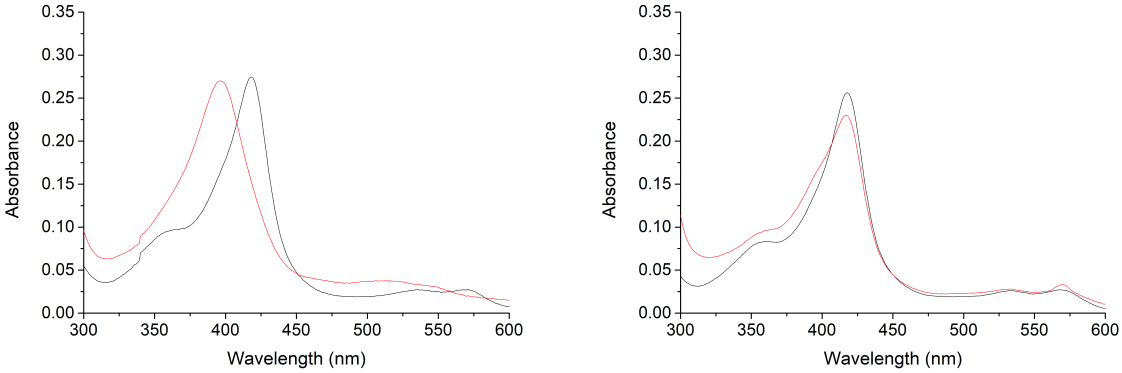

(a) 3-chloro-4-isopropylbenzoic acid **(b)** 3-acetamido-4-isopropylbenzoic acid

Figure 108. Spin state shifts of several 3-X-4-isopropylbenzoic acids with CYP199A4. Black shows CYP199A4 in its resting state, red shows the maximum absorbance shift obtained upon addition of substrate.

This was reinforced by the inability to determine a dissociation constant, due to the low change in absorbance upon addition of this substrate to CYP199A4. The binding affinity of CYP199A4 for the other substrates varied considerably (Figure 109 and Appendix C.2). The chloro and bromo substrates bound with high affinity (0.49 µM and 0.27 µM, respectively), while the hydroxy, nitro and amino substrates bound two orders of magnitude less tightly (52 µM, 35 µM and 34 µM, respectively), inferring that there may be clashes with active site residues or an altered binding position.

The NADH oxidation rate with each substrate was lower than that induced by 4-

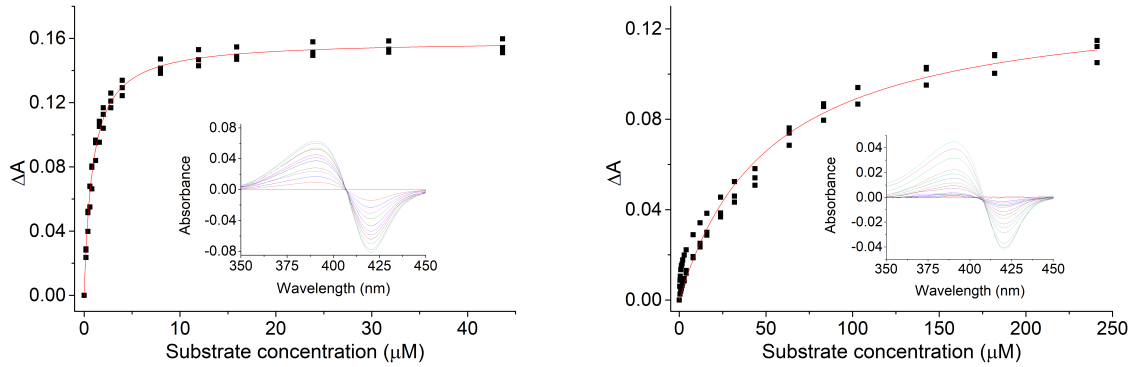

(a) 3-bromo-4-isopropylbenzoic acid (420 nm, 391 nm, 1.3 μM)

(b) 3-hydroxy-4-isopropylbenzoic acid (420 nm, 391 nm, 1.3 μM)

Figure 109. Dissociation constant determination of (a) 3-bromo- and (b) 3-hydroxy-4-isopropylbenzoic acids investigated with CYP199A4. The inset image shows the UV-Vis response to successive addition of substrate aliquots. Shown in brackets are the wavelengths of the trough and peak, and the enzyme concentration used for dissociation constant analysis (trough, peak, μM-P450).

isopropylbenzoic acid, which was 325 min^{-1}. GC-MS analysis of the TMS-derivatised turnovers of each substrate with CYP199A4 showed there were products for the 3-chloro-, 3-bromo-, 3-hydroxy- and 3-nitro-containing substrates (Appendix C.3). Despite displaying higher NADH oxidation activity than the other substrates, no products were observed in the turnovers of the amino or acetamido substrates. Significant levels of H_2O_2 formation were detected in both of these turnovers, and when CYP199A4 was removed the H_2O_2 levels increased (Table 19). This suggested the substrate could be accepting an electron from the ferredoxin and was able to reduce oxygen in the aerobic turnover mixture, as has been described for other aromatic substrates.[221]

In each case where products were observed, the *para*-isopropyl group was oxidised. 3-X-4-(1-methyl-1-hydroxyethyl)benzoic acid was the major product (via α-hydroxylation), as identified by masses which were larger than the substrate mass (substrate + 16 + 72, derivatised OH, or substrate + 16, underivatised OH). The alkene products, 3-X-4-(prop-1-en-2-yl)benzoic acid (α,β-alkene) were identified by the substrate - 2 mass peak. In each case, the alkene was lower yielding than in 4-isopropylbenzoic acid (Figure 110, Appendix C.3). In the cases of 3-chloro- and 3-hydroxy-, there was a small amount of epoxide product from further oxidation of the alkene, identified by a mass of substrate + 14 (3 % and 6 % of total products respectively). The product formation rate and the coupling efficiency of CYP199A4-catalysed oxidation for each of the 3-X-4-isopropylbenzoic acids were lower than 4-isopropylbenzoic acid (Table 19).

The product standards of these *meta*-substituted benzoic acids were unavailable. In order to estimate the product coupling and the ratio of hydroxylation to desaturation, calibration factors were determined using a library of similar compounds. Namely, 4-

ethyl-, 4-(1-hydroxyethyl)-, 4-vinyl-, 4-isopropyl- and the 3-X-4-isopropyl-benzoic acids themselves. The impact of each moiety of the substrate was then assumed to be linear in determining the calibration slopes of the products (Chapter 2.5, Table 2). An epoxide standard was unable to be obtained, so the relevant substrate was used to estimate the amount of epoxide in turnovers where it was observed. In the cases of 3-hydroxy- and 3-nitro-4-isopropylbenzoic acids, the alkene product coeluted with the substrate (Figure 110b, Appendix C.3), and as such the integration of the alkene peak was likely to be less accurate. Additionally, in each GC-MS chromatogram, there were peaks corresponding to partially underivatised hydroxy products, as well as incomplete derivatisation of the *meta*-hydroxy, amino and acetamido groups. This suggested that these *meta*-substituted substrates were difficult to derivatise for GC-MS analysis. The hydroxylated isopropyl moiety must be difficult for the derivatisation agent to access in these substrates, complicating the analysis.

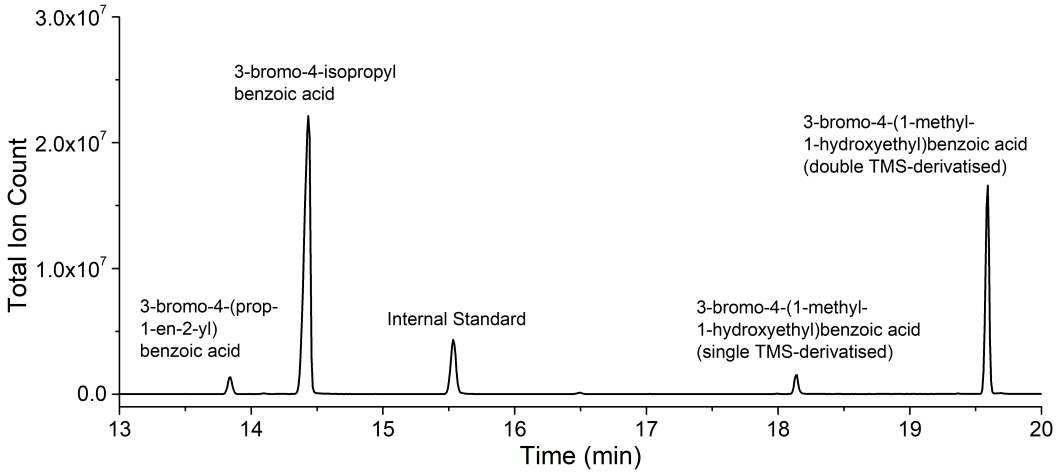

(a) 3-bromo-4-isopropylbenzoic acid

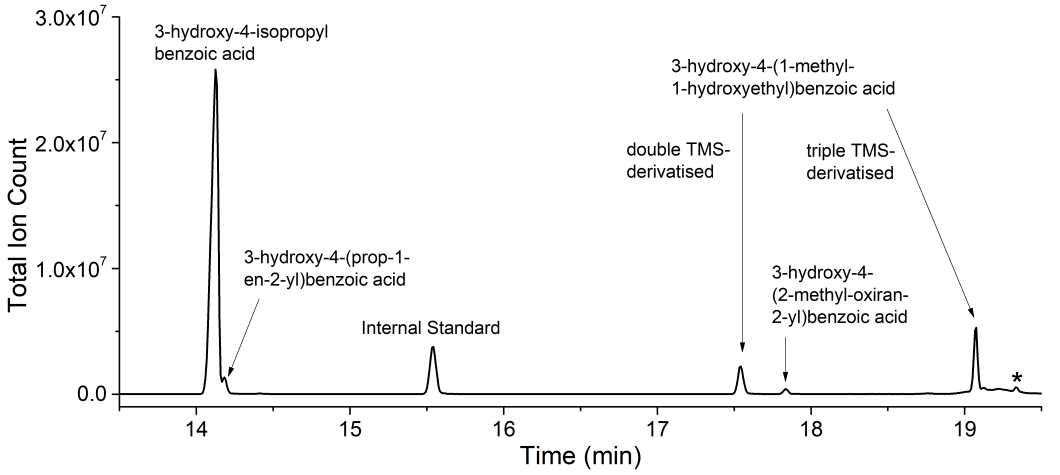

(b) 3-hydroxy-4-isopropylbenzoic acid

Figure 110. GC-MS analyses of TMS-derivatised *in vitro* 3-bromo- and 3-hydroxy-4-isopropylbenzoic acid turnovers with CYP199A4. In (b), an impurity peak (present in substrate controls) is marked with an asterix. Mass spectra of the products are presented in Appendix C.3.

Both the chloro and bromo ligands would be expected to withdraw electron density by induction, and would be resonance donating. 3-Chloro-4-isopropylbenzoic acid displayed the highest product formation rate and coupling of the substrates tested ($48.6\,min^{-1}$, 53 %), and the distribution of products was 77 % hydroxylation, 20 % desaturation and 3 % epoxidation (Table 19, compared to 63 % and 37 % for 4-isopropylbenzoic acid, with no epoxide product). 3-Bromo-4-isopropylbenzoic acid generated a large excess of hydroxylation product (89 % OH, 11 % alkene) but the product formation rate and coupling efficiency were lower than the 3-chloro substrate ($34\,min^{-1}$, 38 %). A hydroxy substituent would be strongly electron donating by resonance to the isopropyl group, but withdrawing by induction effects. The 3-hydroxy-4-isopropylbenzoic acid substrate with CYP199A4 also generated an excess of hydroxylation product over the desaturation product (77 % OH, 16 % alkene, 7 % epoxide). However there was a minimal level of product generated, and the coupling efficiency of the reaction was low ($21.4\,min^{-1}$, 21 %). A nitro substituent would be strongly electron withdrawing. Turnovers of 3-nitro-4-isopropylbenzoic acid showed a greater proportion of hydroxy product (94 % OH, 6 % alkene) relative to the 3-chloro-, 3-bromo- and 3-hydroxy- substrates as well as 4-isopropylbenzoic acid itself. This is in line with the electron withdrawing properties of the nitro group. The coupling efficiency was low, resulting in a very slow rate of product formation ($6.2\,min^{-1}$, 14 %).

These results provided evidence that the *meta*-substitutions were detrimental to enzyme activity. The same P450 oxidations as 4-isopropylbenzoic acid were observed (hydroxylation and desaturation), along with an epoxide product with the 3-chloro- and 3-hydroxy-4-isopropylbenzoic acids. The product formation rate was, in some cases, an order of magnitude lower than 4-isopropylbenzoic acid, and correspondingly the coupling efficiency was reduced in all cases. There was no observable trend between the desaturation-hydroxylation partition and the electronic properties of the *meta*-substituent.

At this stage, it cannot be ruled out that the incorporation of a *meta* functional group is changing the binding orientation of the isopropyl moiety relative to the heme group in CYP199A4. A small change in the relative position of the isopropyl group would affect the partition between hydroxylation and desaturation, masking the electronic effects of the substituents. X-ray crystal structures of CYP199A4 with these substrates would provide important information on how any changes in the distance and orientation of the isopropyl group to the heme iron would effect the partition. It may be that the *meta*-substituted isopropylbenzoic acid substrates bind to the active site of CYP199A4 in a similar orientation to 3,4-dimethoxybenzoic acid, which is itself superimposible with 4-methoxybenzoic acid (Figure 111). The *meta*-methoxy group points towards the F182 residue, which has moved to reduce any steric clashes. Additionally, 3,4-dimethoxybenzoic acid induced a lower spin state shift and bound more weakly than 4-methoxybenzoic acid (70 % vs $\geq$ 95 %; 30 µM vs 0.28 µM, Chapter 3).

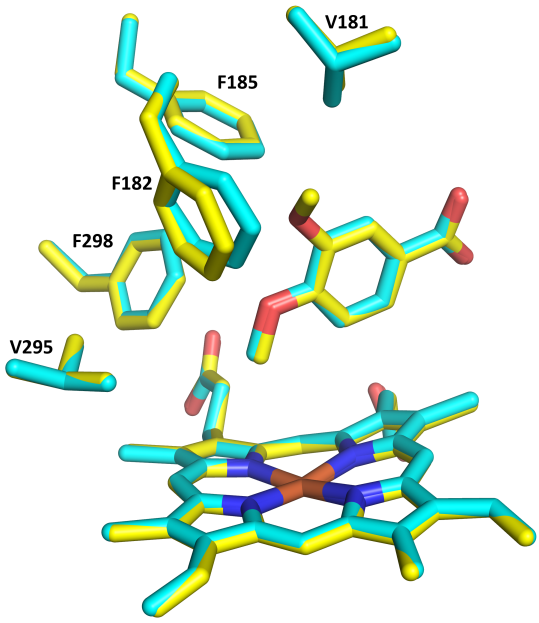

Figure 111. Comparison of the crystal structures of 3,4-dimethoxybenzoic acid-bound CYP199A4 (yellow, PDB: 4EGN) with 4-methoxybenzoic acid (cyan, PDB: 4DO1).

Another approach to investigating the hydroxylation/desaturation partition of 4-isopropylbenzoic acid is required. For example, isotopic substitution at the isopropyl group could be employed (Discussion Chapter 5.3).

5.2.5 Investigation of the carbonyl-containing substrates, 4-propionyl- and 4-(2-oxopropyl)-benzoic acids

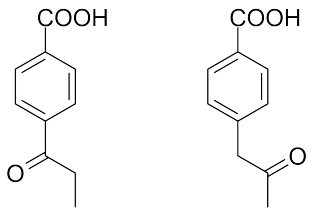

4-propionyl benzoic acid **4-(2-oxopropyl) benzoic acid**

Figure 112. Carbonyl-containing benzoic acids investigated with CYP199A4.

P450 enzymes are known to be capable of catalysing carbon-carbon bond cleavage reactions.[39] This activity can occur at a carbon adjacent to a carbonyl,[109,222] between the carbons of an α,β-hydroxycarbonyl,[115] or between an α,β-diol[113,114] (Chapter 1.4.4). The oxidation of 4-propionyl- and 4-(2-oxopropyl)-benzoic acids by CYP199A4 could generate hydroxycarbonyl products. These could be used as substrates to investigate carbon-carbon bond cleavage reactions (Figure 112).

Table 20. Binding and turnover parameters determined for carbonyl substrates investigated with CYP199A4. Shown are spin state shift and dissociation constant analyses (% HS and K_d, Chapter 2.3), NADH oxidation rates (Chapter 2.4), product formation rates (PFR, Chapter 2.5) and resulting coupling efficiency (%). Rates are mol (molCYP)$^{-1}$ min^{-1}.

Substrate	HS (%)	K_d (µM)	NADH[a]	PFR[b]	Coupling[c]
4-*n*-propylBA[28]	$\geq$ 95	0.04 ± 0.02	688 ± 24	594 ± 72	86 ± 8
4-propionylBA	Type II (420 nm)	9.1 ± 0.4	282 ± 23	29 ± 7	20 ± 2
4-(2-oxopropyl)BA	50	80 ± 3	151 ± 3	123 ± 10	83 ± 3

[a]NADH oxidation rate. [b]PFR: product formation rate. [c]% of NADH consumed that led to formation of substrate metabolite. [d]The dissociation constant was determined using the trough at 414 nm and peak at 430 nm. An absorbance maximum at 379 nm was also observed but was not used (Figure 113a).

4-Propionylbenzoic acid induced a type II spin state shift in CYP199A4 to 420 nm, indicating that the carbonyl oxygen may be interacting with the heme iron (Table 20, Figure 113). A type I, 50 % shift to was observed upon addition of 4-(2-oxopropyl)benzoic acid. The binding affinity of these substrates differed by an order of magnitude (Figure 113); 4-propionylbenzoic acid bound tightly (9.1 µM) while 4-(2-oxopropyl)benzoic acid bound much less tightly (80 µM). Both substrates bound with significantly lower affinity than 4-*n*-propylbenzoic acid ($\geq$ 95 %, 0.04 µM).

The rate of NADH oxidation by CYP199A4 with these substrates was lower than 4-*n*-propylbenzoic acid. The NADH oxidation rate observed with 4-propionylbenzoic acid was 282 min^{-1}, and 4-(2-oxopropyl)benzoic acid was slower than 4-propionylbenzoic acid at 151 min^{-1}. With both substrates, HPLC analysis of the *in vitro* turnovers showed a single oxidation product (Figure 114). *In vivo* cultures were grown (Chapter 2.6) and the products were purified using semi-prep HPLC (Chapter 2.1). NMR characterisation was then used to identify the oxidation product of each.

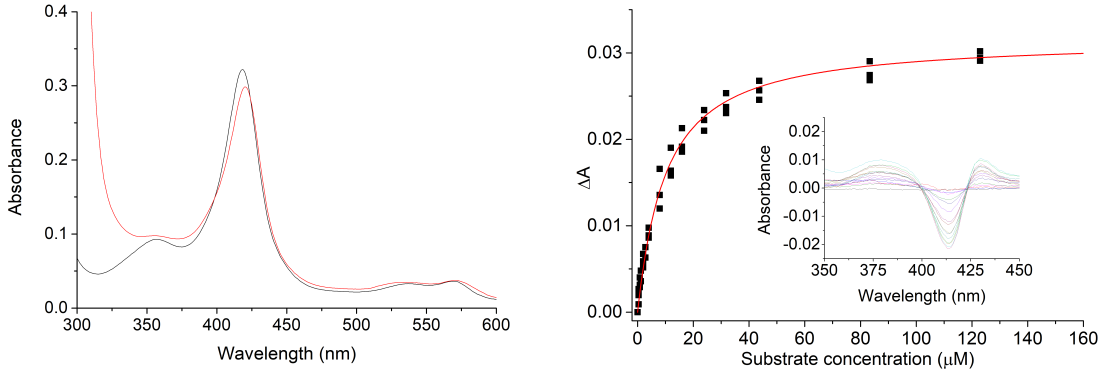

(a) 4-propionylBA (414 nm, 430 nm, 1.6 µM)

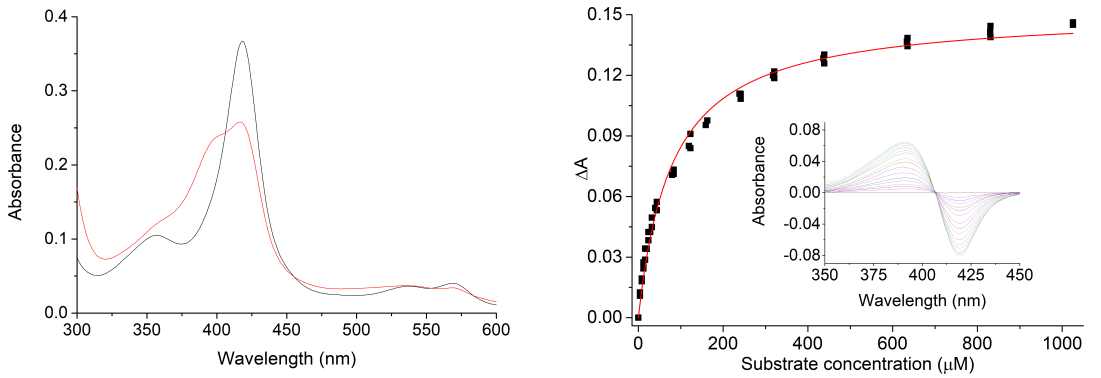

(b) 4-(2-oxopropyl)BA (419 nm, 391 nm, 2.1 µM)

Figure 113. Spin state shift and dissociation constant determination of 4-propionyl and 4-(2-oxopropyl)benzoic acids investigated with CYP199A4. Left column: spin state shift analysis; black shows CYP199A4 in its resting state, red shows the maximum absorbance shift obtained upon addition of substrate. Right column: dissociation constant determination; the inset image shows the UV-Vis response to successive addition of substrate aliquots. Shown in brackets are the wavelengths of the trough and peak, and the enzyme concentration used for dissociation constant analysis (trough, peak, µM-P450).

The product of the 4-propionylbenzoic acid turnover was identified as 4-(2-hydroxypropanoyl)benzoic acid (Figures 114a; 115, left; Appendix C.4). The product formation rate was slow compared to 4-*n*-propylbenzoic acid (29 min^{-1} vs 594 min^{-1}, Table 20) and the resultant coupling efficiency was low (20 %). This would be expected if the substrate α-carbonyl group reduced the oxidation activity of CYP199A4 by inteferring with dioxygen binding through its interaction with the heme iron. It is significant that a product was generated in the turnover, given that type II binding typically results in P450 catalytic cycle inhibition.[202,223]

The *in vitro* reaction of 4-(2-oxopropyl)benzoic acid generated a single product arising from hydroxylation at the substrate α-carbon, which was identified using NMR as 4-(1-hydroxy-2-oxopropyl)benzoic acid (Figures 114b; 115, right; Appendix C.4). The product formation rate (123 min^{-1}) was higher than that of 4-propionylbenzoic acid but lower than CYP199A4 oxidation of 4-*n*-propylbenzoic acid. The coupling efficiency of NADH towards product formation was high (83 %).

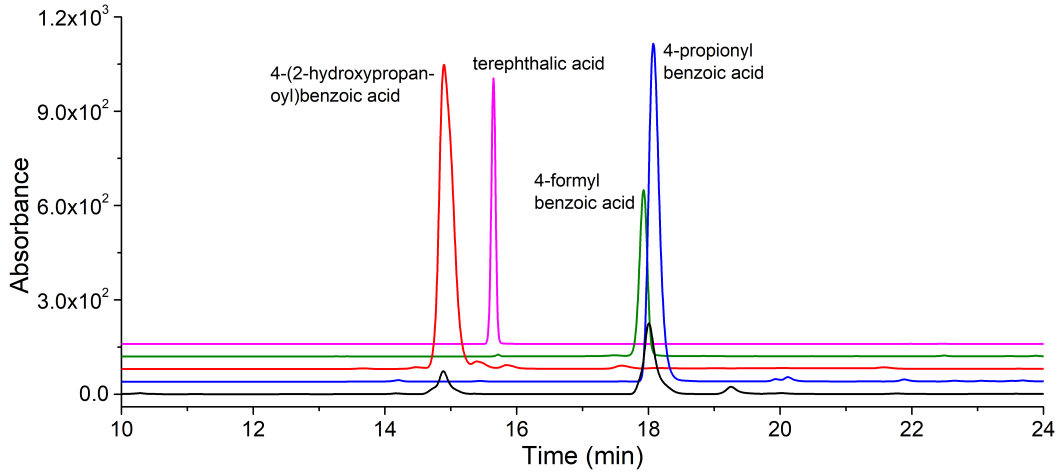

(a)

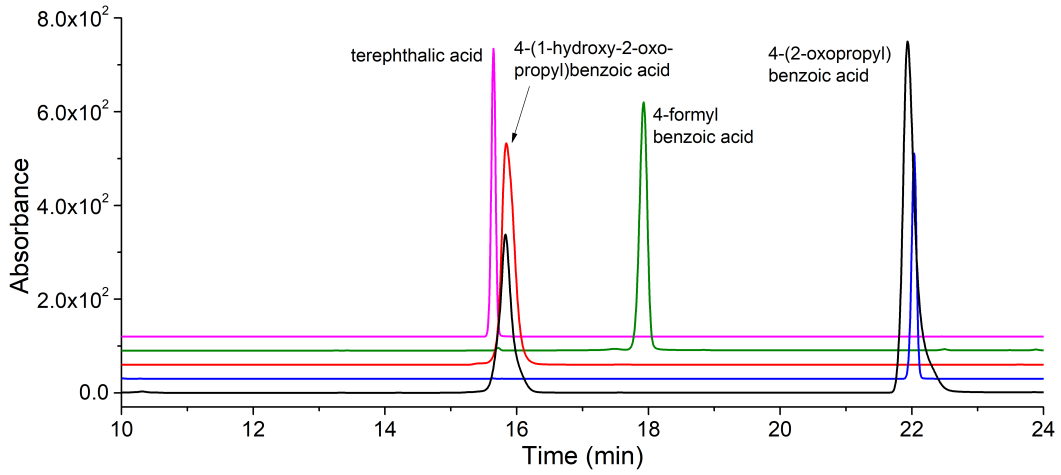

(b)

Figure 114. HPLC analysis of *in vitro* CYP199A4 turnovers of (a) 4-propionyl- and (b) 4-(2-oxopropyl)-benzoic acids. In both, **black**, *in vitro* turnover; green, 4-formylbenzoic acid control, RT = 17.9 min; pink, terephthalic acid control, RT = 15.6 min. The gradient used was 0-50 % H_2O:ACN. The chromatograms were collected at 254 nm.
In (a): blue, substrate control, RT = 18.1 min; red, isolated 4-(2-hydroxypropanoyl)benzoic acid control, RT = 14.9 min.
In (b): blue, substrate control, RT = 22.0 min; red, isolated 4-(1-hydroxy-2-oxopropyl)benzoic acid control, RT = 15.8 min.
Below is shown the reaction scheme of each.

(a) **(b)**

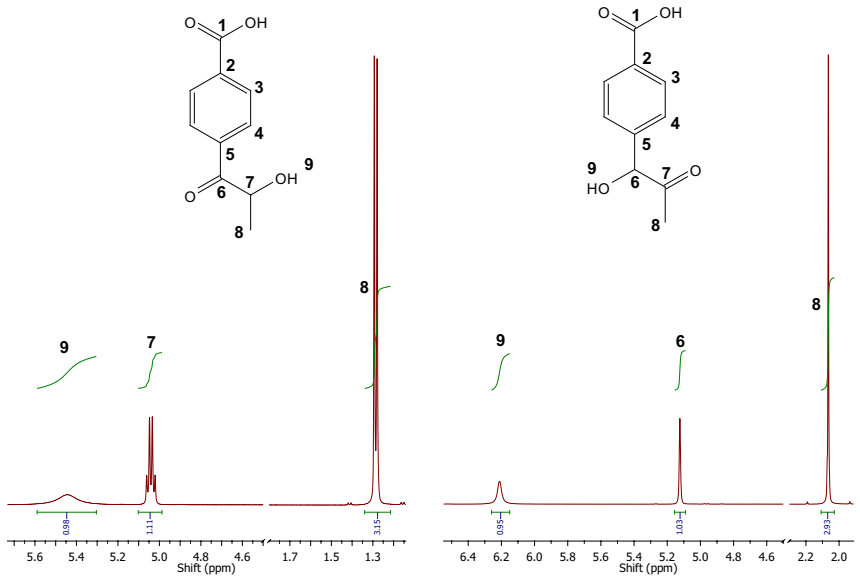

Figure 115. A portion of the ^{1}H NMR spectra of (left) 4-(2-hydroxypropanoyl)- and (right) 4-(1-hydroxy-2-oxopropyl)-benzoic acids. The two hydroxycarbonyls can be clearly distinguished by their splitting patterns.

The expected products of carbon-carbon bond cleavage, 4-formylbenzoic acid and terephthalic acid, could arise from further oxidation of the generated hydroxy products (Figure 116). 4-Formylbenzoic acid and terephthalic acid were not detected in the *in vitro* or *in vivo* turnovers of either of the carbonyl substrates (Figure 114).

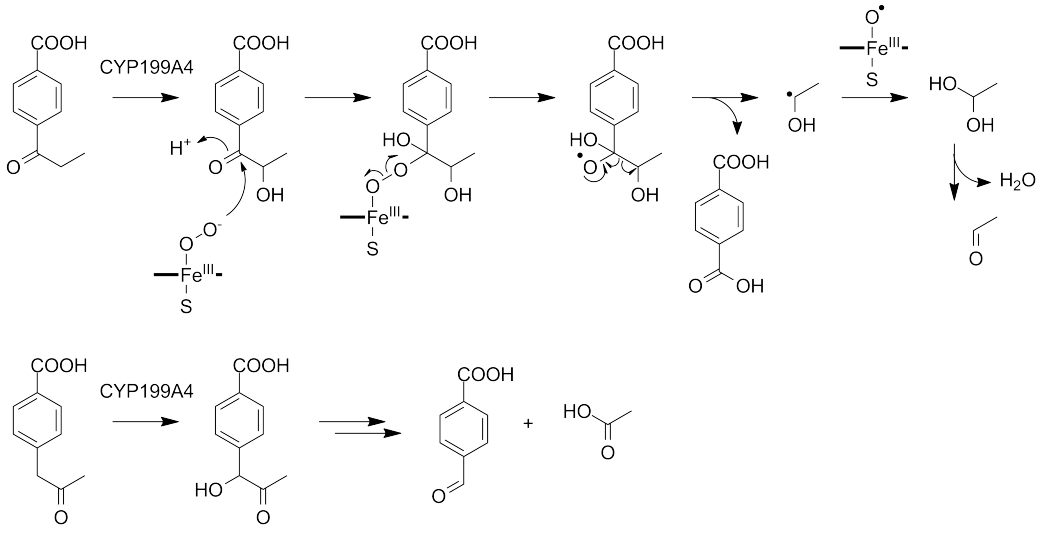

Figure 116. Proposed mechanism for possible carbon-carbon bond cleavage of CYP199A4 substrates.[39,115,224] Top shows the formation of terephthalic acid that would result from C-C cleavage of 4-(2-hydroxypropanoyl)benzoic acid while the bottom shows the formation of 4-formylbenzoic acid from oxidation of 4-(1-hydroxy-2-oxopropyl)benzoic acid. The mechanism proceeds via attack of the carbonyl by the nucleophilic ferric peroxy species, followed by homolytic O-O bond breaking to yield an oxygen radical species. This species undergoes C-C bond cleavage and generates the terephthalic acid and acetaldehyde.

The hydroxylation products could be generated in larger amounts and used as substrates to further investigate carbon-carbon bond cleavage reactions.

In both turnovers, the hydroxylation products would be chiral, and these may form with a preference towards one enantiomer. Further analysis would be required to establish the enantioselectivity of these reactions, and different enantiomers may be able to undergo C-C bond cleavage with P450 enzymes. There was no hydroxylation at the primary γ-carbons, similar to the turnovers of 4-*n*-propylbenzoic acid.

5.3 Discussion

Benzoic acid substrates with *para*-alkyl moieties that were longer or more highly substituted than 4-ethylbenzoic acid were able to be accommodated in the active site of CYP199A4. The chain length did not adversely affect the substrate binding affinity, however the degree of substitution had an effect, as seen with 4-*t*-butylbenzoic acid, which bound ≈ 100-fold less tightly than the other substrates.

The GC-MS or HPLC analysis of all of the CYP199A4-substrate turnovers showed formation of at least one hydroxylation product at the α- or β-carbon. The amount of β-hydroxylation product generated from primary methyl groups was low when a suitable benzylic C−H bond was available. Desaturation of the α- and β-carbons to form an α,β-alkene was observed in the turnovers of all substrates, except for 4-cyclopropylbenzoic acid and 4-*t*-butylbenzoic acid (Table 21).

Table 21. Product distribution of the alkylbenzoic acids. Each product is shown as a % of the total. If there was only a single product, this was considered 100 %. In brackets, the % is shown when further oxidation products, which arise from this product, are included. A dash (-) means there was no formation of this product, and fields marked "N/A" mean that formation of a particular product was not possible.

Substrate	α-OH	β-OH	α,β-alkene	γ-OH
4-ethylBA	42 (43)	3	37 (54)	N/A
4-isopropylBA	63	-	37	N/A
4-*n*-propylBA	40	26	34	-
4-*t*-butylBA	N/A	100	N/A	N/A
4-cyclopropylBA	100	-	-	N/A
4-*n*-butylBA	46	-	50	4
4-isobutylBA	54	41	5	-
4-cyclohexylBA	33	66	< 1	-
4-*n*-heptylBA (*)	60	12	13 (16)	-

(*) The α,β-diol product could potentially have arisen from further oxidation of any of the α-OH, β-OH or α,β-alkene products. The α,β-epoxide was presumed to have arisen from the α,β-alkene.

The strength of C−H bonds is known to decrease with the degree of substitution (Table 22), and the reactivity of a C−H bond adjacent to a benzene ring (benzylic) is also lower than that of an aliphatic C−H (methyl C−H, 439 kJ mol^{-1}; secondary C−H, 404 kJ mol^{-1}; benzylic C−H, 377 kJ mol^{-1}).[53,225] This provided a rationale for the preference towards oxidation at the benzylic α-carbon with most of the alkylbenzoic acids. This is despite the closer proximity of the β-carbon to the heme iron in the majority of the crystal structures (4-*n*-heptylbenzoic acid was the exception; the α-carbon was closest). The higher degree of substitution could contribute to the increased levels of β-hydroxylation with 4-isobutylbenzoic acid (Table 21).

Table 22. Experimentally derived C–H bond dissociation energies (BDE) of alkanes and cycloalkanes. The bond-breaking energies were all determined experimentally in the gas phase at 298 K.[53,225]

C−H bond type	BDE ($kJ\,mol^{-1}$)
Primary[53] (H_3C-H)	439
Secondary[53] (H_3C-CH_2-H)	423
Tertiary[53] ($(CH_3)_3C-H$)	404
Benzylic[53] ($Ph-CH_2-H$)	377
Allylic[53] ($H_2C=CH-CH_2-H$)	372
Cyclopropane[225] (C−H)	456
Cyclohexane[225] (C−H)	418

Hydroxylation at a γ-carbon was observed in the turnover of 4-*n*-butylbenzoic acid but only as a further oxidation product of the alkene metabolite. Many of the hydroxylation products formed by CYP199A4 were chiral, however the enantioselectivity of each needs to be determined. The stereoselectivity of the CYP199A4 catalysed turnover of 4-ethylbenzoic acid was determined (as discussed in Chapter 4.2.3) which revealed that the 4-(1-hydroxyethyl)benzoic acid (S)-enantiomer was formed in excess: S, 87 %; R, 13 % (Appendix B.3). The determination of the enantioselectivity of the other hydroxy metabolites would be of significant interest, especially if these could be related to the position of the substrate in the crystal structure.

In the turnovers of 4-isopropylbenzoic acid by CYP199A4, the oxidation occurred predominantly at the benzylic α-carbon. Despite the close proximity of one of the isopropyl moiety β-carbons to the heme iron in the crystal structure (3.7 Å), there was no β-hydroxylation product. There was also no evidence of β-hydroxylation with 4-*n*-butylbenzoic acid. With these substrates it is possible that the initial hydrogen abstraction, and thus alkene formation, may arise from the α-carbon. Alternatively, β-abstraction may occur, and the rate of radical rebound is slow in comparison to either a second hydrogen abstraction or loss of an electron, accounting for the lack of β-hydroxylation product (Figure 81). In the CYP199A4 turnovers of 4-isobutylbenzoic acid, there was a greater amount of β-hydroxylation product compared to the less substituted substrates (Table 21). However, there was still a larger amount of hydroxylation at the α-carbon compared to the β-carbon (α, 54 %; β, 41 %). The lower levels of alkene formation with 4-isobutylbenzoic acid (5 %) suggests that radical rebound in this substrate is faster than the loss of an electron or second hydrogen abstraction. Despite this, the low coupling efficiency suggested that 4-isobutylbenzoic acid binds in an orientation that is not ideal for C−H bond abstraction. The crystal structures of CYP199A4 with 4-*n*-butylbenzoic acid, 4-isobutylbenzoic acid and their products would provide additional insight into the factors controlling these reactions. It may also provide a rationale for the seemingly sluggish rate of radical rebound in the turnovers

of 4-*n*-butylbenzoic acid, which leads to increased alkene formation.

Cycloalkyl functional groups were able to be oxidised by CYP199A4. In the turnovers of 4-cyclopropylbenzoic acid, there was no evidence of any β-hydroxylation or desaturation activities. The major product of 4-cyclohexylbenzoic acid oxidation was secondary β-hydroxylation rather than the benzylic α-carbon. This was the only substrate where there was a greater amount of β-hydroxylation than α-hydroxylation. There was also only a minimal amount of α,β-alkene product. P450 desaturation metabolites of cyclohexane rings have been reported previously,[226] suggesting their formation is not disfavoured by the strain imposed of forming a double bond.

Cyclohexane C−H bonds are comparable in bond energy to secondary C−H bonds (418 kJ mol^{-1} vs 423 kJ mol^{-1}, Table 22), and in the crystal structure the β-carbon is significantly closer to the heme iron than the α-carbon (4.0 Å vs 5.4 Å), rationalising the observed product distribution. Cyclopropane C−H bonds are stronger than methyl C−H bonds, suggesting they would be harder for Cpd I to abstract (456 kJ mol^{-1} vs 439 kJ mol^{-1}, Table 22).[53,225] The dissociation energy for a benzylic C−H bond is 377 kJ mol^{-1}, and this would presumably be higher for a benzylic cyclopropyl C−H bond. The lowered bond strength at this position relative to the cyclopropyl C_β bonds must contribute to formation of the α-hydroxylated cyclopropyl as the sole turnover product.

A small amount of an α,β-epoxide and an α,β-diol were formed in the 4-*n*-heptylbenzoic acid turnovers by CYP199A4 (Table 21). As with other turnovers of similar substrates the epoxide would result from alkene epoxidation. The diol may have arisen from further oxidation of either the α- or β-hydroxylated products, or alternatively by hydrolysis of the epoxide. In the *in vivo* turnover of 4-*n*-heptylbenzoic acid, there appears to be a reduced amount of the alkene product with a corresponding increase in the α,β-epoxide and an α,β-diol products.

The only instance of oxidation of a γ C−H bond in the substrate turnovers was the further oxidation of the α,β-alkene product of 4-*n*-butylbenzoic acid, which generated (E)-4-(3-hydroxybut-1-en-1-yl)benzoic acid. The α,β-alkene may tightly bind to the active site of CYP199A4 in an orientation where the γ-carbon is close to the heme iron, favouring hydroxylation over double bond epoxidation. Allylic C−H bonds have lower bond dissociation energy than secondary C−H bonds, which may account for the formation of this unusual product (allylic, 372 kJ mol^{-1}; vs secondary, 423 kJ mol^{-1}; Table 22). The alkene metabolites of 4-*n*-butyl- and 4-*n*-heptyl-benzoic acids could be good substrates for CYP199A4. Turnover experiments employing these alkenes as substrates would enable this sequence of steps to be elucidated.

In the crystal structures of 4-cyclohexyl and 4-*n*-heptylbenzoic acids, the orientation of the F298 residue was comparable to that observed in the structure of 4-ethylthiobenzoic acid (Chapter 4). The F298 residue seems to possess more conformational flexibility than the other nearby phenylalanine residues, and thus larger sub-

strates can be accommodated in the active site. Other benzoic acid substrates, such as those possessing *para*-phenyl moieties, could be trialled as substrates for CYP199A4.

The results of the *meta*-substituted 4-isopropylbenzoic acids indicated that the sterics of the *meta* moiety may impact the binding and turnover efficiency of CYP199A4. This could affect the position of the isopropyl group and distort the hydroxylation/desaturation partition. Therefore, the electronic effects of the substituent are negated. An alternate approach is required in order to investigate the factors controlling the partition between hydroxylation and desaturation. A series of enantiomeric 4-isopropylbenzoic acid analogues, containing mono- or tri-deuterated methyl groups, have been synthesised by the research group of James J. De Voss, University of Queensland (Figure 117). Investigation of the desaturation products in the CYP199A4-catalysed turnovers of these substrates, and the resulting kinetic isotope effect (KIE), should reveal whether hydrogen abstraction is stereospecific from one methyl group, and thus if this process is enzyme mediated. The results would also determine if the initial hydrogen abstraction is from the α- or β-carbon.

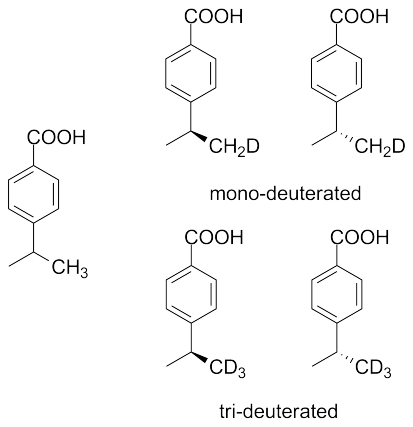

Figure 117. Mono- and tri-deuterated isopropylbenzoic acids developed as probe substrates.

Both 4-propionyl- and 4-(2-oxopropyl)-benzoic acids were regioselectively hydroxylated by CYP199A4, with the α-hydroxylation of 4-(2-oxopropyl)benzoic acid proceeding with higher coupling efficiency than the β-hydroxylation activity of 4-propionylbenzoic acid. Of note is that in the turnovers of 4-propionyl- or 4-(2-oxopropyl)benzoic acids there was no evidence of any further oxidation reactions, arising from carbon-carbon bond cleavage. It is possible that these hydroxycarbonyl products may be poor substrates for CYP199A4, or that the binding orientation of these compounds in the active site may prevent carbon-carbon bond cleavage. The study of these hydroxycarbonyl compounds as substrates for CYP199A4 turnovers and crystallography could establish the potential of this enzyme for catalysing carbon-carbon bond breaking reactions. An example of another system where carbon-carbon bond cleavage might be anticipated is the oxidation of fatty acids by $P450_{BM3}$. These reactions typically yield hydroxylated metabolites as well as α-hydroxycarbonyl metabo-

lites, however, no products could be detected which resulted from carbon-carbon bond cleavage of the hydroxycarbonyl moiety.[227–230] The P450 enzymes which have evolved to catalyse these reactions, such as $P450_{BioI}$ (CYP107H1),[113,114] may have very specific requirements which are not replicated in the CYP199A4 or $P450_{BM3}$ systems with their substrates. For example, $P450_{BioI}$ requires an acyl carrier protein-bound substrate.[231]

Overall, the results demonstrated that CYP199A4 can oxidise a wide range of alkyl substituents. Both the degree of substitution and the proximity of the carbon to the heme iron play a role in controlling the partition between the hydroxylation and desaturation products. The degree of desaturation could possibly be controlled by employing highly substituted substrates. CYP199A4 preferentially oxidises the benzylic α-carbon, however there exist conditions under which the β-carbon can be favoured. The hydroxylation of γ-carbons may require careful substrate selection, such as alkenes. Alternatively, mutagenesis of CYP199A4 active site residues, such as F298, could be employed to modify the substrate selectivity and product distribution of the enzyme.

Chapter 6 Investigation of molecular oxygen activation in CYP199A4

6.1 Introduction

The mechanism of oxygen activation in P450 enzymes implicates a proton relay system (Chapter 1.3). The peroxo-anion (Figure 1, Species V) accepts a proton to form the hydroperoxy intermediate (Cpd 0, Species VI), which upon a second protonation, triggers heterolytic O−O cleavage to form the iron(IV)-oxo species (Cpd I, Species VII). Upon formation, Cpd I reacts rapidly with the substrate to generate hydroxylated product via a radical rebound mechanism[36,39,54–56] (Figure 118).

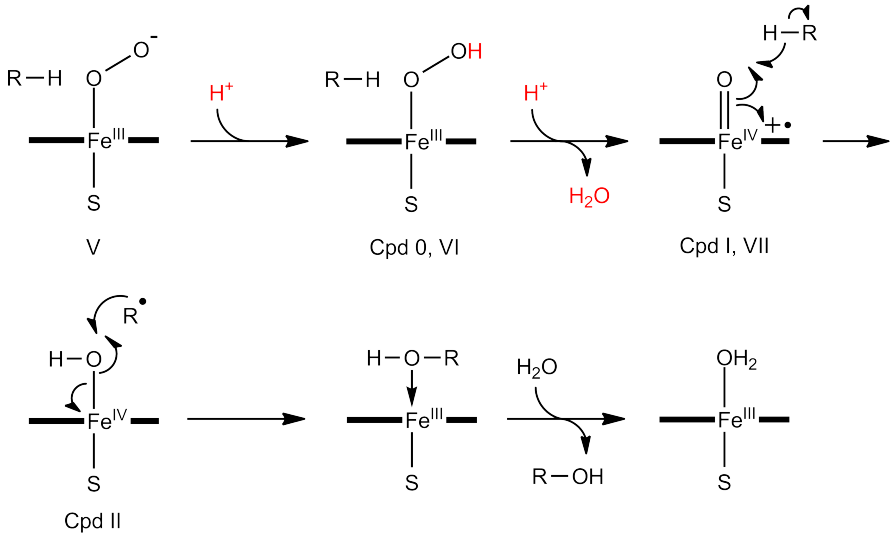

Figure 118. Generation of Cpd I and oxidation of substrate (R−H) via radical rebound. The protonation steps are highlighted in red.

The protonation steps are controlled by a highly conserved pair of residues found in the I-helix, most commonly an acid residue (aspartate or glutamate) and an alcohol residue (threonine or serine). In $P450_{cam}$, the best studied system, these residues are Asp251 and Thr252.[33] The roles of both residues have been investigated by mutagenesis to elucidate the mechanism of oxygen activation in P450s. Wild-type (WT) $P450_{cam}$ displays a fast turnover rate ($\geq 1000\,min^{-1}$) with nearly 100 % coupling efficiency for the conversion of camphor to 5-*exo*-hydroxycamphor. The Thr252 → Ala252 mutant (T252A) displayed 95 % uncoupling to H_2O_2 although the NADH oxidation rate remained comparable to that of the WT $P450_{cam}$.[41,42] Other mutants investigated include Thr252MeO-Thr,[46] Thr252-Asn and Thr252-Ser[33,39] which all displayed camphor hydroxylation activity albeit at a reduced level compared to the WT enzyme. It was proposed that Thr252 stabilises the hydroperoxy intermediate (Cpd 0) via a hydrogen bond with the heme-bound oxygen species.[45,47,48]

The Asp251 → Asn (D251N) mutant of $P450_{cam}$ displayed turnover activity that was two orders of magnitude lower than the WT, but the coupling efficiency of the product formation remained high[49] (Chapter 1.3). The proposed role of Asp251 in $P450_{cam}$ is proton delivery to the heme-bound dioxygen, facilitating protonation of the peroxy intermediate, and subsequently the hydroperoxy intermediate[33] (Figure 118, Species V and VI). The equivalent mutation in other P450s has been shown to have a similar effect on catalytic activity.[232]

The structural studies of $P450_{cam}$ have provided a wealth of structural information on the P450 catalytic cycle. $P450_{cam}$ has been shown to exhibit gating which is controlled by substrate binding,[203,232] as has CYP199A4, although other mechanisms have been proposed.[204] Furthermore, P450 enzymes have been identified in which the transfer of protons does not strictly require the acid-alcohol pair, emphasising the differences between individual systems. For example, $P450_{eryF}$ does not contain the conserved alcohol residue; it is replaced by an alanine (A245). It was proposed that the substrate hydroxyl group performs the same role as the threonine residue in $P450_{cam}$, permitting transfer of protons to a catalytic water molecule in the active site, and thus enabling substrate oxidation.[233–235] Further evidence for the importance of the alcohol residue in P450s was provided by mutation of the $P450_{eryF}$ A245 residue: the A245S[236] and A245T[237] mutants enabled $P450_{eryF}$ to hydroxylate substrates without a hydroxyl group.

Like $P450_{cam}$, CYP199A4 contains a pair of acid-alcohol residues, Asp251 and Thr252. As such these residues are expected to play an important role in the activation of molecular oxygen by this enzyme. CYP199A4 supports an extensive range of mono-oxygenase reactions on benzoic acid substrates with regioselectivity for the *para*-substituent. Examples include the demethylation of 4-methoxy- and 4-methylaminobenzoic acids, sulfoxidation of 4-methylthiobenzoic acid, and the hydroxylation and desaturation of 4-ethyl- and 4-isopropylbenzoic acids (Chapters 3, 4 and 5). While Cpd I is accepted to be the reactive species in the majority of P450 oxidations, there is the potential that other oxidants, such as the nucleophilic Cpd 0, play a role in certain reactions including sulfoxidation (Chapter 1.4.1).[39,69,71,76]

Due to its substrate specificity, CYP199A4 provides a ideal platform to investigate different P450 mono-oxygenase activities while making minimal changes to the size and shape of the substrate. Dealkylation of alkoxy groups is believed to proceed via hydrogen abstraction (HAT) by Cpd I from the carbon adjacent to the oxygen (Chapters 1.4.2, 3.1). Nitrogen dealkylation can occur via HAT or can have an alternative first step of single electron transfer (SET) from the nitrogen (Chapter 4.1). Sulfoxidation has been hypothesised to proceed by several mechanisms. The first proceeds by direct two-electron transfer of the Cpd I oxygen to the sulfur atom. Alternatively, the sulfoxide product can form by single electron transfer from the sulfur, yielding a sulfur radical cation, followed by transfer of the ferryl oxygen to the substrate.[39] It

has been shown computationally that the Fe(III)-H_2O_2 intermediate should be able to facilitate sulfoxidation.[238] It has also been hypothesised that the ferric hydroperoxy species (Cpd 0) plays a role in sulfoxidation reactions.[76] For the alkylbenzoic acids, the partition between hydroxylation and desaturation is thought to be controlled after the initial hydrogen abstraction, by the relative rates of radical rebound versus loss of an electron to form a carbocation or a second H abstraction (Chapter 5).

The activity of each of the substrates described above with WT-CYP199A4 are well characterised (Figure 119). Each of these will be investigated using T252A (Thr252 → Ala252) and D251N (Asp251 → Asn251) mutants of CYP199A4. This will allow the effect of mutating the acid-alcohol pair to be determined for the binding, turnover efficiency, and product distribution of each substrate (Figure 119). The crystal structures of these mutant CYP199A4 isoforms will also be explored in order to determine the role of each of these residues in comparison to other P450 systems.

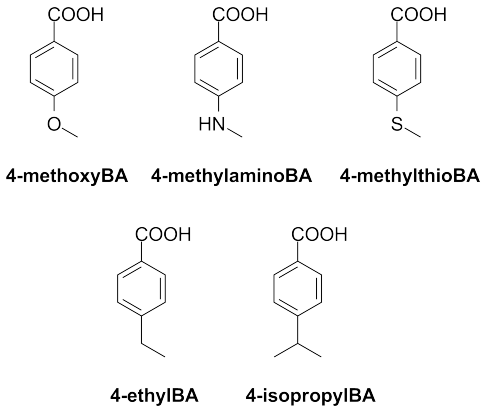

Figure 119. Substrates investigated with T252A and D251N mutants of CYP199A4.

6.2 Results

6.2.1 Substrate binding of the T252A and D251N mutants

The T252A and D251N mutants of CYP199A4 were expressed in *E. coli* and purified using the same methodology as the WT enzyme (Chapter 2.2). There was no discernable difference in the yield of each mutant P450. The ferrous CO spectum for each CYP199A4 mutant was recorded[2,136] (Chapter 2.2.1), and the near complete shift from resting state Fe(III) ($\approx$ 419 nm) to the CO-bound Fe(II) ($\approx$ 450 nm) indicated that each P450 was a viable mono-oxygenase (Figure 120).

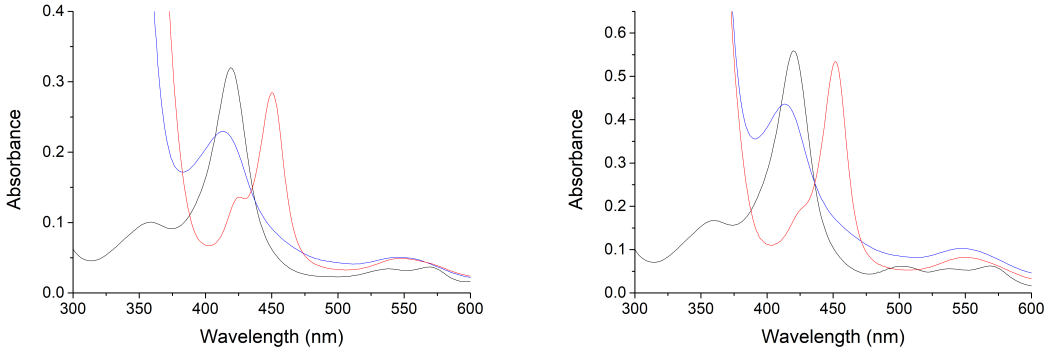

(a) T252A (419, 413, 450 nm) **(b)** D251N (420, 413, 452 nm)

Figure 120. Carbon monoxide binding assays of CYP199A4 mutants. Black shows resting state, Fe(III) CYP199A4, blue shows the reduced Fe(II) form after reduction by sodium dithionite, and red shows the characteristic Soret shift upon binding of CO. The wavelength maximum of each state are in brackets (ferric, ferrous, ferrous-CO). For the WT enzyme, these maxima were: 418, 414, 450 nm.

The spin state shift induced by the selected substrates with each CYP199A4 mutant was analysed, followed by determination of the binding affinity (Chapter 2.3). In most cases, the spin-state shifts of the substrate bound T252A and D251N CYP199A4 variants were comparable to that observed with the WT CYP199A4 (Table 23). 4-Methoxybenzoic acid induced a $\geq$ 95 % spin-state shift with wild-type (WT) CYP199A4 as well as the T252A and D251N mutants, as did the 4-ethyl and 4-isopropylbenzoic acid substrates. With 4-methoxy and 4-ethylbenzoic acids, the substrate binding was tighter with both mutants compared to the WT (Table 23). In contrast, the binding affinity of 4-isopropylbenzoic acid was marginally lower with the two mutated variants than with the WT CYP199A4.

The spin state shift of the T252A mutant with 4-methylaminobenzoic acid was higher than the WT enzyme (90 % vs 70 % respectively), but that of the D251N mutant was only 55 %. However, with both mutants the binding affinity for 4-methylaminobenzoic acid was higher than with the WT (Table 23). 4-Methylthiobenzoic acid shifted 70 % of the heme iron to high spin with the T252A isoform, the same as the WT enzyme. In contrast, the D251N mutant induced a

Table 23. Spin state shift and dissociation constant analyses (% HS and K_d, Chapter 2.3) for several benzoic acid (BA) substrates with mutants of CYP199A4 (Wild-Type, WT; T252A, Thr252 → Ala252; D251N, Asp251 → Asn251).

Substrate	HS (%)	K_d (µM)
4-methoxyBA WT	≥ 95	0.28 ± 0.01
4-methoxyBA T252A	≥ 95	0.22 ± 0.02
4-methoxyBA D251N	≥ 95	0.17 ± 0.01
4-methylaminoBA WT	70	1.6 ± 0.07
4-methylaminoBA T252A	90	0.83 ± 0.08
4-methylaminoBA D251N	55	0.73 ± 0.05
4-methylthioBA WT	70	2.3 ± 0.3
4-methylthioBA T252A	70	1.4 ± 0.1
4-methylthioBA D251N	20	0.83 ± 0.08
4-ethylBA WT	≥ 95	0.34 ± 0.02
4-ethylBA T252A	≥ 95	0.15 ± 0.01
4-ethylBA D251N	≥ 95	0.08 ± 0.03
4-isopropylBA WT	≥ 95	0.29 ± 0.01
4-isopropylBA T252A	≥ 95	0.33 ± 0.07
4-isopropylBA D251N	≥ 95	0.37 ± 0.09

significantly smaller shift (20 % vs WT, 70 %). In line with the majority of the other substrates, the binding affinity for 4-methylthiobenzoic acid was highest with the D251N mutant followed by the T252A mutant, which were both higher than the WT CYP199A4 (Table 23).

Overall, the spin state shifts of the T252A mutant of CYP199A4 were similar to the wild-type, which suggested that mutation of the conserved threonine does not greatly perturb the substrate binding environment of CYP199A4. The D251N mutant displayed reduced spin state shifts with 4-methylamino and 4-methylthiobenzoic acids. The binding affinity of each substrate was similar across the three CYP199A4 isoforms, although with most substrates the tightest binding was observed with the D251N mutant. With 4-isopropylbenzoic acid, the WT displayed slightly tighter binding than the D251N mutant. This suggested that mutation of the conserved aspartate has subtly changed the active site environment of CYP199A4, and this may alter the substrate binding or the spin state preference of the system.

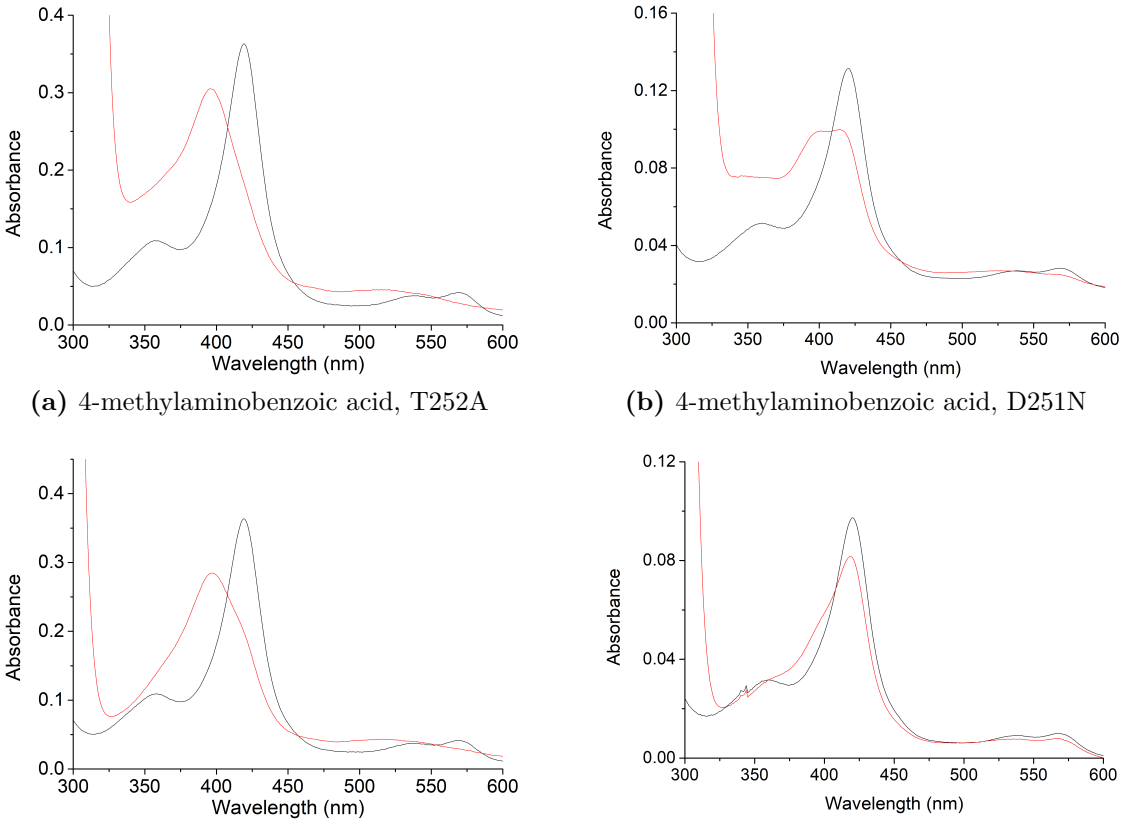

(a) 4-methylaminobenzoic acid, T252A

(b) 4-methylaminobenzoic acid, D251N

(c) 4-methylthiobenzoic acid, T252A

(d) 4-methylthiobenzoic acid, D251N

Figure 121. Spin state shifts of 4-methylamino- and 4-methylthiobenzoic acids with mutant isoforms of CYP199A4. Black shows CYP199A4 in its resting state and red shows the maximum absorbance shift obtained upon addition of substrate.

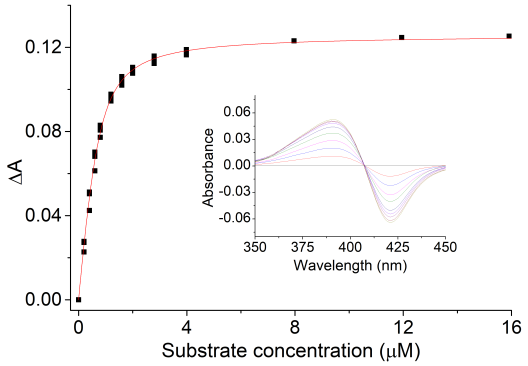

(a) 4-methoxybenzoic acid, T252A (421 nm, 391 nm, 1.3 µM)

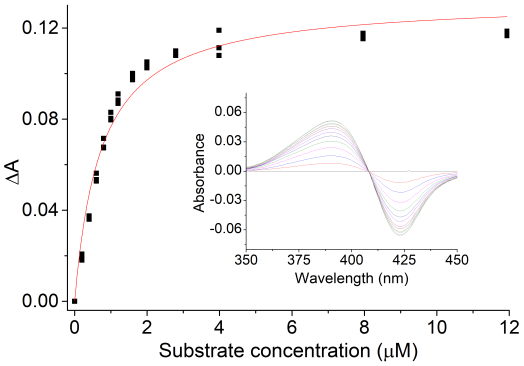

(b) 4-methylaminobenzoic acid, D251N (423 nm, 390 nm, 1.6 µM)

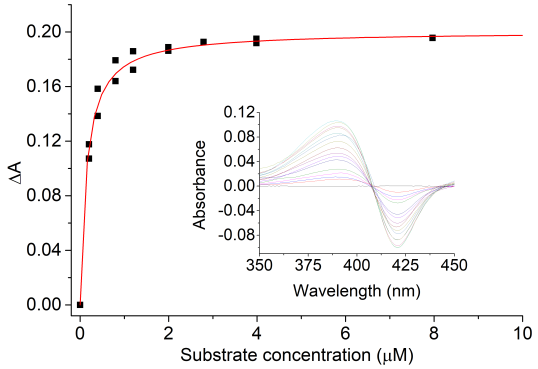

(c) 4-ethylbenzoic acid, T252A (421 nm, 390 nm, 1.8 µM)

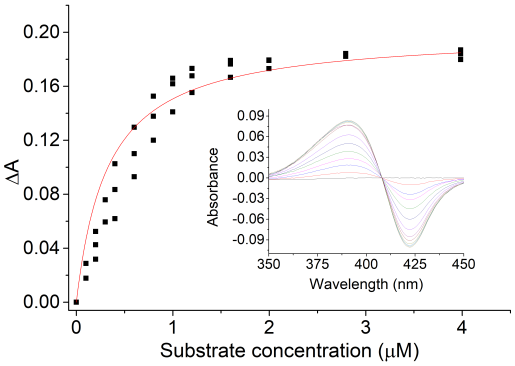

(d) 4-isopropylbenzoic acid, D251N (422 nm, 391 nm, 1.8 µM)

Figure 122. Dissociation constant determination of various substrates with the CYP199A4 mutants. The inset image shows the UV-Vis response to successive addition of substrate aliquots. Shown in brackets are the wavelengths of the trough and peak, and the enzyme concentration used for dissociation constant analysis (trough, peak, µM-P450).

6.2.2 Turnover activity of T252A-CYP199A4

In vitro turnovers of each substrate with the T252A and D251N mutant P450s were then performed (Chapter 2.4). The NADH oxidation activity of T252A-CYP199A4 with the majority of substrates was lower than that of the WT enzyme (Table 24). The exception was 4-isopropylbenzoic acid, where the NADH oxidation rate of T252A-CYP199A4 ($605\,\text{mol}\,(\text{molCYP})^{-1}\,\text{min}^{-1}$, henceforth abbreviated to min^{-1}) was nearly double that of the WT enzyme ($325\,\text{min}^{-1}$, Figure 123a). The most significant reduction in rate was with 4-methylaminobenzoic acid which decreased by a factor of three (WT, $923\,\text{min}^{-1}$; T252A, $273\,\text{min}^{-1}$). This was in spite of the spin state shift of this mutant being higher than that of the WT enzyme. In the case of 4-methoxybenzoic acid, the NADH oxidation rate of the T252A mutant was 62 % of the rate observed with the WT (Figure 123b), while it was 95 % for 4-ethyl- and 74 % for 4-methylthiobenzoic acid (Table 24). These results contrasted with the T252A-P450$_{\text{cam}}$ mutant, where no reduction in NADH consumption compared to the WT was reported.[41,42]

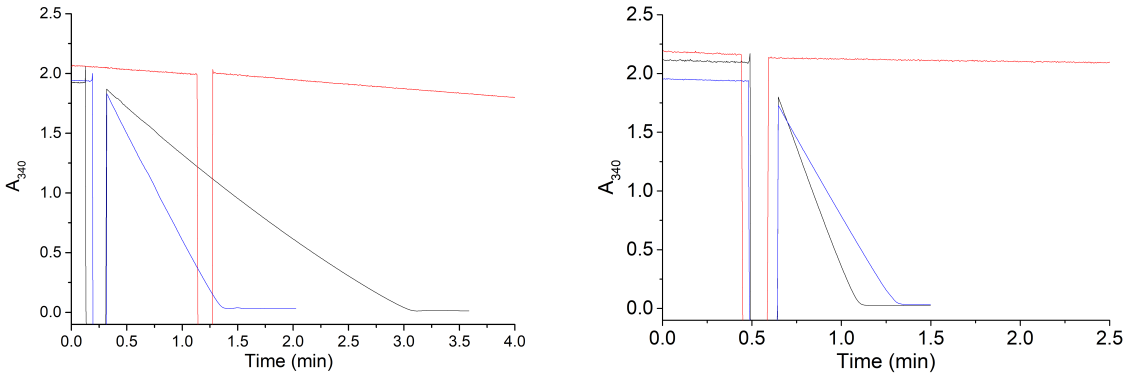

(a) 4-isopropylBA **(b)** 4-methoxyBA

Figure 123. NADH oxidation assays with (a) 4-methoxy- and (b) 4-isopropyl-benzoic acid, employing mutant CYP199A4s. In each is shown: **black**, wild-type; blue, T252A; red, D251N.

Turnovers of each substrate with T252A-CYP199A4 showed formation of the same products as with the WT enzyme, however the turnovers were less efficiently coupled, resulting in lower levels of product formation (Table 24). The most dramatic decrease in the coupling efficiency with the T252A mutant was observed with 4-methylthiobenzoic acid, which dropped to 42 % from 83 % with the WT enzyme. The largest decrease in product formation rate was 4-methylaminobenzoic acid, which dropped from $669\,\text{min}^{-1}$ to $99\,\text{min}^{-1}$ with the T252A mutant. 4-Isopropylbenzoic acid resulted in the smallest reduction in the T252A mutant coupling efficiency (58 % vs WT, 68 %). As a result of the increased NADH oxidation activity, the product formation rate of 4-isopropylbenzoic acid increased over the WT enzyme (T252A, $361\,\text{min}^{-1}$; WT, $221\,\text{min}^{-1}$, Table 24). With all other substrates, the product formation rate decreased due to lower coupling efficiency and NADH oxidation activity.

Table 24. Kinetic and turnover parameters determined for benzoic acid (BA) substrates with CYP199A4 (Wild-Type, WT; T252A, Thr252 → Ala252; D251N, Asp251 → Asn251). Shown are NADH oxidation rates (Chapter 2.4), product formation rates (PFR, Chapter 2.5), resulting coupling efficiency (%) and amount of hydrogen peroxide uncoupling (%, Chapter 2.7). Rates are given as mol (molCYP)$^{-1}$ min^{-1}.

Substrate	NADH[a]	PFR[b]	Coupling[c]	H_2O_2[d]
4-methoxyBA WT	1340 ± 28	1220 ± 120	91 ± 2	1.7 ± 0.2
4-methoxyBA T252A	833 ± 8	472 ± 56	55 ± 5	42 ± 3
4-methoxyBA D251N	7.3 ± 0.8	4.0 ± 1.0	59 ± 3	2.9 ± 0.1
4-methylaminoBA WT	923 ± 200	669 ± 15	64 ± 2	2.6 ± 0.4
4-methylaminoBA T252A	278 ± 12	99 ± 7	35 ± 4	12 ± 0.2
4-methylaminoBA D251N	32 ± 3	7.3 ± 1.5	22 ± 3	0.5 ± 0.1
4-methylthioBA WT	1430 ± 178	1180 ± 133	83 ± 3	1.6 ± 0.4
4-methylthioBA T252A	1060 ± 18	433 ± 29	42 ± 2	38 ± 1
4-methylthioBA D251N	10.3 ± 0.3	3.5 ± 0.1	34 ± 2	1.4 ± 0.1
4-ethylBA WT	812 ± 7	515 ± 32	64 ± 4	2.0 ± 0.1
4-ethylBA T252A	774 ± 12	352 ± 52	46 ± 7	38 ± 1
4-ethylBA D251N	14 ± 4	3.4 ± 0.7	24 ± 1	0.4 ± 0.1
4-isopropylBA WT	325 ± 36	221 ± 27	68 ± 1	1.5 ± 0.2
4-isopropylBA T252A	605 ± 20	361 ± 37	58 ± 5	21 ± 0.5
4-isopropylBA D251N	29 ± 1	10.0 ± 1.0	34 ± 4	0.7 ± 0.1

[a]Rate of turnover of NADH during the reaction. [b]Product formation rate. [c]% of NADH consumed that led to formation of substrate metabolite. [d]% of NADH consumed that led to formation of H_2O_2 via the peroxide uncoupling pathway.

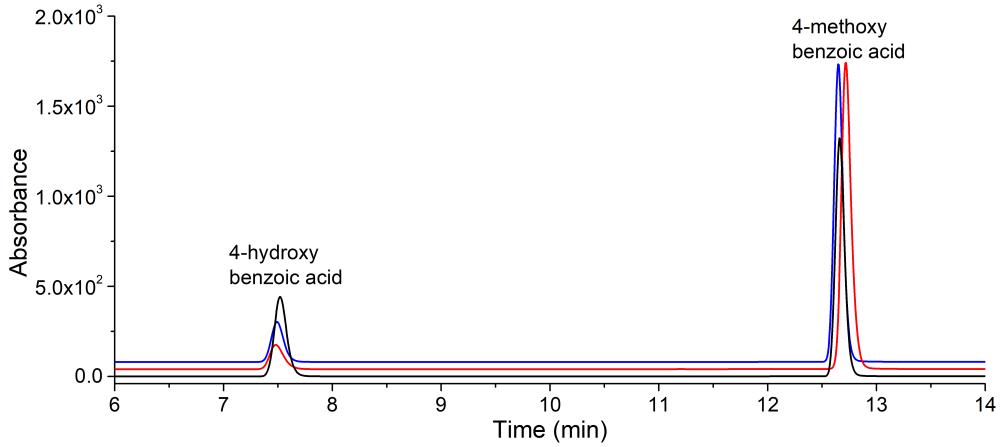

Figure 124. HPLC analysis of 4-methoxybenzoic acid turnover with mutants of CYP199A4. **Black**, wild-type; blue, T252A; red, D251N. The gradient was 20-95 % H_2O:ACN. The chromatogram was monitored at 254 nm.

The turnovers with the T252A mutant showed elevated levels of H_2O_2 formation, which accounted for the majority of uncoupled NADH equivalents (Table 24, Chapter 2.7). In the cases of 4-methoxy- and 4-methylthiobenzoic acids, the remaining NADH equivalents were almost all channelled into H_2O_2 generation (42 % and 38 % respectively). For the remaining substrates, H_2O_2 was observed but in insufficient quantities to account for all the NADH consumed (NADH unaccounted for: methylamino, 53 %; ethyl, 16 %; isopropyl, 21 %).[vii] In these cases, it is likely that the oxidase pathway is involved (Figure 1). These results contrast with that of T252A-$P450_{cam}$, where there was > 95 % uncoupling due to H_2O_2 for camphor hydroxylation. The increased levels of product formation in these T252A-CYP199A4 turnovers relative to T252A-$P450_{cam}$ suggests the effect of the Thr → Ala mutation is different in CYP199A4 and $P450_{cam}$.

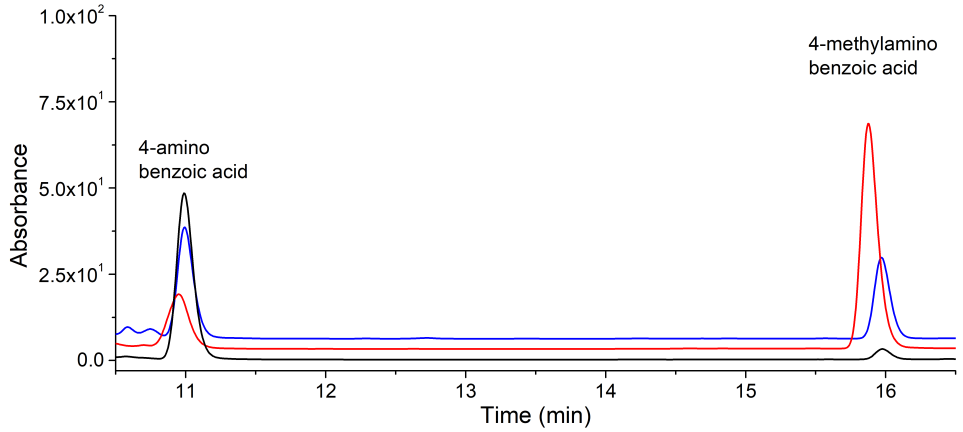

Figure 125. HPLC analysis of 4-methylaminobenzoic acid turnover with mutants of CYP199A4. **Black**, wild-type; blue, T252A; red, D251N. The gradient was 0-50 % of H_2O:ACN and the chromatogram wavelength was 254 nm.

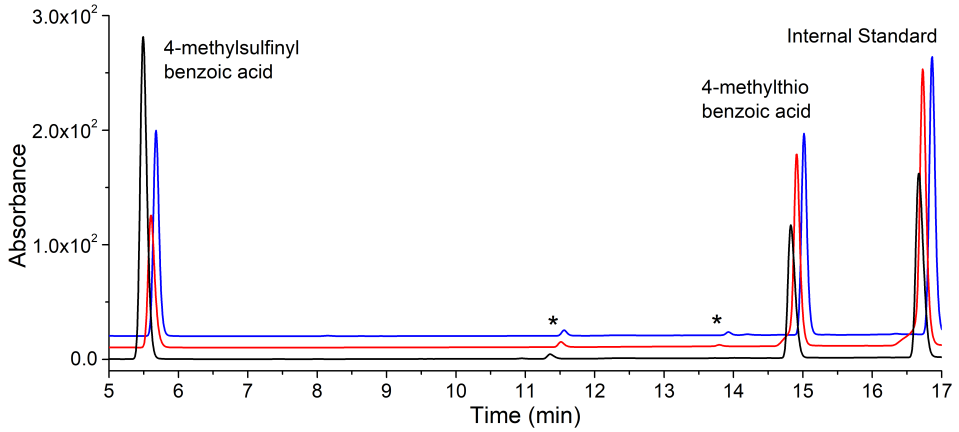

Figure 126. HPLC analysis of 4-methylthiobenzoic acid turnover with mutants of CYP199A4. **Black**, wild-type; blue, T252A; red, D251N. The chromatogram is offset along the x and y axes for additional clarity. Several substrate impurities that appeared in the turnovers are denoted (*). The gradient was 20-95 % H_2O:ACN, monitored at 254 nm.

[vii] In the wild-type enzyme, the % of NADH equivalents unaccounted for: methoxy, 7 %; methylamino, 33 %; methylthio, 15 %; ethyl, 34 %; isopropyl, 30 %.

There was no change in the products observed with 4-methoxy-, 4-methylamino- and 4-methylthio-benzoic acids with the T252A-CYP199A4 mutant. In the turnovers of 4-ethylbenzoic acid, the product distribution showed a reduced proportion of the desaturation metabolite, 4-vinylbenzoic acid, and its further oxidation product 4-(oxiran-2-yl)benzoic acid. There was a compensating increase in the levels of the further oxidation metabolite, 4-acetylbenzoic acid (Table 24, Figure 127). The turnovers of 4-isopropylbenzoic acid with T252A generated a higher yield of the hydroxylation product, 4-(1-methyl-1-hydroxyethyl)benzoic acid compared to the desaturation product, 4-(prop-1-en-2-yl)benzoic acid (T252A, 75:25 %; WT, 63:37 %; Table 25, Figure 128).

Table 25. Product distributions for 4-ethyl- and 4-isopropylbenzoic acids with CYP199A4 isoforms.

Substrate	C_α−OH	C_β−OH	C_α=C_β	C_α=O	epoxide
4-ethylBA WT	42 ± 1	3 ± 0.1	37 ± 0.3	1 ± 0.1	17 ± 1.3
4-ethylBA T252A	37 ± 0.1	7 ± 0.4	26 ± 1.6	25 ± 3.4	6 ± 0.9
4-ethylBA D251N	48 ± 0.5	3 ± 0.3	38 ± 0.1	5 ± 0.1	5 ± 0.4
4-isopropylBA WT	63 ± 1		37 ± 1		
4-isopropylBA T252A	75 ± 0.2		25 ± 0.2		
4-isopropylBA D251N	77 ± 5		23 ± 5		

6.2.3 Turnover activity of D251N-CYP199A4

The NADH oxidation activity of the D251N mutant with each substrate was several orders of magnitude slower than the WT enzyme. 4-Methoxy-, 4-methylthio- and 4-ethyl-benzoic acids consumed NADH at a rate comparable to the passive NADH leak rate ($\approx 9\,\mathrm{min}^{-1}$, Table 24). 4-Methylamino- and 4-isopropyl-benzoic acids displayed slightly higher rates ($32\,\mathrm{min}^{-1}$ and $29\,\mathrm{min}^{-1}$), although both of these were more than an order of magnitude slower than the WT.

The overall coupling efficiency of NADH oxidation towards product formation was reduced with every substrate, the most significant being 4-methylaminobenzoic acid (D251N, 22 % vs WT, 64 %). 4-Methoxybenzoic acid displayed the highest coupling efficiency of the substrates investigated although it was still lower than the WT (D251N, 59 % vs WT, 91 %).

The same products were observed for the D251N variant with each substrate although the 4-ethyl- and 4-isopropyl-benzoic acid metabolites were formed in slightly different ratios (Table 25). In the case of 4-ethylbenzoic acid, there was a decrease in the amount of epoxide product relative to the WT turnovers (D251N, 5 % vs WT, 17 %), with a slight increase in the yield of 4-(1-hydroxyethyl)benzoic acid (D251N, 48 % vs WT, 42 %) and 4-acetylbenzoic acid (D251N, 5 % vs WT, 1 %). The turnovers of D251N with 4-isopropylbenzoic acid also displayed a small change in the partition of the hydroxylation and desaturation metabolites: 4-(1-methyl-1-hydroxyethyl)benzoic acid was 77 % of total product (compared to WT, 63 %), and 4-(prop-1-en-2-yl)benzoic acid was 23 % of total product (WT, 37 %; Table 25).

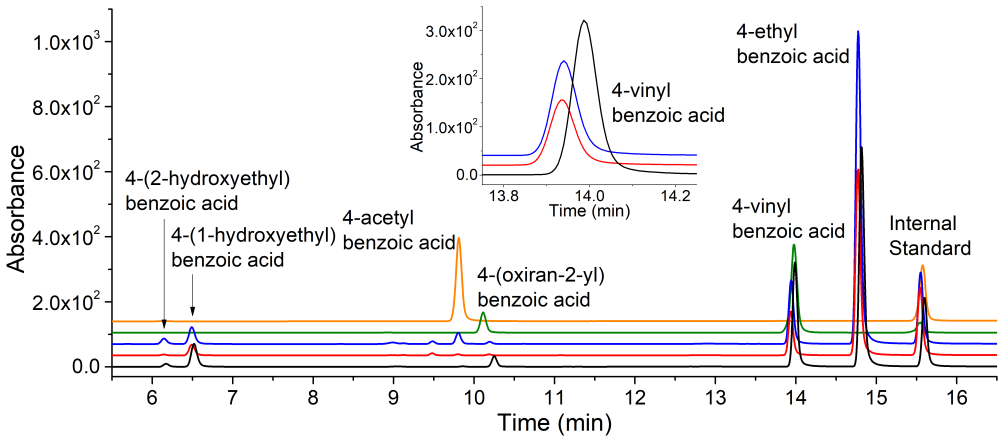

Figure 127. HPLC analysis of 4-ethylbenzoic acid turnover with mutants of CYP199A4. **Black**, wild-type; blue, T252A; red, D251N; green, turnover of 4-vinylbenzoic acid showing epoxide product peak at 10.2 min;[32] orange, 4-acetylbenzoic acid control. The inset shows the relative amounts of 4-vinylbenzoic acid formed in each CYP199A4 turnover. Control chromatograms of the hydroxy products can be found in Figure 86 (Chapter 5.2.2). A 20-95 % gradient of H_2O:ACN was used and the chromatogram was monitored at 254 nm.

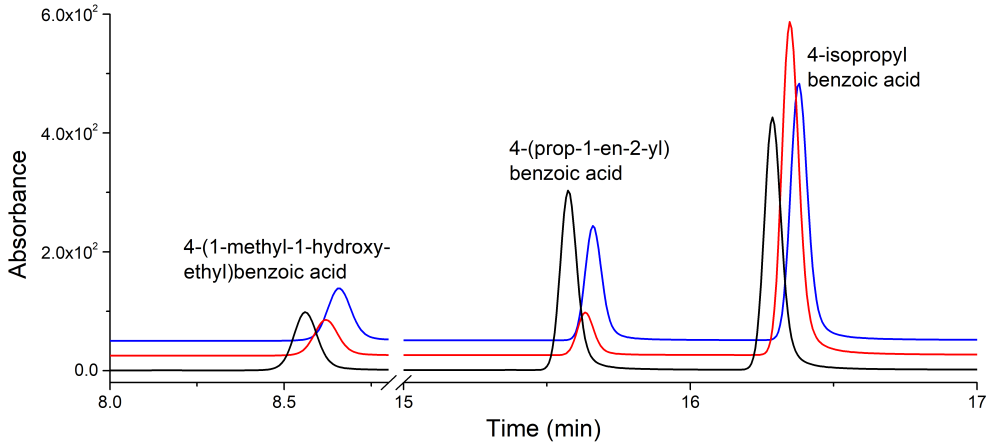

Figure 128. HPLC analysis of 4-isopropylbenzoic acid turnover with mutants of CYP199A4. **Black**, wild-type; blue, T252A; red, D251N. An x-axis break has been applied and the chromatogram has been offset along the x- and y-axes for clarity. A 20-95 % gradient of H_2O:ACN was used, and the chromatogram was monitored at 254 nm.

The formation of H_2O_2 in the turnovers of each substrate with the D251N variant was low and comparable to the amounts observed with the WT enzyme (< 3 % of total NADH equiv., Table 24). This indicated that other uncoupling pathways were consuming the remaining NADH. One possibility is air oxidation of the ferredoxin. Due to the drastically reduced rate of turnover with the D251N variant, air oxidation can compete with the catalytic cycling of the enzyme. The results for D251N-CYP199A4 were comparable to D251N-$P450_{cam}$, where product was still formed but there was a significant decrease in NADH and product formation activity.[44,49,50] It is important to note that the high coupling efficiency reported in the D251N-$P450_{cam}$ system was determined at pH 5.9, as the low NADH oxidation and product formation rates were even slower when the turnovers were performed at pH 7.0.[44] Additionally, the rates reported were corrected for background NADH oxidation, which was similar in magnitude to the NADH oxidation rate by the enzyme itself.

The results suggest that mutation of the threonine has less of an effect on product formation in CYP199A4 than in $P450_{cam}$, where camphor hydroxylation is effectively abolished. The most notable change with D251N-CYP199A4 was the considerably lower oxidation of NADH when compared with wild-type CYP199A4 (Table 24). This implicates a role in proton delivery for the aspartate residue in CYP199A4 in agreement with the results from the $P450_{cam}$ system.

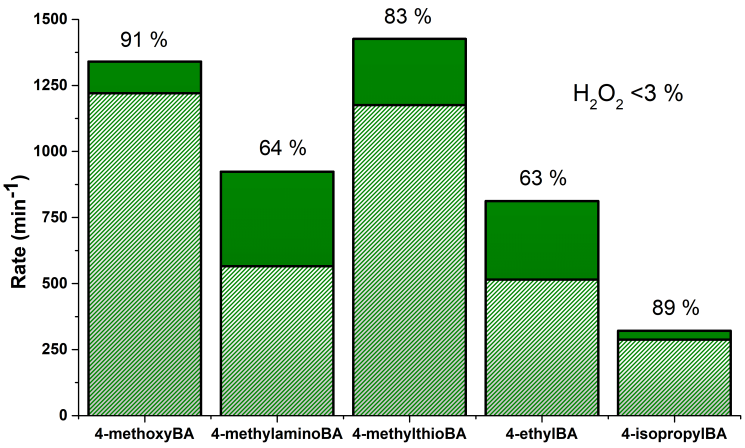

(a) Wild-Type

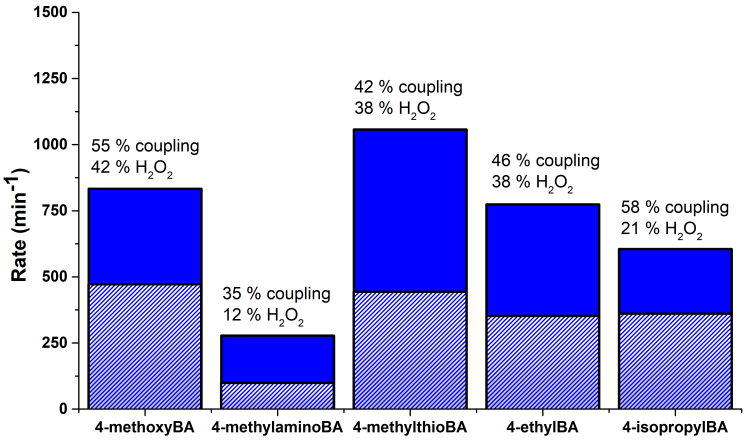

(b) T252A

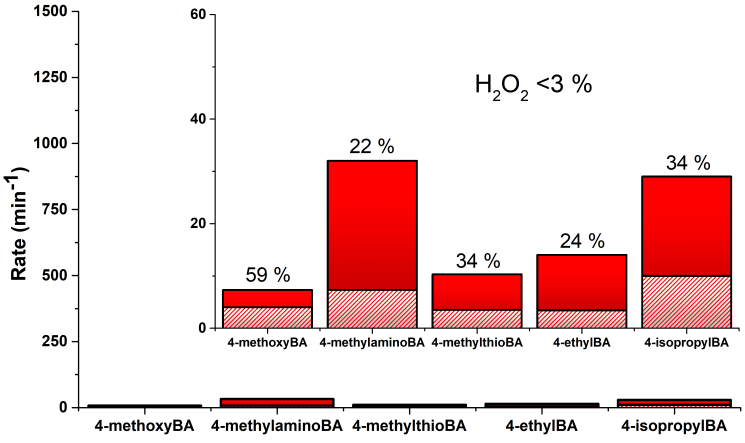

(c) D251N

Figure 129. Turnover parameters for CYP199A4 mutants. Shown are (a) green, wild-type; (b) blue, T252A and (c) red, D251N. The total bar (solid + stripes) represents the NADH oxidation rate (mol (molCYP)$^{-1}$ min^{-1}, which has been shortened to min^{-1}), while the striped portion of the bar represents the product formation rate (same units). The H_2O_2 uncoupling (%) is also shown for each. All are shown on the same y-scale for comparison. The inset in (c) shows a rescaled y-axis highlighting the dramatic reduction in activity.

6.2.4 Crystal structures of the T252A and D251N mutants

In light of the different behaviour of T252A-CYP199A4 compared to the equivalent variant of $P450_{cam}$, both the D251N and T252A mutants of CYP199A4 were investigated in more detail using X-ray crystallography. Both isoforms of CYP199A4 were co-crystallised with 4-methoxybenzoic acid and structures were obtained (Chapter 2.10). Crystals were obtained in 2 weeks from a 500 µL reservoir solution containing 0.2 M magnesium acetate tetrahydrate, 20-23 % w/v PEG-3,350 and 0.1 M Bis-Tris pH 5.25. High resolution data (T252A, 1.42 Å; D251N, 1.59 Å) were obtained at 100 K on the MX1 beamline at the Australian Synchrotron[147,148] and deposited online in the ww-PDB[157,158] (Table 26).

The crystals of the T252A and D251N mutants of CYP199A4 both had $P12_11$ cell symmetry and contained a single molecule in the asymmetric unit, similar to the WT

Table 26. Structural refinement and data collection statistics for CYP199A4 mutants (T252A, D251N) with 4-methoxybenzoic acid. Wild-type (WT) CYP199A4 (PDB: 4DO1) is shown for comparison.[131]

	WT[131]	T252A	D251N
PDB code	4DO1	5KDZ	5KDY
X-ray wavelength (Å)	0.9796	0.9537	0.9537
Unit cell (a/b/c)	107.0/143.5/172.8	41.3/51.3/79.5	44.7/51.4/78.3
($\alpha/\beta/\gamma$)	90/90/90	90/91.9/90	90/93.1/90
Space group	$P2_12_12_1$	$P12_11$	$P12_11$
Molecules per unit cell	4	1	1
Resolution range[a]	50 – 2.0	25.31 – 1.42	39.08 – 1.59
	(2.03 – 2.00)	(1.45 – 1.42)	(1.62 – 1.59)
$<I/\sigma(I)>$[a]	28.5 (5.2)	13.0 (4.0)	12.6 (4.0)
Unique reflections	179187	62253	47965
Completeness[a]	100.0 (100.0)	95.9 (79.9)	97.8 (83.2)
Multiplicity[a]	7.1 (6.1)	4.9 (4.1)	4.8 (3.9)
R_{merge}[a,b] (%)	9.8 (31.9)	6.3 (23.8)	6.6 (25.0)
R_{pim}[a,b] (%)	N/A[c]	3.2 (12.7)	3.3 (13.7)
$CC_{1/2}$[a,d] (%)	N/A[c]	99.8 (91.6)	99.7 (89.6)
R_{work}	0.154	0.135	0.185
R_{free}[e]	0.189	0.178	0.248
Ramachandran plot[f]			
Most favoured	98.5	97.5	97.4
Allowed	1.5	2.5	2.6

[a]Highest resolution shell is shown in parentheses where applicable. [b]all I+ and I-. [c]Not reported in previous work. [d]Half-correlation coefficient.[182,183] [e]5 % of total reflections, randomly selected. [f]% of all amino acid residues.[184] There were no Ramachandran outliers.

CYP199A4s presented in previous chapters (Chapter 3.2.4 and others). The overall topology of each CYP199A4 mutant was similar to that of the 4-methoxybenzoic acid-bound wild-type structure (PDB: 4DO1).[131] The solvent content of each crystal was comparable (T252A, 34.98 %; D251N, 39.07 %). The positions of the peptide backbone of all residues were functionally superimposable to the WT (D251N: rmsd = 0.542 Å; T252A: rmsd = 0.527 Å, both aligned over 392 of 393 residues; Appendix D.3). This indicated that the mutations were not disruptive to the fold of the enzyme. In the active site of each mutant CYP199A4, there was positive electron density corresponding to the 4-methoxybenzoic acid substrate. In the T252A structure, the electron density map confirmed the presence of the alanine residue at the 252 position (Figure 130). The electron density of the 251 residue could plausibly be either an aspartate or asparagine, however the altered position of this residue compared to the WT and T252A variants suggested that it was likely to be the mutated asparagine.

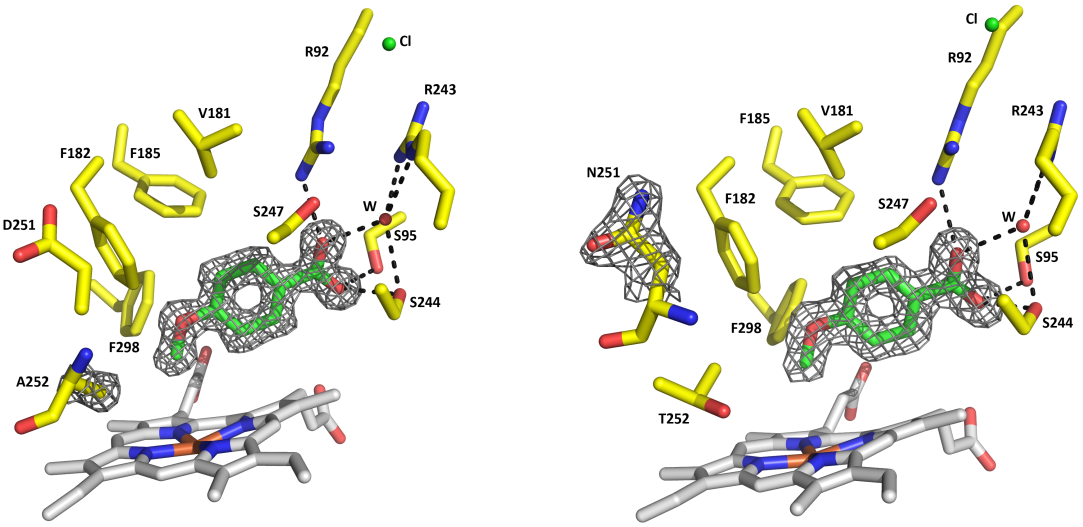

(a) T252A **(b)** D251N

Figure 130. Composite omit maps of 4-methoxybenzoic acid-bound forms of the mutant CYP199A4 enzymes. The electron density of the substrate and the mutated residue are shown contoured as a grey mesh at the 1 σ level using a reduced bias $2mF_o$-DF_c composite omit map.[154]

The positions of the 4-methoxybenzoic acid in the mutant CYP199A4 structures were comparable to that of the wild-type (Figures 131 and 132). In each structure the chloride anion that caps the active site from solvent access was also found in an nearly identical position, as was the water molecule that is part of the substrate carboxylate hydrogen bonding network.[131] In order to make observations on the likely orientation of the substrate relative to the active oxidant, a Cpd I oxygen was modelled at 1.62 Å from the heme iron in the structures of both CYP199A4 mutants[185] (Chapter 2.10). It was found that the angle of the methoxy group C_{Me} to Fe=O was comparable to that of the wild-type (Table 27). There was a small change in the distance from the Cpd I oxygen to the methoxy group C_{Me} or O in either of the mutant CYP199A4s ($\leq$ 0.2 Å).

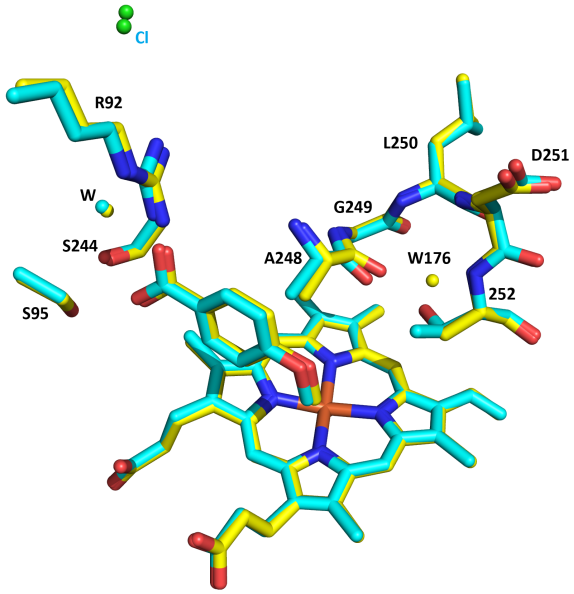

Figure 131. Overlay of the active site and oxygen binding groove of 4-methoxybenzoic acid bound T252A-CYP199A4 with WT CYP199A4. Wild-type CYP199A4 with 4-methoxybenzoic acid (cyan) is overlaid with T252A-CYP199A4 (yellow). The water molecules are shown as spheres in the same colour of their respective structures. The chloride anion is a green sphere.

In the T252A-CYP199A4 crystal structure, the oxygen binding groove from A248 to T252 was slightly narrower than in the wild-type due to a movement of the A248 backbone (Table 28). This was determined by taking measurements between: the G249 N atom to the 252 N atom; the A248 carbonyl to the 252 N atom; and the A248 carbonyl to the 252 side-chain β-carbon (Table 28). Another structural change was the breakage of the A248-T252 hydrogen bond, which allows a water molecule to bind in the space generated by the absence of the threonine hydroxyl group (Figure 131, W176). This water forms hydrogen bonds to the carbonyls of both A248 (2.6 Å) and A249 (3.0 Å), and was 3.4 Å from the A252 C_α and 3.3 Å from the side chain C_β (Table 27). The water was 6.6 Å from the heme iron and 7.8 Å from the methyl group of 4-methoxybenzoic acid.

In WT-P450$_{cam}$, there is a single water molecule bound in the O_2 binding groove (A248 to T252). In the T252A-P450$_{cam}$ structure, there are two water molecules in the groove. The additional water also replaces the threonine hydroxy group but is in a different position compared to that in CYP199A4. It is 5.9 Å from the heme iron and 4.1 Å from the closest methyl of camphor (Figure 4a,b). There are other structural changes as a result of this mutation, and the O_2 binding groove of T252A-P450$_{cam}$ has widened compared to the WT[47] (Discussion Chapter 6.3).

Table 27. Distances of key structural features of 4-methoxybenzoic acid-bound mutant CYP199A4s. The 4-methoxybenzoic acid methoxy group atoms are referred to as C_{Me} and O_{Me}. A ferryl Cpd I oxygen was modelled 1.62 Å from the heme iron (denoted **O**=Fe).

Distance (Å)	WT	T252A	D251N
C_{Me} - Fe	4.1	4.0	4.0
C_{Me} - **O**=Fe	2.7	2.5	2.6
O_{Me} - Fe	5.2	5.1	5.2
O_{Me} - **O**=Fe	3.6	3.4	3.6
A248 - T252 (H-bond)	2.6	-	2.5
New H_2O - A248 (H-bond)	-	2.6	-
New H_2O - Fe	-	6.6	-
New H_2O - **O**=Fe	-	6.2	-
Angle (°)			
Fe=O-C_{Me}	140.7	140.3	143.4
Fe=O-O_{Me}	158.3	161.1	161.1

Table 28. Analysis of the O_2 binding groove in CYP199A4. Shown is a generalised schematic of the loop region from 248 to 252. **1**, **2** and **3** denote the key measurements from one side of the loop to the other (Red denotes atom labels and distances). The label next to each residue indicates the one-letter code and residue number.

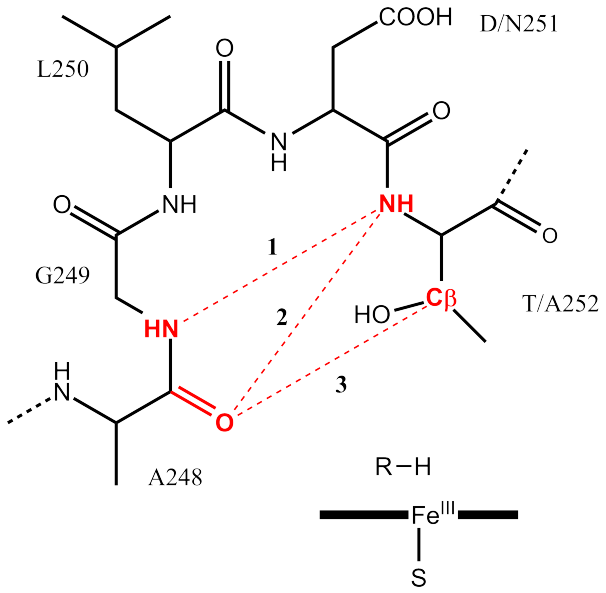

Measurement	WT	Thr → Ala (*)	Asp → Asn
N - - **1** - - N	5.8	5.5 (-0.3)	5.7
O - - **2** - - N	4.2	3.6 (-0.6)	4.3
O - - **3** - - C_β	3.5	3.5 (0)	3.6

(*) The difference between the WT and Thr → Ala mutant is shown in brackets. Distances are Å. In the case of Asp → Asn, the difference was always ≤ 0.1 Å.

As with the equivalent T252A-P450$_{cam}$ variant, there was an increase in the levels of H_2O_2 observed in the T252A-CYP199A4 turnovers, which suggests some build-up or destabilisation of Cpd 0. However, the T252A mutant of CYP199A4 results in lower peroxide uncoupling compared to T252A-P450$_{cam}$. Therefore the changes in the O_2 binding groove must not interfere with protonation of the peroxy intermediate to the same extent as in P450$_{cam}$ (Figure 118, Species V). This could arise, in part, as the water molecule is bound further from the heme iron than in the equivalent T252A-P450$_{cam}$ structure. The structural changes in the oxygen binding groove are also less pronounced in T252A-CYP199A4 and this may alter the stability of the oxy-bound intermediate between the two enzyme variants (Discussion Chapter 6.3).

In the D251N-CYP199A4 crystal structure, there are no obvious changes in the active site near the substrate or heme, nor are there additional water molecules in this region (Figure 132). However, the N251 mutant residue has rotated relative to the D251 side chain in the WT and T252A structures. In addition, the nearby N255 residue has rotated 90°. In the WT, the N255 forms hydrogen bonds to the backbone carbonyl and side chain carboxylate groups of D251, and these hydrogen bonds are broken in the D251N structure (WT, D251-carbonyl - N255 = 2.8 Å, D251-carboxylate - N255 = 3.3 Å vs D251N, N251-carbonyl - N255 = 4.3 Å, N251-carboxylate - N255 = 4.9 Å).

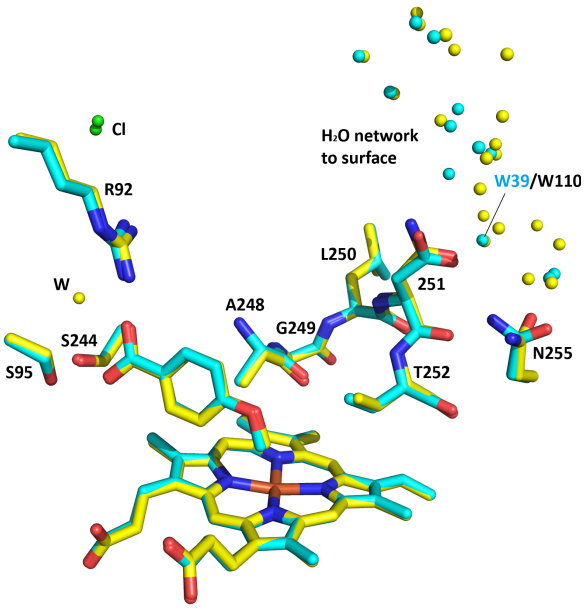

Figure 132. Overlay of the active site of 4-methoxybenzoic acid bound to D251N-CYP199A4 with WT CYP199A4. Wild-type CYP199A4 with 4-methoxybenzoic acid (cyan) is overlaid with D251N-CYP199A4 (yellow). The water molecules are shown as spheres in the colour of their respective structures. The labelled water molecule (WT, W39; D251N, W110) forms hydrogen bonds with the nearby N255 residue (Figures 133 and 134).

In $P450_{cam}$, the D251 side chain forms salt bridges to the side chains of K178 and R186, and forms hydrogen bonds with N255 (Figure 4). In WT-CYP199A4, D251 participates in the above mentioned hydrogen bonding interaction with the nearby N255 residue, and these two residues are hydrogen bonded to a water molecule (W39, Figure 133a). In the D251N structure, there was no water molecule that was directly interacting with both of the N255 and N251 residues, as W39 does in the WT structure (Figure 133). Significantly in CYP199A4, there are no residues available for salt bridge formation with D251N, but this residue is linked to an extensive chain of water molecules which leads to the enzyme surface through a solvent access channel (Figure 134a). This seems likely to be the source of protons employed in oxygen activation by CYP199A4. In the structure of the D251N mutant, the locations of the residues that line this solvent access channel were essentially superimposible with those in the WT (Figures 133b and 134b; Appendix D.3). There was a larger number of water molecules comprising the network in the D251N mutant (D251N, 20 waters, vs WT, 13 waters; T252A, 15 waters, Appendix D.3).

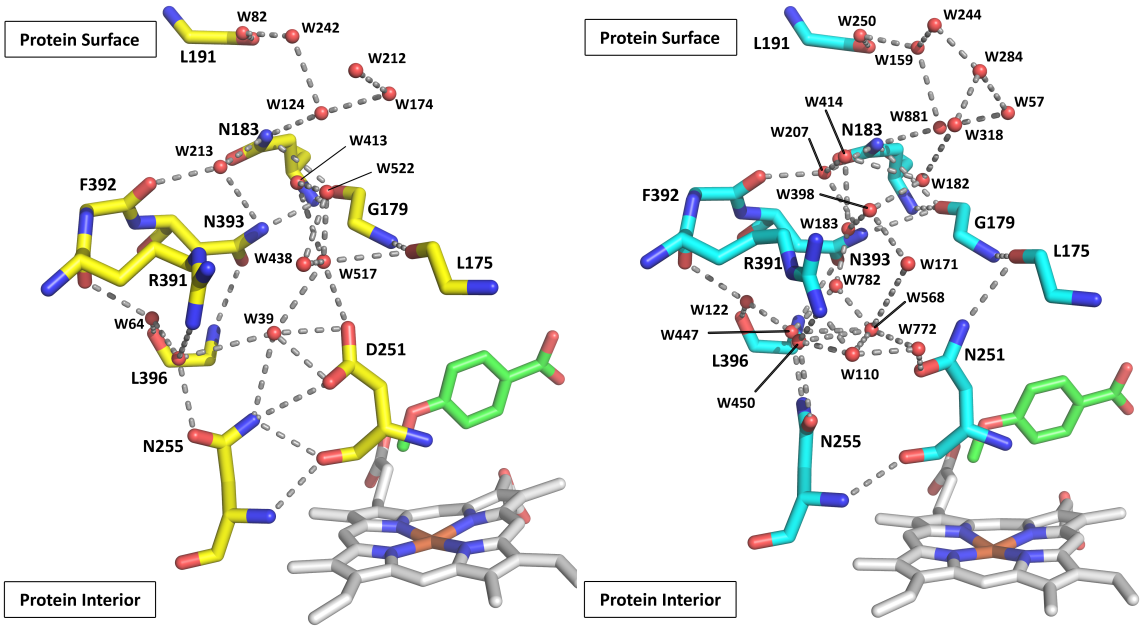

(a) WT-CYP199A4 **(b)** D251N-CYP199A4

Figure 133. (a) The solvent network extending from the 251 residue to the surface of WT-CYP199A4 through a solvent access channel. 4-Methoxybenzoic acid is green, the heme and hydrogen bonds are grey, and water molecules are red spheres. (b) The equivalent network for the D251N-CYP199A4 mutant (residues coloured in cyan). There are more water molecules in the solvent network of D251N-CYP199A4 compared to the WT. In D251N-CYP199A4, the hydrogen bond between the side chains of D251 and N255 is broken.

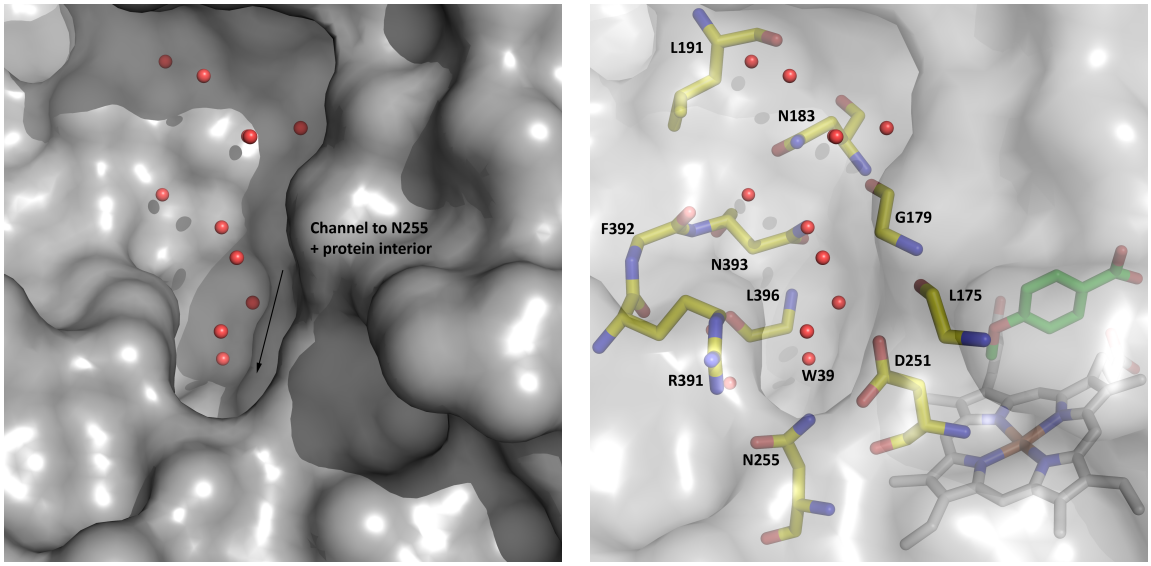

(a) WT-CYP199A4

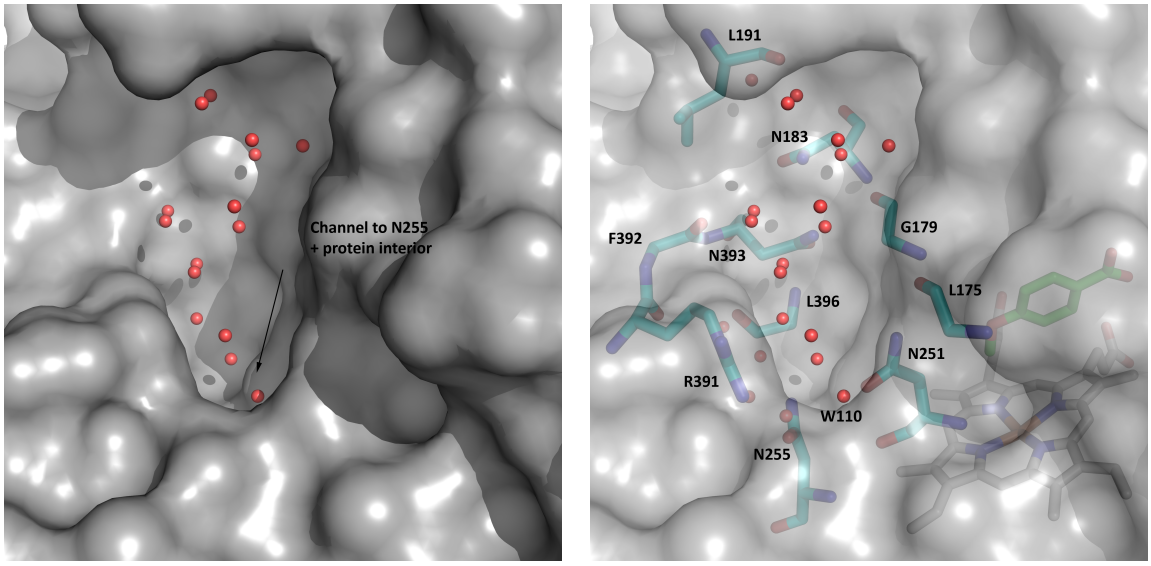

(b) D251N-CYP199A4

Figure 134. Space-filling surface models of the solvent access channel of CYP199A4. The left image shows the outer surface proximal to the access channel, while the right shows the location of residues near the channel. 4-Methoxybenzoic acid is green, the heme is grey and water molecules are red spheres. The side chains of several hydrophobic residues have been omitted for clarity (L175, L191, F392, L396). There were no significant differences in the positions of the residues in the solvent network and access channel for the T252A mutant of CYP199A4.

6.3 Discussion

The decrease in coupling efficiency and product formation activity upon mutation of the conserved threonine are much less dramatic in T252A-CYP199A4 than in T252A-$P450_{cam}$. The T252A-$P450_{cam}$ system displayed only a small change in the rate of NADH oxidation. However, 95 % of the reducing equivalents were channelled towards hydrogen peroxide formation and thus there was little product detected in turnovers.[41,42,47] The large reduction in product formation in T252A-$P450_{cam}$ was hypothesised to arise from an accumulation of the hydroperoxy intermediate (Cpd 0) rather than Cpd I.[41,42] This was used as evidence that Cpd I was the active oxidant in camphor hydroxylation by $P450_{cam}$. Subsequent studies have shown this to be the case for C−H bond oxidation.[33,45,48] Furthermore, the increased epoxidation activity of the T252A mutant of $P450_{cam}$ with 5-methylenecamphor was proposed as evidence of the catalytic epoxidation activity of Cpd 0.[239–241]

Similar results have been observed with the equivalent threonine to alanine mutant of another closely related class I system, CYP101D1 from *Novosphingobium aromaticivorans*. This enzyme, like $P450_{cam}$, oxidises camphor to 5-*exo*-hydroxycamphor.[242] However, other P450 systems display significant differences. For example, the turnovers of the T268A mutant of the class III enzyme $P450_{BM3}$ with C12 and C16 fatty acid substrates displayed a moderate reduction in NADPH oxidation and product formation compared to the wild-type (WT) enzyme.[243–245] It was further demonstrated that high activity could be achieved with the T268A mutant by employing C14 and C15 fatty acid substrates. This suggested a substrate dependence for the activity of $P450_{BM3}$, and a less critical role for Thr268 compared to the conserved threonine in other P450s.[78] $P450_{BM3}$ is unusual in that it is fused to its reductase domain (FAD/FMN cofactors), and it has a sequence which is more similar to that of mammalian P450 enzymes,[20] making direct comparison to $P450_{cam}$ more difficult.

The oxidation of *para*-substituted benzoic acids by the T252A-CYP199A4 class I system displayed more moderate changes in activity than in the $P450_{cam}$ system. With the majority of substrates, there was a decrease in the activity of the enzyme due to lower coupling efficiency and a corresponding increase in hydrogen peroxide formation. The trend with CYP199A4 was more similar to that observed with T268A-$P450_{BM3}$ than that of T252A-$P450_{cam}$. Given that formation of Cpd I is required for P450 C-H bond hydroxylation, Cpd I must form more readily in the Thr → Ala variants of CYP199A4 and $P450_{BM3}$ compared to $P450_{cam}$. This would explain the observation that there is a relatively small decrease in activity in some threonine to alanine mutants.

The available crystal structures of $P450_{cam}$, CYP101D1, $P450_{BM3}$ and now CYP199A4 enable a detailed comparison of the structural changes in the oxygen binding grooves of these enzymes. This allows a better understanding of the mechanism of O_2 activation in different P450 enzymes. The crystal structure of WT $P450_{cam}$ reveals that the side chain of Asp251 forms salt bridges with the nearby Lys178 and Arg186.[44,45,49] The D251 residue of CYP101D1 also participates in a salt bridge network, albeit a less extensive one than that of $P450_{cam}$ (Figure 135). The L178 residue of the latter has been replaced with a glycine but the arginine is conserved.

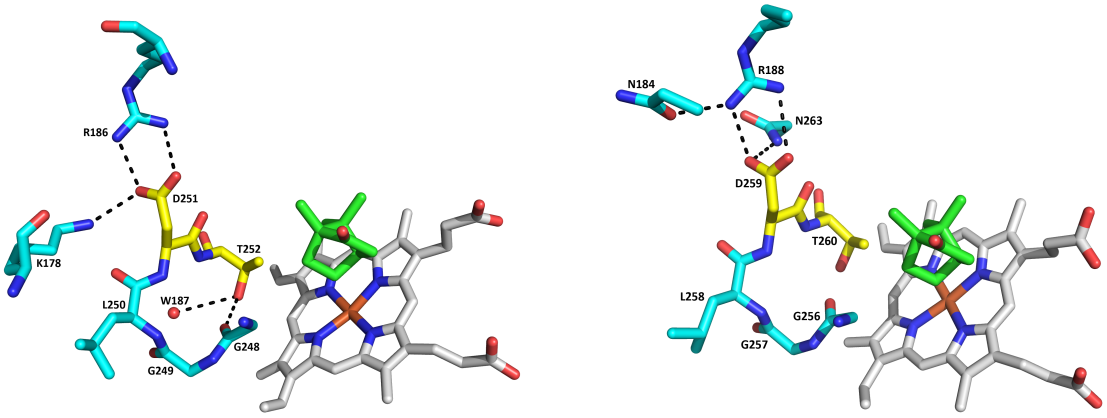

(a) Wild-type $P450_{cam}$ (PDB: 5CP4) **(b)** Wild-type CYP101D1 (PDB: 4C9K)

Figure 135. Comparison of the oxygen binding groove and salt bridge network formed by the conserved acidic residue of $P450_{cam}$ and CYP101D1. Camphor is green, the heme is grey, the conserved acid-alcohol residues are yellow and water molecules are red spheres.

$P450_{BM3}$ contains a glutamate residue rather than aspartate, and this is not involved in a salt bridge network. Instead, it hydrogen bonds to a network of water molecules which leads to the enzyme surface.[246] In CYP199A4, there are hydrogen bonds formed between the D251 and N255 side chains and water molecules (Figure 133).

The oxygen binding groove in the I-helix of $P450_{cam}$ widens upon mutation of the Thr252 to Ala, due to the broken hydrogen bond between the A248 carbonyl and T252 hydroxyl, and entry of an additional water molecule. The oxygen binding groove also widens in the O_2- and CN^--bound crystal structures of WT-$P450_{cam}$ (Figure 136a and Appendix D.3).[viii] In CYP101D1, comparable structural changes are observed in the T260A-CYP101D1 and the CN^--WT structures[242] (Figure 136b and Appendix D.3).

Currently, the PDB does not contain a full complement of crystal structure data for fatty acid-bound $P450_{BM3}$ and its mutants. Substrate free structures, which may not be comparable to the substrate-bound structures, are available for the wild-type[245] and T268A mutant[246] (Figure 137). These indicate that the T268A mutation results in breakage of the G265 carbonyl-T268 hydrogen bond and allows an additional water molecule to enter the oxygen binding groove. However, the resulting structural change

[viii] In the O_2-bound structure of $P450_{cam}$ there is an additional water molecule which is thought to provide access to the external solvent (Figure 4d).[33]

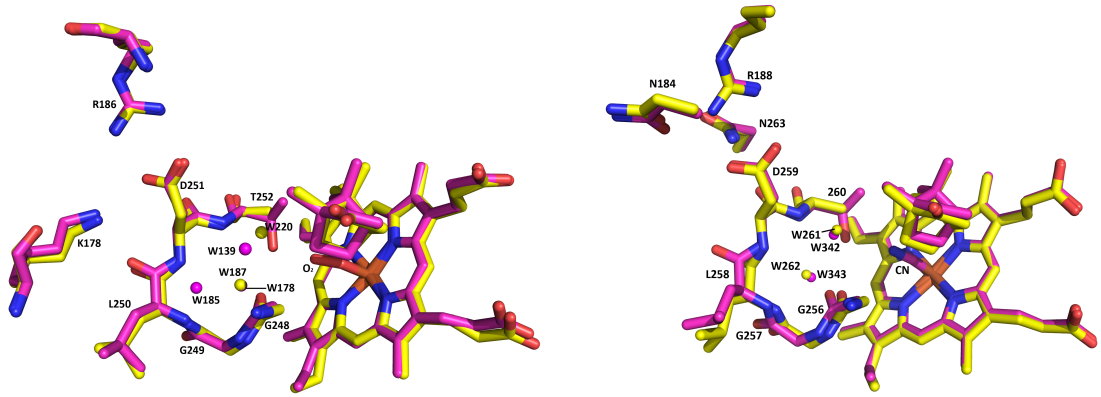

(a) T252A-P450$_{cam}$ (yellow, PDB: 2CP4) overlaid with O_2-bound WT (magenta, PDB: 2A1M)

(b) T260A-CYP101D1 (yellow, PDB: 4C9P) overlaid with CN^--bound WT (magenta, PDB: 4C9L)

Figure 136. Overlays of (a) WT O_2-bound P450$_{cam}$ and (b) WT CN^--bound CYP101D1, both with their respective Thr → Ala mutants. The O_2 and CN^- ligands are believed to induce structural changes in the oxygen binding groove which are comparable to those observed in the Thr → Ala mutants.[232] Refer to Appendix D.3 for a comparison of the O_2- and CN^--bound P450$_{cam}$ structures.

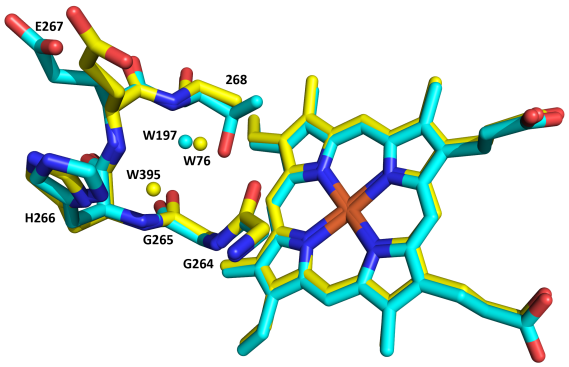

Figure 137. Active site and oxygen binding groove of the substrate-free P450$_{BM3}$ T268A mutant. Wild-type P450$_{BM3}$ (cyan, PDB: 2IJ2),[246] is overlaid with the T268A mutant (yellow, PDB: 1YQO).[245] The water molecules are shown as spheres in the colour of their respective structures. Upon mutation of the Thr268, the oxygen binding groove widens to a lesser extent than in P450$_{cam}$ and CYP101D1.

in the oxygen binding groove of P450$_{BM3}$ is less than that of P450$_{cam}$ and CYP101D1, and is more comparable to CYP199A4 (Table 29).

Mutation of the threonine in CYP199A4 has a lesser effect on turnover uncoupling compared to P450$_{cam}$. The crystal structure of 4-methoxybenzoic acid-bound T252A-CYP199A4 has several features which help to rationalise this observation (Figure 131). The additional water molecule in T252A-CYP199A4, which binds in the space vacated by the broken T252-G248 hydrogen bond, is positioned further away from the heme iron than in the equivalent mutations of P450$_{cam}$ and CYP101D1 (Figure 138, 6.4 Å vs 5.9 Å and 6.0 Å, respectively). The oxygen binding groove of T252A-CYP199A4 opens up to a significantly lesser degree than other class I P450 systems (Figure 139, Table

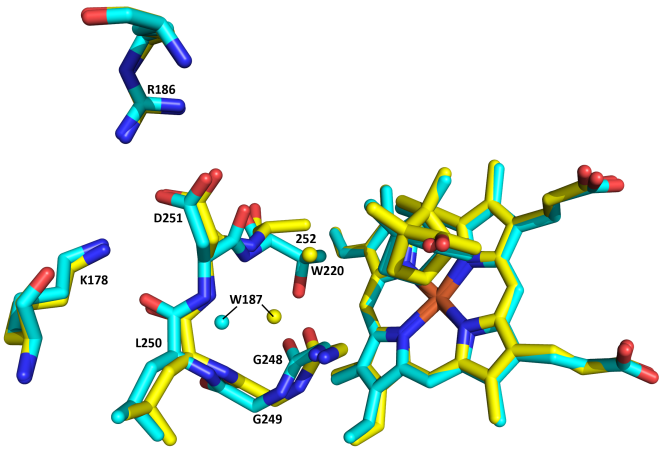

(a) WT-P450$_{cam}$ overlaid with T252A

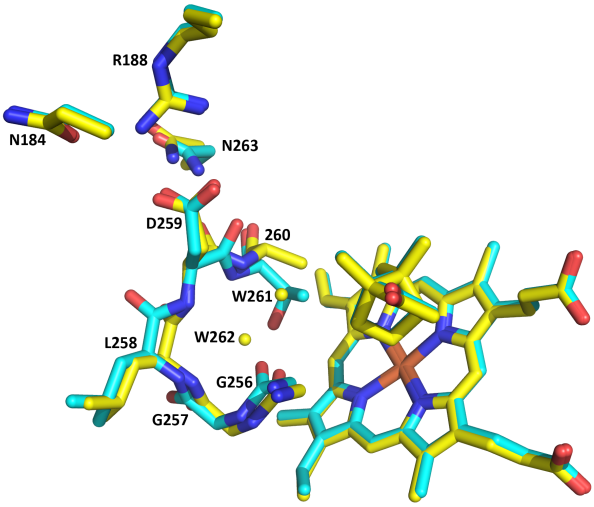

(b) WT-CYP101D1 overlaid with T260A

Figure 138. The active site and oxygen binding groove of Thr → Ala mutants. Wild-type camphor-bound P450$_{cam}$ and CYP101D1 (cyan, PDBs: 5CP4 and 4C9K) are overlaid with their Thr → Ala mutants (yellow, PDBs: 2CP4 and 4C9P). The water molecules are shown as spheres in the colour of their respective structures. In both systems, mutation of the conserved threonine to alanine opens up the oxygen binding groove, and one additional water molecule has entered the groove.

29). Correspondingly, the I-helix hydrogen bonding pattern only undergoes minimal changes (Table 30). In P450$_{cam}$, the structural changes, which occur upon breakage of the A248-T252 hydrogen bond, are hypothesised to allow additional waters to enter the active site (Figure 139b).[33,44] Similar structural modifications are also observed with CYP101D1 (Figure 138b). These changes alter the hydrogen bonding network of the I-helix peptide backbone of P450$_{cam}$, decreasing structural rigidity in the vicinity of the oxygen binding groove. The lack of a salt bridge network in CYP199A4 may allow the I-helix to change its hydrogen-bonding pattern more easily. This could minimise the widening of the oxygen binding groove and this may explain why the structural changes observed in T252A-CYP199A4 are not as substantial as T252A-P450$_{cam}$.

Table 29. Comparison of O_2 binding groove in CYP199A4, CYP101D1 and $P450_{cam}$. Shown is a generalised schematic of the loop region. **1**, **2** and **3** denote the key measurements from one side of the loop to the other (Red denotes atom labels and distances). The label next to each residue indicates the one-letter code and number for the CYP199A4 and $P450_{cam}$ systems (plain text), the middle denotes that of CYP101D1 (**bold** text) and the bottom, $P450_{BM3}$, which is in the substrate free form (*italicised* text).

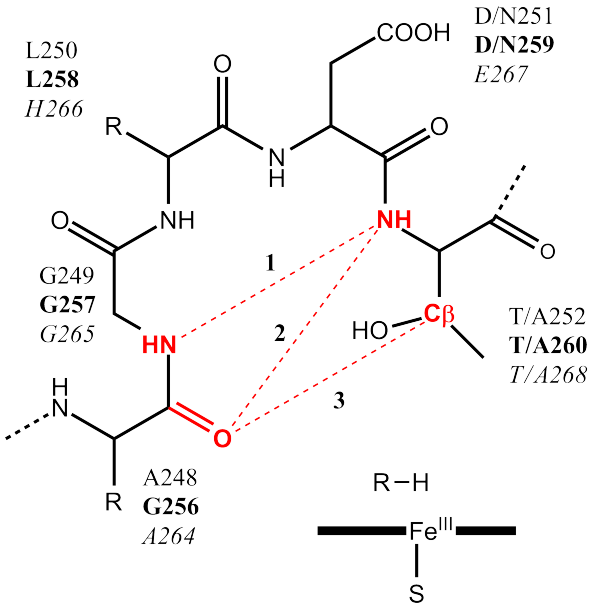

P450	Measurement	WT	Thr → Ala (*)	Asp → Asn (†)
CYP199A4	N - - **1** - - N	5.8	5.5 (-0.3)	5.7
	O - - **2** - - N	4.2	3.6 (-0.6)	4.3
	O - - **3** - - C_β	3.5	3.5 (0)	3.6
$P450_{cam}$	N - - **1** - - N	5.7	6.0 (0.3)	5.7
	O - - **2** - - N	3.9	4.2 (0.3)	3.9
	O - - **3** - - C_β	3.7	4.6 (0.9)	3.7
CYP101D1	N - - **1** - - N	5.8	6.3 (0.5)	5.7
	O - - **2** - - N	3.9	4.6 (0.7)	3.8
	O - - **3** - - C_β	3.5	4.7 (1.2)	3.6
$P450_{BM3}$	N - - **1** - - N	4.5	4.7 (0.2)	($\star$)
	O - - **2** - - N	4.0	3.7 (-0.3)	
	O - - **3** - - C_β	4.5	4.3 (0.2)	

(*) All distances are measured in Å.The difference between the WT and Thr → Ala mutant is shown in brackets. (†) In the case of Asp → Asn, the difference was always ≤ 0.1 Å. ($\star$) $P450_{BM3}$ does not possess an Asp251 residue, instead being replaced with the larger Glu267. A crystal structure of the equivalent mutant, Glu267 → Gln267, has not been deposited in the PDB and thus a comparison could not be made to the Asp → Asn mutants of the other systems.

Table 30. Hydrogen bonding network of the I-helix of CYP199A4. A dash (–) indicates that there were no hydrogen bonds formed by this functional group. A row containing a red star (⋆) indicates there was no change between the wild-type and the mutants. Where there are differences from the wild-type, these interactions are highlighted with light blue. These structures changes are depicted in Figure 139.

Residue		Isoform		
		WT	T252A	D251N
S247	NH	S244 C=O ⋆		
	C=O	– ⋆		
A248	NH	S244 C=O ⋆		
	C=O	T252 Thr-OH	H_2O	T252 Thr-OH
G249	NH	L245 C=O ⋆		
	C=O	–	H_2O	–
L250	NH	– ⋆		
	C=O	T252 NH, V254 NH, T253 Thr-OH ⋆		
251	NH	– ⋆		
	C=O	N255 NH, N255 Asp-NH_2 ⋆		
	Asp/Asn-C=O	[N255 Asp-NH_2]*		–
252	NH	L250 C=O ⋆		
	C=O	N255 NH, G256 NH ⋆		
	Thr-OH	A248 C=O	–	A248 C=O
T253	NH	– ⋆		
	C=O	I257 NH ⋆		
	Thr-OH	L250 C=O ⋆		
V254	NH	L250 C=O ⋆		
	C=O	G258 NH ⋆		
N255	NH	251 C=O, 252 C=O ⋆		
	C=O	I257 NH ⋆		
	Asp-NH_2	[D251 C=O, D251 Asp-C=O]*		–

(*) Both WT and T252A.

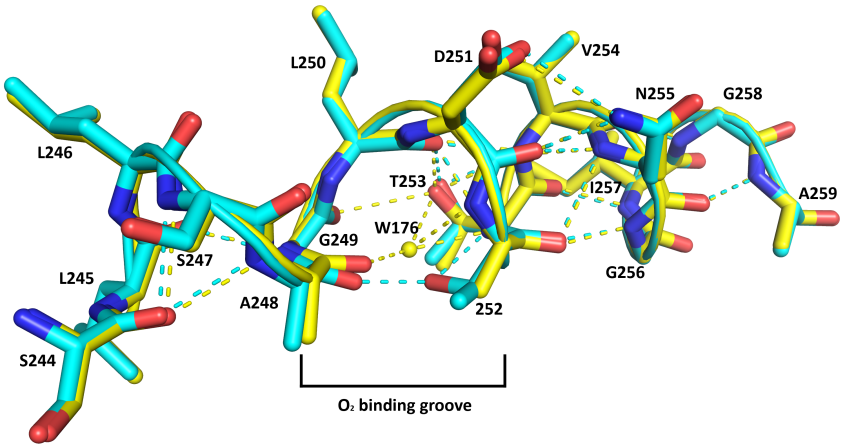

(a) CYP199A4

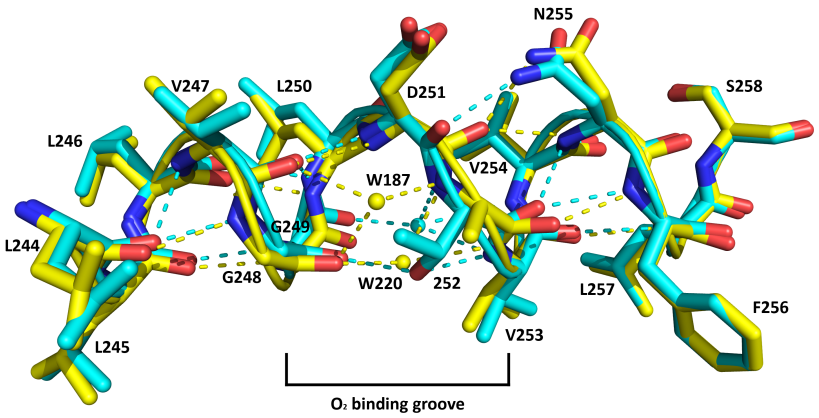

(b) $P450_{cam}$

Figure 139. The hydrogen bonding network of the I-helix of the WT and T252A mutant of (a) CYP199A4 and (b) $P450_{cam}$. In each, the wild-type structure is blue while the T252A mutant is yellow. The I-helix is represented as a ribbon in the same colours. Water molecules (spheres) and hydrogen bonds are depicted in the same colours of their structures. The O_2 binding groove, where the majority of the structural changes occur on mutation of the T252 residue, is indicated. In CYP199A4, very minimal changes in the helix backbone are observed upon mutation. In $P450_{cam}$, the backbone moves most significantly in the vicinity of the Asp251 and Thr/Ala252 residues. Table 30 shows the hydrogen bonding interactions.

The turnovers of benzoic acid substrates by T252A-CYP199A4 all showed reduced NADH oxidation activity, except for the hydroxylation and desaturation of 4-isopropylbenzoic acid. In this case the overall product formation rate was greater due an increase in the turnover of the catalytic cycle (as measure by the NADH oxidation rate). Additionally, there was a lesser degree of uncoupling via the hydrogen peroxide pathway. This may be due to the greater steric bulk of the isopropyl group, which could help stabilise Cpd 0 or reduce solvent access to the proximal oxygen atom of this intermediate, facilitating formation of Cpd I in preference to hydrogen peroxide release. Recently, it has been proposed using computational methods that a ferric-H_2O_2 species is a key intermediate on the route to Cpd I in T252A-$P450_{cam}$-

catalysed epoxidation. The Fe(III)-H_2O_2 is stabilised by the additional steric bulk of the methylene moiety of 5-methylenecamphor.[247] It may be that the isopropyl moiety of 4-isopropylbenzoic acid has a similar stabilising effect on the heme iron oxygen intermediate in T252A-CYP199A4, facilitating Cpd I formation and oxidation, resulting in the coupling efficiency being higher than expected.

The NADH oxidation rate of D251N-CYP199A4 was so low that air oxidation of the ferredoxin may be competing with electron transfer to the P450, which reduces the amount of product formed and therefore the measured coupling efficiency. Subtraction of the leak rate wastage of reducing equivalents would result in a higher coupling efficiency of the P450 catalytic cycle. This would be in agreement with how the results were obtained and reported for $P450_{cam}$.[44] The D251N mutation is hypothesised to slow down proton delivery to the peroxy intermediate (Figure 118, Species V) such that this becomes the rate determining step in the catalytic cycle. The activity of this mutant was very similar to the equivalent Asp → Asn mutation of other P450s. With $P450_{cam}$, $P450_{cin}$ and $P450_{BM3}$, mutation of this residue leads to several orders of magnitude reduction in the NADH oxidation rate and activity.[40,44,49,248]

There was no correlation between the NADH oxidation rate and the spin state shift for the D251N mutant of CYP199A4. This is presumably due to protonation of the peroxy intermediate to Cpd I, rather than the first electron transfer, becoming the rate limiting step (Figure 118). This could be in agreement with the importance of the Asp251 residue in proton delivery for CYP199A4.

The salt bridges formed with the side chain of Asp251 in WT $P450_{cam}$ are hypothesised to play an important role in proton delivery to the active site of this enzyme.[44,45,49] The backbone carbonyl of Asp251 in $P450_{cam}$ adopts an unusual conformation, but rotates upon oxygen binding, such that a conventional helix hydrogen-bonding pattern is observed[33] (Figure 4a,d). Movement of the I-helix is restricted due to the salt bridge interactions of Asp251 with Lys178 and Arg186. However, in D251N-$P450_{cam}$, the salt bridge network is broken, allowing a larger degree of conformational freedom (Figures 140a, 4a,c). In addition, the O_2-bound D251N-$P450_{cam}$ structure shows that the I-helix does not widen as much as in the WT O_2-bound structure, resulting in insufficient space for the new water molecules to enter the active site.[33]

The Asp → Asn mutant of the closely related enzyme CYP101D1 shows a similar reduction in the NADH oxidation rate.[242] It possesses a less extensive salt bridge network than $P450_{cam}$. The Asp259 residue hydrogen bonds to nearby Asn263 (Equivalent to Asn255 in CYP199A4) and forms a salt bridge with Arg188, which in turn hydrogen bonds with Asn184 (Figure 140b). Similar conformational changes are observed in the D259N-CYP101D1 structure as to those observed in $P450_{cam}$: the N259 rotates, disrupting the salt bridge network, however the N259-N263 hydrogen bond remains intact (Figure 140b).

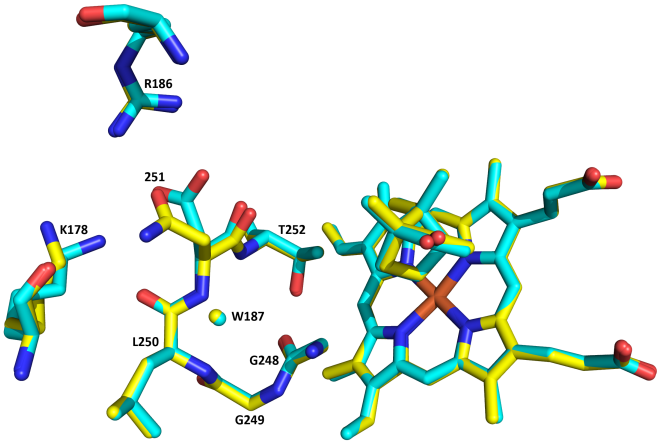

(a) WT-P450$_{cam}$ overlaid with D251N

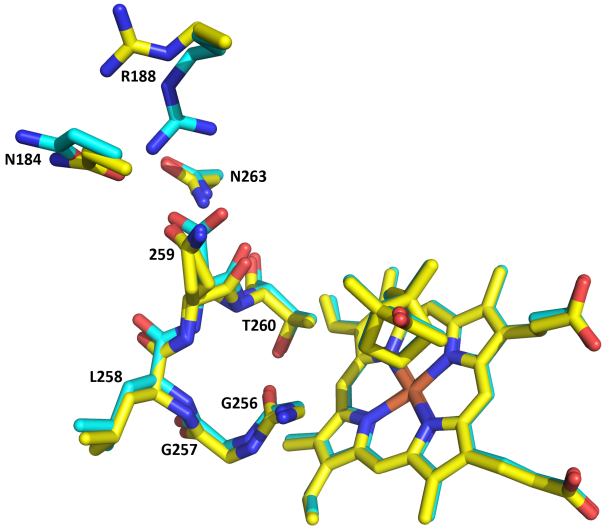

(b) WT-CYP101D1 overlaid with D259N

Figure 140. The active site, oxygen binding network and salt bridges of Asp → Asn mutants of P450$_{cam}$ and CYP101D1. Wild-type camphor-bound (a) P450$_{cam}$ and (b) CYP101D1 (cyan, PDBs: 5CP4 and 4C9K) are overlaid with their respective Asp → Asn mutants (yellow, PDBs: 6CP4 and 4C9N). The water molecules are shown as spheres in the colour of their respective structures.

The CYP199A4 system contains no equivalent salt bridge network and thus the precise details of proton delivery vary between CYP199A4 and P450$_{cam}$. The structures presented here show that D251 in CYP199A4 is instead connected to a chain of water molecules (Figure 133). These interact with residues to form a solvent access channel, which extends to the surface of the enzyme (Figure 134). These observations strongly suggest that the D251 residue in CYP199A4 plays a role in proton delivery. It may be that the W39 water molecule in the solvent network, which hydrogen bonds to D251 and N255, is important (Figure 133).

The product distributions of 4-ethyl- and 4-isopropyl-benzoic acids changed slightly with the mutant variants when compared to the WT. If there was a change in the relative proportions of oxidant species formed, one might expect to see differences in the partition between the hydroxylation and desaturation products. However, the small differences in regioselectivity observed are likely to be due to subtle changes in the position of the substrate alkyl group rather than any change in the active oxidant. Small changes in the location of the methoxy group of 4-methoxybenzoic acid are observed in the mutant crystal structures. Further structures of the substrate-bound mutants (with different substrates), and substrate-bound O_2- or CN^--CYP199A4 forms, would provide valuable information on the structural changes in this P450 system upon oxygen binding and the observed difference in the product distribution.

Chapter 7 Screening of aromatic and heterocyclic substrates

7.1 Introduction

Heterocyclic and aromatic moieties are commonly found in drug molecules. As of 2014, drugs containing nitrogen and sulfur heterocycles comprise > 60 % of all FDA-approved compounds,[249,250] and benzene rings are the most common ring system found in these pharmaceuticals.[251] The metabolism of these functional groups by P450 enzymes is thus of great significance for the pharmaceutical industry.

P450 enzymes are capable of catalysing the oxidation of aromatic systems, usually with hydroxylation as the outcome. The bond dissociation energy of an aromatic C−H bond is significantly higher than that of an alkyl C−H bond,[252] thus it is the aromatic π-electron system, rather than the C−H bond electrons, which interact with Cpd I in these reactions. These reactions are therefore mechanistically different to aliphatic C−H bond hydroxylations. The original mechanistic proposal for aromatic oxidations involves formation of an epoxide intermediate, followed by migration of a hydrogen to form a ketone. Subsequent enolisation regenerates the aromaticity of the product (Figure 141). This mechanism is named the "NIH shift", a reference to its place of formulation.[253]

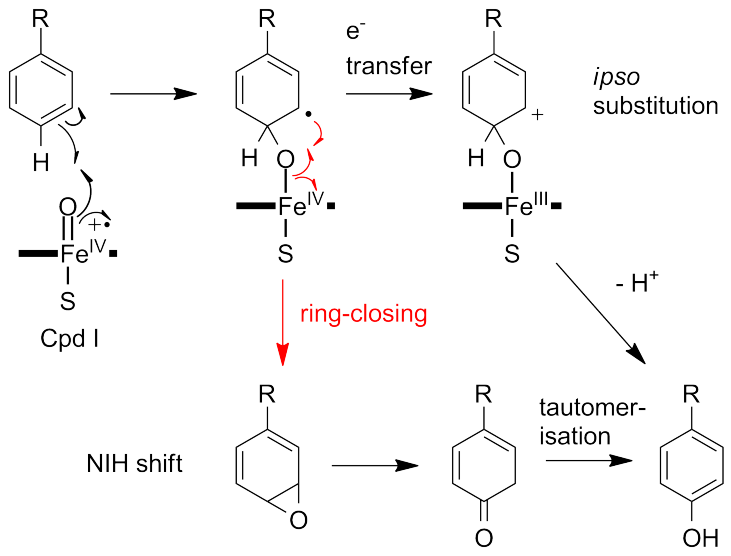

Figure 141. Mechanism of aromatic oxidation by P450 enzymes. The proposed Fe(IV)-O-C intermediate can either gain an electron from the carbon radical to form a cation (top pathway, *ipso*-substitution mechanism), or the ring can close to form an epoxide, and oxidation then proceeds via the classic NIH shift mechanism (bottom).

Subsequent studies have directly observed and characterised epoxides in certain aromatic oxidations, such as the oxidation of benzene.[254] However, other work has demonstrated that there are cases where aromatic oxidation does not seem to involve an NIH shift.[255,256] Based on these results, an alternative mechanism involving a Fe(IV)-O-C intermediate has been proposed, where there is no epoxide formation.[8,39] This reaction mechanism is referred to as *ipso*-substitution. It has been hypothesised that these two mechanistic proposals, the NIH shift and *ipso*-substitution, are two possible pathways branching from the Fe(IV)-O-C reaction intermediate (Figure 141).[39]

Examples of P450-catalysed aromatic oxidations include the oxidation of *para*-substituted phenols by rat liver P450s,[257,258] oxidation of 2-naphthoic acid by CYP199s A2 and A4,[30,167] and indole-2-carboxylic acid by CYP199A2[167] (Figure 142).

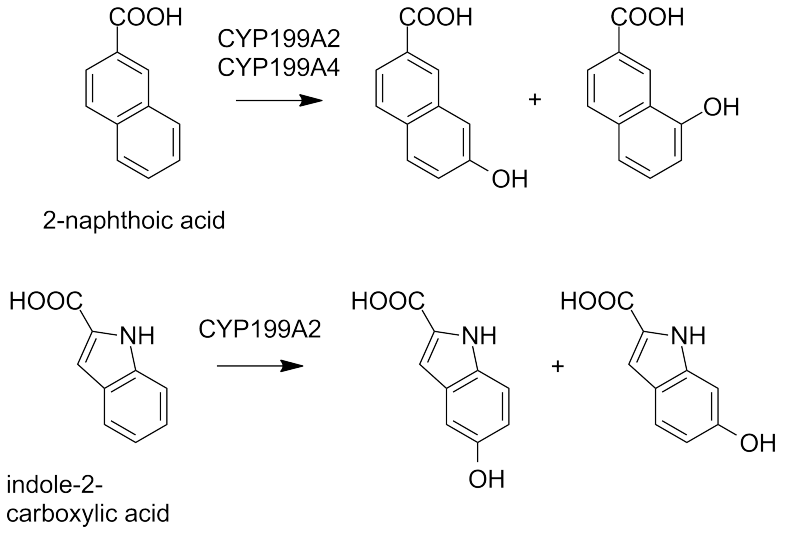

Figure 142. Examples of P450-catalysed aromatic oxidations by members of the CYP199A subfamily.[30,167]

Heterocycles feature prominently in drug metabolism literature.[251] Furan-containing compounds have been shown to function as inhibitors of P450 enzymes, but under certain conditions may undergo metabolism. For example, the furanocoumarin family of compounds can undergo oxidation to furan epoxides, which cause mechanism-based inhibition of CYPs 2A6 and 2B1 (Figure 143a, top).[259–261] More recent studies have shown that the ring-opening metabolism of a simple furan molecule by human and rat liver P450s yields a highly liver-toxic α,β-unsaturated dialdehyde[262] (Figure 143a, bottom).

Thiophenes have been shown to undergo a wide range of activities with P450 enzymes. With certain thiophene substrates, inhibition of P450 enzymes has been observed,[202,263] however there are examples of sulfoxidation reactions.[263–265] Additionally reported are thiophene aromatic C−H hydroxylations[266–268] (Figure 143b), and epoxidations.[264]

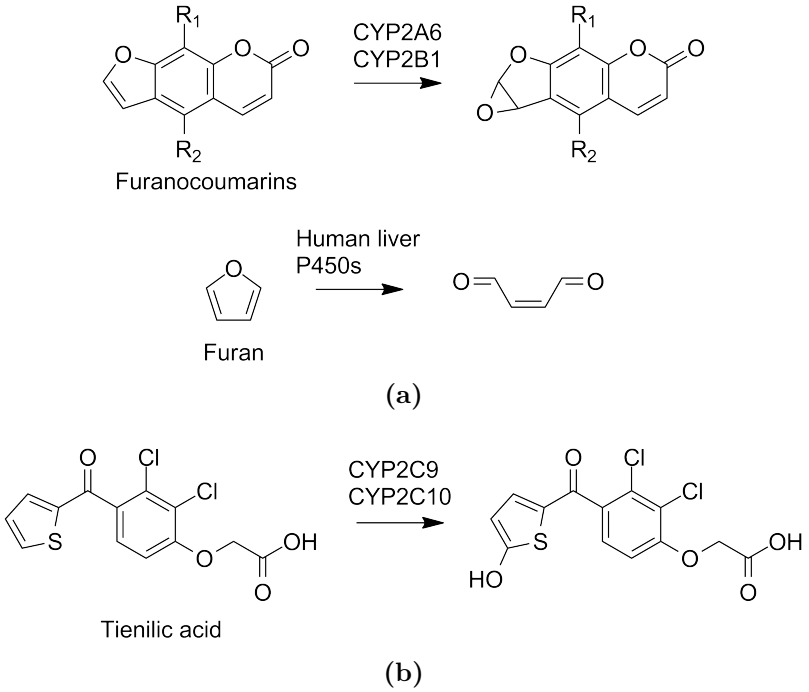

Figure 143. Examples of P450-catalysed oxidation of heterocycles. Shown in (a) are: top, the formation of furan epoxides in the furanocoumarin family; and bottom, the ring-opening metabolism of furan. In (b), the aromatic hydroxylation of the thiophene moiety of tienilic acid is shown. Other metabolites were also observed in the oxidation of these substrates.

Nitrogen-containing heterocycles such as pyridine, pyrrole and imidazole are frequently employed in the design of P450 inhibitors, as nitrogen atoms can strongly coordinate to the ferric heme iron by displacing the distal water ligand.[202,223,269] In these cases, metabolism is not usually observed. Instances in which the nitrogen atom is coordinated to the distal water ligand rather than the ferric heme iron have also been reported. In these cases, P450 function was retained.[202,270–272]

In order to study how these functional groups interact with and are turnover over by P450 enzymes, a range of *para*-phenyl and heterocyclic benzoic acids will be investigated with CYP199A4 (Figure 144). The *para*-phenyl substrates will be employed to determine if CYP199A4 can catalyse aromatic oxidations. Several substrates containing methoxyphenyl groups will allow both aromatic hydroxylation and demethylation to be investigated. 4-Benzylbenzoic acid will be used to probe the competition between alkyl C−H hydroxylation and aromatic oxidation reactions. The effect of replacing the α-carbon C−H bonds with carbonyl and ether groups will be determined using 4-benzoyl- and 4-phenoxy-benzoic acids. Heterocyclic benzoic acid substrates such as 4-(furan-2-yl)benzoic acid, 4-(thiophen-2-yl)benzoic acid and 4-(pyridin-3-yl)benzoic acid, among others, will be screened with CYP199A4 to investigate the binding of these moieties, and to search for oxidation products (Figure 144).

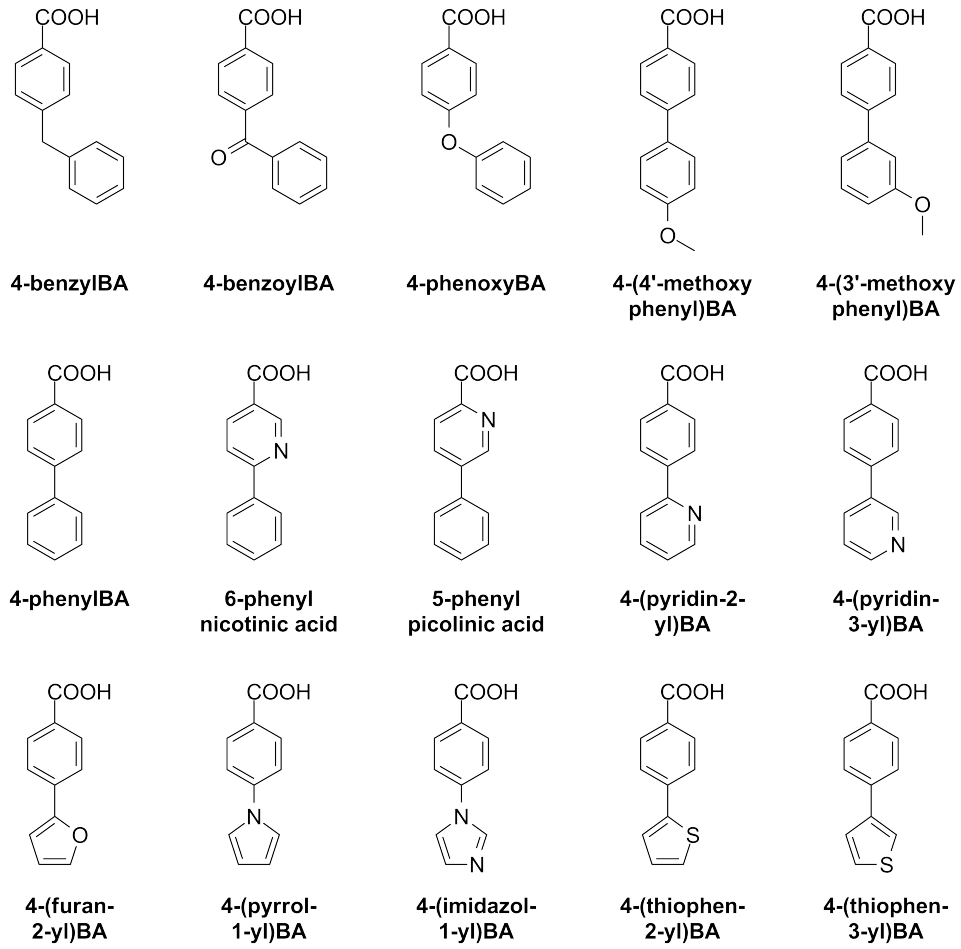

Figure 144. The range of aromatic and heterocyclic substrates investigated with CYP199A4.

7.2 Results

7.2.1 Substrate binding assays

To determine which aromatic and heterocyclic substituents might be accommodated in the active site of CYP199A4, the heme spin state shift was analysed (Chapter 2.3). The binding affinity of CYP199A4 for each substrate was then determined.

The substrates gave a diverse range of spin state shifts, both type I and type II (Table 31). Addition of 4-benzylbenzoic acid shifted the spin state of CYP199A4 to 90 % high spin heme and it bound tightly to CYP199A4 (5.2 µM, Figure 146a). 4-Benzoylbenzoic acid, which contains a carbonyl group at the bridging methylene, gave a type II shift (421 nm, Figure 145). This implied that the carbonyl group was interacting with the heme iron. A dissociation constant could not be determined for 4-benzoylbenzoic acid with CYP199A4, due to the small absorbance change on addition of substrate aliquots (Table 31).

Table 31. Spin state shift, dissociation constant analyses (% HS and K_d, Chapter 2.3) and the NADH oxidation rate (Chapter 2.4) of CYP199A4 with substrates containing aromatic and heterocyclic functional groups. Benzoic acid is abbreviated to BA.

Substrate	HS (%)	K_d (µM)	NADH
4-benzylBA	90	5.2 ± 0.3	549 ± 6
4-benzoylBA	Type II (421 nm)	-[a]	9.2 ± 1.1
4-phenoxyBA	< 5	-[a]	10.7 ± 1.2
4-(3′-methoxyphenyl)BA	≥ 95	0.57 ± 0.02	703 ± 65
4-(4′-methoxyphenyl)BA	10	100 ± 10	62.3 ± 2.1
4-phenylBA	90	1.7 ± 0.1	902 ± 34
6-phenylnicotinic acid	< 10	-[a]	45.3 ± 0.7
5-phenylpicolinic acid	55	240 ± 20	332 ± 26
4-(pyridin-2-yl)BA	Type II (422 nm)	1.0 ± 0.1[b]	9.8 ± 2.1
4-(pyridin-3-yl)BA	Type II (424 nm)	2.3 ± 0.1[b]	30.0 ± 2.8
4-(furan-2-yl)BA	35	4.3 ± 0.2	200 ± 6
4-(pyrrol-1-yl)BA	70	3.5 ± 0.1	92.4 ± 5.7
4-(imidazol-1-yl)BA	Type II (421 nm)	1.6 ± 0.2[b]	40.7 ± 0.4
4-(thiophen-2-yl)BA	75	2.0 ± 0.1	118 ± 3
4-(thiophen-3-yl)BA	90	1.8 ± 0.1	19.4 ± 0.9

[a]Not able to be determined due to low spin state shift and low detector response to addition of substrate. [b]The dissociation constant for these substrates were determined using the trough at ≈ 413 nm and peak at ≈ 430 nm (Figure 146b, Appendix E.2). In each, an absorbance maximum at ≈ 375 nm was also observed but was not used for determining the change in absorbance.

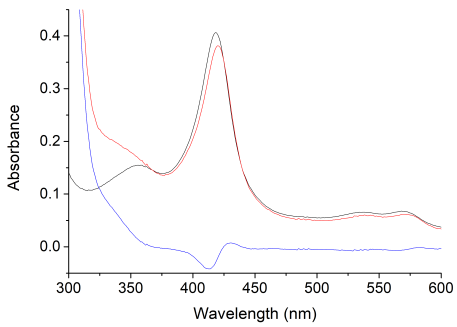

Figure 145. Spin state shift of 4-benzoylbenzoic acid. **Black**, resting state; red, maximum absorbance shift, blue, difference spectrum (trough, 413 nm; peak, 430 nm).

4-Phenoxybenzoic acid, in which the methylene bridge of 4-benzylbenzoic acid is replaced with an oxygen, barely shifted the spin state of CYP199A4 (< 5 %), and a dissociation constant could not be determined (Appendix E.1). 4-(3′-Methoxyphenyl)benzoic acid generated a ≥ 95 % shift to high spin in CYP199A4, but with 4-(4′-methoxyphenyl)benzoic acid a much lower 10 % shift was observed (Both Appendix E.1). The 3′-methoxy- substrate bound with significantly higher affinity than the 4′-methoxy isomer (0.57 µM vs 100 µM, both Appendix E.2).

The substrates containing *para*-phenyl moieties gave a range of spin state shifts and binding affinities when added to CYP199A4. 4-Phenylbenzoic acid shifted the spin state to 90 % and the binding affinity was 1.7 µM (Appendix E.1). In contrast, 6-phenylnicotinic acid, which contained a nitrogen at the *meta* position of the benzoic acid moiety, yielded < 10 % of high spin heme, and the binding affinity was not able to be determined (Table 31). When the nitrogen atom was *ortho* to the carboxylic acid, as in the case of 5-phenylpicolinic acid, a 55 % shift was observed along with a dissociation constant of 240 µM, which was an order of magnitude lower than 4-phenylbenzoic acid. Importantly, these results indicated that a *para*-phenyl ring could be accommodated in the enzyme active site. Both 4-(pyridin-2-yl)- and 4-(pyridin-3-yl)benzoic acids both induced type II shifts with CYP199A4 (422 nm and 424 nm respectively), revealing that the pyridine nitrogen was interacting with the heme iron. The binding affinity for 4-(pyridin-2-yl)benzoic acid was higher than that of 4-(pyridin-3-yl)benzoic acid (1.0 µM vs 2.3 µM, Figure 146b and Appendix E.1). The type II binding inferred that these pyridine substrates may inhibit the P450 catalytic cycle.

The substrates containing heterocyclic moieties displayed a wide range of spin state shifts and dissociation constants when investigated with CYP199A4. 4-(Furan-2-yl)benzoic acid displayed a 35 % type I spin state shift and the binding affinity was 4.3 µM (Appendix E.2). The spin state of CYP199A4 with 4-(pyrrol-1-yl)benzoic acid was shifted to 70 % high spin heme, and the substrate bound tightly (1.6 µM, Figure 146c). 4-(Imidazol-1-yl)benzoic acid, which contained an additional nitrogen in its 5-membered ring compared to 4-(pyrrol-1-yl)benzoic acid, displayed a type II shift (421 nm). This indicated that the 3′-position nitrogen atom was interacting with the heme iron and that the substrate may be an inhibitor of CYP199A4. The dissociation constant was determined to be 1.6 µM (Table 31, Appendix E.2).

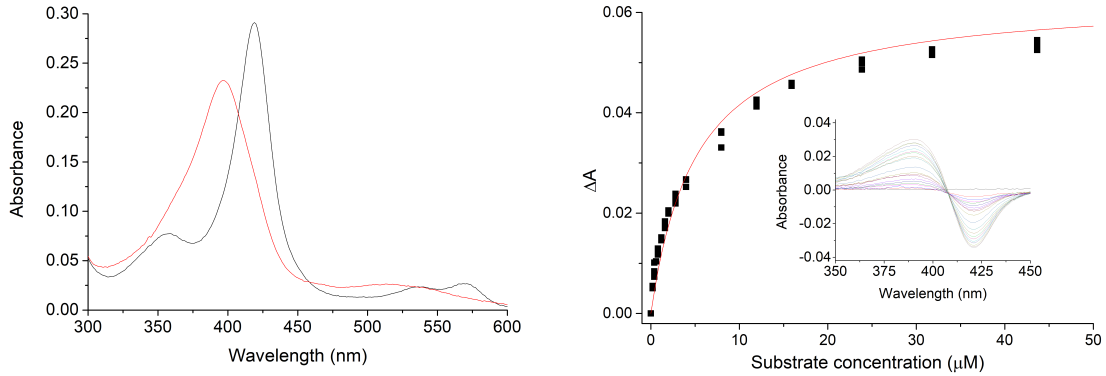

(a) 4-benzylBA (421 nm, 390 nm, 0.8 µM)

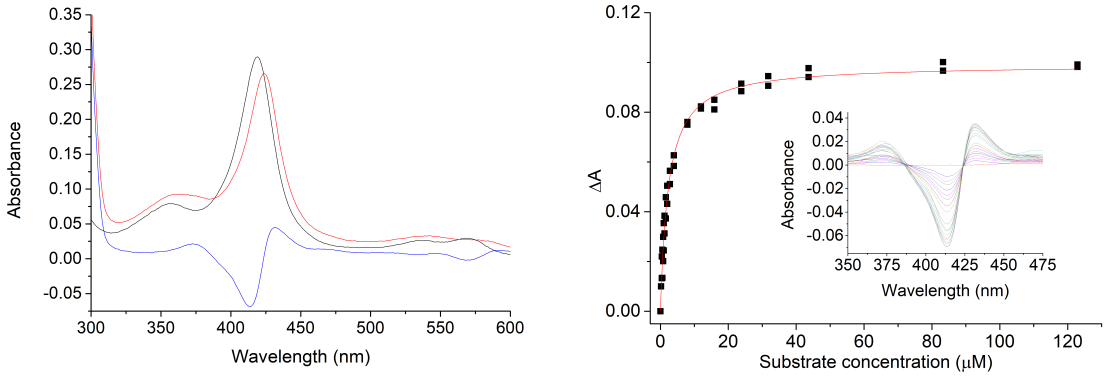

(b) 4-(pyridin-3-yl)BA (413 nm, 431 nm, 2.6 µM)

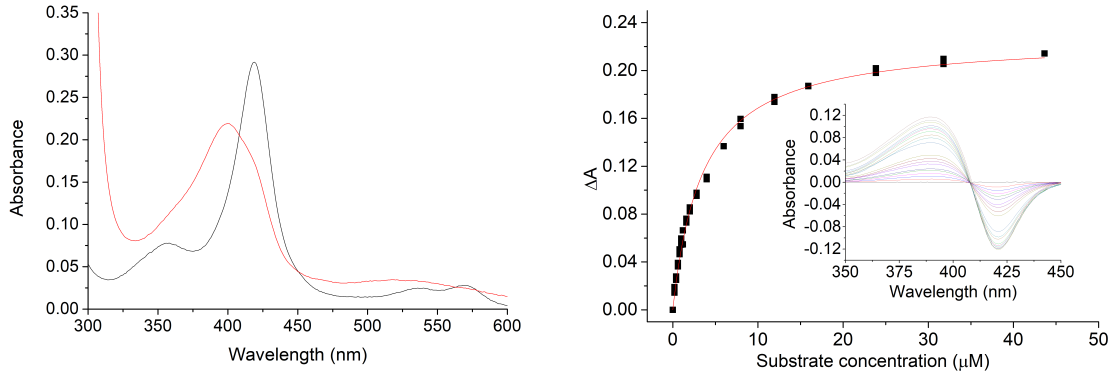

(c) 4-(pyrrol-1-yl)BA (421 nm, 389 nm, 2.7 µM)

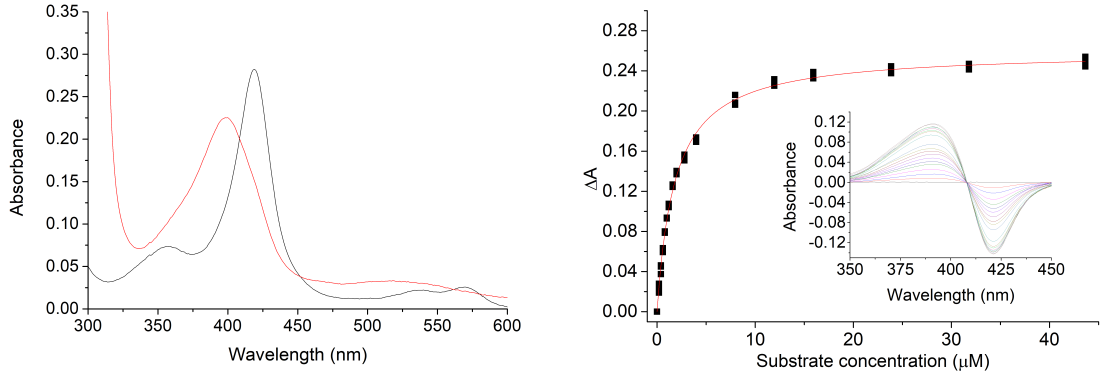

(d) 4-(thiophen-3-yl)BA (421 nm, 391 nm, 2.5 µM)

Figure 146. Spin state shift and dissociation constant determination of aromatic and heterocyclic substrates. Left column: spin state shift analysis. Black, resting state; red, maximum absorbance shift obtained; blue, difference spectrum. Right column: dissociation constant determination; the inset image shows the UV-Vis response to successive addition of substrate aliquots. Shown in brackets are the wavelengths of the trough and peak, and the enzyme concentration used for dissociation constant analysis (trough, peak, µM-P450).

Large spin state shifts were observed when both thiophene substrates were added to CYP199A4. 4-(Thiophen-3-yl)benzoic acid gave a 90 % shift to high spin heme (Figure 146d), which was larger than that of 4-(thiophen-2-yl)benzoic acid (75 %, Appendix E.2). The binding affinities displayed by both substrates were similar (thiophen-2-yl, 2.0 µM; thiophen-3-yl, 1.8 µM). Overall, a wide variety of functional groups *para* to the benzoic acid moiety could be accommodated in the active site of CYP199A4. As such this enzyme can be used to investigate how these functional groups are metabolised by P450 enzymes, and how different substrates may interact with the heme iron component of these enzymes.

7.2.2 Turnover activity and product formation

The oxidation of each substrate by CYP199A4 was investigated using *in vitro* oxidation assays (Chapter 2.4), followed by analysis using HPLC and GC-MS (Chapter 2.1). In cases where there were metabolites, *in vivo* turnovers were employed in an attempt to generate increased amounts of product for characterisation by HPLC, GC-MS and NMR (Chapter 2.6).

When 4-benzylbenzoic acid was added to CYP199A4, a fast NADH oxidation rate was observed (549 min^{-1}, Table 31). HPLC analysis indicated there was a single oxidation product (Figure 147), while the *in vivo* turnover showed the formation of an additional product. The metabolites from the *in vivo* turnover were extracted and purified using semi-prep HPLC (Chapter 2.1). The major product, which was the sole product in the *in vitro* turnover, was identified as 4-(hydroxyphenylmethyl)benzoic acid using NMR (Appendix E.5). This arose via hydroxylation at the benzylic α-carbon, producing a chiral metabolite (Figure 147). The additional product which appeared only in the whole-cell turnovers was identified as 4-benzoylbenzoic acid, by HPLC coelution with an authentic product standard (Figure 147) and NMR (Appendix E.5). The hydroxylation product was calibrated using HPLC, which enabled the product formation rate and coupling efficiency of the turnover to be determined as 522 min^{-1} and 95 % respectively (Table 31). There were no products arising from aromatic oxidation at the phenyl substituent.

Addition of 4-benzoylbenzoic acid to CYP199A4 generated a type II spin state shift to 421 nm, indicating the carbonyl oxygen was binding to the heme iron. This would be expected to inhibit the catalytic cycle of the enzyme. The NADH oxidation rate was comparable to the rate of passive oxidation of NADH ($\approx$ 9 min^{-1}), and HPLC analysis of both *in vitro* and *in vivo* turnovers indicated there were no P450 oxidation products (Appendix E.3).

4-Phenoxybenzoic acid caused the CYP199A4 turnover system to oxidise NADH at a rate of only 10.7 min^{-1} (Table 31). This was comparable to the passive NADH oxidation rate ($\approx$ 9 min^{-1}) and was in line with the $<$ 5 % spin state shift observed.

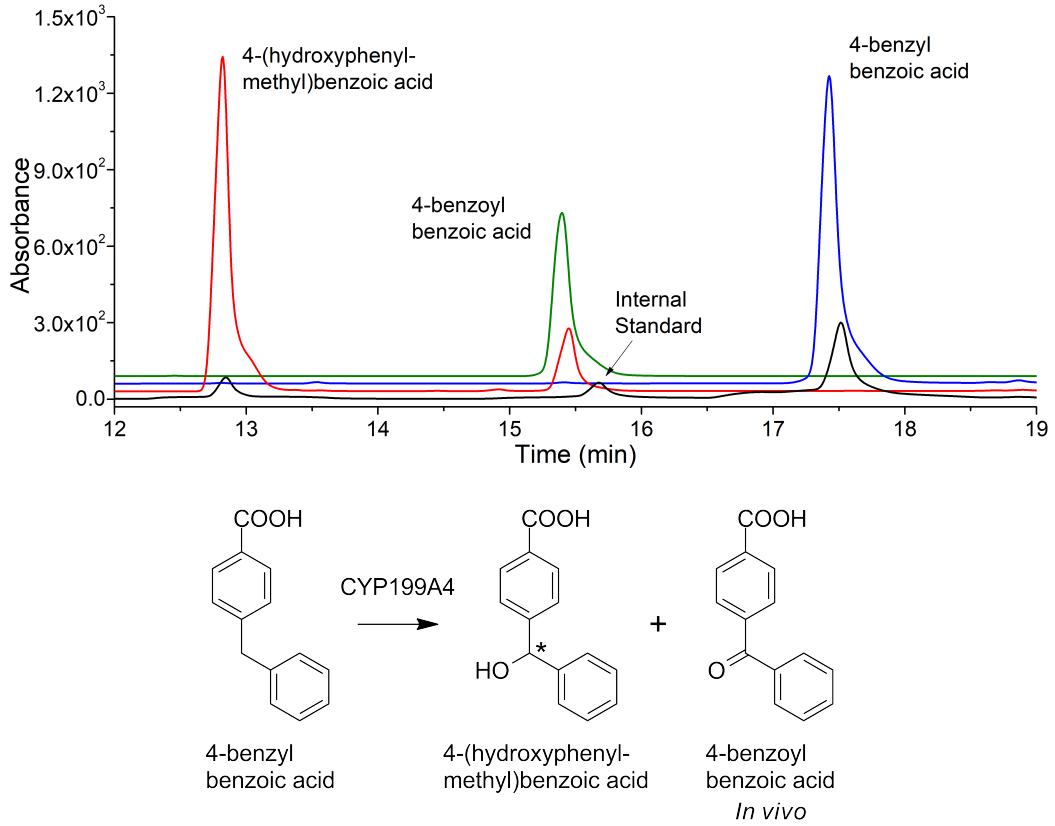

Figure 147. HPLC analysis of 4-benzylbenzoic acid turnover with CYP199A4. **Black**, *in vitro* turnover (internal standard: 15.7 min); red, *in vivo* turnover (no internal standard was added); blue, substrate control, RT = 17.5 min; green, 4-benzoylbenzoic acid control, RT = 15.5 min. A 20-95 % gradient of H_2O:ACN was used, and the chromatogram was monitored at 254 nm.

HPLC and GC-MS analysis of the *in vitro* and *in vivo* turnovers did not show any peaks which were P450 oxidation products (Figure 148).

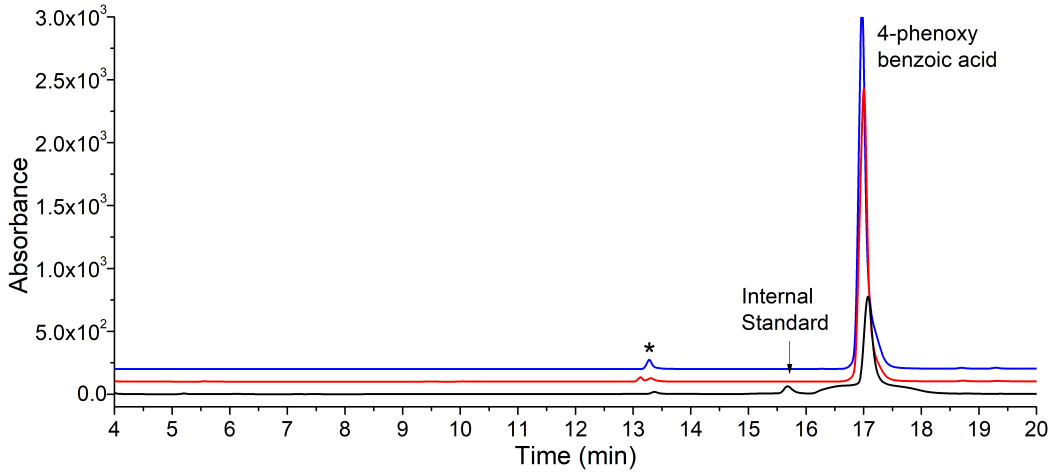

Figure 148. HPLC analysis of 4-phenoxybenzoic acid turnover with CYP199A4. **Black**, *in vitro* turnover; red, *in vivo* turnover; blue, substrate control, RT = 17.0 min. Denoted (*) is an impurity peak which appeared in the substrate control. A 20-95 % gradient of H_2O:ACN was used, and the chromatogram at 254 nm was monitored.

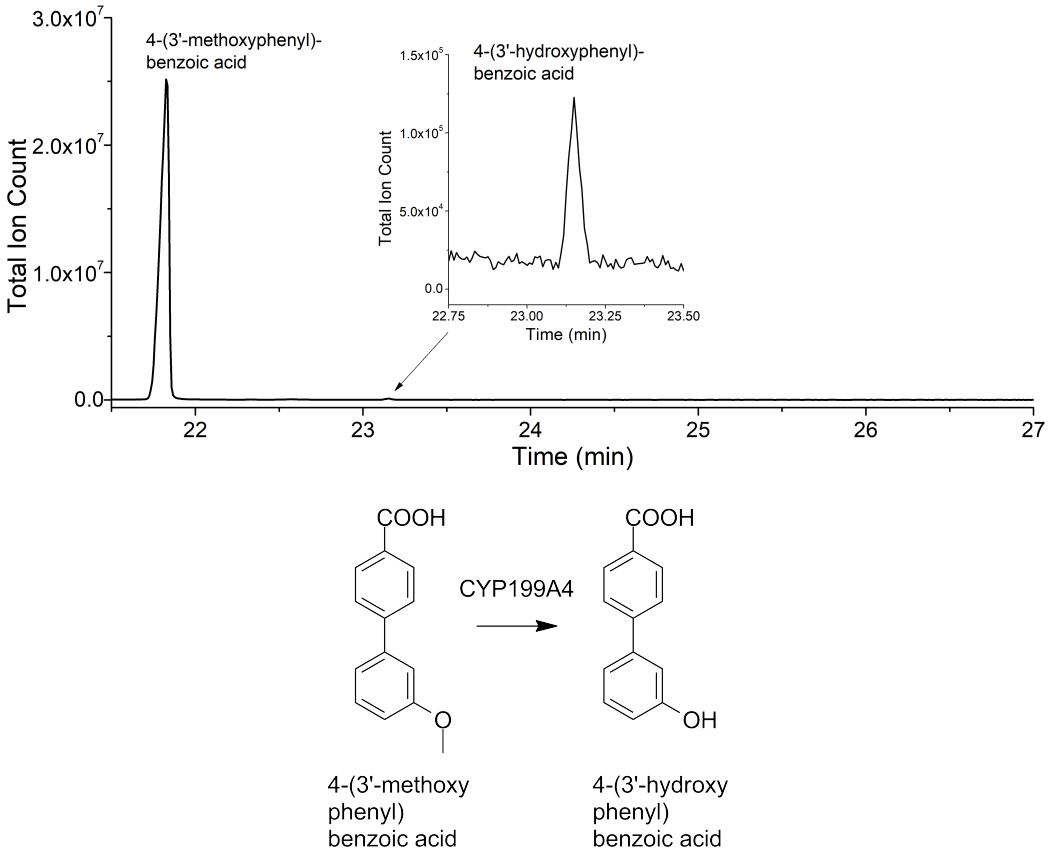

Figure 149. GC-MS analysis of TMS-derivatised 4-(3′-methoxyphenyl)benzoic acid *in vitro* turnover with CYP199A4. The mass spectrum of the product is presented in Appendix E.4.

Addition of 4-(3′-methoxyphenyl)benzoic acid induced a fast NADH oxidation rate in the CYP199A4 turnover system, indicative of efficient substrate oxidation (703 min^{-1}, Table 31). HPLC analysis, however, did not reveal a peak that could be readily assigned as an oxidation product in either the *in vitro* or *in vivo* turnovers (Appendix E.3). A small peak was detected by GC-MS analysis of the *in vitro* and *in vivo* turnovers, whose mass was indicative of a demethylation metabolite, which could only have arisen at the 3′-methoxy position (m/z = 358.30, Figure 149, Appendix E.4).

The NADH oxidation rate observed during the CYP199A4 turnover of 4-(4′-methoxyphenyl)benzoic acid was 62.3 min^{-1}, which was significantly lower than the 4-(3′-methoxyphenyl)- substrate (Table 31). The HPLC chromatograms of the *in vitro* turnover with 4-(4′-methoxyphenyl)benzoic acid indicated there was an oxidation product (RT = 16.3 min, Appendix E.3). In the *in vivo* turnover there was a potential further oxidation product at 14.3 min. A single product peak was observed in the GC chromatogram of the *in vitro* and *in vivo* turnovers, and the mass spectrum of this peak was indicative of a demethylation at the 4′-methoxy position (m/z = 358.15, Figure 150, Appendix E.4). The results indicated that CYP199A4 could demethylate methoxyphenyl moieties, but with low product yields.

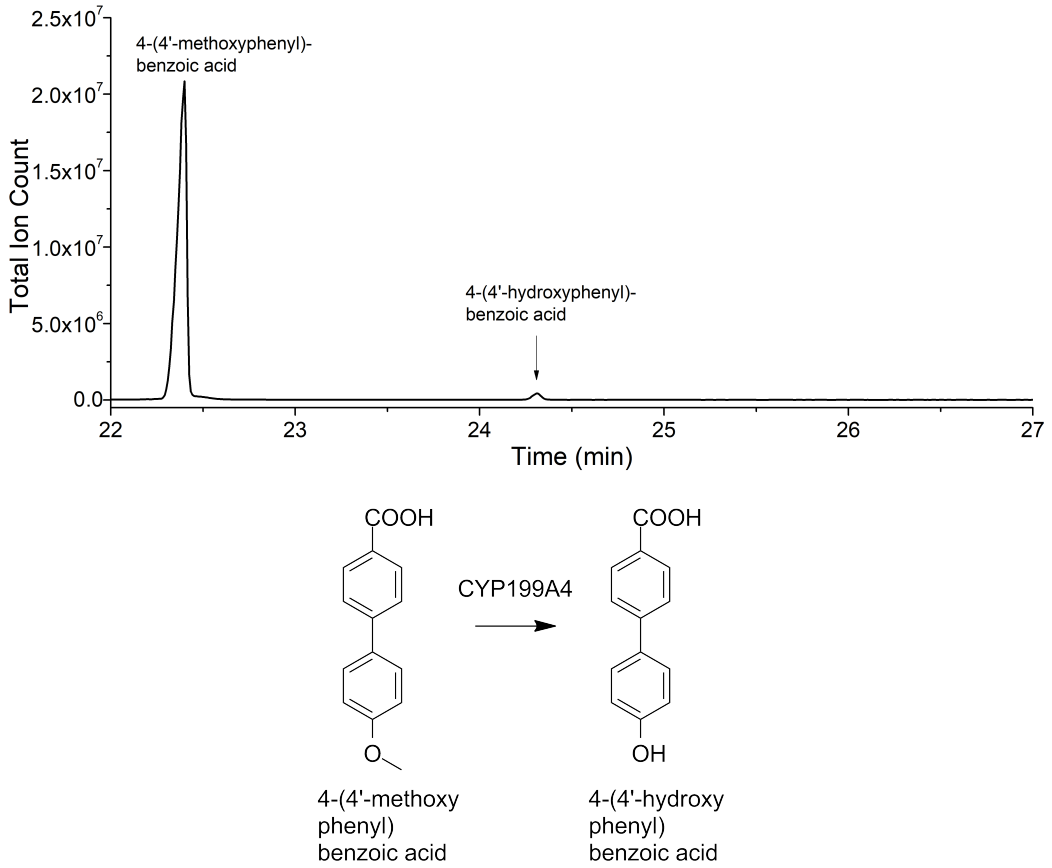

Figure 150. GC-MS analysis of TMS-derivatised 4-(4′-methoxyphenyl)benzoic acid turnover with CYP199A4. The mass spectrum of the product is presented in Appendix E.4.

The *in vitro* turnovers of the *para*-phenyl substrates were then investigated. 4-Phenylbenzoic acid caused CYP199A4 to rapidly oxidise NADH at $902\,\mathrm{min}^{-1}$, faster than any of the other substrates investigated in this chapter (Table 31). The NADH oxidation rate of CYP199A4 induced by 5-phenylpicolinic acid was $332\,\mathrm{min}^{-1}$, and with 6-phenylnicotinic acid it was $45.3\,\mathrm{min}^{-1}$ (Table 31). These rates followed the same trend as the magnitude of the spin state shifts induced by these substrates. The *in vitro* turnovers of 4-(pyridin-2-yl)- and 4-(pyridin-3-yl)-benzoic acids with CYP199A4 proceeded with slow NADH oxidation rates ($9.8\,\mathrm{min}^{-1}$ and $30.0\,\mathrm{min}^{-1}$ respectively, Table 31). These low rates could be rationalised by the type II binding observed (422 nm and 424 nm), which would be expected to result in the inhibition of P450 catalysis.

Analysis of the turnovers of any of these substrates by HPLC and GC-MS did not reveal any P450 oxidation products (Figure 151, Appendices E.3 and E.4). Turnover mixtures with no P450 enzyme were performed with 4-phenylbenzoic acid, and these displayed an NADH oxidation rate comparable to the passive leak rate ($\approx 9\,\mathrm{min}^{-1}$). This indicated that substrate-bound CYP199A4 was required in order to initiate NADH consumption. The hydrogen peroxide content of the *in vitro* turnovers of 4-phenylbenzoic acid accounted for 24 % of the total NADH, with the oxidase pathway presumed to

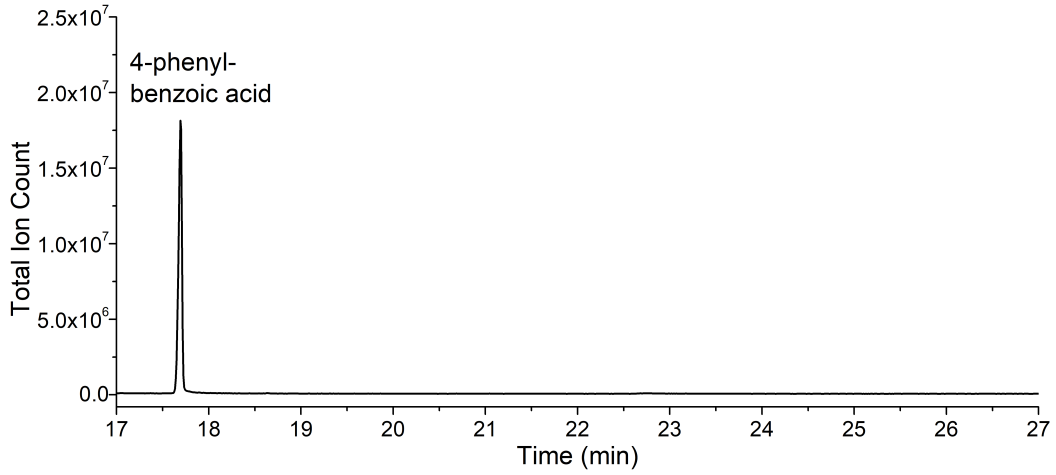

Figure 151. GC-MS analysis of TMS-derivatised 4-phenylbenzoic acid turnover with *in vitro* CYP199A4. The mass spectrum of the substrate is presented in Appendix E.4.

be responsible for the remainder (Chapter 2.7). In the cases of 5-phenylpicolinic acid, 6-phenylnicotinic acid, 4-(pyridin-2-yl)benzoic acid and 4-(pyridin-3-yl)benzoic acid there were no significant levels of hydrogen peroxide generated in the turnovers.

CYP199A4 did not catalyse aromatic hydroxylation with any of the phenyl-containing benzoic acid substrates, despite the majority of these shifting the spin state of CYP199A4 and inducing oxidation of NADH. These results are in agreement with those of the 4-benzyl-, 4-benzoyl- and 4-phenoxy-benzoic acids, where there was no observed aromatic oxidation. The lack of aromatic oxidation could be due to the orientation of the aromatic ring relative to the heme iron. The pyridine substrates did not undergo oxidation by CYP199A4, which would be expected given the type II binding spectrum exhibited, and suggested that they were CYP199A4 inhibitors with the nitrogen binding to the heme iron.

The turnovers of substrates containing 5-membered heterocycles were then investigated. The NADH oxidation rate of the CYP199A4 turnover of 4-(furan-2-yl)benzoic acid was 200 min^{-1} (Table 31). The HPLC and GC-MS chromatograms of the *in vitro* turnover did not show any peaks apart from the substrate, suggesting that CYP199A4 was not capable of metabolising a furan-2-yl moiety (Figure 152). The *in vivo* turnover, however, contained several peaks which could potentially be CYP199A4 oxidation products. In the *in vivo* turnover GC-MS, a peak corresponding to 2 mass units above the substrate was observed at 16.3 min (m/z = 262.15 vs substrate, 260.20, Figure 153, Appendix E.4). This was suspected to be a dihydrofuran, formed by reduction of one of the double bonds by an endogenous *E. coli* ene reductase.[273,274] Its absence in the *in vitro* turnovers suggests that it is not a product arising from P450 mono-oxygenase activity. There were two peaks in the *in vivo* turnovers which could potentially be P450 oxidation products. At 21.02 min, a peak with m/z = 348.55 was observed, which corresponds to a TMS-derivatised hydroxylated furan. Additionally, at 20.18 min a peak with m/z = 352.25 was observed which may correspond to hydroxylation of a fully

reduced tetrahydrofuran moiety (Figure 153).

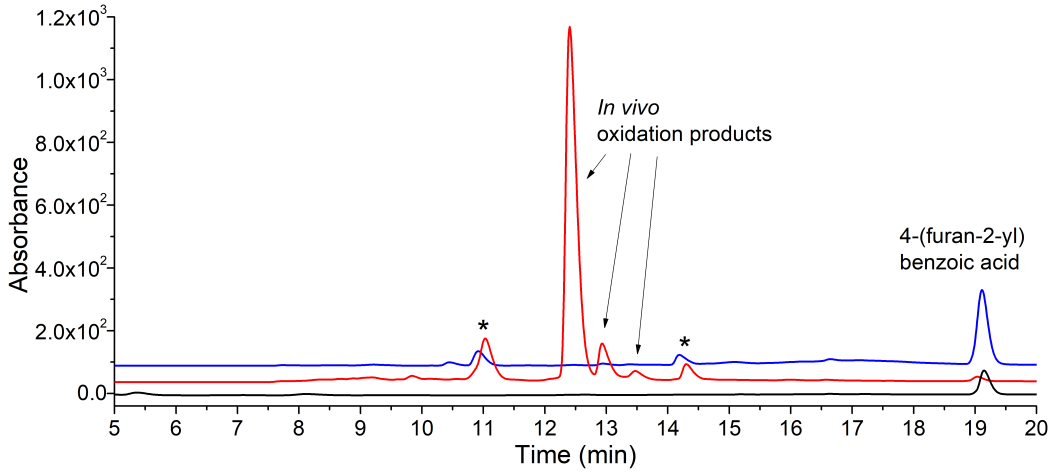

Figure 152. HPLC analysis of 4-(furan-2-yl)benzoic acid turnover with CYP199A4. **Black**, *in vitro* turnover; red, *in vivo* turnover; blue, substrate control, RT = 19.1 min. A 20-95 % gradient of H_2O:ACN was used, and it was monitored at 249 nm. There were no *in vitro* products generated. Peaks which are denoted (*) were found in the substrate control and thus were not products.

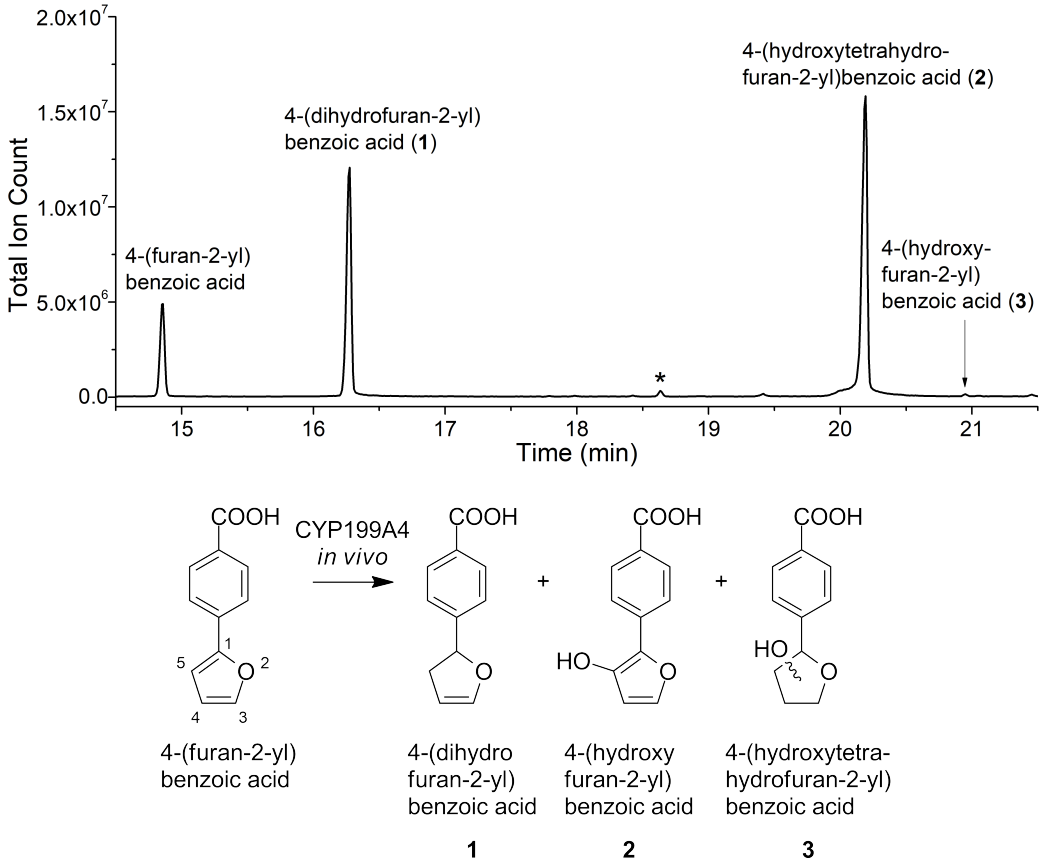

Figure 153. GC-MS analysis of *in vivo* TMS-derivatised 4-(furan-2-yl)benzoic acid turnover with CYP199A4. The position of each oxidation is speculated based on previous results with alkylbenzoic acids (Chapter 5). The mass spectrum of each peak is presented in Appendix E.4. A substrate impurity is denoted (*).

The major product, as determined using the GC-MS peak integrations, was thought to be a hydroxylated tetrahydrofuran (60 %), followed by a dihydrofuran (39 %) and the remainder was a hydroxylated furan (<1 %). The hydroxylation was speculated to be at the furan 5-position, while for the hydroxylated tetrahydrofuran the oxidation was hypothesised to be at the 1- or 5-position (Figure 153, bottom). This assignment was based on the observation that CYP199A4 preferentially oxidises the benzylic α- or β-carbons of the *para* substituent (Chapter 5). The position of the hydroxylation would be able to be elucidated by purification of the turnover mixture followed by characterisation using NMR spectroscopy.

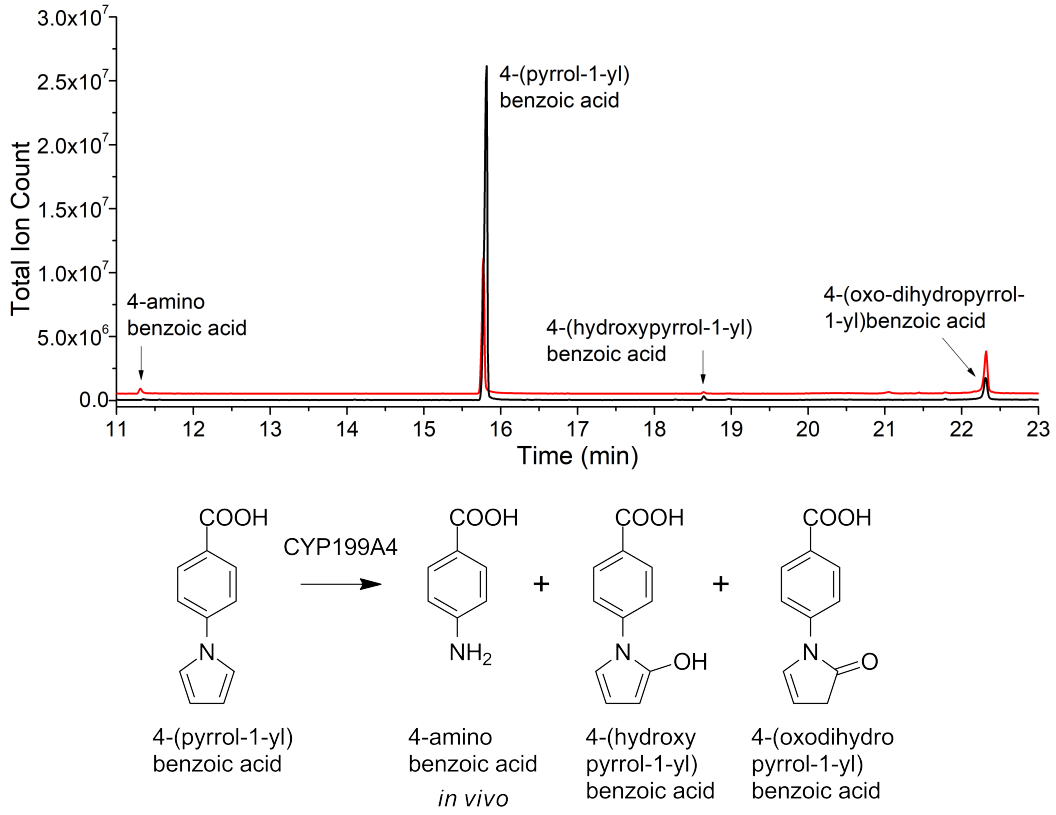

Figure 154. GC-MS analysis of TMS-derivatised 4-(pyrrol-1-yl)benzoic acid turnover with CYP199A4. **Black**, *in vitro* turnover; red, *in vivo* turnover. The mass spectrum of each peak is presented in Appendix E.4. The position of each oxidation is speculated (Chapter 5).

With 4-(pyrrol-1-yl)benzoic acid, the NADH turnover rate of CYP199A4 was 92.4 min^{-1} (Table 31). In the GC-MS chromatogram of both the *in vitro* and *in vivo* turnovers, a small peak was observed whose mass spectrum could be assigned to a hydroxylation product (RT = 18.7 min, m/z = 347.30, Figure 154, Appendix E.4). It was suspected the site of hydroxylation was at the 2-position (β-carbon), adjacent to the pyrrole nitrogen. The major peak in the turnovers, at 22.3 min, displayed a mass spectrum peak of 275.25 (substrate + 16) which was indicative of an oxidation product. This could be the keto tautomer of the enol (i.e. hydroxylation) product at 18.7 min (Figure 154). The partition in the *in vitro* turnover was 13 % enol to 87 % keto product, using the GC-MS peak integrals. Additionally, in the *in vivo* turnover,

a small peak could be assigned to 4-aminobenzoic acid (RT = 11.30 min).

4-(Thiophen-2-yl)benzoic acid caused an NADH oxidation rate of 118 min^{-1} when combined with CYP199A4 (Table 31). When the turnovers were analysed using GC-MS, a small peak with a mass corresponding to a hydroxylated thiophenyl could be detected at 21.8 min (m/z = 374.20, Figure 155, Appendix E.4). This product was speculated to be 4-(5-hydroxythiophen-2-yl)benzoic acid. Both the *in vivo* and *in vitro* turnovers showed two peaks in the HPLC chromatogram (Figure 156). Given that only a single product peak was observed in the GC-MS chromatogram, it was postulated that the two peaks were the hydroxylation product in its carboxylate and carboxylic acid forms (Figure 156). In both the GC and HPLC analyses of the *in vivo* turnover, there was no substrate remaining. Presumably all of the 4-(thiophen-2-yl)benzoic acid had been consumed or otherwise degraded. The *in vivo* turnover was separated using semi-prep HPLC in an attempt to characterise the hydroxylation product. When the peak was collected and analysed by ^{1}H NMR, there was very little compound which could not be characterised. This product might be able to be characterised using a larger scale *in vivo* or *in vitro* turnover.

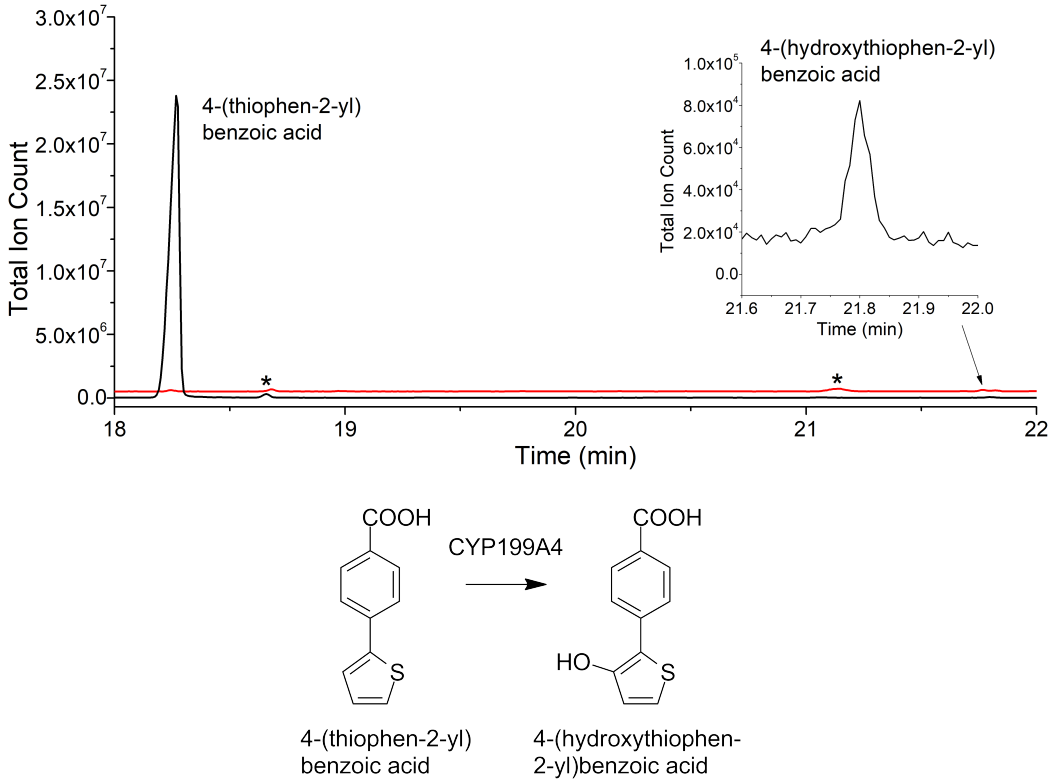

Figure 155. GC-MS analysis of TMS-derivatised 4-(thiophen-2-yl)benzoic acid *in vitro* turnover with CYP199A4. **Black**, *in vitro* turnover; red, *in vivo* turnover. Impurities, which were present in the substrate control, are marked with an asterix (*). The mass spectra are presented in Appendix E.4. The position of the hydroxyl group shown in the product has not been confirmed.

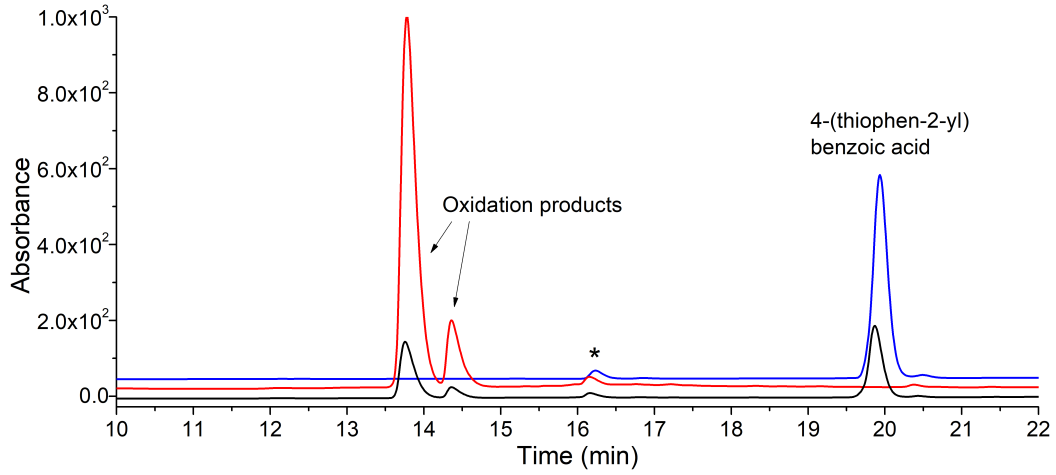

Figure 156. HPLC analysis of 4-(thiophen-2-yl)benzoic acid turnover with CYP199A4. **Black**, *in vitro* turnover; red, *in vivo* turnover; blue, substrate control, RT = 20.0 min. A 20-95 % gradient of H_2O:ACN was used and the chromatogram was monitored at 271 nm. An impurity that was present in the substrate is denoted (*).

The NADH oxidation rate of CYP199A4 with 4-(thiophen-3-yl)benzoic acid was lower than the thiophen-2-yl (19.4 min^{-1} vs 118 min^{-1}, Table 31), despite the higher % spin state shift of the former. When the turnovers were analysed by HPLC, there was a peak at 9.7 min that could be an oxidation product (Figure 158). When the turnovers were analysed using GC-MS, however, no peaks which displayed masses indicative of P450 oxidation products could be observed (Figure 157). A larger scale *in vivo* turnover may allow significant amounts of this potential product to be obtained for characterisation.

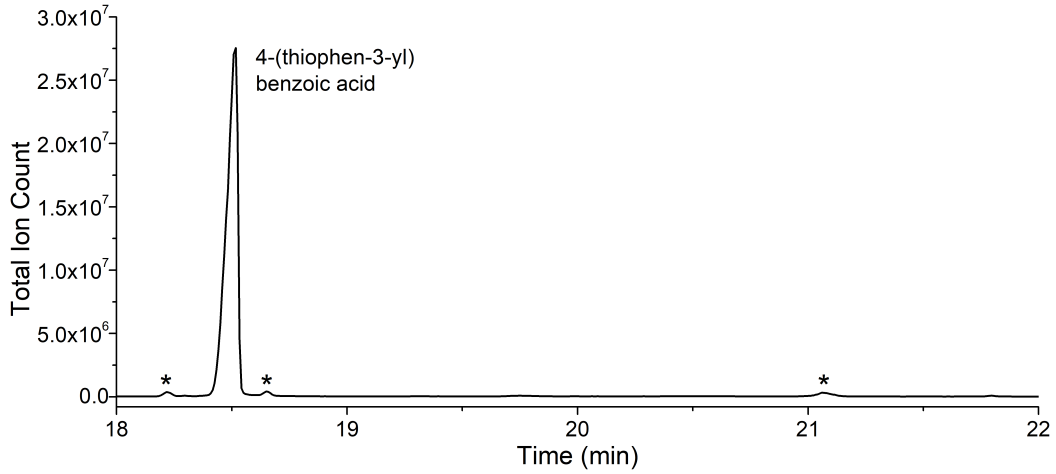

Figure 157. GC-MS analysis of TMS-derivatised 4-(thiophen-3-yl)benzoic acid turnover with *in vitro* CYP199A4. Impurities, also present in the substrate control, are marked with an asterix (*).

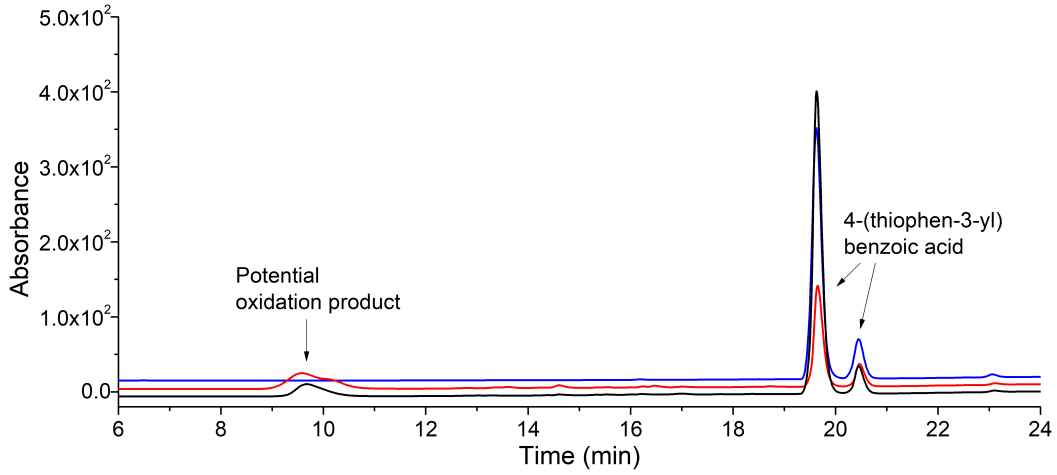

Figure 158. HPLC analysis of 4-(thiophen-3-yl)benzoic acid turnover with CYP199A4. **Black**, *in vitro* turnover; red, *in vivo* turnover; blue, substrate control, RT = 19.7 min. A 20-95 % gradient of H_2O:ACN was employed and the chromatogram was monitored at 271 nm.

In vitro CYP199A4 turnovers showed limited NADH oxidation activity with 4-(imidazol-1-yl)benzoic acid (40.7 min^{-1}), as expected due to the type II binding observed. HPLC analysis of the *in vitro* and *in vivo* turnovers indicated there were no product peaks, and the absence of a substrate peak in both seemed to indicate that 4-(imidazol-1-yl)benzoic acid readily degraded (Appendix E.3).

Turnover studies of the heterocyclic substituted benzoic acids showed that CYP199A4 was able to catalyse the oxidation of pyrrol-1-yl and thiophen-2-yl moieties, albeit with low product yields. Further experiments are required to characterise these metabolites. There was no *in vitro* enzyme activity with the furan-2-yl substrate, although *in vivo* turnovers generated multiple oxidation products. The products that were speculated to have been generated by endogenous *E. coli* enzymes seemed to be more readily oxidised by CYP199A4 than 4-(furan-2-yl)benzoic acid. The imidazole substrate did not undergo any P450-catalysed oxidation, suggesting it was an inhibitor of CYP199A4.

7.2.3 Crystal structure of 4-(thiophen-3-yl)benzoic acid-bound CYP199A4

The crystallographic screening conditions developed and employed previously (Chapter 3.2.4, and others) were employed with the substrates studied here (Figure 144). Of this set, crystals were obtained for 4-(thiophen-2-yl)benzoic acid, 4-(thiophen-3-yl)benzoic acid and 4-(3′-methoxyphenyl)benzoic acid. X-ray diffraction data for each were collected at the Australian Synchrotron as described previously (Chapter 2.10).

The crystals obtained for 4-(3′-methoxyphenyl)benzoic acid did not diffract. The data obtained for 4-(thiophen-2-yl)benzoic acid was highly anisotropic and was not able to be solved. The 4-(thiophen-3-yl)benzoic acid dataset was able to be solved to a high resolution (Table 32, 1.66 Å) and was deposited online in the wwPDB[157,158] with accession code 6C3J.

Table 32. Structural refinement and data collection statistics for CYP199A4 with 4-(thiophen-3-yl)benzoic acid. Data were collected using 0.9537 Å X-rays and the space group was $P12_11$. There was one molecule in the asymmetric unit.

	4-(thiophen-3-yl)BA
PDB code	6C3J
Unit cell (a/b/c)	44.3/51.6/79.5
($\alpha/\beta/\gamma$)	90/92.0/90
Resolution range[a]	44.26 - 1.66
	(1.69 - 1.66)
$<I/\sigma(I)>$[a]	11.8 (2.0)
Unique reflections	41408
Completeness[a]	99.9 (80.2)
Multiplicity[a]	7.6 (7.5)
R_{merge}[a,b] (%)	10.0 (78.6)
R_{pim}[a,b] (%)	3.9 (30.6)
$CC_{1/2}$[a,c] (%)	99.9 (80.6)
R_{work}	0.145
R_{free}[d]	0.182
Ramachandran plot[e]	
Most favoured	96.9
Allowed	3.1

[a]Highest resolution shell is shown in parentheses where applicable. [b]all I+ and I-. [c]Half-correlation coefficient.[182,183] [d]5 % of total reflections, randomly selected. [e]% of all amino acid residues.[184] There were no Ramachandran outliers.

The structure crystallised with a single subunit with $P12_11$ symmetry, and the overall protein fold was very similar to the structures solved previously (Figure 159a, rmsd = 0.344 Å). There was electron density in the active site that was modelled as 4-(thiophen-3-yl)benzoic acid (Figure 159b). The orientation of the sulfur in the thiophenyl moiety was determined by examining the electron density map at the 3 σ

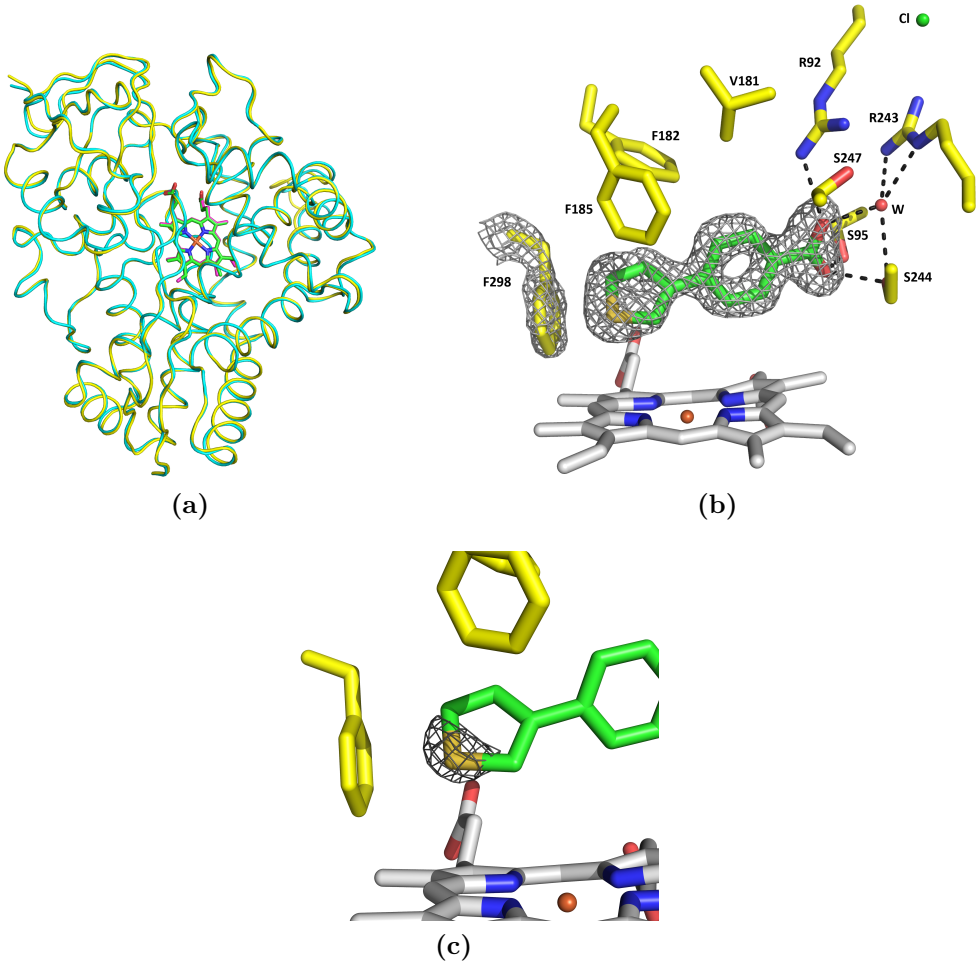

Figure 159. Crystal structure of 4-(thiophen-3-yl)benzoic acid-bound CYP199A4 solved at 1.66 Å resolution. Depicted in (a) is the three-dimensional fold (yellow tube and magenta heme) overlaid with structure of 4-ethylbenzoic acid (cyan tube and green heme). Shown in (b) and (c) are reduced bias $2mF_o$-DF_c composite omit maps[154] of 4-(thiophen-3-yl)benzoic acid-bound CYP199A4. In (b), the electron density map for 4-(thiophen-3-yl)benzoic acid and the F298 residue are shown contoured as a grey mesh at the 1 σ level. In (c) the map for the thiophenyl moiety of 4-(thiophen-3-yl)benzoic acid is contoured at the 3 σ level, indicating the location of the sulfur atom.

level, which revealed there was a very high electron density region corresponding to the position of the sulfur atom (Figure 159c).

The 4-(thiophen-3-yl)benzoic acid substrate is held in a significantly different binding orientation to 4-ethylbenzoic acid in the active site of CYP199A4 (Figure 160a). The benzoic acid is angled slightly away from the heme in comparison to that of the 4-ethylbenzoic acid structure, resulting in the thiophenyl moiety being held further away from the heme iron. The thiophenyl ring C_β is 4.2 Å from the heme iron, compared to the C_β of 4-ethylbenzoic acid which is only 3.2 Å away. The thiophenyl sulfur atom is held 5.2 Å from the heme iron.

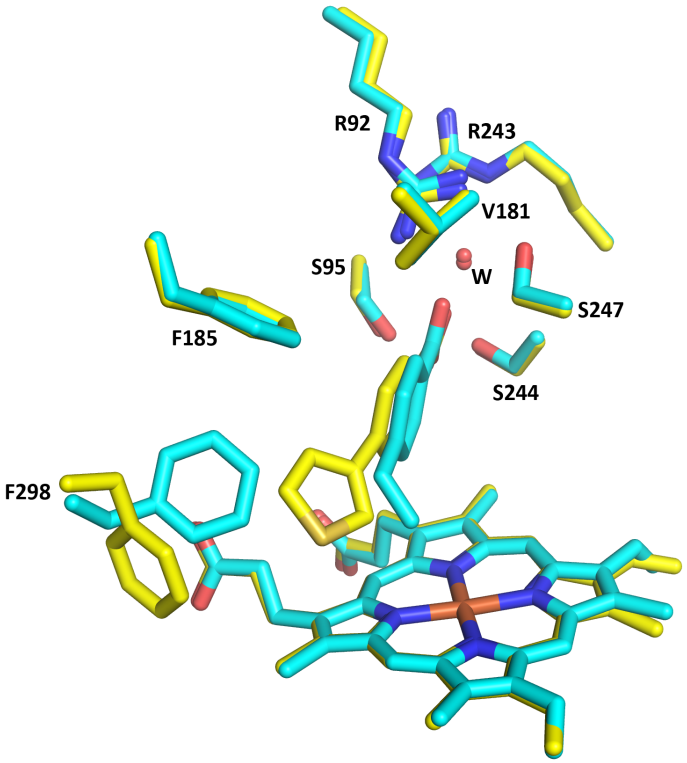

(a) Overlay with 4-ethylbenzoic acid

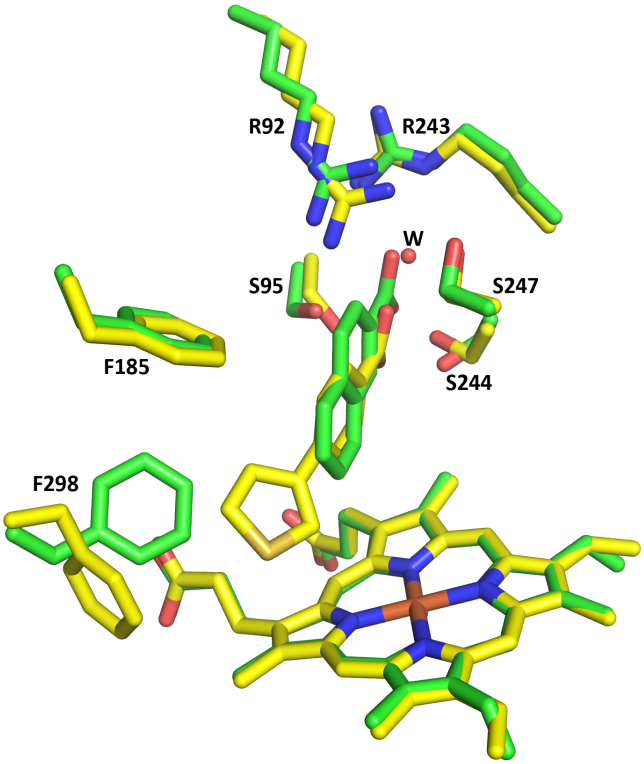

(b) Overlay with 2-naphthoic acid

Figure 160. Comparisons of the active site of 4-(thiophen-3-yl)benzoic acid CYP199A4 complex (yellow) with (a) 4-ethylbenzoic acid (cyan, PDB: 4EGM) and (b) 2-naphthoic acid (green, PDB: 4EGP).[30] Water molecules are shown as red spheres.

The thiophene ring is oriented so that its edge is pointing at the heme. This contrasted with 2-naphthoic acid, which is held at a different angle to the heme iron (Figure 160b). 2-Naphthoic acid undergoes aromatic oxidation by CYP199A2 at the C7 and C8 position carbons, which are 4.7 Å and 5.4 Å away from the heme iron respectively[30,167] (Table 32, bottom schematic). The difference in orientation of these aromatic groups may account for the different reactivities of 4-(thiophen-3-yl)benzoic acid and 2-naphthoic acid.

Similarly to the crystal structures of 4-ethylthiobenzoic acid (Chapter 4), 4-cyclohexylbenzoic acid and 4-heptylbenzoic acid (Both Chapter 5), the F298 residue has moved in order to accommodate the thiophenyl moiety in the active site of the enzyme. The $C_{\gamma'}$ of 4-(thiophen-3-yl)benzoic acid is 1.2 Å from the closest carbon of the F298 residue in the 4-ethylbenzoic acid structure, while it is 3.9 Å from the closest F298 carbon in the 4-(thiophen-3-yl)benzoic acid structure (Figure 160a).

When the Cpd I oxygen was modelled 1.62 Å from the heme iron, the distances from the oxygen atom to the thiophene ring were larger than that of 4-ethylbenzoic acid (C_α-O, 4.0 Å; C_β-O, 2.9 Å; S-O, 4.1 Å vs C_β-O, 2.0 Å; C_α-O, 3.5 Å, Table 33). In comparison, the C7 and C8 carbons of 2-naphthoic acid are further away from the Cpd I oxygen than the thiophene carbons (C7-O, 3.3 Å; C8-O, 4.2 Å; Table 33).

The angle of the Fe=O to the substrate was much lower for the thiophene ring of 4-(thiophen-3-yl)benzoic acid than the *para*-ethyl group of 4-ethylbenzoic acid (C_α, 143.8°; C_β, 123.8°; S, 135.1° vs C_α, 161.6°; C_β, 162.1°). However, these angles were comparable to that of 2-naphthoic acid (C7, 141.3°; C8, 131.3°). The small approach angle, along with the significant distance of the thiophenyl from the heme iron, and the lower reactivities of the non-benzylic positions could rationalise the lack of any P450 oxidation products with this substrate.

Table 33. Distances and angles between structural features of 4-(thiophen-3-yl)benzoic acid-bound CYP199A4. Comparisons to 4-ethylbenzoic acid and 2-naphthoic acid are also shown.

Distance (Å)	4-ethylBA	2-naphthoic acid	4-(thiophen-3-yl)BA
C_α - Fe	4.7	(C8) 5.4	5.4
C_α - **O**=Fe	3.5	(C8) 4.2	4.0
C_β - Fe	3.2	(C7) 4.7	4.2
C_β - **O**=Fe	2.0	(C7) 3.3	2.9
S - Fe	-	-	5.2
S - **O**=Fe	-	-	4.1
C_X - F298	(X = α) 3.9	(X = C6) 4.2	(X = γ') 3.9
Angle (°)			
C_{04}-C_α-C_β	113.7	-	128.6
C_α-C_β-S	-	-	105.2
Dihedral C_{09}-C_{04}-C_α-C_β	50.2	0.8 (*)	50.0
Fe=O-C_α	161.6	(C7) 141.3	143.8
Fe=O-C_β	162.1	(C8) 131.3	123.8
Fe=O-S	-	-	135.1

(*) This dihedral angle was measured using C_{09}-C_{10}-C_{05}-C_{06}.

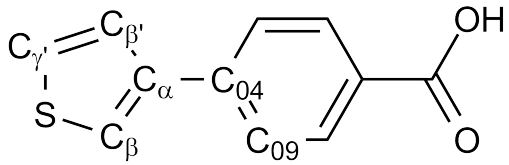

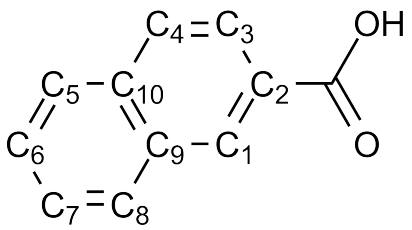

7.3 Discussion

In the present study of *para*-phenyl benzoic acids, hydroxylation at the α-carbon of 4-benzylbenzoic acid proceeded readily, while there was no activity observed with the substrates where the α-carbon lacked C−H bonds. This reactivity can be rationalised by the proximity of the benzylic C−H bond of this substrate to the heme iron, which was confirmed by the type II spin state shift induced by 4-benzoylbenzoic acid, indicating the carbonyl oxygen was binding to the heme iron. There was a limited amount of demethylation of methoxyphenyl substituents but no aromatic oxidation. The tight binding and high NADH oxidation activity of 4-phenylbenzoic acid, which did not generate any products, provides evidence that CYP199A4 was not able to catalyse the efficient aromatic oxidation of phenyl moieties. This contrasted with 2-naphthoic acid, whose aromatic C−H bonds were reported to be oxidised by CYP199A2 and CYP199A4 albeit with low activity.[30,167]

The lack of aromatic oxidation may be due to the binding orientation of the substrate in the active site of CYP199A4. The phenyl ring of a substrate may be required to face towards the heme iron in order for Cpd I to access the aromatic π-electrons. It may be that the substrates examined here, such as 4-phenylbenzoic acid, bind in an orientation where this is not the case. One face of 2-naphthoic acid is oriented towards the space above the site of oxygen binding, although it is held far from the heme iron (Figures 160b, 161). This substrate has a constrained nature due to the rings comprising the naphthalene moiety.

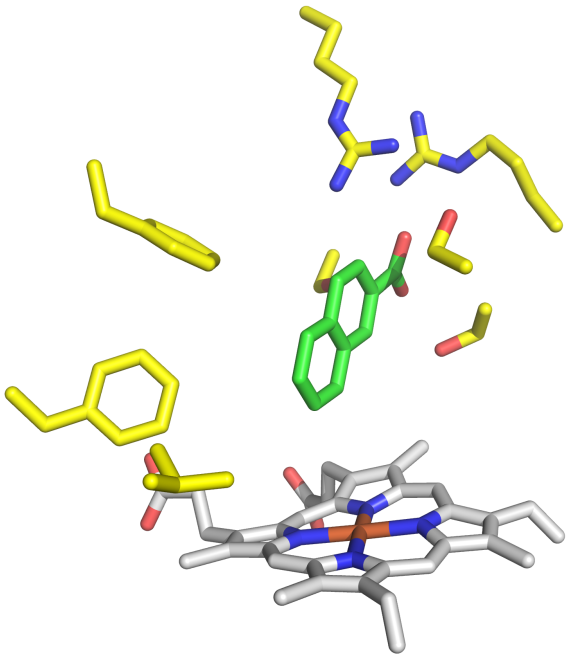

Figure 161. Binding orientation of 2-naphthoic acid in the active site of CYP199A4 (PDB: 4EGP), highlighting the orientation of the aromatic system relative to the heme iron. Several active site residues have been omitted for clarity.

CYP199A4 was able to oxidise heterocyclic *para*-position moieties, but with relatively low activity. The substrates that exhibited type II binding were not oxidised by CYP199A4. This was indicative of coordination between the heme iron and substrate heteroatom, resulting in inhibition of the P450 catalytic cycle. The thiophene and furan-containing substrates did not display type II binding, indicating that these moieties were not interacting with the heme iron of CYP199A4.

The absence of any easily detectable products in the turnover of 4-(thiophen-3-yl)benzoic acid was rationalised by the crystal structure. The thiophen-3-yl moiety is angled away from the heme, such that the ferryl oxygen of Cpd I may not be able to access the π-electrons in order to abstract an aromatic C−H bond (Figure 160). 4-(Pyrrol-1-yl)benzoic acid and 4-(thiophen-2-yl)benzoic acid, where hydroxylation was observed in CYP199A4 turnovers, may have subtlely different binding orientations that are more comparable to that of 2-naphthoic acid (Figure 161) or 4-cyclohexylbenzoic acid (Figure 5.2.3).

The turnovers of 4-(furan-2-yl)benzoic acid indicated that CYP199A4 was not able to easily metabolise the furan moiety, unlike other P450 systems where ring-opening and epoxidation products have been observed (Figure 143a).[259–261] The turnovers indicated that products only arose when *E. coli* enzymes, most likely ene reductases, were involved.[273,274] The dihydrofuran product, resulting from initial reduction of a furan double bond by an ene reductase, may be a better substrate for CYP199A4 (Figure 162). It would be of further interest to investigate this mechanism by employing dihydro- and tetrahydrofuran substrates with *in vitro* CYP199A4.

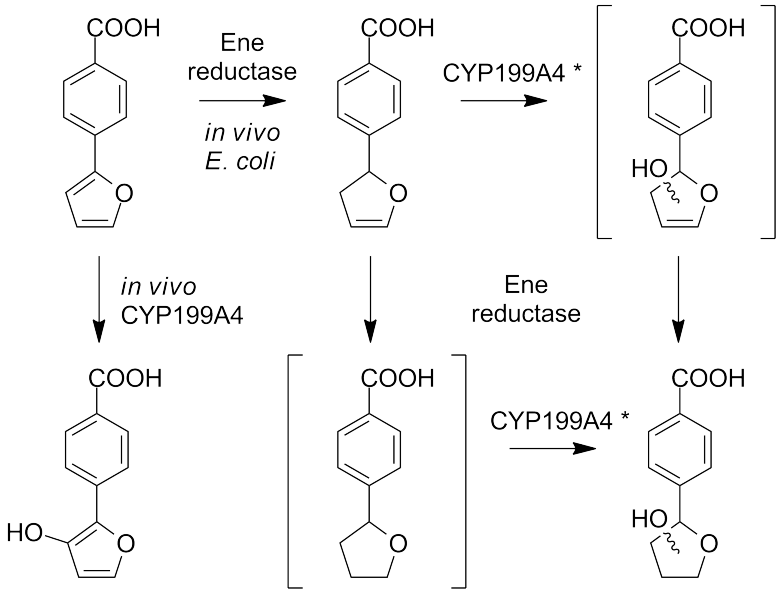

Figure 162. Proposed mechanism for *in vivo* metabolism of 4-(furan-2-yl)benzoic acid by CYP199A4 and *E. coli* ene reductase enzymes. The species shown in brackets were not observed in turnovers. It is currently unknown if the CYP199A4 oxidation steps denoted (*) function independently of the *in vivo* ene reductases.

Chapter 8 Conclusions and future directions

General conclusions to the thesis

The cytochrome P450 enzyme CYP199A4 preferentially binds *para*-substituted benzoic acids and regioselectively oxidises the *para*-substituent. The range of substrates that can be accommodated by CYP199A4 and the activities that can be catalysed have been explored by performing binding and turnover studies. It was found that the nature of the substituents, and their positions on the benzene ring, influence the binding affinity of the enzyme. CYP199A4 is selective for *para*-substituted benzoic acids, however limited activity at certain *meta*-substituents can also be catalysed. Furthermore, a wide range of mono-oxygenase activities were able to be catalysed. Reported for the first time were examples of CYP199A4 catalysing ethylenedioxy bridge hydroxylation, synthesis of amides from hemiaminals, dehalogenation and the aromatic oxidation of heterocycles. The diversity of these activities highlight this enzyme's potential for investigating poorly understood P450 mechanistic pathways. Crystallographic structures were determined for various substrate-bound forms of CYP199A4 and were able to provide information on the binding orientation of each substrate in the enzyme active site.

The mechanism of oxygen activation in CYP199A4 was investigated using *in vitro* substrate turnovers and crystallography of the T252A and D251N mutants. It was found that the T252 residue plays a less critical role in this enzyme and that the active oxidant, Cpd I, forms more readily in this mutant, compared to $P450_{cam}$. The D251N mutant of CYP199A4 showed a comparable drop in activity to that of D251N-$P450_{cam}$, suggesting that the D251 residue of CYP199A4 has a similar role in proton delivery. Overall, these results suggest that the activation of molecular oxygen by P450 enzymes can differ between systems.

Chapter 3 – Dealkylation of *para*-methoxy substituted benzoic acids by CYP199A4

Substrates with various substituents related to oxidative demethylation were explored using CYP199A4. The binding and kinetic properties of CYP199A4 were determined with a range of mono-, di- and tri-substituted methoxybenzoic acid substrates, with differently sized substituents at the *ortho*-, *meta*- and *para*-positions. Demethylation products were observed with the majority of substrates with *para*-functional groups, however both the size and position of the other substituents were important for enzyme activity. For 3,5-dimethoxybenzoic acid, there was a limited amount of *meta*-demethylation, which suggested that this sterically bulky substrate must adopt a dif-

ferent binding orientation in the enzyme active site. Likewise, a small amount of demethylation was observed for 2,3,4-trimethoxybenzoic acid. Other catalytic transformations were also achieved using CYP199A4. Deethylation activity was observed with 4-ethoxybenzoic acid, albeit with lower activity than demethylation. CYP199A4 catalysed the ring-opening of 3,4-(methylenedioxy)benzoic acid, releasing formic acid. However, hydroxylation activity was observed for 3,4-(ethylenedioxy)benzoic acid. From this finding it was concluded that the stabilisation of the hemiacetal product may be analogous to the stability of cyclic sugars, which are in equilibrium with a ring-opened form.

It was also demonstrated that replacement of the benzoic acid moiety by a nicotinic acid could be accommodated by CYP199A4, although the activity and product formation were reduced. A broader range of nicotinic and picolinic acid substrates could be employed to investigate their electronic effects on CYP199A4-catalysed reactions (Figure 163).

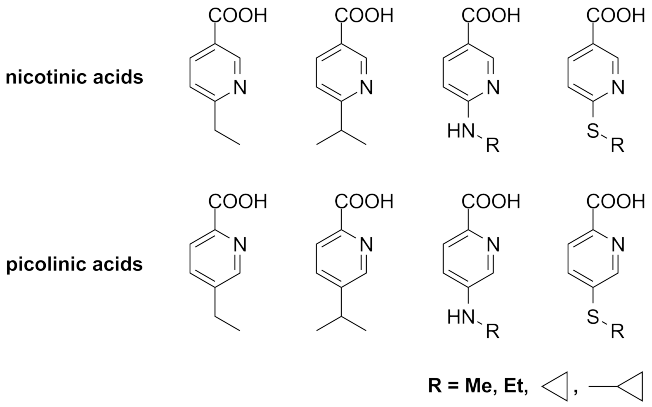

Figure 163. Nicotinic and picolinic acid substrates that could be employed as probes for the electronic effect of various CYP199A4-catalysed oxidations. The magnitude of the electron withdrawing effect differs between nicotinic and picolinic acids due to the position of the nitrogen atom relative to the *para* substituent.

For example, 6-ethylnicotinic acid could be used to probe the partition between desaturation and hydroxylation activities as investigated in Chapter 5. The 6-methylthio- and 6-methylamino- analogues could be used to probe the hydrogen abstraction and single electron transfer mechanisms in the heteroatom oxidation and dealkylation pathways.

Chapter 4 – Heteroatom dealkylation and oxidation by CYP199A4

Nitrogen-containing substrates exclusively underwent N-dealkylation, with no competing N-oxidation observed. 4-Aminomethylbenzoic acid substrates were not effectively oxidised by CYP199A4. In the turnovers of the ethylamino-containing substrates, there was formation of an acetamide metabolite in addition to the expected deethylation product. This acetamide is hypothesised to arise from CYP199A4-catalysed oxidation of a hemiacetal intermediate, although imine intermediates have also been proposed.[275] Future turnover studies employing $^{18}O_2$ would allow the nature of this intermediate to be investigated by determining the origin of the acetamide oxygen atom. If the acetamide oxygen atom is derived from dioxygen, the metabolite would be isotopically labelled (^{18}O) and this would imply that the reaction proceeded by further oxidation of a hemiaminal (Figure 164, top). Conversely, if ^{16}O is detected in the metabolite, this implicates an imine intermediate, as the oxygen atom must be derived from water. Alternatively, if the reaction proceeds by the imine intermediate, turnovers performed in ^{18}O-labelled water ($H_2{}^{18}O$) would result in an ^{18}O labelled acetamide (Figure 164, bottom).

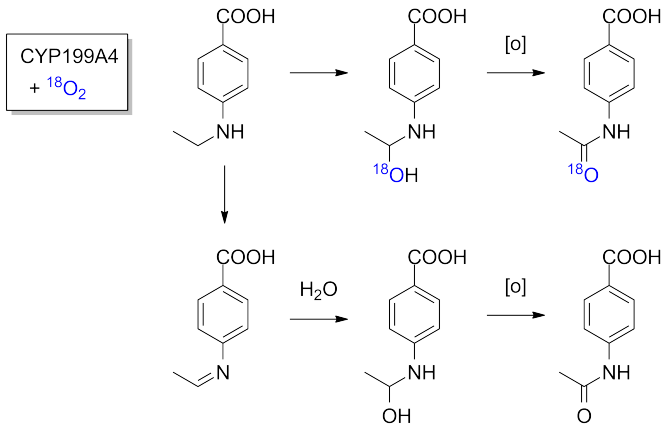

Figure 164. The possible intermediates in the mechanism of acetamide formation.[275] The mechanism proceeds by one of two possible initial steps. Top: P450-catalysed hydroxylation to a hemiaminal. Bottom: desaturation to an imine followed by hydration to the hemiaminal. If $^{18}O_2$ is used in turnover experiments (shown in blue), the oxygen isotope incorporated into the final product would allow determination of the intermediate.

It has been suggested that hemiaminals possess high stability in mildly acidic or neutral conditions (pH $\leq$ 7).[209] If a hemiaminal intermediate is involved, turnovers at different pH may result in a change to the ratio of acetamide and deethylation products. 4-Acetamidobenzoic acid has been shown to induce type II binding to CYP199A4, which suggests this substrate disrupts enzyme catalysis.[32] As the turnover of ethylaminobenzoic acids progresses, the acetamide may accumulate and bind to the heme iron, resulting in a decrease in the turnover activity of CYP199A4.

Previously, cyclopropylamine moieties have been employed to investigate the intermediates in nitrogen dealkylation and oxidation reactions.[276–278] Substrates containing these groups undergo metabolism by P450 enzymes to form a complex mixture of products. The products formed are dependant on whether the first step of the mechanism is single electron transfer from the nitrogen or hydrogen abstraction from the adjacent carbon. The cyclopropyl group can undergo ring-opening when a radical forms at the adjacent carbon, via either mechanism. The ring-opening metabolites can also potentially inhibit P450 enzymes (Figure 165).[277] Benzoic acid substrates containing cyclopropylamine *para* substituents may provide valuable insight into the intermediates involved in N-dealkylation and acetamide formation by CYP199A4. 4-Cyclopropylmethylaminobenzoic acid can potentially undergo dealkylation and amide formation as well as cyclopropyl ring-opening (Figure 165).

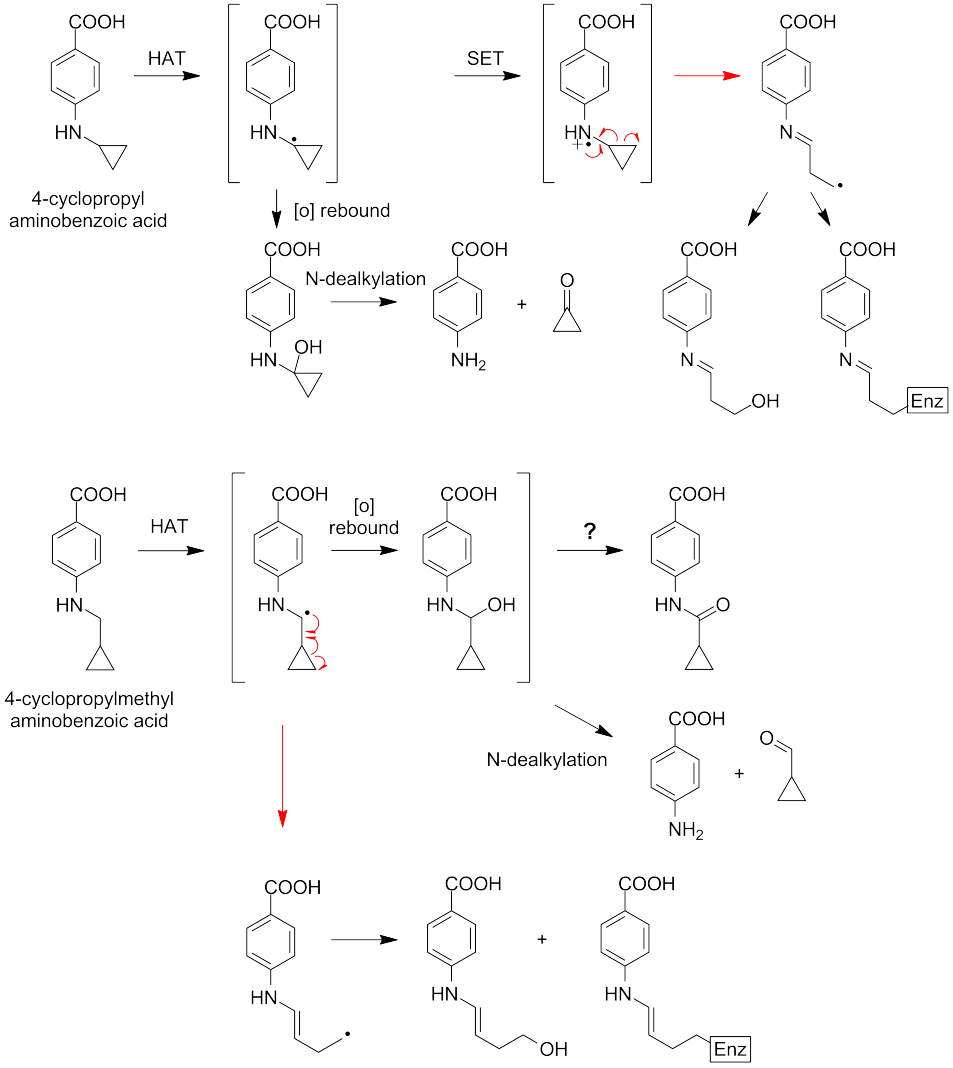

Figure 165. Cyclopropylamine benzoic acid substrates that could be investigated with CYP199A4. The ratio of metabolites would provide information on the relative importance of the HAT and SET mechanisms. Shown in boxes labelled "Enz" are possible ring-opened metabolites where the radical species covalently bonds to the enzyme, inhibiting further activity.[277]

CYP199A4 catalysed the sulfoxidation but not the S-dealkylation of alkylsulfur substrates, and chiral sulfoxides were formed. One enantiomer of 4-ethylsulfinylbenzoic acid was formed in excess, which was postulated to be the (S)-enantiomer by analogy to the enantioselectivity of 4-ethylbenzoic acid turnovers, which favoured the (S)-enantiomer of 4-(1-hydroxyethyl)benzoic acid. The crystal structures of CYP199A4 with bound 4-methylamino-, 4-methylthio- and 4-ethylthio-benzoic acids showed that the reactivity of the heteroatom was more important than the distance it was held from the heme iron. Potentially, more substituted alkylthio substrates, such as 4-isopropylthiobenzoic acid, could be used to explore if S-dealkylation reactions can be catalysed by CYP199A4. Alternatively, the position of the sulfur atom along the alkyl chain could be modified to investigate the effects on reaction selectivity and efficiency (Figure 166). Cyclopropylthiobenzoic acids may also allow determination of the character of the S-oxidation intermediates for this enzyme (Figure 166). If ring-opening metabolites are observed in turnovers of 4-cyclopropylthiobenzoic acid, this would suggest the involvement of a radical cation species.

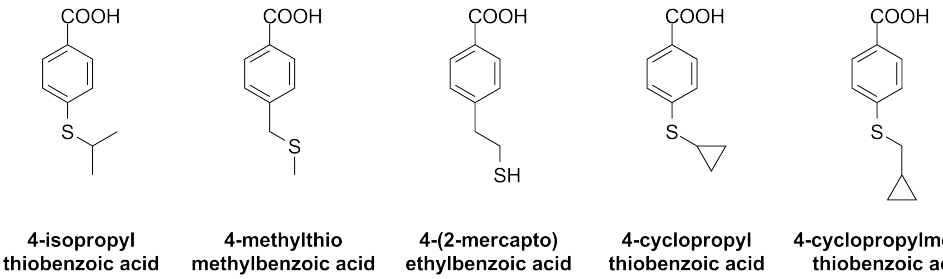

Figure 166. Examples of thiobenzoic acid probe substrates that could be used to investigate sulfoxidation and S-dealkylation activities.

CYP199A4 was unable to oxidise 4-halobenzoic acids. However, dehalogenation products were observed as the metabolites of 4-halomethylbenzoic acid substrates. 4-(2-Haloethyl)benzoic acids underwent hydroxylation and desaturation, and a limited amount of dehalogenation, but with much lower turnover efficiency compared to 4-ethylbenzoic acid. These results revealed that halogen oxidation reactions by CYP199A4 may require specific substrates. Investigating the turnovers of chiral 4-(1-haloethyl)benzoic acids would provide a useful comparison to the 4-(2-haloethyl)benzoic acid substrates, because specific enantiomers may be more likely to undergo dehalogenation.

Reactions such as the anaerobic reduction of hexachloroethane to tetrachloroethene by $P450_{cam}$ have also been reported previously.[212–214] These haloalkylbenzoic acid substrates could be used to investigate reductive dehalogenation activities with CYP199A4.

Chapter 5 – Investigation of the partition of desaturation and hydroxylation

The alkylbenzoic acid substrates investigated in this study all bound to CYP199A4. The degree of substitution was observed to have a negative effect on binding affinity; however, the effect of the alkyl group length was minimal. Each substrate underwent hydroxylation at the α-carbon, where there was a suitable benzylic C−H bond for hydrogen abstraction. In the absence of a C−H bond for α-carbon abstraction, hydroxylation activity at the adjacent carbon (C_β) was observed instead. This desaturation of α- and β-carbons to form an alkene was observed for the majority of substrates. CYP199A4 was also capable of hydroxylating cyclic alkyl moieties; however, there was minimal desaturation observed. Hydroxylation at a γ-carbon was observed only as a further oxidation metabolite of the 4-*n*-butylbenzoic acid alkene, suggesting that alkene substrates may favour this activity.

The crystal structures of the alkylbenzoic acids were able to provide information of the binding orientation of each substrate in the active site of CYP199A4 (Chapter 5.2.3). Further crystallographic investigation of compounds, such as 4-*n*-butylbenzoic acid and its alkene product, will assist in determining the factors controlling the desaturation pathway. For the structures of 4-cyclohexyl- and 4-*n*-heptyl-benzoic acid, the F298 residue moved to accommodate the large *para*-substituent. Mutants of CYP199A4 with the phenylalanine replaced with a smaller aliphatic residue (Phe298 → Gly, Ala, Val, Ile) could be tested using larger substrates, to determine the changes in binding, enzyme activity and product partition (Figure 167).

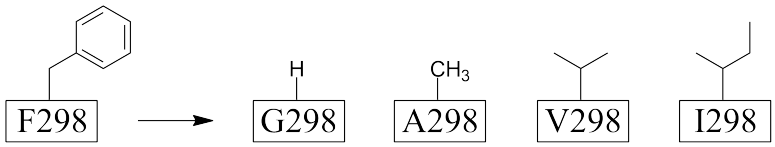

Figure 167. Mutagenesis targets of the F298 residue to investigate the size of substrates that can be incorporated by CYP199A4.

The *meta*-substituted 4-isopropylbenzoic acids were, for the majority of substrates, able to bind to CYP199A4. Hydroxylation and desaturation activities were observed for all, with the exception of the 3-amino- and 3-acetamido- substrates. There was no obvious correlation with the electronic properties of the substituent. It was hypothesised that the *meta*-substituents modified the binding of these substrates, preventing them from being used as probes for the electronic properties of the hydroxylation-desaturation partition. Deuterated substrates, such as deuterated 4-isopropyl- and 4-*n*-propyl-benzoic acids, may be able to circumvent these issues by minimising changes to the size of the substrate. This will hopefully allow the determination of the enantioselectivity of hydrogen abstraction and the nature of the intermediate involved in

the desaturation pathway (Figure 168). These substrates could be used in combination with the nicotinic and picolinic acid probes discussed earlier (Figure 163) to further investigate the desaturation of substrates by CYP1994.

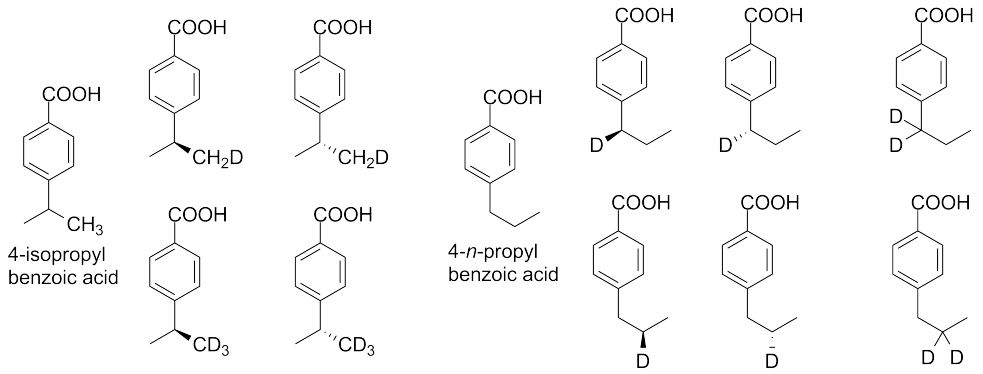

Figure 168. Deuterated 4-isopropyl- and 4-*n*-propyl-benzoic acids to be employed as probe substrates for the desaturation mechanism of CYP199A4.

The oxidation of 4-propionyl- and 4-(2-oxopropyl)-benzoic acids by CYP199A4 yielded α-hydroxycarbonyl metabolites. These metabolites may themselves be substrates for CYP199A4, and hence used to determine if carbon-carbon bond cleavage reactions can be catalysed by this enzyme (Chapter 5.2.5, Figure 114). Specific enantiomers of each may be required to fully assess the mechanism of action.

Chapter 6 – Investigation of molecular oxygen activation in CYP199A4

The T252A mutant showed a decrease in activity and an increase in hydrogen peroxide formation for all substrates, with the exception of 4-isopropylbenzoic acid. Conversely, this substrate was more active with the T252A mutant. The T252A crystal structure contained an extra water molecule in the active site oxygen binding groove, similar to that observed in T252A-P450$_{cam}$. The widening of the oxygen binding groove in CYP199A4 caused by the T252A mutation was less dramatic compared to that of T252A-P450$_{cam}$ (Chapter 6.3, Figure 139). Overall, the T252 residue of CYP199A4 seems to be less crucial for productive activity than its equivalent in P450$_{cam}$. The activity of the D251N mutant of CYP199A4 also decreased by several orders of magnitude for all substrates compared to the wild-type enzyme. For all substrates, both the T252A and D251N mutants of CYP199A4 yielded the same reaction products as the wild-type enzyme.

The crystal structures of the CYP199A4 isoforms revealed a water channel, which extended from the surface of the enzyme to the D251 residue in the active site. As a result of the D251N mutation, the D251-N255 side chain interaction was broken, and the N255 side chain had rotated (Chapter 6.2.4, Figures 133 and 134). These changes may affect the rate of controlled delivery of protons to the active site.

Further mutagenesis of the acid-alcohol pair may reveal more details of the oxygen activation mechanism of CYP199A4 (Figure 169). The Thr252 residue could be mutated to a Ser or Asn, to determine which interactions are important in stabilising the oxygen binding groove. Some P450 enzymes have also been shown to employ H_2O_2 to generate compound I via a peroxide shunt pathway, rather than using O_2, NAD(P)H and electron transfer partner proteins.[279] This is facilitated through a carboxylate residue that coordinates to the heme iron. The equivalent mutations, T252D and T252E, could be investigated with CYP199A4, to determine whether the enzyme is able to perform substrate oxidation using H_2O_2.

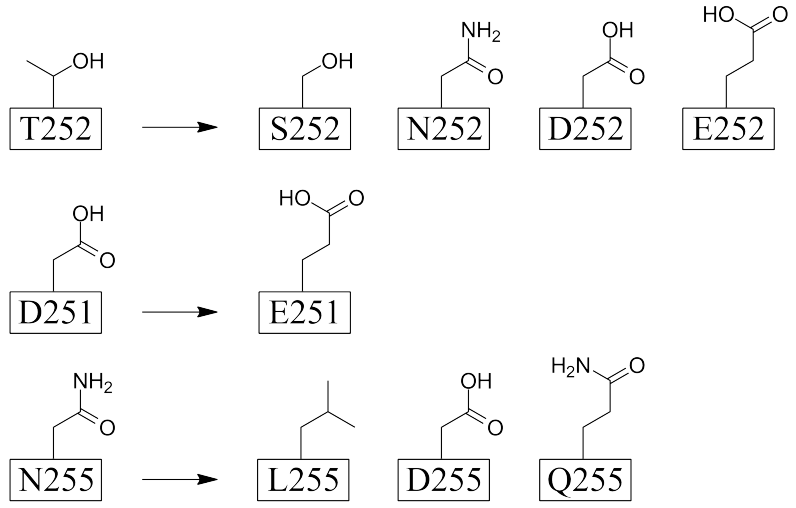

Figure 169. Mutagenesis targets for the acid-alcohol pair and investigation of the oxygen activation mechanism of CYP199A4.

Additionally, conversion of the D251 residue to a glutamic acid (D251E) could identify if comparable activity to the wild-type aspartic acid can be achieved with a larger, more flexible residue. Furthermore, the side chain of the N255 residue formed hydrogen bonds with the D251 side chain, which may play a role in proton transfer to molecular oxygen in CYP199A4. This could be further investigated using a series of mutants such as Asn255 → Leu, Asp and Gln (Figure 169). Double or triple mutants of D251, T252 and N255 could be used to further investigate if particular oxidants or activities can be favoured with certain substrates.

Chapter 7 – Screening of aromatic and heterocyclic substrates

The potential substrate range of CYP199A4 was explored and expanded to include phenyl ring and heterocycle-containing substrates. There was no aromatic oxidation of any of the phenyl-containing substrates, and benzylic α-carbons were hydroxylated in preference, as was the case with 4-benzylbenzoic acid. There was a limited amount of demethylation of methoxyphenyl substrates. From these results, it may be possible to design substrates which undergo different oxidations at the benzylic α-carbon, such as

oxidation of heteroatoms and alkenes (Figure 170). It is hypothesised that CYP199A4-catalysed aromatic oxidation may be facilitated by the benzene ring being positioned perpendicularly to the heme. Investigation of more phenyl and heterocyclic substrates by crystallography may provide additional insight into the requirements for aromatic oxidation reactions.

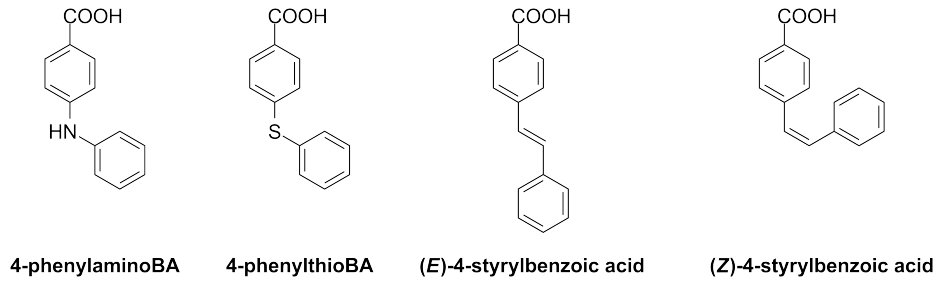

Figure 170. Phenyl-containing substrates to be investigated with CYP199A4. These may display different modes of binding and activity to the substrates investigated previously.

Several heterocyclic substrates, including 4-(thiophen-2-yl)- and 4-(pyrrol-1-yl)-benzoic acids, underwent limited aromatic oxidation. The pyridine and carbonyl-containing substrates displayed type II binding and no product formation, which suggested they were inhibiting the P450 catalytic cycle.[202] 4-(Furan-2-yl)benzoic acid was not oxidised by *in vitro* CYP199A4, however it underwent several hydroxylation and double bond reduction reactions when an *in vivo* CYP199A4 system was employed. The furan moiety may require reduction by *E. coli* proteins expressed in the recombinant system prior to oxidation by CYP199A4. The isolation and characterisation of these products would be of significant interest, as they could be suitable substrates for CYP199A4.

Other drug moieties could be incorporated at the *para*-position of benzoic acid substrates. Morpholine rings, which are prevalent in drug molecules,[251] have been shown to undergo ring-opening reactions with P450 enzymes.[280] Hence, 4-morpholinobenzoic acid could be used to investigate this activity with CYP199A4 (Figure 171). Azides have been shown to undergo reduction to amines in certain P450 systems, and this reaction appears to occur when either P450 reductases are involved,[281] or under anaerobic conditions.[282,283] The metabolism of azides could be further investigated, both aerobically and anaerobically, using the *in vitro* CYP199A4-HaPux-HaPuR system with 4-azidomethylbenzoic acid (Figure 171).

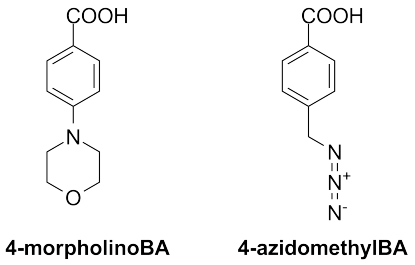

Figure 171. Drug moiety substrates to be investigated with CYP199A4.

EPR spectroscopy provides information on whether the water coordinated to the heme iron has been displaced by a substrate molecule.[211] This data is complementary to that obtained from optical spectrophotometry (such as UV-Vis spectroscopy as employed in this thesis). Binding of aromatic and heterocyclic substrates to the heme iron

could be probed using EPR spectroscopy. This method would be useful for substrates that display type II binding to CYP199A4, as this binding mode typically indicates that a substrate heteroatom is interacting with the heme iron.

Closing remarks

CYP199A4 catalyses a broad range of reactions and thus can be used to investigate various P450 oxidation mechanisms. Although many questions were answered during the course of this research, many new avenues of inquiry have opened up. The potential of this P450 enzyme as a tool to investigate the metabolism of various functional groups is anticipated to inform the future design of drug molecules, and the development of new biocatalytic systems.

References

(1) Poulos, T. L.; Johnson, E. F. In *Cytochrome P450: Structure, Mechanism, and Biochemistry*, 4th ed.; Ortiz de Montellano, P., Ed.; Springer: New York, 2015; Chapter 1, pp 3–32.

(2) Omura, T.; Sato, R. *J. Biol. Chem.* **1964**, *239*, 2370–8.

(3) Garfinkel, D. *Arch. Biochem. Biophys.* **1958**, *77*, 493–509.

(4) Klingenberg, M. *Arch. Biochem. Biophys.* **1958**, *75*, 376–86.

(5) Guengerich, F. P. In *Cytochrome P450: Structure, Mechanism, and Biochemistry*, 4th ed.; Ortiz de Montellano, P., Ed.; Springer: New York, 2015; Chapter 9, pp 523–785.

(6) Schuler, M. A.; Werck-Reichhart, D. *Annu. Rev. Plant Biol.* **2003**, *54*, 629–667.

(7) McLean, K. J.; Munro, A. W. *Drug Metab. Rev.* **2008**, *40*, 427–446.

(8) Guengerich, F. P. *Chem. Res. Toxicol.* **2001**, *14*, 611–650.

(9) Mao, W.; Rupasinghe, S. G.; Johnson, R. M.; Zangerl, A. R.; Schuler, M. A.; Berenbaum, M. R. *Comp. Biochem. Physiol. B, Biochem. Mol. Biol.* **2009**, *154B*, 427–434.

(10) Mao, W.; Schuler, M. A.; Berenbaum, M. R. *Proc. Natl. Acad. Sci. USA* **2011**, *108*, 12657–12662.

(11) Nelson, D. R.; Schuler, M. A. *Tropical Plant Biology* **2013**, *6*, 138–151.

(12) Nelson, D. R. The cytochrome P450 homepage.
URL: http://drnelson.uthsc.edu/cytochromeP450.html, 2009.

(13) Lamb, D. C.; Lei, L.; Warrilow, A. G. S.; Lepesheva, G. I.; Mullins, J. G. L.; Waterman, M. R.; Kelly, S. L. *J. Virol.* **2009**, *83*, 8266–8269.

(14) McLean, M. A.; Maves, S. A.; Weiss, K. E.; Krepich, S.; Sligar, S. G. *Biochem. Biophys. Res. Commun.* **1998**, *252*, 166–172.

(15) Wright, R. L.; Harris, K.; Solow, B.; White, R. H.; Kennelly, P. J. *FEBS Lett.* **1996**, *384*, 235–239.

(16) Nelson, D. R. *Biochim. Biophys. Acta* **2017**, *1866*, 141–154.

(17) Nelson, D. R. *Methods Mol. Biol.* **1998**, *107*, 15–24.

(18) Nelson, D. R. *Biochim. Biophys. Acta* **2011**, *1814*, 14–18.

(19) Poulos, T. L.; Raag, R. *FASEB J.* **1992**, *6*, 674–9.

(20) Hannemann, F.; Bichet, A.; Ewen, K. M.; Bernhardt, R. *Biochem. Biophys. Acta, Gen. Subj.* **2007**, *1770*, 330–344.

(21) Kelly, S. L.; Lamb, D. G.; Baldwin, B. C.; Corran, A. J.; Kelly, D. E. *J. Biol. Chem.* **1997**, *272*, 9986–9988.

(22) Miners, J. O.; Birkett, D. J. *Br. J. Clin. Pharmacol.* **1998**, *45*, 525–538.

(23) Bell, S. G.; Hoskins, N.; Xu, F.; Caprotti, D.; Rao, Z.; Wong, L.-L. *Biochem. Biophys. Res. Commun.* **2006**, *342*, 191–196.

(24) Prosser, D. E.; Jones, G. *Trends Biochem. Sci.* **2004**, *29*, 664 – 673.

(25) Chen, K. S.; Prahl, J. M.; DeLuca, H. F. *Proc. Natl. Acad. Sci. USA* **1993**, *90*, 4543–4547.

(26) Ohyama, Y.; Noshiro, M.; Okuda, K. *FEBS Lett.* **1991**, *278*, 195 – 198.

(27) Bell, S. G.; Tan, A. B.; Johnson, E. O.; Wong, L. L. *Mol. Biosyst.* **2010**, *6*, 206–14.

(28) Coleman, T. Investigation of the Substrate Range and Mechanism of CYP199A4 Catalysed Oxidations. Honours Thesis, The University of Adelaide, 2013.

(29) Cryle, M. J.; Hayes, P. Y.; De Voss, J. J. *Chem. Eur. J.* **2012**, *18*, 15994–15999.

(30) Bell, S. G.; Zhou, R.; Yang, W.; Tan, A. B.; Gentleman, A. S.; Wong, L. L.; Zhou, W. *Chem. Eur. J.* **2012**, *18*, 16677–88.

(31) Chao, R. R.; De Voss, J. J.; Bell, S. G. *RSC Adv.* **2016**, *6*, 55286–55297.

(32) Chao, R. Utilising CYP199A4 from Rhodopseudomonas palustris HaA2 for Biocatalysis and Mechanistic Studies. M.Sc. thesis, The University of Adelaide, 2016.

(33) Poulos, T. L. *Chem. Rev.* **2014**, *114*, 3919–62.

(34) Rittle, J.; Green, M. T. *Science* **2010**, *330*, 933–937.

(35) Mak, P. J.; Denisov, I. G. *Biochim. Biophys. Acta* **2018**, *1866*, 178–204.

(36) Groves, J. T.; McClusky, G. A. *J. Am. Chem. Soc.* **1976**, *98*, 859–861.

(37) Puchkaev, A. V.; Ortiz de Montellano, P. R. *Arch. Biochem. Biophys.* **2005**, *434*, 169–177.

(38) Nishida, C. R.; Ortiz de Montellano, P. R. *Biochem. Biophys. Res. Commun.* **2005**, *338*, 437–45.

(39) Ortiz de Montellano, P. In *Cytochrome P450: Structure, Mechanism, and Biochemistry*, 4th ed.; Ortiz de Montellano, P., Ed.; Springer: New York, 2015; Chapter 4.

(40) Stok, J. E.; Yamada, S.; Farlow, A. J.; Slessor, K. E.; De Voss, J. J. *Biochim. Biophys. Acta* **2013**, *1834*, 688–96.

(41) Imai, M.; Shimada, H.; Watanabe, Y.; Matsushima-Hibiya, Y.; Makino, R.; Koga, H.; Horiuchi, T.; Ishimura, Y. *Proc. Natl. Acad. Sci. USA* **1989**, *86*, 7823–7.

(42) Martinis, S. A.; Atkins, W. M.; Stayton, P. S.; Sligar, S. G. *J. Am. Chem. Soc.* **1989**, *111*, 9252–3.

(43) Gerber, N. C.; Sligar, S. G. *J. Am. Chem. Soc.* **1992**, *114*, 8742–3.

(44) Vidakovic, M.; Sligar, S. G.; Li, H.; Poulos, T. L. *Biochemistry* **1998**, *37*, 9211–9219.

(45) Nagano, S.; Poulos, T. L. *J. Biol. Chem.* **2005**, *280*, 31659–63.

(46) Kimata, Y.; Shimada, H.; Hirose, T.; Ishimura, Y. *Biochem. Biophys. Res. Commun.* **1995**, *208*, 96–102.

(47) Raag, R.; Martinis, S. A.; Sligar, S. G.; Poulos, T. L. *Biochemistry* **1991**, *30*, 11420–9.

(48) Raag, R.; Poulos, T. L. *Biochemistry* **1991**, *30*, 2674–84.

(49) Gerber, N. C.; Sligar, S. G. *J. Biol. Chem.* **1994**, *269*, 4260–6.

(50) Gerber, N. C.; Sligar, S. G. *Cytochrome P450 Int. Conf., 8th* **1994**, 753–6.

(51) Sligar, S. G.; Aikens, J.; Gerber, N.; McLean, M.; Suslick, K.; Benson, D. *Cytochrome P450 Int. Conf., 8th* **1994**, 373–8.

(52) Zhang, W.; Pochapsky, S. S.; Pochapsky, T. C.; Jain, N. U. *J. Mol. Biol.* **2008**, *384*, 349–363.

(53) Blanksby, S.; Ellison, G. *Acc. Chem. Res.* **2003**, *36*, 255–63.

(54) Groves, J. T.; McClusky, G. A.; White, R. E.; Coon, M. J. *Biochem. Biophys. Res. Commun.* **1978**, *81*, 154–60.

(55) Krauser, J. A.; Guengerich, F. P. *J. Biol. Chem.* **2005**, *280*, 19496–506.

(56) Kim, K.-H.; Isin, E. M.; Yun, C.-H.; Kim, D.-H.; Guengerich, F. P. *FEBS J.* **2006**, *273*, 2223–2231.

(57) Gelb, M. H.; Heimbrook, D. C.; Malkonen, P.; Sligar, S. G. *Biochemistry* **1982**, *21*, 370–7.

(58) White, R. E.; Miller, J. P.; Favreau, L. V.; Bhattacharyya, A. *J. Am. Chem. Soc.* **1986**, *108*, 6024–31.

(59) Auclair, K.; Hu, Z.; Little, D. M.; Ortiz de Montellano, P. R.; Groves, J. T. *Journal of the American Chemical Society* **2002**, *124*, 6020–6027, PMID: 12022835.

(60) Bowry, V. W.; Lusztyk, J.; Ingold, K. U. *Journal of the American Chemical Society* **1991**, *113*, 5687–5698.

(61) Bowry, V. W.; Ingold, K. U. *Journal of the American Chemical Society* **1991**, *113*, 5699–5707.

(62) Atkinson, J. K.; Ingold, K. U. *Biochemistry* **1993**, *32*, 9209–14.

(63) Newcomb, M.; Chandrasena, R. E. P.; Lansakara-P., D. S. P.; Kim, H.-Y.; Lippard, S. J.; Beauvais, L. G.; Murray, L. J.; Izzo, V.; Hollenberg, P. F.; Coon, M. J. *The Journal of Organic Chemistry* **2007**, *72*, 1121–1127, PMID: 17288366.

(64) Newcomb, M.; Le Tadic, M.-H.; Putt, D. A.; Hollenberg, P. F. *J. Am. Chem. Soc.* **1995**, *117*, 3312–13.

(65) Newcomb, M.; Le Tadic-Biadatti, M.-H.; Chestney, D. L.; Roberts, E. S.; Hollenberg, P. F. *J. Am. Chem. Soc.* **1995**, *117*, 12085–91.

(66) Newcomb, M.; Shen, R.; Choi, S.-Y.; Toy, P. H.; Hollenberg, P. F.; Vaz, A. D. N.; Coon, M. J. *J. Am. Chem. Soc.* **2000**, *122*, 2677–2686.

(67) Newcomb, M.; Shen, R.; Lu, Y.; Coon, M. J.; Hollenberg, P. F.; Kopp, D. A.; Lippard, S. J. *J. Am. Chem. Soc.* **2002**, *124*, 6879–6886.

(68) Hiroya, K.; Murakami, Y.; Shimizu, T.; Hatano, M.; de Montellano, P. R. O. *Arch. Biochem. Biophys.* **1994**, *310*, 397–401.

(69) Vaz, A. D.; Pernecky, S. J.; Raner, G. M.; Coon, M. J. *Proc. Natl. Acad. Sci. USA* **1996**, *93*, 4644–8.

(70) Vaz, A. D.; McGinnity, D. F.; Coon, M. J. *Proc. Natl. Acad. Sci. USA* **1998**, *95*, 3555–60.

(71) Coon, M. J.; Vaz, A. D. N.; Mcginnity, D. F.; Peng, H.-M. *Drug Metab. Dispos.* **1998**, *26*, 1190–1193.

(72) Toy, P. H.; Newcomb, M.; Coon, M. J.; Vaz, A. D. N. *J. Am. Chem. Soc.* **1998**, *120*, 9718–9719.

(73) Jin, S.; Makris, T. M.; Bryson, T. A.; Sligar, S. G.; Dawson, J. H. *J. Am. Chem. Soc.* **2003**, *125*, 3406–7.

(74) Davydov, R.; Perera, R.; Jin, S.; Yang, T.-C.; Bryson, T. A.; Sono, M.; Dawson, J. H.; Hoffman, B. M. *J. Am. Chem. Soc.* **2005**, *127*, 1403–1413.

(75) Keizers, P. H. J.; Schraven, L. H. M.; De Graaf, C.; Hidestrand, M.; Ingelman-Sundberg, M.; Van Dijk, B. R.; Vermeulen, N. P. E.; Commandeur, J. N. M. *Biochem. Biophys. Res. Commun.* **2005**, *338*, 1065–1074.

(76) Cryle, M. J.; De Voss, J. J. *Angew. Chem. Int. Ed.* **2006**, *45*, 8221–8223.

(77) Kerber, W. D.; Ramdhanie, B.; Goldberg, D. P. *Angew. Chem. Int. Ed.* **2007**, *46*, 3718–3721.

(78) Cryle, M. J.; De Voss, J. J. *ChemBioChem* **2008**, *9*, 261–266.

(79) Shaik, S.; Kumar, D.; de Visser, S. P.; Altun, A.; Thiel, W. *Chem. Rev.* **2005**, *105*, 2279–328.

(80) Shaik, S.; Hirao, H.; Kumar, D. *Nat. Prod. Rep.* **2007**, *24*, 533–52.

(81) Shaik, S.; Cohen, S.; Wang, Y.; Chen, H.; Kumar, D.; Thiel, W. *Chem. Rev.* **2010**, *110*, 949–1017.

(82) Sharma, P. K.; De Visser, S. P.; Shaik, S. *J. Am. Chem. Soc.* **2003**, *125*, 8698–9.

(83) Kumar, D.; De Visser, S. P.; Shaik, S. *J. Am. Chem. Soc.* **2004**, *126*, 5072–5073.

(84) Kumar, D.; de Visser, S. P.; Shaik, S. *J. Am. Chem. Soc.* **2003**, *125*, 13024–13025.

(85) Kumar, D.; de Visser, S. P.; Sharma, P. K.; Cohen, S.; Shaik, S. *J. Am. Chem. Soc.* **2004**, *126*, 1907–20.

(86) Shaik, S. A tale of two states: Reactivity of cytochrome P450 enzymes. Modelling Molecular Structure and Reactivity in Biological Systems. 2006; pp 233–248.

(87) de Visser, S. P.; Porro, C. S.; Quesne, M. G.; Sainna, M. A.; Munro, A. W. *Curr. Top. Med. Chem.* **2013**, *13*, 2218–2232.

(88) Li, C.; Zhang, L.; Zhang, C.; Hirao, H.; Wu, W.; Shaik, S. *Angew. Chem. Int. Ed.* **2007**, *46*, 8168–8170.

(89) Park, M. J.; Lee, J.; Suh, Y.; Kim, J.; Nam, W. *J. Am. Chem. Soc.* **2006**, *128*, 2630–2634.

(90) Ogliaro, F.; de Visser, S. P.; Cohen, S.; Sharma, P. K.; Shaik, S. *J. Am. Chem. Soc.* **2002**, *124*, 2806–17.

(91) de Visser, S. P.; Ogliaro, F.; Harris, N.; Shaik, S. *J. Am. Chem. Soc.* **2001**, *123*, 3037–47.

(92) de Visser, S. P.; Ogliaro, F.; Shaik, S. *Angew. Chem. Int. Ed.* **2001**, *40*, 2871–2874.

(93) Guengerich, F. P. *Chem. Res. Toxicol.* **2008**, *21*, 70–83.

(94) Ortiz de Montellano, P. R. *Chem. Rev.* **2010**, *110*, 932–948.

(95) Guengerich, F. P.; Yun, C. H.; Macdonald, T. L. *J. Biol. Chem.* **1996**, *271*, 27321–27329.

(96) Bhakta, M. N.; Wimalasena, K. *J. Am. Chem. Soc.* **2002**, *124*, 1844–5.

(97) Guengerich, F. P.; Macdonald, T. L. *Advances in Electron Transfer Chemistry*; Elsevier, 1993; pp 191–241.

(98) Bell-Parikh, L. C.; Guengerich, F. P. *J. Biol. Chem.* **1999**, *274*, 23833–40.

(99) Meunier, B.; de Visser, S. P.; Shaik, S. *Chem. Rev.* **2004**, *104*, 3947–80.

(100) Li, C.; Wu, W.; Kumar, D.; Shaik, S. *J. Am. Chem. Soc.* **2006**, *128*, 394–5.

(101) Wang, Y.; Kumar, D.; Yang, C.; Han, K.; Shaik, S. *J. Phys. Chem. B* **2007**, *111*, 7700–10.

(102) Rettie, A. E.; Boberg, M.; Rettenmeier, A. W.; Baillie, T. A. *J. Biol. Chem.* **1988**, *263*, 13733–8.

(103) Reilly, C. A.; Yost, G. S. *Drug Metab. Dispos.* **2005**, *33*, 530–6.

(104) Rettie, A. E.; Sheffels, P. R.; Korzekwa, K. R.; Gonzalez, F. J.; Philpot, R. M.; Baillie, T. A. *Biochemistry* **1995**, *34*, 7889–95.

(105) Wong, S. H.; Bell, S. G.; De Voss, J. J. *Pure Appl. Chem.* **2017**, *89*, 841–852.

(106) Lai, W.; Shaik, S. *J. Am. Chem. Soc.* **2011**, *133*, 5444–52.

(107) Lai, W.; Chen, H.; Cohen, S.; Shaik, S. *J. Phys. Chem. Lett.* **2011**, *2*, 2229–2235.

(108) Ji, L.; Faponle, A. S.; Quesne, M. G.; Sainna, M. A.; Zhang, J.; Franke, A.; Kumar, D.; van Eldik, R.; Liu, W.; de Visser, S. P. *Chem. Eur. J.* **2015**, *21*, 9083–9092.

(109) Mitropoulos, K. A.; Gibbons, G. F.; Reeves, B. E. A. *Steroids* **1976**, *27*, 821–9.

(110) Shyadehi, A. Z.; Lamb, D. C.; Kelly, S. L.; Kelly, D. E.; Schunck, W. H.; Wright, J. N.; Corina, D.; Akhtar, M. *J. Biol. Chem.* **1996**, *271*, 12445–50.

(111) Burstein, S.; Middleditch, B. S.; Gut, M. *J. Biol. Chem.* **1975**, *250*, 9028–37.

(112) Byon, C.-Y.; Gut, M. *Biochem. Biophys. Res. Commun.* **1980**, *94*, 549–52.

(113) Cryle, M. J.; Matovic, N. J.; De Voss, J. J. *Org. Lett.* **2003**, *5*, 3341–3344.

(114) Cryle, M. J.; De Voss, J. J. *Chem. Comm.* **2004**, 86–87.

(115) Hosoda, H.; Fishman, J. *J. Am. Chem. Soc.* **1974**, *96*, 7325–9.

(116) He, X.; Cryle, M. J.; De Voss, J. J.; Ortiz de Montellano, P. R. *J. Biol. Chem.* **2005**, *280*, 22697–22705.

(117) Kim, D.; Cryle, M. J.; De Voss, J. J.; Ortiz de Montellano, P. R. *Arch. Biochem. Biophys.* **2007**, *464*, 213–220.

(118) Pohl, L. R.; Nelson, S. D.; Krishna, G. *Biochem. Pharmacol.* **1978**, *27*, 491–6.

(119) Pohl, L. R.; Krishna, G. *Biochem. Pharmacol.* **1978**, *27*, 335–41.

(120) Guengerich, F. P. *J. Biol. Chem.* **1989**, *264*, 17198–205.

(121) Harwood, C. Harwood Lab: *Rhodopseudomonas palustris*.
URL: https://depts.washington.edu/cshlab/html/organisms/rhodopseudomonas.html.

(122) Larimer, F. W. et al. *Nat. Biotechnol.* **2004**, *22*, 55–61.

(123) Huang, J. J.; Heiniger, E. K.; McKinlay, J. B.; Harwood, C. S. *Appl. Environ. Microbiol.* **2010**, *76*, 7717–7722.

(124) Guo, D.; Xu, F.; Bell, S. G.; Pang, X.; Bartlam, M.; Wong, L.-L. *Protein Pept. Lett.* **2008**, *15*, 423–426.

(125) Pang, X.; Xu, F.; Bell, S. G.; Guo, D.; Wong, L. L.; Rao, Z. *Acta Crystallogr. F* **2007**, *63*, 342–345.

(126) Peng, Y.; Xu, F.; Bell, S. G.; Wong, L. L.; Rao, Z. *Acta Crystallogr. F* **2007**, *63*, 422–425.

(127) Harwood, C. S.; Gibson, J. *Appl. Environ. Microbiol.* **1988**, *54*, 712–17.

(128) Oda, Y.; Larimer, F. W.; Chain, P. S. G.; Malfatti, S.; Shin, M. V.; Vergez, L. M.; Hauser, L.; Land, M. L.; Braatsch, S.; Beatty, J. T.; Pelletier, D. A.; Schaefer, A. L.; Harwood, C. S. *Proc. Natl. Acad. Sci. USA* **2008**, *105*, 18543–18548.

(129) Oda, Y.; Wanders, W.; Huisman, L. A.; Meijer, W. G.; Gottschal, J. C.; Forney, L. J. *Appl. Environ. Microbiol.* **2002**, *68*, 3467–3477.

(130) Coleman, T.; Wong, S. H.; Podgorski, M. N.; Bruning, J. B.; De Voss, J. J.; Bell, S. G. *ACS Catal.* **2018**, *8*, 5915–5927.

(131) Bell, S. G.; Yang, W.; Tan, A. B.; Zhou, R.; Johnson, E. O.; Zhang, A.; Zhou, W.; Rao, Z.; Wong, L. L. *Dalton Trans.* **2012**, *41*, 8703–14.

(132) Coleman, T.; Chao, R.; De Voss, J.; Bell, S. *Biochim. Biophys. Acta* **2016**, *1864*, 667–75.

(133) Chao, R. R.; Lau, I. C.-K.; De Voss, J. J.; Bell, S. G. *ChemCatChem* **2016**, *8*, 3626–3635.

(134) Bell, S. G.; Xu, F.; Johnson, E. O.; Forward, I. M.; Bartlam, M.; Rao, Z.; Wong, L. L. *J. Biol. Inorg. Chem.* **2010**, *15*, 315–28.

(135) de Marco, A.; Vigh, L.; Diamant, S.; Goloubinoff, P. *Cell Stress & Chaperones* **2005**, *10*, 329–339.

(136) Omura, T.; Sato, R. *J. Biol. Chem.* **1964**, *239*, 2379–85.

(137) Michaelis, L.; Menten, M. *Biochemistry Zeitung* **1913**, *49*, 333–369.

(138) Briggs, G. E.; Haldane, J. B. *Biochem. J.* **1925**, *19*, 338–339.

(139) Williams, J. W.; Morrison, J. F. *Methods Enzymol.* **1979**, *63*, 437–467.

(140) Chen, M. M.; Snow, C. D.; Vizcarra, C. L.; Mayo, S. L.; Arnold, F. H. *Protein Eng. Des. Sel.* **2012**, *25*, 171–8.

(141) Dickinson, R. G.; Jacobsen, N. W. *J. Chem. Soc. D* **1970**, 1719–1720.

(142) Quesenberry, M. S.; Lee, Y. C. *Anal. Biochem.* **1996**, *234*, 50–5.

(143) Schaller, K. H.; Triebig, G. In *Methods of Enzymatic Analysis*, 3rd ed.; Bergmeyer, H. U., Ed.; VCH Publishers: Cambridge, UK, 1988; Vol. 6; pp 668–672.

(144) Emsley, P.; Lohkamp, B.; Scott, W.; Cowtan, K. *Acta Crystallogr. D* **2010**, *66*, 486–501.

(145) Adams, P. et al. *Acta Crystallogr. D* **2010**, *66*, 213–21.

(146) Rhodes, G. In *Crystallography Made Crystal Clear (Third Edition)*, third edition ed.; Rhodes, G., Ed.; Complementary Science; Academic Press: Burlington, 2006; Chapter 3, pp 31 – 47.

(147) Cowieson, N. P.; Aragao, D.; Clift, M.; Ericsson, D. J.; Gee, C.; Harrop, S. J.; Mudie, N.; Panjikar, S.; Price, J. R.; Riboldi-Tunnicliffe, A.; Williamson, R.; Caradoc-Davies, T. *J. Synchrotron Radiat.* **2015**, *22*, 187–190.

(148) McPhillips, T.; McPhillips, S.; Chiu, H.; Cohen, A.; Deacon, A.; Ellis, P.; Garman, E.; Gonzalez, A.; Sauter, N.; Phizackerley, R.; Soltis, S.; Kuhn, P. *J. Synchrotron Radiat.* **2002**, *1*, 401–6.

(149) Battye, T.; Kontogiannis, L.; Johnson, O.; Powell, H.; Leslie, A. *Acta Crystallogr. D* **2011**, *67*, 1204–14.

(150) Otwinowski, Z.; Minor, W. *Methods Enzymol.* **1997**, *276*, 307–326.

(151) Evans, P.; Murshudov, G. *Acta Crystallogr. D* **2013**, *67*, 1204–14.

(152) Winn, M. et al. *Acta Crystallogr. D* **2011**, *67*, 235–42.

(153) McCoy, A.; Grosse-Kunstleve, R.; Adams, P.; Winn, M.; Storoni, L.; Read, R. *J. Appl. Cryst.* **2007**, *40*, 658–74.

(154) Terwilliger, T. C.; Grosse-Kunstleve, R. W.; Afonine, P. V.; Moriarty, N. W.; Adams, P. D.; Read, R. J.; Zwart, P. H.; Hung, L. W. *Acta Crystallogr. D* **2008**, *64*, 515–524.

(155) Afonine, P. V.; Moriarty, N. W.; Mustyakimov, M.; Sobolev, O. V.; Terwilliger, T. C.; Turk, D.; Urzhumtsev, A.; Adams, P. D. *Acta Crystallogr. D* **2015**, 646–666.

(156) Liebschner, D.; Afonine, P. V.; Moriarty, N. W.; Poon, B. K.; Sobolev, O. V.; Terwilliger, T. C.; Adams, P. D. *Acta Crystallographica. Section D, Structural Biology* **2016**, *73*, 148–157.

(157) Berman, H. M.; Westbrook, J.; Feng, Z.; Gilliland, G.; Bhat, T. N.; Weissig, H.; Shindyalov, I. N.; Bourne, P. E. *Nucleic Acids Res.* **2000**, *28*, 235–242.

(158) Berman, H. M.; Henrick, K.; Nakamura, H. *Nat. Struct. Biol.* **2003**, *10*, 980.

(159) Schrodinger LLC. The PyMOL Molecular Graphics System, Version 1.8. 2015.

(160) Bathelt, C. M.; Zurek, J.; Mulholland, A. J.; Harvey, J. N. *J. Am. Chem. Soc.* **2005**, *127*, 12900–12908.

(161) Lonsdale, R.; Oláh, J.; Mulholland, A. J.; Harvey, J. N. *J. Am. Chem. Soc.* **2011**, *133*, 15464–15474.

(162) Chen, H.; Hirao, H.; Derat, E.; Schlichting, I.; Shaik, S. *J. Phys. Chem. B* **2008**, *112*, 9490–9500.

(163) Gumiero, A.; Metcalfe, C. L.; Pearson, A. R.; Raven, E. L.; Moody, P. C. E. *Journal of Biological Chemistry* **2011**, *286*, 1260–1268.

(164) Bell, S. G.; Xu, F.; Forward, I.; Bartlam, M.; Rao, Z.; Wong, L. L. *J. Mol. Biol.* **2008**, *383*, 561–74.

(165) Furuya, T.; Kino, K. *Biosci. Biotechnol. Biochem.* **2009**, *73*, 2796–9.

(166) Furuya, T.; Kino, K. *ChemSusChem* **2009**, *2*, 645–9.

(167) Furuya, T.; Kino, K. *Appl. Microbiol. Biotechnol.* **2010**, *85*, 1861–8.

(168) Arisawa, M.; Nihei, Y.; Suzuki, T.; Yamaguchi, M. *Org. Lett.* **2012**, *14*, 855–7.

(169) Parker, K. A.; Petraitis, J. J. *Tetrahedron Lett.* **1981**, *22*, 397–400.

(170) Kawamura, Y.; Takatsuki, H.; Torii, F.; Horie, T. *Bull. Chem. Soc. Jpn.* **1994**, *67*, 511–15.

(171) Trost, B. M. On inventing new reactions for atom economy. Pacifichem 2010, International Chemical Congress of Pacific Basin Societies. 2010; pp ORGN–27.

(172) Trost, B. M. *Handbook of Green Chemistry*; Wiley-VCH Verlag GmbH & Co. KGaA, 2012; Vol. 7; pp 1–33.

(173) Ikezawa, N.; Iwasa, K.; Sato, F. *FEBS J.* **2007**, *274*, 1019–35.

(174) Mizutani, M.; Sato, F. *Arch. Biochem. Biophys.* **2011**, *507*, 194–203.

(175) Fukuto, J. M.; Kumagai, Y.; Cho, A. K. *J. Med. Chem.* **1991**, *34*, 2871–6.

(176) Skerjanec, A. *Clin. Pharmacokinet.* **2006**, *45*, 325–350.

(177) Coleman, T.; Chao, R.; Bruning, J.; De Voss, J.; Bell, S. *RSC Adv.* **2015**, *5*, 52007–18.

(178) Bertelsen, K. M.; Venkatakrishnan, K.; Von Moltke, L. L.; Obach, R. S.; Greenblatt, D. J. *Drug Metab. Dispos.* **2003**, *31*, 289–93.

(179) Raag, R.; Poulos, T. L. *Biochemistry* **1989**, *28*, 917–22.

(180) Chau, N. T. T.; Nguyen, T. H.; Castanet, A.-S.; Nguyen, K. P. P.; Mortier, J. *Tetrahedron* **2008**, *64*, 10552–10557.

(181) Clayden, J.; Greeves, N.; Warren, S. *Organic Chemistry*, 2nd ed.; Oxford University Press, 2012.

(182) Karplus, P. A.; Diederichs, K. *Science* **2012**, *336*, 1030–1033.

(183) Karplus, P. A.; Diederichs, K. *Current Opinion in Structural Biology* **2015**, *34*, 60–68, Carbohydrate-protein interactions; Biophysical and molecular biological methods.

(184) Ramachandran, G.; Ramakrishnan, C.; Sasisekharan, V. *J. Mol. Biol.* **1963**, *7*, 95–99.

(185) de Visser, S. P. *J. Am. Chem. Soc.* **2006**, *128*, 15809–15818.

(186) Hinson, J.; Mitchell, J.; Jollow, D. *Mol. Pharmacol.* **1975**, *11*, 462–469.

(187) Hinson, J.; Nelson, S.; Gillette, J. *Mol. Pharmacol.* **1979**, *15*, 419–27.

(188) Alexson, S.; Diczfalusy, M.; Halldin, M.; Swedmark, S. *Drug Metab. Dispos.* **2002**, *30*, 643–47.

(189) Oguri, K.; Tanimoto, Y.; Yoshimura, H. *Xenobiotica* **1989**, *19*, 171–8.

(190) Ghassabian, S.; Rawling, T.; Zhou, F.; Doddareddy, M.; Tattam, B.; Hibbs, D.; Edwards, R.; Cui, P.; Murray, M. *Biochem. Pharmacol.* **2012**, *84*, 215–23.

(191) Kelly, W. L.; Townsend, C. A. *Journal of the American Chemical Society* **2002**, *124*, 8186–8187.

(192) Gunsior, M.; Breazeale, S. D.; Lind, A. J.; Ravel, J.; Janc, J. W.; Townsend, C. A. *Chemistry & Biology* **2004**, *11*, 927–938.

(193) Hansen, C. H.; Wittstock, U.; Olsen, C. E.; Hick, A. J.; Pickett, J. A.; Halkier, B. A. *Journal of Biological Chemistry* **2001**, *276*, 11078–11085.

(194) Reintanz, B.; Lehnen, M.; Reichelt, M.; Gershenzon, J.; Kowalczyk, M.; Sandberg, G.; Godde, M.; Uhl, R.; Palme, K. *Plant Cell* **2001**, *13*, 351–367.

(195) Chen, S.; Glawischnig, E.; Jorgensen, K.; Naur, P.; Jorgensen, B.; Olsen, C.-E.; Hansen, C. H.; Rasmussen, H.; Pickett, J. A.; Halkier, B. A. *Plant Journal* **2003**, *33*, 923–937.

(196) Rydberg, P.; Ryde, U.; Olsen, L. *J. Chem. Theory Comput.* **2008**, *4*, 1369–1377.

(197) Mazel, P.; Henderson, F.; Axelrod, J. *J. Pharmacol. Exp. Ther.* **1964**, *143*, 1–6.

(198) Henderson, J. F.; Mazel, P. *Biochem. Pharmacol.* **1964**, *13*, 1471–4.

(199) Henderson, J. F.; Mazel, P. *Biochem. Pharmacol.* **1964**, *13*, 207–10.

(200) Lin, H.-l.; Zhang, H.; Medower, C.; Hollenberg, P. F.; Johnson, W. W. *Drug Metab. Dispos.* **2011**, *39*, 345–350.

(201) Holland, H. L.; Chernishenko, M. J.; Conn, M.; Munoz, A.; Manoharan, T. S.; Zawadski, M. A. *Can. J. Chem.* **1990**, *68*, 696–700.

(202) Correia, M. A.; Hollenberg, P. F. In *Cytochrome P450: Structure, Mechanism, and Biochemistry*, 4th ed.; Ortiz de Montellano, P., Ed.; Springer: New York, 2015; Chapter 5.

(203) Sligar, S. G. *Biochemistry* **1976**, *15*, 5399–406.

(204) Honeychurch, M. J.; Hill, H. A. O.; Wong, L. L. *FEBS Lett.* **1999**, *451*, 351–353.

(205) Shea, J. P.; Valentine, G. L.; Nelson, S. D. *Biochem. Biophys. Res. Commun.* **1982**, *109*, 231–5.

(206) Kedderis, G. L.; Dwyer, L. A.; Rickert, D. E.; Hollenberg, P. F. *Mol. Pharmacol.* **1983**, *23*, 758–60.

(207) Ibe, B. O.; Raj, J. U. *Exp. Lung Res.* **1994**, *20*, 207–22.

(208) Upthagrove, A. L.; Nelson, W. L. *Drug Metab. Dispos.* **2001**, *29*, 1114–22.

(209) Perrin, L.; Loiseau, N.; Andre, F.; Delaforge, M. *FEBS J.* **2011**, *278*, 2167–78.

(210) Rodriguez-Antona, C.; Ingelman-Sundberg, M. *Oncogene* **2006**, *25*, 1679–1691.

(211) Harbort, J. S.; De Voss, J. J.; Stok, J. E.; Bell, S. G.; Harmer, J. R. In *Future Directions in Metalloprotein and Metalloenzyme Research*; Hanson, G., Berliner, L., Eds.; Springer International Publishing, 2017; pp 103–142.

(212) Castro, C. E.; Wade, R. S.; Belser, N. O. *Biochemistry* **1985**, *24*, 204–210.

(213) Li, S.; Wackett, L. P. *Biochemistry* **1993**, *32*, 9355–9361.

(214) Walsh, M. E.; Kyritsis, P.; Eady, N. A. J.; Hill, H. A. O.; Wong, L.-L. *Eur. J. Biochem.* **2000**, *267*, 5815–5820.

(215) Bernhardt, R. *J. Biotechnol.* **2006**, *124*, 128–145, BioPerspectives-From basic research to industrial production.

(216) Guengerich, F. P.; Munro, A. W. *J. Biol. Chem.* **2013**, *288*, 17065–17073.

(217) Zhu, N.; Zhao, J.; Bao, H. *Chem. Sci.* **2017**, *8*, 2081–2085.

(218) Denmark, S. E.; Kallemeyn, J. M. *J. Am. Chem. Soc.* **2006**, *128*, 15958–15959.

(219) Zhou, W.; Zhang, T. Crystal structure of CYP199A4 with 4-*n*-propylbenzoic acid. Unpublished (PDB: 5YQA).

(220) Roberts, J. D.; Mazur, R. H. *J. Am. Chem. Soc.* **1951**, *73*, 2509–2520.

(221) Hall, E. A.; Sarkar, M. R.; Bell, S. G. *Catal. Sci. Technol.* **2017**, *7*, 1537–1548.

(222) Alexander, K.; Akhtar, M.; Boar, R. B.; McGhie, J. F.; Barton, D. H. R. *J. Chem. Soc. Chem. Commun.* **1972**, 383–5.

(223) Schenkman, J. B.; Sligar, S. G.; Cinti, D. L. *Pharmacol. Ther.* **1981**, *12*, 43–71.

(224) Varfaj, F.; Zulkifli, S. N. A.; Park, H.-G.; Challinor, V. L.; De Voss, J. J.; Ortiz de Montellano, P. R. *Drug Metab. Dispos.* **2014**, *42*, 828–838.

(225) Tian, Z.; Fattahi, A.; Lis, L.; Kass, S. R. *J. Am. Chem. Soc.* **2006**, *128*, 17087–17092.

(226) Johnson, K. M.; Phan, T. T. N.; Albertolle, M. E.; Guengerich, F. P. *J. Biol. Chem.* **2017**, *292*, 13672–13687.

(227) Boddupalli, S. S.; Estabrook, R. W.; Peterson, J. A. *Journal of Biological Chemistry* **1990**, *265*, 4233–4239.

(228) Li, H.; Poulos, T. L. *Biochimica et Biophysica Acta (BBA) - Molecular and Cell Biology of Lipids* **1999**, *1441*, 141–149.

(229) Cryle, M. J.; Matovic, N. J.; Voss, J. J. D. *Tetrahedron Letters* **2007**, *48*, 133–136.

(230) McLean, K. J.; Leys, D.; Munro, A. W. In *Cytochrome P450: Structure, Mechanism, and Biochemistry*, 4th ed.; Ortiz de Montellano, P., Ed.; Springer: New York, 2015; Chapter 6.

(231) Cryle, M. J.; Schlichting, I. *Proc Natl Acad Sci USA* **2008**, *105*, 15696.

(232) Sligar, S.; Denisov, I. In *Cytochrome P450: Structure, Mechanism, and Biochemistry*, 4th ed.; Ortiz de Montellano, P., Ed.; Springer: New York, 2015; Chapter 3.

(233) Cupp-Vickery, J. R.; Poulos, T. L. *Nature Structural Biology* **1995**, *2*, 144–53.

(234) Cupp-Vickery, J. R.; Han, O.; Hutchinson, R.; Poulos, T. L. *Nature Structural Biology* **1996**, *3*, 632–637.

(235) Cupp-Vickery, J. R.; Poulos, T. L. *Steroids* **1997**, *62*, 112–116.

(236) Choonkeun, K.; Haeyoung, K.; Oksoo, H. *Bioorganic Chemistry* **2000**, *28*, 306–314.

(237) Xiang, H.; Tschirret-Guth, R. A.; De Montellano, P. R. O. *Journal of Biological Chemistry* **2000**, *275*, 35999–36006.

(238) Wang, B.; Li, C.; Cho, K. B.; Nam, W.; Shaik, S. *J. Chem. Theory Comput.* **2013**, *9*, 2519–25.

(239) Modi, A. R.; Dawson, J. H. *Adv. Exp. Med. Biol.* **2015**, *851*, 63–81.

(240) Jin, S.; Bryson, T. A.; Dawson, J. H. *J. Biol. Inorg. Chem.* **2004**, *9*, 644–53.

(241) Gelb, M. H.; Malkonen, P.; Sligar, S. G. *Biochem. Biophys. Res. Commun.* **1982**, *104*, 853–858.

(242) Batabyal, D.; Poulos, T. L. *Biochemistry* **2013**, *52*, 8898–8906.

(243) Yeom, H.; Sligar, S. G.; Li, H.; Poulos, T. L.; Fulco, A. J. *Biochemistry* **1995**, *34*, 14733–40.

(244) Truan, G.; Peterson, J. A. *Arch. Biochem. Biophys.* **1998**, *349*, 53–64.

(245) Clark, J. P.; Miles, C. S.; Mowat, C. G.; Walkinshaw, M. D.; Reid, G. A.; Daff, S. N.; Chapman, S. K. *J. Inorg. Biochem.* **2006**, *100*, 1075–90.

(246) Girvan, H. M.; Seward, H. E.; Toogood, H. S.; Cheesman, M. R.; Leys, D.; Munro, A. W. *J. Biol. Chem.* **2007**, *282*, 564–572.

(247) Wang, B.; Li, C.; Dubey, K. D.; Shaik, S. *J. Am. Chem. Soc.* **2015**, *137*, 7379–90.

(248) Yeom, H.; Sligar, S. G. *Arch. Biochem. Biophys.* **1997**, *337*, 209–216.

(249) Vitaku, E.; Smith, D. T.; Njardarson, J. T. *J. Med. Chem.* **2014**, *57*, 10257–10274.

(250) Ilardi, E. A.; Vitaku, E.; Njardarson, J. T. *J. Med. Chem.* **2014**, *57*, 2832–2842.

(251) Taylor, R. D.; MacCoss, M.; Lawson, A. D. G. *J. Med. Chem.* **2014**, *57*, 5845–5859.

(252) Davico, G. E.; Bierbaum, V. M.; DePuy, C. H.; Ellison, G. B.; Squires, R. R. *J. Am. Chem. Soc.* **1995**, *117*, 2590–9.

(253) Guroff, G.; Daly, J. W.; Jerina, D. M.; Renson, J.; Witkop, B.; Udenfriend, S. *Science* **1967**, *157*, 1524–30.

(254) Lovern, M. R.; Turner, M. J.; Meyer, M.; Kedderis, G. L.; Bechtold, W. E.; Schlosser, P. M. *Carcinogenesis* **1997**, *18*, 1695–1700.

(255) Tomaszewski, J. E.; Jerina, D. M.; Daly, J. W. *Biochemistry* **1975**, *14*, 2024–31.

(256) Preston, B. D.; Miller, J. A.; Miller, E. C. *J. Biol. Chem.* **1983**, *258*, 8304–11.

(257) Ohe, T.; Mashino, T.; Hirobe, M. *Arch. Biochem. Biophys.* **1994**, *310*, 402–9.

(258) Ohe, T.; Mashino, T.; Hirobe, M. *Drug Metab. Dispos.* **1997**, *25*, 116–22.

(259) Koenigs, L. L.; Trager, W. F. *Biochemistry* **1998**, *37*, 13184–13193.

(260) Koenigs, L. L.; Trager, W. F. *Biochemistry* **1998**, *37*, 10047–10061.

(261) Khojasteh-Bakht, S. C.; Chen, W.; Koenigs, L. L.; Peter, R. M.; Nelson, S. D. *Drug Metab. Dispos.* **1999**, *27*, 574–580.

(262) Gates, L. A.; Lu, D.; Peterson, L. A. *Drug Metab. Dispos.* **2012**, *40*, 596–601.

(263) Lopez-Garcia, M. P.; Dansette, P. M.; Mansuy, D. *Biochemistry* **1994**, *33*, 166–75.

(264) Dansette, P. M.; Bertho, G.; Mansuy, D. *Biochem. Biophys. Res. Commun.* **2005**, *338*, 450–455.

(265) Rademacher, P. M.; Woods, C. M.; Huang, Q.; Szklarz, G. D.; Nelson, S. D. *Chem. Res. Toxicol.* **2012**, *25*, 895–903.

(266) Mansuy, D.; Dansette, P. M.; Foures, C.; Jaouen, M.; Moinet, G.; Bayer, N. *Biochem. Pharmacol.* **1984**, *33*, 1429–35.

(267) Neau, E.; Dansette, P. M.; Andronik, V.; Mansuy, D. *Biochem. Pharmacol.* **1990**, *39*, 1101–7.

(268) Mansuy, D.; Dansette, P. M. *Adv. Exp. Med. Biol.* **1996**, *387*, 1–6.

(269) Jefcoate, C. R. *Methods Enzymol.* **1978**, *52*, 258–79.

(270) Sadek, B. *Pharma Chemica* **2011**, *3*, 410–419.

(271) Rock, D.; Wienkers, L. C. *Drug Metabolism Handbook*; John Wiley & Sons, Inc., 2009; pp 479–534.

(272) Hollenberg, P. F. *Drug Metabolism Handbook*; John Wiley & Sons, Inc., 2009; pp 343–358.

(273) Grau, M. M.; van der Toorn, J. C.; Otten, L. G.; Macheroux, P.; Taglieber, A.; Zilly, F. E.; Arends, I. W. C. E.; Hollmann, F. *ASC* **2009**, *351*, 3279–3286.

(274) Mueller, N. J.; Stueckler, C.; Hauer, B.; Baudendistel, N.; Housden, H.; Bruce, N. C.; Faber, K. *ASC* **2010**, *352*, 387–394.

(275) Zheng, D.; Zhou, X.; Cui, B.; Han, W.; Wan, N.; Chen, Y. *ChemCatChem* **2017**, *9*, 937–940.

(276) Shaffer, C. L.; Harriman, S.; Koen, Y. M.; Hanzlik, R. P. *J. Am. Chem. Soc.* **2002**, *124*, 8268–74.

(277) Cerny, M. A.; Hanzlik, R. P. *Arch. Biochem. Biophys.* **2005**, *436*, 265–275.

(278) Cerny, M. A.; Hanzlik, R. P. *J. Am. Chem. Soc.* **2006**, *128*, 3346–54.

(279) Shoji, O.; Wiese, C.; Fujishiro, T.; Shirataki, C.; Wunsch, B.; Watanabe, Y. *J. Biol. Inorg. Chem.* **2010**, *15*, 1109–15.

(280) Combourieu, B.; Poupin, P.; Besse, P.; Sancelme, M.; Veschambre, H.; Truffaut, N.; Delort, A.-M. *Biodegradation* **1998**, *9*, 433–442.

(281) Cretton, E. M.; Sommadossi, J. P. *Drug Metab. Dispos.* **1993**, *21*, 946–50.

(282) Eagling, V. A.; Howe, J. L.; Barry, M. J.; Back, D. J. *Biochem. Pharmacol.* **1994**, *48*, 267–76.

(283) Pan-Zhou, X.-R.; Cretton-Scott, E.; Zhou, X.-J.; Yang, M.-X.; Lasker, J. M.; Sommadossi, J.-P. *Biochem. Pharmacol.* **1998**, *55*, 757–766.

(284) Coleman, T.; Chao, R. R.; Stok, J. E.; Bruning, J. B.; De Voss, J. J.; Bell, S. G. Title: *Investigating the role of the acid-alcohol pair of CYP199A4 during oxidative demethylation, alkene epoxidation, hydroxylation and desaturation reactions.* Under Preparation.

(285) Coleman, T.; Zhang, T.; Bruning, J. B.; Zhou, W.; De Voss, J. J.; Bell, S. G. Title: *Examining the regioselectivity of oxidation and the hydroxylation/desaturation partition of alkyl substituted benzoic acids with CYP199A4.* Under Preparation.

Publications

This thesis is based on the following publications (currently published and under preparation as of 14th June, 2018) that detail some of the research undertaken during the period of candidature.

(177) **Coleman, T.**, Chao, R.R., Bruning, J.B., De Voss, J.J. and Bell, S.G. *CYP199A4 catalyses the efficient demethylation and demethenylation of para-substituted benzoic acid derivatives.* RSC Adv. **2015**, 5, 52007-18.

(130) **Coleman, T.**, Wong, S.H., Podgorski, M.N., Bruning, J.B., De Voss, J.J. and Bell, S.G. *Cytochrome P450 CYP199A4 from Rhodopseudomonas palustris Catalyzes Heteroatom Dealkylations, Sulfoxidation, and Amide and Cyclic Hemiacetal Formation.* ACS Catal. **2018**, 8, 5915-5927.

(284) **Coleman, T.**, Chao, R.R., Stok, J.E., Bruning, J.B., De Voss, J.J. and Bell, S.G. Title: *Investigating the role of the acid-alcohol pair of CYP199A4 during oxidative demethylation, alkene epoxidation, hydroxylation and desaturation reactions.* Under preparation.

(285) **Coleman, T.**, Zhang, T., Bruning, J.B., Weihong, Z., De Voss, J.J. and Bell, S.G. Title: *Examining the regioselectivity of oxidation and the hydroxylation/desaturation partition of alkyl substituted benzoic acids with CYP199A4.* Under preparation.

Additionally, the following publication was based in significant part on work conducted during the period of candidature.

(132) **Coleman, T.**, Chao, R.R., De Voss, J.J. and Bell, S.G. *The importance of the benzoic acid carboxylate moiety for substrate recognition by CYP199A4 from Rhodopseudomonas palustris HaA2.* Biochimica et Biophysica Acta **2016**, 1864, 667-75.

Appendix A Supplementary data for Chapter 3

A.1 Spin state shifts

Spin state shifts of substituted benzoic acid substrates tested with CYP199A4. Black shows CYP199A4 in its resting state, red shows the maximum absorbance shift obtained upon addition of substrate.

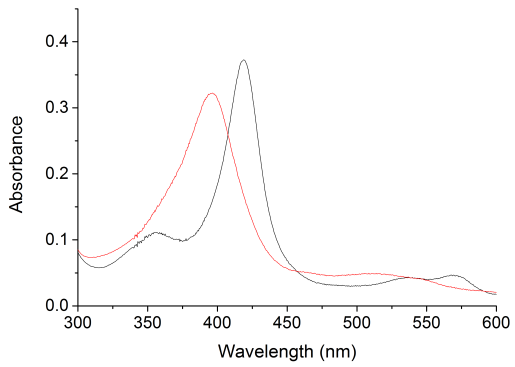

(a) 4-methoxybenzoic acid

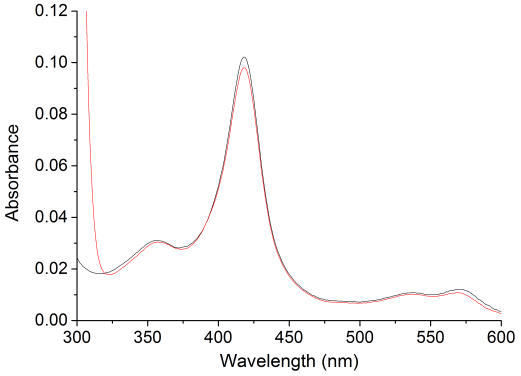

(b) 2-methoxybenzoic acid

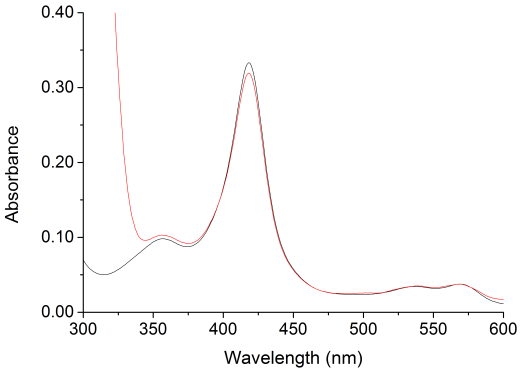

(c) 2,5-dimethoxybenzoic acid

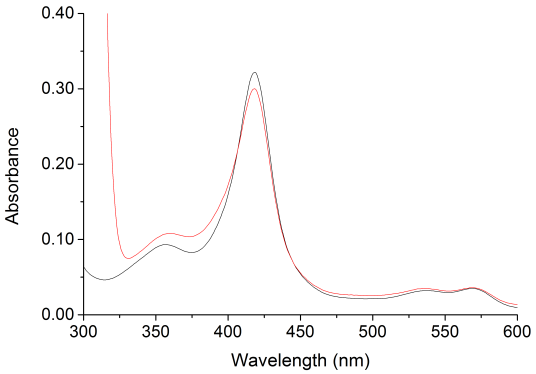

(d) 3,5-dimethoxybenzoic acid

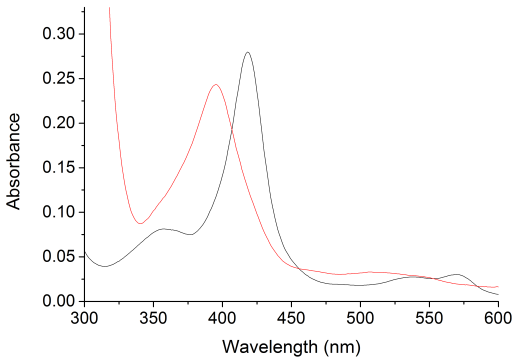

(e) 2-hydroxy-4-methoxybenzoic acid

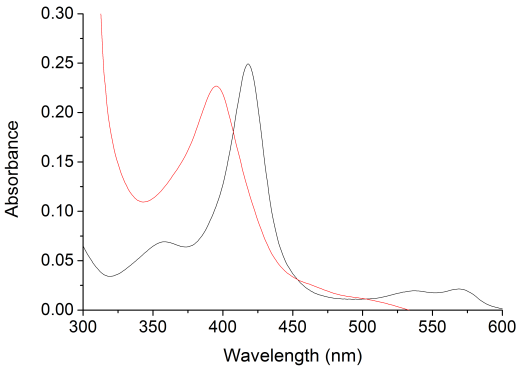

(f) 3-hydroxy-4-methoxybenzoic acid

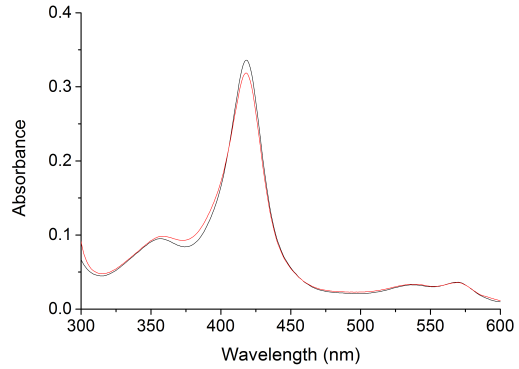

(g) 2,3,4-trimethoxybenzoic acid

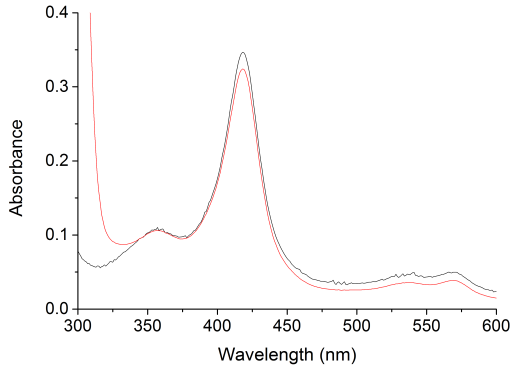

(h) 3,5-dihydroxy-4-methoxybenzoic acid

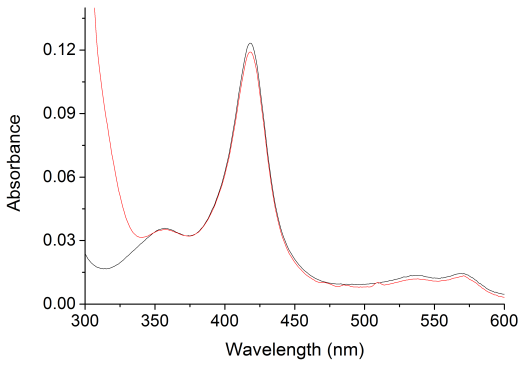

(i) 3,5-dimethoxy-4-hydroxybenzoic acid

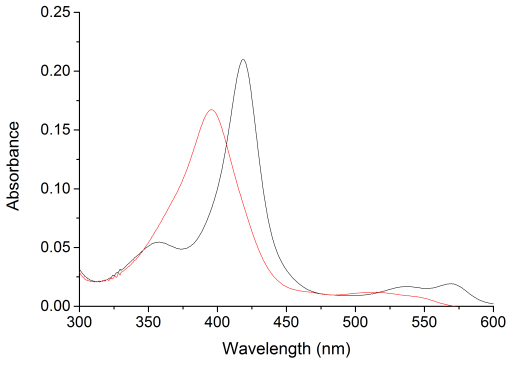

(j) 6-methoxynicotinic acid[28]

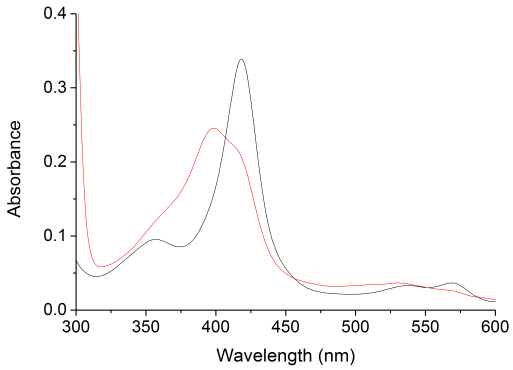

(k) 3,4-(ethylenedioxy)benzoic acid

A.2 Dissociation constant analysis

Analysis of dissociation constants for CYP199A4-bound substrates. Shown in brackets are the wavelengths of the trough and peak, and the enzyme concentration used for dissociation constant analysis (trough, peak, [P450]).

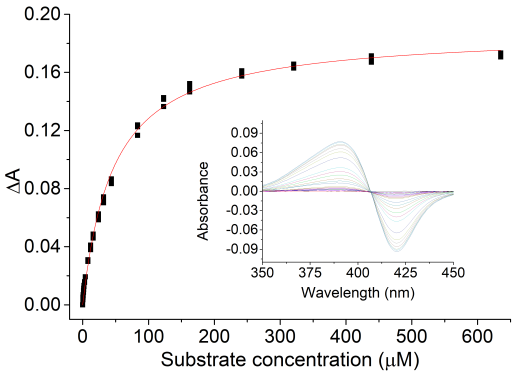

(a) 2,4-dimethoxybenzoic acid (421 nm, 391 nm, 1.5 μM)

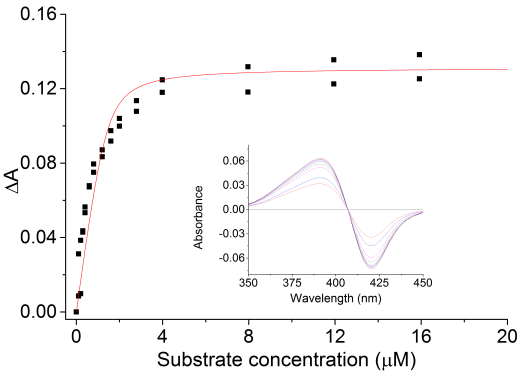

(b) 2-hydroxy-4-methoxybenzoic acid (421 nm, 391 nm, 1.5 μM)

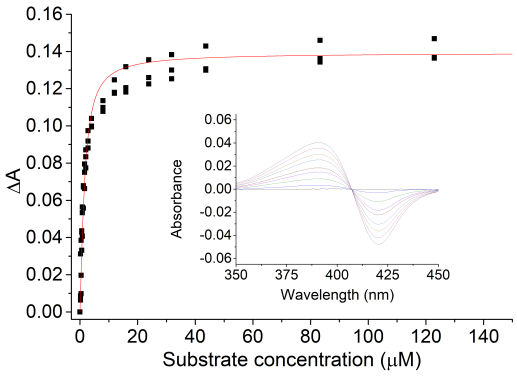

(c) 3-hydroxy-4-methoxybenzoic acid (420 nm, 391 nm, 1.5 μM)

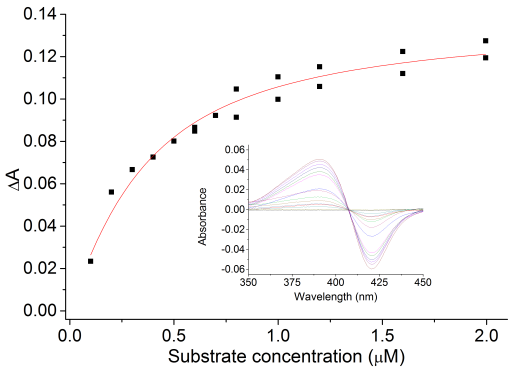

(d) 6-methoxynicotinic acid[28] (421 nm, 391 nm, 1.2 μM)

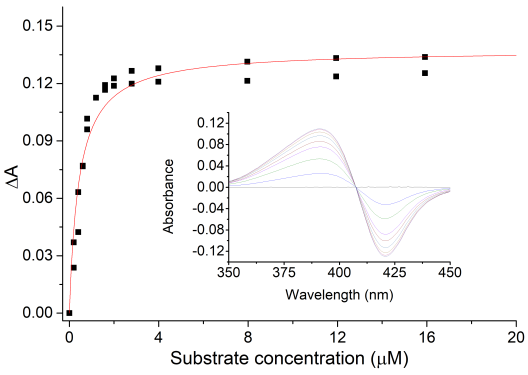

(e) 4-trifluoromethoxybenzoic acid (421 nm, 391 nm, 1.5 μM)

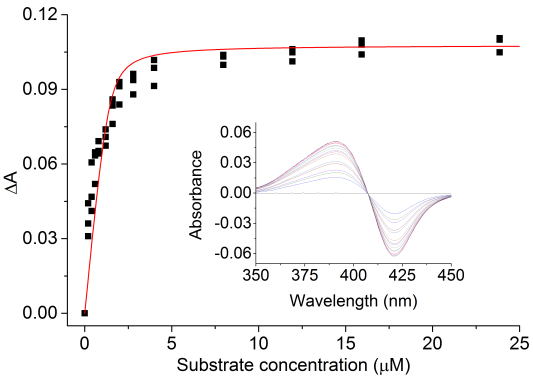

(f) 3,4-(methylenedioxy)benzoic acid (421 nm, 391 nm, 1.3 μM)

A.3 HPLC analysis

All gradients are H_2O:ACN, monitored at 254 nm.

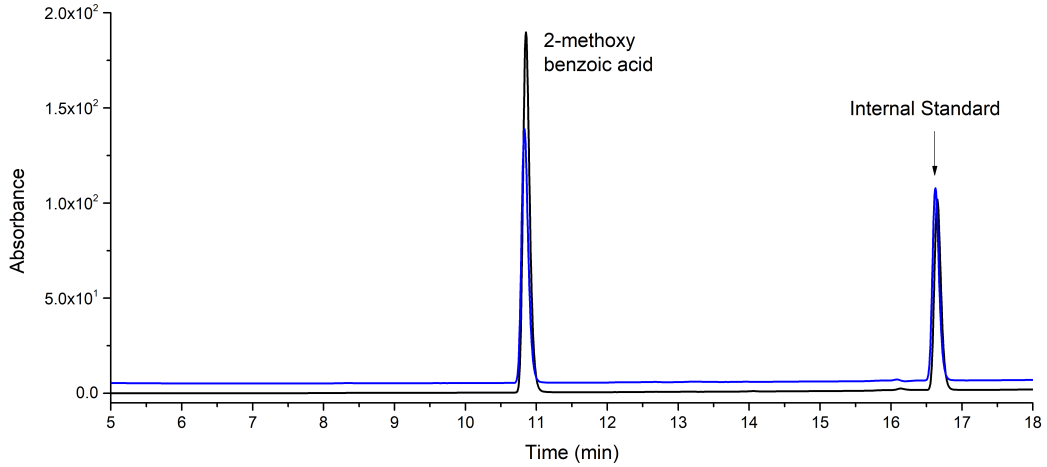

(a) 2-methoxybenzoic acid. **Black**, *in vitro* turnover; blue, substrate control, RT = 10.9 min. Gradient, 20-95 %.

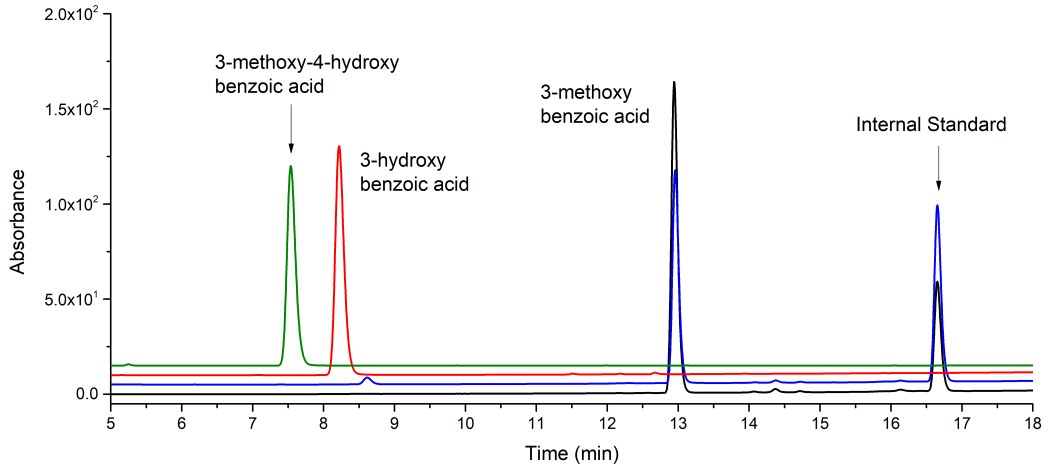

(b) 3-methoxybenzoic acid. **Black**, *in vitro* turnover; blue, substrate control, RT = 13.0 min; red, 3-hydroxybenzoic acid control, RT = 8.3 min; green, 3-methoxy-4-hydroxybenzoic acid, RT = 7.6 min. Gradient, 20-95 %.

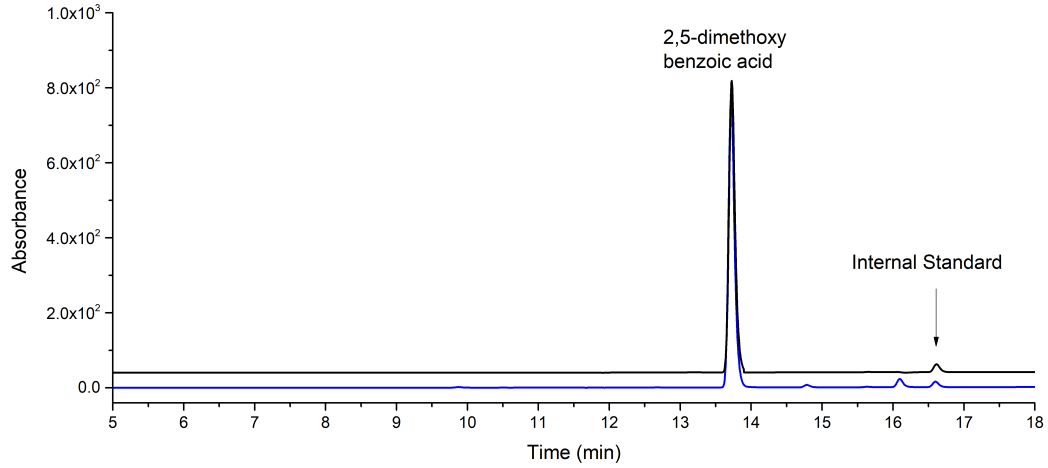

(c) 2,5-dimethoxybenzoic acid. **Black**, *in vitro* turnover; blue, substrate control, RT = 13.7 min. Gradient, 20-95 %.

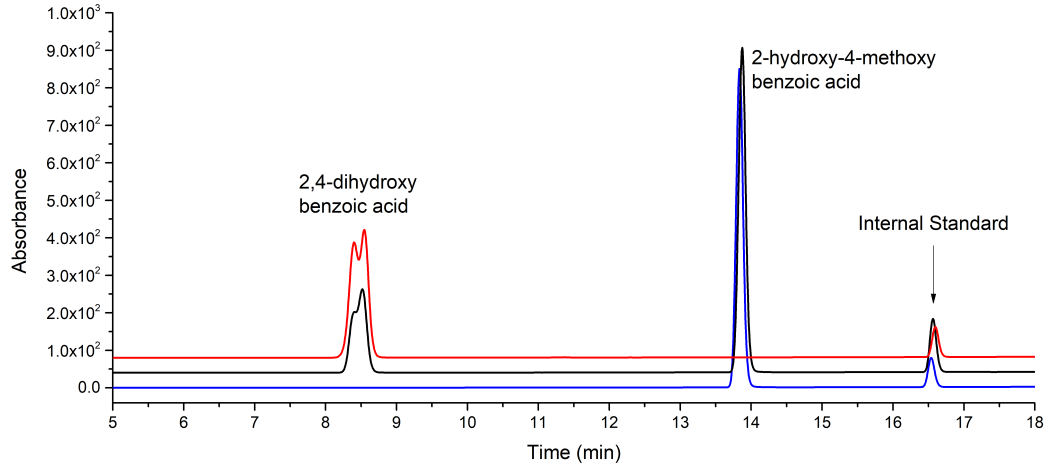

(d) 2-hydroxy-4-methoxybenzoic acid. **Black**, *in vitro* turnover; blue, substrate control, RT = 13.9 min; red, 2,4-dihydroxybenzoic acid control, RT = 8.5 min. Gradient, 20-95 %.

No product peaks were observed in the GC-MS chromatograms of the trimethoxybenzoic acids presented below.

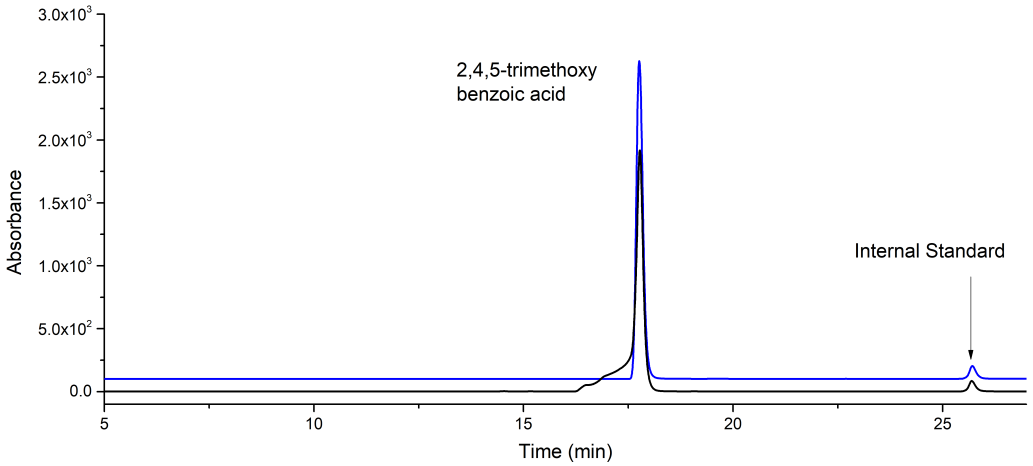

(e) 2,4,5-trimethoxybenzoic acid. **Black**, *in vitro* turnover; blue, substrate control, RT = 17.8 min. Gradient, 0-50 %.

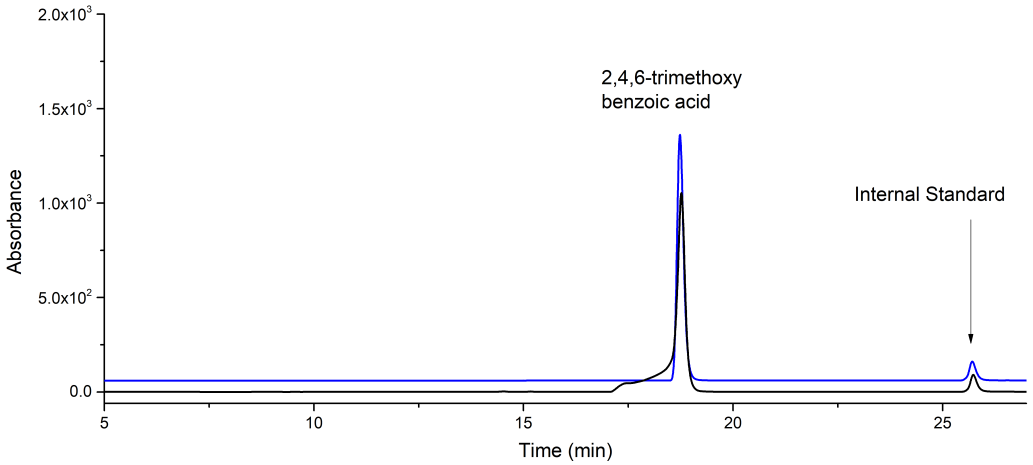

(f) 2,4,6-trimethoxybenzoic acid. **Black**, *in vitro* turnover; blue, substrate control, RT = 18.7 min. Gradient, 0-50 %.

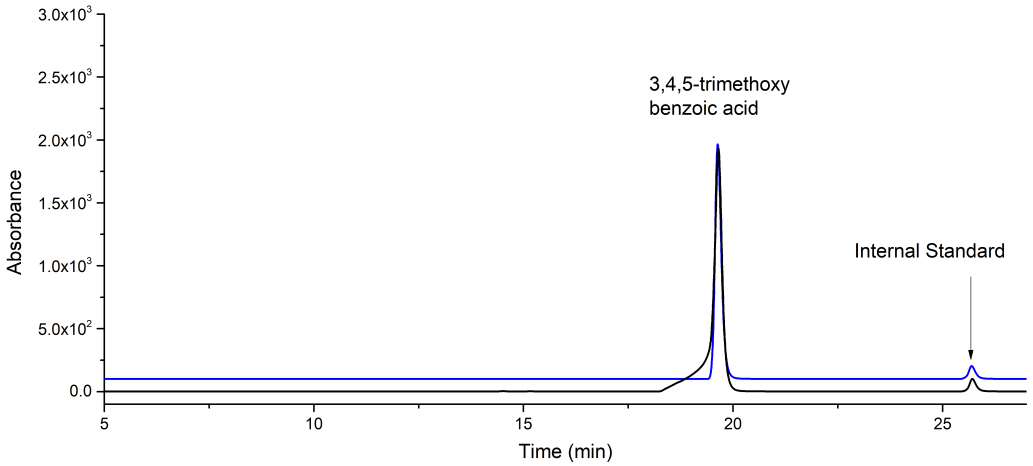

(g) 3,4,5-trimethoxybenzoic acid. **Black**, *in vitro* turnover; blue, substrate control, RT = 19.7 min. Gradient, 0-50 %.

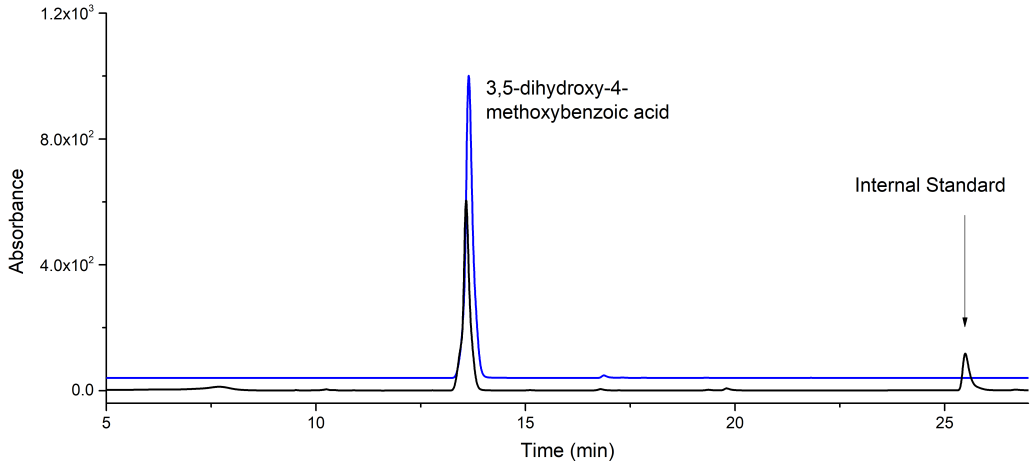

(h) 3,5-dihydroxy-4-methoxybenzoic acid. **Black**, *in vitro* turnover; blue, substrate control, RT = 13.6 min. Gradient, 0-50 %.

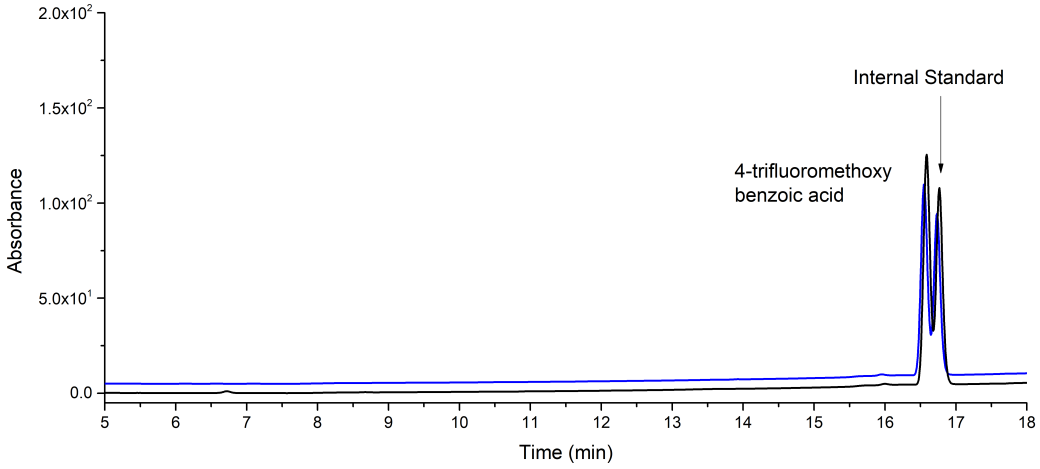

(i) 4-trifluoromethoxybenzoic acid. **Black**, *in vitro* turnover; blue, substrate control, RT = 16.6 min. Gradient, 20-95 %. There were no products observed in the GC analysis.

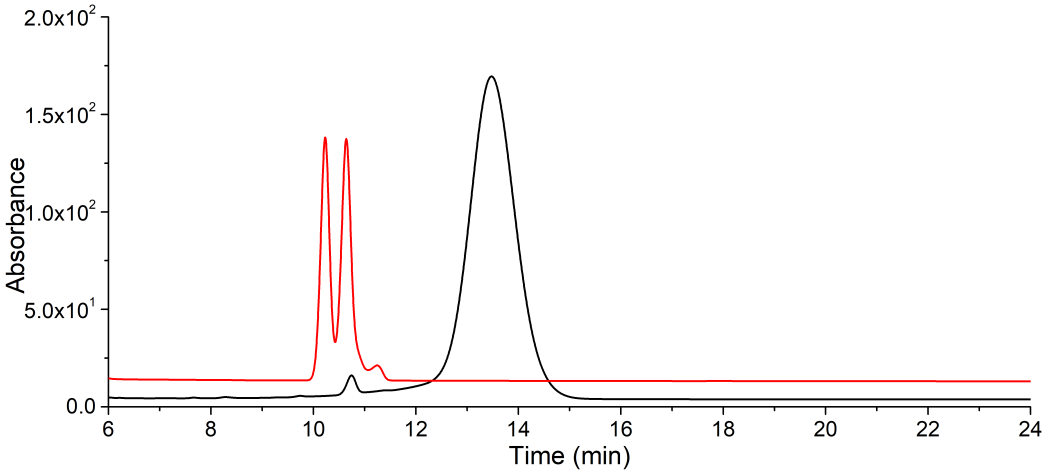

(j) Chiral HPLC of 3,4-(ethylenedioxy)benzoic acid. A 20 % H_2O:ACN isocratic solvent system was used (Chapter 2.1). **Black**, purified 3,4-(2′-hydroxy-ethylenedioxy)benzoic acid product (enantiomers did not appear to separate); red, control of chiral 4-(1-hydroxyethyl)benzoic acid (enantiomers are resolved).

A.4 GC-MS analysis

GC-MS analysis of 3,5-dimethoxy-4-hydroxybenzoic acid with CYP199A4.

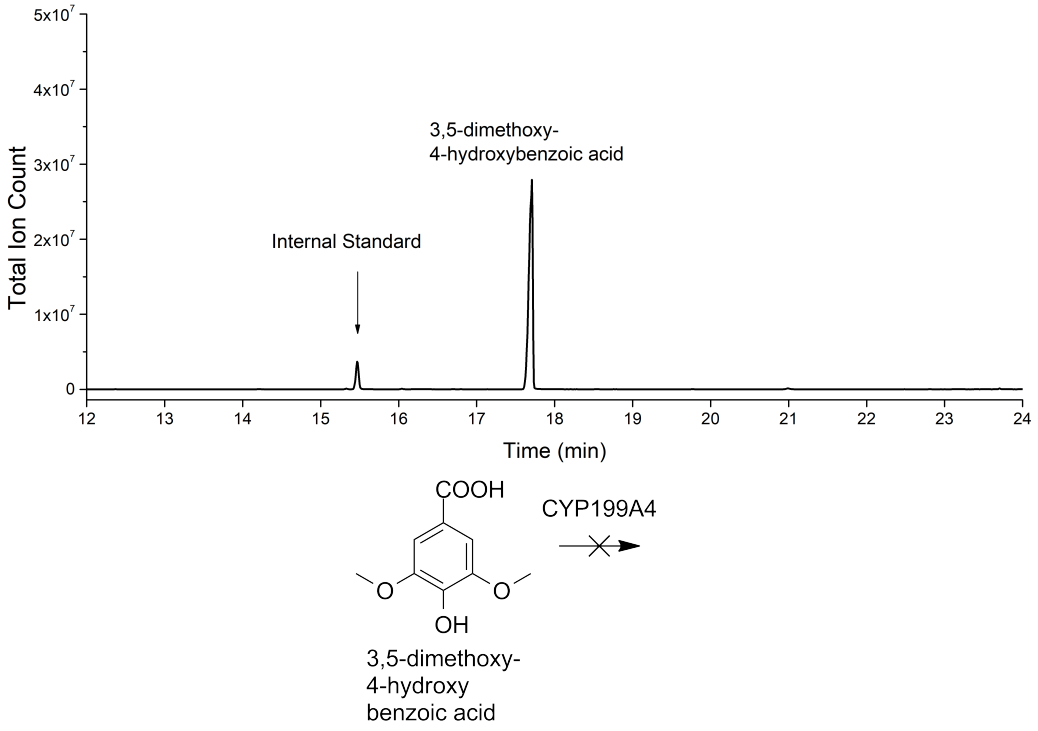

There were no products observed in the GC analysis of 2,4,5-, 2,4,6- and 3,4,5-trimethoxybenzoic acids, 4-trifluoromethoxybenzoic acid.

Mass spectra of the products of TMS-derivatised CYP199A4 turnovers.
Shown are: (a) 3,5-dimethoxybenzoic acid (product is 3-hydroxy-5-methoxybenzoic acid); (b) 2,4-dimethoxybenzoic acid (product is 2-hydroxy-4-methoxybenzoic acid). In both cases, observed m/z = 312.05 vs expected 312.12; (c) the mass spectrum of the isolated product of the turnover of 2,3,4-trimethoxybenzoic acid, 2,3-dimethoxy-4-hydroxybenzoic acid (MS m/z = 342.35 vs expected 342.13).

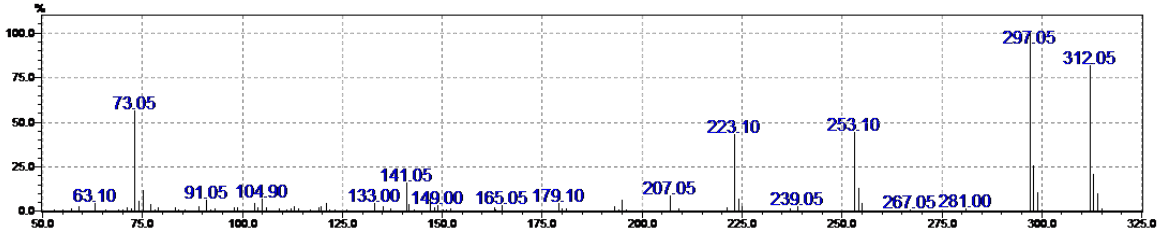

(a) 3-hydroxy-5-methoxybenzoic acid

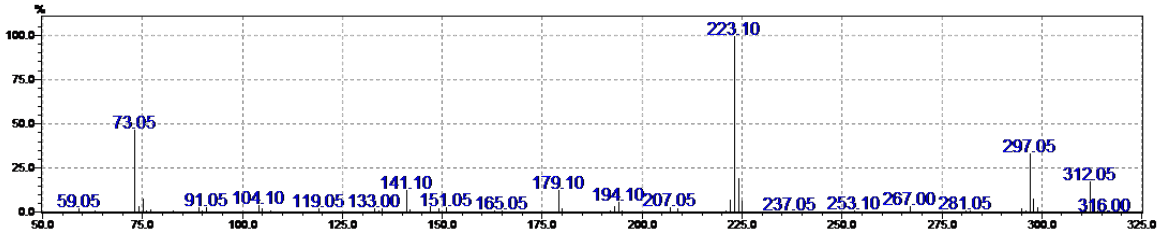

(b) 2-hydroxy-4-methoxybenzoic acid

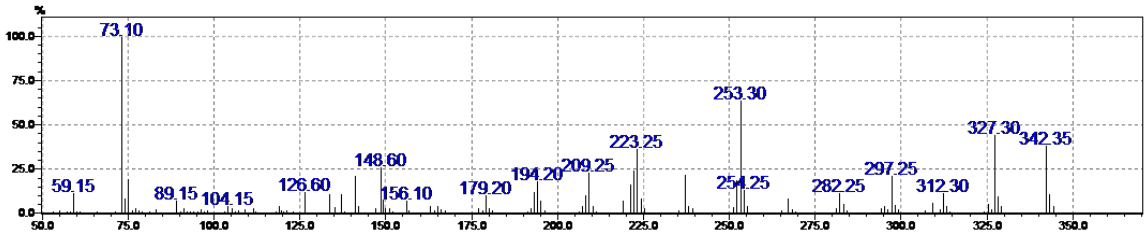

(c) 2,3-dimethoxy-4-hydroxybenzoic acid

A.5 NMR analysis

Product of 2,3,4-trimethoxybenzoic acid

2,3-dimethoxy-4-hydroxybenzoic acid: 500 MHz, d_6-DMSO.

^{1}H: δ 3.74 (s, 3H, **8/9**), 3.77 (s, 3H, **8/9**), 6.65 (d, 1H, J = 8.7 Hz, **6**), 7.36 (d, 1H, J = 8.7 Hz, **7**).

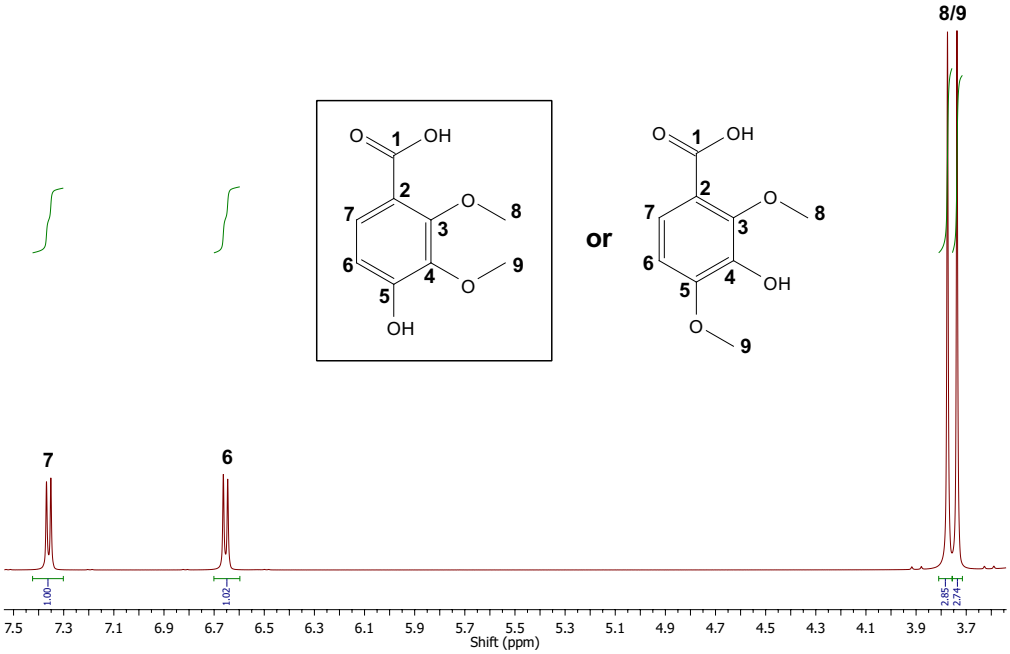

^{13}C: δ 63.40 (**8/9**), 64.42 (**8/9**), 114.69 (**6**), 119.67, 129.63 (**7**), 144.35, 157.55, 158.06, 169.55 (**1**).

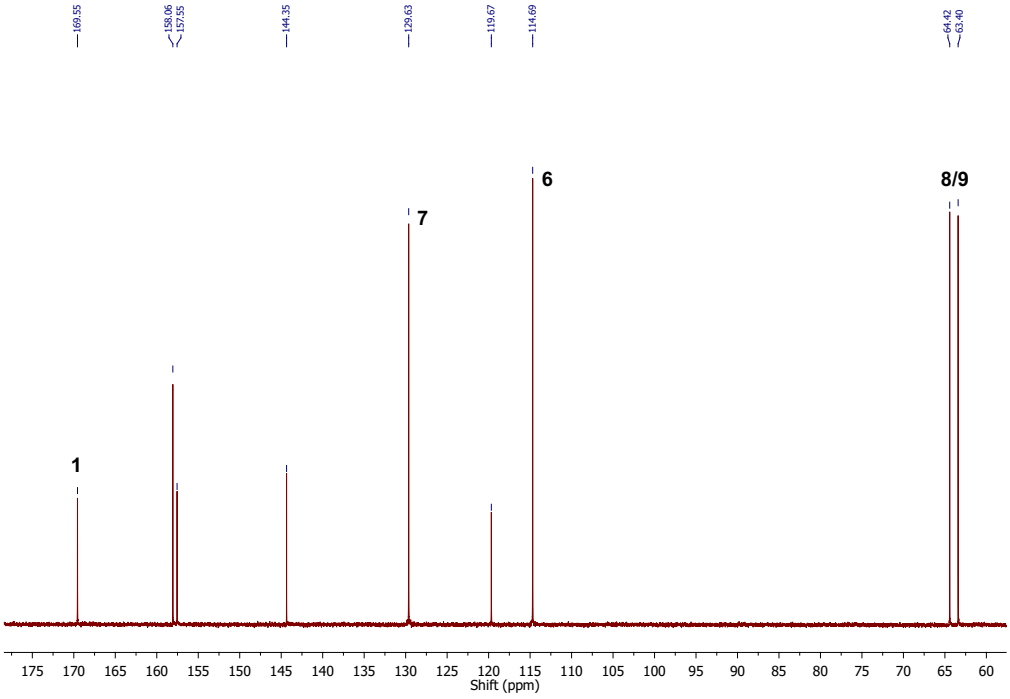

^{1}H-^{13}C HSQC:

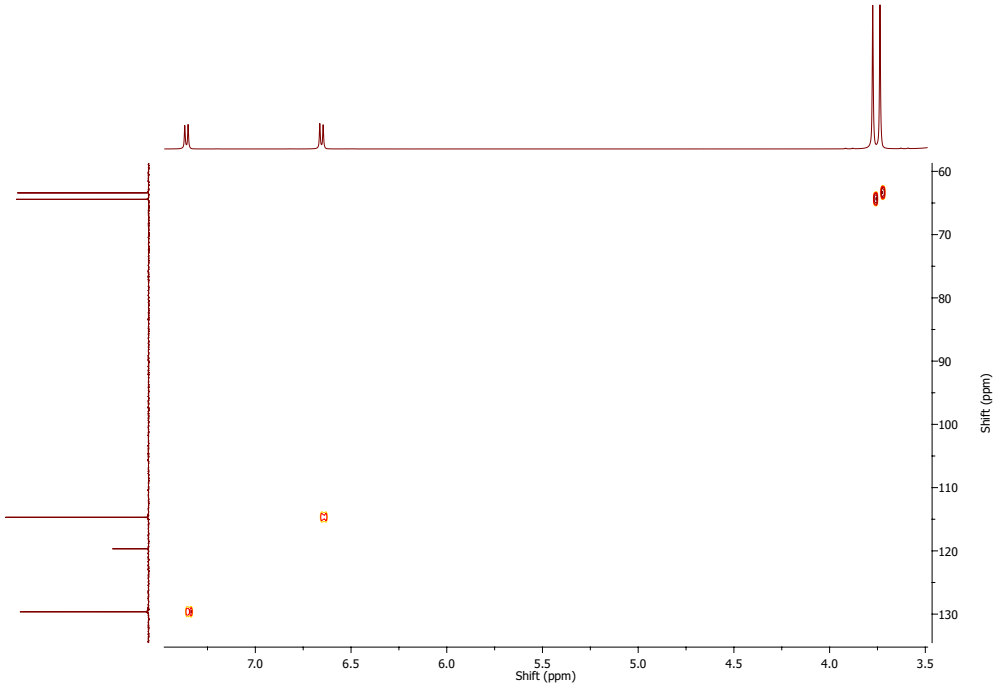

^{1}H-^{13}C HMBC:

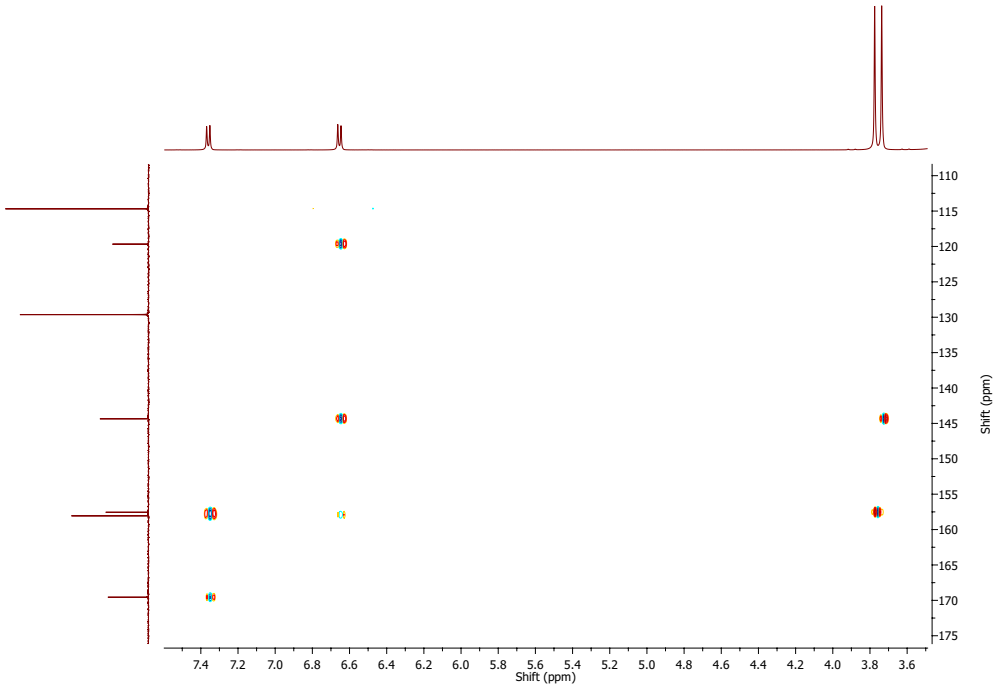

Product of 3,4-(ethylenedioxy)benzoic acid

3,4-(2′-hydroxyethylenedioxy)benzoic acid: 500 MHz, d_6-DMSO.

^{1}H: δ 3.99 (dd, 1H, J = 3.7, 11.3 Hz, **8**), 4.11 (dd, 1H, J = 1.7, 11.3 Hz, **8**), 5.54 (d, 1H, J = 1.7 Hz, **9**), 6.93 (d, 1H, J = 8.4 Hz, **6**), 7.38 (d, 1H, J = 2.0 Hz, **3**), 7.46 (dd, 1H, J = 2.0, 8.4 Hz, **7**).

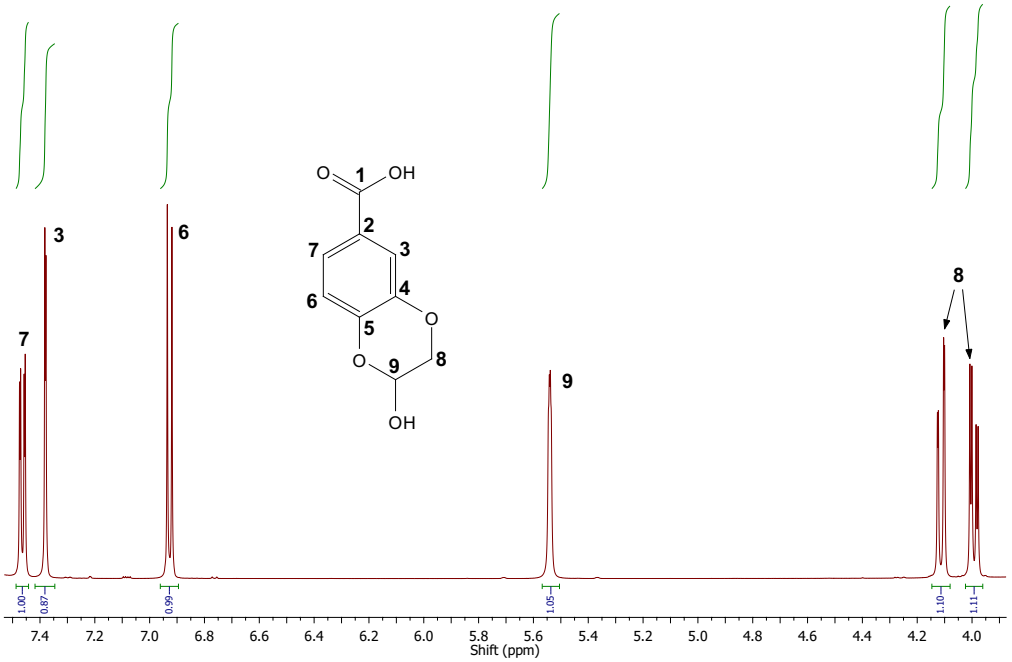

^{13}C: δ 69.88 (**8**), 92.16 (**9**), 120.35 (**3/6**), 120.69 (**3/6**), 126.41 (**7**), 126.87 (**2**), 145.53 (**4**), 148.90 (**5**), 169.86 (**1**).

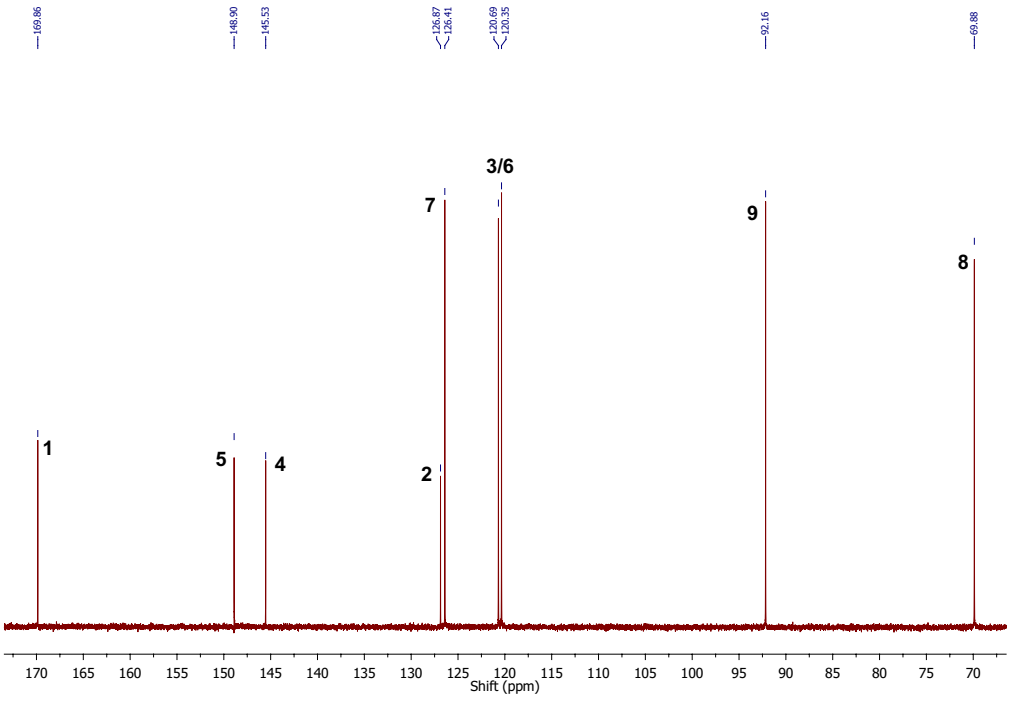

^{1}H-^{1}H COSY:

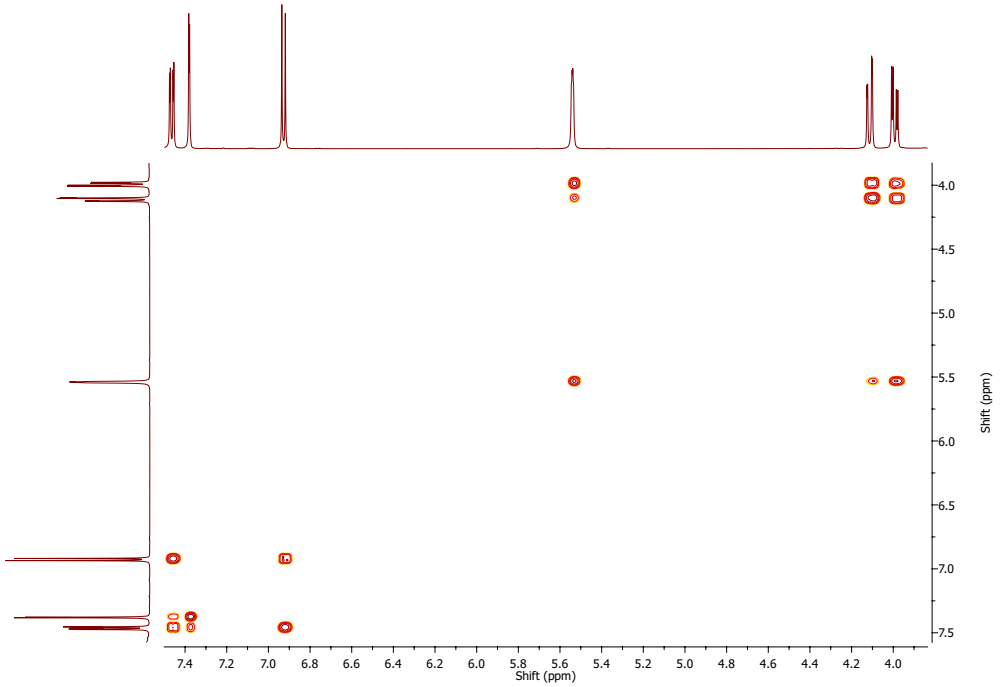

^{1}H-^{13}C HSQC:

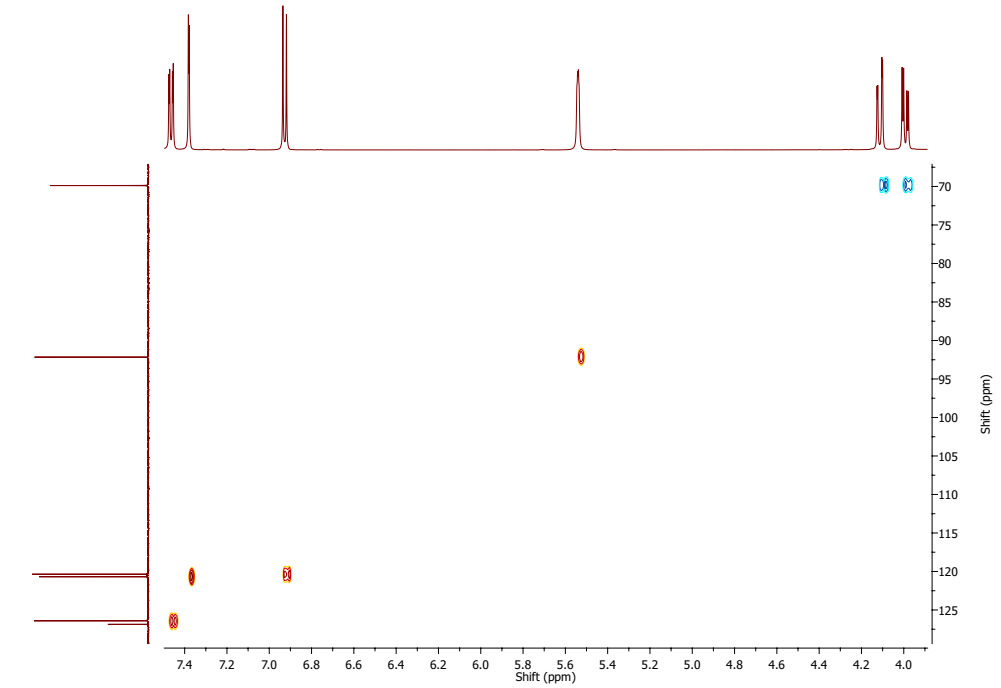

^{1}H-^{13}C HMBC:

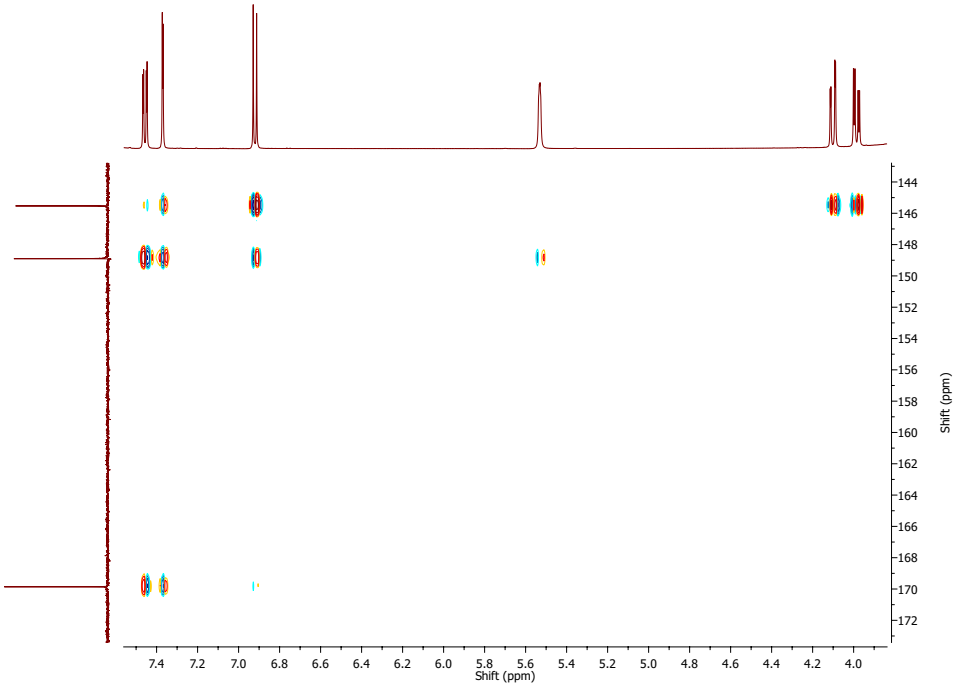
144
146
148
150
152
154
156
158
160
162
164
166
168
170
172
Shift (ppm)
7.4
7.2
7.0
6.8
6.6
6.4
6.2
6.0
5.8
5.6
5.4
5.2
5.0
4.8
4.6
4.4
4.2
4.0
Shift (ppm)

Appendix B Supplementary data for Chapter 4

B.1 Spin state shifts

Spin state shifts of benzoic acid substrates tested with CYP199A4. Black shows CYP199A4 in its resting state, red shows the maximum absorbance shift obtained upon addition of substrate.

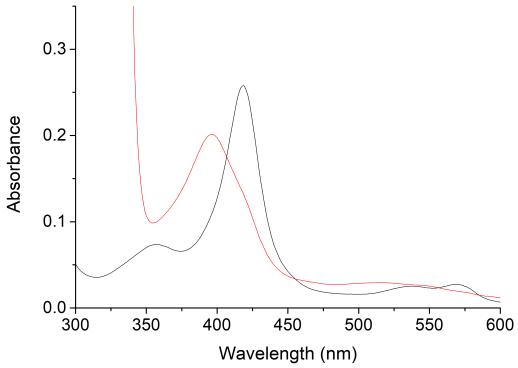

(a) 4-diethylaminobenzoic acid

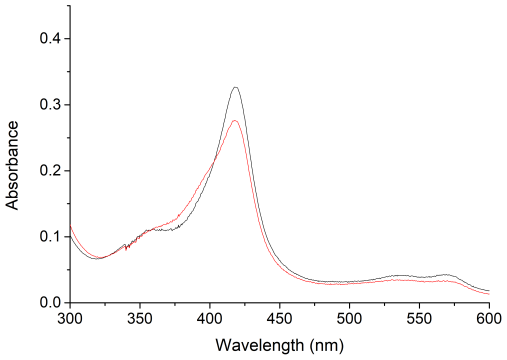

(b) 4-aminomethylbenzoic acid[28]

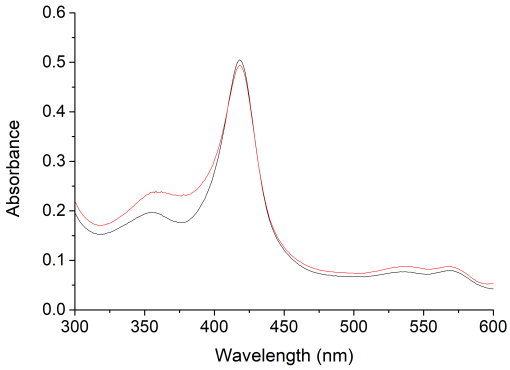

(c) 4-(ethylamino)methylbenzoic acid

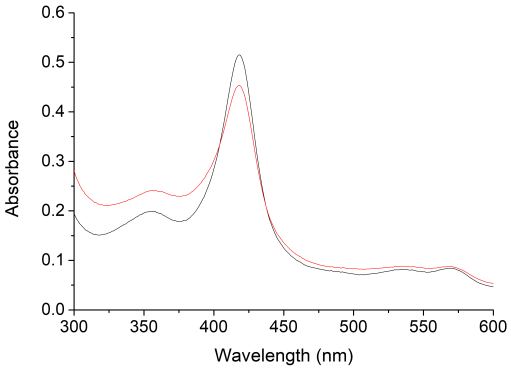

(d) 4-(dimethylamino)methylbenzoic acid

B.2 Dissociation constant analysis

Analysis of the dissociation constant for 4-aminomethylbenzoic acid.[28] Shown in brackets are the wavelengths of the trough and peak, and the enzyme concentration used for dissociation constant analysis (trough, peak, [P450]).

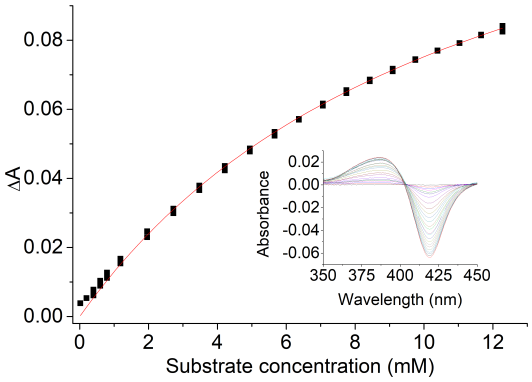

(419 nm, 387 nm, 3.4 µM)

B.3 HPLC analysis

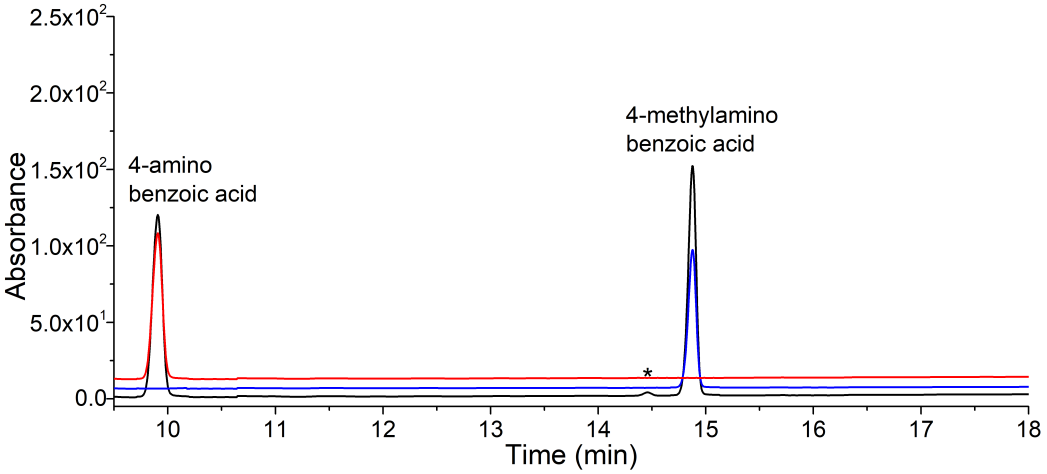

(a) 4-Methylaminobenzoic acid. **Black**, *in vitro* turnover; blue, substrate control, RT = 14.9 min; red, 4-aminobenzoic acid control, RT = 9.9 min. Labelled (*) is a peak which was present in a control turnover containing no P450. The gradient was 0-50 %, and the chromatogram at 254 nm was monitored.

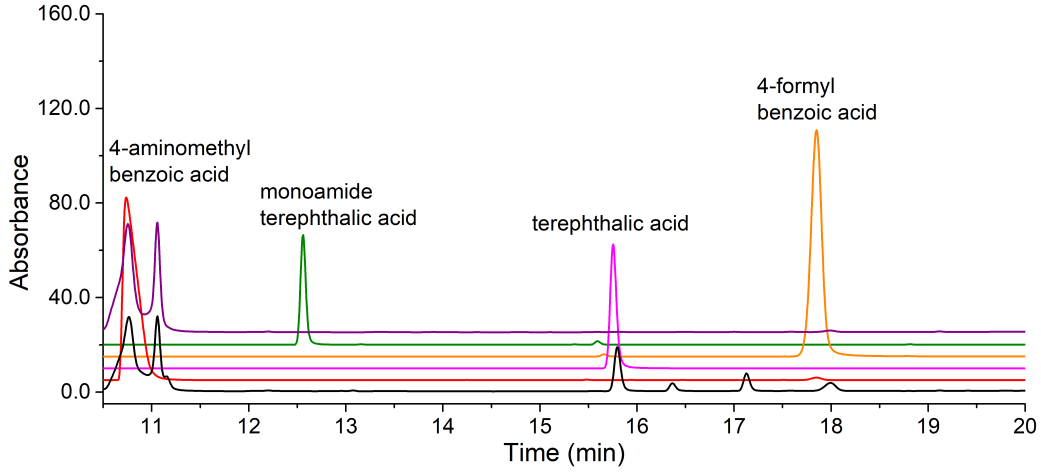

(b) HPLC analysis of 4-aminomethylbenzoic acid turnover with CYP199A4. **Black**, *in vitro* turnover, substrate appeared as a double peak; red, 4-aminomethylbenzoic acid control, RT = 10.8 min; pink, terephthalic acid control, RT = 15.8 min; orange, 4-formylbenzoic acid control, RT = 17.8 min; green, monoamide terephthalic acid control, RT = 12.6 min; purple, no P450 control reaction. There were additional peaks at 16.4 min and 17.2 min that could not be identified. A 0-50 % gradient of H_2O:ACN was employed, and the chromatogram was monitored at 254 nm.

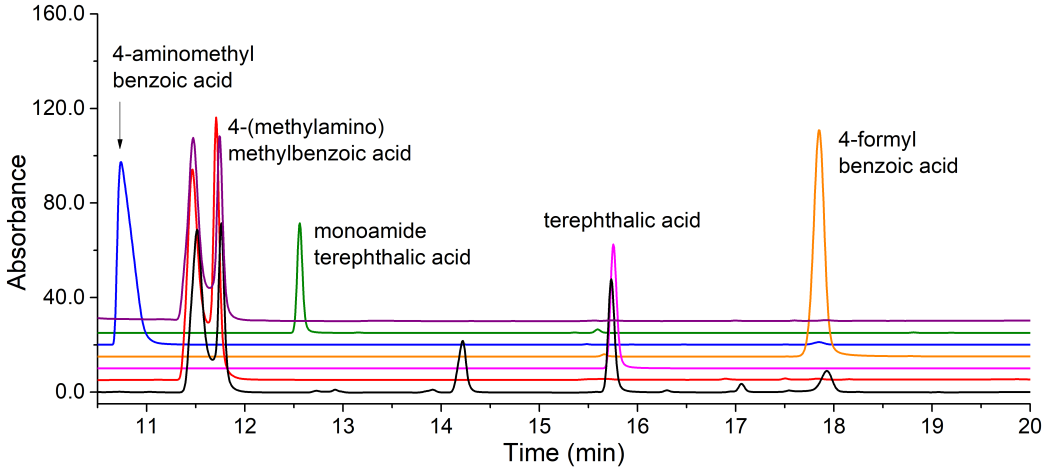

(c) HPLC analysis of 4-(methylamino)methylbenzoic acid turnover with CYP199A4. **Black**, *in vitro* turnover; red, substrate control, RT = 11.5 min and 11.8 min double peak; pink, terephthalic acid control, RT = 15.8 min; orange, 4-formylbenzoic acid control, RT = 17.8 min; blue, 4-aminomethylbenzoic acid control, 10.8 min; green, monoamide terephthalic acid control, RT = 12.6 min; purple, no P450 control reaction). There was an additional peak at 14.2 min that could not be identified. The peaks at 16.4 min and 17.2 min were also observed in the turnover of 4-aminomethylbenzoic acid. The gradient was 0-50 % H_2O:ACN. The chromatogram was monitored at 254 nm.

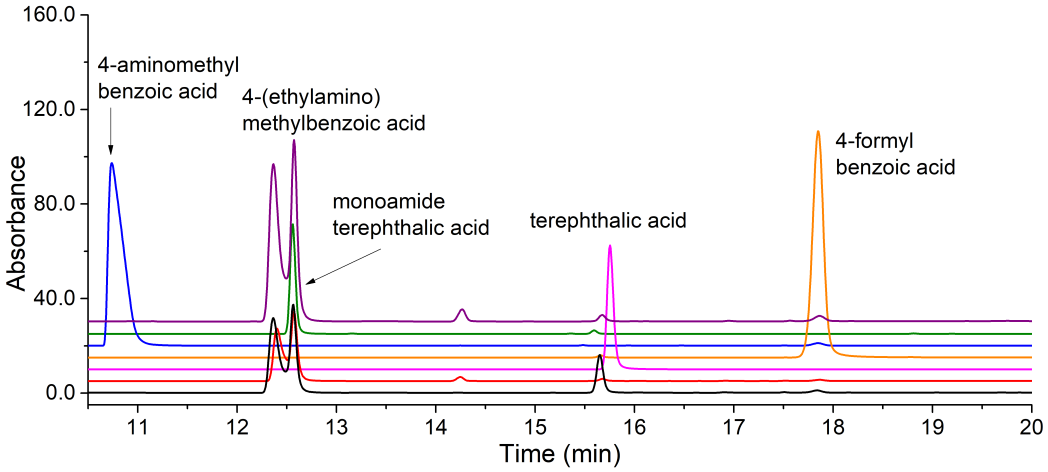

(d) HPLC analysis of 4-(ethylamino)methylbenzoic acid turnover with CYP199A4. **Black**, *in vitro* turnover; red, substrate control, RT = 12.4 min and 12.6 min double peak; pink, terephthalic acid control, RT = 15.8 min; orange, 4-formylbenzoic acid control, RT = 17.8 min; blue, 4-aminomethylbenzoic acid control, 10.8 min; green, monoamide terephthalic acid control, RT = 12.6 min; purple, no P450 control reaction. The gradient was 0-50 % H_2O:ACN, and the chromatogram was monitored at 254 nm.

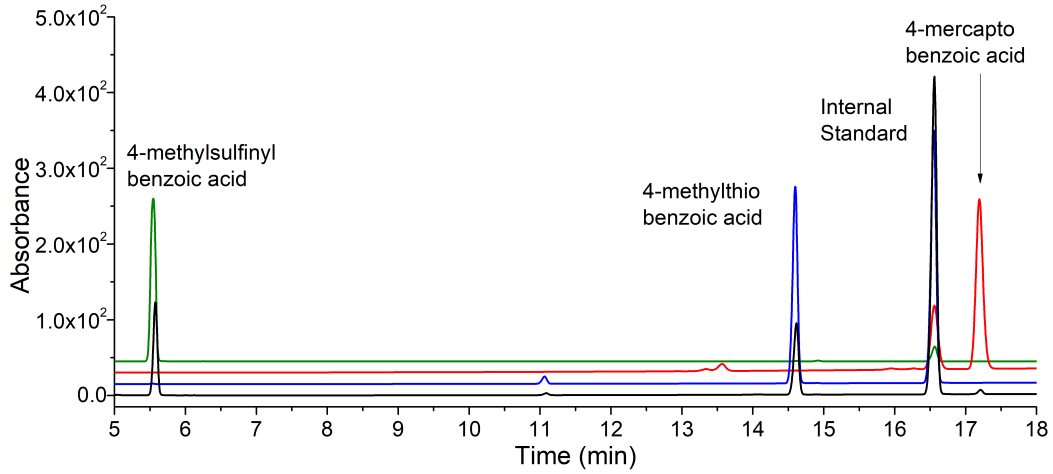

(e) 4-methylthiobenzoic acid. **Black**, *in vitro* turnover; blue, substrate control, RT = 14.6 min; red, 4-mercaptobenzoic acid control, RT = 17.2 min; green, 4-methylsulfinylbenzoic acid control, RT = 5.6 min. The 4-mercaptobenzoic acid was also present in a control turnover containing no P450. The gradient was 20-95 % H_2O:ACN, and the chromatogram was monitored at 254 nm.

Chiral HPLC analysis of 4-ethylthiobenzoic acid. The samples were derivatised to methyl esters before injection. The solvent system was 5 % isopropanol in hexane, isocratically for 60 min.

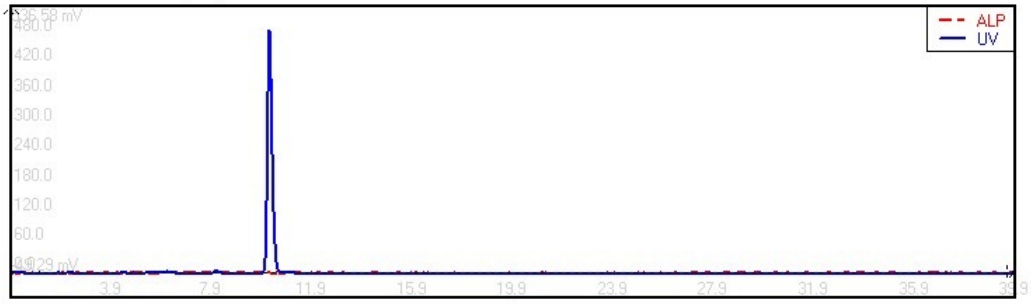

(a) 4-ethylthiobenzoic acid substrate (RT = 10.3 min)

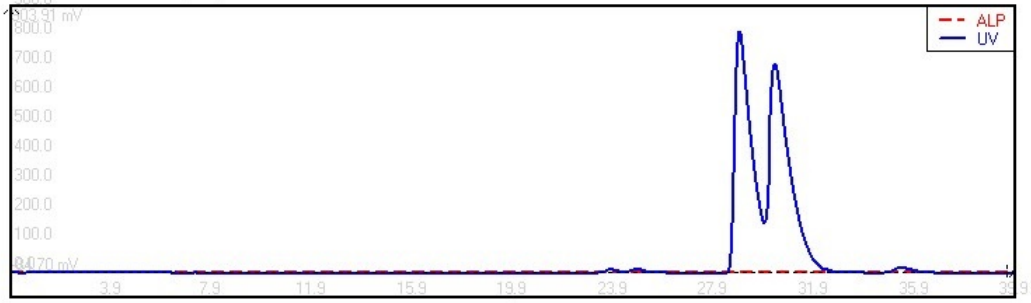

(b) racemic mixture of R and S enantiomers (RT = 29.0 and 31.5 min)

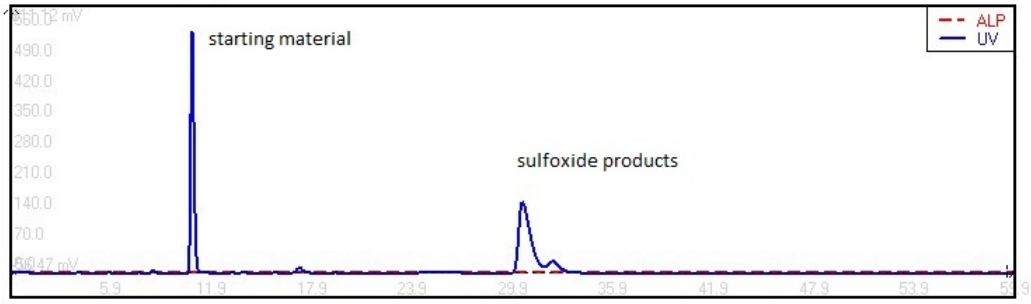

(c) CYP199A4 turnover of 4-ethylthiobenzoic acid (RT = 30.6 min and 32.3 min)

Chiral HPLC analysis of 4-ethylbenzoic acid. The samples were derivatised to methyl esters before injection. The solvent system was 5 % isopropanol in hexane, isocratically for 60 min.

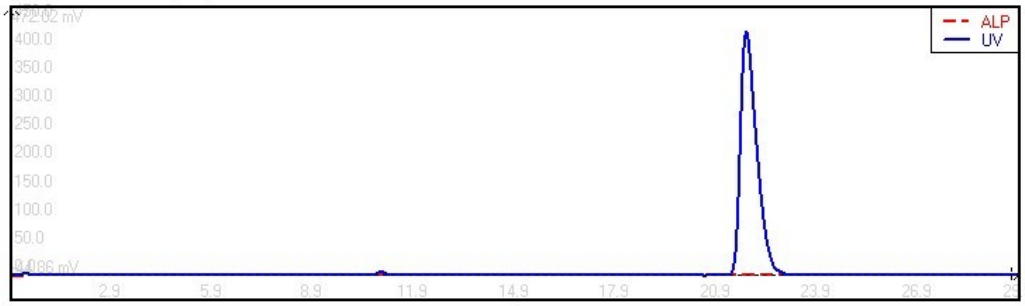

(a) 4-ethylbenzoic acid (S)-enantiomer (RT = 21.9 min)

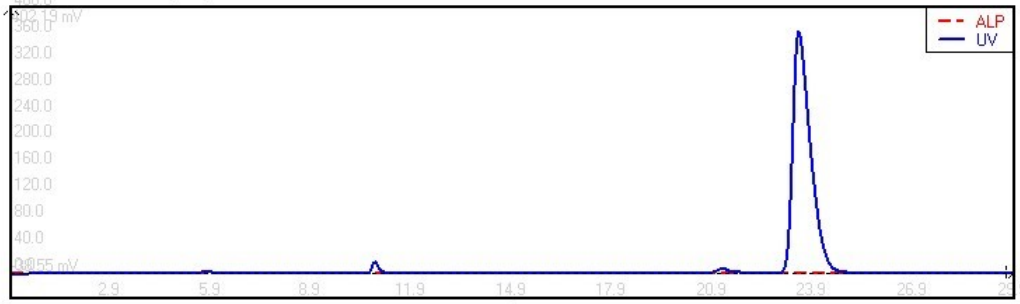

(b) 4-ethylbenzoic acid (R)-enantiomer (RT = 23.6 min)

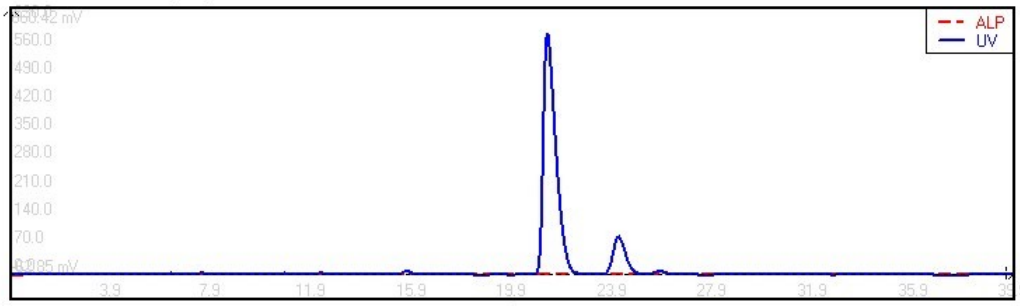

(c) CYP199A4 turnover of 4-ethylbenzoic acid (RT = 21.4 min and 24.3 min)

HPLC analysis of 4-halobenzoic acids (Chapter 4.2.5). All gradients are H_2O:ACN, monitored at 254 nm.

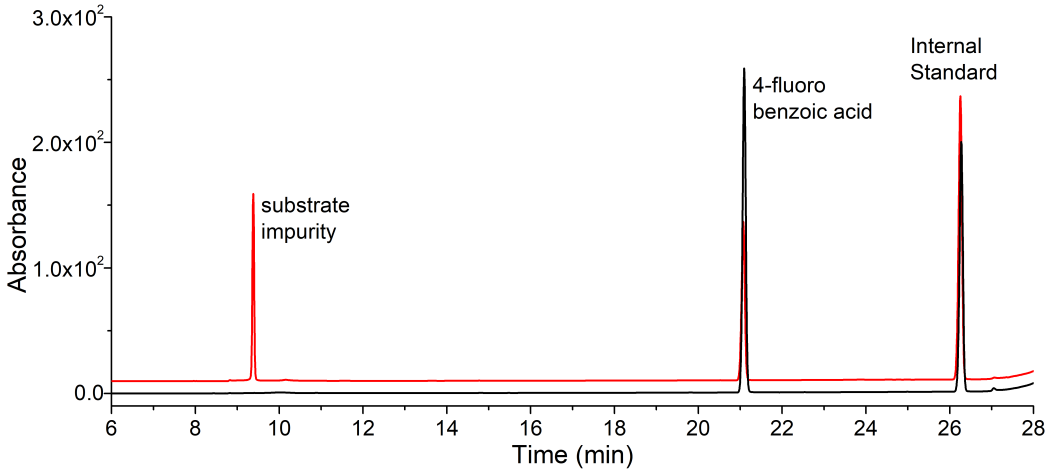

(a) 4-fluorobenzoic acid. **Black**, *in vitro* turnover; red, substrate control, RT = 21.1 min. 0-50 %.

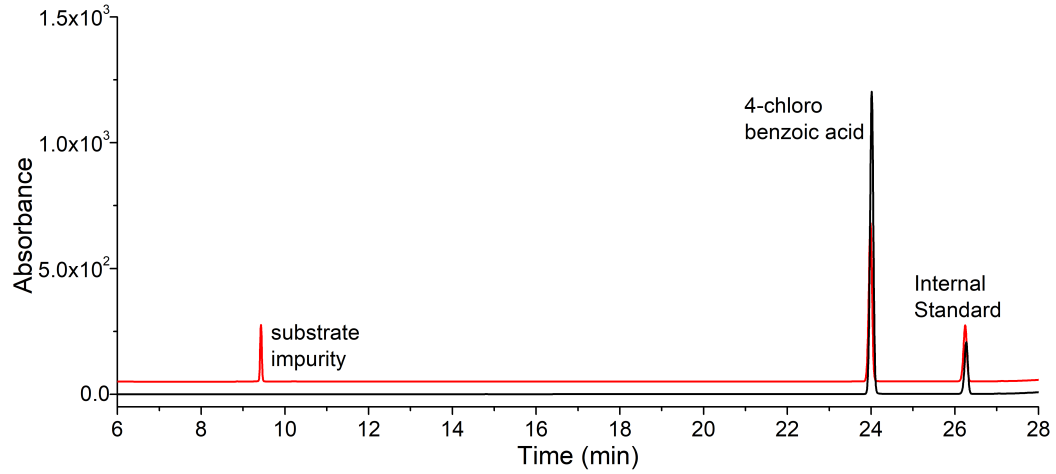

(b) 4-chlorobenzoic acid. **Black**, *in vitro* turnover; red, substrate control, RT = 24.0 min. 0-50 %.

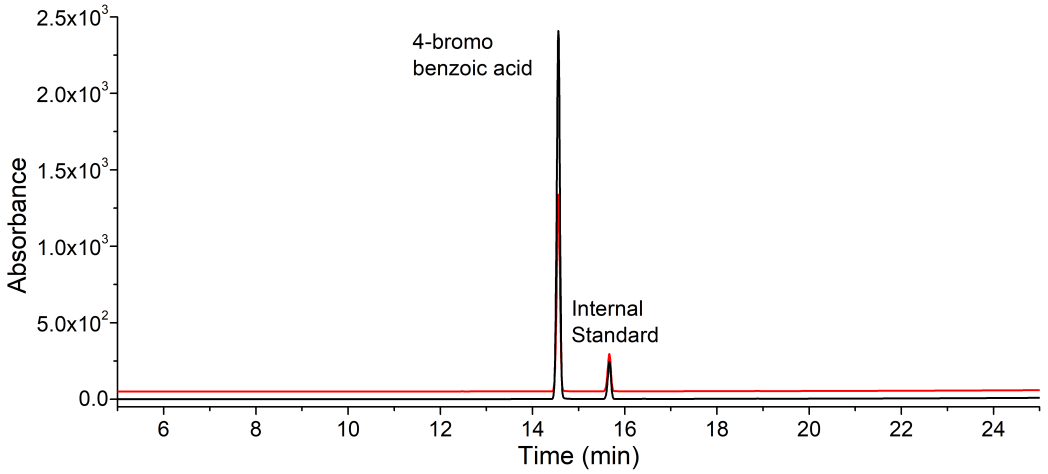

(c) 4-bromobenzoic acid. **Black**, *in vitro* turnover; red, substrate control, RT = 14.6 min. 20-95 %.

B.4 GC-MS analysis

All turnovers were TMS-derivatised before analysis using excess BSTFA/TMCS (99:1).

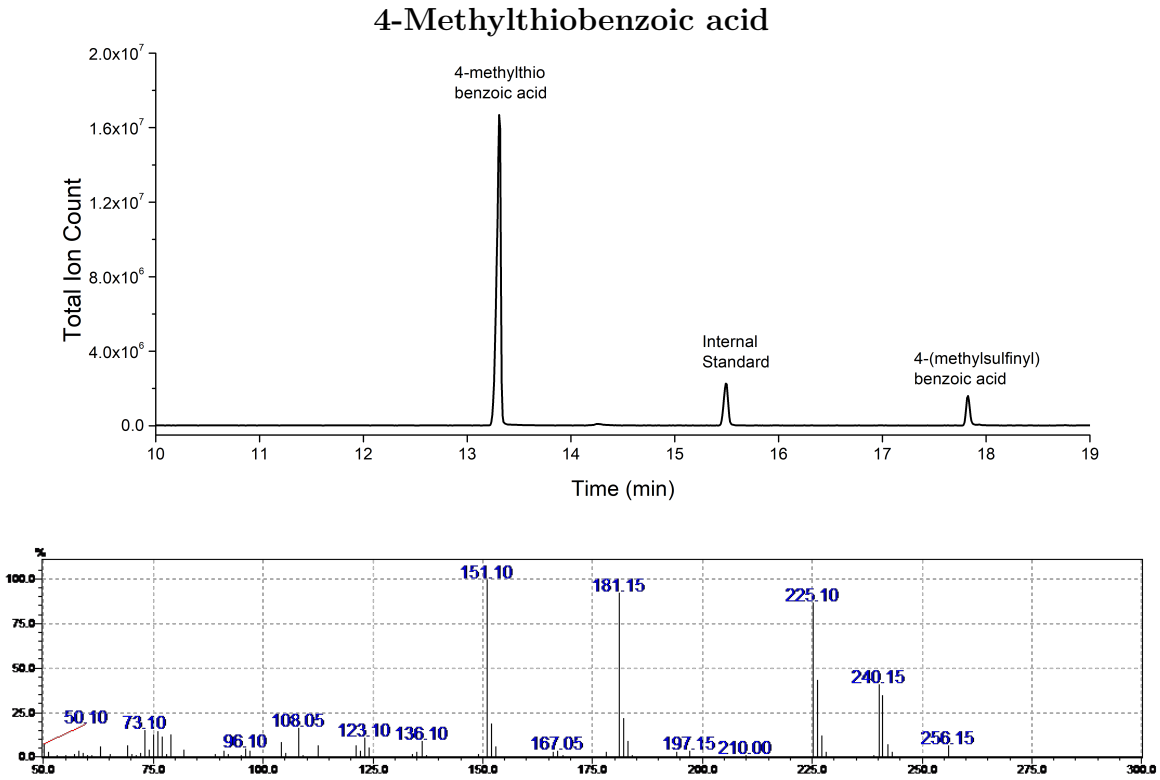

(a) 4-(methylsulfinyl)benzoic acid. RT = 17.8 min. Observed m/z = 256.15 vs expected 256.06.

Halomethyl substrates

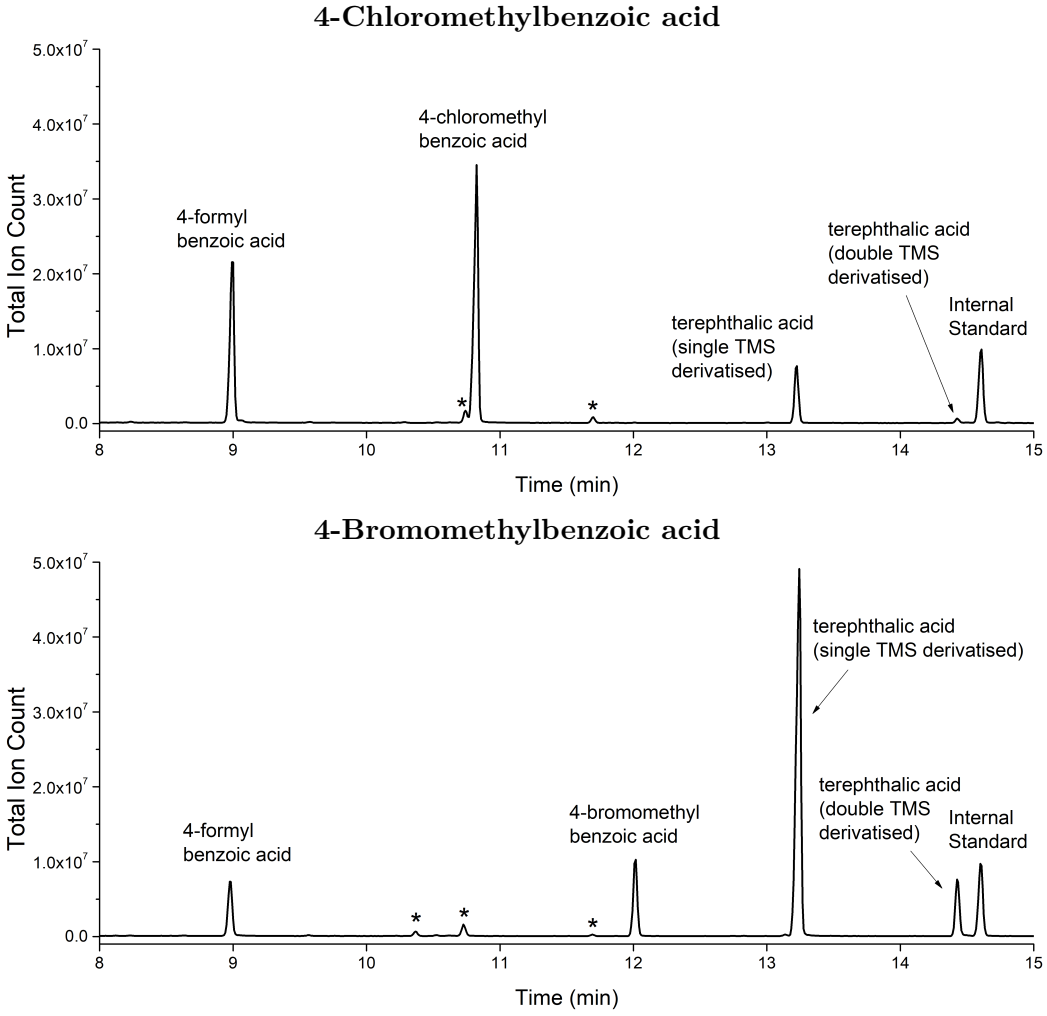

There was a significant amount of singly TMS-derivatised terephthalic acid in each turnover, indicating incomplete derivatisation of the sample. In each, several substrate impurities were present, which are denoted (*).

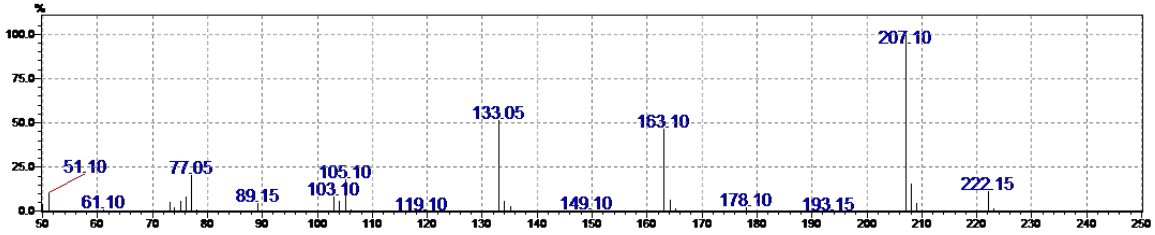

(a) 4-Formylbenzoic acid. RT = 9.0 min. Observed m/z = 222.15 vs expected 222.07.

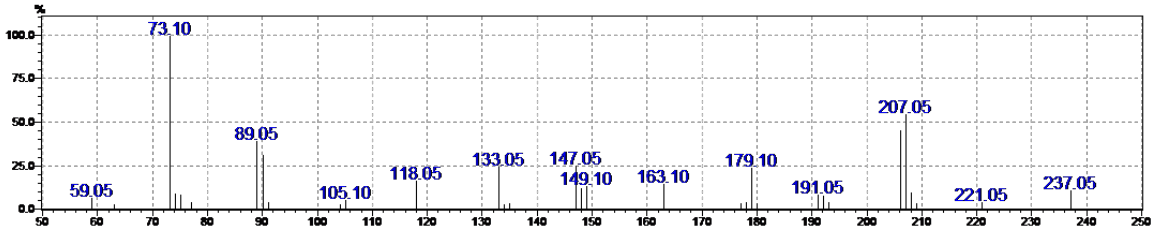

(b) Single-TMS derivatised terephthalic acid. RT = 13.2 min. Observed m/z = 237.05 vs expected 238.07.

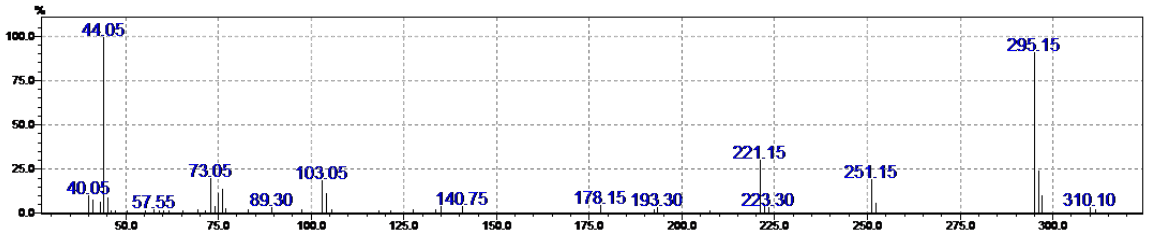

(c) Double-TMS derivatised terephthalic acid. RT = 14.4 min. Observed m/z = 310.10 vs expected 310.11.

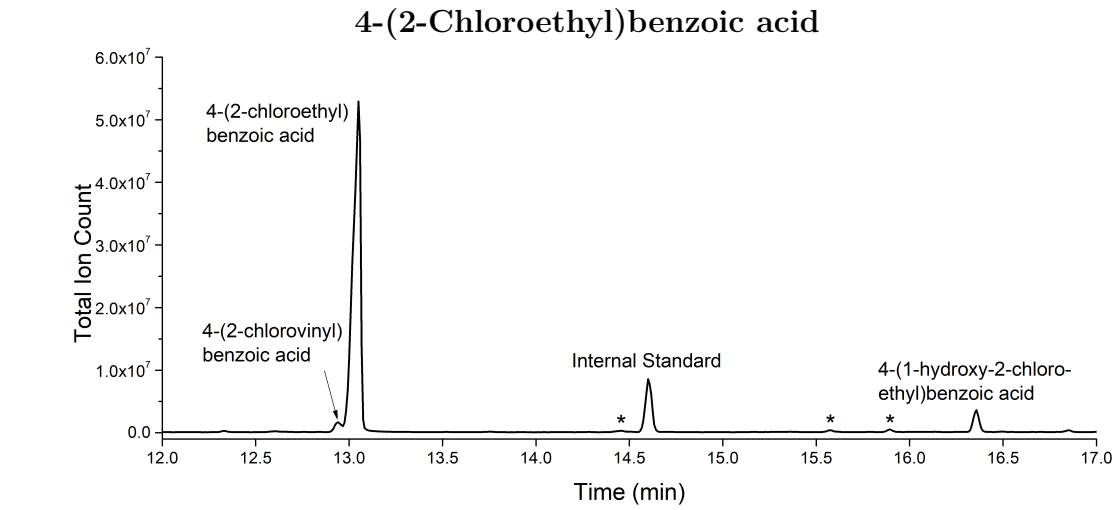

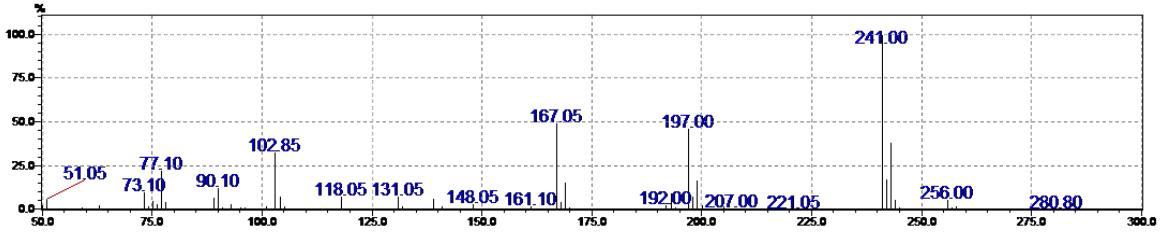

(a) 4-(2-Chloroethyl)benzoic acid. RT = 13.1 min. Observed m/z = 256.00 vs expected 256.07.

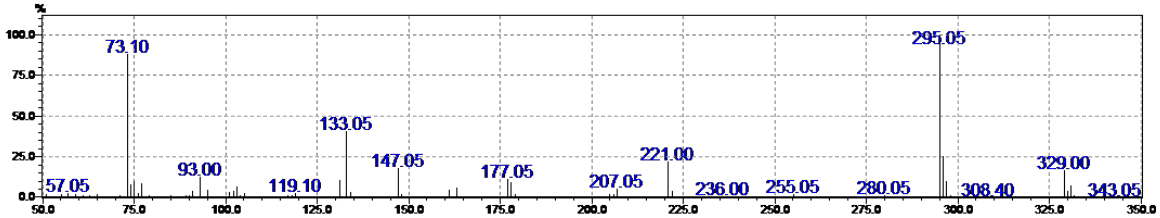

(b) 4-(1-Hydroxy-2-chloroethyl)benzoic acid. RT = 16.4 min. Observed m/z = 343.05 vs expected 344.10.

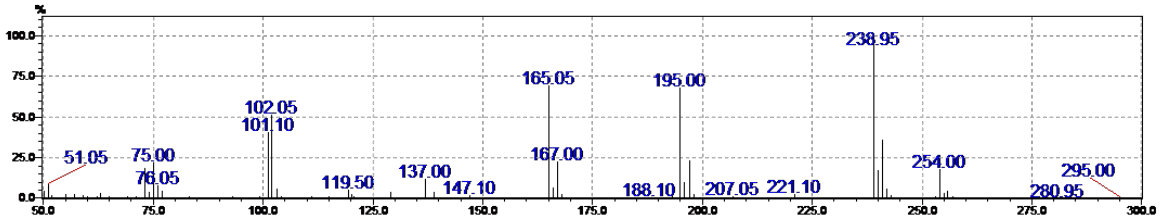

(c) 4-(2-Chlorovinyl)benzoic acid. RT = 13.0 min. Observed m/z = 254.00 vs expected 254.05.

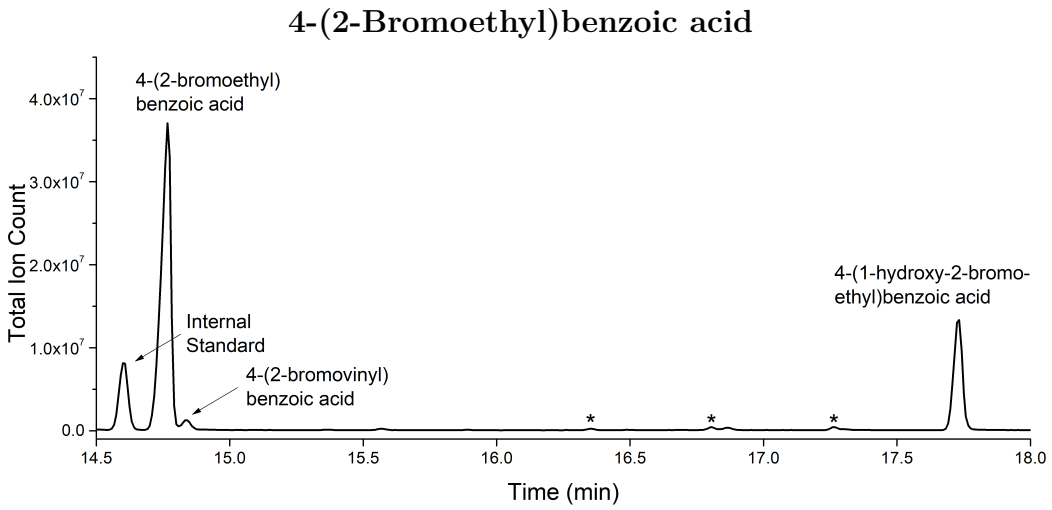

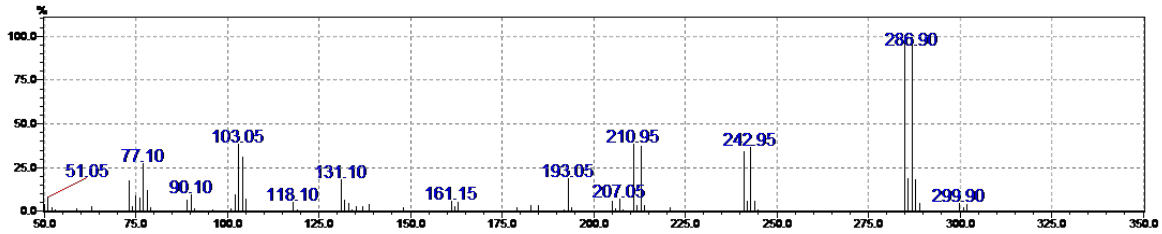

(a) 4-(2-Bromoethyl)benzoic acid. RT = 14.7 min. Observed m/z = 299.90/301.90 (1:1) vs expected 300.02/302.02.

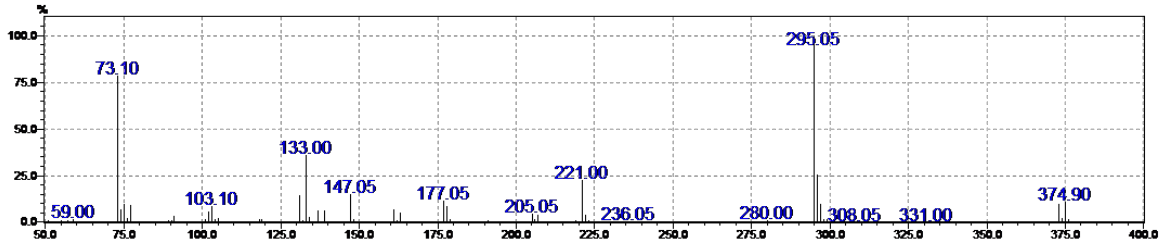

(b) 4-(1-Hydroxy-2-bromoethyl)benzoic acid. RT = 17.7 min. Observed m/z = 372.90/374.90 (1:1, -Me) vs expected 388.05/390.05.

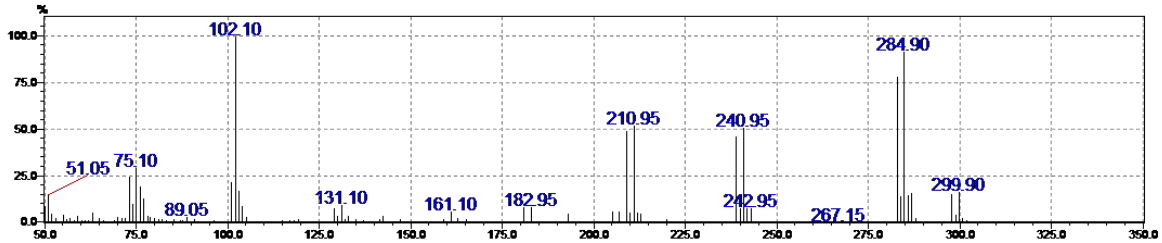

(c) 4-(2-Bromovinyl)benzoic acid. RT = 14.8 min. Observed m/z = 297.90/299.90 (1:1) vs expected 298.00/300.00.

B.5 NMR analysis

Product of 4-ethylamino- and 4-diethylamino-benzoic acids

4-Acetamidobenzoic acid: 500 MHz, d_6-DMSO.
^{1}H: δ 2.07 (s, 3H, **7**), 7.68 (d, 2H, J = 8.7 Hz, **4**), 7.86 (d, 2H, J = 8.7 Hz, **3**).

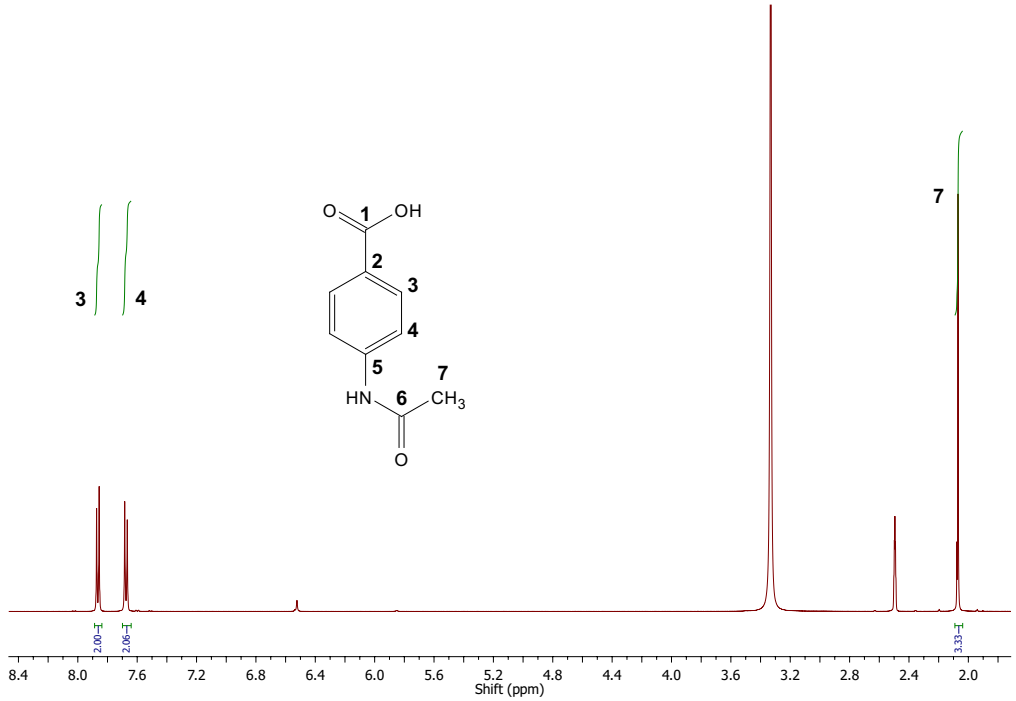

^{13}C: 27.27 (**7**), 121.27 (**4**), 127.99 (**5**), 133.47 (**3**), 146.43 (**2**), 170.03 (**6**), 171.97 (**1**).

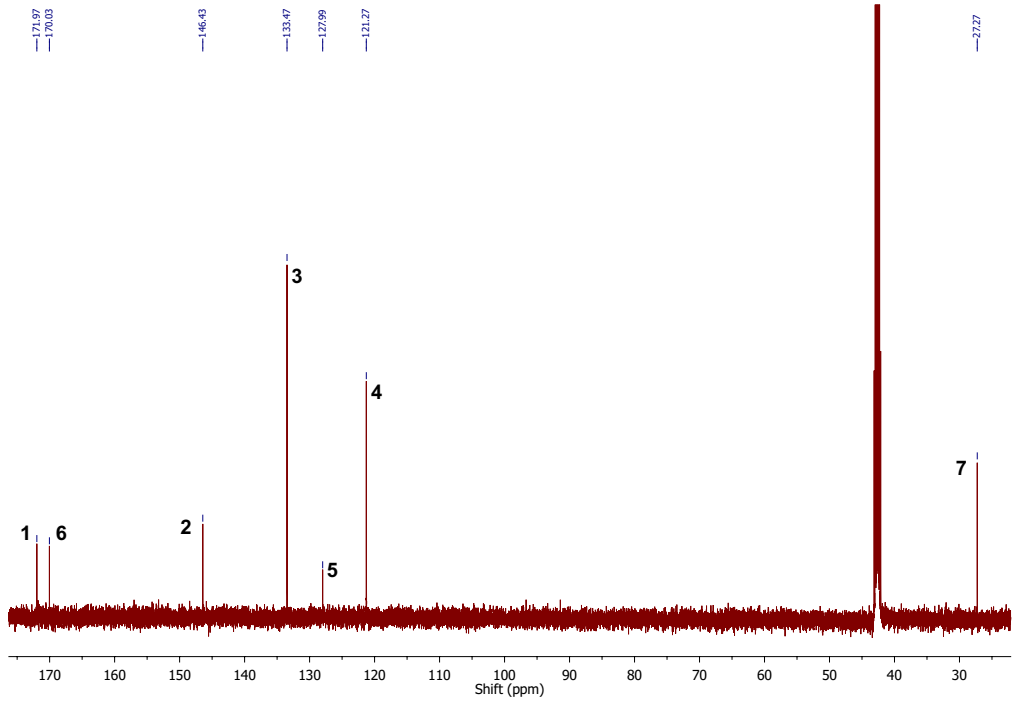

^{1}H-^{1}H COSY:

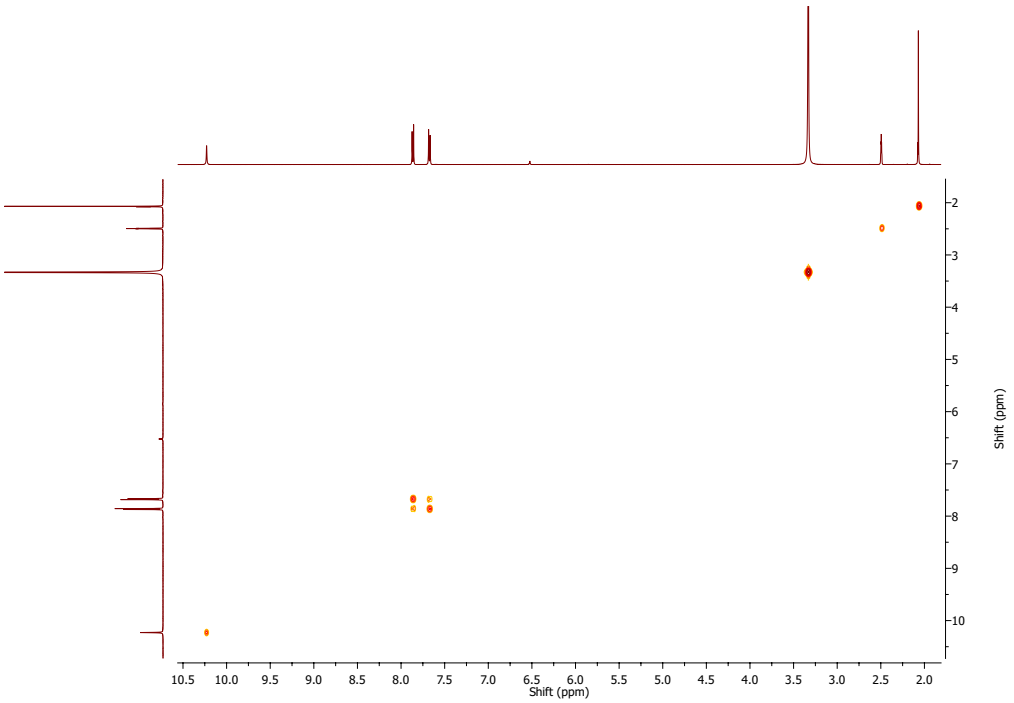

^{1}H-^{13}C HSQC:

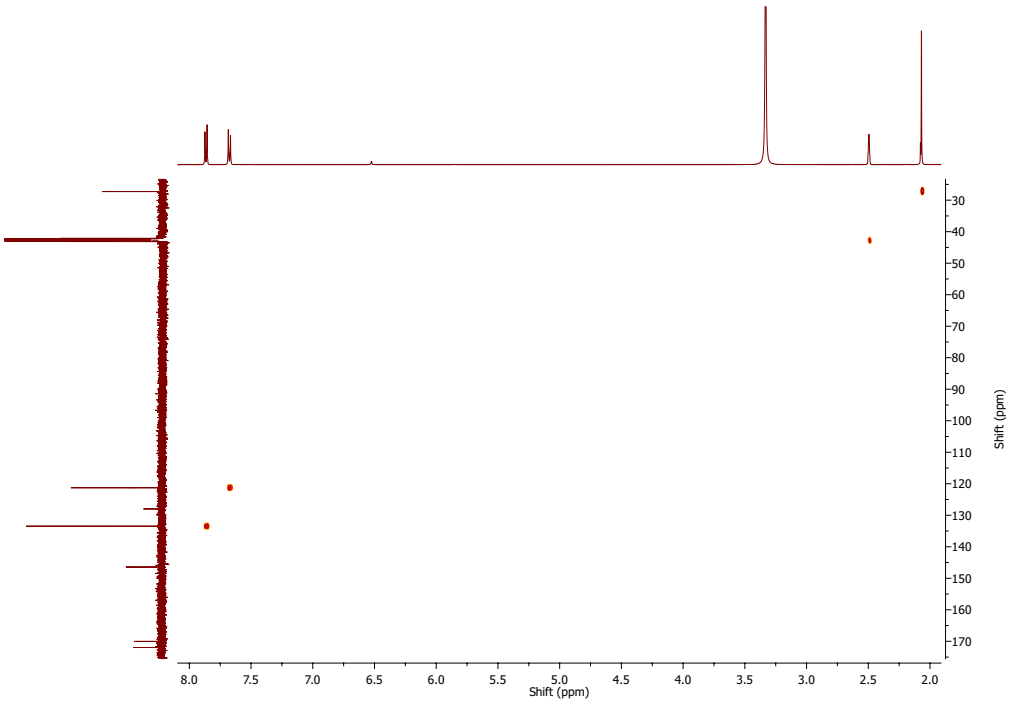

Products of 4-(2-chloroethyl)benzoic acid

4-(2-hydroxyethyl)benzoic acid: 500 MHz, d_6-DMSO.
^{1}H: δ 2.78 (t, 2H, J = 6.8 Hz, **6**), 3.62 (dt, 2H, J = 5.2, 6.8 Hz, **7**), 4.66 (t, 1H, J = 5.1 Hz, **8**), 7.33 (d, 2H, J = 8.1 Hz, **4**), 7.84 (d, 2H, J = 8.1 Hz, **3**). A ^{13}C spectrum could not be assigned due to insufficient sample. Despite this, HSQC cross-peaks were observed.

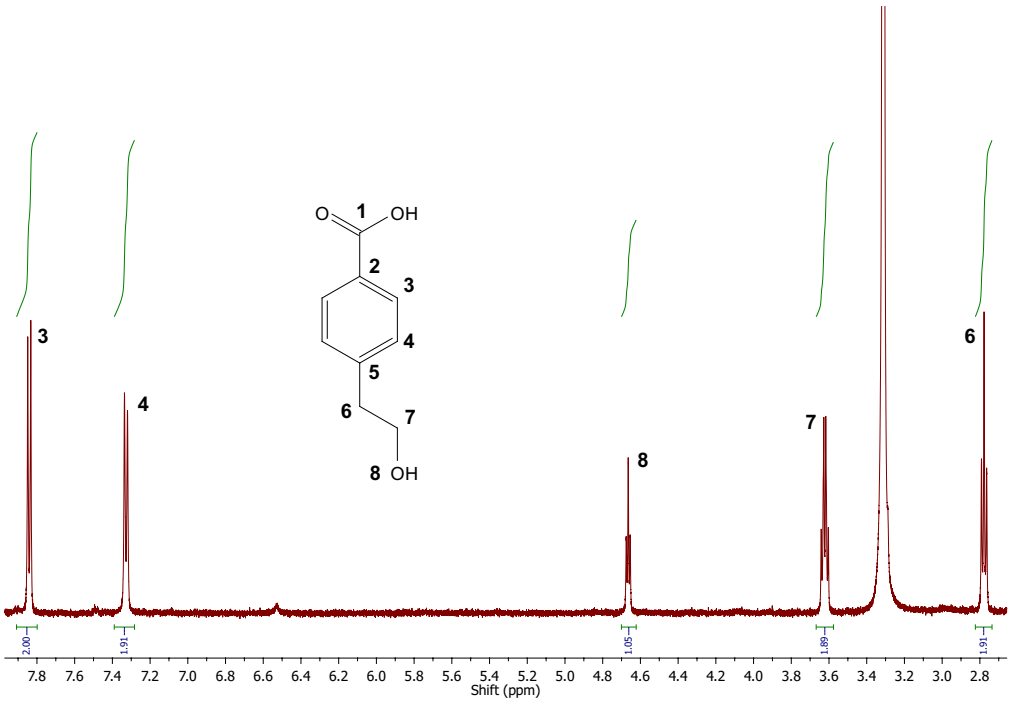

^{1}H-^{1}H COSY:

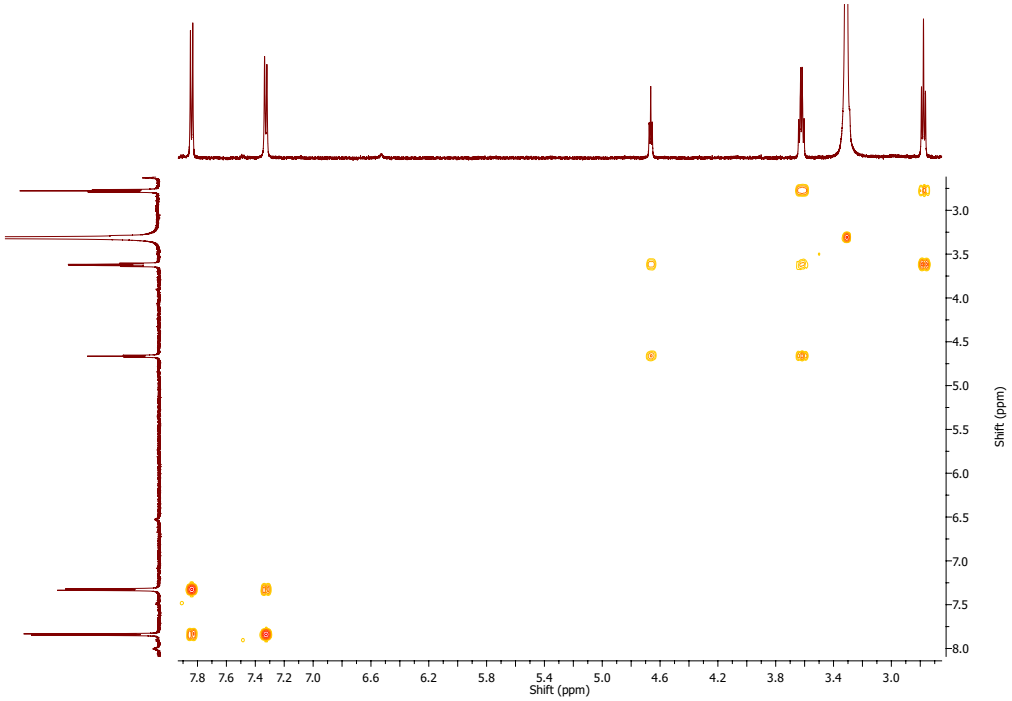

^{1}H-^{13}C HSQC:

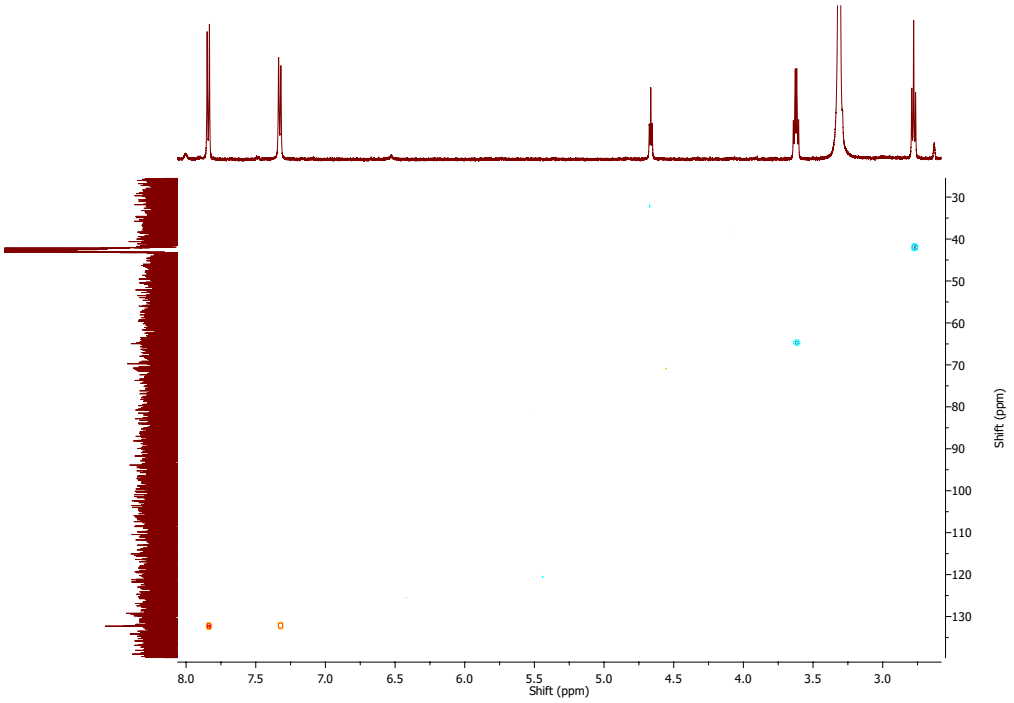
30
40
50
60
70
80
90
100
110
120
130
Shift (ppm)
8.0
7.5
7.0
6.5
6.0
5.5
5.0
4.5
4.0
3.5
3.0
Shift (ppm)

4-(1-hydroxy-2-chloroethyl)benzoic acid: 500 MHz, d_6-DMSO.
^{1}H: δ 3.70 (dd, 1H, J = 6.7, 11.1 Hz, **8**), 3.78 (dd, 1H, J = 4.1, 11.1 Hz, **8**), 4.84-4.88 (m, 1H, **6**), 5.91 (d, 1H, J = 4.2 Hz, **7**), 7.50 (d, 2H, J = 8.2 Hz, **4**), 7.90 (d, 2H, J = 8.2 Hz, **3**). A ^{13}C spectrum could not be assigned due to insufficient sample. An interpretable HSQC spectrum was still able to be obtained.

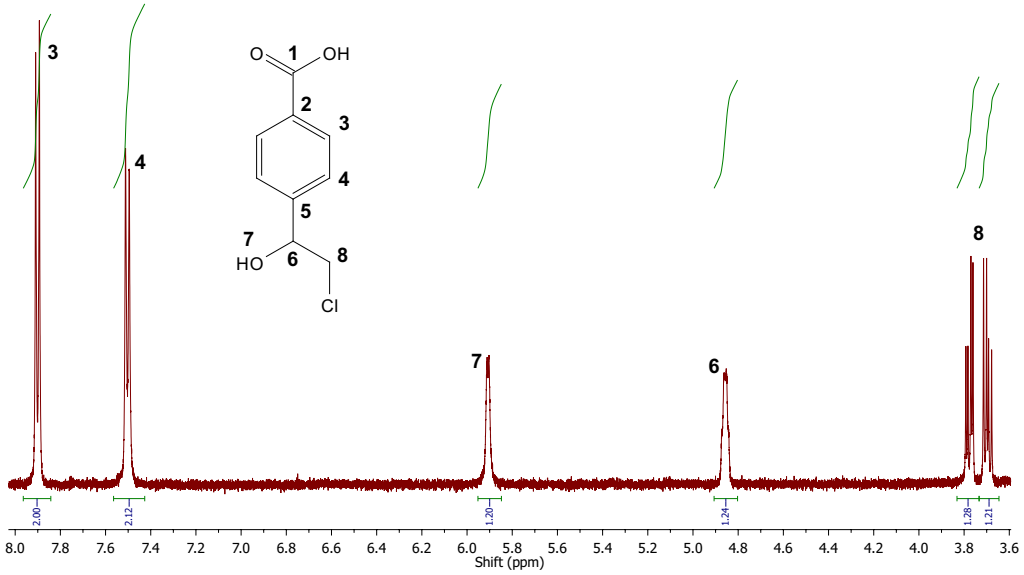

^{1}H-^{1}H COSY:

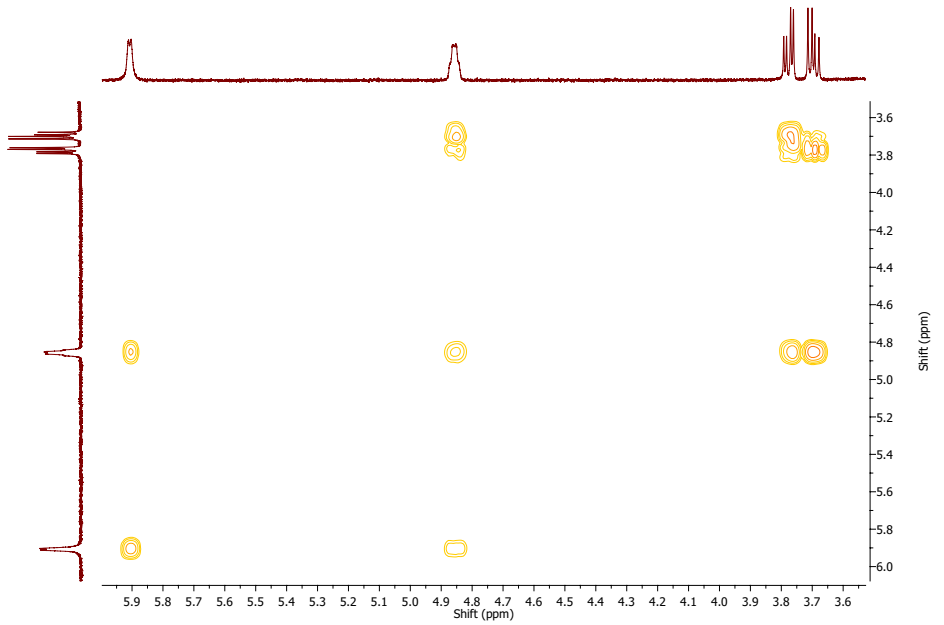

^{1}H-^{13}C HSQC:

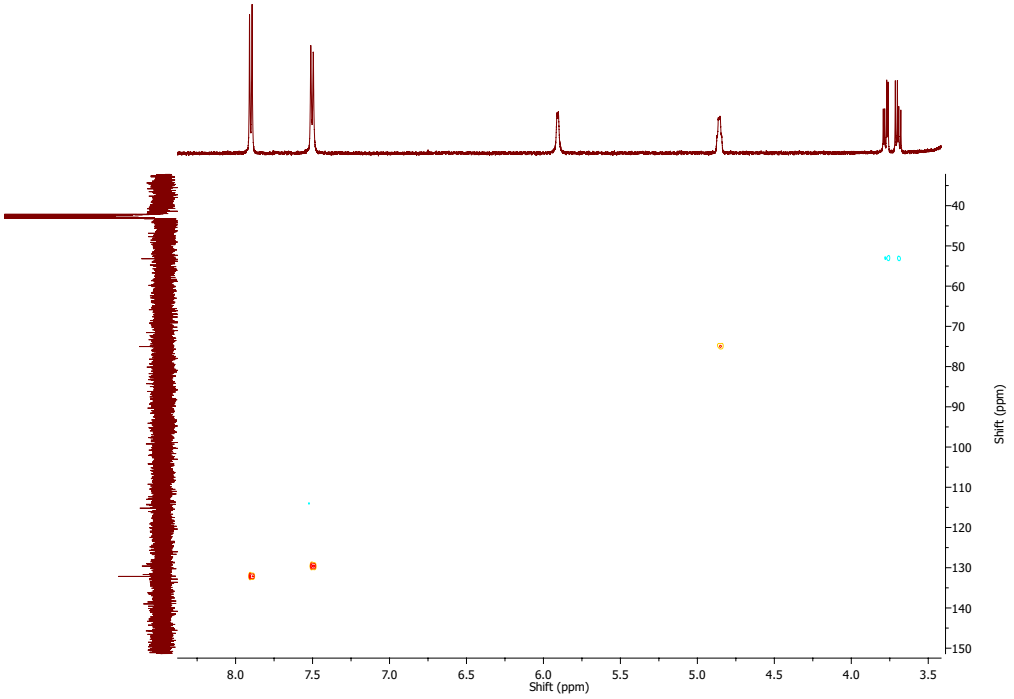
40
50
60
70
80
90
100
110
120
130
140
150
Shift (ppm)
8.0
7.5
7.0
6.5
6.0
5.5
5.0
4.5
4.0
3.5
Shift (ppm)

Product of 4-(2-bromoethyl)benzoic acid

4-(1-hydroxy-2-bromoethyl)benzoic acid: 500 MHz, d_6-DMSO.
^{1}H: δ 3.60 (dd, 1H, J = 6.7, 10.3 Hz, **8**), 3.69 (dd, 1H, J = 4.5, 10.3 Hz, **8**), 4.87-4.90 (m, 1H, **6**), 5.95 (d, 1H, J = 2.7 Hz, **7**), 7.51 (d, 2H, J = 8.2 Hz, **4**), 7.91 (d, 2H, J = 8.2 Hz, **3**).

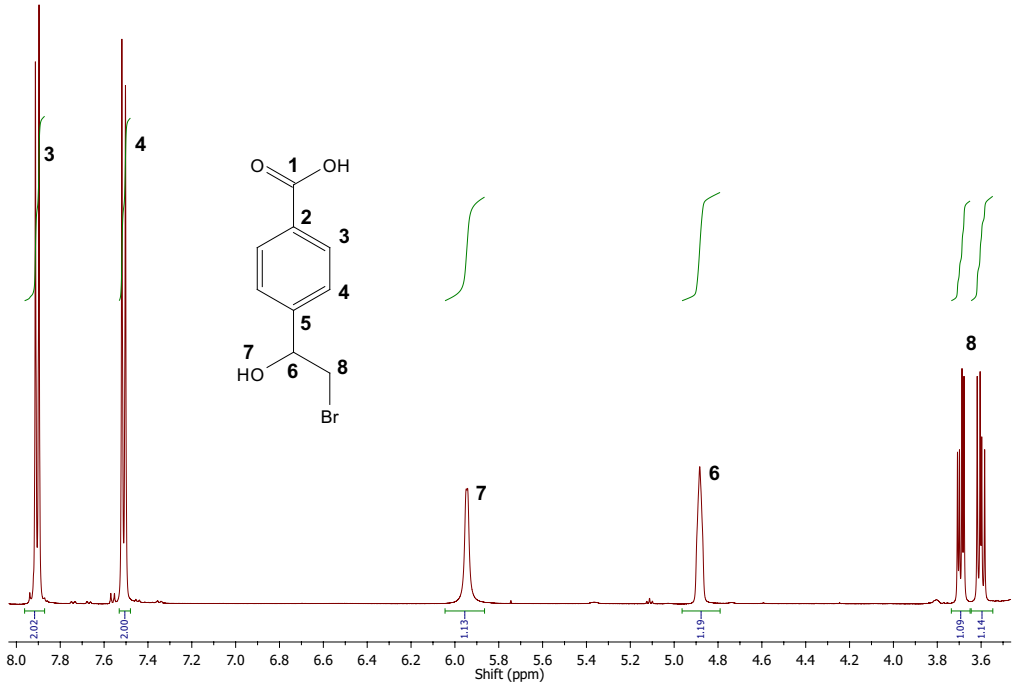

^{13}C: δ 43.00 (**8**, shown in expansion), 74.64 (**6**), 129.61 (**4**), 132.19 (**3**), 133.02 (**5**), 150.63 (**2**), 170.27 (**1**).

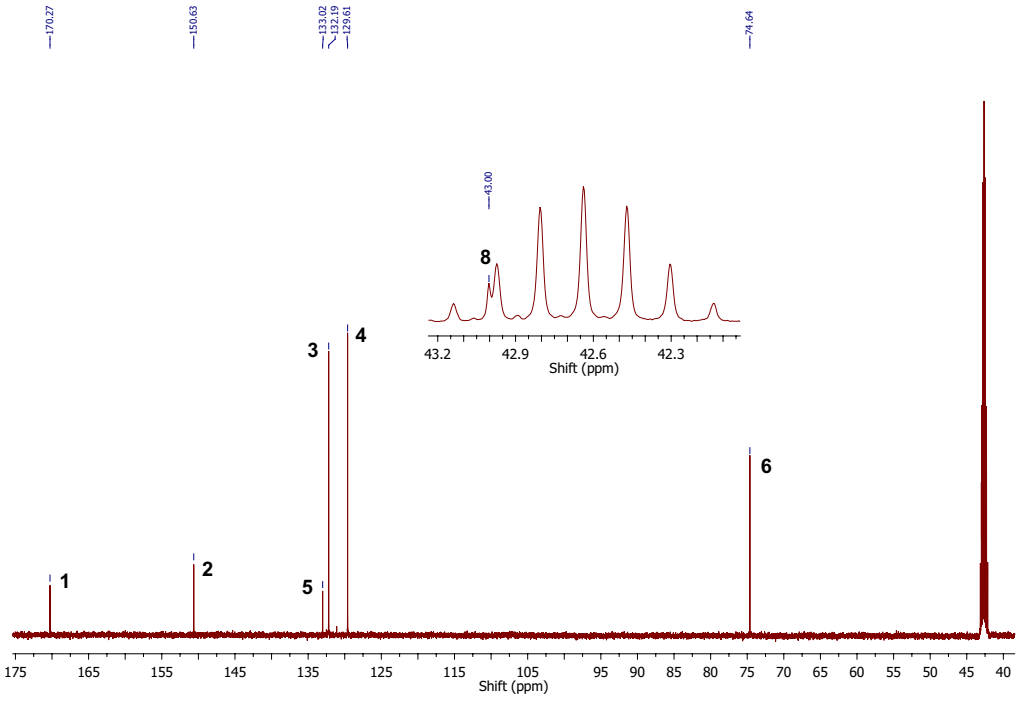

^{1}H-^{1}H COSY:

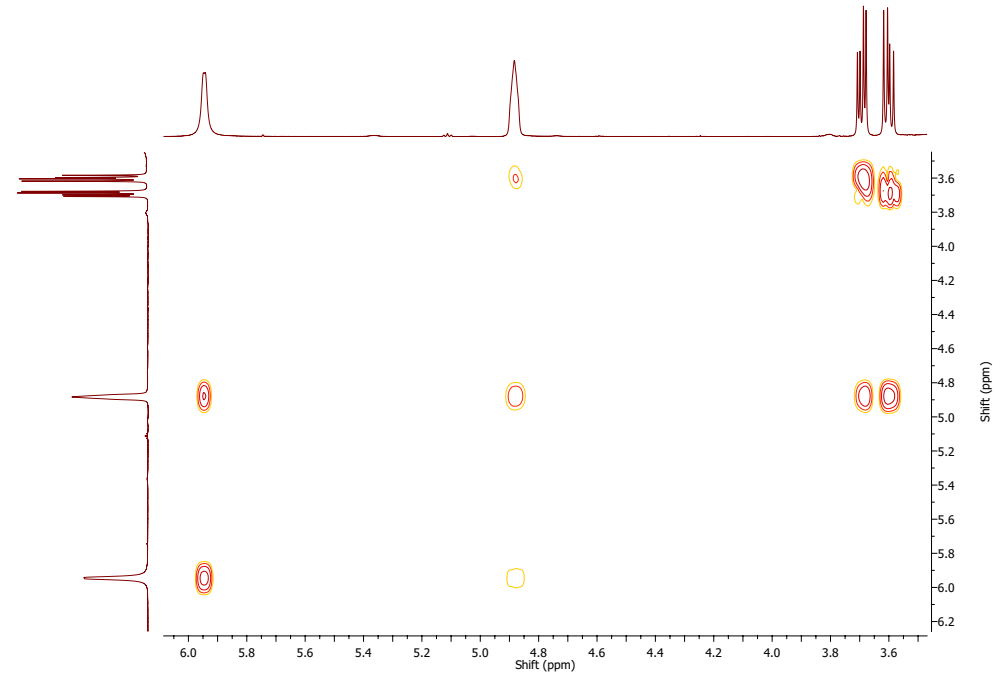

^{1}H-^{13}C HSQC:

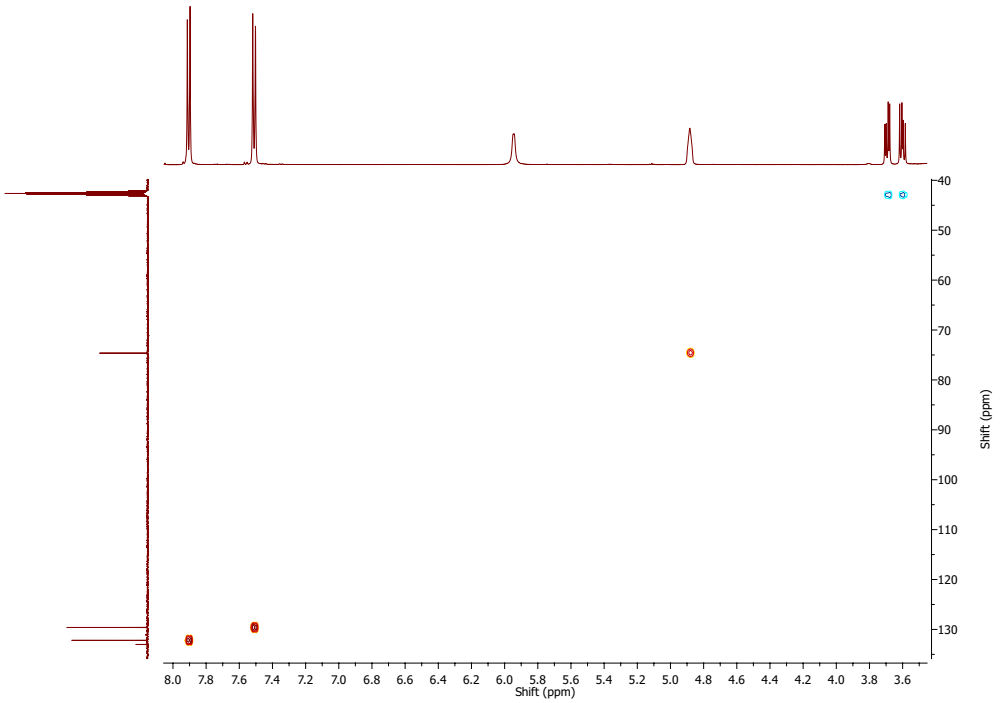

B.6 X-ray crystallography

Data collection statistics for 4-ethylaminobenzoic acid with CYP199A4. The overall data collection statistics were considered satisfactory, however significant problems occurred during the phasing step. The resulting electron density maps were poor quality. The data set may be improved by truncation or by merging with another full data set. Alternatively, the crystal growth conditions may need to be optimised further.

	4-ethylaminoBA
X-ray wavelength (Å)	0.9537
Unit cell (a/b/c)	42.6/51.7/79.9
($\alpha/\beta/\gamma$)	90/92.3/90
Space group	$P12_11$
Molecules per unit cell	1
Resolution range[a]	51.72 - 2.07
	(2.13 - 2.07)
$<I/\sigma(I)>$[a]	2.0 (0.7)
Unique reflections	21318
Completeness[a]	99.6 (98.0)
Redundancy[a]	4.5 (3.8)
R_{merge}[a,b] (%)	48.9 (145.6)
R_{pim}[a,b] (%)	26.7 (85.9)

[a]Highest resolution shell is shown in parentheses where applicable. [b]all I+ and I-.

Appendix C Supplementary data for Chapter 5

C.1 Spin state shifts

Spin state shifts of alkyl benzoic acid substrates tested with CYP199A4 in Chapter 5.2. Black shows CYP199A4 in its resting state, red shows the maximum absorbance shift obtained upon addition of substrate.

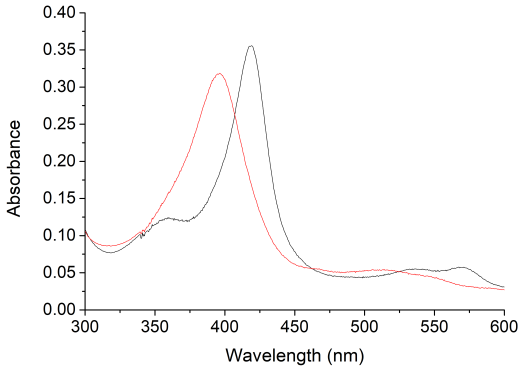

(a) 4-isopropylbenzoic acid[28]

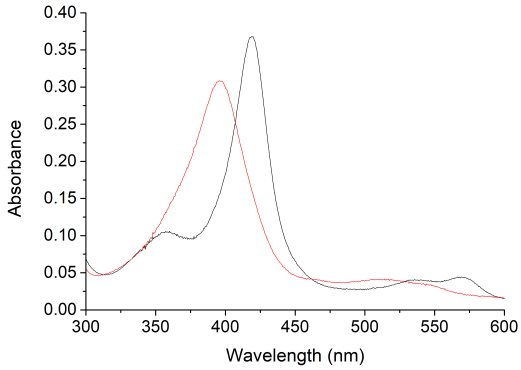

(b) 4-*n*-propylbenzoic acid[28]

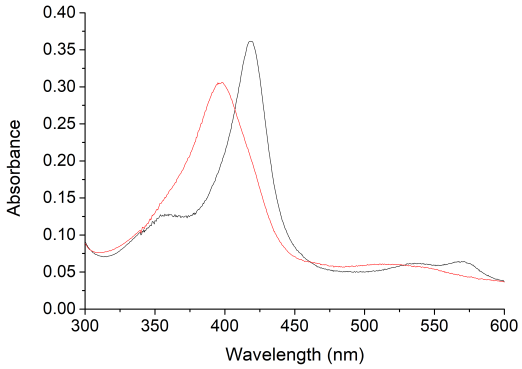

(c) 4-*t*-butylbenzoic acid[28]

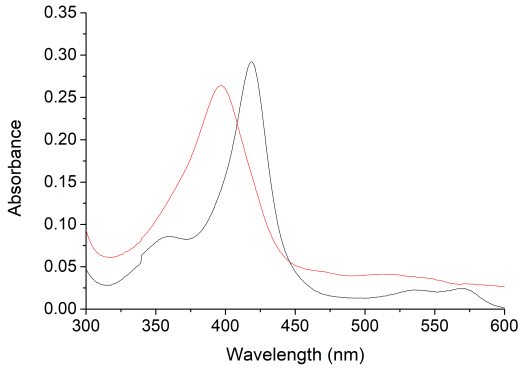

(d) 4-isobutylbenzoic acid

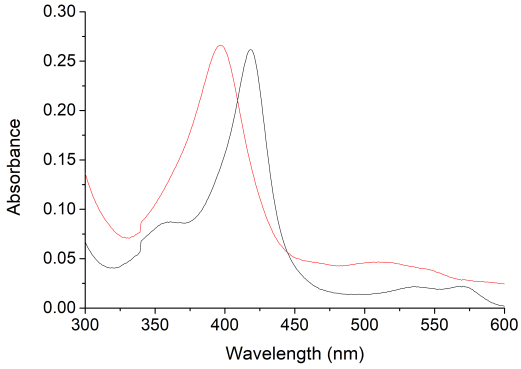

(e) 4-cyclohexylbenzoic acid

Spin state shifts of related alkyl benzoic acid substrates presented in Chapters 5.2.4 and 5.2.5.

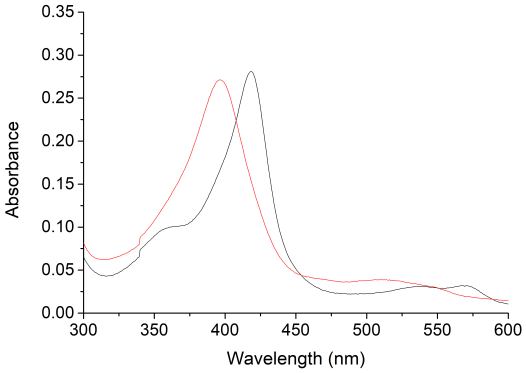

(a) 3-bromo-4-isopropylbenzoic acid

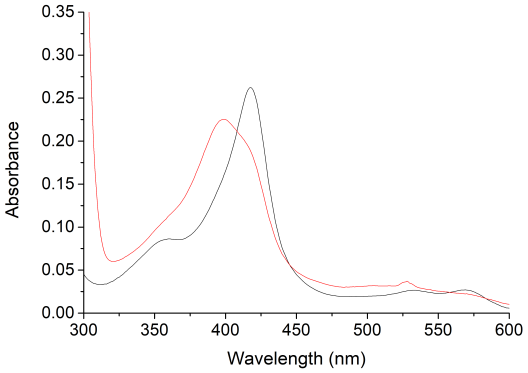

(b) 3-hydroxy-4-isopropylbenzoic acid

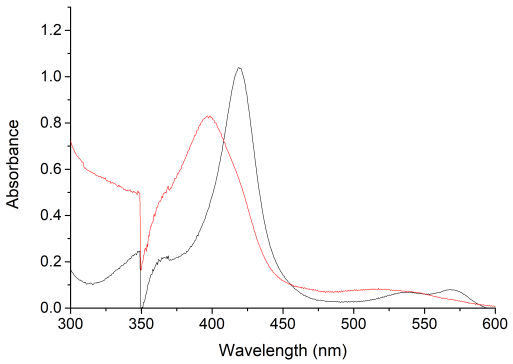

(c) 3-nitro-4-isopropylbenzoic acid

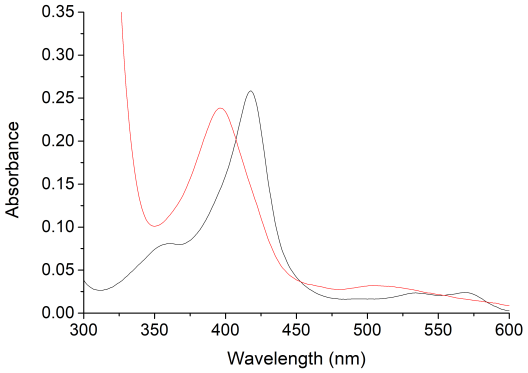

(d) 3-amino-4-isopropylbenzoic acid

C.2 Dissociation constant analysis

Analysis of dissociation constants for CYP199A4-bound substrates presented in Chapter 5.2. (a) to (c), Chapter 5.2.1 ((a) and (b) were previously published[28]); (d) to (f), Chapter 5.2.4. Shown in brackets are the wavelengths of the trough and peak, and the enzyme concentration used for dissociation constant analysis (trough, peak, [P450]).

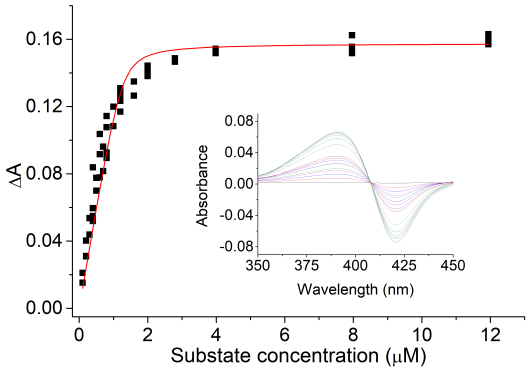

(a) 4-*n*-propylbenzoic acid[28] (421 nm, 391 nm, 1.5 µM)

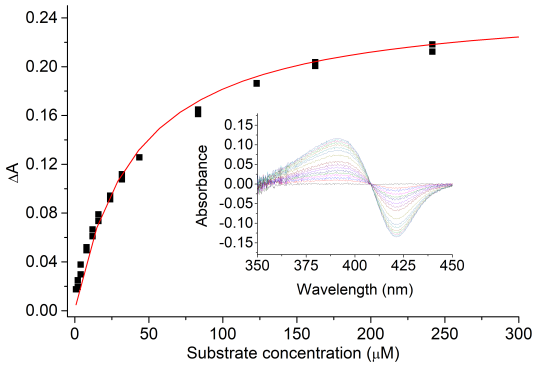

(b) 4-*t*-butylbenzoic acid[28] (421 nm, 391 nm, 1.8 µM)

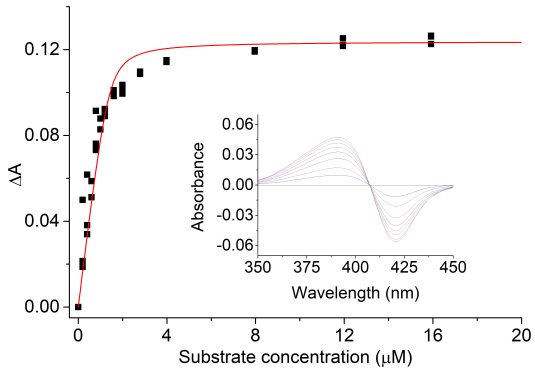

(c) 4-isobutylbenzoic acid (421 nm, 391 nm, 1.1 µM)

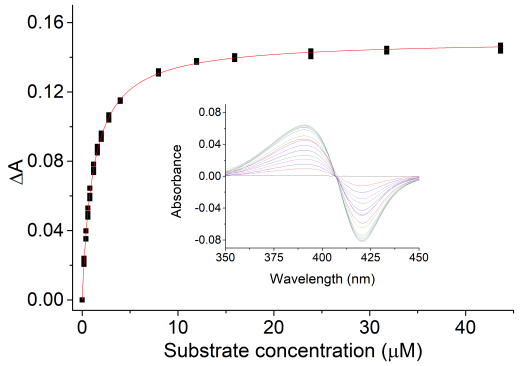

(d) 3-chloro-4-isopropylbenzoic acid (421 nm, 391 nm, 1.3 µM)

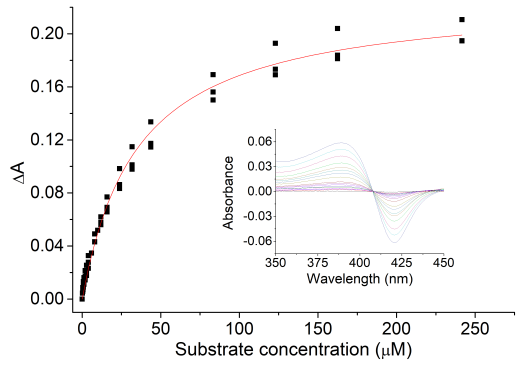

(e) 3-nitro-4-isopropylbenzoic acid[28] (421 nm, 389 nm, 1.9 µM)

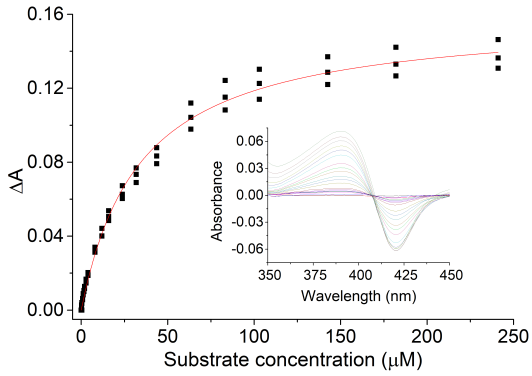

(f) 3-amino-4-isopropylbenzoic acid (420 nm, 390 nm, 1.2 µM)

C.3 GC-MS analysis

GC-MS analysis of substrates presented in Chapter 5. All turnovers were TMS-derivatised before analysis using excess BSTFA/TMCS (99:1).

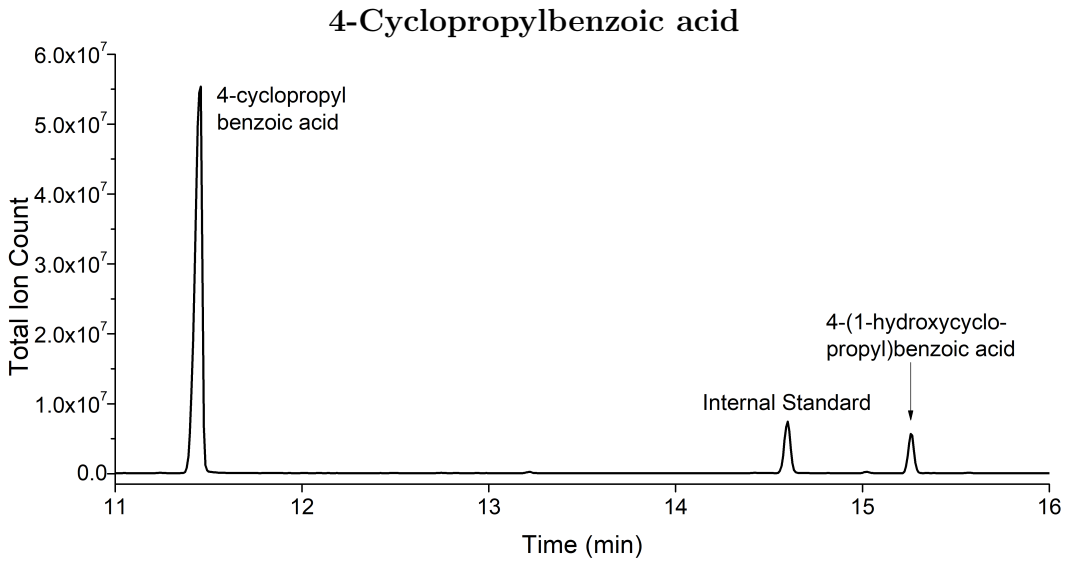

GC-MS analysis of *in vitro* 4-cyclopropylbenzoic acid turnover with CYP199A4.

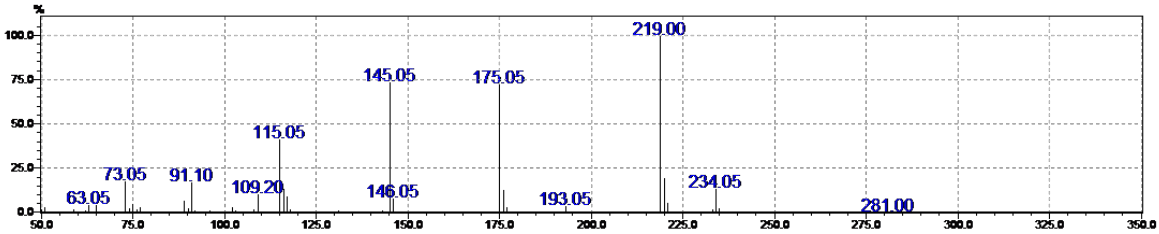

(a) 4-cyclopropylbenzoic acid. RT = 11.4 min. Observed m/z = 234.05 vs expected 234.11.

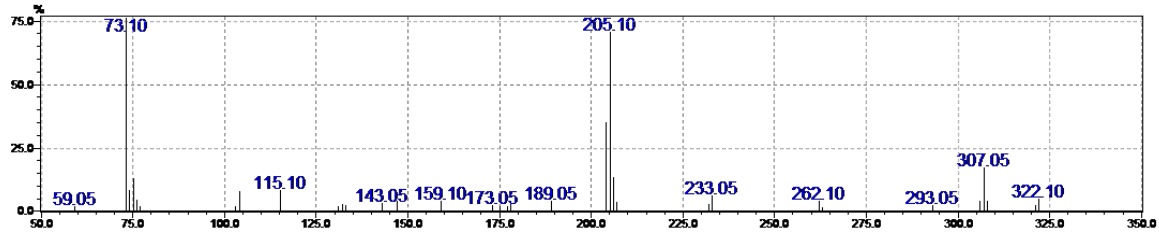

(b) 4-(1-hydroxycyclopropyl)benzoic acid. RT = 15.3 min. Observed m/z = 322.10 vs expected 322.14.

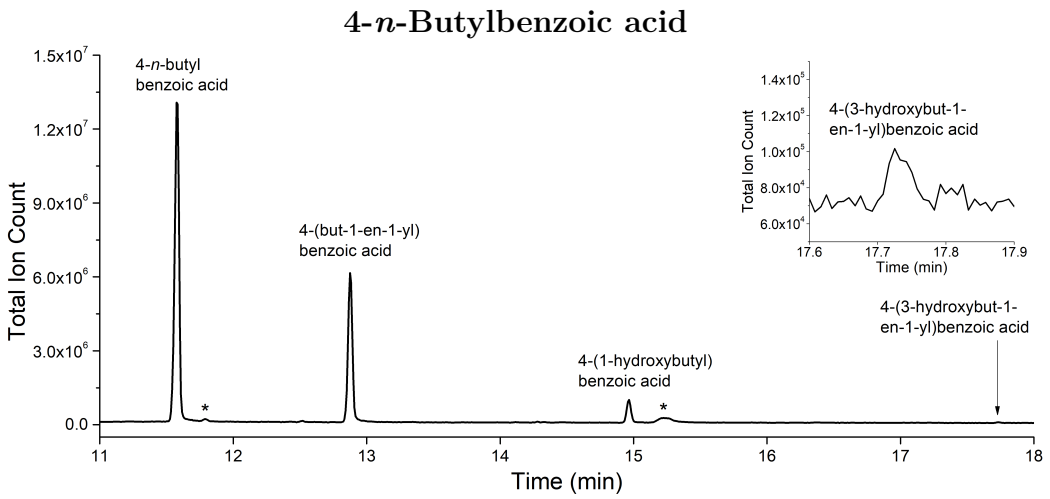

GC-MS analysis of *in vitro* 4-*n*-butylbenzoic acid turnover with CYP199A4. Impurity peaks (present in substrate controls) are marked with an asterix.

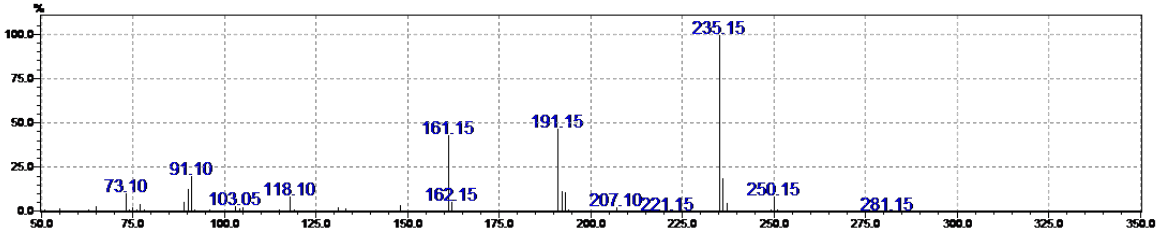

(a) 4-*n*-butylbenzoic acid. RT = 11.6 min. Observed m/z = 250.15 vs expected 250.14.

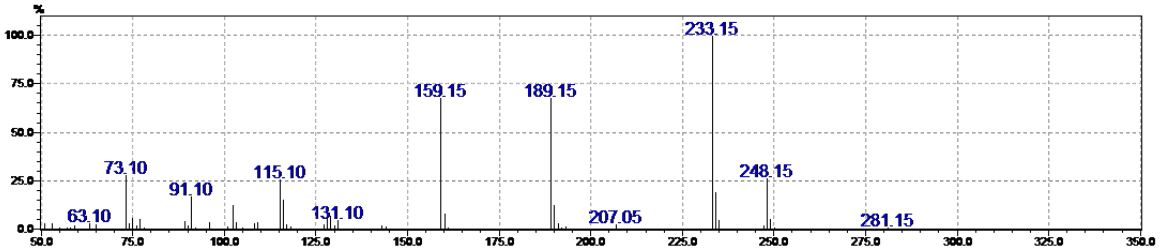

(b) 4-(but-1-en-1-yl)benzoic acid. RT = 12.9 min. Observed m/z = 248.15 vs expected 248.12.

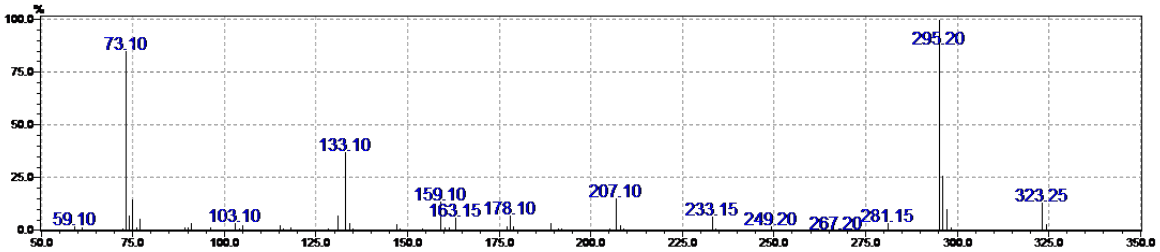

(c) 4-(1-hydroxybutyl)benzoic acid. RT = 15.0 min. Observed m/z = 323.25 (- Me) vs expected 338.17.

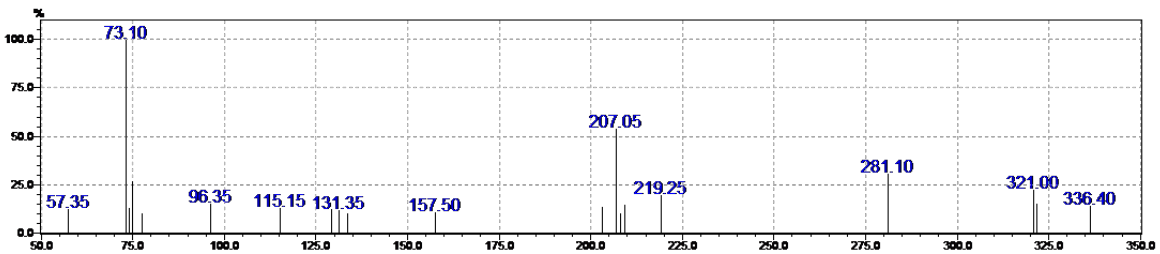

(d) 4-(3-hydroxybut-1-en-1-yl)benzoic acid. RT = 17.7 min. Observed m/z = 336.40 vs expected 336.16.

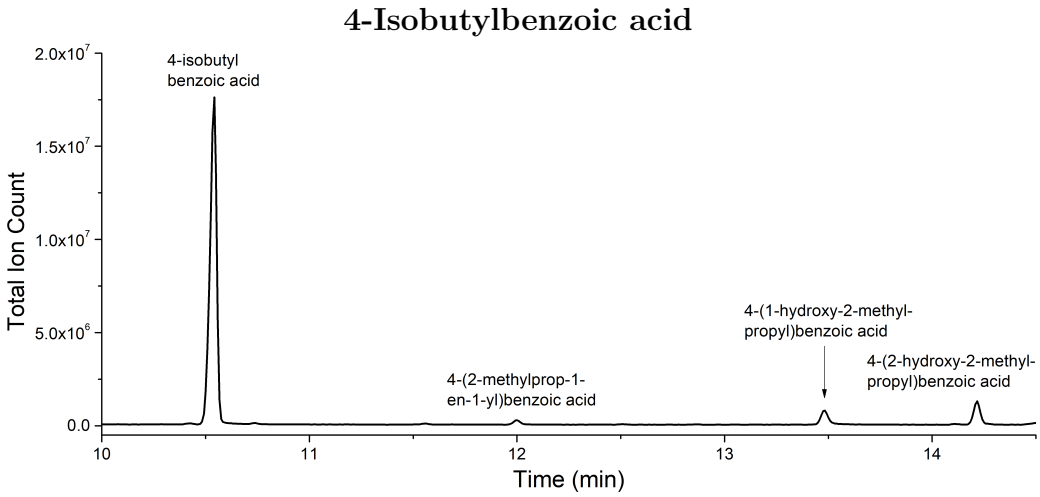

GC-MS analysis of *in vitro* 4-isobutylbenzoic acid turnover with CYP199A4.

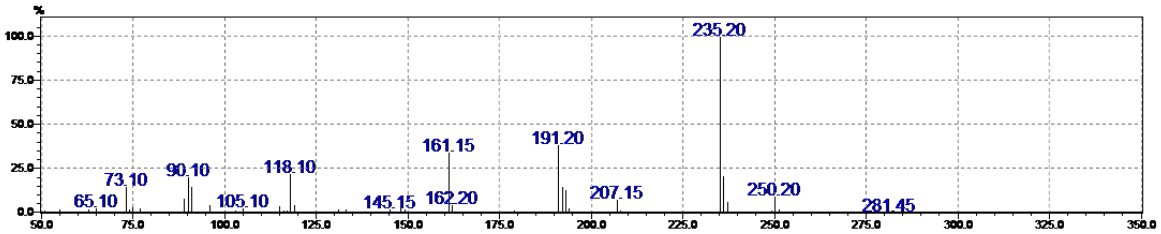

(a) 4-isobutylbenzoic acid. RT = 10.5 min. Observed m/z = 250.20 vs expected 250.14.

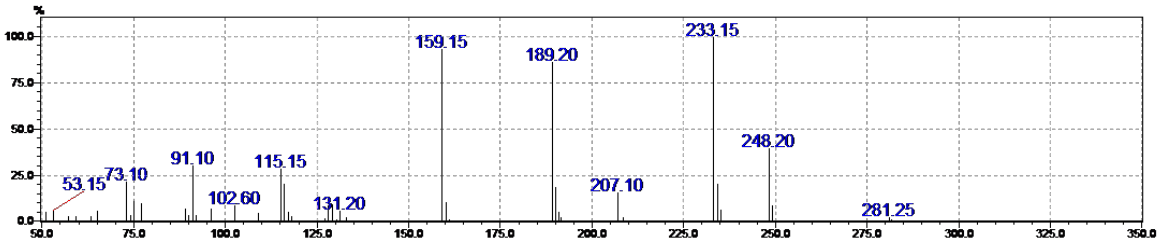

(b) 4-(2-methylprop-1-en-1-yl)benzoic acid. RT = 12.0 min. Observed m/z = 248.20 vs expected 248.12.

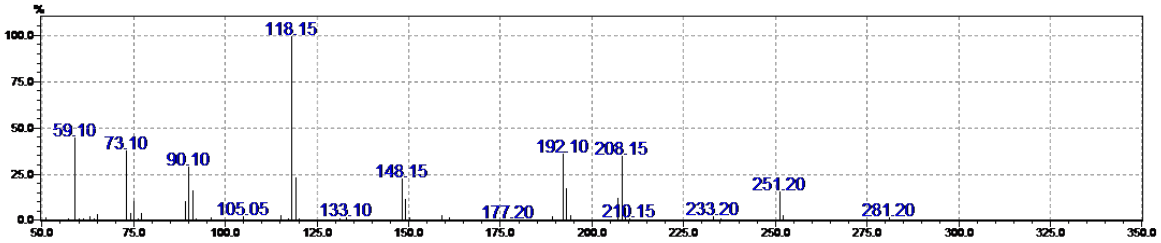

(c) 4-(2-hydroxy-2-methylpropyl)benzoic acid, single TMS-derivatised. RT = 13.5 min. Observed m/z = 251.20 (- Me) vs expected 266.13. No double derivatised peak was observed.

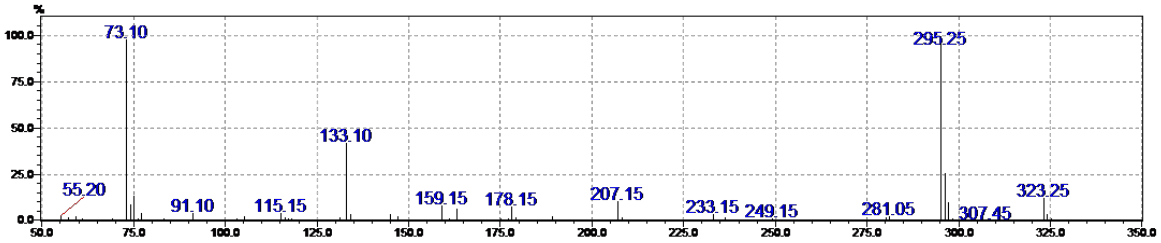

(d) 4-(1-hydroxy-2-methylpropyl)benzoic acid. RT = 14.2 min. Observed m/z = 323.25 vs expected 338.17.

4-Cyclohexylbenzoic acid

Refer to Figure 93 (Chapter 5.2.2).

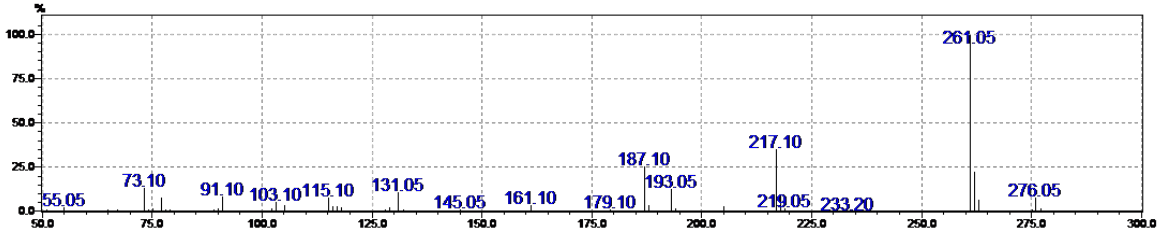

(a) 4-cyclohexylbenzoic acid. RT = 17.3 min. Observed m/z = 276.05 vs expected 276.15.

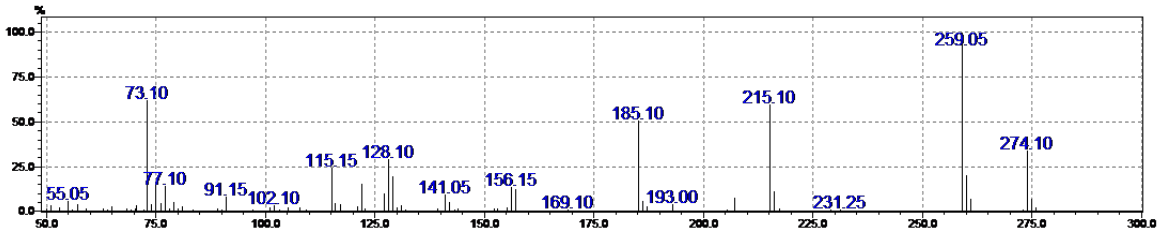

(b) 4-(cyclohex-1-en-1-yl)benzoic acid. RT = 18.6 min. Observed m/z = 274.10 vs expected 274.14.

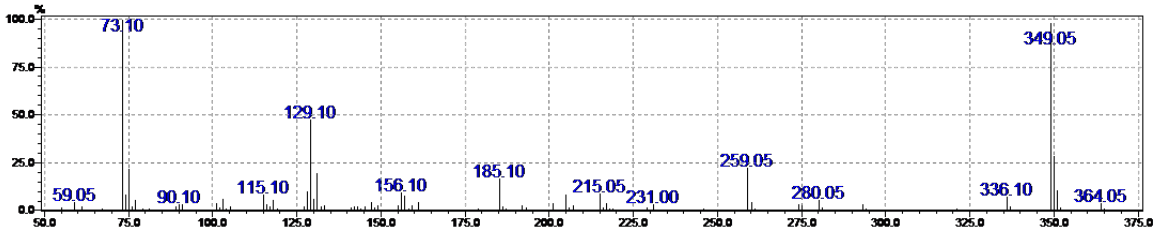

(c) 4-(2-hydroxycyclohexyl)benzoic acid. RT = 19.5 min. Observed m/z = 364.05 vs expected 364.19.

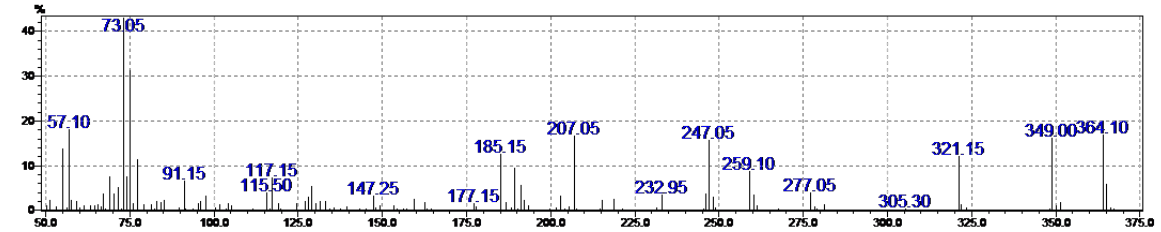

(d) 4-(1-hydroxycyclohexyl)benzoic acid, double TMS-derivatised. RT = 20.0 min. Observed m/z = 364.10 vs expected 364.19.

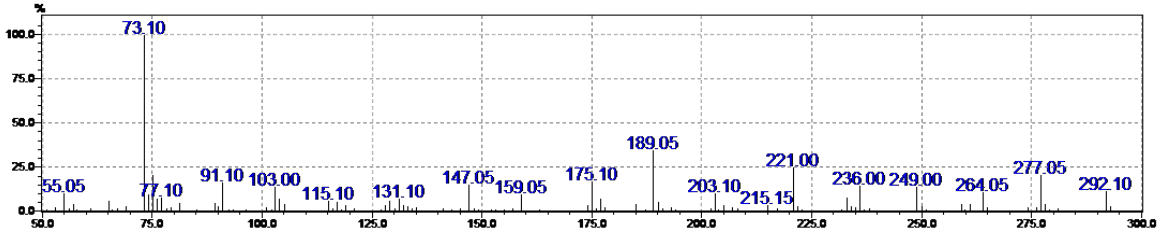

(e) 4-(1-hydroxycyclohexyl)benzoic acid, single TMS-derivatised. RT = 20.2 min. Observed m/z = 292.10 vs expected 292.15.

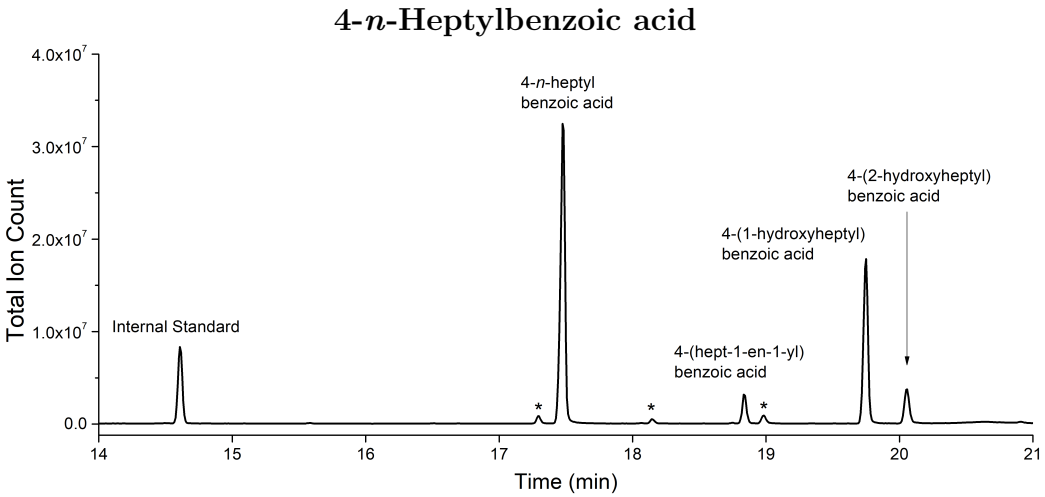

GC-MS analysis of *in vitro* 4-*n*-heptylbenzoic acid turnover with CYP199A4. Impurity peaks (present in substrate controls) are marked with an asterix.

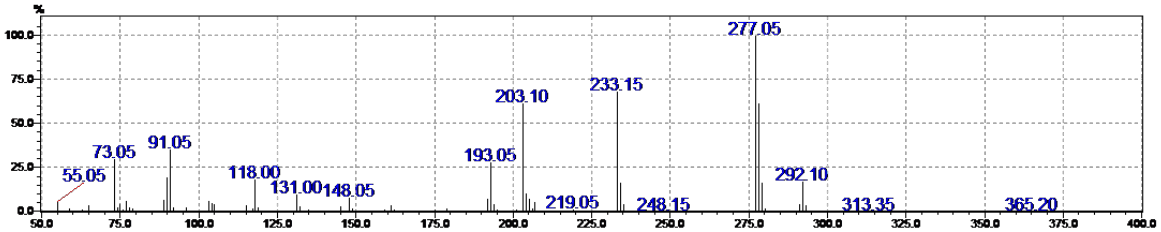

(a) 4-*n*-heptylbenzoic acid. RT = 17.4 min. Observed m/z = 292.10 vs expected 292.19.

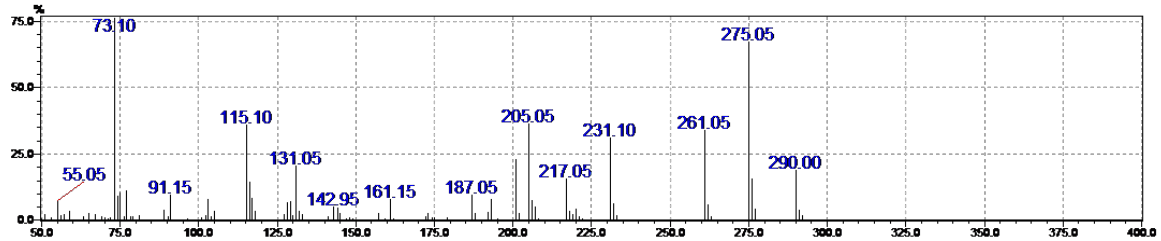

(b) 4-(hept-1-en-1-yl)benzoic acid. RT = 18.8 min. Observed m/z = 290.00 vs expected 290.17.

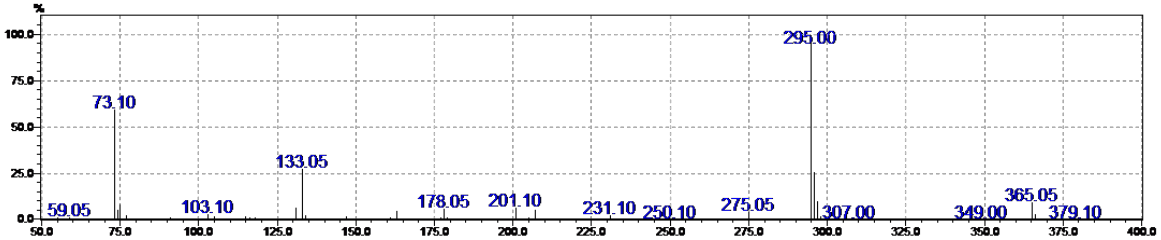

(c) 4-(1-hydroxyheptyl)benzoic acid. RT = 19.7 min. Observed m/z = 379.10 vs expected 380.22.

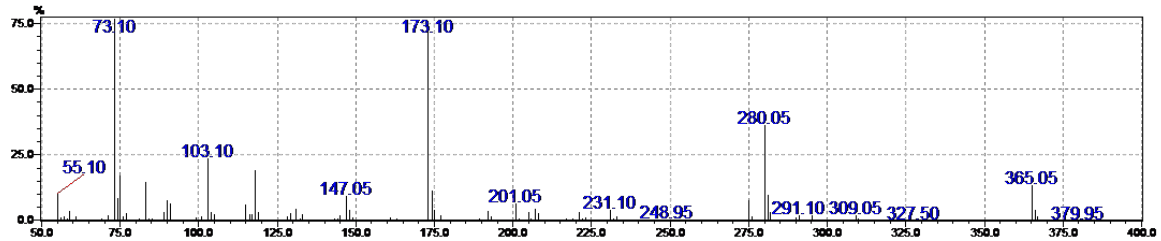

(d) 4-(2-hydroxyheptyl)benzoic acid. RT = 20.1 min. Observed m/z = 379.95 vs expected 380.22.

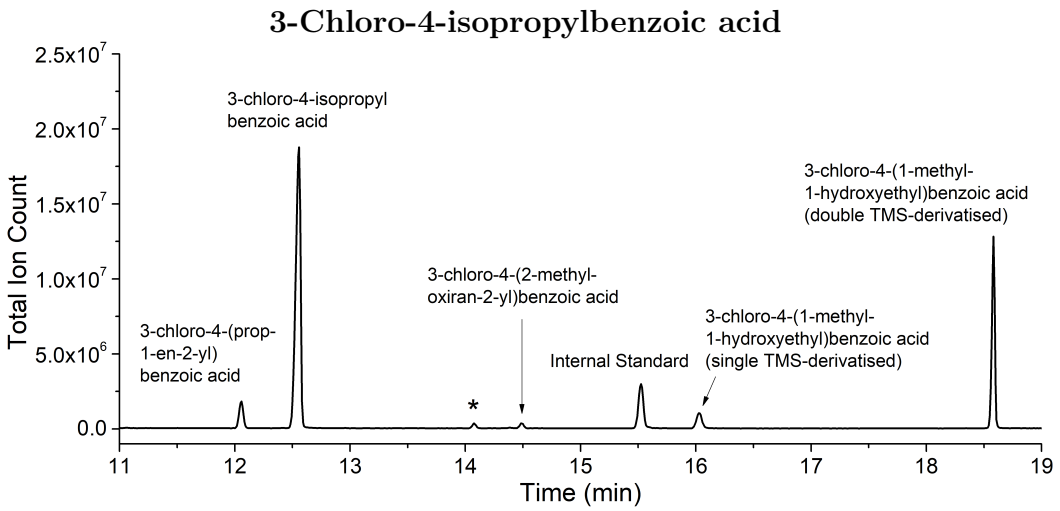

GC-MS analysis of *in vitro* 3-chloro-4-isopropylbenzoic acid turnover with CYP199A4. An impurity peak (present in controls containing no P450) is marked with an asterix.

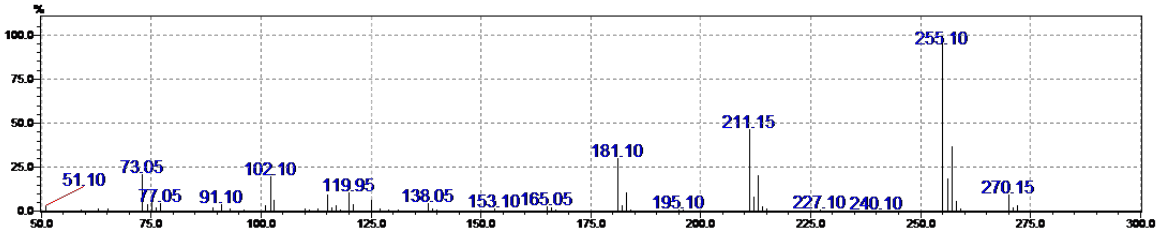

(a) 3-chloro-4-isopropylbenzoic acid. Observed m/z = 270.15 vs expected 270.08.

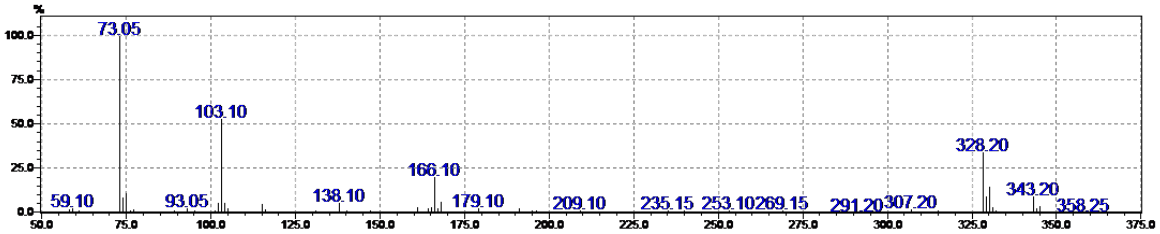

(b) 3-chloro-4-(1-methyl-1-hydroxyethyl)benzoic acid, double TMS-derivatised. Observed m/z = 358.25 vs expected 358.12.

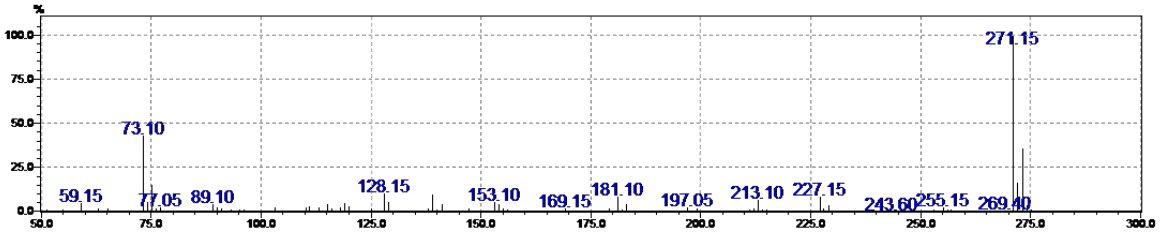

(c) 3-chloro-4-(1-methyl-1-hydroxyethyl)benzoic acid, single TMS-derivatised. Observed m/z = 271.15 (- Me) vs expected 286.08.

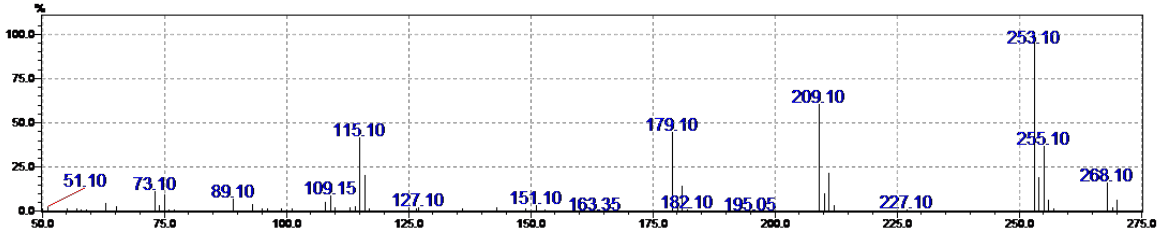

(d) 3-chloro-4-(prop-1-en-2-yl)benzoic acid. Observed m/z = 268.10 vs expected 268.07.

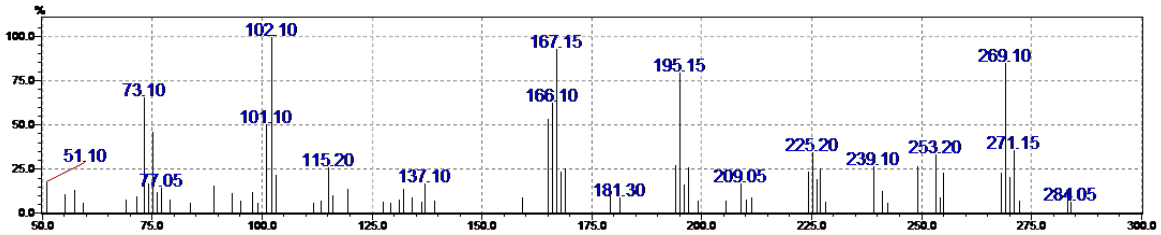

(e) 3-chloro-4-(2-methyloxiran-2-yl)benzoic acid. Observed m/z = 284.05 vs expected 284.06.

3-Bromo-4-isopropylbenzoic acid

Refer to Figure 110a (Chapter 5.2.4).

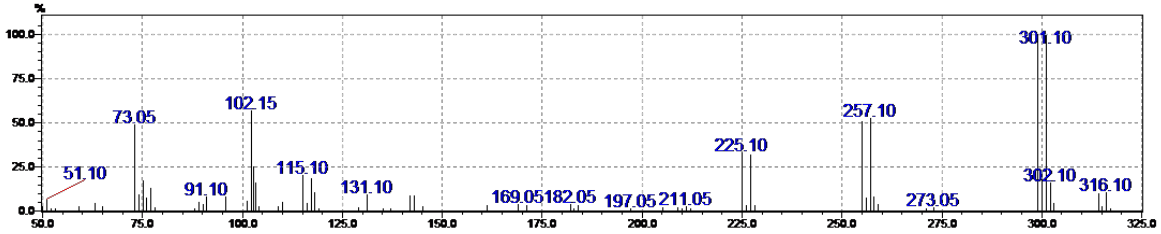

(a) 3-bromo-4-isopropylbenzoic acid. Observed m/z = 314.10/316.10 vs expected 314.03/316.03.

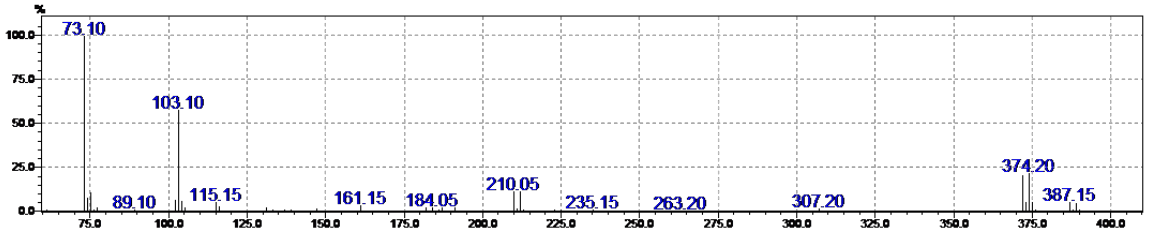

(b) 3-bromo-4-(1-methyl-1-hydroxyethyl)benzoic acid, double TMS-derivatised. Observed m/z = 387.15/389.15 (- Me) vs expected 402.07/404.07.

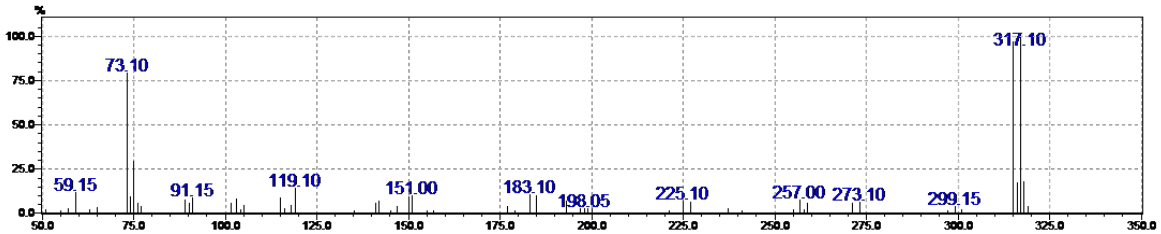

(c) 3-bromo-4-(1-methyl-1-hydroxyethyl)benzoic acid, single TMS-derivatised. Observed m/z = 315.10/317.10 (- Me) vs expected 330.03/332.03.

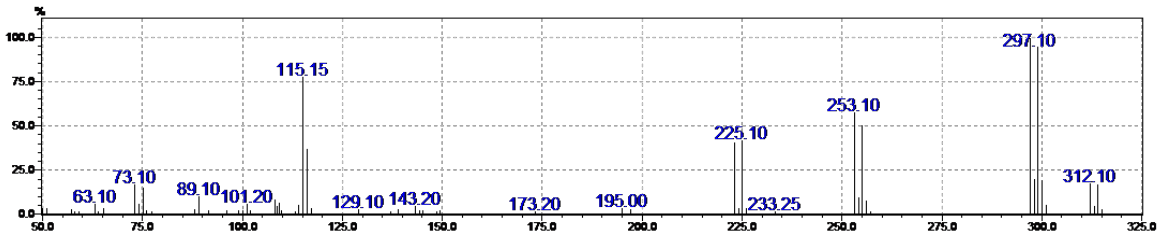

(d) 3-bromo-4-(prop-1-en-2-yl)benzoic acid. Observed m/z = 312.10/314.10 vs expected 312.02/314.02.

3-Hydroxy-4-isopropylbenzoic acid

Refer to Figure 110b (Chapter 5.2.4).

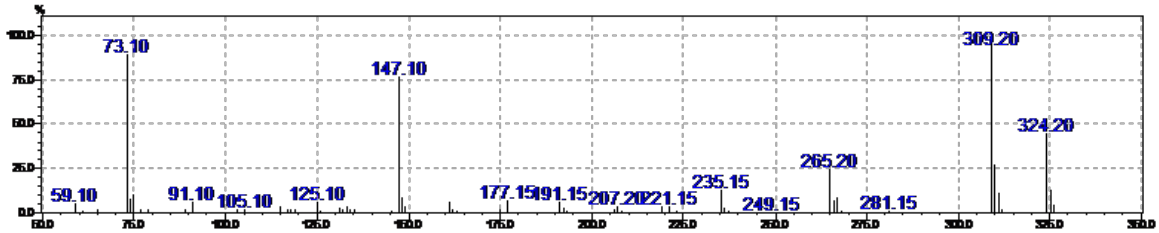

(a) 3-hydroxy-4-isopropylbenzoic acid. Observed m/z = 324.20 vs expected 324.16.

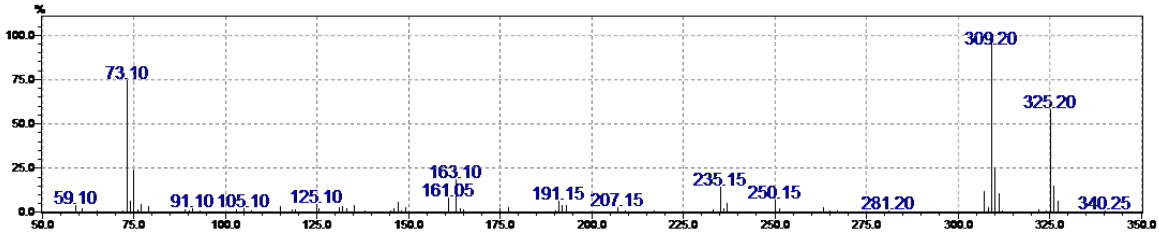

(b) 3-hydroxy-4-(1-methyl-1-hydroxyethyl)benzoic acid, double TMS-derivatised. Observed m/z = 340.25 vs expected 340.15.

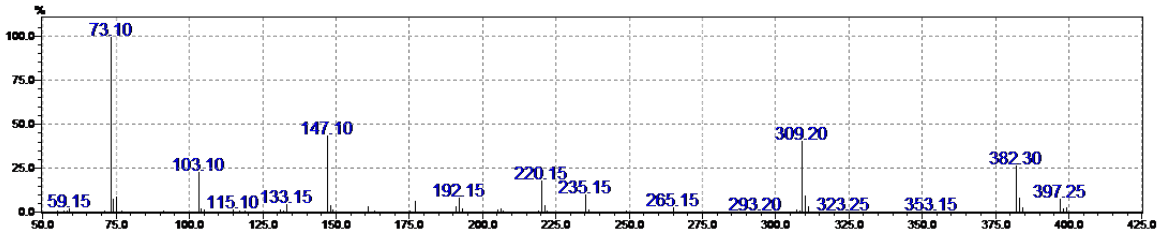

(c) 3-hydroxy-4-(1-methyl-1-hydroxyethyl)benzoic acid, triple TMS-derivatised. Observed m/z = 397.25 (- Me) vs expected 412.19.

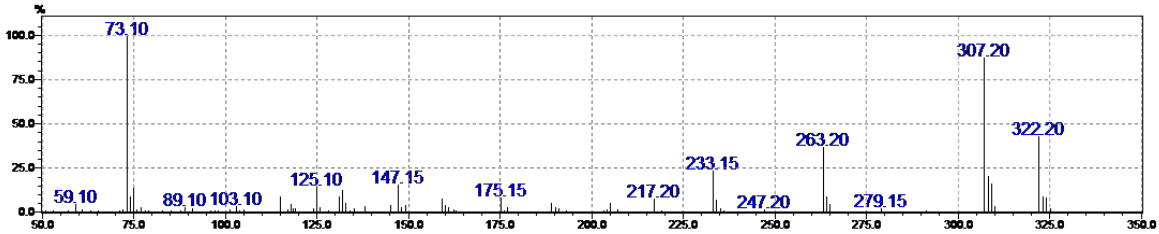

(d) 3-hydroxy-4-(prop-1-en-2-yl)benzoic acid. Observed m/z = 322.20 vs expected 322.14.

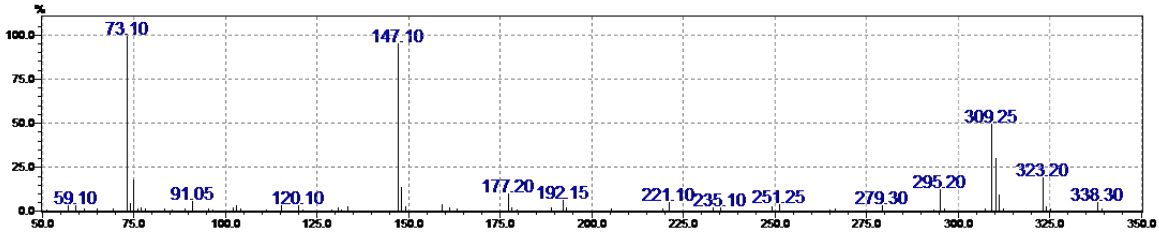

(e) 3-hydroxy-4-(2-methyloxiran-2-yl)benzoic acid. Observed m/z = 338.30 vs expected 338.14.

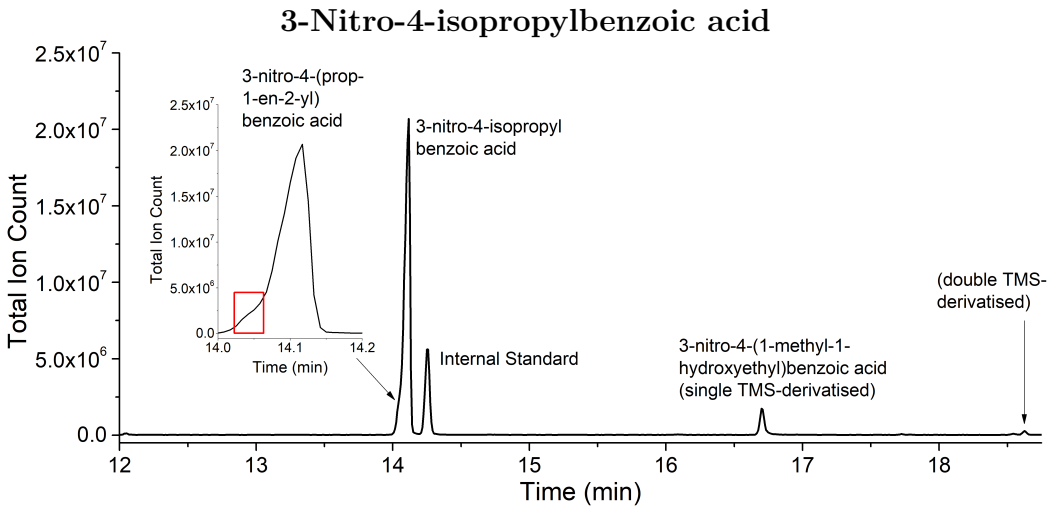

GC-MS analysis of *in vitro* 3-nitro-4-isopropylbenzoic acid turnover with CYP199A4.

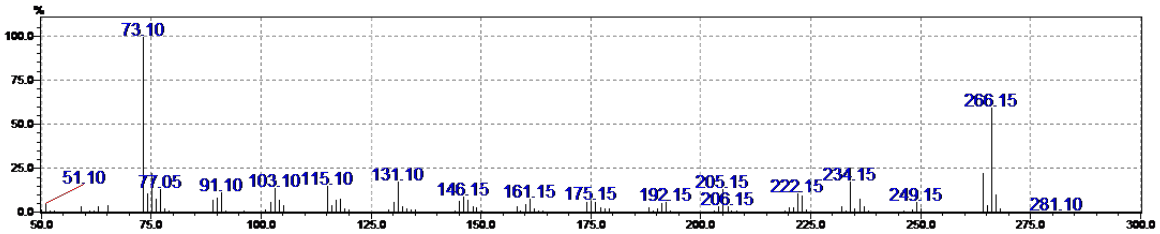

(a) 3-nitro-4-isopropylbenzoic acid. Observed m/z = 281.10 vs expected 281.11.

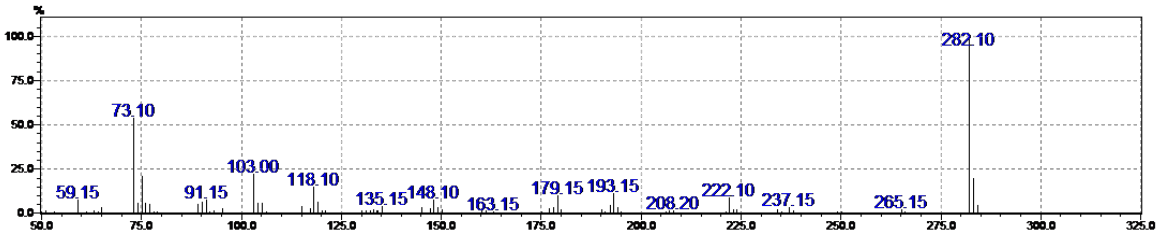

(b) 3-nitro-4-(1-methyl-1-hydroxyethyl)benzoic acid, single TMS-derivatised. Observed m/z = 282.10 (- Me) vs expected 297.10.

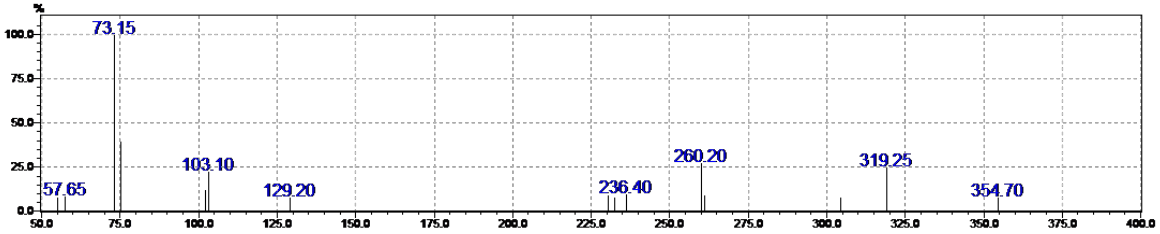

(c) 3-nitro-4-(1-methyl-1-hydroxyethyl)benzoic acid, double TMS-derivatised. Observed m/z = 354.70 (- Me) vs expected 369.14.

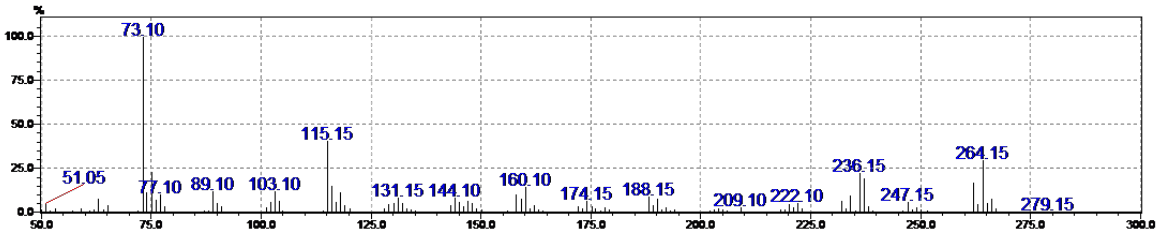

(d) 3-nitro-4-(prop-1-en-2-yl)benzoic acid. Observed m/z = 279.15 vs expected 279.09.

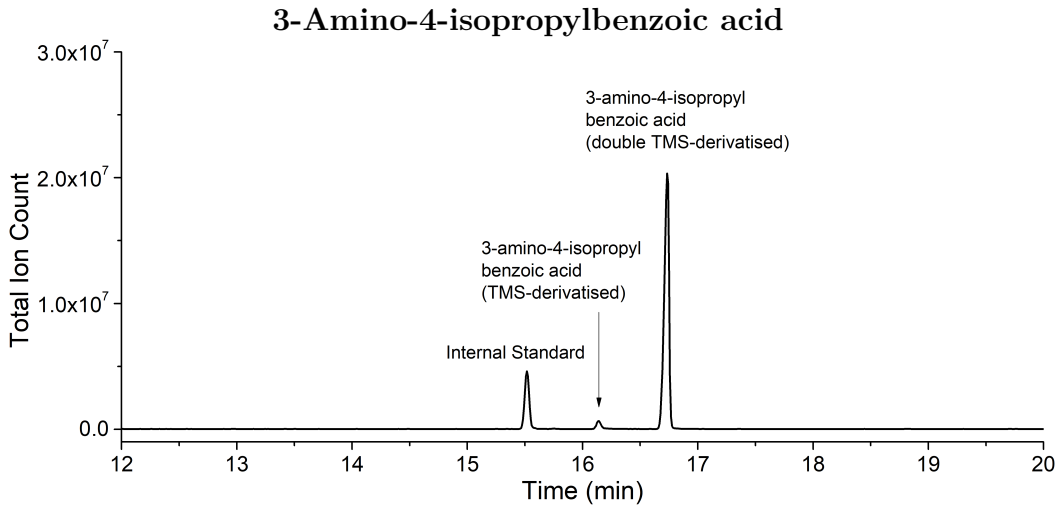

GC-MS analysis of *in vitro* 3-amino-4-isopropylbenzoic acid turnover with CYP199A4. No product peaks were observed.

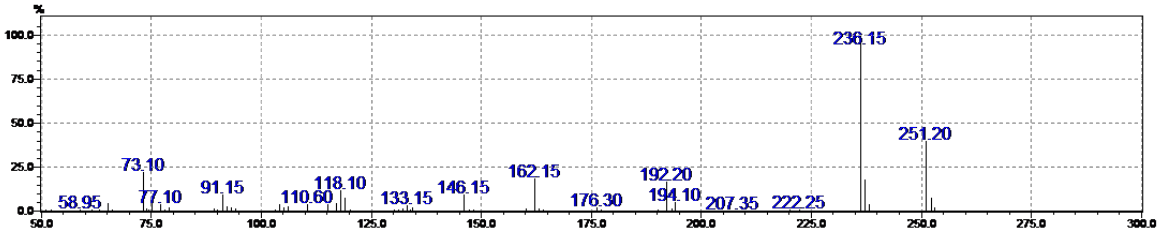

(a) 3-amino-4-isopropylbenzoic acid, single TMS-derivatised. Observed m/z = 251.20 vs expected 251.13.

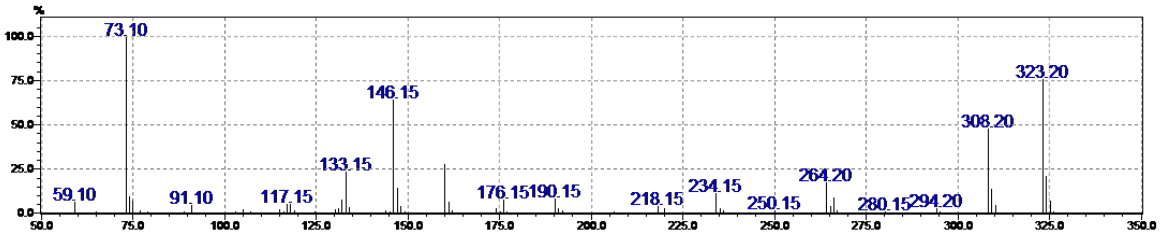

(b) 3-amino-4-isopropylbenzoic acid, double TMS-derivatised. Observed m/z = 323.20 vs expected 323.17.

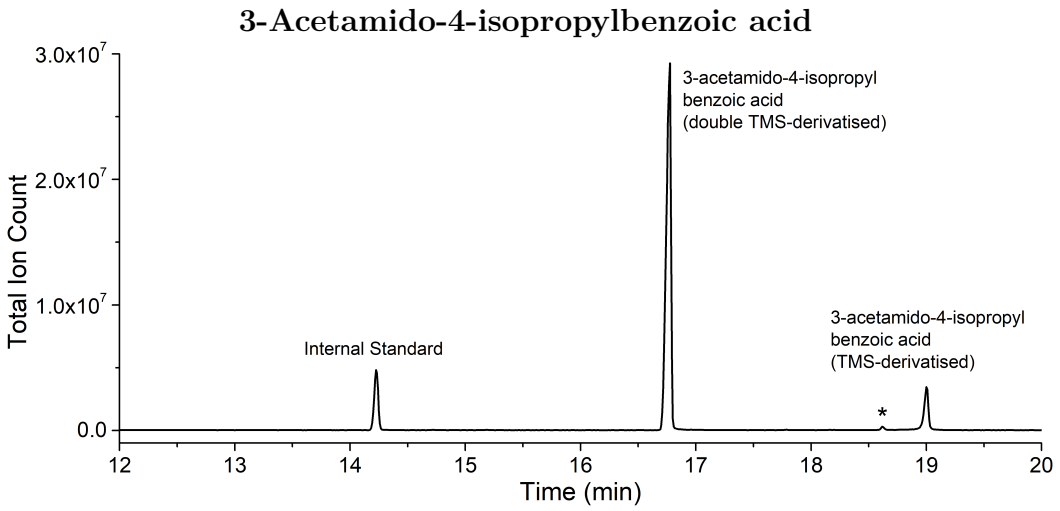

GC-MS analysis of *in vitro* 3-acetamido-4-isopropylbenzoic acid turnover with CYP199A4. No product peaks were observed.

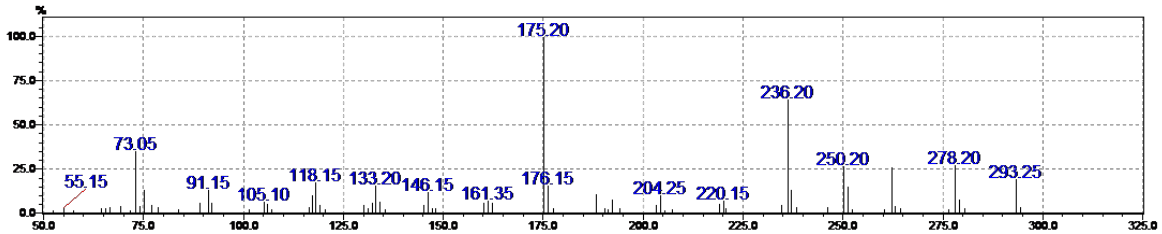

(a) 3-acetamido-4-isopropylbenzoic acid, single TMS-derivatised. Observed m/z = 293.25 vs expected 293.14.

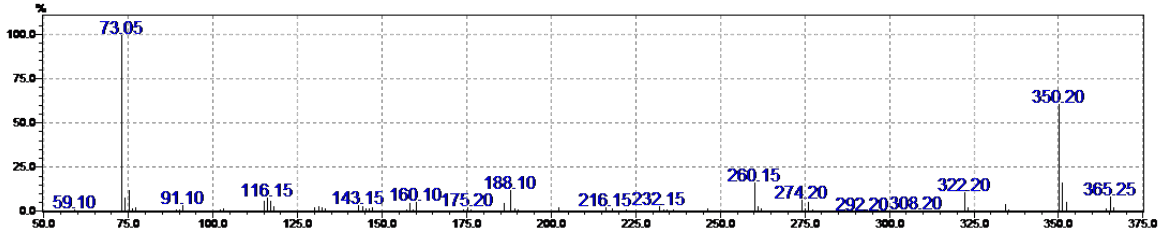

(b) 3-acetamido-4-isopropylbenzoic acid, double TMS-derivatised. Observed m/z = 365.25 vs expected 365.18.

C.4 NMR analysis

Product of 4-cyclopropylbenzoic acid

4-(1-Hydroxycyclopropyl)benzoic acid: 500 MHz, d_6-DMSO.

^{1}H: δ 1.02 (dd, 2H, J = 5.0, 7.1 Hz, **7**), 1.17 (dd, 2H, J = 5.0, 7.1 Hz, **7**), 6.09 (s, 1H, **8**), 7.32 (d, 2H, J = 8.2 Hz, **3**), 7.85 (d, 2H, J = 8.2 Hz, **4**).

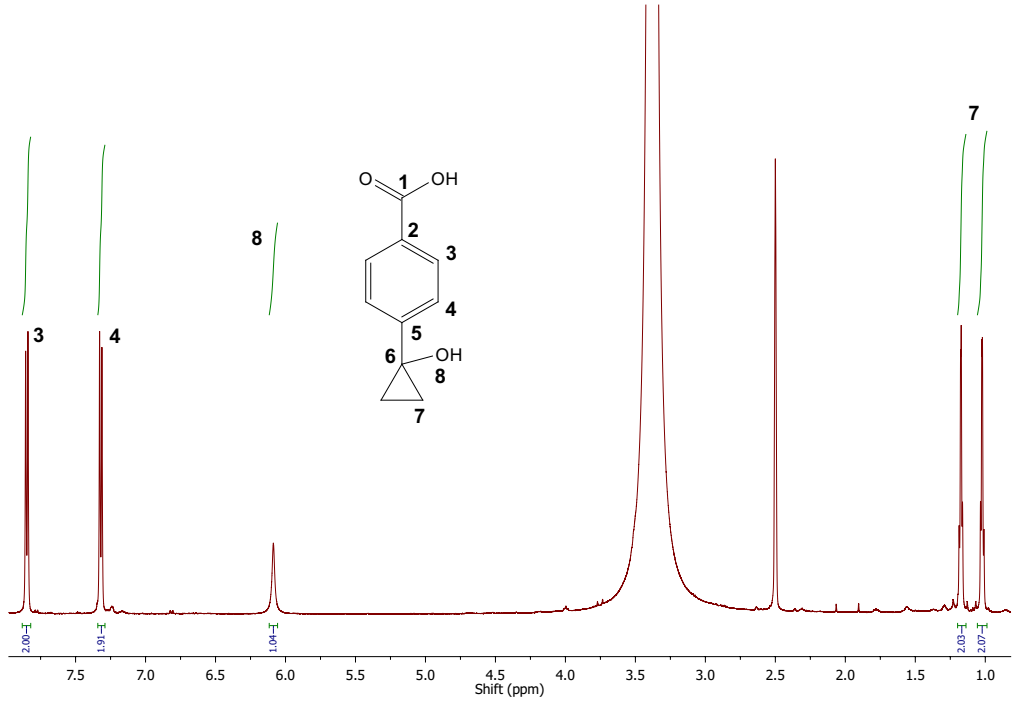

^{13}C: δ 22.4 (**7**), 57.4 (**6**), 126.7 (**4**), 130.8 (**5**), 132.2 (**3**), 154.9 (**2**), 170.5 (**1**).

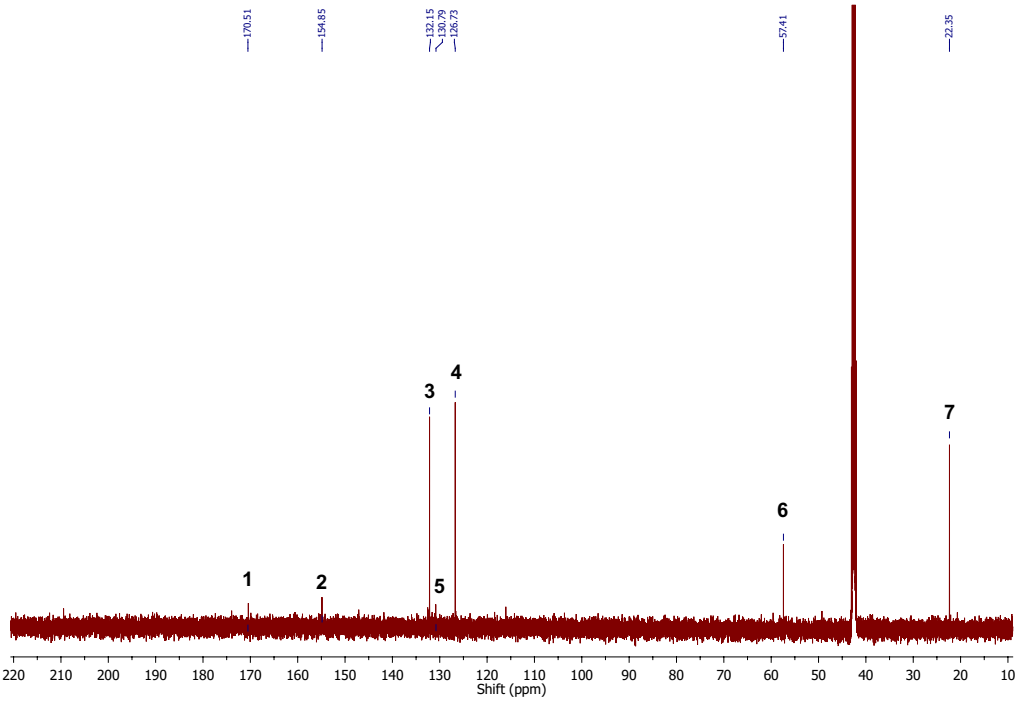

^{1}H-^{1}H COSY:

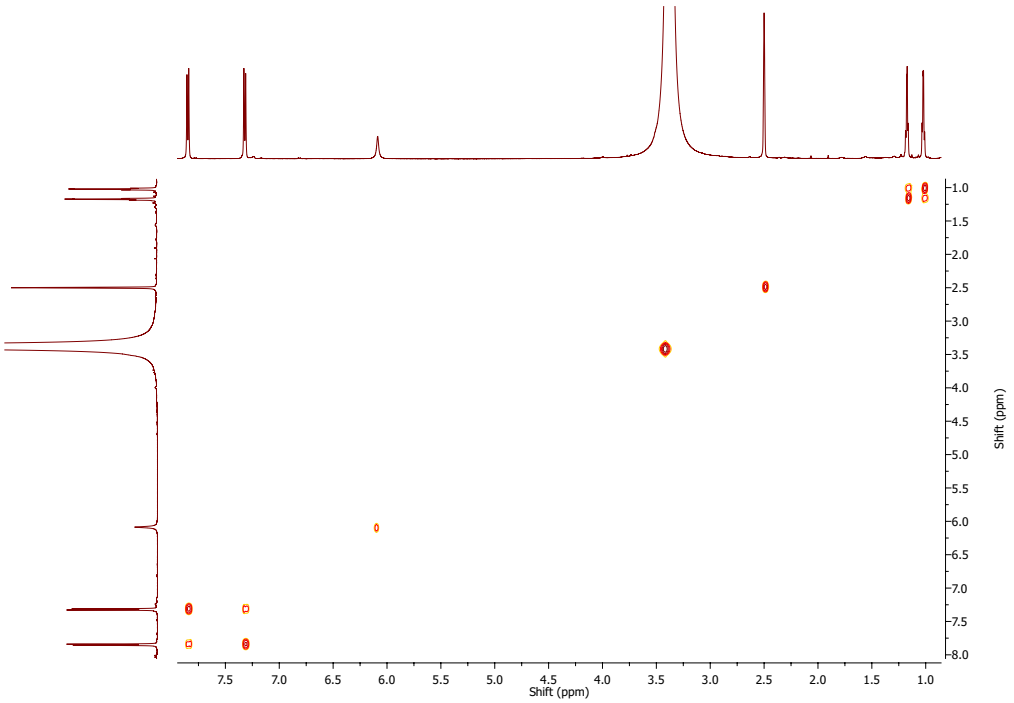

^{1}H-^{13}C HSQC:

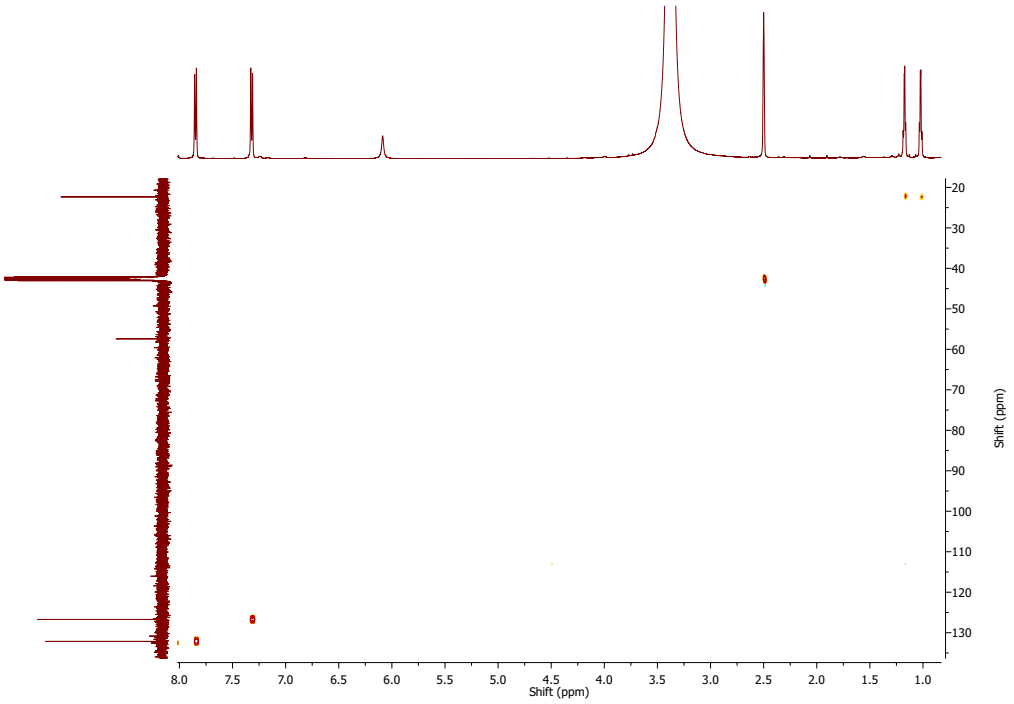

Products of 4-*n*-butylbenzoic acid

4-(E)-4-(3-hydroxybut-1-en-1-yl)benzoic acid: 500 MHz, $CDCl_3$.
^{1}H: δ 1.40 (d, 3H, J = 6.4 Hz, **9**), 4.52-4.57 (m, 1H, **8**), 6.42 (dd, 1H, J = 15.9, 6.0 Hz, **7**), 6.66 (d, 1H, J = 15.9 Hz, **6**), 7.47 (d, 2H, J = 8.2 Hz, **4**), 8.05 (d, 2H, J = 8.2 Hz, **3**).

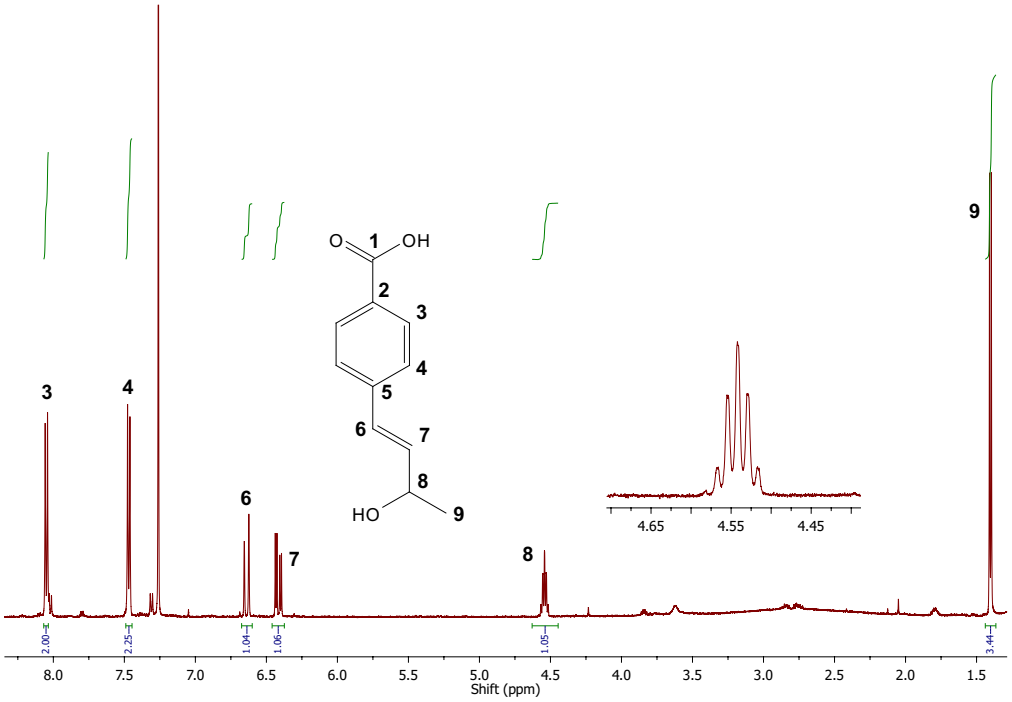

^{13}C: δ 23.4 (**9**), 68.7 (**8**), 126.4 (**4**), 127.9 (**5**), 128.2 (**6**), 130.6 (**3**), 136.6 (**7**), 142.0 (**2**). The quartenary COOH carbon was not observed.

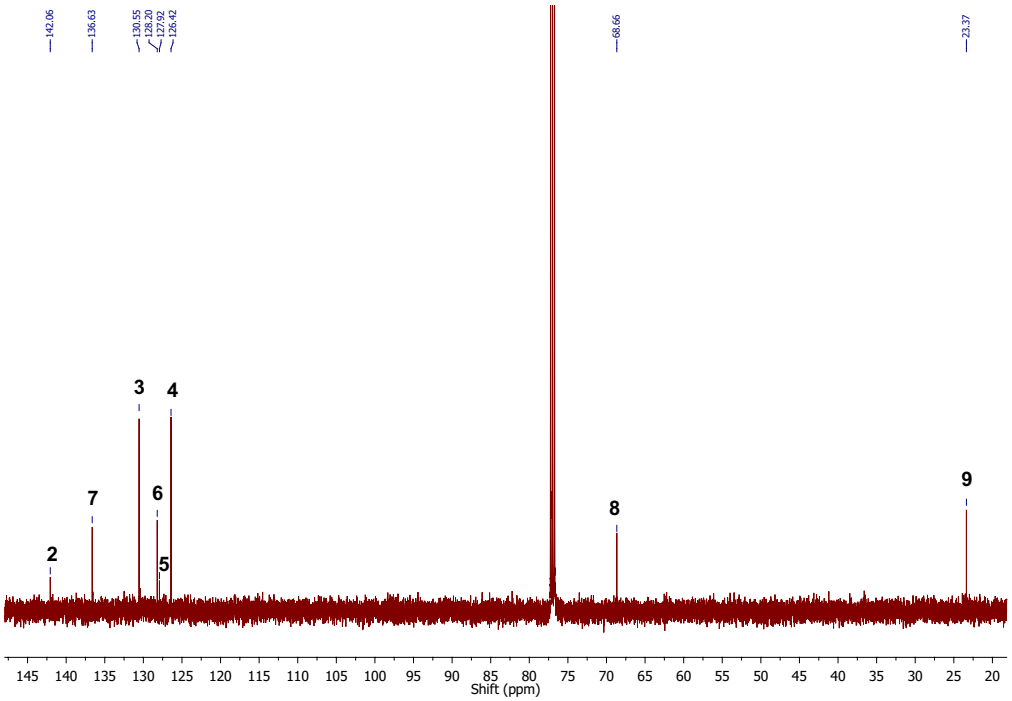

^{1}H-^{1}H COSY:

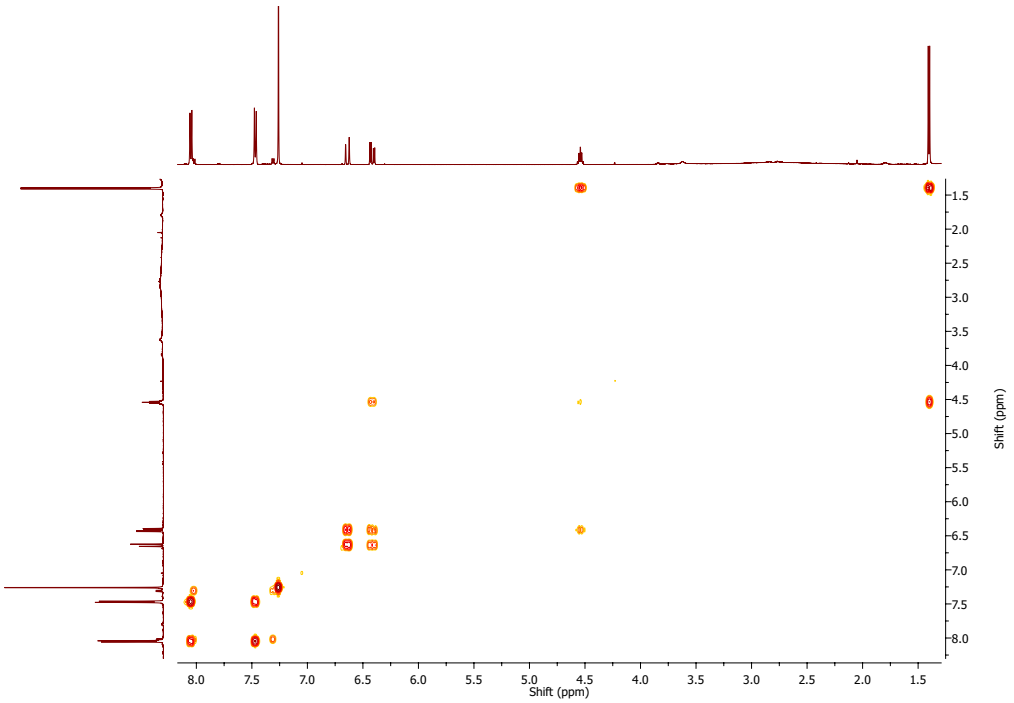

^{1}H-^{13}C HSQC:

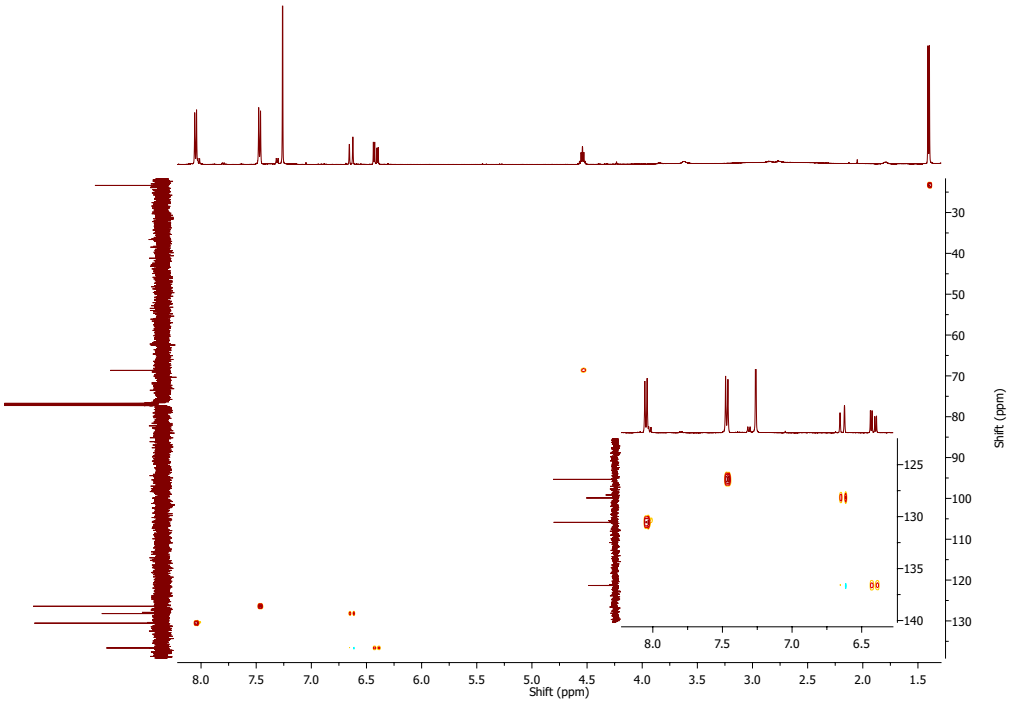

4-(1-hydroxybutyl)benzoic acid: 500 MHz, $CDCl_3$.
^{1}H: δ 0.95 (t, 3H, J = 7.4 Hz, **9**), 1.30-1.50 (m, 2H, **8**), 1.67-1.82 (m, 2H, **7**), 4.79 (dd, 1H, J = 5.9, 7.2 Hz, **6**), 7.46 (d, 2H, J = 8.2 Hz, **4**), 8.09 (d, 2H, J = 8.2 Hz, **3**).

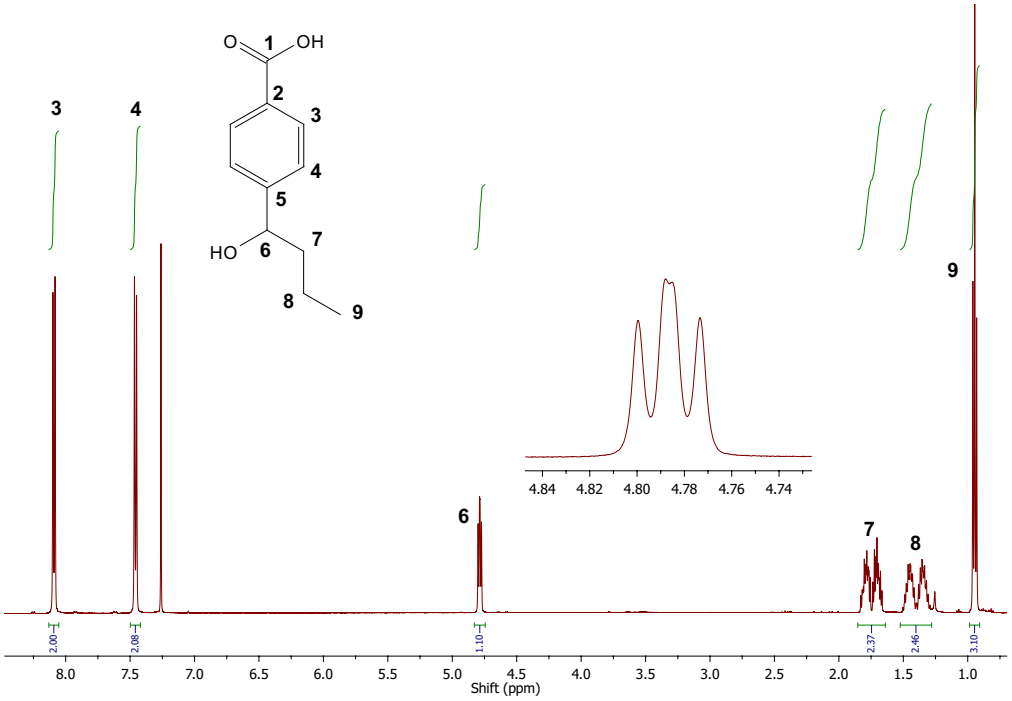

^{13}C: δ 13.9 (**9**), 18.8 (**8**), 41.3 (**7**), 73.9 (**6**), 125.9 (**4**), 128.3 (**5**), 130.4 (**3**), 151.0 (**2**), 171.2 (**1**).

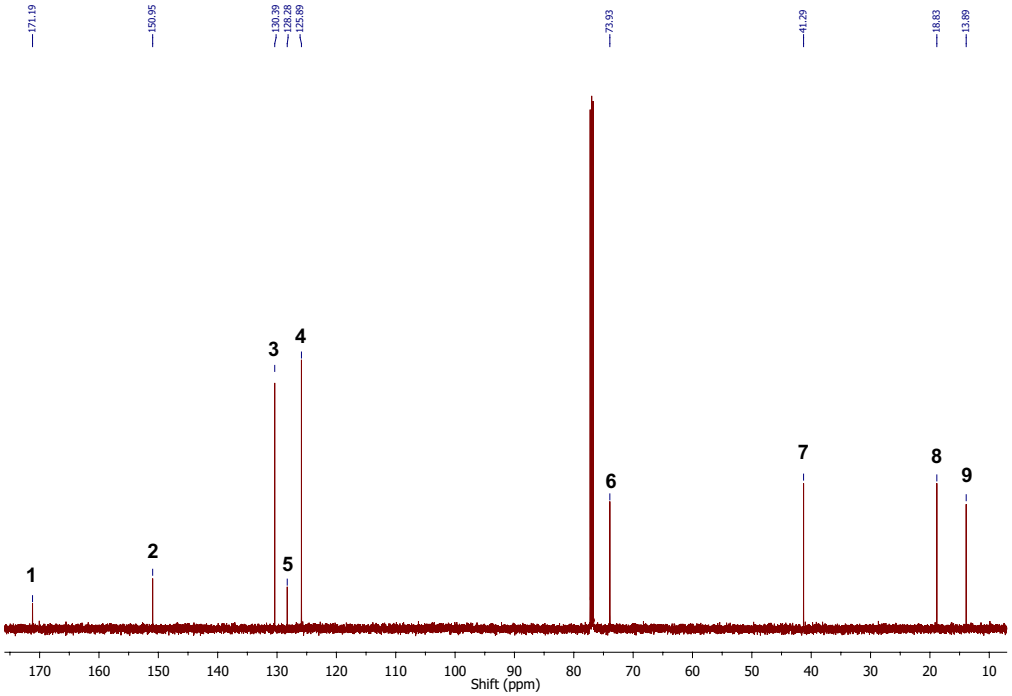

^{1}H-^{1}H COSY:

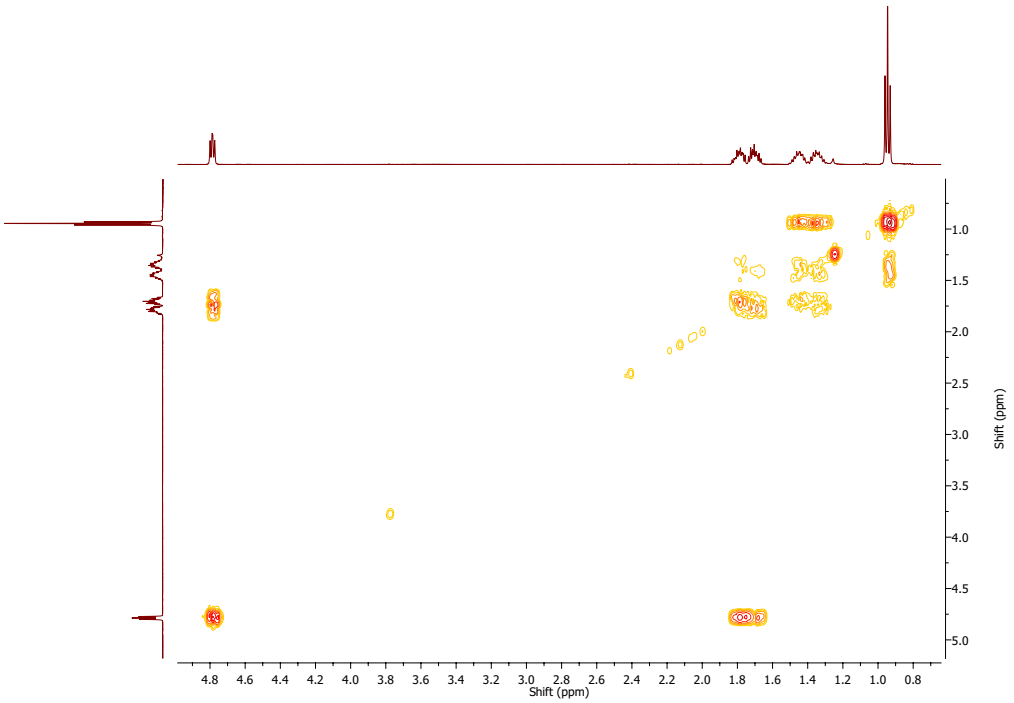
1.0
1.5
2.0
2.5
3.0
3.5
4.0
4.5
5.0
Shift (ppm)
4.8 4.6 4.4 4.2 4.0 3.8 3.6 3.4 3.2 3.0 2.8 2.6 2.4 2.2 2.0 1.8 1.6 1.4 1.2 1.0 0.8
Shift (ppm)

(E)-4-(but-1-en-1-yl)benzoic acid: 500 MHz, $CDCl_3$.
^{1}H: δ 1.12 (t, 3H, J = 7.4 Hz, **9**), 2.28 (dq, 2H, J = 4.7, 7.4 Hz, **8**), 6.42-6.44 (m, 2H, **6/7**), 7.43 (d, 2H, J = 8.3 Hz, **4**), 8.04 (d, 2H, J = 8.3 Hz, **3**).

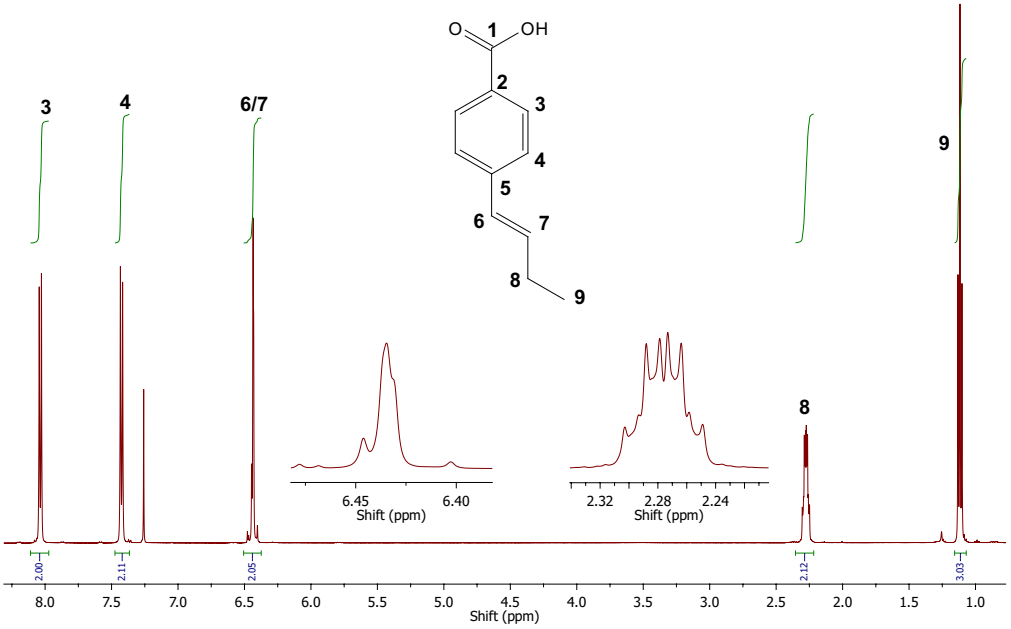

^{13}C: δ 13.4 (**9**), 26.2 (**8**), 125.8 (**4**), 127.3 (**5**), 128.1 (**6**), 130.5 (**3**), 136.1 (**7**), 143.4 (**2**), 171.8 (**1**).

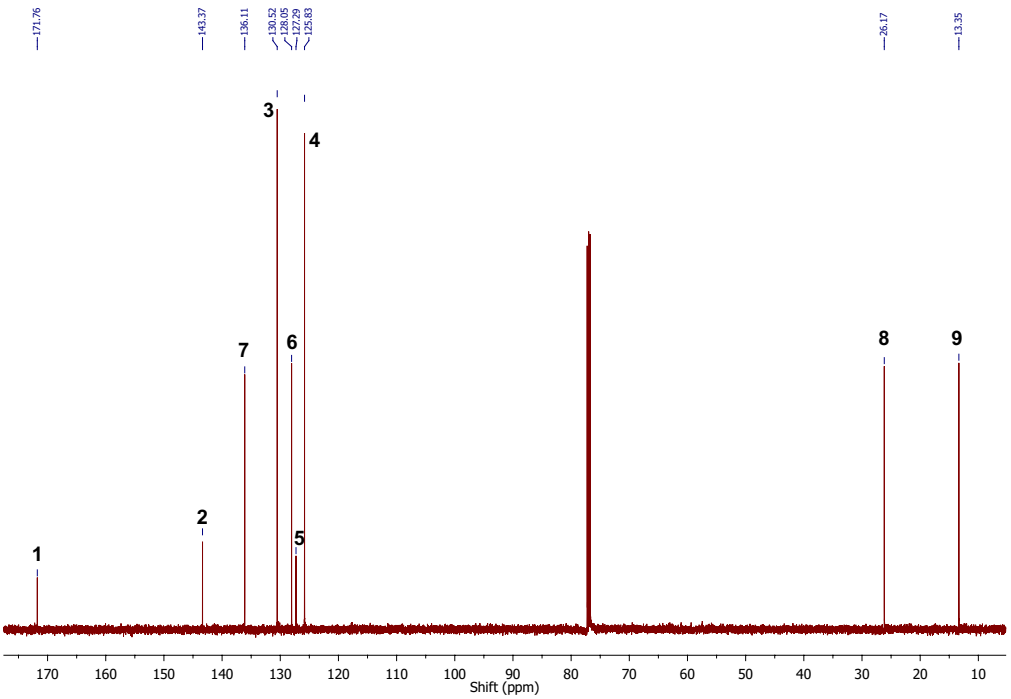

^{1}H-^{1}H COSY:

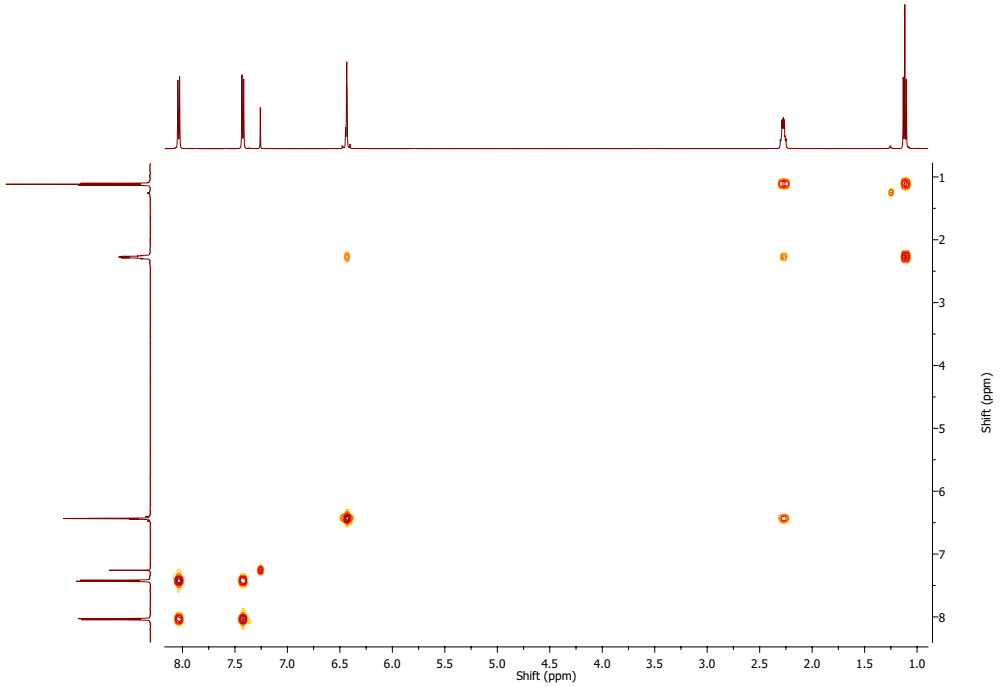
8.0
7.5
7.0
6.5
6.0
5.5
5.0
4.5
4.0
3.5
3.0
2.5
2.0
1.5
1.0
Shift (ppm)
1
2
3
4
5
6
7
8
Shift (ppm)

Products of 4-isobutylbenzoic acid

4-(2-hydroxy-2-methylpropyl)benzoic acid: 500 MHz, $CDCl_3$.
^{1}H: δ 1.26 (s, 6H, **8**), 2.85 (s, 2H, **6**), 7.34 (d, 2H, J = 8.1 Hz, **4**), 8.05 (d, 2H, J = 8.1 Hz, **3**).

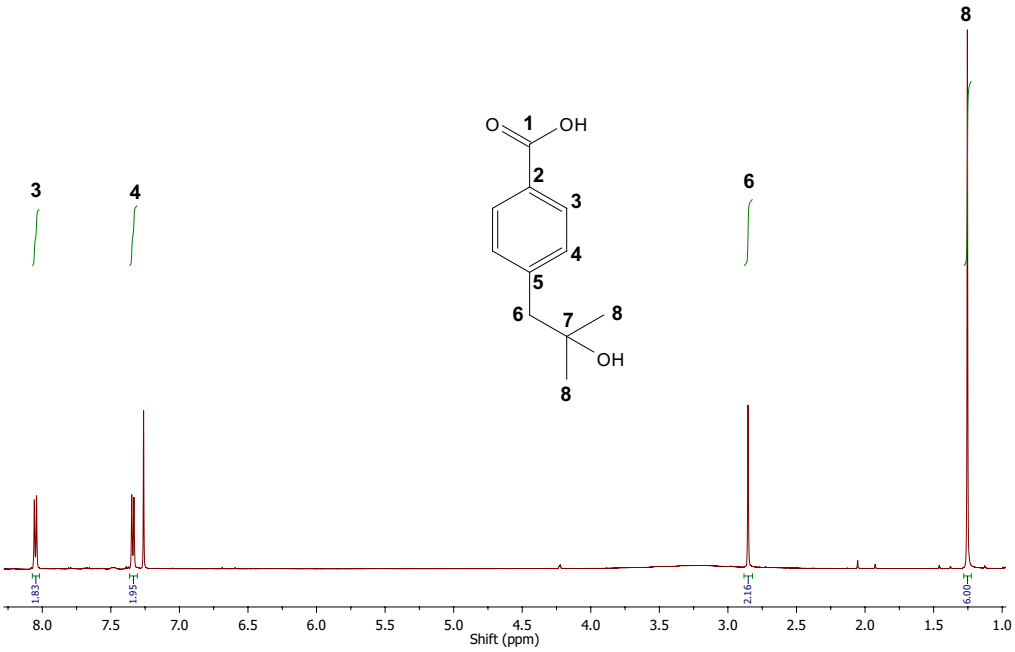

^{13}C: δ 29.3 (**8**), 49.7 (**6**), 71.0 (**7**), 127.5 (**5**), 130.0 (**4**), 130.6 (**3**), 144.3 (**2**), 171.1 (**1**).

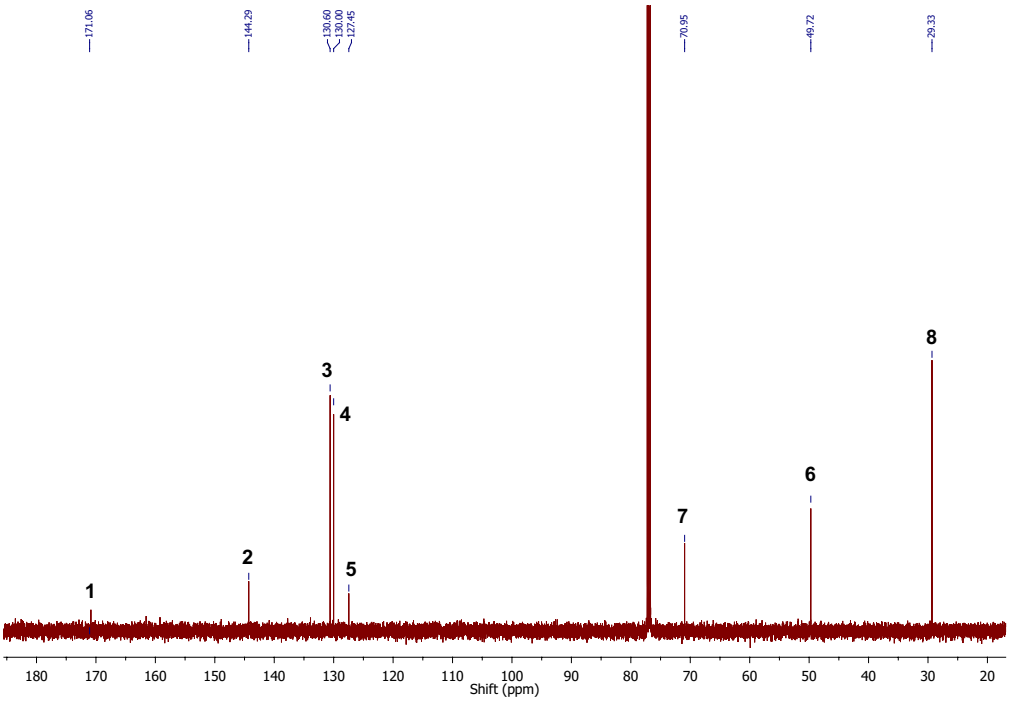

^{1}H-^{1}H COSY:

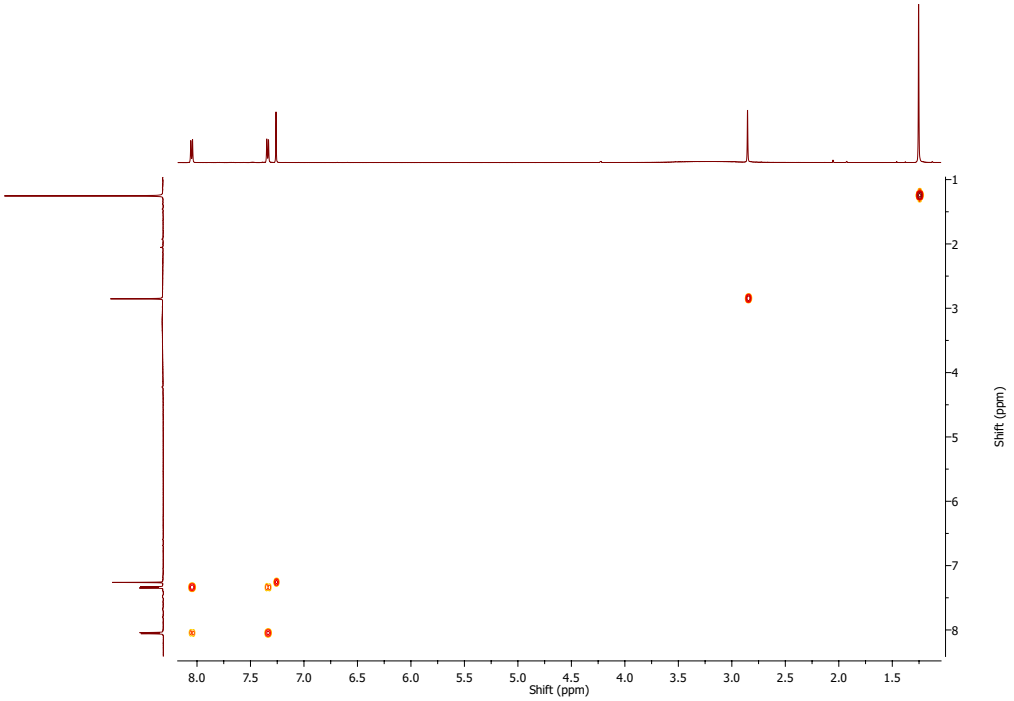
8.0
7.5
7.0
6.5
6.0
5.5
5.0
4.5
4.0
3.5
3.0
2.5
2.0
1.5
Shift (ppm)
1
2
3
4
5
6
7
8
Shift (ppm)

4-(1-hydroxy-2-methylpropyl)benzoic acid: 500 MHz, $CDCl_3$.
^{1}H: δ 0.85 (d, 3H, J = 6.8 Hz, **8/9**), 0.98 (d, 3H, J = 6.7 Hz, **8/9**), 1.99 (dq, 1H, J = 6.5, 6.6 Hz, **7**), 4.50 (d, 1H, J = 6.3 Hz, **6**), 7.43 (d, 2H, J = 8.1 Hz, **4**), 8.09 (d, 2H, J = 8.1 Hz, **3**).

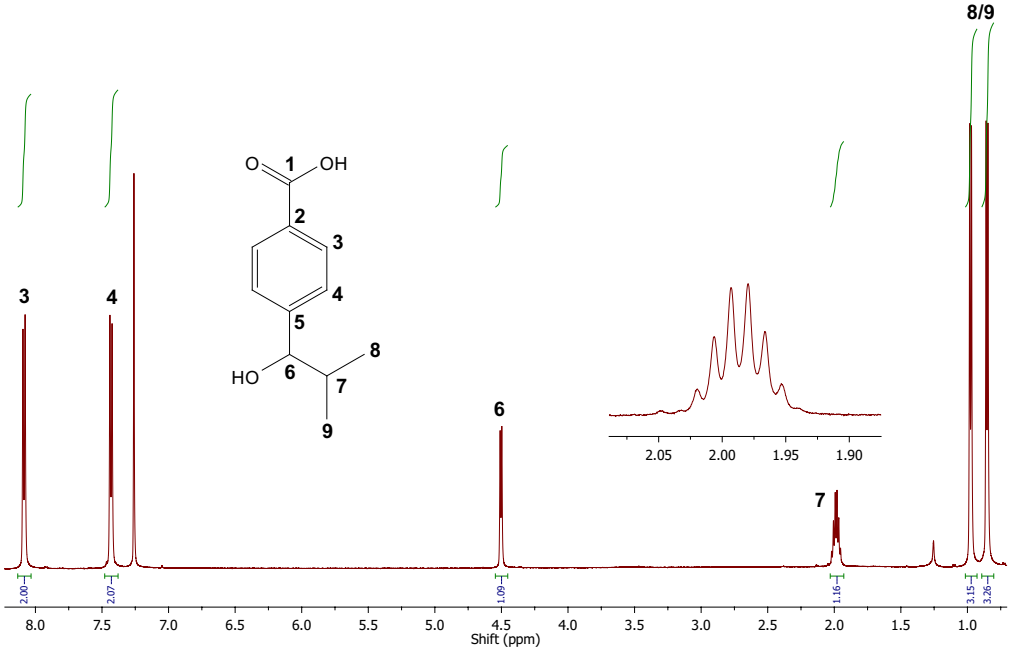

^{13}C: δ 17.7 (**8/9**), 18.9 (**8/9**), 36.3 (**7**), 79.3 (**6**), 126.6 (**4**), 128.2 (**5**), 130.1 (**3**), 149.7 (**2**), 171.0 (**1**).

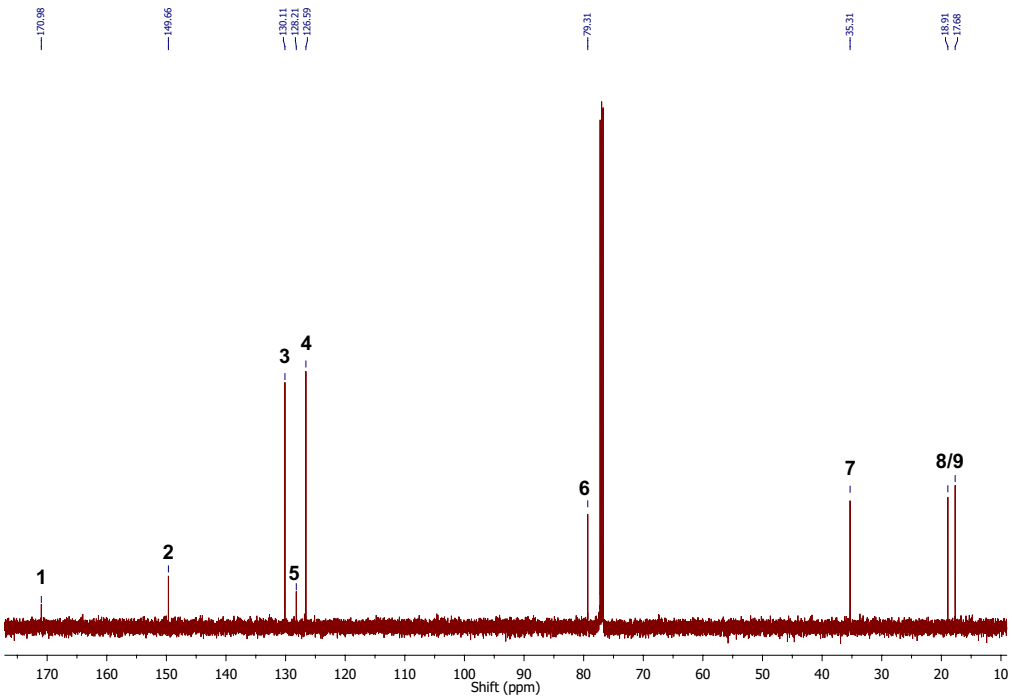

^{1}H-^{1}H COSY:

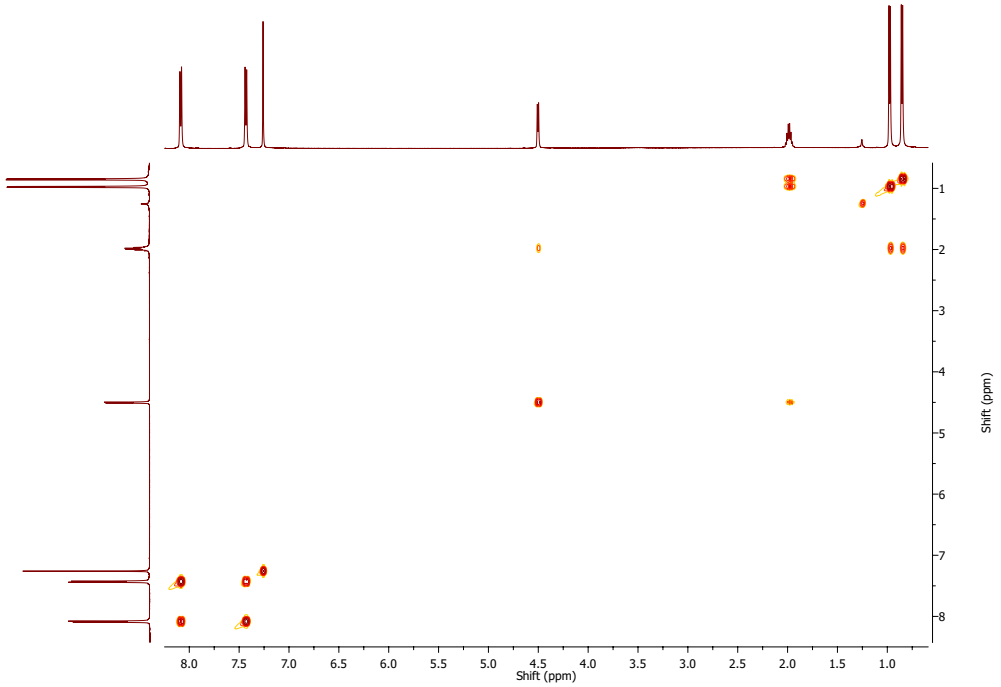
Shift (ppm)
8.0
7.5
7.0
6.5
6.0
5.5
5.0
4.5
4.0
3.5
3.0
2.5
2.0
1.5
1.0
Shift (ppm)
1
2
3
4
5
6
7
8

4-(2-methylprop-1-en-1-yl)benzoic acid: 500 MHz, $CDCl_3$.

A ^{13}C spectrum was not able to be obtained.

^1H: δ 1.90 (s, 3H, **8/9**), 1.94 (s, 3H, **8/9**), 6.31 (s, 1H, **6**), 7.31 (d, 2H, **4**), 8.03 (d, 2H, **3**).

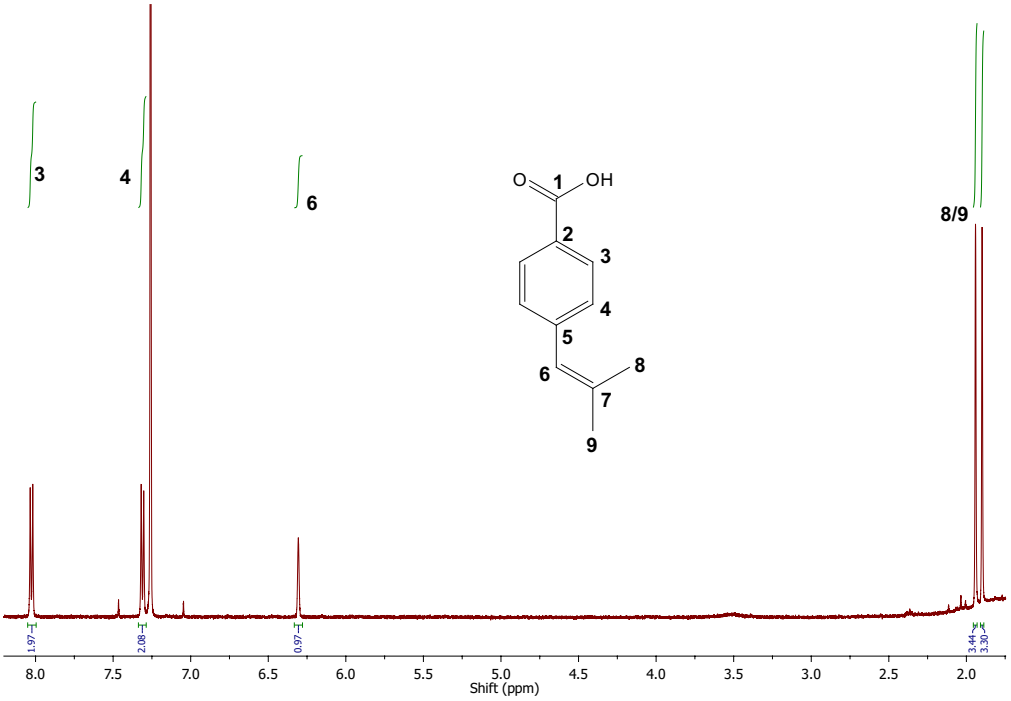

^1H-^1H COSY:

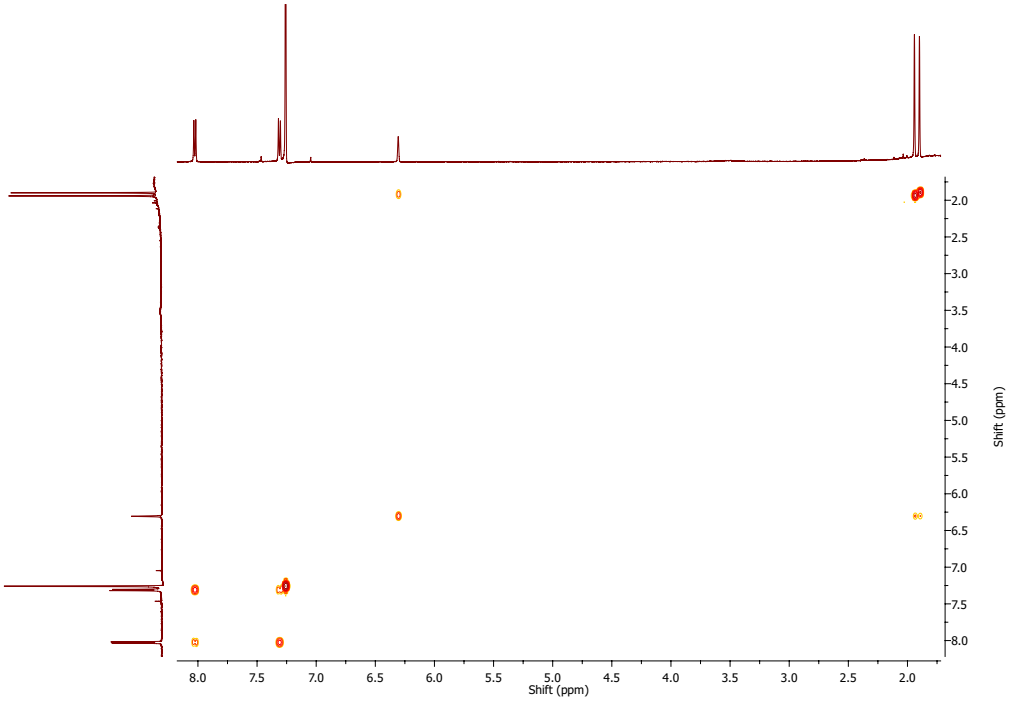

Products of 4-cyclohexylbenzoic acid

4-(2-hydroxycyclohexyl)benzoic acid: 500 MHz, d_6-DMSO.
^{1}H: δ 1.22-1.28 (m, 2H), 1.31-1.37 (m, 1H), 1.43 (dq, 1H, J = 2.7, 12.6 Hz), 1.95 (dd, 1H, J = 2.7, 12.0 Hz), 2.42 (ddd, 1H, J = 2.9, 11.1, 11.1 Hz, **6**), 3.51 (m, 1H, **7**), 4.36 (d, 1H, J = 5.7 Hz, **12**), 7.33 (d, 2H, J = 8.1 Hz, **4**), 7.84 (d, 2H, J = 8.1 Hz, **3**).

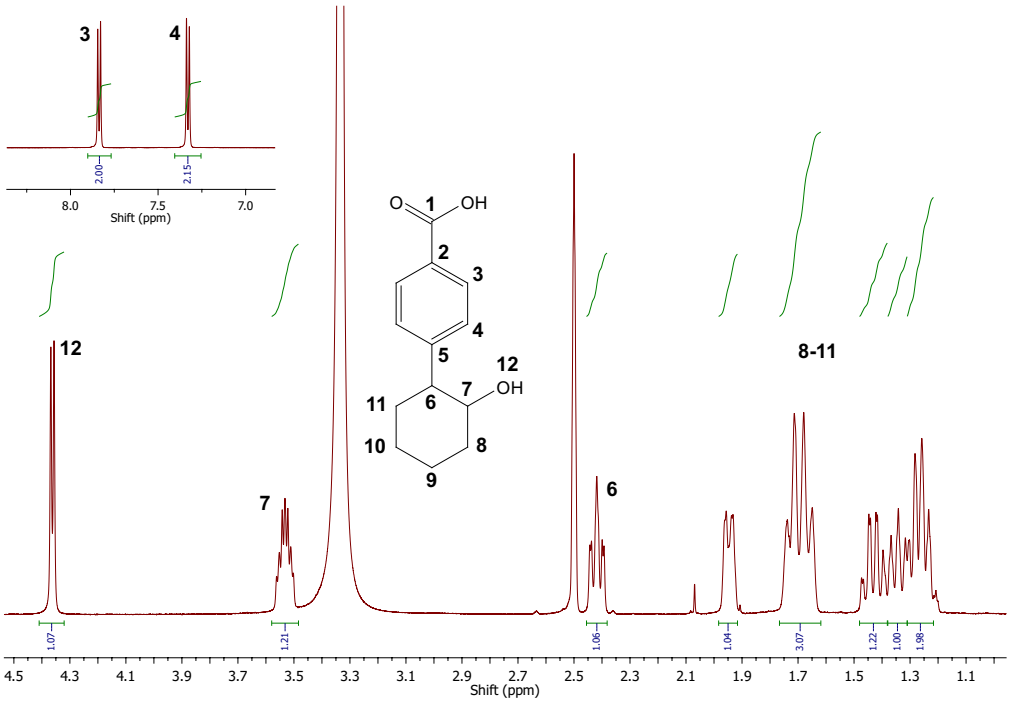

^{13}C: δ (27.8, 28.8, 36.6, 39.2 - **8-11**), 55.4 (**6**), 75.3 (**7**), 131.1 (**4**), 131.4 (**5**), 132.2 (**3**), 153.9 (**2**), 170.5 (**1**).

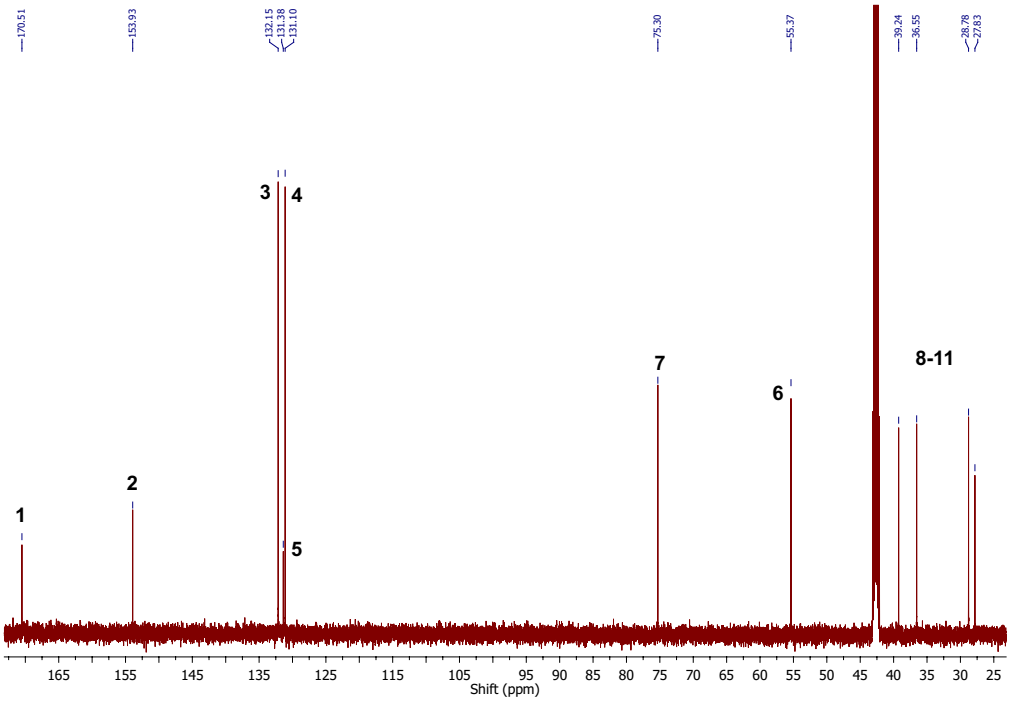

^{1}H-^{1}H COSY:

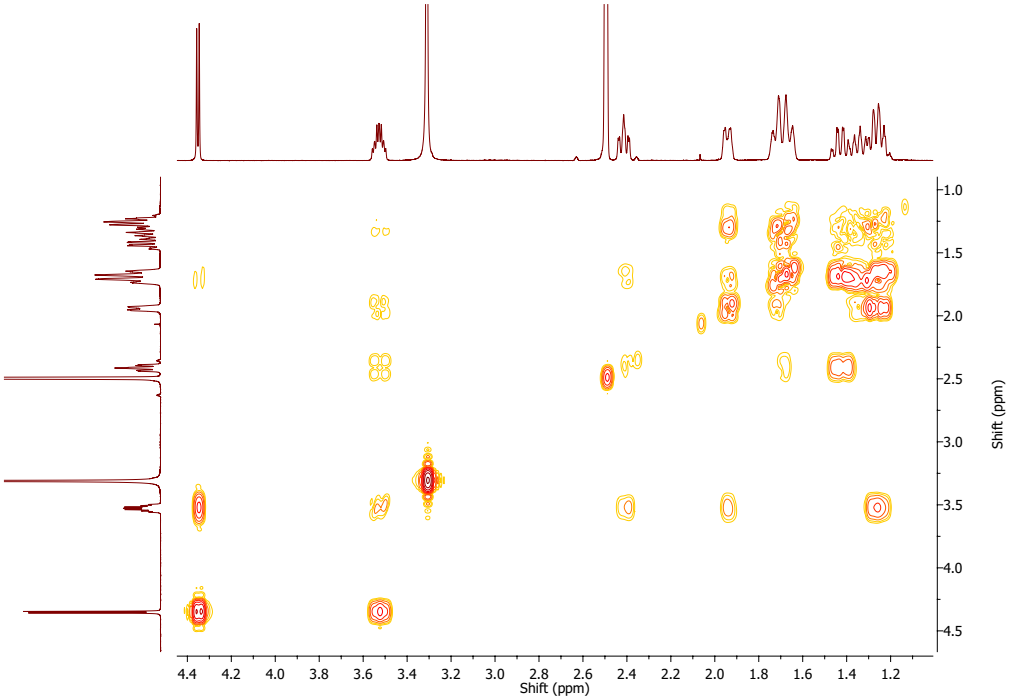

^{1}H-^{13}C HSQC:

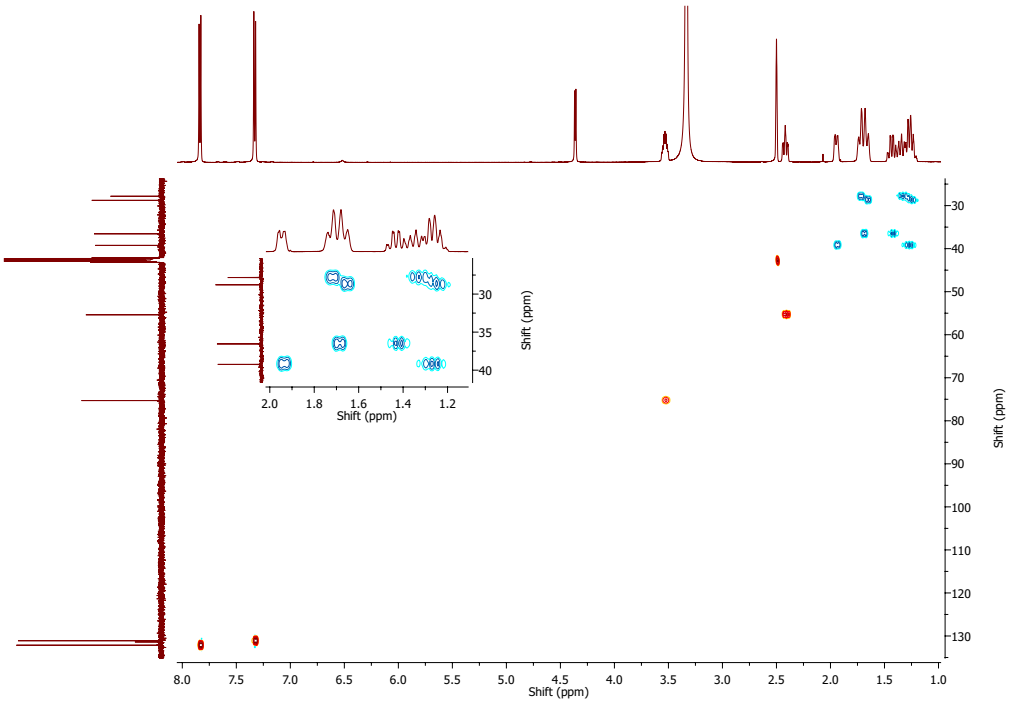

4-(1-hydroxycyclohexyl)benzoic acid: 500 MHz, d_6-DMSO.
^{1}H: δ 1.21-1.29 (m, 1H, **9**), 1.47-1.52 (m, 2H, **8** x 2), 1.57-1.61 (m, 2H, **7** x 2), 1.63-1.67 (m, 1H, **9**) 1.68-1.76 (m, 4H, **7,8** x 2 each), 4.83 (s, 1H, **10**), 7.59 (d, 2H, J = 8.3 Hz, **4**), 7.87 (d, 2H, J = 8.3 Hz, **3**).

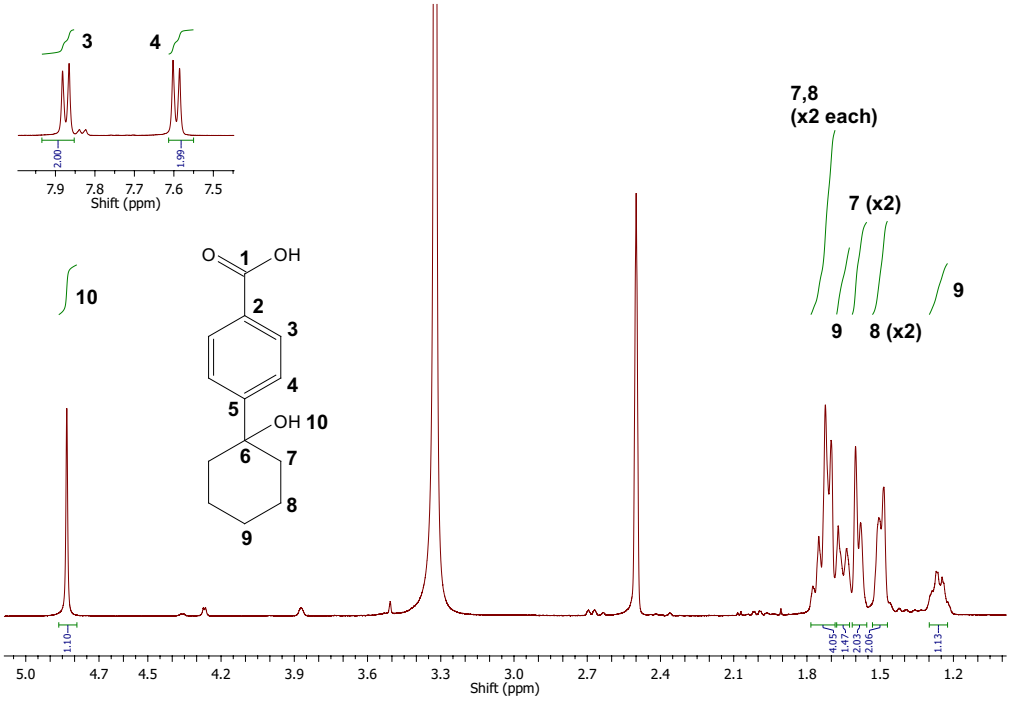

^{13}C: δ 24.7 (**8**), 28.2 (**9**), 41.2 (**7**), 74.8 (**6**), 128.1 (**4**), 131.6 (**5**), 132.0 (**3**), 159.3 (**2**), 170.4 (**1**).

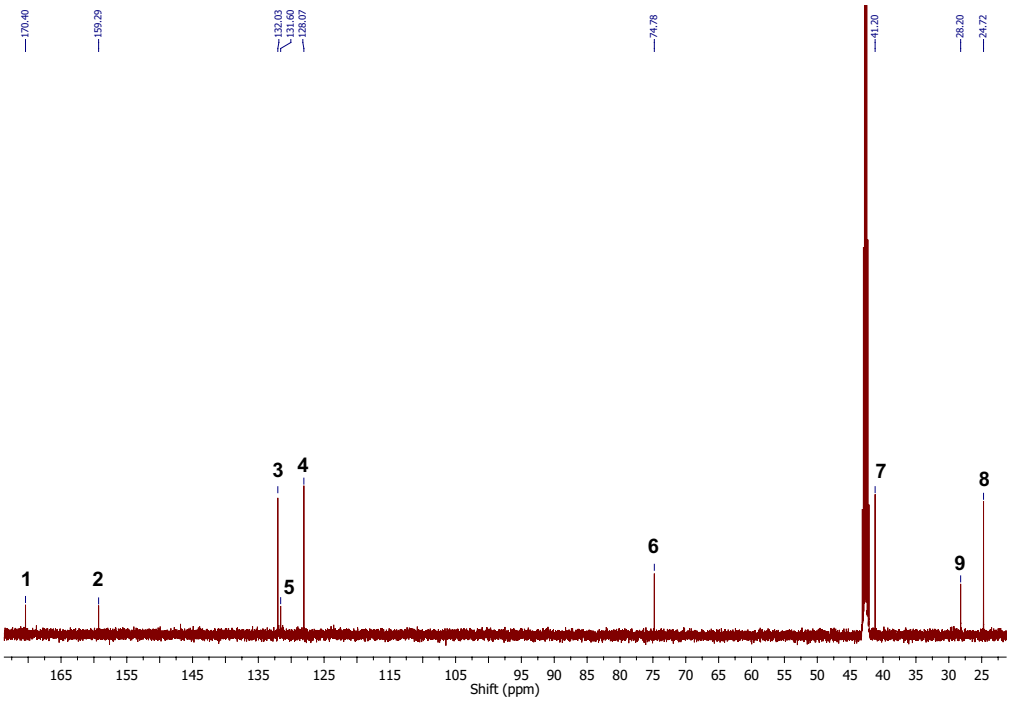

^{1}H-^{1}H COSY:

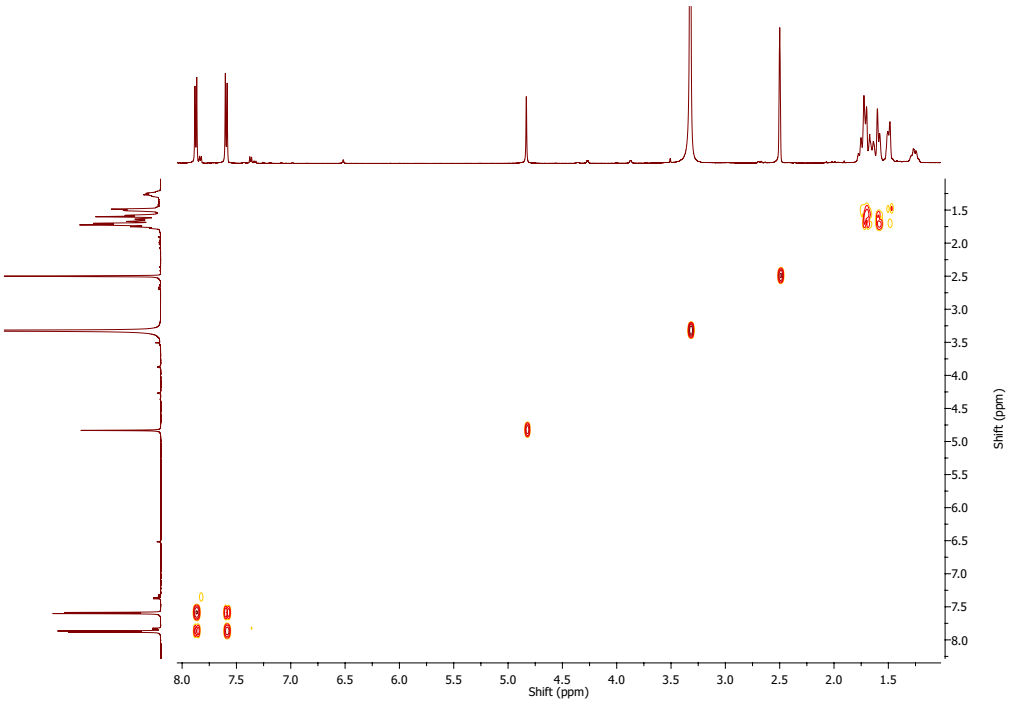

^{1}H-^{13}C HSQC:

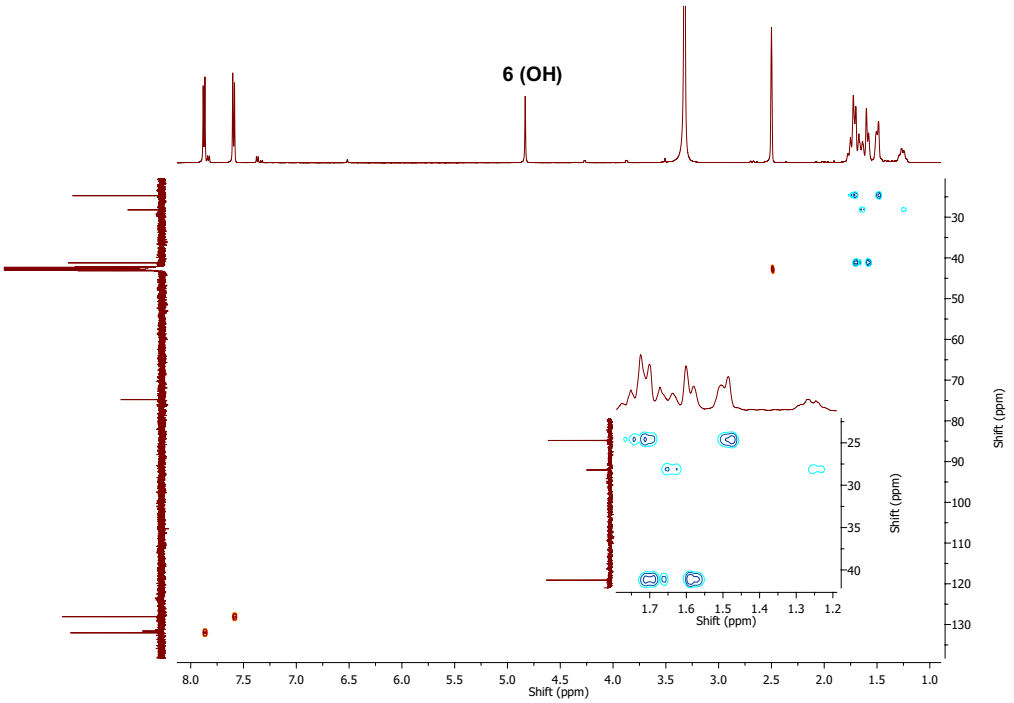

Products of 4-*n*-heptylbenzoic acid

4-(2-hydroxyheptyl)benzoic acid: 500 MHz, $CDCl_3$.
^{1}H: δ 0.91 (t, 3H, J = 6.8 Hz, **12**), 1.27-1.40 (m, 5H, **9-11**), 1.48-1.55 (m, 3H, **8,10**) 2.77 (dd, 1H, J = 8.3, 13.6 Hz, **6**), 2.91 (dd, 1H, J = 4.3, 13.6 Hz, **6**), 3.86-3.91 (m, 1H, **7**), 7.35 (d, 2H, J = 8.1 Hz, **4**), 8.06 (d, 2H, J = 8.1 Hz, **3**).

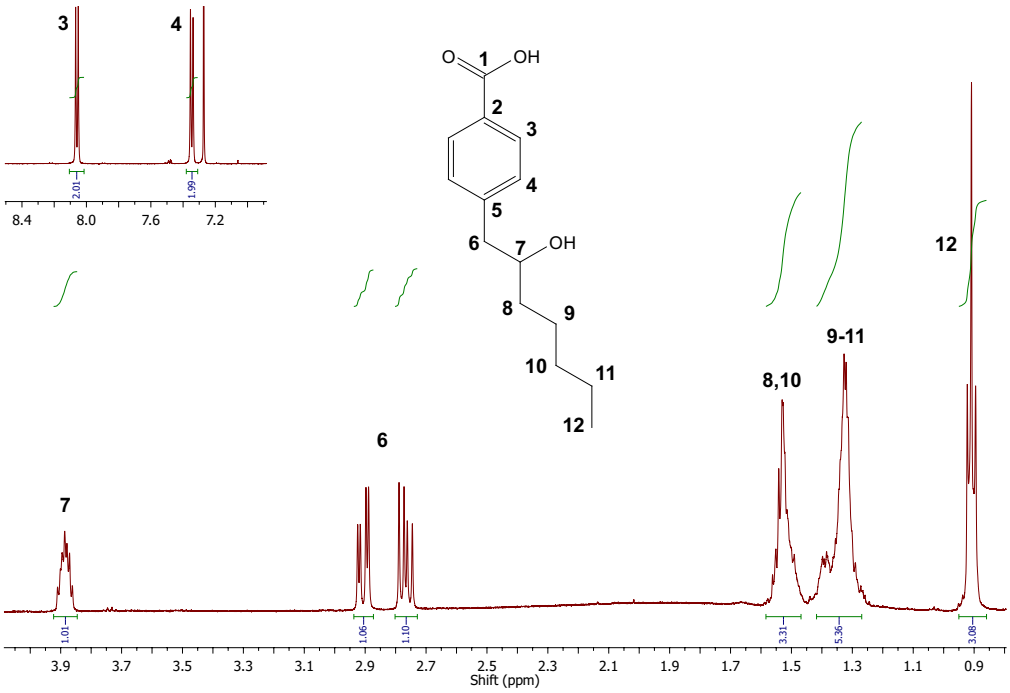

^{13}C: δ 16.7 (**12**), 25.3 (**11**), 28.0 (**10**), 34.4 (**9**), 39.7 (**8**), 46.7 (**6**), 75.2 (**7**), 130.0 (**5**), 132.3 (**4**), 133.1 (**3**), 148.0 (**2**). The quartenary COOH carbon was not observed.

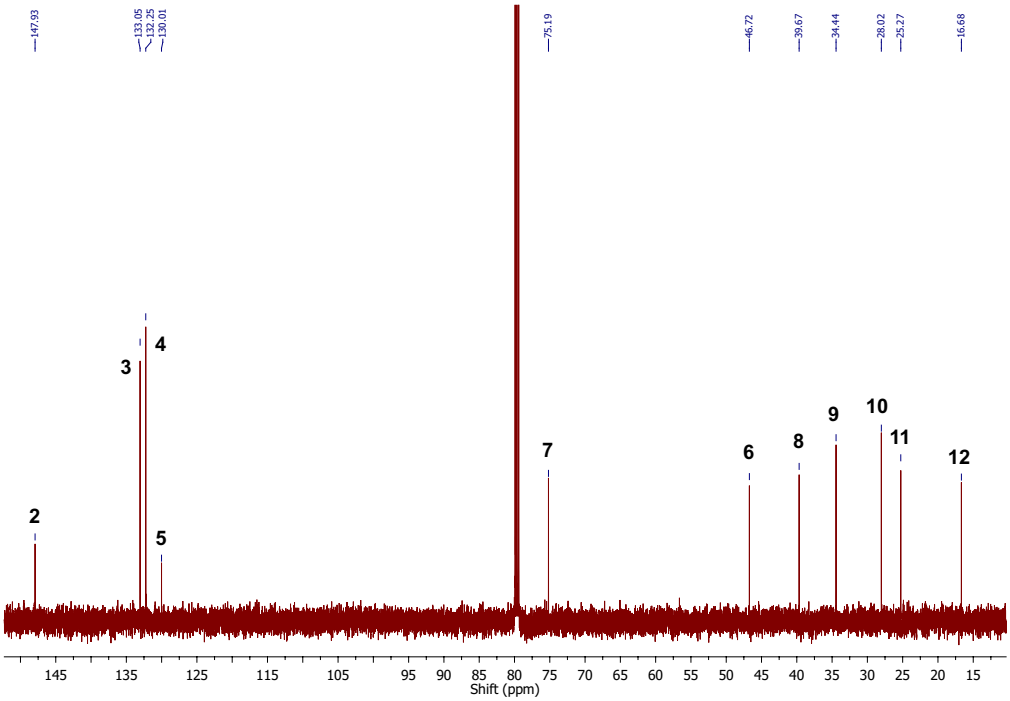

^{1}H-^{1}H COSY:

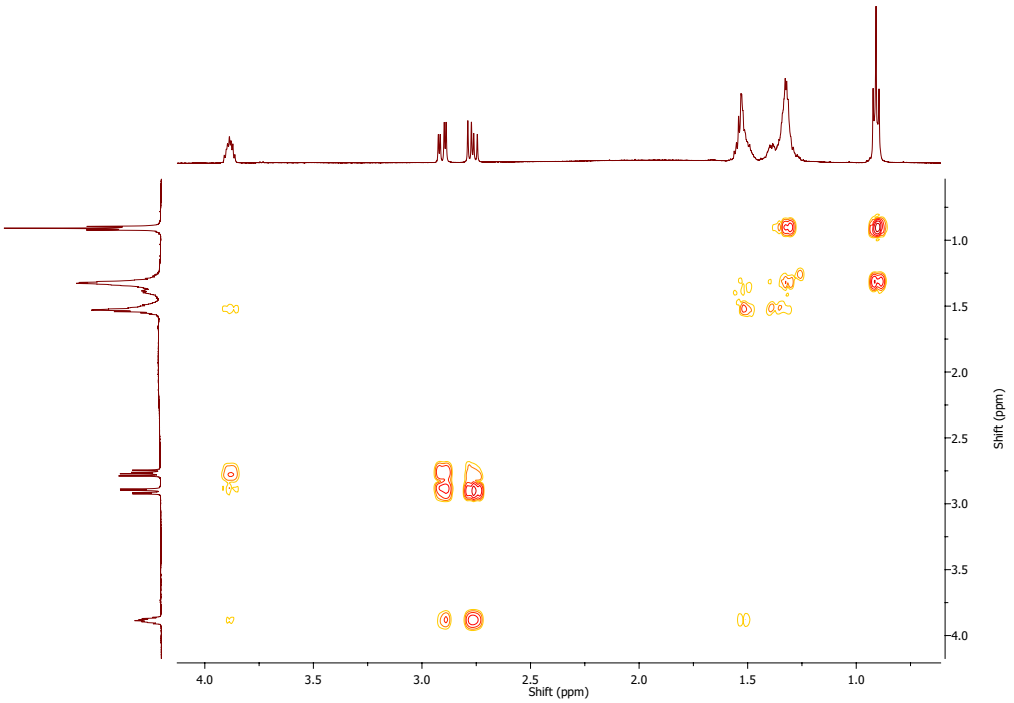

^{1}H-^{13}C HSQC:

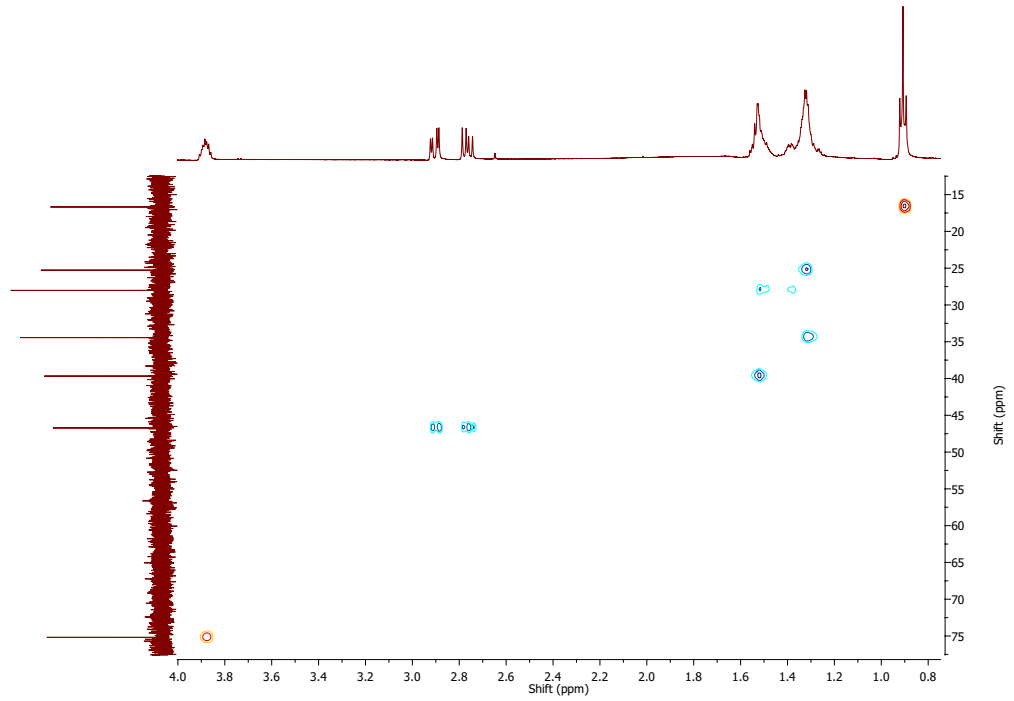

4-(1-hydroxyheptyl)benzoic acid: 500 MHz, $CDCl_3$.
^{1}H: δ 0.88 (t, 3H, J = 6.8 Hz, **12**), 1.23-1.35 (m, 7H, **8-11**), 1.38-1.45 (m, 1H, **10**) 1.70-1.84 (m, 2H, **7**), 4.78 (dd, 1H, J = 2.5, 5.9 Hz, **6**), 7.46 (d, 2H, J = 8.1 Hz, **4**), 8.09 (d, 2H, J = 8.1 Hz, **3**).

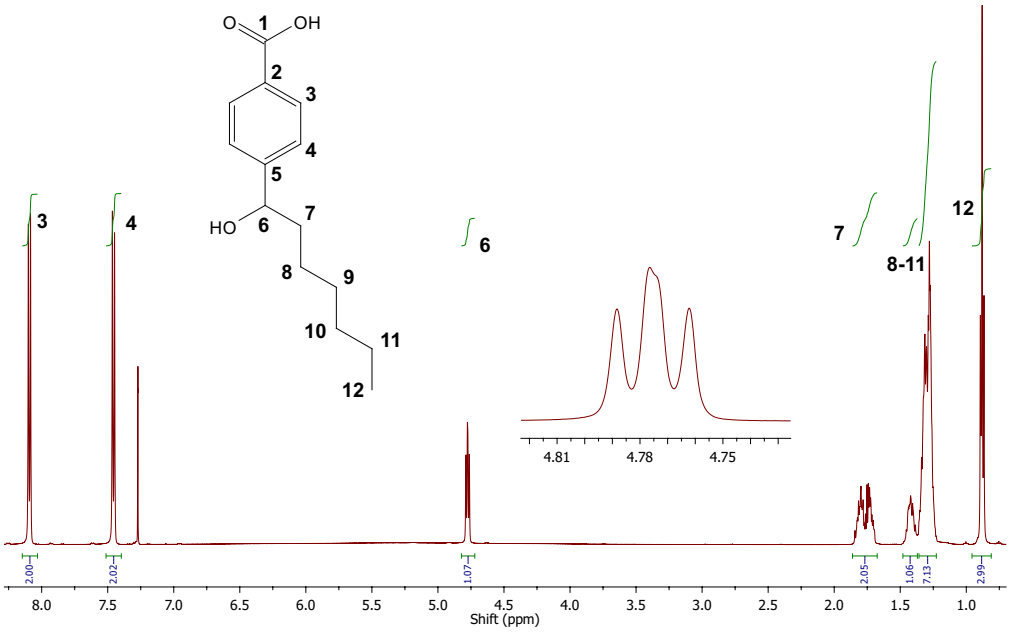

^{13}C: δ 16.7 (**12**), 25.2 (**11**), 28.2 (**10**), 31.8 (**9**), 34.4 (**8**), 41.8 (**7**), 76.9 (**6**), 128.6 (**4**), 131.0 (**5**), 133.1 (**3**), 153.6 (**2**), 174.2 (**1**).

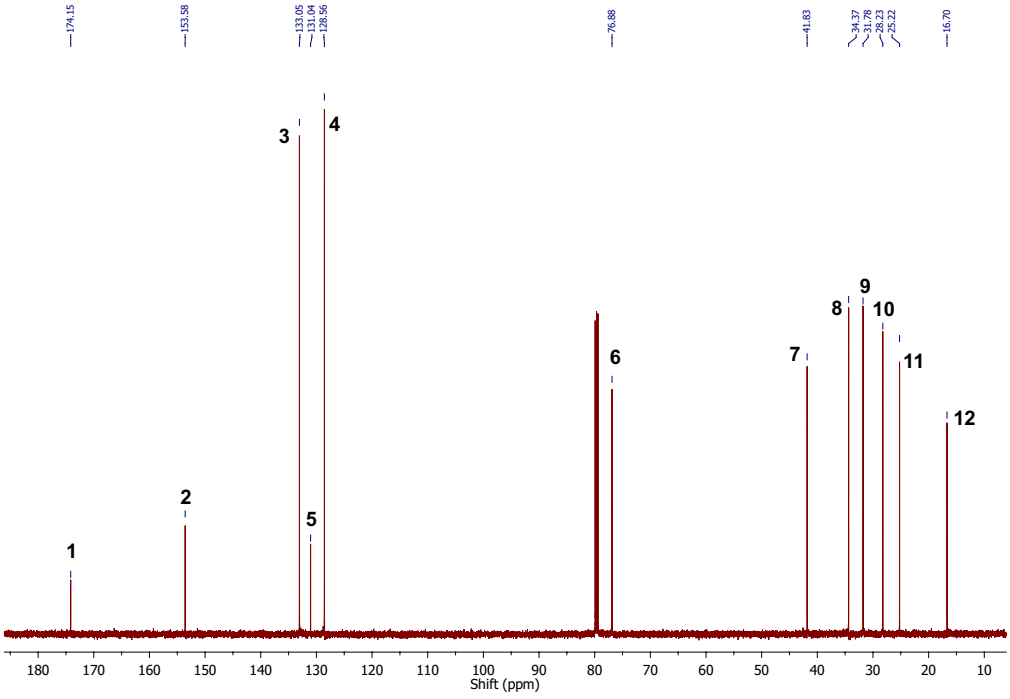

^{1}H-^{1}H COSY:

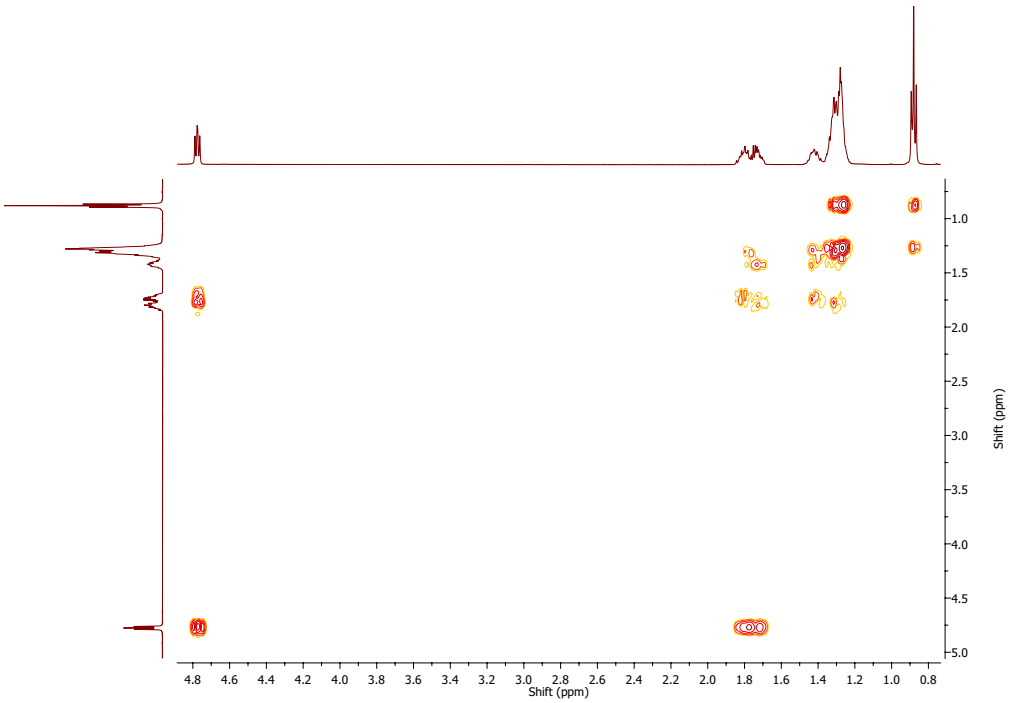

^{1}H-^{13}C HSQC:

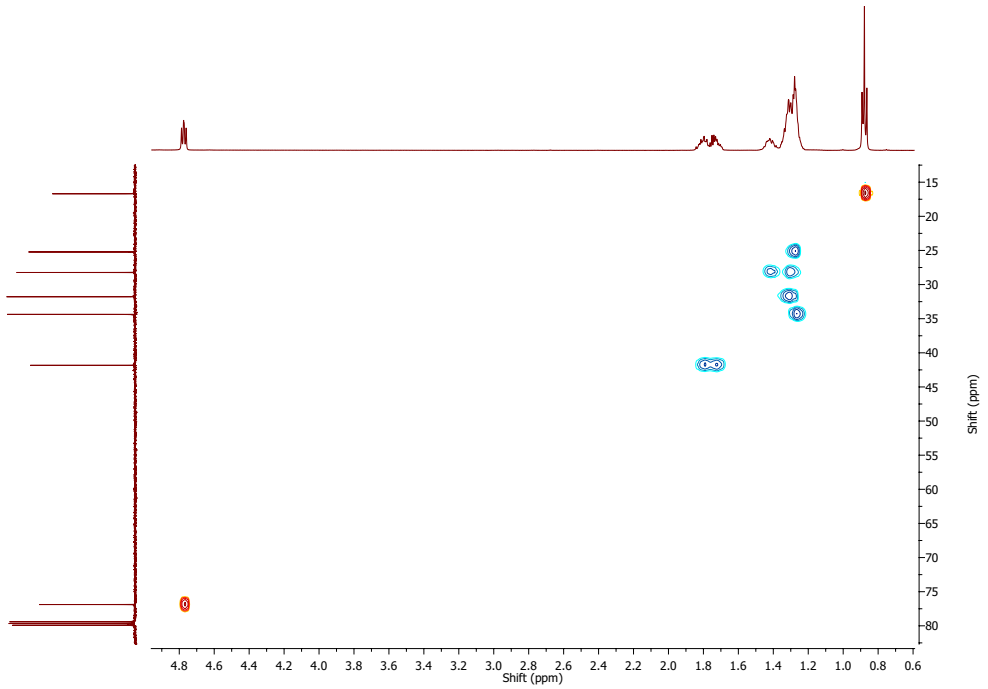

4-(3-pentyloxiran-2-yl)benzoic acid: 500 MHz, $CDCl_3$.
^{1}H: δ 0.83 (t, 3H, J = 6.9 Hz, **12**), 1.17-1.25 (m, 5H, **8-11**), 1.35-1.45 (m, 3H, **8-11**) 3.28 (dt, 1H, J = 4.4, 6.0 Hz, **7**), 4.13 (d, 1H, J = 4.2 Hz, **6**), 7.46 (d, 2H, J = 8.2 Hz, **4**), 8.09 (d, 2H, J = 8.2 Hz, **3**).

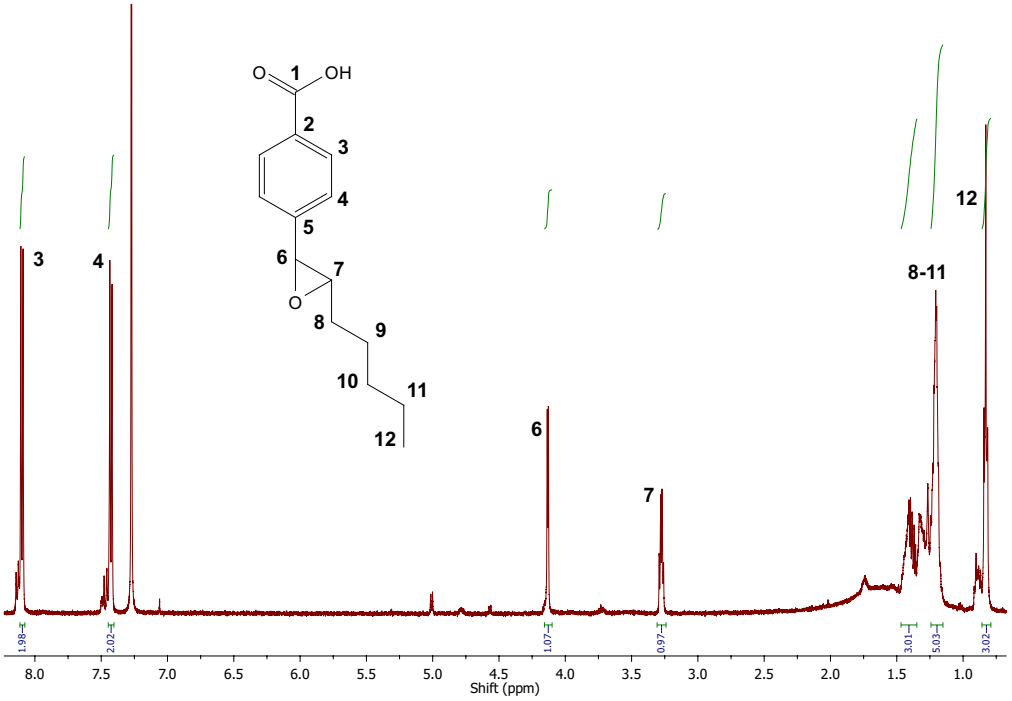

^{13}C: δ 16.5 (**12**), 25.0 (**11**), 28.2 (**10**), 29.3 (**9**), 34.0 (**8**), 59.8 (**6**), 62.5 (**7**), 129.3 (**4**), 132.6 (**3**). The **1** and **5** quartenary carbons were not observed.

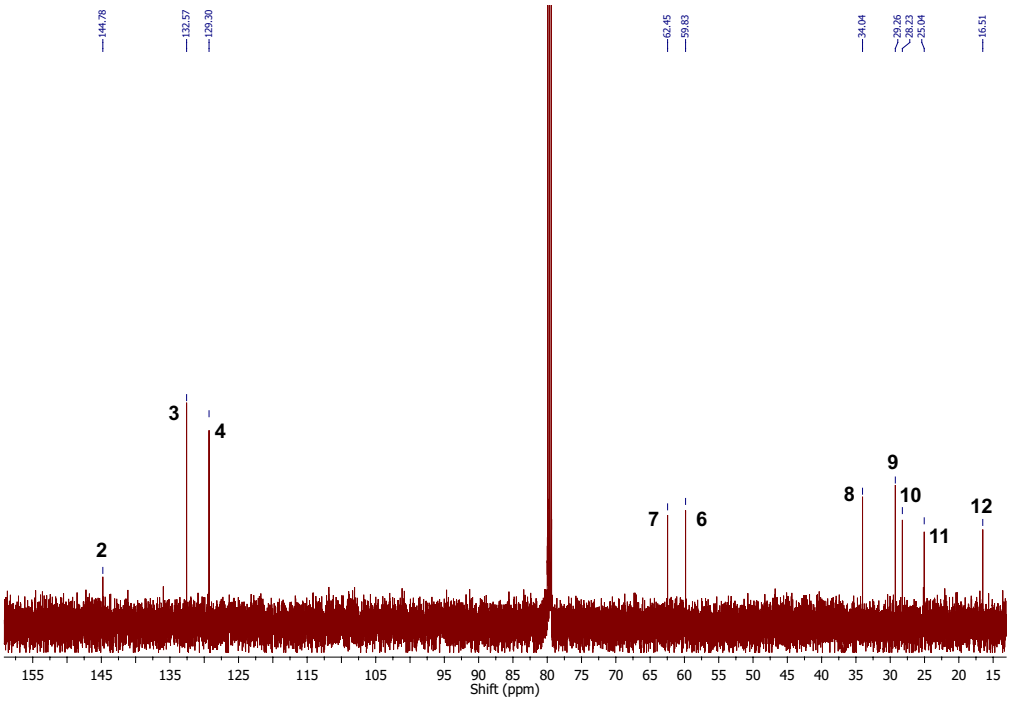

^{1}H-^{1}H COSY:

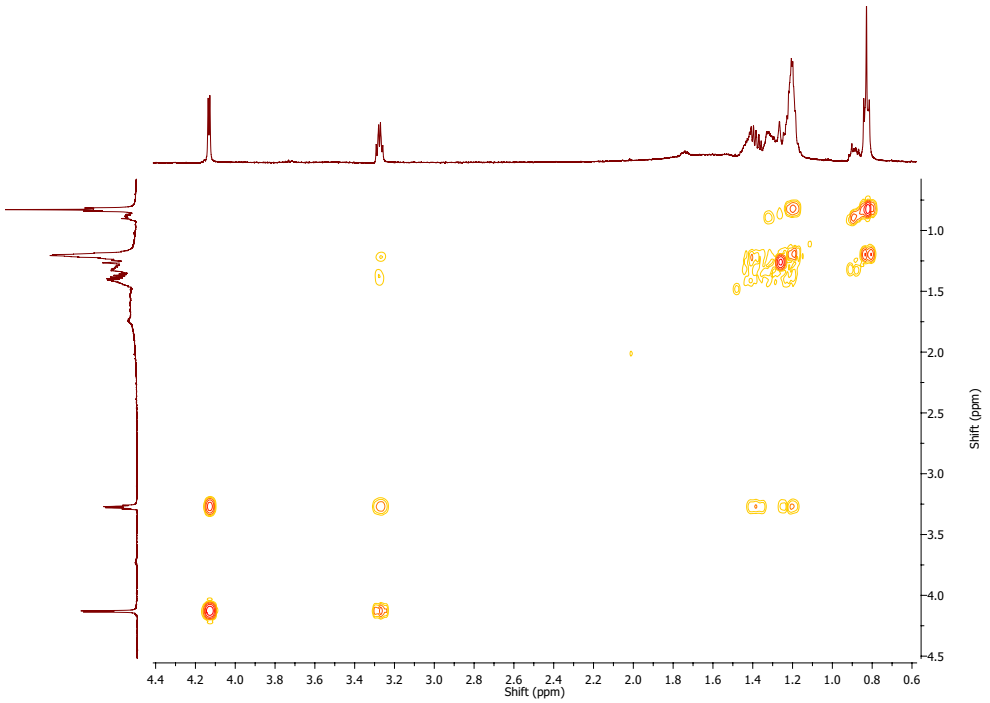

^{1}H-^{13}C HSQC:

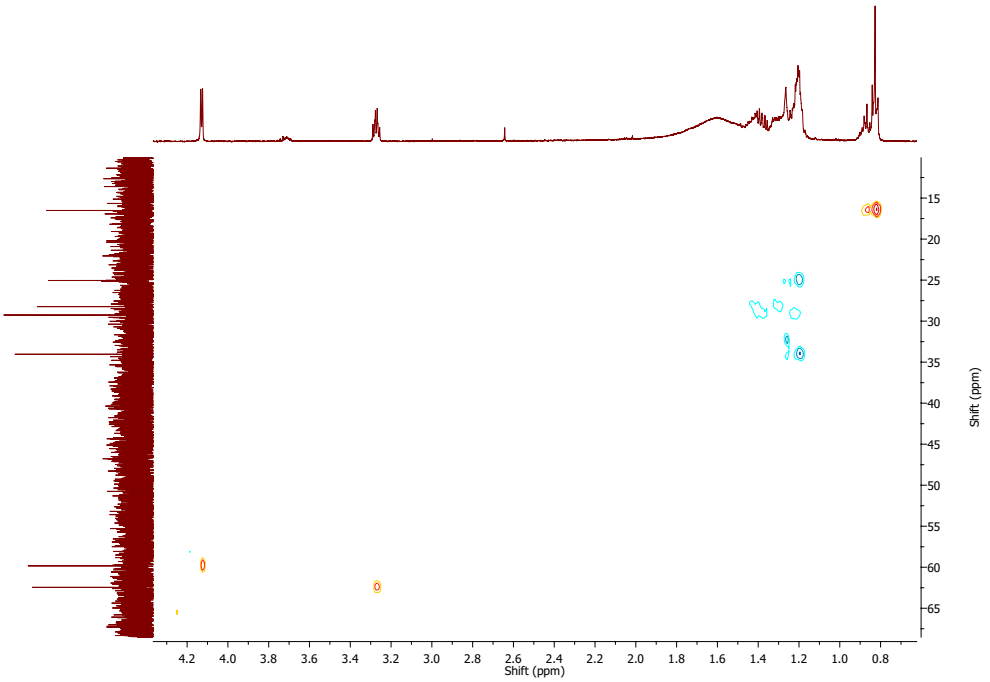

4-(1,2-dihydroxyheptyl)benzoic acid: 500 MHz, d_6-DMSO.

^{1}H: δ 0.83 (t, 3H, J = 6.7 Hz, **12**), 1.12-1.26 (m, 4H, **8-11**), 1.40-1.46 (m, 2H, **8-11**) 3.42-3.48 (m, 1H, **7**), 4.38-4.43 (m, 2H, **6, 14**), 5.29 (d, 1H, J = 4.3 Hz, **13**), 7.42 (d, 2H, J = 8.0 Hz, **4**), 7.86 (d, 2H, J = 8.0 Hz, **3**).

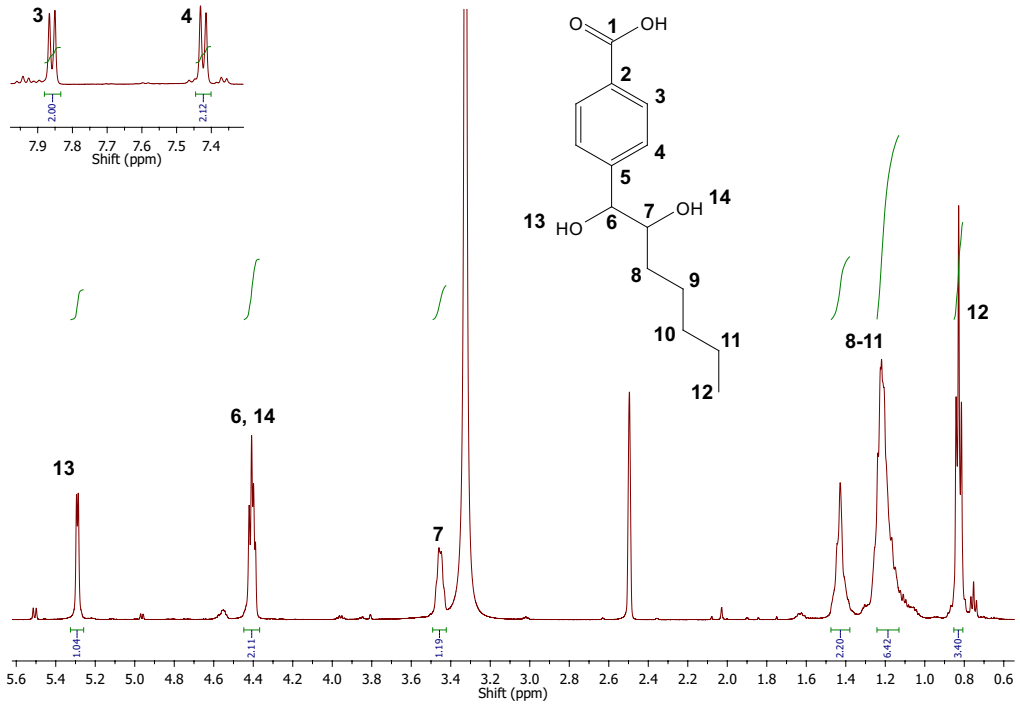

^{13}C: δ 17.1 (**12**), 25.2 (**11**), 28.1 (**10**), 34.6 (**9**), 35.2 (**8**), 77.3 (**7**), 79.2 (**6**), 130.3 (**4**), 131.7 (**3**), 132.1 (**5**), 152.2 (**2**), 170.1 (**1**).

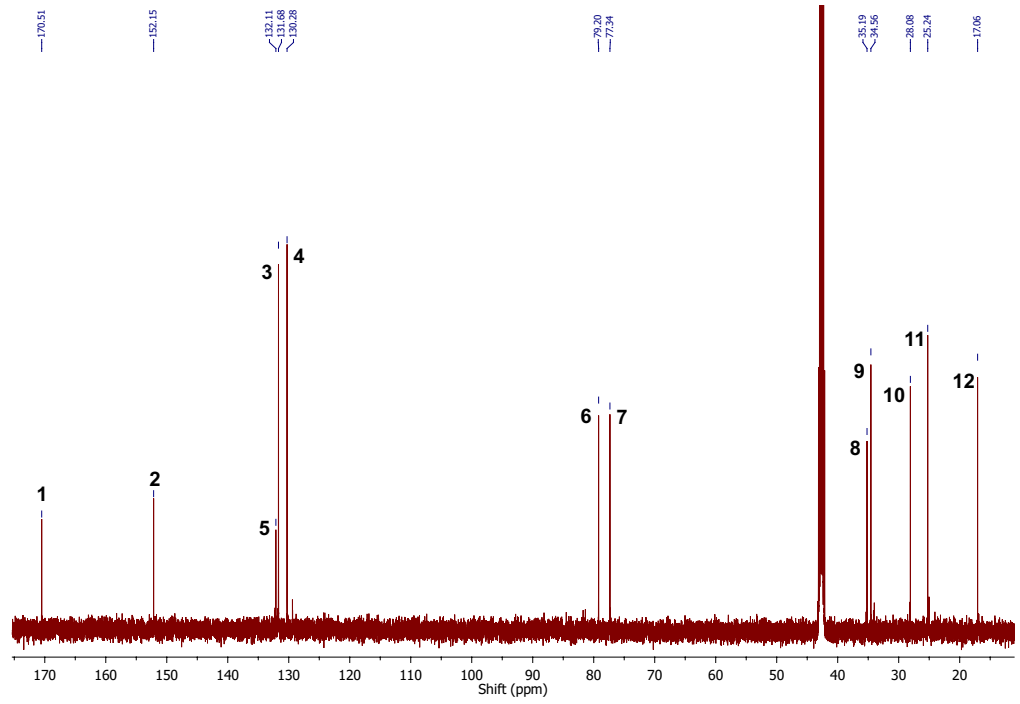

^{1}H-^{1}H COSY:

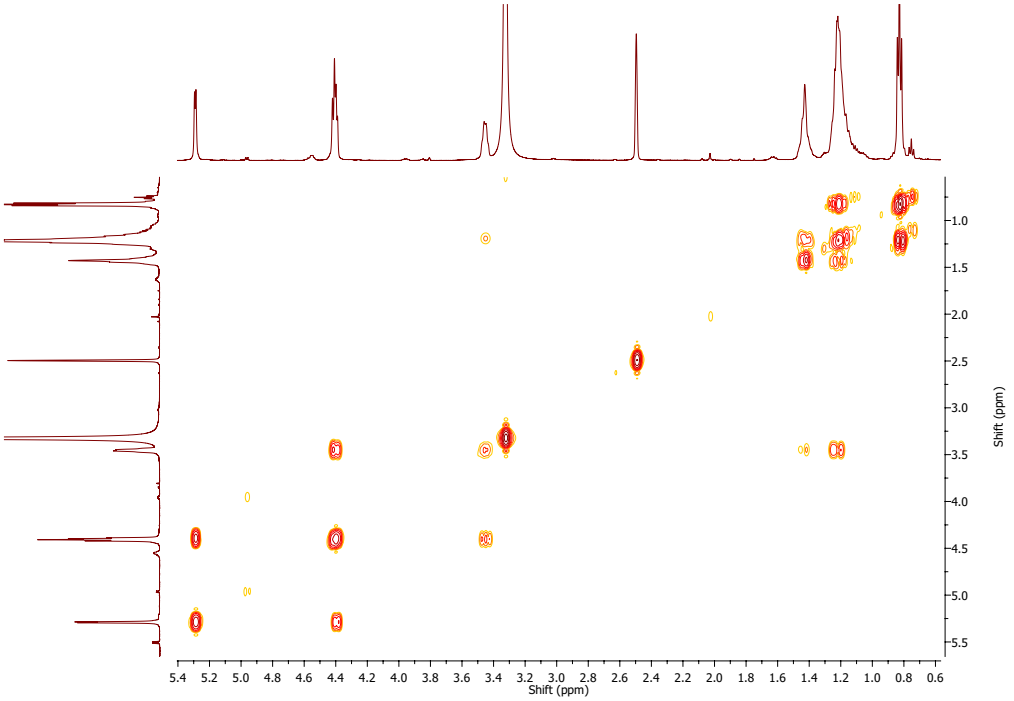

^{1}H-^{13}C HSQC:

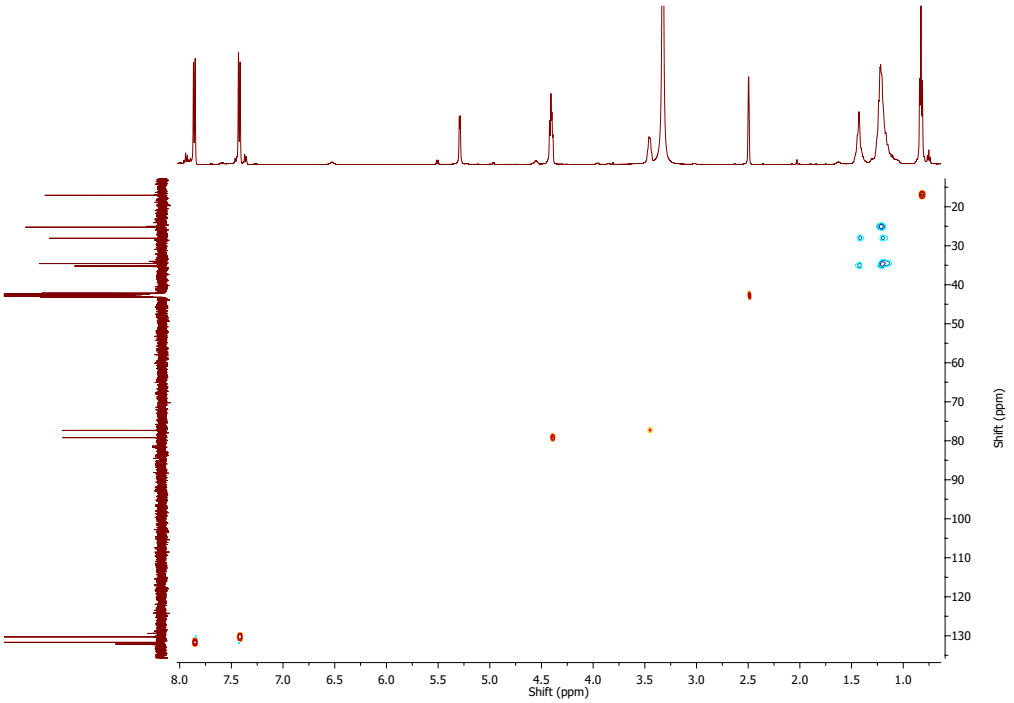

4-(hept-1-en-1-yl)benzoic acid: 500 MHz, d_6-DMSO.
^{1}H: δ 0.86 (t, 3H, J = 6.9 Hz, **12**), 1.25-1.31 (m, 4H, **10,11**), 1.42-1.46 (m, 2H, **9**) 2.18-2.22 (m, 2H, **8**), 6.45-6.47 (m, 2H, **6,7**), 7.49 (d, 2H, J = 8.3 Hz, **4**), 7.85 (d, 2H, J = 8.3 Hz, **3**).

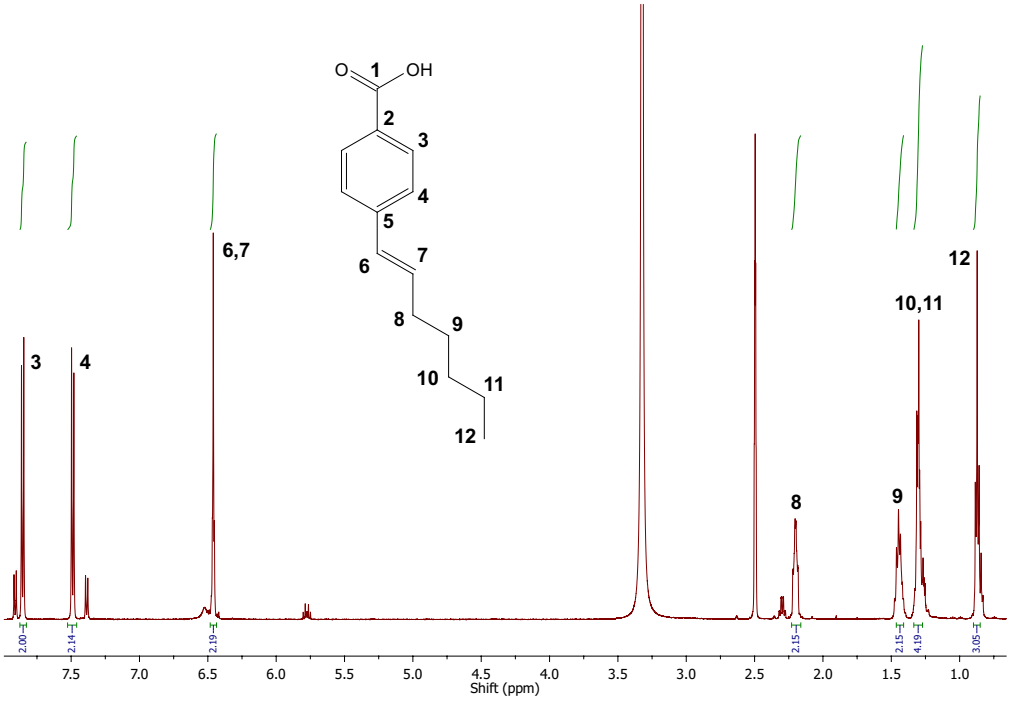

^{13}C: δ 17.0 (**12**), 25.1 (**11**), 31.4 (**9**), 34.0 (**10**), 35.6 (**8**), 128.9 (**4**), 131.7 (**5**), 131.9 (**7**), 132.8 (**3**), 137.1 (**6**), 144.8 (**2**), 170.2 (**1**).

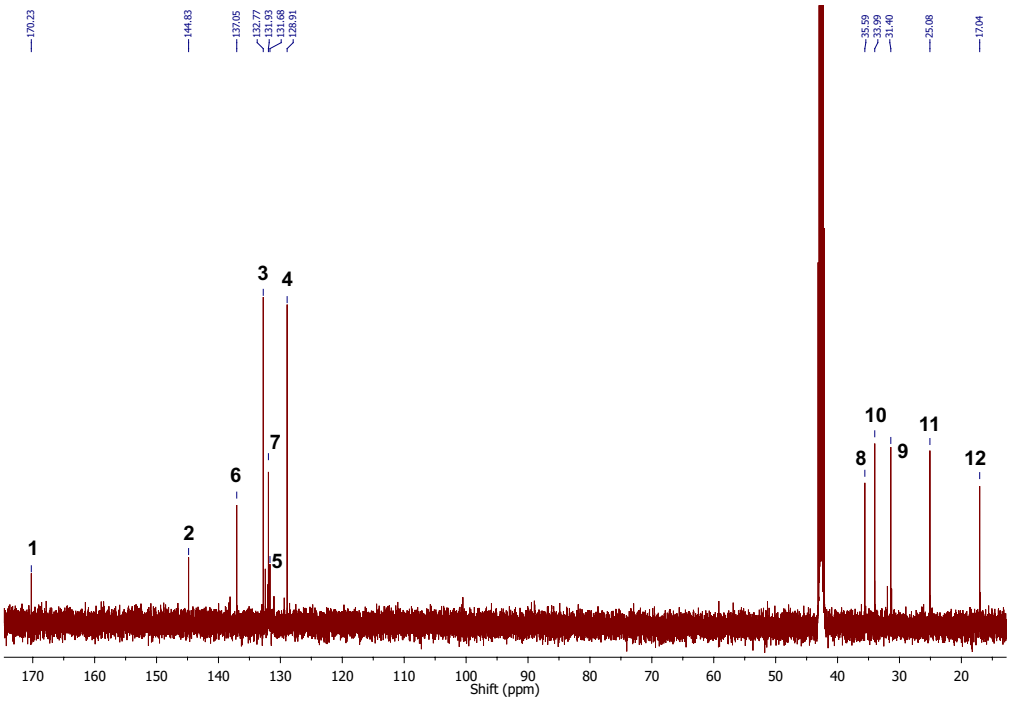

^{1}H-^{1}H COSY:

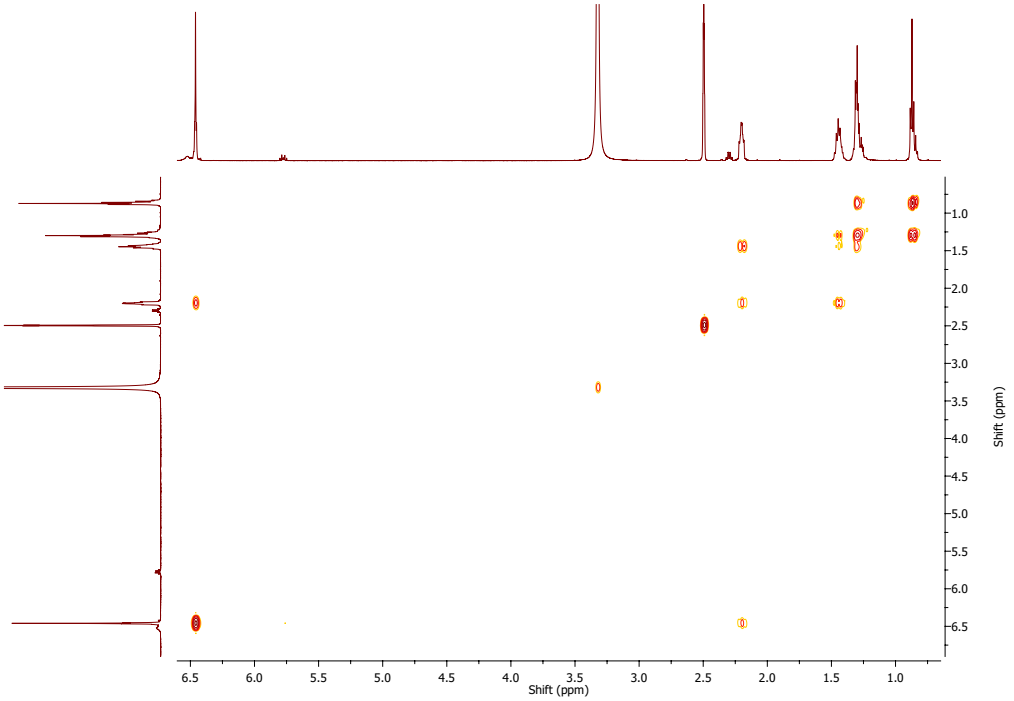

^{1}H-^{13}C HSQC:

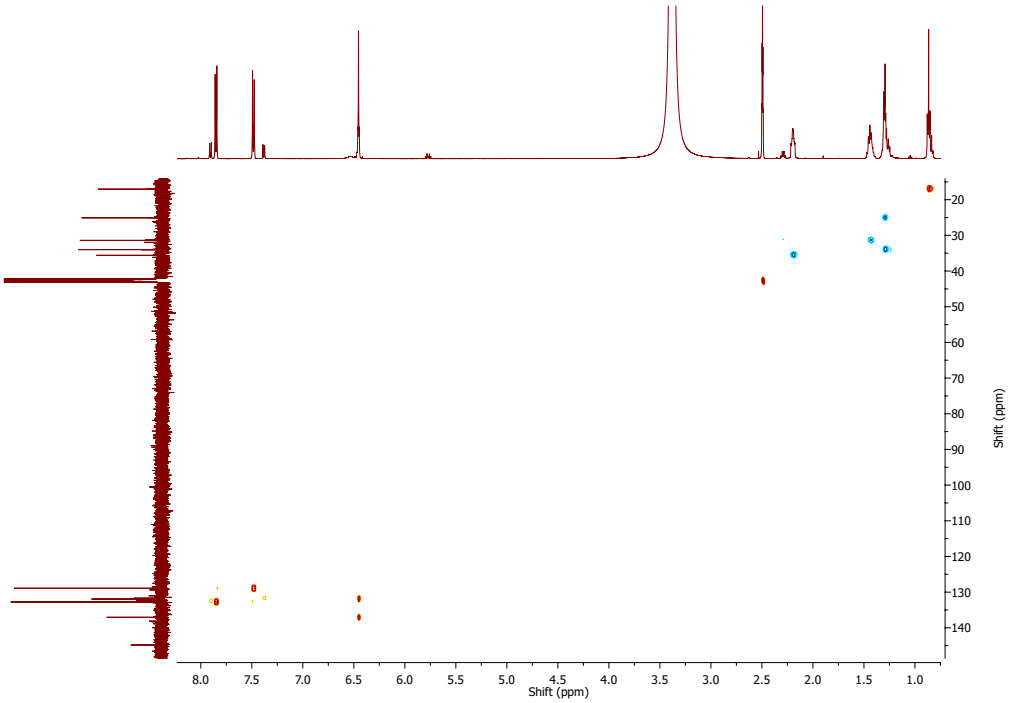

Product of 4-propionylbenzoic acid

4-(2-hydroxypropanoyl)benzoic acid: 500 MHz, d_6-DMSO.
^{1}H: δ 1.29 (d, 3H, J = 6.8 Hz, **8**), 5.04 (q, 1H, J = 6.8 Hz, **7**), 5.44 (s, 1H, **9**), 8.05 (d, 2H, J = 8.3 Hz, **3/4**), 8.06 (d, 2H, J = 8.3 Hz, **3/4**).

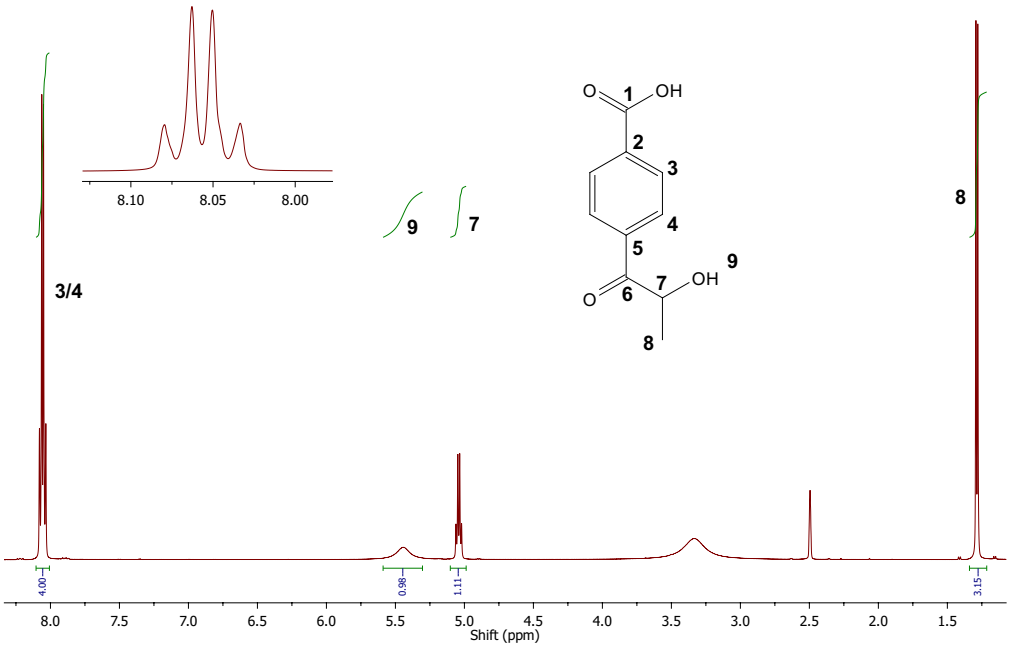

^{13}C: δ 23.3 (**8**), 72.2 (**7**), 131.9 (**3/4**), 132.6 (**3/4**), 137.6 (**5**), 141.3 (**2**), 169.8 (**1**), 204.5 (**6**).

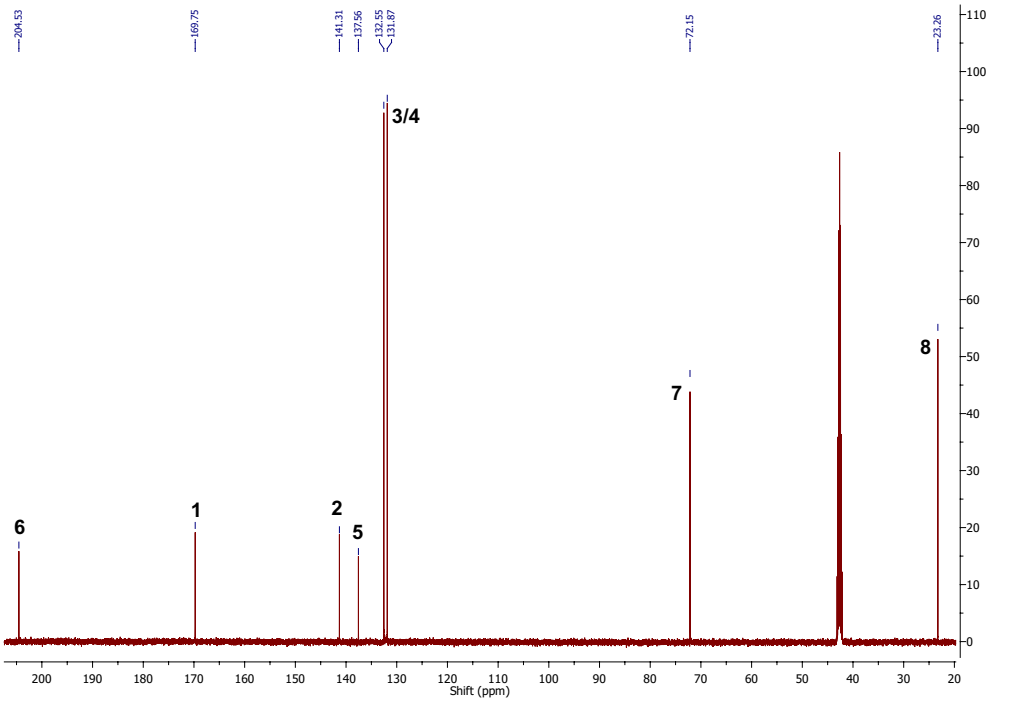

^{1}H-^{1}H COSY:

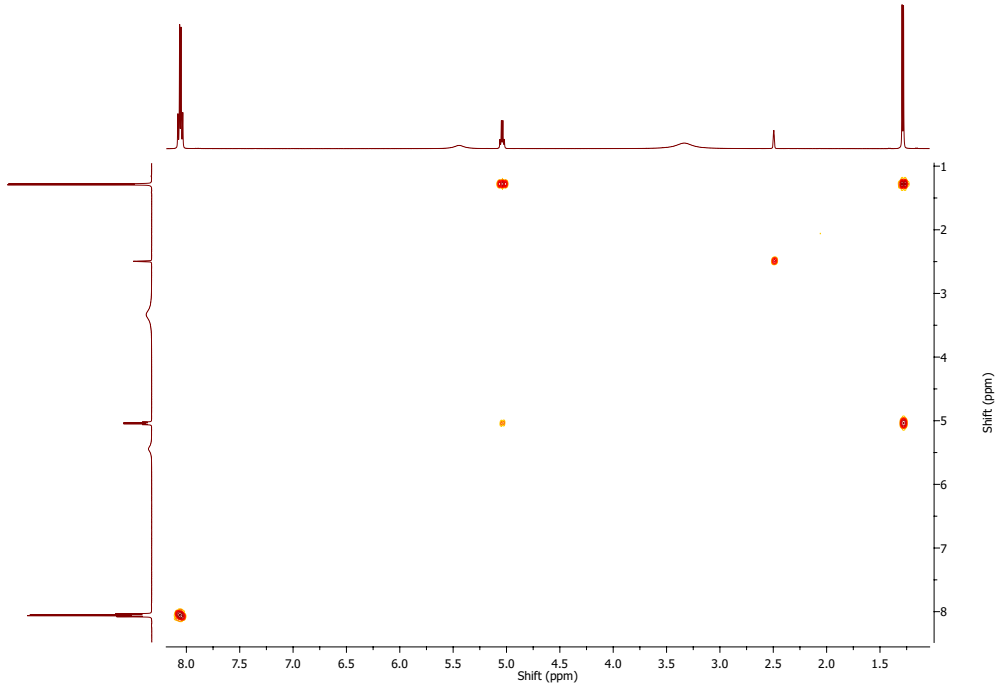
1
2
3
4
5
6
7
8
Shift (ppm)
8.0
7.5
7.0
6.5
6.0
5.5
5.0
4.5
4.0
3.5
3.0
2.5
2.0
1.5
Shift (ppm)

Product of 4-(2-oxopropyl)benzoic acid

4-(1-hydroxy-2-oxopropyl)benzoic acid: 500 MHz, d_6-DMSO.
^{1}H: δ 2.06 (s, 3H, **8**), 5.12 (s, 1H, **6**), 6.21 (s, 1H, **9**), 7.50 (d, 2H, J = 8.2 Hz, **4**), 7.93 (d, 2H, J = 8.2 Hz, **3**).

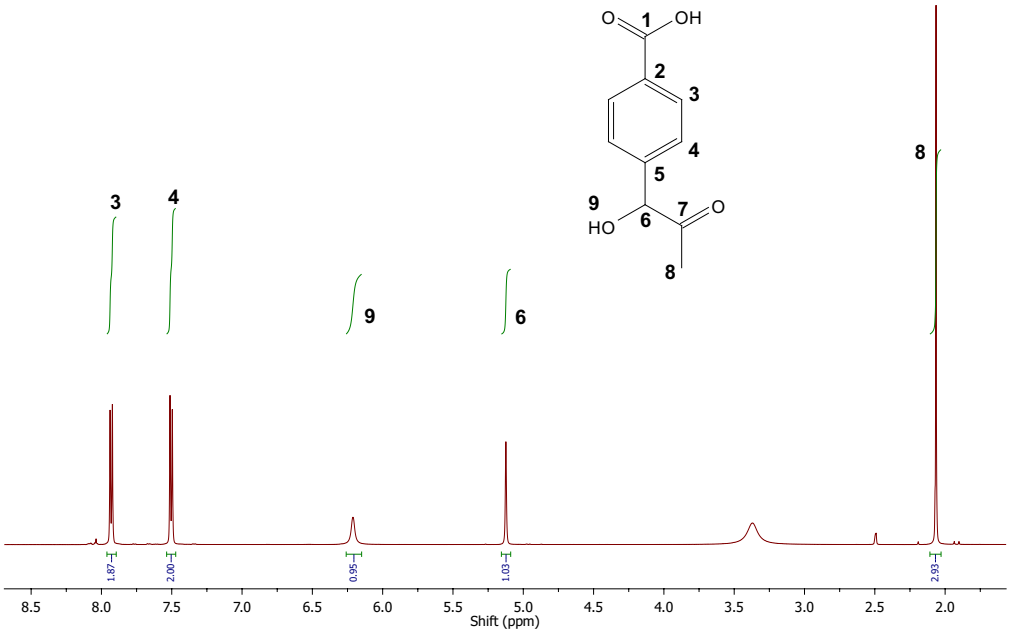

^{13}C: δ 28.2 (**8**), 82.0 (**6**), 129.8 (**4**), 132.5 (**3**), 133.3 (**5**), 147.3 (**2**), 170.2 (**1**), 211.4 (**7**).

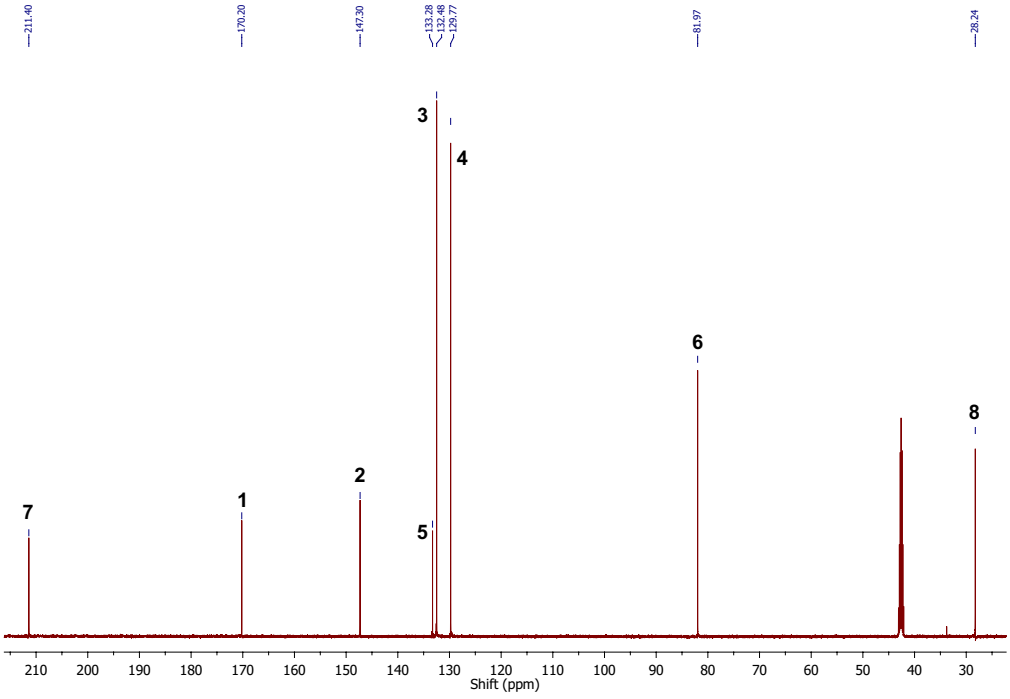

^{1}H-^{1}H COSY:

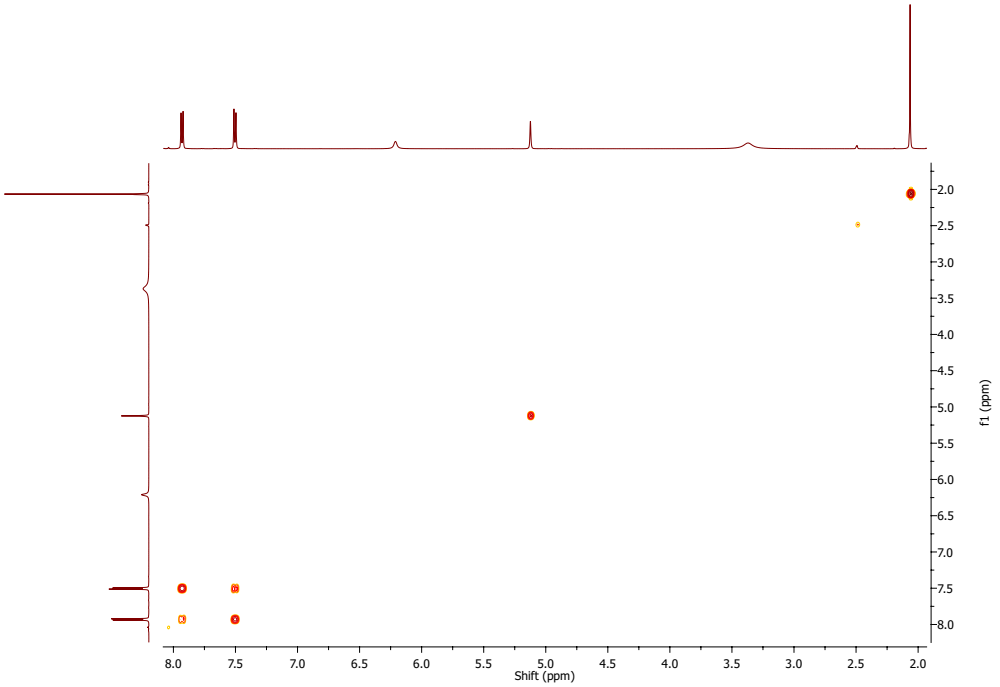
8.0
7.5
7.0
6.5
6.0
5.5
5.0
4.5
4.0
3.5
3.0
2.5
2.0
Shift (ppm)
2.0
2.5
3.0
3.5
4.0
4.5
5.0
5.5
6.0
6.5
7.0
7.5
8.0
f1 (ppm)

C.5 X-ray crystallography

Cartoon representations of 4-alkylbenzoic acid CYP199A4 complexes showing overall conservation of fold. In each, the reference structure, 4-ethylbenzoic acid-CYP199A4 (PDB: 4EGM) is shown as a cyan tube with the heme in green; the new alkyl structure is shown as a yellow tube with the heme in magenta.

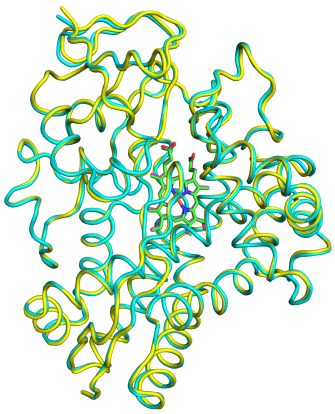

(a) 4-isopropylbenzoic acid

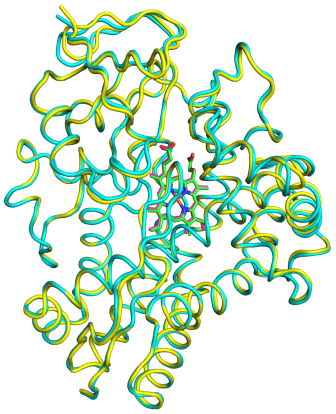

(b) 4-cyclopropylbenzoic acid

(c) 4-cyclohexylbenzoic acid

(d) 4-*n*-heptylbenzoic acid

Structural refinement and data collection statistics for CYP199A4 with 4-*n*-propylbenzoic acid. Data were collected using 1.000 Å X-rays and the space group for the structure was $P12_11$. There was one molecule in the asymmetric unit. The data is unpublished work by the group of Weihong Zhou.

	4-*n*-propylBA
PDB code	5YQA
Unit cell (a/b/c)	43.9/51.4/79.6
($\alpha/\beta/\gamma$)	90/92.1/90
Resolution range[a]	50.0 - 1.38
	(1.40 - 1.38)
$<I/\sigma(I)>$[a]	30.6 (4.5)
Completeness[a]	98.9 (95.5)
Redundancy[a]	3.6 (2.9)
R_{merge}[a,b] (%)	4.0 (22.5)
R_{work}	0.178
R_{free}[c]	0.196
Ramachandran plot[d]	
Most favoured (%)	98.5
Allowed (%)	1.5

[a]Highest resolution shell is shown in parentheses where applicable. [b]all I+ and I-. [c]5 % of total reflections, randomly selected. [d]% of all amino acid residues.[184] There were no Ramachandran outliers (0 %).

Appendix D Supplementary data for Chapter 6

D.1 Spin state shifts

Spin state shifts of benzoic acid substrates tested with mutant isoforms of CYP199A4 (D251N, T252A). Black shows CYP199A4 in its resting state, red shows the maximum absorbance shift obtained upon addition of substrate.

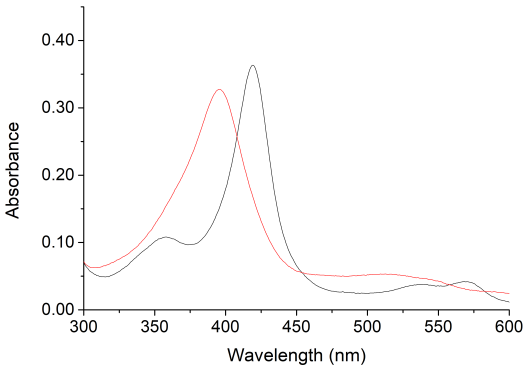

(a) 4-methoxybenzoic acid, T252A

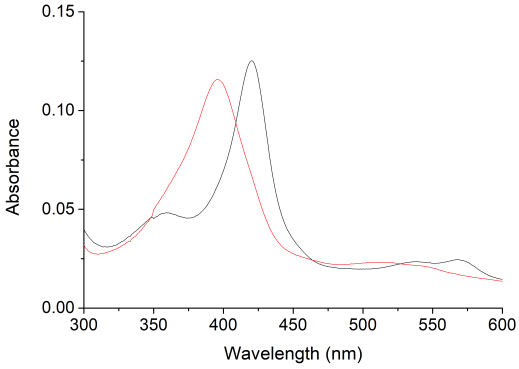

(b) 4-methoxybenzoic acid, D251N

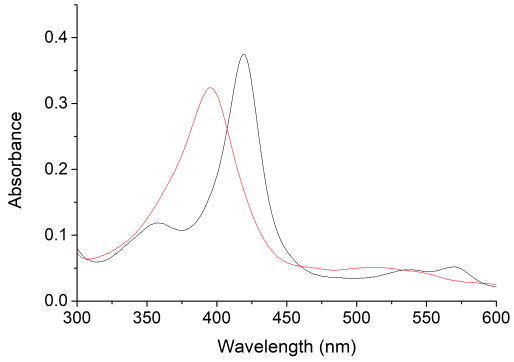

(c) 4-ethylbenzoic acid, T252A

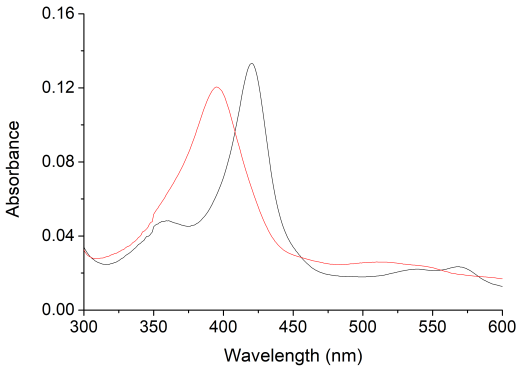

(d) 4-ethylbenzoic acid, D251N

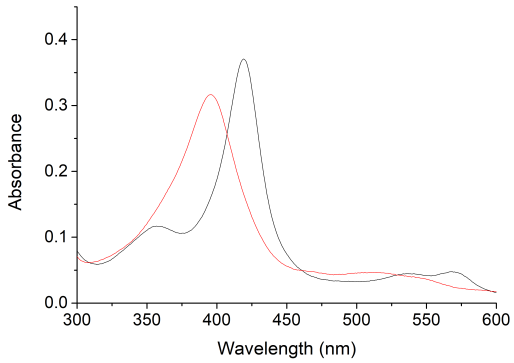

(e) 4-isopropylbenzoic acid, T252A

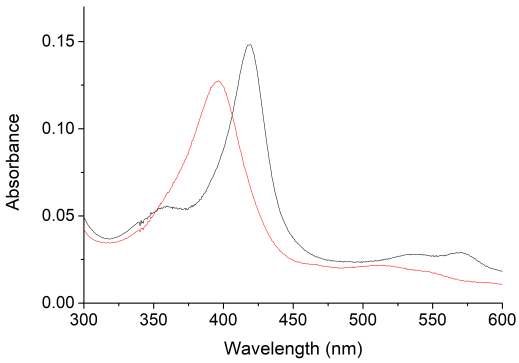

(f) 4-isopropylbenzoic acid, D251N

D.2 Dissociation constant analysis

Analysis of dissociation constants for substrates with mutant isoforms (T252A, D251N) of CYP199A4. Shown in brackets are the wavelengths of the trough and peak, and the enzyme concentration used for dissociation constant analysis (trough, peak, [P450]).

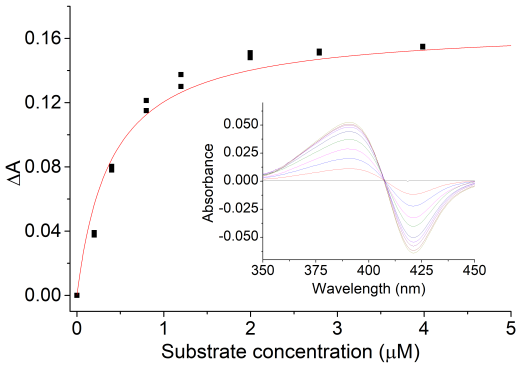

(a) 4-methoxybenzoic acid, D251N (421 nm, 391 nm, 1.7 µM)

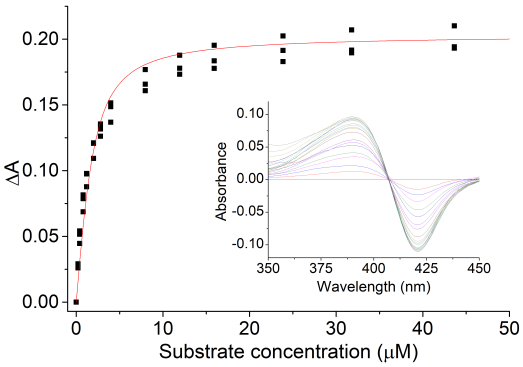

(b) 4-methylaminobenzoic acid, T252A (421 nm, 390 nm, 1.8 µM)

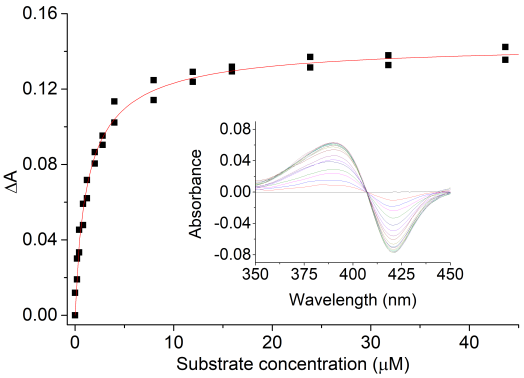

(c) 4-methylthiobenzoic acid, T252A (421 nm, 390 nm, 1.3 µM)

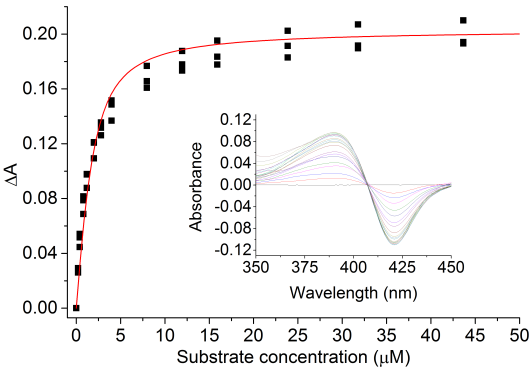

(d) 4-methylthiobenzoic acid, D251N (421 nm, 390 nm, 1.7 µM)

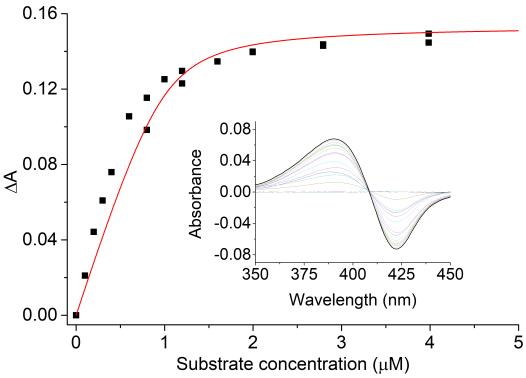

(e) 4-ethylbenzoic acid, D251N (422 nm, 390 nm, 1.7 µM)

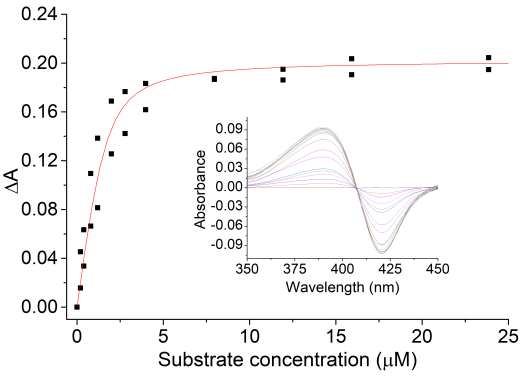

(f) 4-isopropylbenzoic acid, T252A (421 nm, 391 nm, 1.8 µM)

D.3 X-ray crystallography

Cartoon representations of 4-methoxybenzoic acid CYP199A4 mutant complexes showing overall conservation of fold. In each, the reference structure, 4-methoxybenzoic acid (wild-type CYP199A4, PDB: 4DO1) is shown as a cyan tube with the heme in green; the new mutant structure is shown as a yellow tube with the heme in magenta.

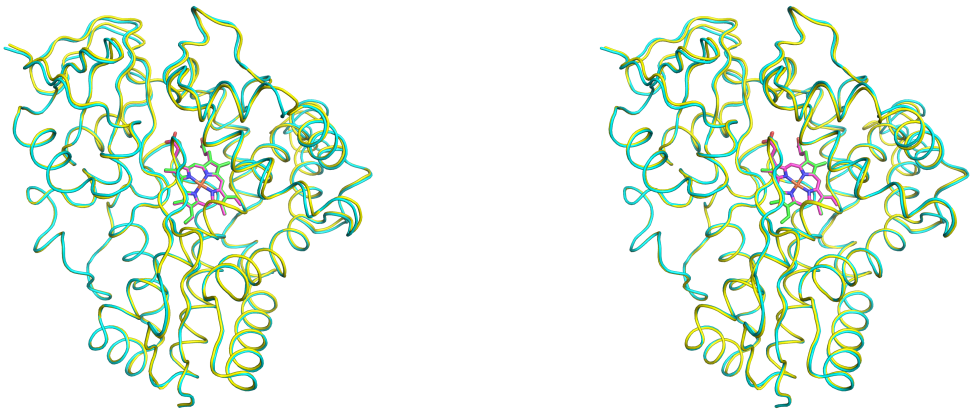

(a) T252A **(b)** D251N

Overlay of the water networks of WT (yellow) and D251N (cyan) CYP199A4 isoforms. The water molecules are shown as spheres in the colour of their respective structure.

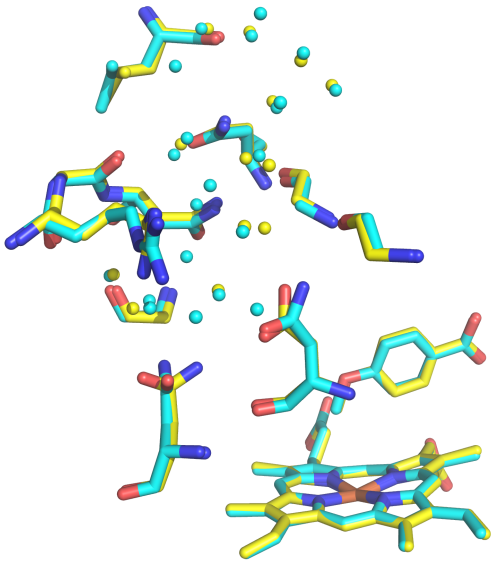

The solvent network extending from the D251 residue to the surface of T252A-CYP199A4 through a solvent access channel. 4-Methoxybenzoic acid is green, the heme and hydrogen bonds are grey, and water molecules are red spheres. There are 15 water molecules in the solvent network of T252A-CYP199A4 compared to 20 for the D251N mutant.

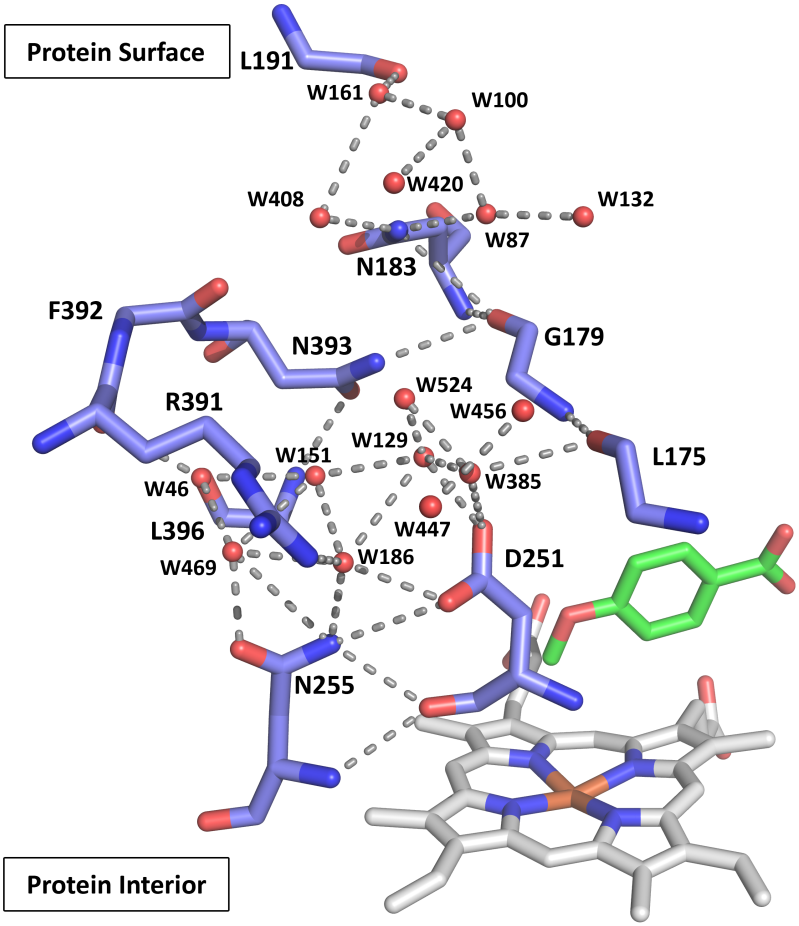

The binding of CN^- and O_2 ligands to the heme of wild-type camphor-bound $P450_{cam}$, and the CN^--bound wild-type structure of CYP101D1, which shows comparable changes to a O_2-bound structure. Camphor is green, the heme group is grey, the conserved acid-alcohol pair of residues are yellow and water molecules are red spheres.

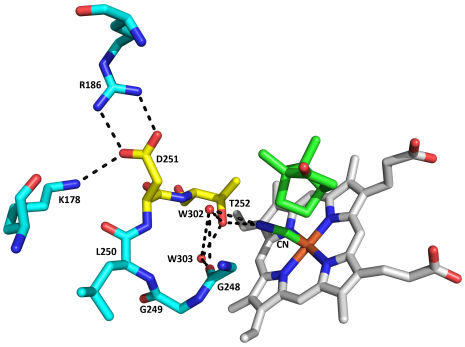

(a) Cyano-bound wild-type $P450_{cam}$ (PDB: 1O76)

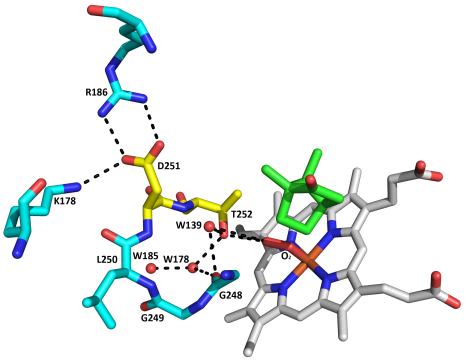

(b) Oxygen-bound wild-type $P450_{cam}$ (PDB: 2A1M)

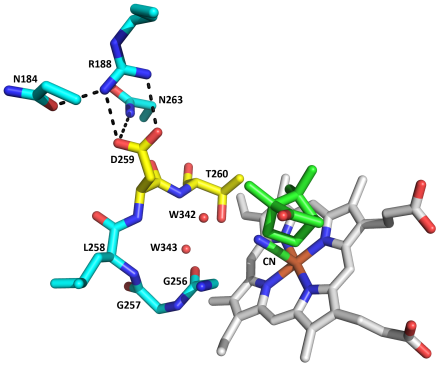

(c) CN^--bound wild-type CYP101D1 (PDB: 4C9L)

Appendix E Supplementary data for Chapter 7

E.1 Spin state shifts

Spin state shifts of benzoic acid substrates tested with CYP199A4. Black shows CYP199A4 in its resting state, red shows the maximum absorbance shift obtained upon addition of substrate. When the spin state shift assignment was ambiguous, blue shows the difference spectrum between the black and red traces.

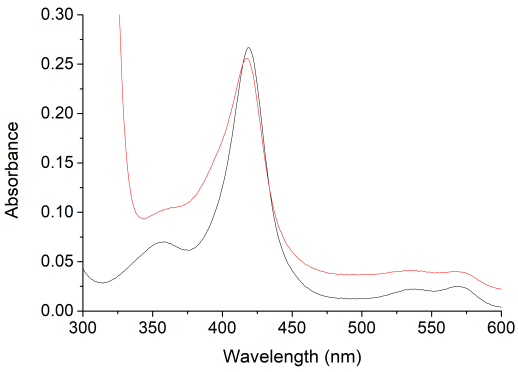

(a) 4-(4′-methoxyphenyl)benzoic acid

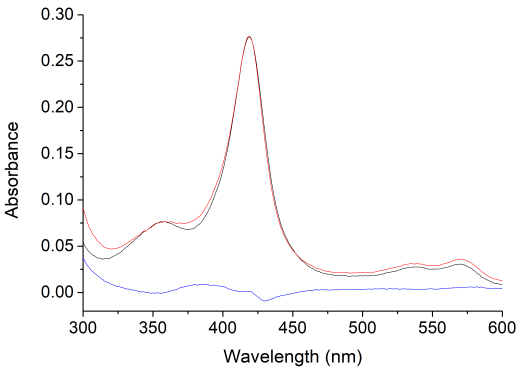

(b) 4-phenoxybenzoic acid (419 nm)

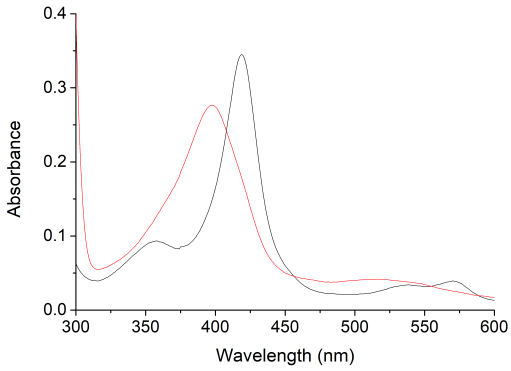

(c) 4-phenylBA

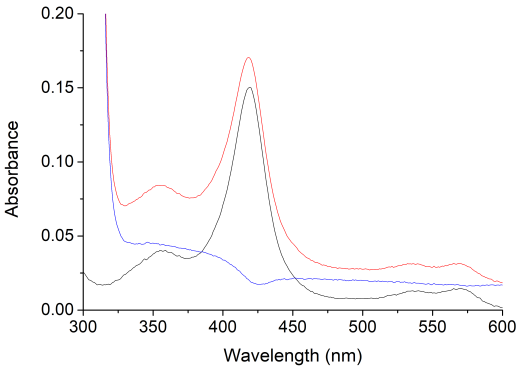

(d) 6-phenylnicotinic acid (419 nm → 418 nm)

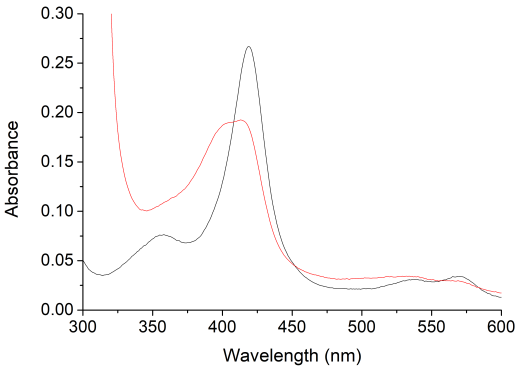

(e) 5-phenylpicolinic acid

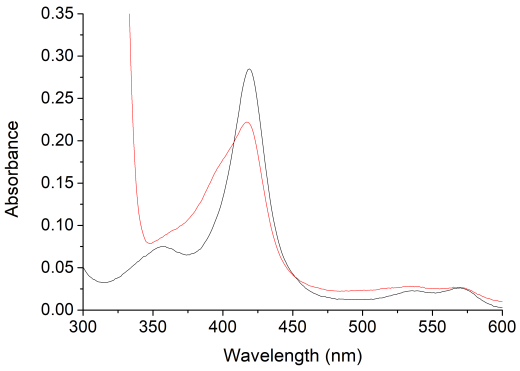

(f) 4-(furan-2-yl)benzoic acid

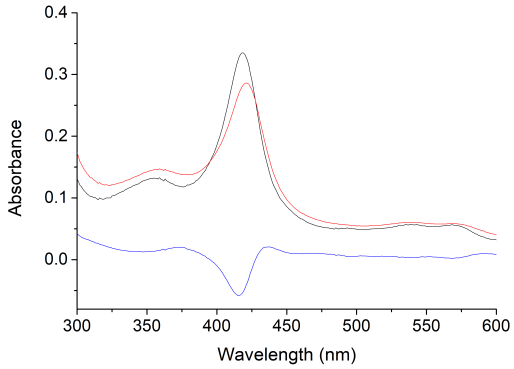

(g) 4-(imidazol-1-yl)benzoic acid (419 nm → 421 nm)

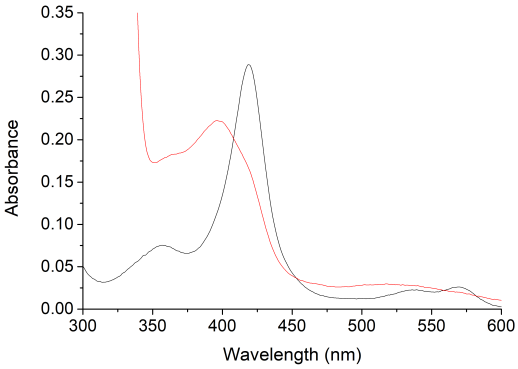

(h) 4-(thiophen-2-yl)benzoic acid

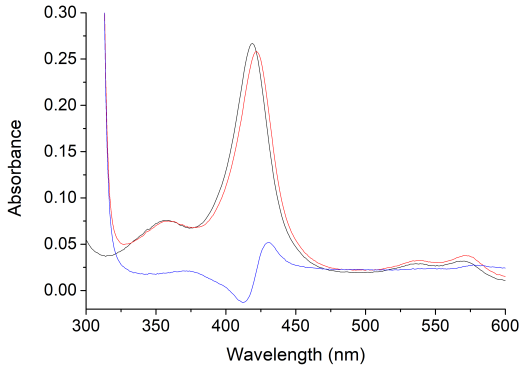

(i) 4-(pyridin-2-yl)benzoic acid (419 nm → 422 nm)

E.2 Dissociation constant analysis

Dissociation constant analysis for the range of substrates investigated in Chapter 7. Shown in brackets are the wavelengths of the peak and trough, and the enzyme concentration used for dissociation constant analysis (LS, HS, [P450]).

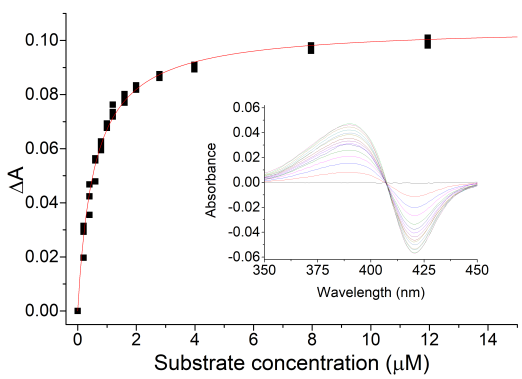

(a) 4-(3′-methoxyphenyl)benzoic acid (421 nm → 390 nm, 0.9 μM)

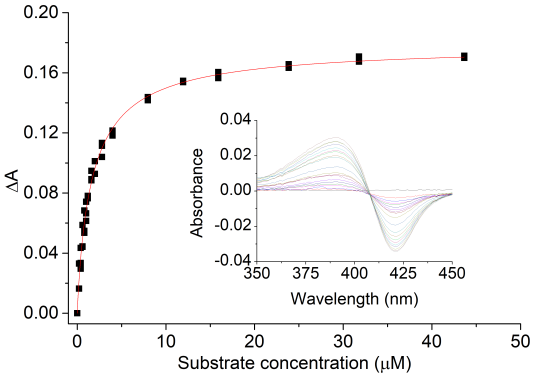

(b) 4-phenylbenzoic acid (421 nm → 390 nm, 1.7 μM)

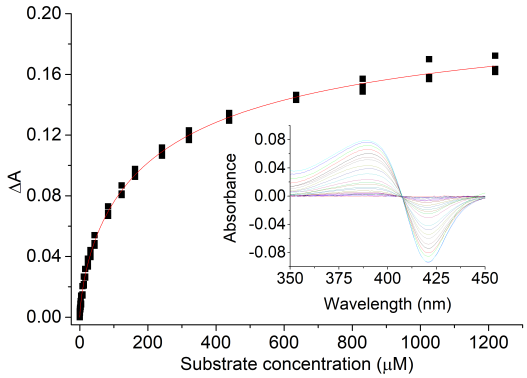

(c) 5-phenylpicolinic acid (421 nm → 390 nm, 2.3 μM)

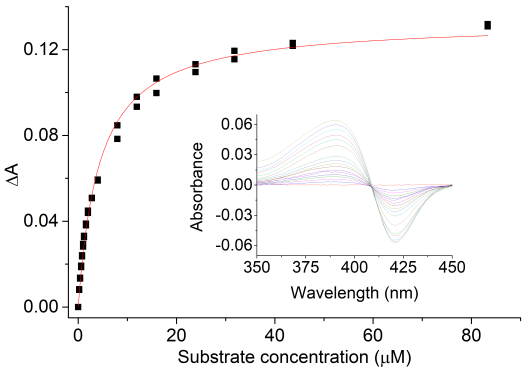

(d) 4-(furan-2-yl)benzoic acid (421 nm → 390 nm, 2.6 μM)

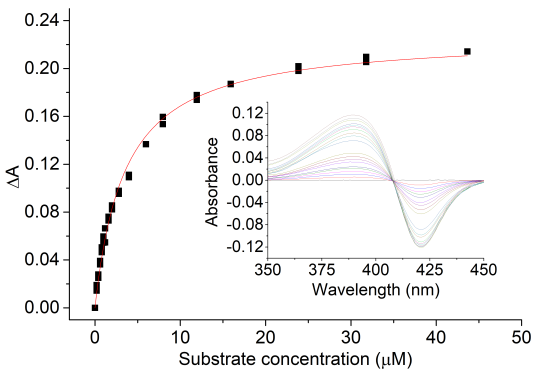

(e) 4-(pyrrol-1-yl)benzoic acid (421 nm → 391 nm, 2.7 µM)

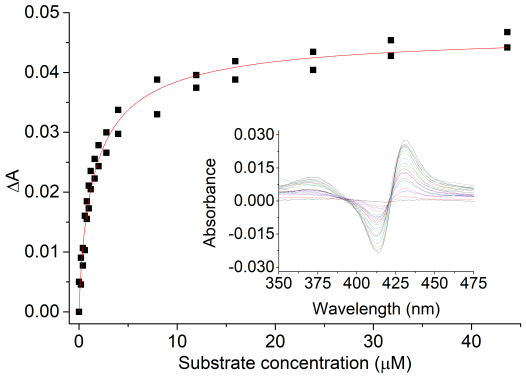

(f) 4-(imidazol-1-yl)benzoic acid (413 nm → 431 nm, 3.1 µM)

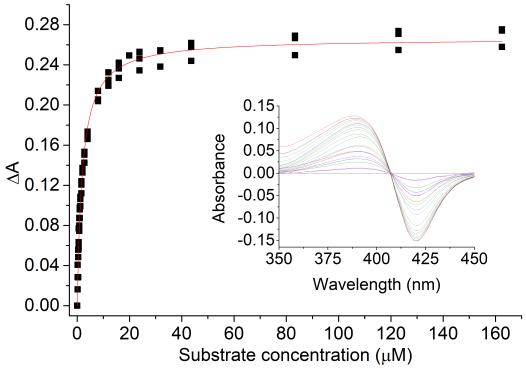

(g) 4-(thiophen-2-yl)benzoic acid (420 nm → 389 nm, 2.9 µM)

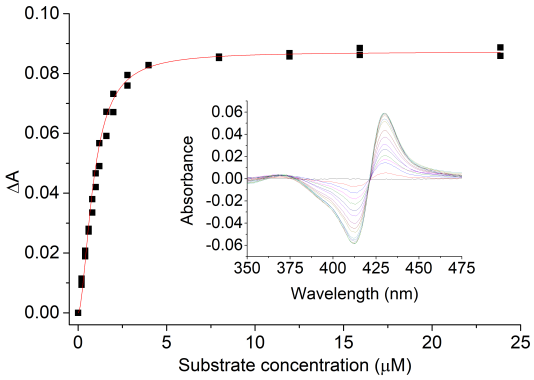

(h) 4-(pyridin-2-yl)benzoic acid (412 nm → 430 nm, 4.3 µM)

E.3 HPLC analysis

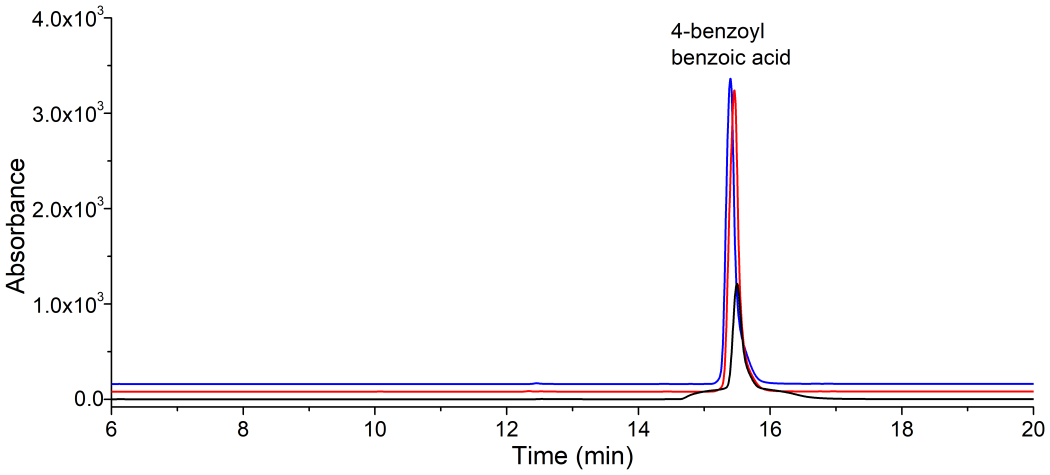

(a) HPLC analysis of 4-benzoylbenzoic acid turnover with CYP199A4. **Black**, *in vitro* turnover; red, *in vivo* turnover; blue, substrate control, RT = 15.5 min. 20-95 % gradient of H_2O:ACN, monitored at 254 nm.

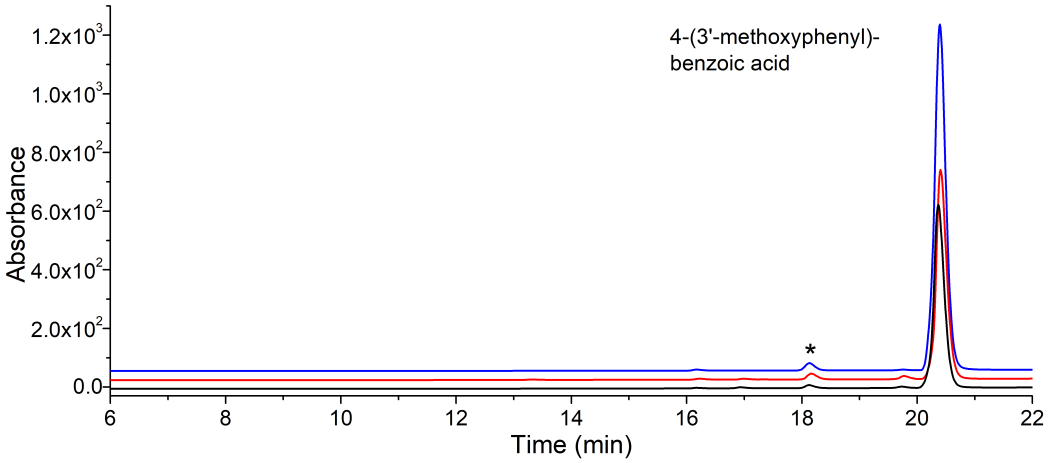

(b) HPLC analysis of 4-(3′-methoxyphenyl)benzoic acid turnover with CYP199A4. **Black**, *in vitro* turnover; red, *in vivo* turnover; blue, substrate control, RT = 20.4 min. 20-95 % gradient of H_2O:ACN, monitored at 239 nm.

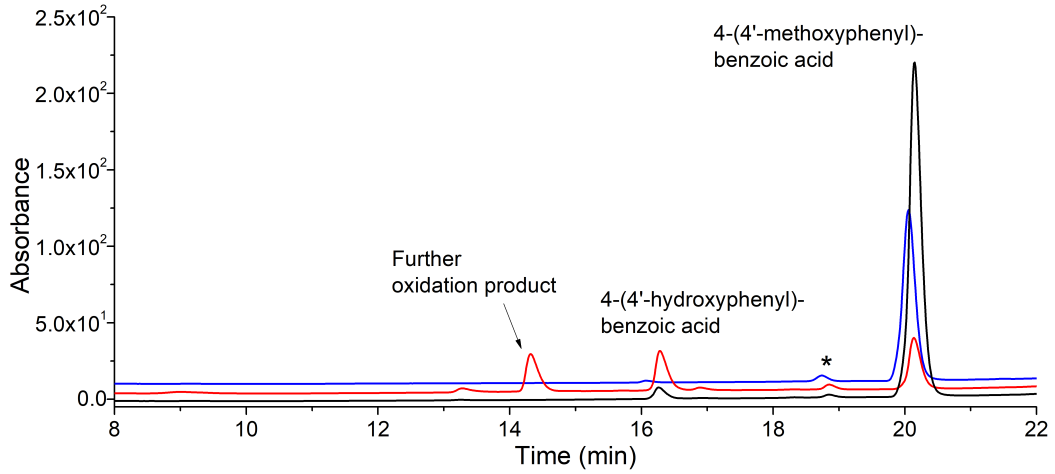

(c) HPLC analysis of 4-(4′-methoxyphenyl)benzoic acid turnover with CYP199A4. **Black**, *in vitro* turnover; red, *in vivo* turnover; blue, substrate control, RT = 20.4 min. Denoted (*) is an impurity peak, present in the substrate control. A 20-95 % gradient of H_2O:ACN was used. The chromatogram was monitored at 299 nm.

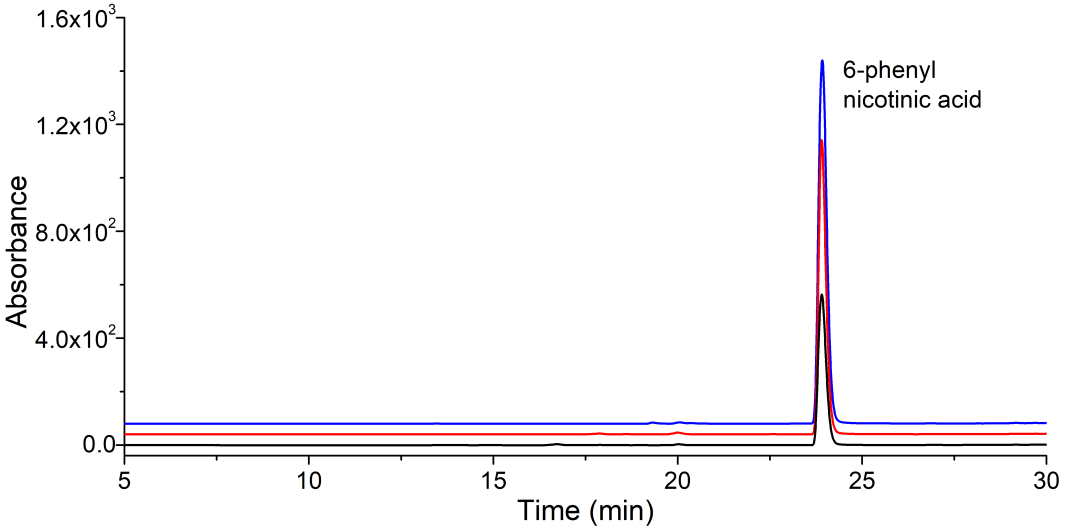

(d) HPLC analysis of 6-phenylnicotinic acid turnover with CYP199A4. **Black**, *in vitro* turnover; red, *in vivo* turnover; blue, substrate control, RT = 24.0 min. A 0-50 % gradient of H_2O:ACN was employed. The chromatogram was collected at 254 nm.

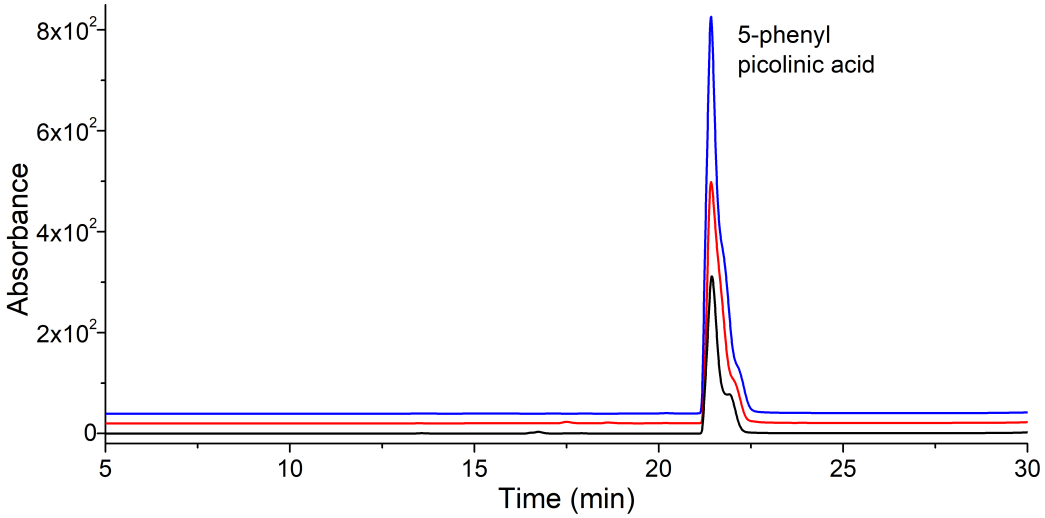

(e) HPLC analysis of 5-phenylpicolinic acid turnover with CYP199A4. **Black**, *in vitro* turnover; red, *in vivo* turnover; blue, substrate control, RT = 21.5 min. A 0-50 % gradient of H_2O:ACN was used. The chromatogram was collected at 254 nm.

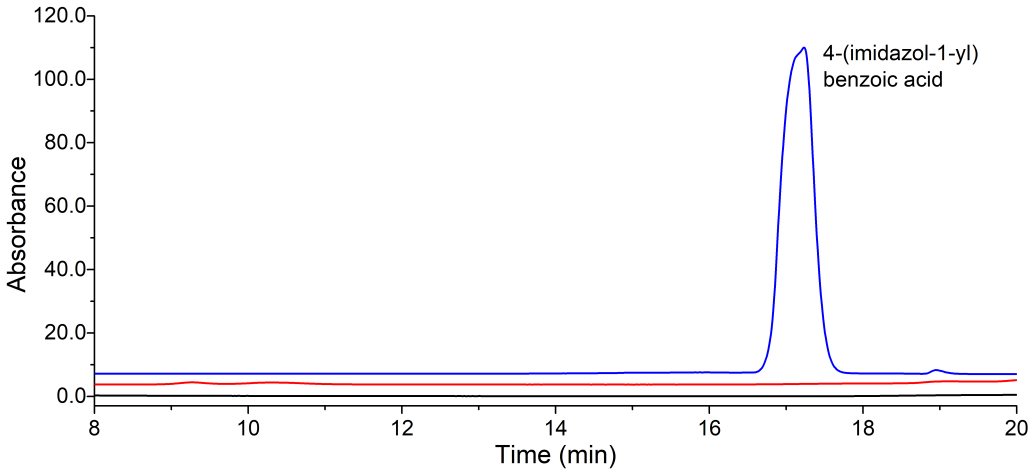

(f) HPLC analysis of 4-(imidazol-1-yl)benzoic acid turnover with CYP199A4. **Black**, *in vitro* turnover; red, *in vivo* turnover; blue, substrate control, RT = 17.2 min. A 0-50 % gradient of H_2O:ACN was used, and the chromatogram was monitored at 254 nm.

E.4 GC-MS analysis

GC-MS analysis of substrates presented in Chapter 7.2.2. All turnovers were TMS-derivatised prior to analysis using excess BSTFA/TMCS (99:1).

4-(3′-Methoxyphenyl)benzoic acid

Refer to Figure 149.

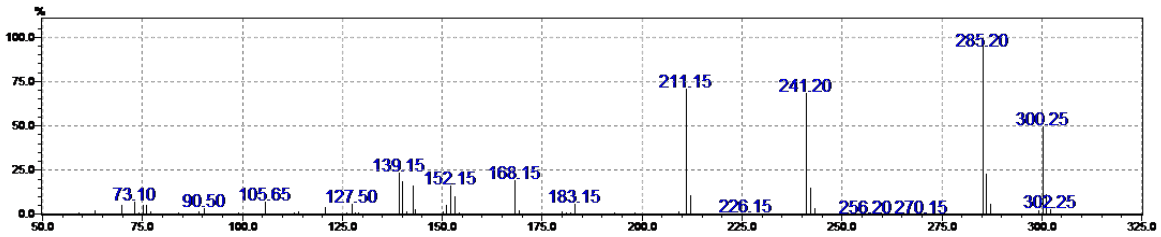

(a) 4-(3′-methoxyphenyl)benzoic acid. RT = 21.8 min. Observed m/z = 300.25 vs expected 300.12.

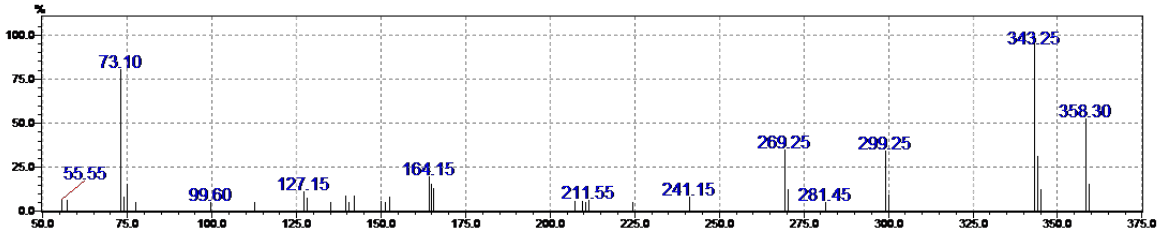

(b) 4-(3′-hydroxyphenyl)benzoic acid. RT = 23.2 min. Observed m/z = 358.30 vs expected 358.14.

4-(4′-Methoxyphenyl)benzoic acid

Refer to Figure 150.

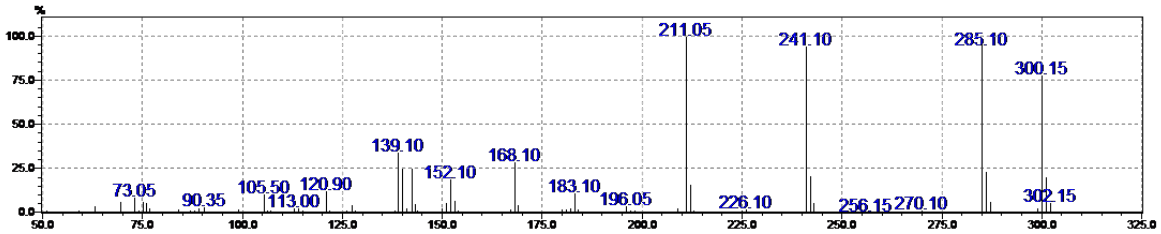

(a) 4-(4′-methoxyphenyl)benzoic acid. RT = 22.4 min. Observed m/z = 300.15 vs expected 300.12.

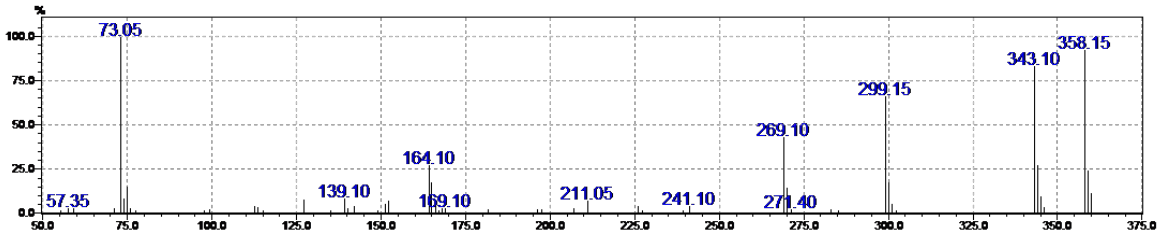

(b) 4-(4′-Hydroxyphenyl)benzoic acid. RT = 24.3 min. Observed m/z = 358.15 vs expected 358.14.

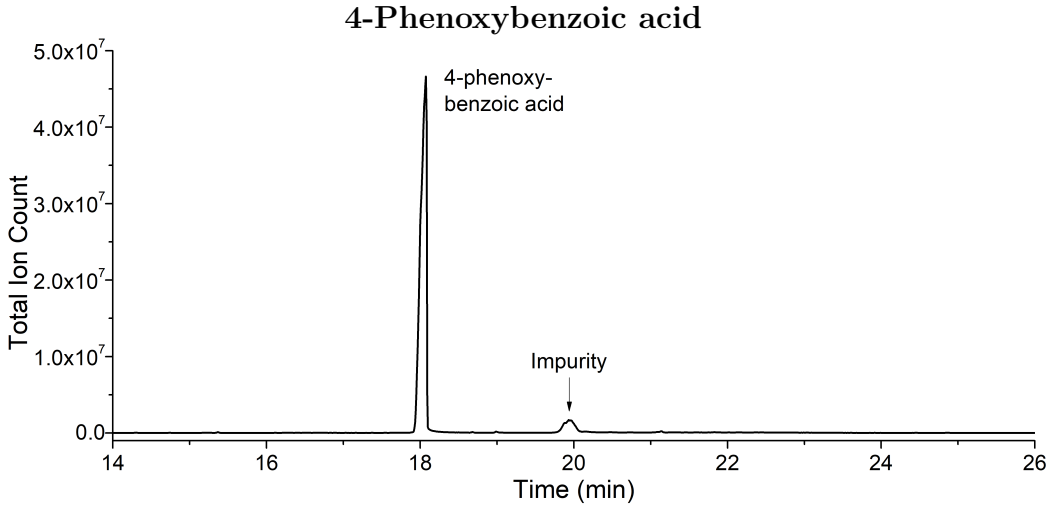

GC-MS analysis of 4-phenoxybenzoic acid *in vitro* turnover with CYP199A4. A impurity which was present in a substrate control is marked (*).

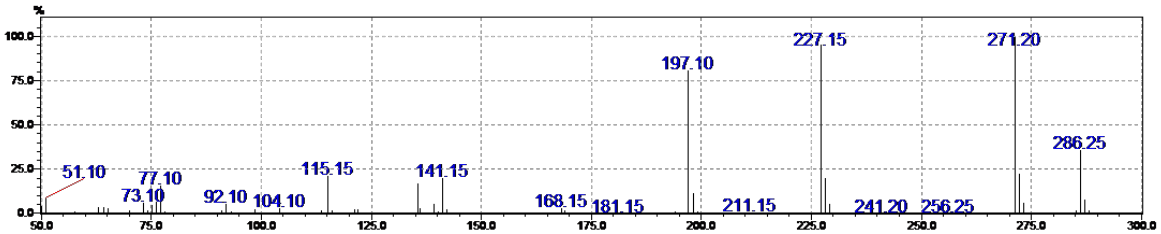

(a) 4-phenoxybenzoic acid. RT = 18.1 min. Observed m/z = 286.25 vs expected 286.103.

4-Phenylbenzoic acid

Refer to Figure 151.

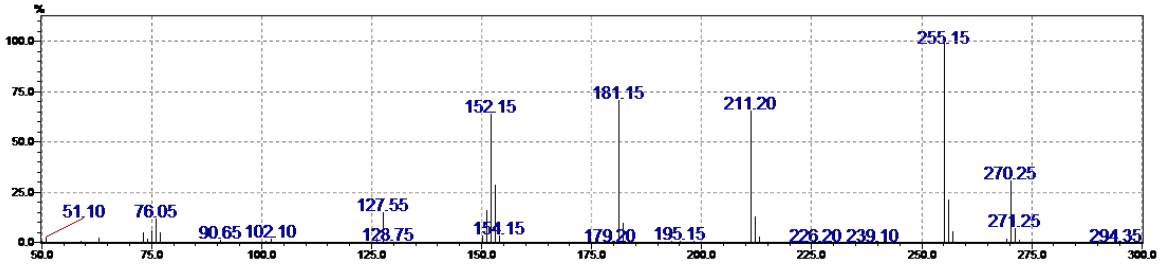

(a) 4-phenylbenzoic acid. RT = 17.7 min. Observed m/z = 270.25 vs expected 270.108.

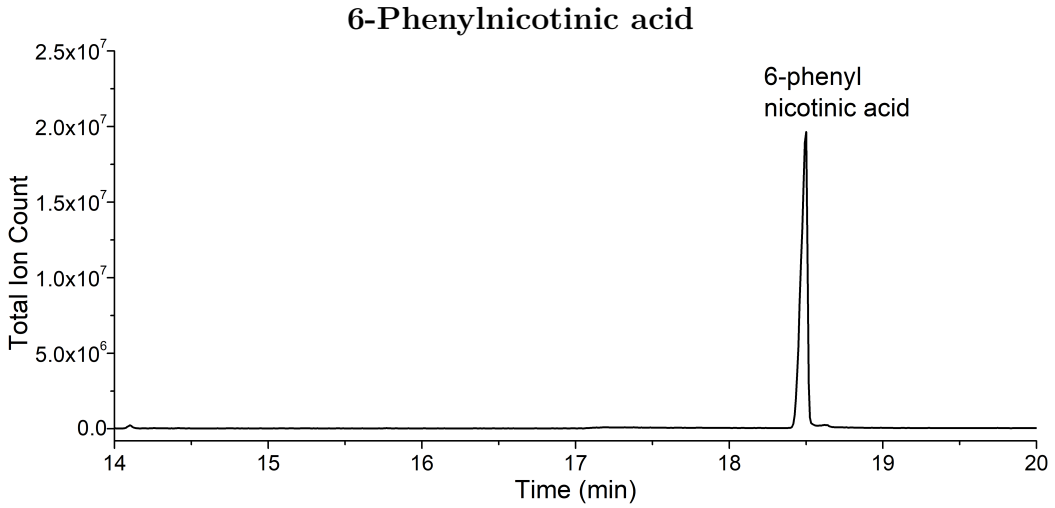

GC-MS analysis of 6-phenylnicotinic acid turnover with CYP199A4.

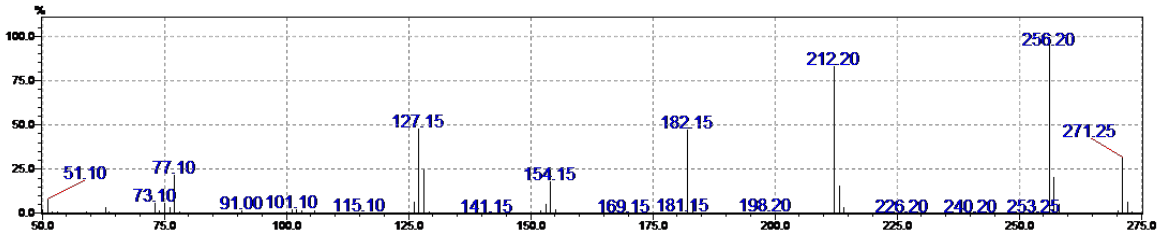

(a) 6-phenylnicotinic acid. RT = 18.5 min. Observed m/z = 271.25 vs expected 271.103.

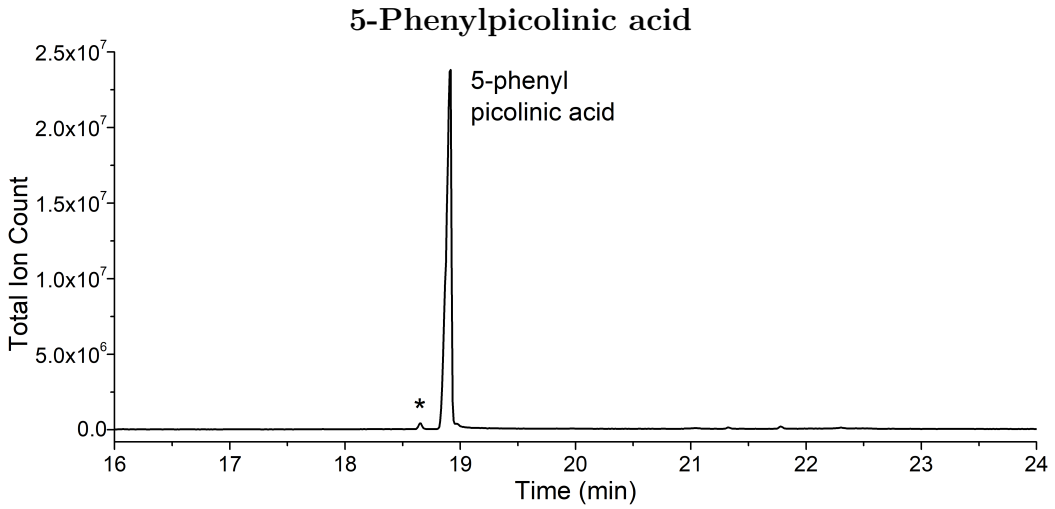

GC-MS analysis of 5-phenylpicolinic acid turnover with CYP199A4. A impurity which was present in a substrate control is marked (*).

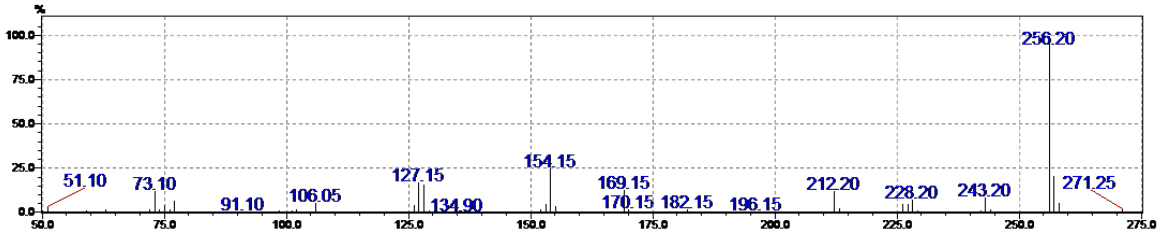

(a) 5-phenylpicolinic acid. RT = 18.9 min. Observed m/z = 271.25 vs expected 271.103.

4-(Furan-2-yl)benzoic acid

Refer to Figure 153.

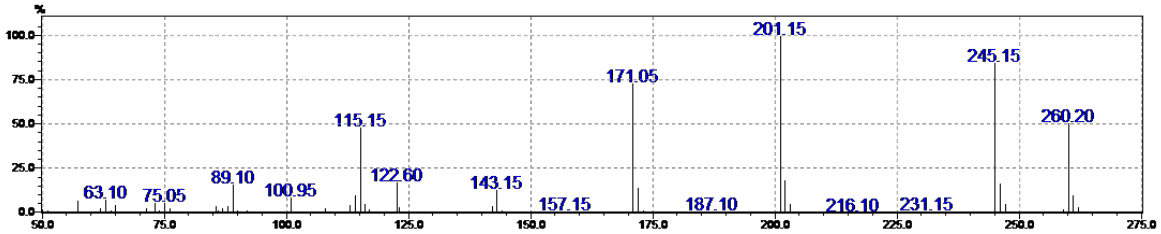

(a) 4-(furan-2-yl)benzoic acid. RT = 14.9 min. Observed m/z = 260.20 vs expected 260.087.

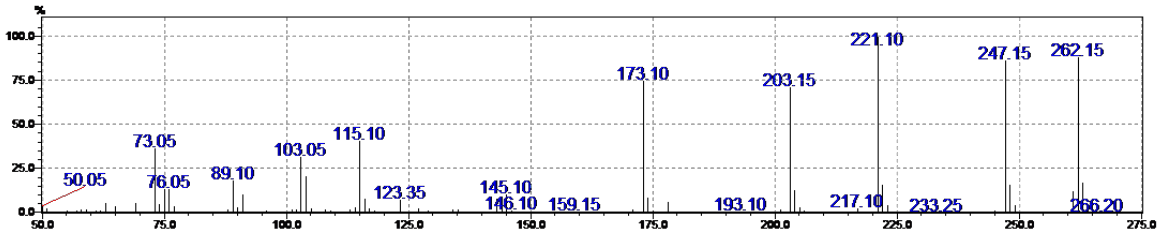

(b) 4-(dihydrofuran-2-yl)benzoic acid. RT = 16.3 min. Observed m/z = 262.15 vs expected 262.103.

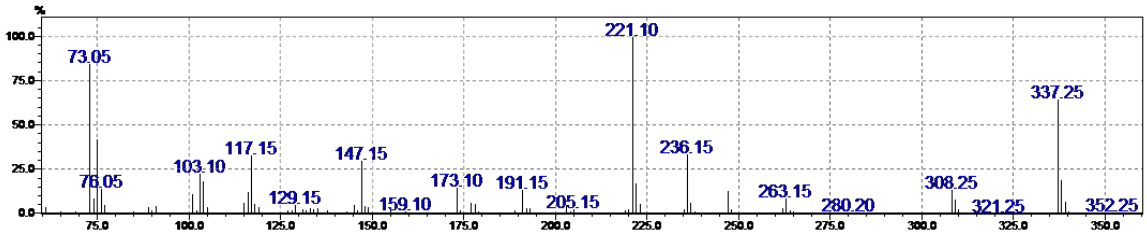

(c) 4-(hydroxytetrahydrofuran-2-yl)benzoic acid. RT = 20.2 min. Observed m/z = 352.25 vs expected 352.153.

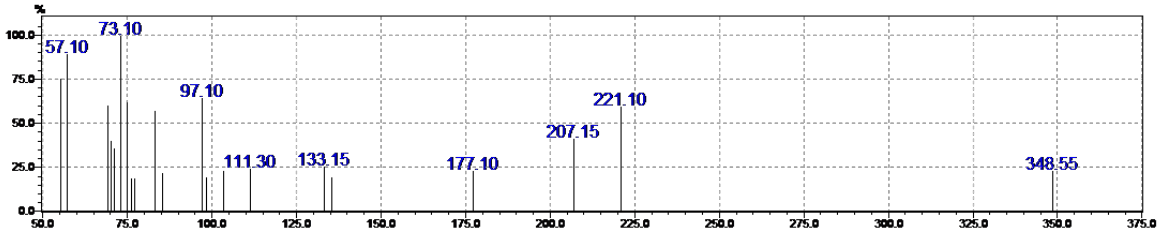

(d) 4-(hydroxyfuran-2-yl)benzoic acid. RT = 20.9 min. Observed m/z = 348.55 vs expected 348.121.

4-(Pyrrol-1-yl)benzoic acid

Refer to Figure 154.

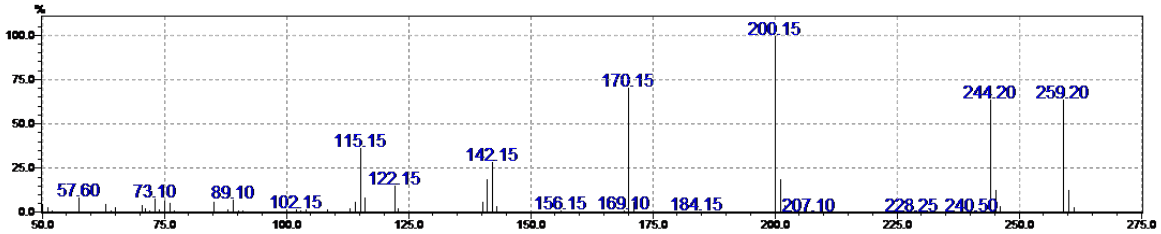

(a) 4-(pyrrol-1-yl)benzoic acid. RT = 15.7 min. Observed m/z = 259.20 vs expected 259.103.

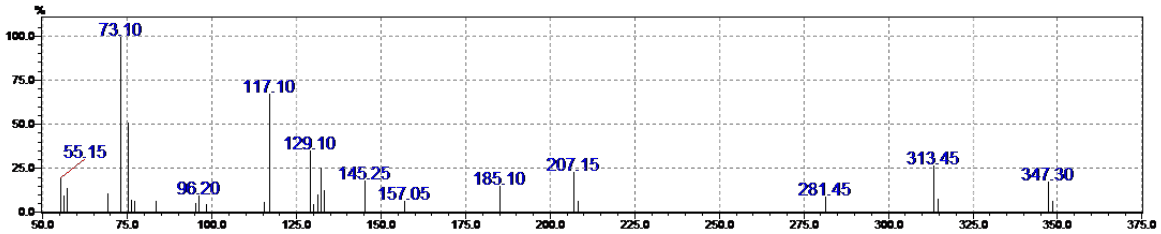

(b) 4-(hydroxypyrrol-1-yl)benzoic acid. RT = 18.6 min. Observed m/z = 347.30 vs expected 347.137.

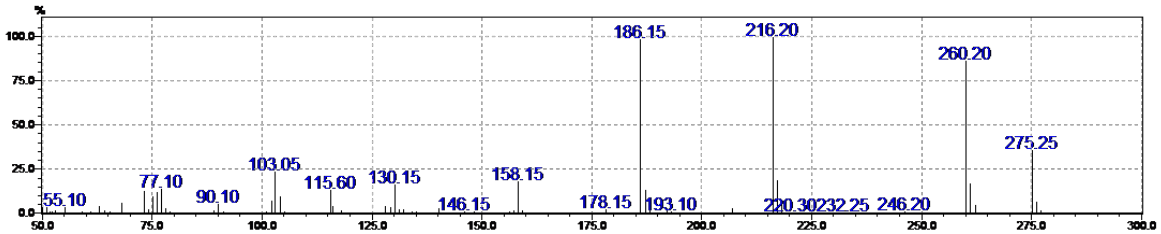

(c) 4-(oxo-dihydropyrrol-1-yl)benzoic acid. RT = 22.3 min. Observed m/z = 275.25 vs expected 275.098.

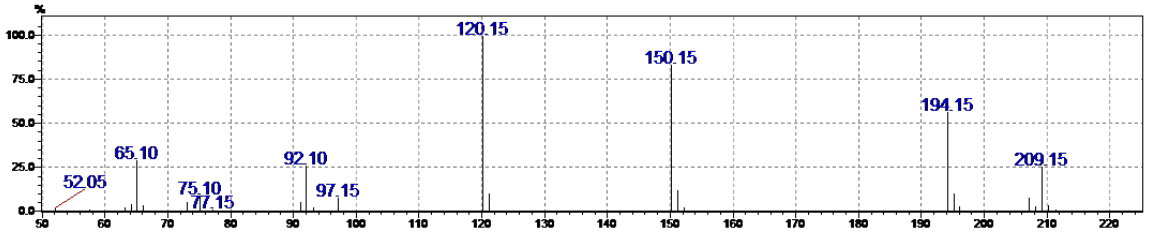

(d) 4-aminobenzoic acid. RT = 11.3 min. Observed m/z = 209.15 vs expected 209.087.

4-(Thiophen-2-yl)benzoic acid

Refer to Figure 155.

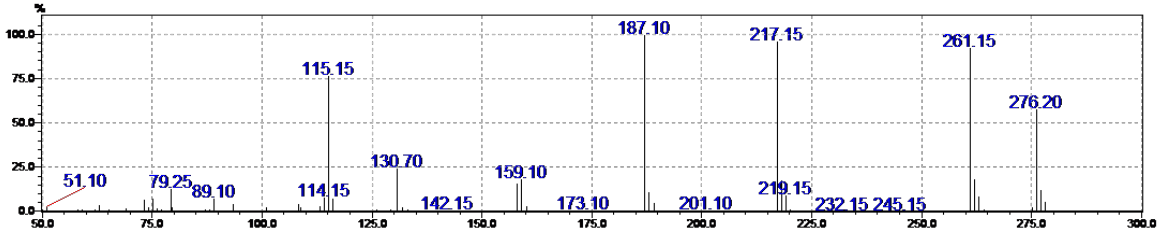

(a) 4-(thiophen-2-yl)benzoic acid. RT = 18.3 min. Observed m/z = 276.20 vs expected 276.064.

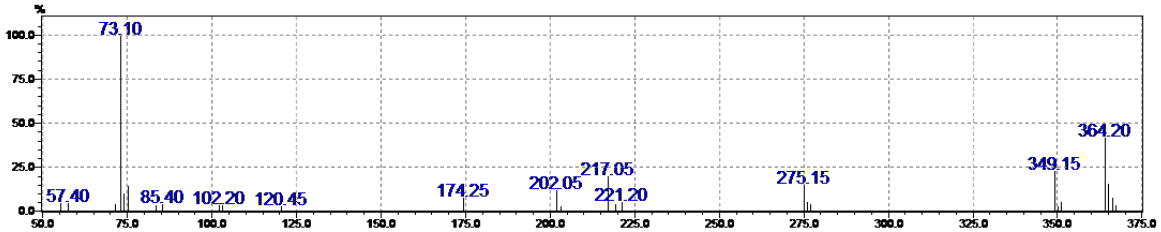

(b) 4-(hydroxythiophen-2-yl)benzoic acid. RT = 21.8 min. Observed m/z = 364.20 vs expected 364.099.

4-(Thiophen-3-yl)benzoic acid

Refer to Figure 157.

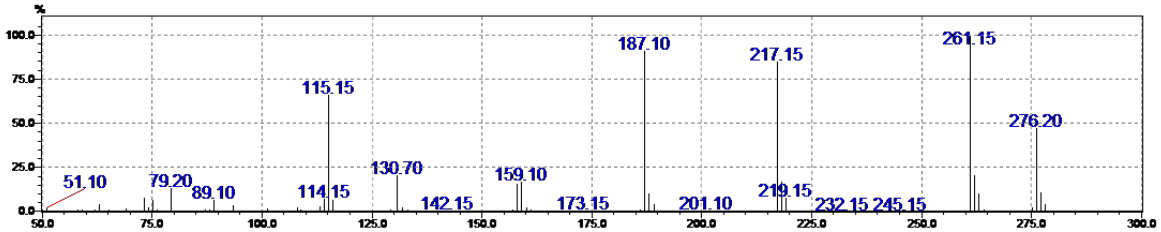

(a) 4-(thiophen-3-yl)benzoic acid. RT = 18.5 min. Observed m/z = 276.20 vs expected 276.064.

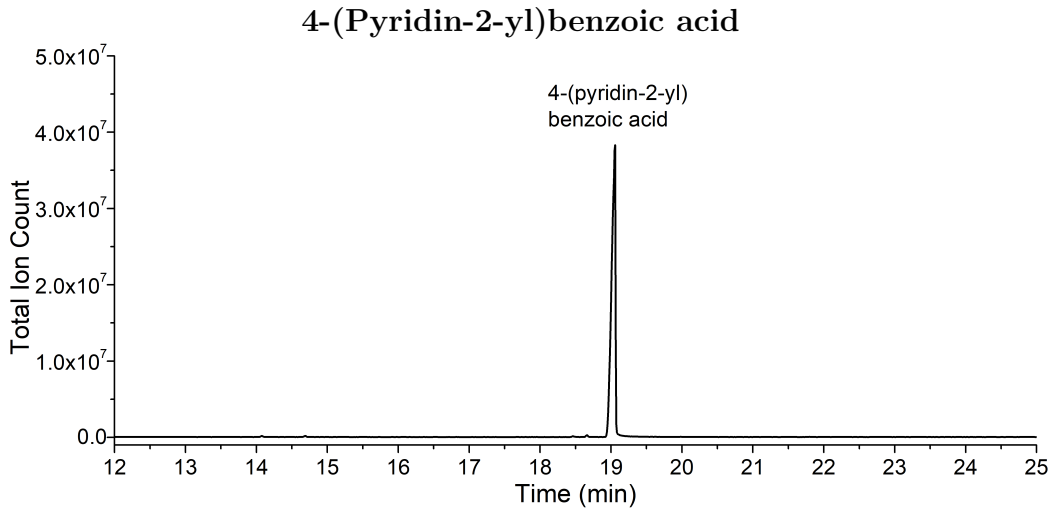

GC-MS analysis of 4-(pyridin-2-yl)benzoic acid *in vivo* turnover with CYP199A4.

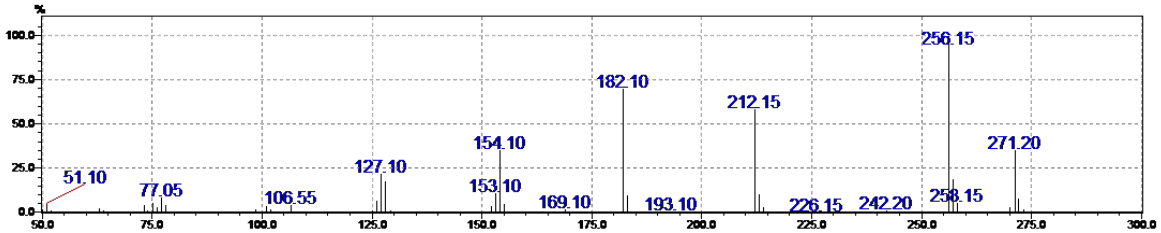

(a) 4-(pyridin-2-yl)benzoic acid. RT = 19.0 min. Observed m/z = 271.20 vs expected 271.103.

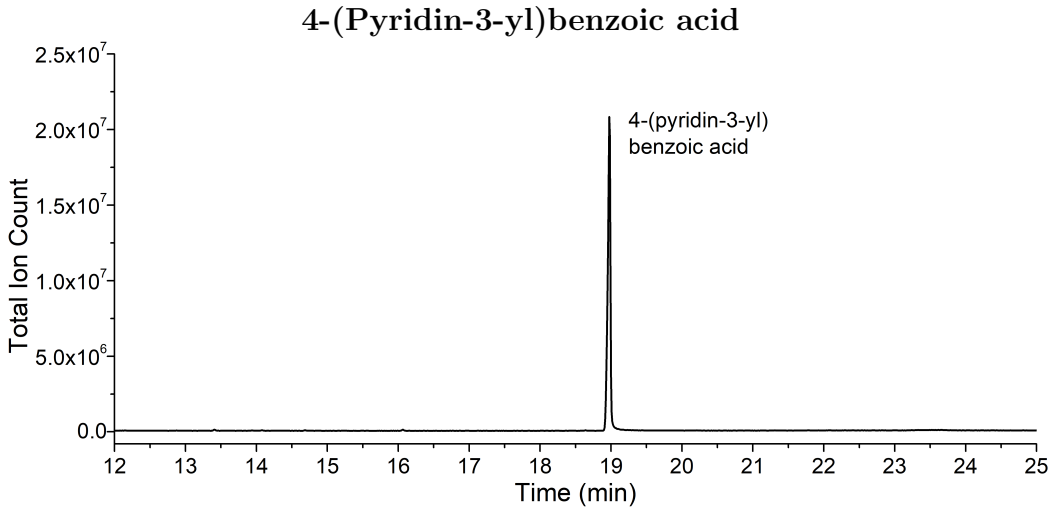

GC-MS analysis of 4-(pyridin-3-yl)benzoic acid *in vivo* turnover with CYP199A4.

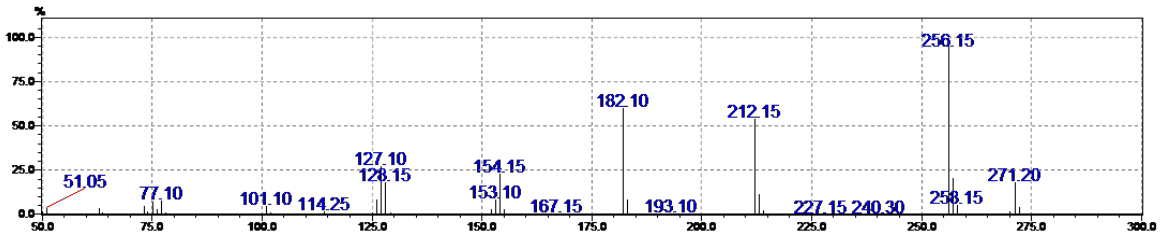

(a) 4-(pyridin-3-yl)benzoic acid. RT = 19.0 min. Observed m/z = 271.20 vs expected 271.103.

E.5 NMR analysis

Products of 4-benzylbenzoic acid

4-(hydroxyphenylmethyl)benzoic acid: 500 MHz, d_6-DMSO.

^{1}H: δ 5.76 (s, 1H, **6**), 6.03 (s, 1H, **6 (OH)**), 7.20 (t, 1H, **10**), 7.30 (t, 2H, **9**), 7.37 (d, 2H, **8**), 7.49 (d, 2H, **4**), 7.87 (d, 2H, **3**).

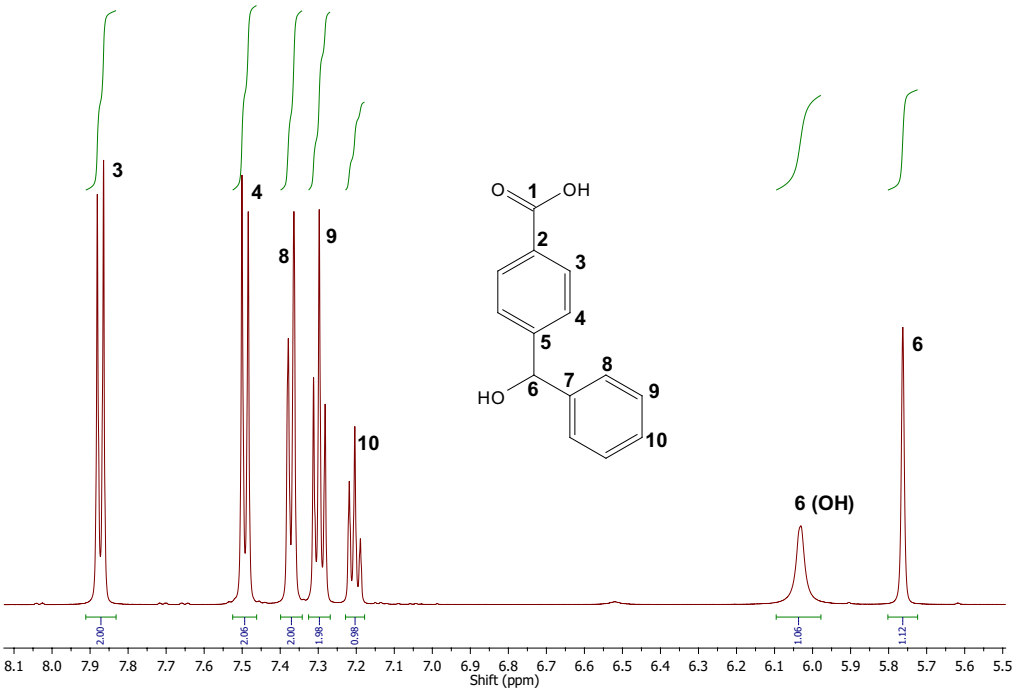

^{13}C: δ 77.01 (**6**), 129.34 (**3**/**4**), 129.42 (**3**/**4**), 130.06 (**10**), 131.30 (**4**), 132.30 (**7**), 132.35 (**3**), 148.18 (**5**), 153.71 (**2**), 170.29 (**1**).

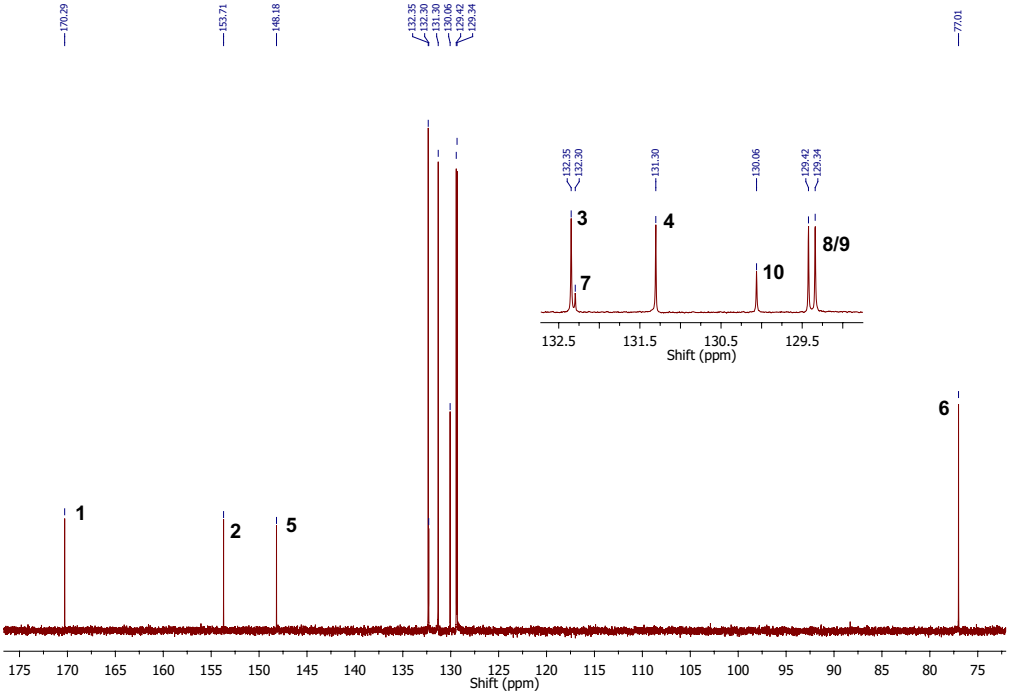

^{1}H-^{1}H COSY:

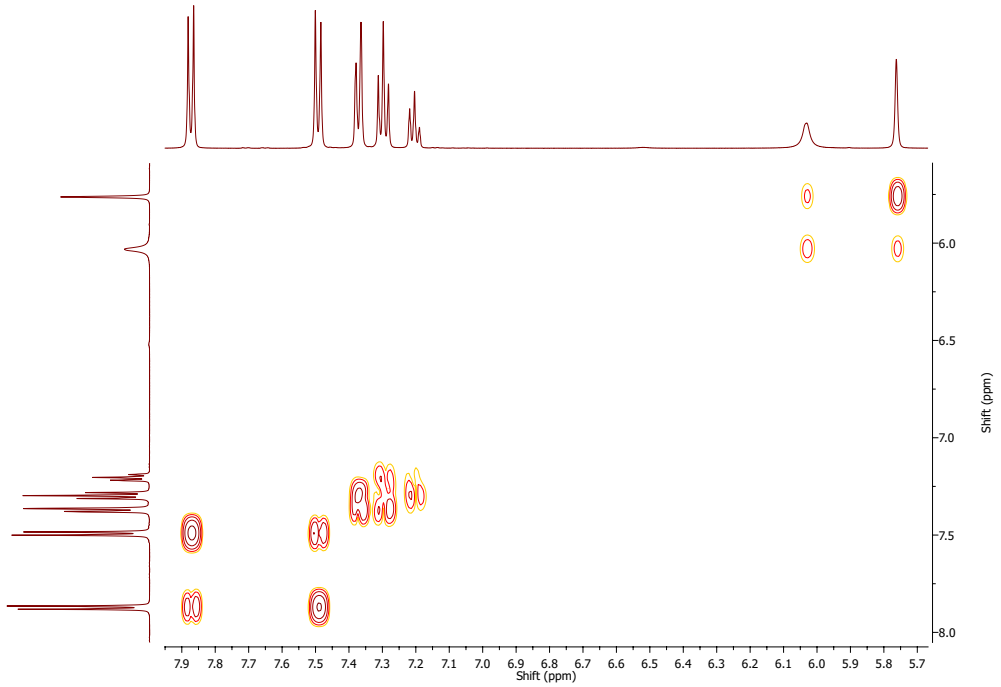
6.0
6.5
7.0
7.5
8.0
Shift (ppm)
7.9 7.8 7.7 7.6 7.5 7.4 7.3 7.2 7.1 7.0 6.9 6.8 6.7 6.6 6.5 6.4 6.3 6.2 6.1 6.0 5.9 5.8 5.7
Shift (ppm)

4-benzoylbenzoic acid: 500 MHz, d_6-DMSO.
^{1}H: δ 7.58 (t, 2H, **9**), 7.71 (t, 1H, **10**), 7.76 (d, 2H, **8**), 7.82 (d, 2H, **4**), 8.09 (d, 2H, **3**).

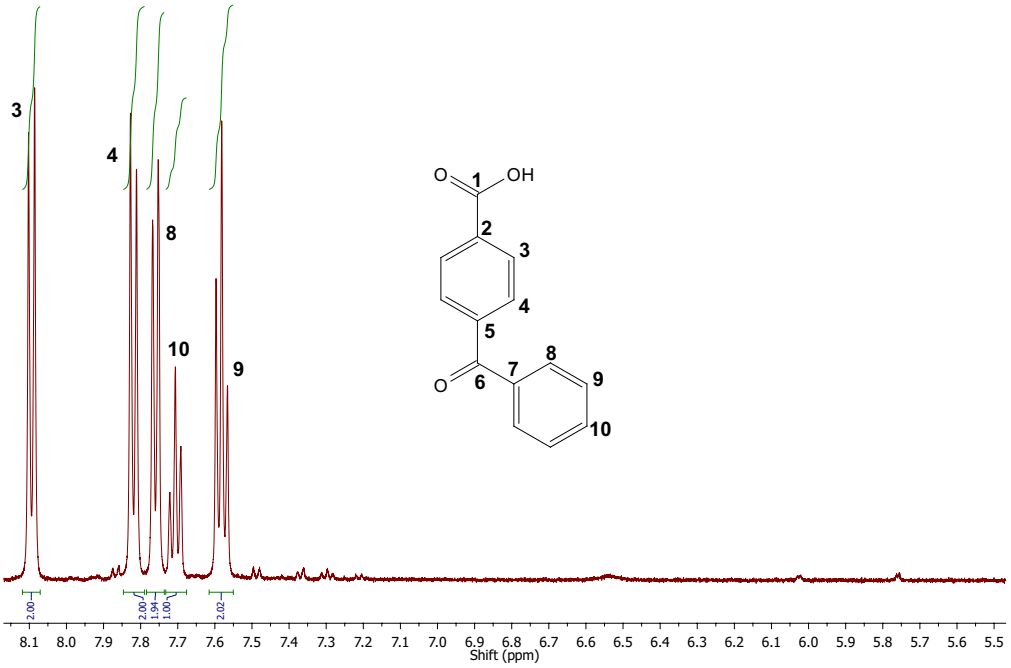

^{1}H-^{1}H COSY: